UNIVERSITÉ DE GENÈVE

Archive ouverte UNIGE
https://archive-ouverte.unige.ch

Thèse 2011

Open Access

This version of the publication is provided by the author(s) and made available in accordance with the copyright holder(s).

Constraints on planetary formation from the discovery & study of transiting Extrasolar Planets

Triaud, Amaury

How to cite

TRIAUD, Amaury. Constraints on planetary formation from the discovery & study of transiting Extrasolar Planets. Doctoral Thesis, 2011. doi: 10.13097/archive-ouverte/unige:18065

This publication URL: https://archive-ouverte.unige.ch/unige:18065
Publication DOI: 10.13097/archive-ouverte/unige:18065

© This document is protected by copyright. Please refer to copyright holder(s) for terms of use.

UNIVERSITÉ DE GENÈVE
Département d'Astronomie

FACULTÉ DES SCIENCES
Professeur Didier Queloz

Constraints on Planetary Formation from the Discovery & Study of Transiting Extrasolar Planets

THÈSE

présentée à la Faculté des sciences de l'Université de Genève pour obtenir le grade de Docteur ès sciences, mention Astronomie et Astrophysique

par

Amaury H.M.J. TRIAUD

de

Bordeaux (France)

Thèse N° 4342

GENÈVE
Observatoire Astronomique de l'Université de Genève
2011

UNIVERSITÉ
DE GENÈVE
FACULTÉ DES SCIENCES

Doctorat ès sciences
Mention astronomie et astrophysique

Thèse de *Monsieur Amaury TRIAUD*

intitulée :

"Contraints on Planetary Formation from Discovery & Study of Transiting Extrasolar Planets"

La Faculté des sciences, sur le préavis de Messieurs D. QUELOZ, professeur associé et directeur de thèse (Département d'astronomie – Observatoire de Sauverny), G. MEYNET, professeur ordinaire (Département d'astronomie – Observatoire de Sauverny), W. BENZ, professeur (Universität Bern – Physikalisches Institut – Bern, Schweiz), et A. COLLIER CAMERON, professeur (Scottish Universities Physics Alliance – School of Physics and Astronomy – University of St Andrews – St Andrews, Scotland), autorise l'impression de la présente thèse, sans exprimer d'opinion sur les propositions qui y sont énoncées.

Genève, le 28 août 2011

Thèse - 4342 -

Le Doyen, Jean-Marc TRISCONE

N.B. - La thèse doit porter la déclaration précédente et remplir les conditions énumérées dans les "Informations relatives aux thèses de doctorat à l'Université de Genève".

Ce travail de thèse a donné lieu à des publications dont la liste se trouve à la page 265.



UNIVERSITÉ
DE GENÈVE

Contraintes sur la Formation Planétaire grâce à la Découverte et l'Étude de Planètes Extrasolaires en Transit

Après des siècles de questionnement sur la présence d'autres mondes en dehors de notre Système Solaire, les premières planètes extrasolaires ont été découvertes il y a une quinzaine d'années. Depuis, la quête a continué. La plus grande découverte de notre nouvelle ligne de recherche scientifique, l'*exoplanétologie*, a sans aucun doute été la grande diversité que ces nouveaux mondes nous offrent ; une diversité en masse, en taille, en périodes orbitales ainsi que sur l'architecture de ces systèmes que nous découvront. Des planètes bien différentes que celles composant notre système ont été détectées. Ainsi nous connaissons l'existence des *Jupiters chauds*, géantes gazeuses dont la période orbitale n'est que de quelques jours, des *mini-Neptunes*, corps de cinq à dix fois la masse de notre Terre mais couvertes d'une épaisse couche gazeuse, des *super-Terres*, planètes de masse similaire mais rocheuses, des mondes de lave, et récemment, peut-être la première planète océan. D'autres surprise nous attendent sûrement.

Cette thèse se porte sur une classe de planètes bien particulière : les Jupiters chauds. Ces mondes étonnants sont encore mal compris. Mais, grâce à l'évolution des techniques d'observation et du traitement de leurs signaux, nous en connaissons maintenant autant que ce que nous connaissions de nos propres géantes gazeuses avant leur visite par des sondes spatiales. Ce sont des laboratoires pour toute une série de phénomènes physiques intenses causés par leur proximité avec leur étoile. Notamment, ces planètes sont en moyenne bien plus large qu'attendu. Au-delà de ces étrangetées, leur présence si proche de leur étoile est anormale, les conditions nécessaires pour former des planètes aussi massive, aussi proche, ne semblant pas réalisables. Dès lors il est plus raisonnable d'expliquer leurs orbites actuelles par une formation loin de l'étoile suivie d'une migration orbitale. C'est sur ce dernier sujet que porte cette thèse : l'origine des Jupiters chauds.

Les lois de la physique sont universelles. Ainsi utilisant les mêmes phénomènes physiques nous devons pouvoir expliquer l'existence des Jupiters chauds tout en expliquant pourquoi le Jupiter de notre Système Solaire se trouve à cinq fois la distance Terre-Soleil. En Astronomie, on ne peut faire d'expérience - nous en faisons partie. À la place, nous cherchons et caractérisons plusieurs objets similaires afin de dégager statistiquement des informations. Pour répondre à notre question il faut ainsi trouver plusieurs objets et détecter les indices de leur histoire passée afin de pouvoir remonter aux processus qui ont mené à leur formation.

Il y a plusieurs manières de trouver des planètes. Pour cette thèse, la méthode dite des transits a été employée. Elle consiste à detecter une perte périodique de la lumière originant d'une étoile devant laquelle une planète passe : un transit. Cette méthode est particulièrement sensible à la présence de Jupiters chauds. Pendant cette thèse une cinquantaine de nouvelles planètes de ce type ont ainsi été découvertes, consistant près d'un tiers des Jupiters chauds connus. Ces planètes

sont confirmées grâce des mesures de vitesses radiales, ces-mêmes qui menèrent à la découverte de la première planète extrasolaire, autour de l'étoile 51 Pegasi. L'analyse de l'ensemble des signaux lumineux produits par la présence d'une planète autour de son étoile, notamment ceux reçus pendant un transit permettent de connaître la masse, la taille de la planète, sa période orbitale, la forme de son orbite, sa température, même la composition chimique de son atmosphère. Par ailleurs ces observations permettent aussi d'étudier l'étoile autour de laquelle se trouve cette planète, comme sa masse, sa taille, sa vitesse de rotation ainsi que son âge dans une certaine mesure.

Un type d'observation en particulier fut employé : l'effet Rossiter-McLaughlin. Lors du transit, cet effet crée une anomalie par rapport aux vitesses radiales attendues. Par la modélisation de cette anomalie, il est possible de mesurer la projection de l'angle entre le plan orbital de la planète et le plan équatorial de l'étoile, sur le ciel.

Dans notre Système, toutes les planètes se situent dans un même plan à peu de chose près : l'écliptique. Le plan équatorial du Soleil est aussi presque aligné avec l'écliptique. Cette observation mena Kant et Laplace à postuler sur la formation de planètes à partir de matériaux disposés dans la forme d'un disque primordial entourant le Soleil, disques observés de nos jours autour d'étoiles jeunes.

Cet angle orbital a été mesuré pour les planètes découvertes, et, de manière surprenante, au lieu d'observer des planètes en orbite au dessus de l'équateur de leur étoile, une énorme variété a été trouvée. Certaines planètes sont même en orbite dans le sens contraire de celui attendu. Ces observations combinées avec d'autres du même type, ainsi qu'avec les autres paramètres déja connus de cette étonante population de planètes, permettent d'explorer les phénomènes s'étant produit sans doute peu de temps après leur formation.

Ces Jupiter chauds ont eu une histoire mouvementée. Lorsque le disque dans lequel ils se sont formés s'est dissipé, des interactions gravitationelles avec d'autres planètes au sein du même système, ou causées par la présence d'une seconde étoile dans le système, ont mené ces géantes gazeuses sur des orbites inclinées voire rétrogrades, et très elliptiques. Lors de leurs passages au plus proche de l'étoile, la dissipation des forces de marées au sein de ces planètes ainsi que dans l'étoile ont progressivement mené à une circularisation et une réduction de leurs périodes orbitales, sur lesquelles nous les observons de nos jours.

Forewords

After centuries of wondering about the presence of other worlds outside our Solar System, the first extrasolar planets were discovered about fifteen years ago. Since the quest continued. The greatest discovery of our new line of research, *exoplanetology*, has probably been the large diversity that those new worlds have brought forward; a diversity in mass, in size, in orbital periods, as well as in the architecture of the systems we discover. Planets very different from those composing our system have been detected. As such, we found *hot Jupiters*, gas giants which orbital period is only of a few days, *mini-Neptunes*, bodies five to ten time the mass of the Earth but covered by a thick gas layer, *super-Earths* of similar masses but rocky, lava worlds, and more recently, maybe the first ocean planet. Many more surprises probably await us.

This thesis has for subject this very particular planet class: the hot Jupiters. Those astonishing worlds are still badly understood. Yet, thanks to the evolution of observational techniques and of the treatment of their signals, we probably have gathered as much knowledge from these worlds, than what was known of our own gas giants prior to their visit by probes. They are laboratories for a series of intense physical phenomena caused by their proximity to their star. Notably, these planets are found in average much larger than expected. In addition to these curiosities, their presence so close to their star is abnormal, the necessary conditions for the formation of such massive bodies, this close, not being plausible. Thus it is more reasonable to explain their current orbits by a formation far from their star, followed by an orbital migration. It is on this last subject that this thesis is on: the origin of hot Jupiters.

The laws of physics are universal. Therefore, using the same physical phenomena, we need to explain the existence of hot Jupiters, while explaining why the Jupiter within our Solar System is found five times the Earth-Sun distance. In Astronomy, we cannot do experiments; we are a part of it. Instead, we search and characterise several similar objects in order to extract information out of them statistically. To answer our question, we needed to find several objects and detect the clues from their past history bringing us back to the processes that led to their formation.

There are several manners with which one can find planets. For this thesis, the so-called transit method was used. It consists in detecting a periodic loss of light from a star in front of which a planet passes: a transit. This method is particularly sensitive to the presence of hot Jupiters. During this thesis, about fifty planets of such type have been discovered, about a third of the known hot Jupiters. Those planets are confirmed thanks to radial velocity measurements, the same technique that led to the discovery of the first extrasolar planet, around the star 51 Pegasi. The analysis of the stellar light affected by the presence of a planet around it, notably the light received during transit, allows us to know about the mass, the size of the planet, its orbital period, the shape of its orbit, its temperature, even the chemical composition of its atmosphere. Furthermore, these observations give us the occasion to study the star around which is found the planet, such as its mass, its size, its rotation speed, as well as give estimates on its age.

One type of observations was employed in particular: the Rossiter-McLaughlin effect. During transit, this effect creates an anomaly compared to the expected radial velocities. Through a modelisation of this anomaly, it is possible to measure the projection of the angle between the orbital plane of the planet and the equatorial plane of the star, on the sky.

In our System, all planets are located more or less in a same plane : the ecliptic. The equatorial plane of the Sun is also almost aligned with the ecliptic. This observation led Kant and Laplace to postulate on the formation of planets from matter spread in the form of a primordial disc around the Sun; such discs are nowadays observed around young stars.

This angle was measured for the newly discovered planets, and, surprisingly, instead of observing planets in orbit above the equator of their star, a wide variety was found. Some planets are even in orbit in the direction counter to that which was expected. Those observations, combined with others of similar type, as well as with those already known parameters from that astonishing planet population, allow us to explore the phenomena that occurred probably soon after their formation.

Those hot Jupiters have had an eventful history. When the disc in which they formed dissipated, gravitational interactions with other planets in the same system, or caused by the presence of another star in the system, have led those gas giants on inclined, some retrograde, and very elliptic orbits. During their regular passage at the closest point with their star, the dissipation of tidal forces within the planet and the star induced a circularisation and a reduction of their orbital periods, on which we observe them nowadays.

Thanks

A thesis is often seen as the work of a single person. The title only carries my name, and that of my supervisor, in small on the top left. No one else. Yet without the help and support of many people, this work would not have been realised. Newton said that he rested on the shoulders of giants, being no Newton, I have many a giant carrying me.

I will start by giving thanks to the technical staff of the observatory, often overlooked (for example absent from our scientific papers). Yet, how often have I been happy to have someone to phone to when all things broke at the telescope, or when using the automated reduction softwares giving ample time to focus on other things. Generally speaking, the conviviality, availability and help from people at the mécanique or from administration and IT made my time in Genève very pleasant.

My greatest thanks go to Didier who gave me much independence and freedom during those four years, especially that of trusting me and leaving me develop and test out ideas on the Swiss Telescope in La Silla, leading to new observing programs. This was while teaching me how to research, and helping me politically, by smoothing the mess I sometimes found myself in, or by suggesting my name to various conference scientific committees. He is also responsible for pushing me to learn how to drive, something even my Grandma did not manage to convince me of doing.

The planet's group is boiling with enthusiasm, ideas and help. To work in such an environment, with such availability of telescope time, data, analysing tools and expertise, along with friendship was simply extraordinary. Special thanks go to Damien Ségransan, Pedro Figuiera and Maxime Marmier and our far reaching discussions and debates, often not astronomical, to Johannes Sahlmann, sharing my office, for introducing me to astrometry and for suffering my instant bursts of enthusiasm at any random new result, article or email appearing on my screen (sorry for the ever growing mess on my desk), to Michaël Gillon for the close, fruitful and continuing collaboration, to Nami Mowlavi for his help, work and presence about the Geneva stellar evolution tracks, to Michel Mayor and Stéphane Udry for keeping an interest on my work, to Roi Alonso, Anahí Granada, Richard Anderson, Monika Lendl and all the members of the good company of people regularly going out for dancing, eating, drinking, laughing...

I still cannot entirely comprehend the chance to have work along with the WASP consortium, notably David Anderson, Barry Smalley, Andrew Collier Cameron, Elaine Simpson, Don Pollacco, and Coel Hellier. The easy-going and friendly approach you applied during our collaboration and the quality of your work certainly helped make mine much better.

I also have to acknowledge the many discussions with colleagues (sometimes also competitors) from other universities, met on the conference trail. Again the chance to talk and exchange ideas, have raised my interest for many subjects and prevented many misinterpretations. I would like to especially name Christoph Mordasini, Soko Matsumura, Rosemary Mardling, Dan Fabrycky, Greg Laughlin and Willy Kley on the theoretical side, Josh Winn, Leslie Hebb, Rachel Street, François Bouchy, Isabelle Boisse, Simon Albrecht and Norio Narita on the observational side.

To Günther Wuchterl I owe an early interest for planetary orbital migration, to Andrew Collier Cameron my introduction to WASP and the correction of this document, to Caroline Soubiran the beginning of my astronomical work and to Thomas Robitaille, the emergence of my interest in Astronomy and the revelation that one could actually follow it.

Finally, I thank my parents for the education they gave me and the support during my studies, notably by giving me the opportunity to study abroad. They allowed me to develop a much treasured critical thinking.

THE JURY THAT ASSESSED THIS THESIS WAS COMPOSED BY:

GEORGES MEYNET & DIDIER QUELOZ,
UNIVERSITÉ DE GENÈVE, SWITZERLAND

WILLY BENZ,
UNIVERSITÄT BERN, SWITZERLAND

AND

ANDREW COLLIER CAMERON
UNIVERSITY OF ST ANDREWS, SCOTLAND, UK

À la source de toute science se trouve la surprise que les choses soient comme elles sont
ARISTOTE

At the beginning of all science is the surprise that things are the way they are
ARISTOTLE

Contents

Résumé en français i

Forewords iii

Thanks v

1 Introduction & Basic Principles 1
- 1.1 Historical Background . . . 1
- 1.2 Orbits, Spectroscopy & Binary stars . . . 4
  - 1.2.1 Orbital motion . . . 4
  - 1.2.2 Spectroscopy and the Doppler effect . . . 5
  - 1.2.3 Binary stars . . . 7
- 1.3 Extrasolar Planets . . . 8
  - 1.3.1 Direct detection method . . . 9
  - 1.3.2 Indirect detection methods . . . 10
  - 1.3.3 Characterisation methods . . . 15
  - 1.3.4 State of the field . . . 20
- 1.4 Organisation of the Thesis . . . 21

2 Tools to Study Extrasolar Planets 23
- 2.1 The Models . . . 23
  - 2.1.1 A planetary transit . . . 23
  - 2.1.2 The Rossiter-McLaughlin effect . . . 26
- 2.2 Adjusting Models to Data and Extracting Meaningful Error Bars . . . 27
  - 2.2.1 A Markov chain Monte Carlo . . . 28
  - 2.2.2 Adapting the models . . . 31
  - 2.2.3 Inserting priors . . . 35
  - 2.2.4 Extracting statistics . . . 35
  - 2.2.5 A toy model . . . 36
- 2.3 First Applications on Photometry & Radial Velocities . . . 50
  - 2.3.1 Improved parameters for HD 17156 b . . . 50
  - 2.3.2 Improved parameters for WASP-4 b & WASP-5 b . . . 56
- 2.4 Planetary Occultations . . . 66
- 2.5 Applications Using the Rossiter-McLaughlin Effect . . . 76
  - 2.5.1 The Rossiter-McLaughlin effect of CoRoT-2b . . . 76
  - 2.5.2 Exploring the limits of fitting the Rossiter-McLaughlin effect . . . 81
- 2.6 Adding Stellar Isochrones . . . 89
  - 2.6.1 Description of the method . . . 89

2.6.2 Case study on WASP-8 & WASP-23 . . . 99

3 Discovering Transiting Extrasolar Planets 105
3.1 The WASP Survey . . . 105
3.2 Using *Euler* to Confirm Transiting Hot Jupiters . . . 108
3.3 From a Candidate to a Confirmed Planet . . . 114
3.3.1 *On/Off* photometry . . . 115
3.3.2 Checking the spectrum . . . 116
3.3.3 No variations, or another period . . . 120
3.3.4 Bissector, FWHM & mask variations . . . 120
3.3.5 Doppler imaging for odd cases . . . 121
3.4 Using the Tool for Discovery & Immediate Characterisation . . . 122
3.4.1 WASP-6 b . . . 122
3.4.2 Discovery of CoRoT-5 b . . . 131
3.4.3 The WASP-8 triple star system . . . 138
3.4.4 Analysing WASP-23 b . . . 143
3.5 The Southern WASP Planet Collection . . . 156
3.6 Summary of the WASP/CORALIE Survey . . . 181
3.6.1 WASP results in numbers . . . 181
3.6.2 Evolution of results and detection capacity . . . 188
3.7 The Rossiter-McLaughlin Effect as a Detection Tool . . . 191

4 Rossiter-McLaughlin Observations 199
4.1 The Change that Came . . . 200
4.2 Newer Results . . . 224

5 Interpretation regarding the Origins of hot Jupiters 233
5.1 The Origins of hot Jupiters . . . 233
5.2 Observational Clues . . . 242
5.2.1 Using the multiplicity argument . . . 242
5.2.2 The metallicity correlation . . . 247
5.2.3 The eccentricity distribution . . . 247
5.2.4 The study of our own Solar System . . . 247
5.2.5 Spin/orbit angles . . . 248
5.3 Planets' history . . . 255

6 Conclusion 259
6.1 Prospects . . . 261
6.1.1 The future of WASP . . . 261
6.1.2 WASP and binaries . . . 261
6.1.3 The WASP transiting M-dwarfs . . . 262
6.1.4 Treating the Rossiter-McLaughlin effect better . . . 262
6.1.5 Calibrating stellar evolution models . . . 263

A Publications related to this thesis 265

List of Figures 272

List of Tables 273

References 275

Chapter 1

Introduction & Basic Principles

One has to start somewhere. I have decided to take that starting point as far in the past as I could, from knowledge that was gathered, not for this production but for public performances, mostly given at the Observatoire in the course of public visits. Having gathered this historical material in order to answer the multiple questions that inevitably come from the public, I thought it would make a good starting point to this thesis by positioning it in the long and slow evolution of our species' understanding of the Universe.

1.1 Historical Background

The definition of the word *planet* has changed a few times throughout human history. Semantically, *planet*, in most European languages, comes from the ancient Greek *planetos* meaning a wandering star; a star, a point of light in the night sky, that moves a contrario with the others that do not. Those wandering stars are fairly easy to spot in the sky thanks to their brightness, their lack of scintillation and their position: aligned with the evening and morning zodiacal lights, very evident in a clear and dark night. Astronomy was born from that dichotomy between the motion of planets and the apparently eternal position of stars.

Traditionally (at least since Babylonian times), and for the majority of human history, there has been seven planets: the Sun, the Moon, Mercury, Venus, Mars, Jupiter and Saturn. They appear to have been known by most civilisations and have probably given the number of days in a week. A planet then was not considered the same as a *world*. The Earth was not considered a planet: for its apparent lack of motion and its lack of light emission. So, in the third century BC, when the Greek philosopher Epicurus wrote to Herodotus:

> [...] there is an infinite number of worlds, some like this world, others unlike it. [...] Hence there will be nothing to hinder an infinity of worlds.
>
> [...] we must not suppose that the worlds have necessarily one and the same shape. For nobody can prove that in one sort of world there might not be contained, whereas in another sort of world there could not possibly be, the seeds out of which animals and plants arise and all the rest of the things we see.

the worlds that he writes about are not the planets of then. For planets to be considered as worlds we have to wait for the Galilean revolution, happening during the European Renaissance, and

marking the beginning of modern science. Before this, Astronomy could only rely on one sole type of measurement: astrometry; positioning.

From the position of planets and from clear reasoning, the ancients modelled mathematically the apparent motion of the planets in the night sky to an incredible level of sophistication which lead to their mechanical modelisation in a geocentric orrery called the Antikythera mechanism[1]. It comprised many wheels for each planet, some used as epicycles in order to reproduce the apparent retrograde motion of the outer planets in the sky, but also the analemma, the varying distance between Earth and Moon and the phases of the Moon. This machine intended for use on Earth therefore reproduced accurately the position of the planets in the night sky and the coming of solar and lunar eclipses.

Heliocentric ideas permeate history, from Greece in the III$^{\text{rd}}$ century BC, to India in the V$^{\text{th}}$ century, Persia in the XII$^{\text{th}}$ century, Andalucia in the XIV$^{\text{th}}$ and Nikolaus Copernicus in XVI$^{\text{th}}$ century Poland. A probable reason why they never took a hold was that none could answer its main criticism: that if Earth is hurtling through space around the Sun, why are the stars not showing a parallax. The answer we now give to this question is that stars are incredibly far away, but this argument was not receivable then since it could be perceived as a completely unconstrained fudge factor: one could always place the stars further than the current best astrometric measurements.

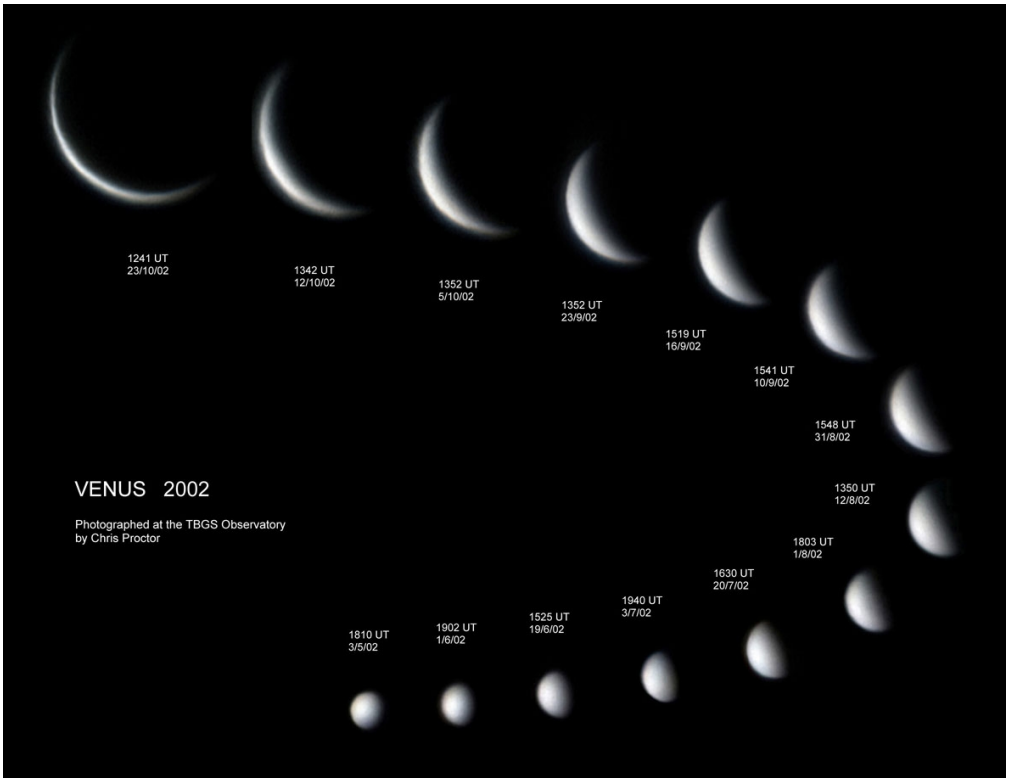
Galileo Galilei, having improved the optics of a Dutch spyglass for the count of the Venetian navy, proved that the image the instrument showed was not an alternate reality by accurately reporting details such as the type of ships and crews approaching the Serenisssime Republic. His observations of mountains on the Moon's surface in contradiction with the held belief of its perfectly uniform sphericity gave a first blow to Aristotelian philosophy. Turning to Jupiter he became the first known human to record the presence of unknown wanderers by discovering the four satellites that now bear his name. His careful observation of that system lead quickly to a unique conclusion: these wanderers had to orbit Jupiter, in contradiction, again, to Aristotelian principles.

Let's remark here that thus far nothing that was shown is against planets orbiting around the Earth; these observations alone nevertheless meant a great deal: it ushered a new era by demonstrating that not everything is explained and mentioned in philosophical or religious texts, thus, that one needs systematic, independent and objective checks. It was also the beginning of a new era for Astronomy, for Galileo invented a new manner with which to look at the heavens: Galileo invented imaging.

His images showed moving spots on the Sun and Jupiter as well as stars in the Milky Way. But above else, he showed the shape of a crescent on Venus which slowly turned to full and then waned again, while its angular diameter changed. Galileo solved a long standing Greek philosophical problem about why Venus was changing so much in brightness by demonstrating for the first time, that a wanderer other than the Moon was merely reflecting light and not producing it. Venus became a world. More importantly it showed the direction of the unique source of light: the Sun and its position inside Venus's motion. Venus around the Sun, to explain all other planetary motion, the Earth must orbit the Sun. Therefore, indeed, stars were pushed so incredibly far away that we couldn't measure their parallax until 200 years later. Galileo's observations made of Earth a planet, and made of all the other wanderers, worlds (except for the Sun).

In fact one could probably have proven the geocentric model prior to Galileo's observations. Tycho Brahe had remarked that comets crossed the wanderers' orbits at odds with the Aristotelian concept of crystalline celestial spheres bearing the planets in their course around the Earth. He had also reported a Nova, while Kepler observed a supernova: the heavens were dynamic and not

[1] http://www.antikythera-mechanism.gr/



The phases of Venus

still. The precision of Tycho Brahe's astrometry was used by Johannes Kepler who deduced the laws of planetary motion from these exquisite measurements.

From then on thoughts evolved quite rapidly. The scientific method became the philosophy through which one could make sense of the Universe. Kepler's notion of force was extended by Newton by postulating on the universality of natural laws and producing the mathematical description of the force of gravitational attraction. Newton's postulate led to the various successes of science to understand the workings the world around us and the use of those to create newer technologies.

Advances in Optics led to better telescopes, the development of mathematics allowed a precise calculation of planetary ephemerides which lead to Halley's prediction for the return of a comet. These also permitted the improvement of clock making and time measurement which in turn were used during the international campaign launched for Venus' transits in front of the Sun and the first meaningful estimate of celestial distances. Then came Herschel's discovery of Uranus in 1781 from whose perturbed orbit, predictions were made for the presence of an eighth planet, Neptune, first observed in 1846 near its predicted position[2] and whose first orbit since detection will close in July this year.

The XIX$^{\text{th}}$ century saw the development of two new techniques that revolutionised astronomy: multiband photometry & spectroscopy and photography. Both multi-band photometry and spectroscopy are new ways to look at the heavens, the first was allowing image comparison between

[2]I have to mention an unease at this prediction since both Le Verrier and Adams apparently used Titius-Bode law as a help in their calculations. A colleague reflected recently on this: how valid is a prediction relying on wrong principles. Yet the proximity of Neptune to the calculated position is a little astonishing if we consider this prediction was bogus. See Greg Laughlin's oklo.org http://oklo.org/2011/01/17/neptune-after-one-orbit/

different regimes in the light spectrum, the other by breaking the picture into its distribution in wavelength. Both are at the source of the principles located at the heart of contemporary astrophysics: the deduction of physical processes from a distance through the manipulation of the light we receive. Photography made possible the archiving of data in a more accurate and objective way with the possibility of reanalysis for mistakes or time variation as well as estimating systematic errors by comparing several independent plates.

Although there have been many a spectacular discovery in the last century, for what matters to the subject treated in this thesis there has been one revolution: the computer. The capacity to compute fast and store information turned astronomy from a science that was mostly concerned about humanly manageable numbers of objects to the prospect of doing meaningful statistics, to estimate our biases, to store information like nothing before. In parallel, it also rendered possible the computation of equations on scale unimagined earlier, the solution of complex problems and the capacity to start doing experiments in astronomy where one can produce simulation of nature and by twitching parameters and initial conditions, produce different, testable results. Those results can be compared with observations to vindicate the science on which they are based. They have also provided an additional driver for observers by showing which of the many observable parameters hold the keys to distinguish between competing scenarii.

The computer also allowed the adjustment of models on data with the possibility of varying parameters, the estimation of the likelihood of solutions between different hypotheses and the determination of accurate intervals of confidence.

1.2 Orbits, Spectroscopy & Binary stars

This section will very briefly describe the physics that is necessary to detect extrasolar planets. The physics has been well described and formalised in the XIX$^{\text{th}}$ and XX$^{\text{th}}$ centuries.

1.2.1 Orbital motion

Galileo and Kepler's discoveries led Isaac Newton to formalise physically the processus behind planetary motion. In most of what is of concern to us in this thesis, Newtonian physics is sufficient because the vast majority of the systems dealt with here are single planets around a star. In the case where more than one body is discovered one might want to apply the perturbation theory, but in most cases found in the Genève and California search for extrasolar planets, the level of precision on individual measurements and the small timespan of observations makes it an unnecessary treatment for most systems, even those in which some planets are in a mean motion resonance (famous exceptions are GJ 876 (Correia et al. 2010) and Kepler 9 (Holman et al. 2010)). One of the indirect methods of detection, transit timings, relies on this perturbation theory (see section 1.3.2).

In addition, while General Relativity is needed to explain the full motion of Mercury's orbital precession, it is also in most cases unneeded to describe extrasolar planet systems.

Thus, for the moment we will stick with the classical description. Kepler's first law states that orbits are ellipses whose equation is, in polar coordinates:

$$r = \frac{a(1-e^2)}{1+e\cos\theta} \tag{1.1}$$

where r is the separation, a the semimajor axis of an ellipse with eccentricity e. θ is the true anomaly. In an infinitesimal time we can write a change of area as

$$\dot{A} = r^2\frac{\dot{\theta}}{2} \tag{1.2}$$

Integrating to the total area of an ellipse (πab) in a time P we reach Kepler's second law:

$$r^2\dot{\theta} = \frac{2\pi a^2(1-e^2)}{P} = constant \tag{1.3}$$

Using Newton's laws, the total angular momentum is given as:

$$J = \mu r^2\dot{\theta} = \sqrt{GM_\star M_\mathrm{p}\mu a(1-e^2)} \tag{1.4}$$

with $\mu = M_\star M_\mathrm{p}/(M_\star + M_\mathrm{p})$ the reduced mass of the system. Replacing in equation 1.3 and reorganising we obtain Kepler's third law:

$$P^2 = \frac{4\pi^2}{G(M_\star + M_\mathrm{p})}a^3 \tag{1.5}$$

1.2.2 Spectroscopy and the Doppler effect

Coincidentally, spectroscopy also originates from Newton, credited to be the first to study the dispersion of white light into its colour components through a prism. He called this phenomenon the light spectrum. The XIX$^{\mathrm{th}}$ century saw the discovery of the infrared (Herschel) and the ultraviolet (Ritter) as two regions of the spectrum unseen by the eye. About the same time the first wavelength measurements were also done (Young).

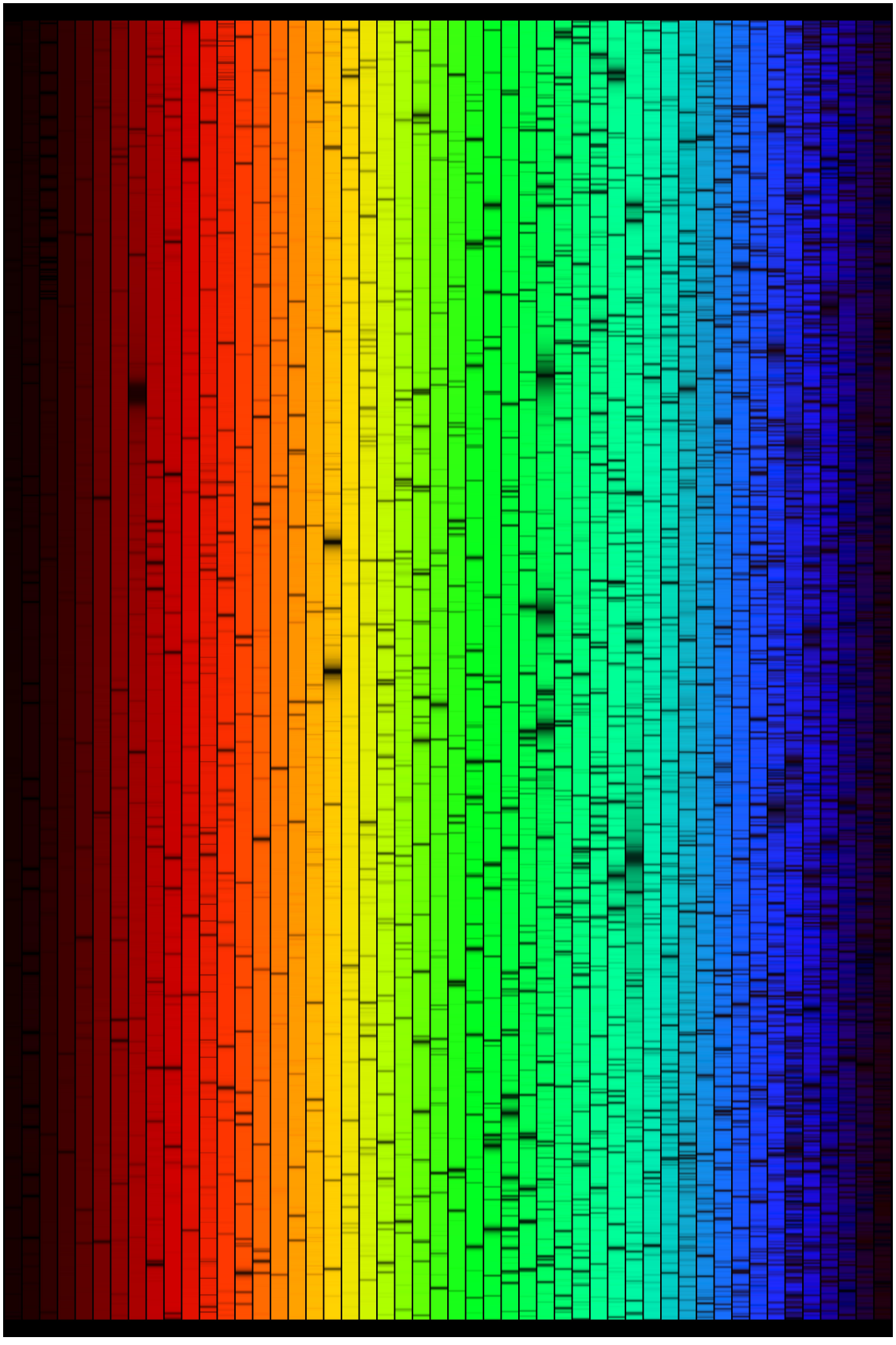
Quickly after, Fraunhofer building the first spectroscope, observed that instead of having an uninterrupted stream of light, some dark bands appeared in the light spectrum, what we now call absorption lines. He started to measure precisely at which wavelength these laid. In the meantime, physicists such as Wheatstone, Alter, and Ångström, realised that heated metals were emitting light at particular wavelengths, now called emission lines. Later, Bunsen and Kirchhoff realised the wavelengths of metallic emission lines corresponded to the Fraunhofer absorption lines and thus appeared the possibility of studying the chemical composition of the Sun. Kirchhoff formalised his findings into three laws that bear his name

1. A hot solid object produces light with a continuous spectrum, a so called black body
2. A hot tenuous gas produces light with spectral lines at discrete wavelengths which depend on the energy levels of the atoms in the gas.
3. A hot solid object surrounded by a cooler tenuous gas produces light with an almost continuous spectrum which has gaps at discrete wavelengths depending on the energy levels of the atoms in the gas

This lead in time to the discovery of a unknown atomic element present in emission line in the solar spectrum, by Janssen: Helium.

Fraunhofer not just turned his instrument on the Sun, but also observed several stars including Sirius and realised that their spectra were different from the Sun's. Astronomical spectroscopic analyses originate from this work. Relying on the postulate that the laws of Physics are universal, the spectral lines observed in a star can be compared to that of chemical elements in a lab on Earth and one can determine the chemical composition of stars and of any absorbing or emitting medium in the Universe.

In the mid XIX$^{\mathrm{th}}$ century, Doppler derived equation showing that the determination of frequencies emitted by a moving source are affected by its motion (he sought through this work the explanation of why some binary stars have such different colour). It was experimentally verified with sound and quickly put in practice in Astronomy with the first velocity determination done on Sirius. What we measure is the velocity on our line of sight, the so-called radial velocity.



The solar spectrum. Credits N.A.Sharp, NOAO/NSO/Kitt Peak FTS/AURA/NSF.

Doppler's equation can be written as

$$f_{\rm obs} = \left(1 - \frac{v_\star - v_{\rm obs}}{c}\right).f_i \tag{1.6}$$

where,$f_{\rm obs}$ is the observed frequency; $v_\star$ is the velocity of the star, or the source; $v_{\rm obs}$ is the velocity of the observer; c, is the velocity of light and f_i is the initially emitted frequency. We thus can rearrange and get the velocity of a star as a function of wavelength:

$$v_\star = \frac{\lambda_i - \lambda_{\rm obs}}{\lambda_i} c + v_{\rm obs} \tag{1.7}$$

λ_i can be determined from laboratory experiments. A reddening is caused by an object receding from our point of view. A reddening also corresponds to a positive velocity. The above equation shows that one needs to take into account the radial velocity of the observer. In order to get precise and accurate radial velocities we therefore need to know well the motion of the Earth around the barycentre of the solar system.

Careful analysis of stellar spectra allow the determination of the effective temperature of the star, its rotation projected in the line of sight, the amount of metals on its surface and its gravity at surface.

1.2.3 Binary stars

The tools used to search for extrasolar planets come directly from the study of binary stars. Binary, or multiple stars (when more than two components inhabit the system) are defined as stars on orbits around a common centre of mass.

Spectroscopically we can distinguish two types of binaries. A double-lined binary, or SB2, is a system where the light of both stars is shone onto one spectrum. If both components have a different velocity, they will imprint absorption lines at two different shifts from rest. Thus the velocity of both can be estimated[3] (see also figure 3.11). An SB1, or single line binary, is a system were one the components does not contribute enough to the combined spectrum (because of its rotation, or lack of flux), we therefore only see one set of lines.

Observing spectroscopically an SB2, we can determine from the amplitude and period of the motion, the mass ratio of both components since they orbit around a common centre of mass. We can transform the equation presented earlier in section 1.2.1 and express them in terms of velocity.

Using the formalism presented in Hilditch (2001) our object has orbital polar coordinates $r\cos(\theta+\omega)$ and $r\sin(\theta+\omega)$. We observe the projection of that second component on its orbit, giving us $r\sin(\theta+\omega)\sin i$ of which we take the time derivative to obtain:

$$V_{\rm rad} = \sin i\,(sin(\theta+\omega)\dot{r} + r\cos(\theta+\omega)\dot{\theta}) \tag{1.8}$$

where θ is the true anomaly. The longitude of periastron is noted here as ω. Using r defined in equation 1.1 and Kepler's 2$^{\rm nd}$ law (eq 1.3) we finally get:

$$V_{\rm rad} = K(\cos(\theta+\omega) + e\cos\omega) + \gamma \tag{1.9}$$

with

$$K = \frac{2\pi a \sin i}{\sqrt{P(1-e^2)}} \tag{1.10}$$

called the semi amplitude. This is directly measurable from as half the peak to peak variation in velocity. γ is called the systemic velocity: the velocity of that system in space with respect to the Solar System's barycentre.

[3] An SB3, would be a system where we have three spectra combined: three stars at least in the system

In a double lined binary we can measure K_1 and K_2 and obtain:

$$a_1 \sin i = \frac{\sqrt{1-e^2}}{2\pi} K_1 P$$
$$a_2 \sin i = \frac{\sqrt{1-e^2}}{2\pi} K_2 P \tag{1.11}$$

Kepler's third law give us:

$$(M_1 + M_2) = \frac{4\pi^2}{G} \frac{a^3}{P^2} \tag{1.12}$$

since $M_1 a_1 = M_2 a_2$ we can solve the equations and get to the minimum masses $M_1 \sin i$ and $M_2 \sin i$. Since we cannot solve for the semi major axis a or the inclination i but only their combination we have to settle for the mass ratio.

If both components are in our line of the sight, they will eclipse periodically. Thanks to this the inclination, i is known and thus a as well and the real masses can be measured. Alternatively, we can make astrometric measurement and observe the orbital motion of the target being drawn on the sky with respect to background stars, assumed immobile. There, i and a are resolved. Similarly to spectroscopic binaries one can observe one, two or more components.

In the case of an SB1, we can only measure K_1. The only quantity one can estimate is the mass function:

$$f(m) = \frac{M_2^3 \sin^3 i}{M_1 + M_2} \tag{1.13}$$

Having a measurement of i is not sufficient to solve the system and one need to assume for a certain M_1 that one can try to estimate from other observables. Again, if you want to know more, consult Hilditch (2001).

Extrasolar planets are essentially the same as SB1s: something that will cause a periodic motion of its host star around their common centre of mass. Because the planet does not emit light, only reflecting it, we see no secondary set of lines. One can search for planets in the same way that one can search and study binary stars, the only difference being the mass ratio.

As instruments got more and more precise, it was possible to detect smaller amplitudes, leading to greater mass ratios and a discovery by Latham et al. (1989) of an object with a minimum mass of 11.2 Jovian masses around HD 114762 [4]. The old spectrographs just reached about the precision needed to discover planets. A newer, more precise and stable generation of instruments was designed to push further down and enter fully into the planet realm.

1.3 Extrasolar Planets

In a quest to check Epicurus' intuition and answering if life is ubiquitous in the Universe or not, it was logical to search for planets. That search for other worlds started with William Herschel in our own Solar System. Results from the currently flying WISE satellite[5] are placing enormous

[4] For $i > 60^\circ$ the mass of that object is well into the Brown Dwarf regime, and thus was not considered a planet candidate then. Now, witth better knowledge of the mass distribution of substellar objects around stars, it has been included, though doubts remain as to its exact nature.

[5] A NASA infrared, all sky survey http://wise.ssl.berkeley.edu/

constraints on the absence of other as-of-yet undetected planets in our system. The search had to go elsewhere. According to the universality of physical laws nothing should prevent planets from forming around other stars, but also under the principles ruling the scientific method, one had to check. Furthermore, other questions relating to the uniqueness of our Solar System and the position of Earth - and of our humanity - in the Universe, needed answering. In addition, and it has proven so, the more one observes, the more one can discover. Nature is a giver of surprises. Those surprises, also called outliers when first found, are what constrain theories most efficiently as even those need explaining and thus, too, help answering the debate on our origins. In this context the discovery of the first extrasolar planet being a Jupiter-like planet orbiting the star 51 Pegasi in a four day orbit by Mayor & Queloz (1995) came somewhat as a surprise and strongly shaped the way planet formation and orbital evolution became thought of. It is not always that one starts exploration by detecting outliers. This detection is a direct result of the method of detection used: the *radial velocity method*, an indirect way of identifying a planet with which this object, and others of the same type, are easiest to find. Each detection method is plagued with the same problem: the easiest objects are detected first but are not necessarily representative of the overall, then undetected, distribution. 51 Peg b became the first object in a new planet class, absent from our Solar System: the *hot Jupiters*.

1.3.1 Direct detection method

The most simple manner one can imagine in order to search for planets is to look, literally, much as William Herschel did: to do what is called *direct imaging*. This method, working well within our system, is nevertheless probably one of the hardest to use in the context of extrasolar planets because of the enormous contrast between the light emitted by the star and the reflected light from the planet. One also has to achieve high angular resolution, therefore needing a large mirror or a powerful interferometric system. In addition one has to tackle the atmospheric distortion and all the various and many inaccuracies originating from the instrument, the way it is built and residual effects from applied corrections. Direct imaging has found a few planet candidates in recent years, probably massive and on the outer regions of their system, mostly around cold stars and brown dwarfs. The most emblematic objects are probably the quadruple planet system around HR 8799 (Marois et al. 2008, 2010) and the planet candidates around β Pictoris (Lagrange et al. 2009, 2010) and Fomalhaut (Kalas et al. 2008).

An alternative direct detection was recently claimed on the already known planet HD 189733 b. Snellen et al. (2010) claimed having detected the planet's signal similarly to that of an SB2. The work focused on the detection of CO absorption lines that moved across the combined spectrum of the star and the planet by several tens of km s^{-1}.

The direct method is possible but being currently too challenging for a wide survey because of the time needed to integrate at the telescope in order to detect the tiny contrast between a star and its planetary companions, astronomers circumvented the problem and envisioned several indirect methods to start searching for exoplanets; all of those are currently being used. Direct detections nevertheless have a very promising future for the discovery of long period planets whose orbital motion are so slow (let's think here of Neptune's 160 year cycle[6]) that they would practically be undetectable by indirect methods relying on time series.

[6] and let's imagine a PhD thesis with the aim to find one!

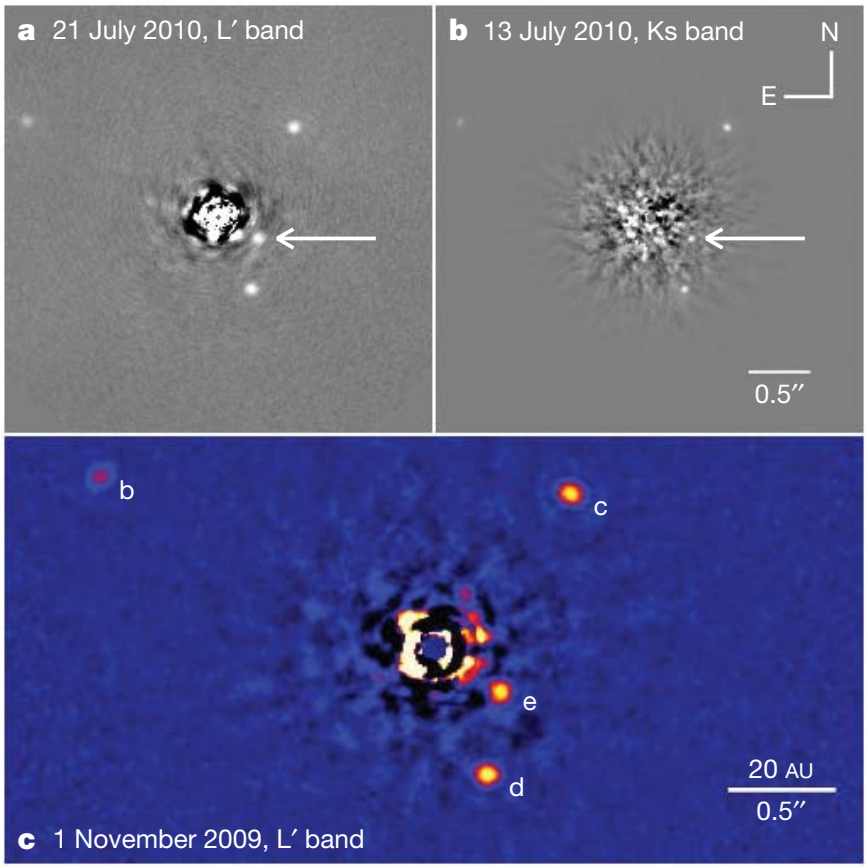


Figure 1.1: Direct detection of four planets around the star HR 8799. Figure obtained from Marois et al. (2010)

1.3.2 Indirect detection methods

Most indirect methods rely on one principle: the manner with which the target star will be affected by the presence of a planet. Pulsar timing, radial velocities, astrometric measurements and transit time delays all use the propriety that an applied force causes an equal and opposite reaction. Both planet and star attract each others; both orbit a common centre of mass called barycentre. In our solar system, the barycentre is located near the surface of the Sun.

radial velocities

Widely used in the case of binary star, we saw that with HD 114762 b (Latham et al. 1989) the planet limit was approached. One only needed to improve this well proven method to a precision allowing the detection of planets treating them as SB1 (see section 1.2.3). It has been the most successful method until 2011 when NASA's *Kepler* satellite released a host of planets candidates discovered via the transit method. Nevertheless, the radial velocity method remains one of the most efficient means to search for planets and the most reliable and accepted manner with which one can check results from other methods. The results from *Kepler* are being confirmed progressively via radial velocity measurements, and until a mass determination (also measurable via transit timing) remain planet candidates.

The reason for the resilience of that method in an age of fast discovery thanks to planetary transits is largely due to its sensitivity to longer periods and smaller masses, the capacity to obtain most orbital parameters such as the eccentricity, the ability to search brighter and nearer stars, and the information it gives to prevent a false detection.

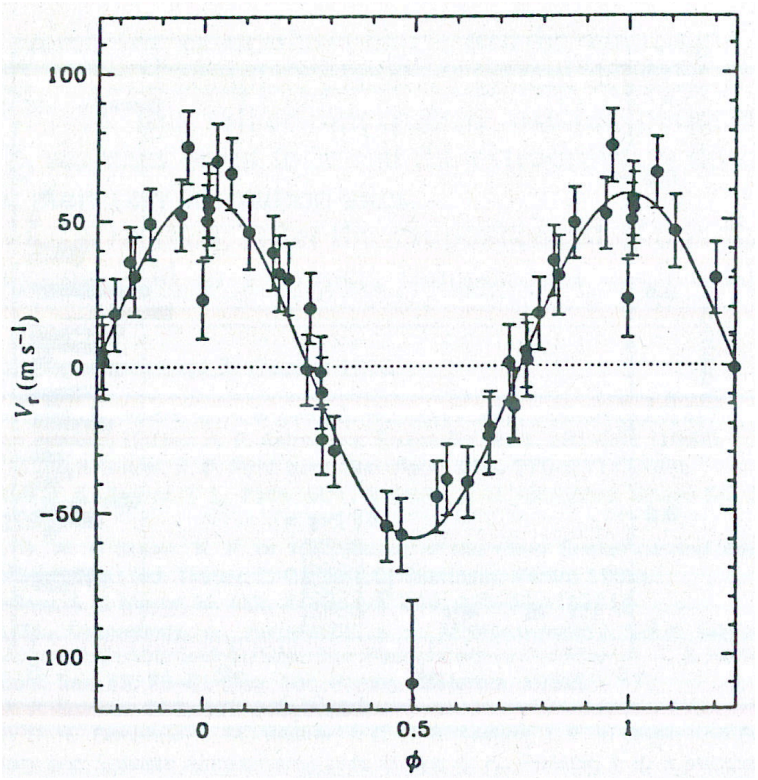


Figure 1.2: Radial velocity announcing the detection of 51 Peg b, the first extrasolar planet, the first *hot Jupiter*. Figure obtained from Mayor & Queloz (1995)

Its major results are: the first detection of a planet around a solar type star (Mayor & Queloz 1995); the detection of the smallest mass planet[7] (Mayor et al. 2009a); the discovery of a vast distribution of planet less massive than Neptune but more than Earth located closer to their star than is Mercury to the Sun (Mayor et al. 2009b) and of packed planetary systems (Lovis et al. 2011). These have subsequently been confirmed by *Kepler*.

Used alone, unfortunately this method suffers from two drawbacks: that a stellar mass, a notably hard quantity to accurately determine for field stars, needs to be assumed in order to get to the companion's mass. Then, only a minimum mass, $M_{\rm p} \sin i$ is determined.

From equation 1.10 we can deduce the type of signal this method is likely to deliver:

$$K = \frac{28.4\,\mathrm{m\,s^{-1}}}{\sqrt{1-e^2}} \frac{M_p \sin i}{M_{\rm Jup}} \left(\frac{M_\star}{M_\odot}\right)^{-2/3} \left(\frac{P}{1\,\mathrm{yr}}\right)^{-1/3} \tag{1.14}$$

expressed in terms of Jovian masses $M_{\rm Jup}$ and solar masses $M_\odot$ [8].

planetary transits

Only when 51 Peg b was discovered did this method became seriously considered. Prior to that, the knowledge about the presence of planets near to their stars was lacking. Mercury, with its 88 day period was the closest planet known to its star then. A posteriori, this method is probably one of the easiest with which one can expect to detect exoplanet candidates: one hopes to observe a planet transit in front of its host star. It only requires a light detector with a good enough precision to obtain reliable photometry, a large number of stars (achieved either by observing a small, deep field, or a wide and shallower field), time, and the capacity to sort through the photometric

[7] minimum mass that is

[8] obtained from Allen's Astrophysical Quantities (Cox 2000)

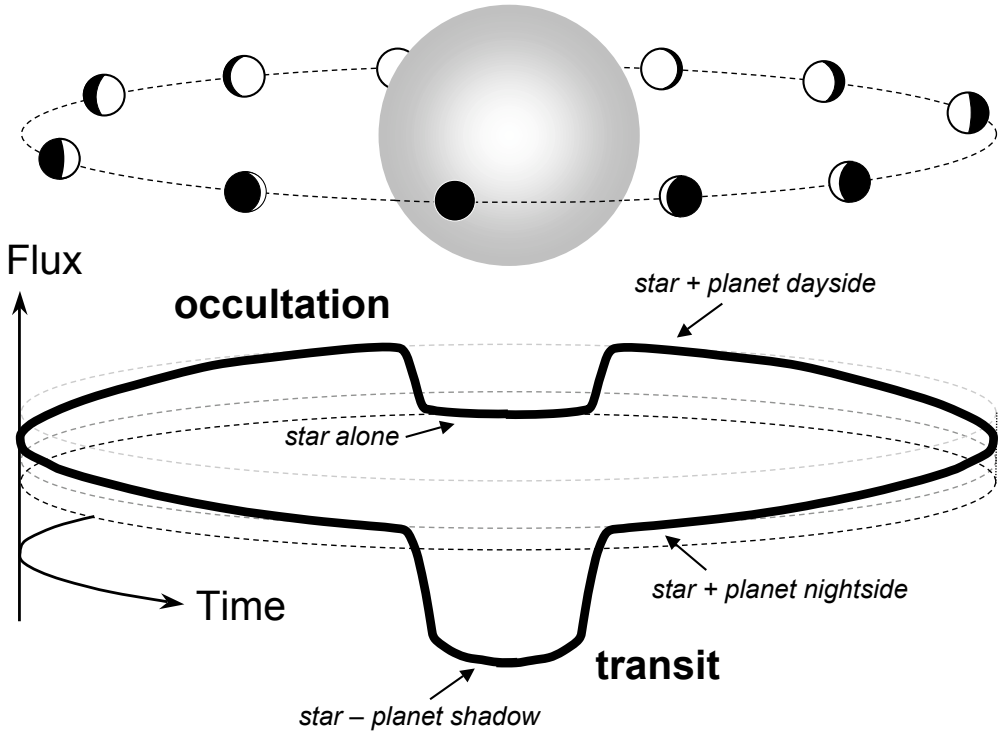


Figure 1.3: Diagram showing the change in flux received on Earth as a planet orbits its star. Figure taken from Winn (2010).

timeseries comprising thousands of data points on thousands of stars. Because of geometrical constraints, this method is mostly concerned with the detection of short-period planets. It also suffers from quite a number of false positives. This thesis relies on data acquired with a transit survey and thus will be described at length later.

Transits also provide another means to look for planets via the timing of those events. There are two manners to use that timing. The easiest, similar to pulsar timing is to check for a variation in the middle of transit time due to the motion of the star around its barycentre, caused by another undetected companion. This is mostly used in the context of eclipsing binaries around which planets are searched. The second manner relies on the dynamical perturbation two planets can cause on each other's orbit, especially when located in a mean motion resonance. This perturbation will be observed as a transit time variation caused by a planet being early or late due to its interactions with a second one, that is or is not transiting (see section on timing).

On a first order the signal we expect: a drop in flux F, can be described from the radii of the planet $R_{\rm p}$ and of the star $R_\star$ as:

$$\begin{aligned}\frac{\Delta F}{F} &= \frac{\pi R_{\rm p}^2 B_\star}{\pi R_\star^2 B_\star + \pi R_{\rm p}^2 B_{\rm p}} \\ &\simeq \left(\frac{R_{\rm p}}{R_\star}\right)^2 \sim \frac{1}{100}\left(\frac{R_{\rm p}}{R_{\rm Jup}}\right)^2 \left(\frac{R_\odot}{R_\star}\right)^2 \end{aligned} \tag{1.15}$$

where we assume the planet's brightness $B_\star$ to be null during transit. In order for a transit to happen we need a special geometrical configuration, something most other methods do not suffer from as much (except microlensing, see later). Let us now estimate the probability that a planet

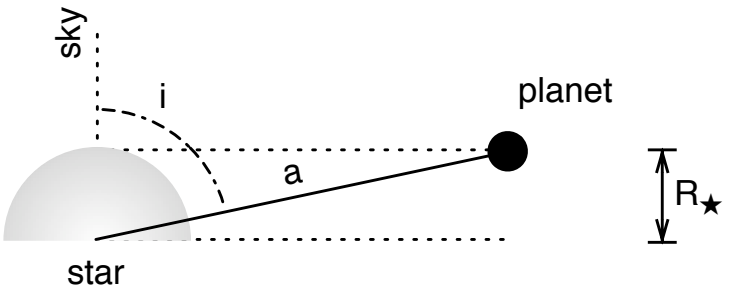


Figure 1.4: Diagram showing some of the quantities in the text. Observer would on the right hand side, looking towards the star

does transit its host star. For that, the projection of the separation between planet and star needs to be smaller than the sum of their radii:

$$a \cos i < R_{\rm p} + R_\star \tag{1.16}$$

where a is the semimajor axis, i is the inclination of the orbital plane with respect to the sky (see figure 1.4). This means there is a band drawn around each star on the sky where transit would be visible to far away observers. Now, assuming planetary systems are randomly orientated in space (uniform in $\cos i$) we expect the probability of a transit to be simply:

$$\begin{aligned} Prob &= \frac{R_{\rm p} + R_\star}{a} \simeq \frac{R_\star}{a} \\ &\sim \frac{1}{10} \left(\frac{R_\star}{R_\odot}\right) \left(\frac{P}{3\,\text{days}}\right)^{-2/3} \left(\frac{M_\star}{M_\odot}\right)^{-1/3} \end{aligned} \tag{1.17}$$

assuming for a complete transit rather than grazing. We immediately see that we are sensitive to large planets at small orbital separation.

The first exoplanetary transit was observed on HD 209458, by Charbonneau et al. (2000) and formally confirmed that those radial velocity signals found by Doppler surveys were indeed those of planets and not of stellar binaries in nearly face-on orbits as some were arguing then.

While all other methods are solely detection methods, transits also give us physical information about the planets and brought a treasure trove of observables which led to an intensive theoretical development about the physics happening on those planets. Check Winn (2010) for a review on all what one can do when a planet is known to transit. Eventually, direct imaging will provide such opportunities as well.

timing method

Under this term are gathered various manner to observe a single physical phenomenon. As a planet orbits the centre of mass of the system, so does the central object, which we are observing. If that object emits regular pulsations, then sometimes that pulsation is emitted as the object is closer to Earth and other times when it is further thus creating a periodic signal in the arrival time of the pulsations.

Pulsars, shortened of *pulsating stars* are understood to be fast rotating neutron star emitting radiation in a focused beam in the direction of the object's magnetic poles. We can detect this emission for those objects whose beam is sometimes directed towards Earth. An unseen body in orbit around such an object will cause it to oscillate around the barycentre. Thus sometimes pulses will appear to be late as coming from a little further way, and sometime early. The precision of those instrument, the otherwise regularity of the pulses and the number of events one

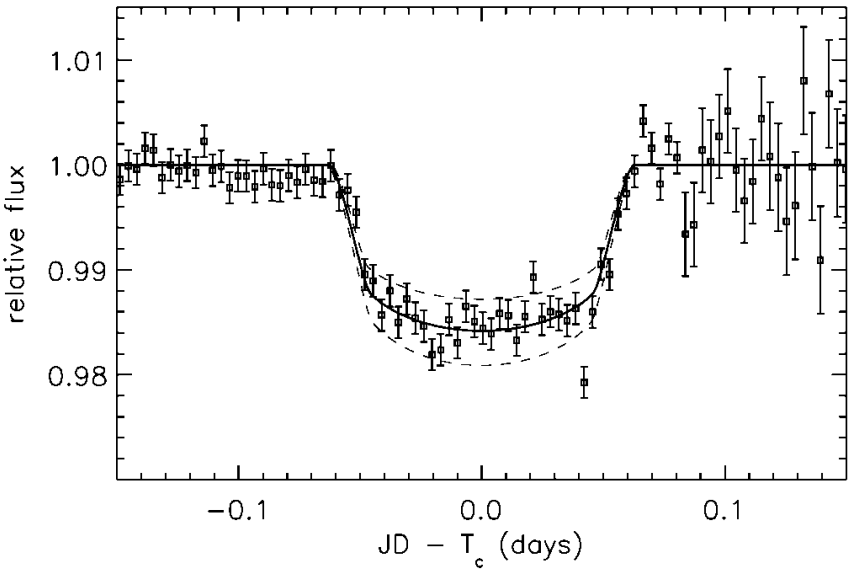


Figure 1.5: Composite of two transits showing the change in flux with time of the first observed transit by an extrasolar planet: HD 209458 b, as presented in Charbonneau et al. (2000)

gets thanks to the rapidity of pulsars' rotation allows very fine measurements. Four planets have been found around two pulsars (Wolszczan & Frail 1992; Wolszczan & Kuchner 2010). They have small masses. Although prior, the impact of their discovery was never as big as that of 51 Peg b because of the unusual nature of the central-most object: a supernova remnant and the paucity of such objects. It is thought those planets may have form from dust accretion, dust ejected during the supernova event and reorganised into a disc later. A few other scenarii are investigated (see Wolszczan & Kuchner (2010) for references).

Similar to pulsar timing is the detection of a variable signal in the oscillations of V391 Peg compatible with a gas giant giant orbiting at a few AU (Silvotti et al. 2007). The planet yield from these techniques is small, but interesting as they explore the future of planetary systems, after stars evolved off the main sequence.

Another way to use timing is through eclipse or transit timing. The idea is that one uses the transit/eclipse mid transit time as the frequency on which one attempts to detect a periodic change in arrival time. Search on planet transit have a successful detection only on the multiplanetary systems found using the *Kepler* satellite (eg. Holman et al. (2010)). They are used as a way to estimate the mass of planets, not yet as a detection tool. Other photometric, ground based surveys, have produced mainly hot Jupiters. Those are, for reasons explained later, found most of the time alone. Transit timing detections have thus far showed no credible detections. A few signals have been found, but associated with stellar rotation (Alonso et al. 2009).

One detection of a slow shift of about 30 seconds in the eclipses' mid time of the binary CM Draconis, over 30 years, could be caused by a circumbinary planetary body (Deeg et al. 2008). More observations are needed to conclude on that system.

astrometry

In a similar fashion to work on binary stars, it is possible to measure accurately the position of a star to others in the field assumed to have fixed positions during the required length of the observations. Progressively the orbit can draw itself on the sky, on top of the star's proper motion and of its parallax. The big advantage of this method is to obtain information on the semimajor axis and inclination of the orbit. Another very important point of interest is that its highest sensitivity

is for gas giants orbiting at a few AU from their star. It is thus more sensitive to Solar System analogues than radial velocities are. So far it has not detected any planets, but showed a few planet candidate are in fact stellar, places some upper limits on some masses (Sahlmann et al. 2011b) and possible confirmation of a few planets (eg ϵ Eridani (Benedict et al. 2006)).

A large investment is underway to make precise astrometric measurement. This method is key to probe the outer reaches of stellar systems for which neither the radial velocities, let alone the transit method, can reach. Ultimately, astrometry, very much as Doppler surveys will suffer from the time an orbit takes to close, when that time is of comparable size to one's lifetime.

microlensing

Microlensing is a method yielding few results due to the low probability of catching an event. Its principles are outlined in: Gaudi (2010). Credited with a dozen planet discoveries, this method detects the light amplification caused by a planet passing in the line of sight of a background star. The planet acts as a lens thanks to the deflection of light due to its mass. It is most sensitive to planets located at a few AU from their host, and to planets around low mass stars, as these are in greater numbers in our galaxy than solar type stars. Often deemed of interest to probe the distribution of the planets at large orbital separation and build a statistical picture, this technique is plagued by the lack of detection. This said, thanks to better alert systems, detection rates should augment. These will help fill a gap in parameter space which is hard to reach by other detection methods. Unfortunately, the objects that have been detected are also useless for further studies, notably, because the short time events occur for, means that only in special circumstances does one measure orbital motion and get constrains on eccentricity. Microlensing events are a one-off. Most of the time the host star is not even detected; only its effect on the background star is. This makes any characterisation practically impossible.

1.3.3 Characterisation methods

If, from 1995, the number of researchers aiming to detect new planets has increased enormously, what has progressed dramatically is the effort to characterise those new worlds and learn the most one can about them. New physics in regime beforehand unreachable is being theorised and checked. This effort is truly remarkable and some say that what we now know on those far away hot Jupiters has reached a similar level to what we knew about the gas giants in our own solar system prior to their visit by the *Voyager* probes.

high precision photometry

Be it for checking whether a planet detected in radial velocity could be transiting, or for planet founds by transit surveys, the initial photometry is usually obtained from small telescope, thus poor. The first effort one can achieve after detection, is to obtain better photometry. The range of telescope and opportunities varies on the means and ability of researchers. One can ask time on a space telescope such as *Hubble*, as was the case for HD 189733b (Pont et al. 2007), but its short orbit around the Earth forces one to only take bits of transit, rather than a complete transit, or use a VLT, as will be presented in section 2.3.2.

Another efficient way is to use a well built machine, not necessarily big and observe a lot of events, as demonstrated by *KeplerCam* on the 1.2m at Fred L. Whipple Observatory (eg. Winn et al. (2009a), or more recently by the 60 cm robotic telescope TRAPPIST build in a collaboration between

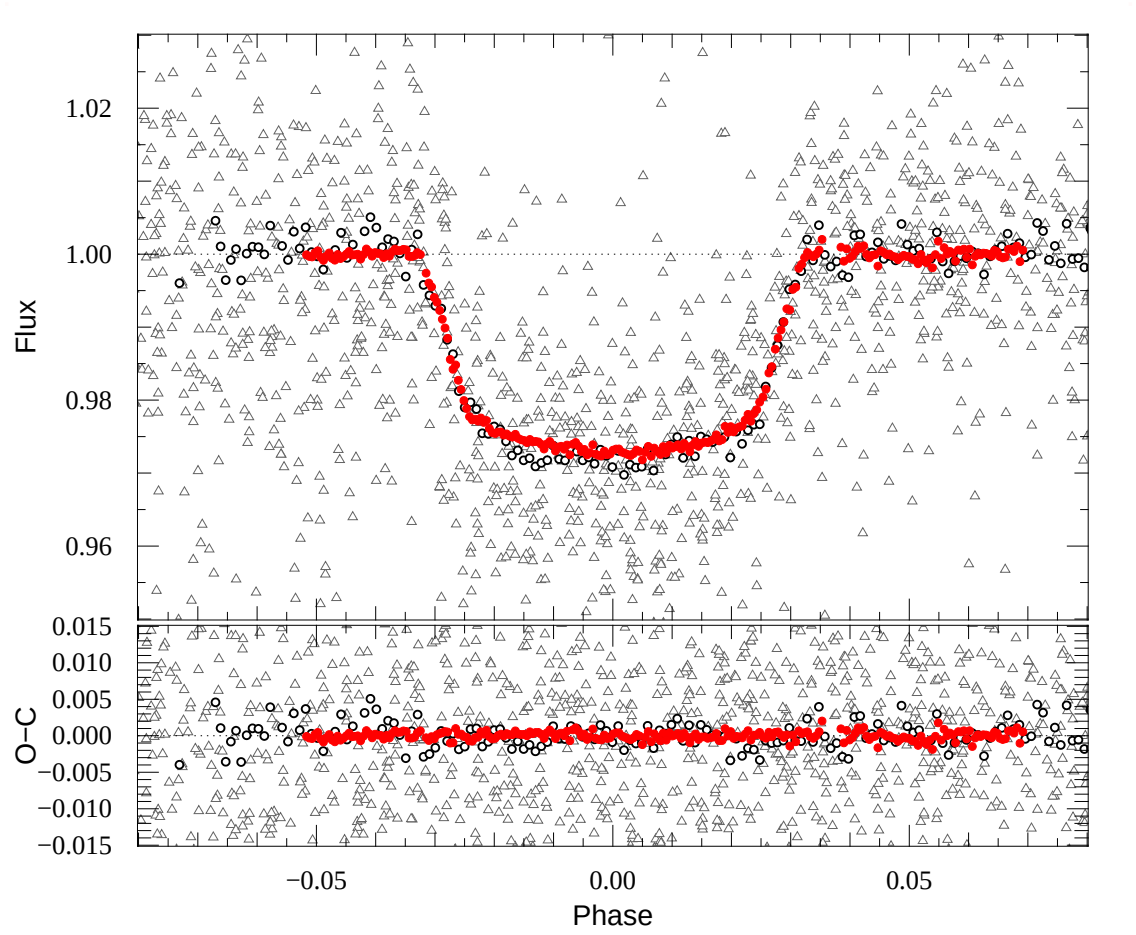


Figure 1.6: Example of characterisation on WASP-4: grey open triangles: WASP discovery photometry; black open circles: *Euler* telescope confirmation of the transit; red full discs: VLT FORS2 data. Residuals from the best fit are displayed. Data from Gillon et al. (2009b), see section 2.3.2.

Genève and Liège astronomy departments. Our own *EulerCam* on the 1.2m Swiss telescope at La Silla is used for the same reasons; that work is part of Monika Lendl's thesis.

In all cases one can obtain an exquisite lightcurve, and precise estimates of the ratio of radii, impact parameter, limb darkening, and on the presence of stellar spots. If observed on a long timespan, it also helps producing reliable ephemeris. One is still limited while extracting physical parameters of the planet, by our knowledge on the star's mass. Work presented in this thesis will show how the addition of precise transit lightcurves can lead to accurate determination of the stellar density (using eq. 2.10) can lead to the determination of a star's age (see section 2.6).

In the case of a series of transit, one can use their mid transit point to search for transit timing variation as explained briefly earlier, or search for a variation in impact parameter which could also be caused by the interactions with another planet. If the planet happens to cross stellar spots one can try to estimate the spin/orbit angle, like done in the case of WASP-4 by Sanchis-Ojeda et al. (2011).

Finally one can detect a change in transit depth from which can be estimated the area of the star covered with stellar spots (Huber et al. 2010). This is of particular concern. Planet radii are estimated using eq. 1.15, assuming $F_\star$ is not hidden by any other component.

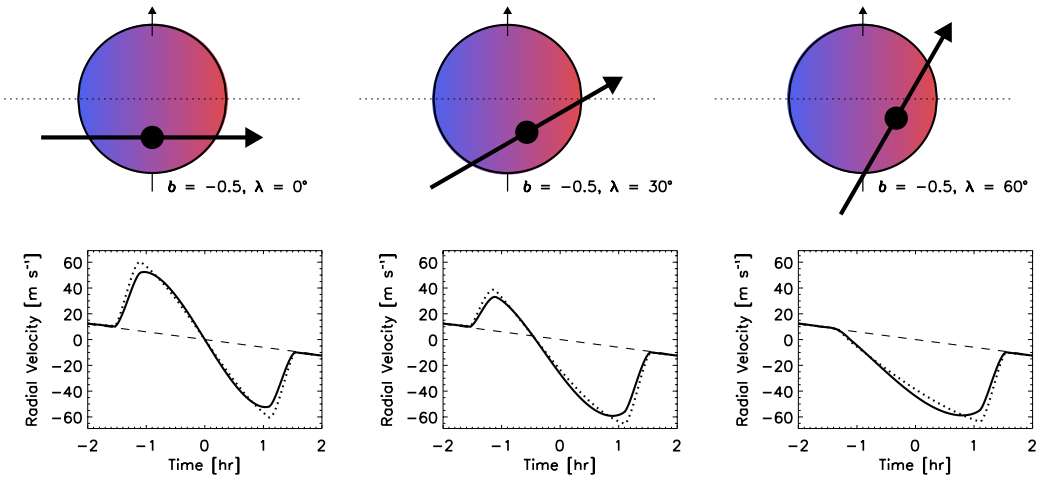


Figure 1.7: Different configurations for the Rossiter-McLaughlin effect. In this thesis we will use the projected spin/orbit angle as β instead of λ on the figure. $\beta = -\lambda$. Figure taken from Gaudi & Winn (2007) and coloured.

the Rossiter-McLaughlin effect

In a proposition to have an estimate of stellar rotation, Holt (1893) predicted that would a star eclipse partially another star, if their rotation axes are aligned with their orbital axes, it would cover first the approaching, blue shifted, hemisphere of the eclipsed thus making the overall light appear redder. As it made it way across, the transiter would reach the red-shifted hemisphere and covering it would create an anomalous blue shift in the radial velocities. Holt proposed that from this change in colour one could estimate the rotation of star, at a time when there was no other estimator.

It was observed not too long afterwards by Schlesinger (1910); Rossiter and McLaughlin both observed it deliberately (Rossiter 1924; McLaughlin 1924). Attempts were quickly made to model it (Petrie 1938; Kopal 1942; Hosokawa 1953) but its adjustment was troublesome. One interest of observing this effect is not only about gathering information on the rotation of stars but rather, to estimate the angle between the rotation spin of the primary and the secondary's orbital spin. A non coplanar case would produce an asymmetric colour anomaly in the radial velocities. Several Rossiter-McLaughlin effects observed on eclipsing binaries are mentioned in the literature all of them symmetric except one observation of Algol (despite other symmetric observations) reported in Kopal (1942), but I could not find the data.

Then this effect almost disappears from the literature. Probably because of the difficulties about modelling it, observers deliberately avoided taking data during transit, else this data is not presented. It reappears on the scene in 1999 when Michel Mayor hears a presentation by Jean Schneider about it in Antofagasta, Chile. His conclusions were that only for fast rotators would this effect be measureable. Michel thought otherwise and shortly after the announce of the first transiting planet, HD 209458 b, the first Rossiter-McLaughlin effect is measured for a planetary system by Queloz et al. (2000).

Applications to binary stars are still rare, but recently a paper clearly demonstrated that the components of the eclipsing binary DI Herculis were on pole-on orbits and thus reconciled the observed apsidal motion with the predictions of General Relativity (Albrecht et al. 2009).

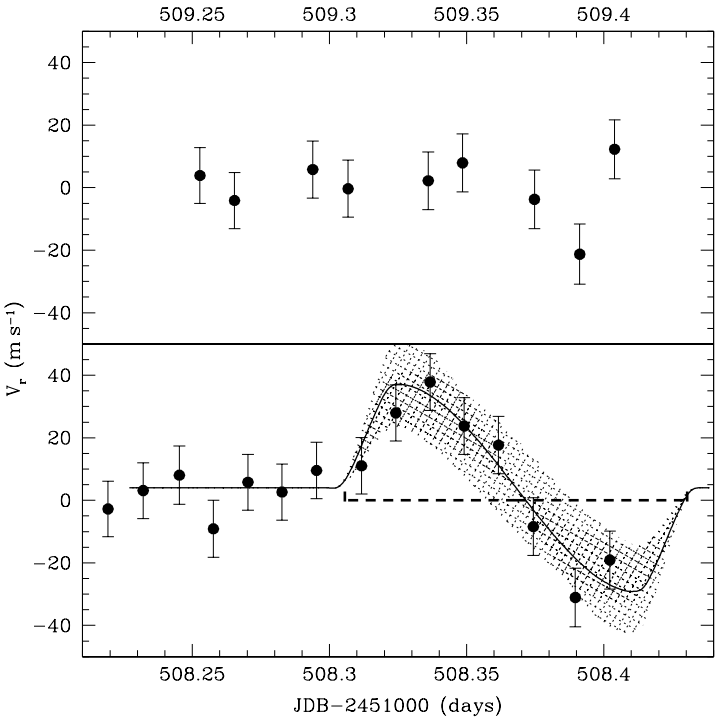


Figure 1.8: Two radial velocity time-series, one during transit (bottom), one a night later (top) after the Doppler reflex motion caused by HD 209458 b's motion on its star has been removed. The anomaly that appears during transit is the first Rossiter-McLaughlin effect observed for an extrasolar planet, as presented in Queloz et al. (2000)

Since this thesis is mostly about this effect, more attention will be spent on its intimate workings, the results that we obtained and their implications. A first order expression for the semi-amplitude of a symmetric Rossiter-McLaughlin effect is:

$$\delta v \simeq 15 \frac{V \sin I}{2.2\,\mathrm{km\,s^{-1}}} \left(\frac{R_\mathrm{p}}{R_\mathrm{Jup}}\right)^2 \left(\frac{R_\odot}{R_\star}\right)^2 \sqrt{1-b^2} \qquad \mathrm{m\,s^{-1}} \tag{1.18}$$

With the Rossiter-McLaughlin effect we obtain two observables, the $V \sin I$, the projected rotation velocity of the star (whose spin axis is inclined by I degrees to the sky) but above else, the projection of the obliquity ψ which is the angle between the stellar spin axis and the planet's orbital spin. That projected angle is called β.

searching for other companions

This is done basically using the same detection techniques, direct or indirect. Except for systems in which hot Jupiters are present, it appears that the probability of a finding a 2$^{\mathrm{nd}}$ planet in a system where we have one is very high, especially when looking at planets with masses comparable or smaller to that of Neptune. It is likely that this is a function of stellar mass, which is linked to the disc mass, intrinsically linked to the presence of planets.

In our case the search for other planets was done using radial velocity measurements to search for additional periodic changes, or trends. We also monitored the lightcurves we obtained, but so far no other transit signal has appeared.

secondary occultation

Similar to the transit technique, we expect a change in received flux as the planet is occulted by a star. When we have confirmed the presence of a transiting planet on a circular orbit, it has

to be occulted by the star. The thermal radiation, and reflected stellar light from the planet will disappear as the planet occults. This allows a determination of a planet's albedo and temperature. Similarly one can measure the flux during the orbit and hope to detect its phase curve (Knutson et al. 2009) (see figure 1.3). Because the planet is colder than the star, the planet will reemit thermally at longer wavelength than the star (thus at longer wavelength than the reflected light).

Detecting an occultation also allows a determination of the eccentricity of the system. Those will be treated later in section 2.4

transmission and reflection spectroscopy

Stellar light crossing the planet's atmosphere during transit, or being reflected or reemitted during occultation will be affected by the atmospheric composition of the planet. This of course is one intense field of research as it opens the opportunity to study the atmospheric composition of planets. In the search for the detection of life on other worlds, that knowledge is paramount. More and more measurements are done on bright targets, but to this day, the field of exoplanet's atmosphere is a hard one. The needed precision is extreme and the interpretation of the data is a complex problem.

In transmission spectroscopy one plays with apparent changes in the depth of the transit. If certain species are present in the atmosphere, they might absorb stellar light more than if they were not and their presence at certain heights in the atmosphere will make the transit appear more or less deeper and wider. The spectrum of the planet is thus reconstructed from the apparent size of the planet.

As the planet occults, the variation in flux depends on the ratio of the two brightness, which, through the Planck function is linked to the brightness temperature of the planet. From several measurements at several wavelength, one can also recreate the planet's spectrum.

In transmission spectroscopy, the spectrum that is obtained is created in the upper atmosphere of the planet, while in reflection spectroscopy, the spectrum is that integrated over the whole disc of the planet. For more information, see for example Seager (2011).

knowing the star

Be it for radial velocity, or transits, or really any method, we are dominated by the star's flux. Any variation in it will affect our measurements. Furthermore, the precise and accurate determination of stellar parameters for field single stars has traditionally been hard, yet, from those parameters are derived the planets' parameters. Thus characterising planets, means characterising the host star. This is something which is often missed, as we are still in an intense discovery age with people focused more in building a statistical sample. But as efforts to understand better the physics involved in planetary systems are increasing, so will efforts in understanding the star. This is paramount especially if one wants to have an accurate understanding of planet's spectra as described just previous section. Knutson et al. (2011) show that transits taken at different times but at the same wavelength show variation in depth, probably caused by a varying stellar spot coverage.

In another twist, as instruments increased their precision, stars that appeared stable turned out not to be. In order to detect smaller transit, and smaller mass planets, one also now needs to

understand how the star behaves. Because of the precision used in the survey described in this document, I have not been very worried with this. (not yet)

1.3.4 State of the field

September 2007 was when I have started working in Genève for this thesis. According to the Extrasolar Planet Encyclopaedia[9] there were about 230 known exoplanets, of which about 25 were known to transit their star. All of those were hot Jupiters but for one, GJ 436b (Gillon et al. 2007), a hot Neptune, which we will see may not be so different from the majority of hot Jupiters in origin. I arrived at a ripe moment in the still short history of that new field of science. The many surveys to discover transiting planets had just started producing results promising many detection to come and the capacity to draw statistics from the distribution and do what has been progressively called *comparative planetology*. The WASP survey (Pollacco et al. 2006), without which collaboration this thesis would have been completely different, had detected their first two objects (Cameron et al. 2007a) and about to publish three more (Pollacco et al. 2008; Wilson et al. 2008; Anderson et al. 2008). The HAT network (Bakos et al. 2004) had announced their first candidates of many; the OGLE, TrES, SWEEPS and XO surveys completed the collection.

Those planets are found in average too large to be explained by the equation of state of a heated Hydrogen and Helium ball (Bodenheimer et al. 2003). Various processes have been invoked to explain the hot Jupiters' inflated radii, one of the most promising is the so-called Ohmic dissipation (Batygin & Stevenson 2010).

A widely accepted idea was that gas giants cannot form in the inner parts of a stellar system, but only where ices have not sublimated: where they can be used as building blocks to create the cores of future gas giants. The observations of so many gas giants within the traditionally accepted *snow line* (about 3 to 5 AU) meant that planets have moved between the location of their birth and their current location. The most emblematic population are the so-called *hot Jupiters*, gas giants of mass comparable to Jupiter's but on orbits < 5 days.

An equally widely accepted idea was that planets migrate from interactions with the protoplanetary disc (Lin et al. 1996; Ward 1997). Actually the process behind this *disc migration* is so effective at bringing in planets that we should expect that all should have fallen into their stars, contradicting our detections, and also, our mere existence. People thus started looking into refining this theory and finding a stopping mechanism. As more multiplanetary systems were discovered, the hot Jupiters looked increasingly lonely which led Doug Lin to propose that maybe we were seeing the *lasts of the Mohicans* where the last migrating planet pushes all the others into the star and remains as the only one left. The consequences of many gas giants falling into a star have been studied by Garaud (2011). We shall see later that we may indeed observe a surviving population of hot Jupiters, but for entirely different reasons.

Alternative theories[10] have been competing with disc migration such as *planet-planet scattering* (Rasio & Ford 1996), or *Kozai migration* (Wu & Murray 2003). The migrating mechanism here is a mix of dynamical interactions and of an orbital decay due to the dissipation of angular momentum through tides.

The distinction between both migration pathways was hard to bring out from the data. This thesis attempts to provide that distinction through a use of a new observable: the projected spin/orbit

[9] http://www.exoplanet.eu

[10] alternative is good (please, do not see this just as a political statement)

angle β. At the time only five measurements of the Rossiter-McLaughlin effect had been measured, all five appeared aligned, in accordance with disc migration.

As I write these words, the number of extrasolar planets is between 500 and 600 of which about 130 are known to transit. In addition the satellite *Kepler* has announced a thousand candidates, of all sizes. The rate of discovery continues to increase. Those worlds continue to surprise us by the immense diversity they have.

1.4 Organisation of the Thesis

It is not always an easy task to arrange the work of several years in an order. Chronologically, it makes no sense since different topics are treated alongside without necessary have much in common. In the meantime some things are intrinsically linked, but more importantly, they evolve. Thus what was done at some time may no longer be used later on. Yet the papers included in this work are there as snapshots of how things were perceived then. How best then to capture the new and old, and various concepts in one document?

I have chosen to give a brief introduction, especially regarding the description of the physical phenomena, in order to develop on them later. In chapter 2, the models for those phenomena are better described, as well their inclusion into a fitting algorithm and a description of that algorithm. After describing a piece of code, it seemed logical to show it at work and thus, papers using the code in various circumstances are presented. Those papers also should reflect on the evolution of the code as newer needs and refinements appeared.

The biggest achievement of this thesis is the work regarding the Rossiter-McLaughlin. This work is presented in chapter 4 along with the current state of affairs regarding the distribution of the projected spin/orbit angle β. Following this is the interpretation, in chapter 5; I felt it necessary to separate observations from interpretation. The earlier should remain true, while the latter will change with additional observations and newer observables since it only shows a reflection from an incomplete description of nature. Moreover, the theoretical ideas that provide the backbone for the interpretation are likely to change.

But prior to presenting all that work, one needed to find the targets on which to observe the Rossiter-McLaughlin effect. Without the many southern transiting planets that we discovered, it would have been impossible task. Thus, the many discoveries made by the collaboration of Genève and the WASP consortium are described prior to the Rossiter-McLaughlin work: in chapter 3. There, will be given a description of the project, how planets were discovered and an outlook onto our achievements over these past four years.

A short conclusion will be given in chapter 6, notably including a part about other projects on which work has started, or might, in the near future.

Several papers are included in the text. For each of them I have written a short introduction to outline the historical context in which they were written, which part I had in them, and how they influenced my thoughts, for example leading to improvements into my fitting algorithm.



The Transit of Venus, taken at the Observatoire de Paris.

Chapter 2

Tools to Study Extrasolar Planets

One one hand we have data and on the other, a mathematical model linked to a physical phenomenon. We want to compare both and see if the physics can reproduce the observations. This model has a number of parameters that can vary and change the model. For instance, if one changes the orbital separation and the mass of a planet, the period and the amplitude of the radial velocity signal will change. When models can be linearised, equations can be solved and a solution can be found. However sometimes this is not possible. We remind here that since we cannot be sure that we have all the information necessary about a system, we cannot prove a particular model is true. We can only compare it with another model, say a random distribution and have information that one is better than the next. This chapter is dedicated to the manner with which a model and its parameters are searched so as to find the best model to the currently available data.

2.1 The Models

After a quick introduction to the type of signal one can expect from various planet finding methods, we will here go a little more into their details. Since the Keplerian orbit has already been described (section 1.2.1) and its application in the context of radial velocity measurements also explained, I won't go into further details. It is also something well known in Genève and a number of other thesis have this covered in more details than I would. The focus will therefore be on what happens while a planet transits. The following equations can found in Seager & Mallén-Ornelas (2003) or in Winn (2010).

2.1.1 A planetary transit

Transits occur when the true anomaly $\theta = \pi/2 - \omega$. Occultation would be at $\theta = -\pi/2 - \omega$. A note while on the subject: for RV planets phase $\phi = 0$ is traditionally at periastron passage (circular orbit have by convention $\omega = \pi/2$), for transits we often used $\phi = 0$ as the transit mid point.

We saw in the introduction that for a transit to happen, once must fulfil the following criterion:

$$a \cos i < R_{\rm p} + R_\star \tag{2.1}$$

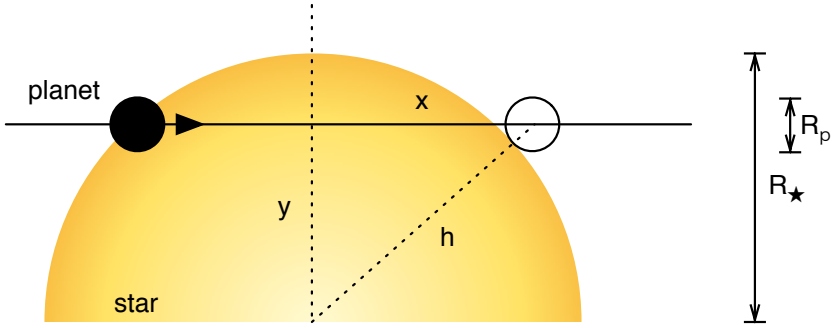


Figure 2.1: Diagram showing a transiting extrasolar planet with the quantities used in the various equations included in the text.

This is for a grazing transit where only part of the planet covers the stellar disc. For a full transit this criterion changes to

$$a\cos i < R_{\rm p} - R_\star \tag{2.2}$$

Using these one can define the impact parameter b as the closest approach to the centre of the star as:

$$b = \frac{a\cos i}{R_\star}\left(\frac{1-e^2}{1+e\sin\omega}\right) \tag{2.3}$$

b is in units of stellar radii $R_\star$. Thus for a transit b cannot exceed $1+R_{\rm p}/R_\star$. For a circular orbit, and from the total time T of the transit, we can estimate the scaled size of the star $R_\star/a$ geometrically (see figure 2.1):

$$\begin{aligned} h &= R_{\rm p} + R_\star \\ &= R_\star\left(1+\frac{R_{\rm p}}{R_\star}\right) \end{aligned} \tag{2.4}$$

$$2x = 2\sqrt{h^2-y^2} \quad \text{with} \quad y = bR_\star \tag{2.5}$$

$$\text{but also} \qquad = a\sin\left(\frac{2\pi T}{P}\right) \tag{2.6}$$

equating both and assuming a small sine:

$$\frac{R_\star}{a} \sim \frac{T}{P}\frac{\pi}{\sqrt{\left(1+\frac{R_{\rm p}}{R_\star}\right)^2 - b^2}} \tag{2.7}$$

From the change in flux, we obtained $R_{\rm p}/R_\star$. We therefore also have the scaled size of the planet $R_{\rm p}/a$. For eccentric orbit we have to add to correct for the fact that the planet-star instant separation is no longer the semi-major axis. We can approximate to:

$$\frac{R_\star}{a} \sim \frac{T}{P}\frac{\pi}{\sqrt{\left(1+\frac{R_{\rm p}}{R_\star}\right)^2 - b^2}}\frac{1+e\sin\omega}{\sqrt{1-e^2}} \tag{2.8}$$

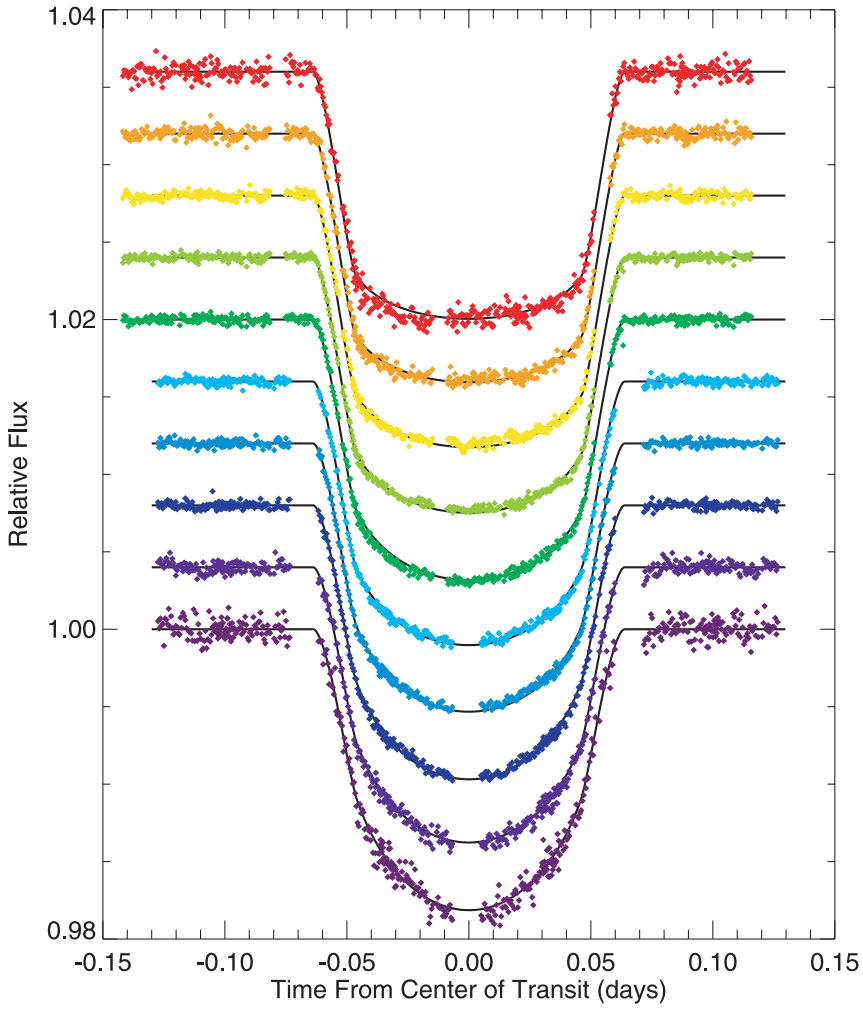


Figure 2.2: Multiband observations of the planet HD 209458 b transiting its star, in several bands, using *Hubble*. One clearly sees the effect of limb darkening, more marked at 0.32 μm (bottom) than at 0.97 μm (top). Figure obtained from Knutson et al. (2007).

The full shape of a transit is obtained by estimating the depth for a changing h. That quantity is called δ, the projected distance between the two bodies, which is described in units of semimajor axis as:

$$\delta = \frac{1-e^2}{1+e\cos\theta}\sqrt{1-\cos^2(\theta+\omega)\sin^2 i} \tag{2.9}$$

The time for which the planet's disc is entering the stellar disc is called the *ingress*. As the planet exits, the time between the moment where last the planet's disc is entirely above the star and the moment where no part of the planet covers the star is called the *egress*. Because stars have a limb darkening, we also have to estimate the stellar intensity that is effectively covered at each position of the planet. Limb darkening is usually much weaker as one observes in the infrared, thus approaching the equations displayed above. Several papers show how to integrate various limb darkening laws such as Giménez (2006a).

We saw in the introduction that we get directly from the transit (eq 1.15), the ratio of radii $R_{\rm p}/R_\star$; if we obtain radial velocities, we get the ratio of masses. Transforming quickly Kepler's

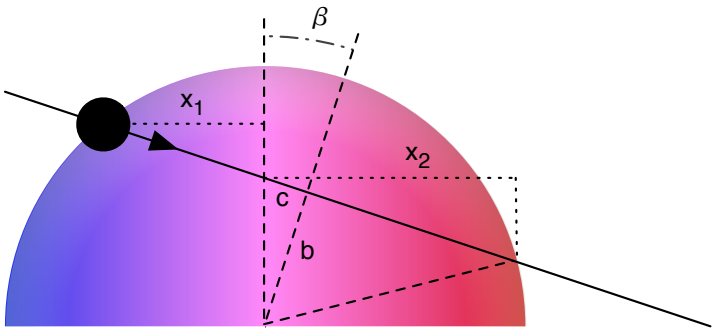


Figure 2.3: Diagram representing a planet transiting in front of a rotating star and showing the quantities used in the equations displayed in the text.

law (eq. 1.12) and as used in Sozzetti et al. (2007), we can get to the stellar density:

$$\frac{M_\star}{R_\star^3} = \frac{4\pi^2}{GP^2}\left(\frac{a}{R_\star}\right)^3 - \frac{M_\mathrm{p}}{R_\star^3} \tag{2.10}$$

where the second term on the right hand side can be approximated to zero. Assuming for a $M_\star$ thus solves for the stellar radius which helps us get to R_p. This same assumption on $M_\star$ leads us to the planet's mass thanks to radial velocity measurements.

Stellar density is something that stellar evolution models can predict. Section 2.6 will attempt to use this equation in order to obtain stellar masses without making too many assumptions. Other quantities of interest can be obtained directly from the transit lightcurve, independently from stellar parameters assumptions: Southworth et al. (2007) showed for example that once you have a radial velocity confirmation of the transiting planet, one can determine the planet's gravity directly too:

$$g_\mathrm{p} = \frac{2\pi}{P}\frac{K\sqrt{1-e^2}}{\left(\frac{R_\mathrm{p}}{a}\right)^2 \sin i} \tag{2.11}$$

2.1.2 The Rossiter-McLaughlin effect

The description of the effect is well described in Giménez (2006b) and Ohta et al. (2005), but a recent paper by Albrecht et al. (2011) provided an elegant way to explain the Rossiter-McLaughlin effect pedagogically. In my work, I have been using the formalism from Giménez (2006b) which denotes the spin/orbit angle as β while Ohta et al. (2005) takes the opposite and names it λ (thus two different notations in the literature). That difference is not interesting as all the interpretation needs to be done in absolute values, between 0 and $180°$, anyway.

Using figure 2.3, we have, geometrically, and in units of stellar radius $R_\star$:

$$c = b\tan\beta \tag{2.12}$$

$$x_1 = \left(\sqrt{1-b^2} - c\right)\cos\beta = \sqrt{1-b^2}\cos\beta - b\sin\beta \tag{2.13}$$

$$x_2 = \left(\sqrt{1-b^2} + c\right)\cos\beta = \sqrt{1-b^2}\cos\beta + b\sin\beta \tag{2.14}$$

According to Gray (2008) the apparent velocity of a point on the stellar surface is:

$$v(x) = x\,(v_\star \sin I) \tag{2.15}$$

with x estimated from the stellar spin axis. Extrema are thus at $(v_\star \sin I)\, x_1$ and $(v_\star \sin I)\, x_2$. Their sum will give the maximum change in velocity that the planet covers. The shift in velocity of the centre of the effect is estimated by taking the difference. This second quantity gives an idea of the departure from the *usual* double peaked, symmetric effect. Those relations are:

$$v_\star \sin I\, (x_1 + x_2) = 2\sqrt{1 - b^2}\, (v_\star \sin I\, \cos\beta) \tag{2.16}$$

$$v_\star \sin I\, (x_1 - x_2) = 2\, b\, (v_\star \sin I\, \sin\beta) \tag{2.17}$$

We see that for $\beta = \pm 90°$ we have no change in velocity, but a large shift in the velocity for the centre of the transit. For $\beta = \pm 90°$, equation 2.17 gives the amplitude of the effect. Those equations are a simplified truth: in fact the Rossiter-McLaughlin effect will show a change in velocity as the planet covers progressively some part of the velocity information from the star. The limb darkening will also play a role.

When the impact parameter $b \to 0$, relation 2.17 $\to 0$. We thus only have information from relation 2.16. The effect is symmetric; $v_\star \sin I$ and β are linked into one quantity creating a degeneracy between both quantities. The only way to measure β is to have an independent measure of $v_\star \sin I$. This can be obtained for example from analysing the broadening of spectral lines.

This problem can also be solved by modelling the way the rotationally broadened spectral lines are affected by the planet by retrieving the part of velocity space that the planet hides. This has been done by Albrecht et al. (2009) in the context of binaries and Cameron et al. (2010a) for exoplanets.

2.2 Adjusting Models to Data and Extracting Meaningful Error Bars

The ultimate adjustment tool is to search all of parameter space at infinitesimal steps, building a slightly different model every time which can be compared to the data. Because the range over which we need to search those parameters can be arbitrary and because of the number of parameters that need to vary can be important, this not usually done: it is not practical and would require too much computation. Several algorithms have been devised to search for a likely solution and then approach it, each has some qualities and some issues.

For the work presented in this thesis, two fitting tools were used, one, developed by Damien Ségransan and Maxime Marmier, called YORBIT, solves linearly equations when possible and otherwise searches parameter space with a *genetic algorithm* (Ségransan et al. 2011 in prep). This tool for the moment only accepts radial velocity measurements as input.

For the majority of the work here presented I used a *Markov Chain Monte Carlo* with a *Metropolis-Hastings* algorithm. I started its development while doing by Masters thesis at the University of St Andrews under supervision by Andrew Collier Cameron. The beauty of the MCMC as it will now referred to (or sometimes simply as a Markov Chain, or a chain) is to explore parameters around the solution and produce confidence intervals on each parameters. Its issue is on how to find the most likely solution. One needs a few other tools in order to guide it. YORBIT served some of that purpose as its genetic algorithm is very efficient at finding a good solution (while being poor at

producing robust error bars except when the data constrains the model very well[1]). This chapter is dedicated to this MCMC, on how it works, and what it can do. Following this, a series of papers for which an evolution of the code was needed are presented.

The specificity of that MCMC is that it allows us to adjust several signals caused by the same physical phenomenon: that of a planet orbiting over the disc of its host star. By combining all those different manners of observing the same object we reduce the total number of parameters that we need to use per datapoint and ensure that the solution we get is the best compromise. In essence in the case of our planet search with the WASP survey, the period is well determined by the long timespan of the photometric observations. Thus the adjustment of the semi-amplitude of the Doppler reflex motion caused by the planet has a smaller parameter space to explore and we get finer error bars on the planet's mass than if we were only fitting the radial velocities.

2.2.1 A Markov chain Monte Carlo

The algorithms and underlying theorems will not be discussed here, only their implications. For reference read for example, Gregory (2005) or Tegmark et al. (2004). A Markov Chain Monte Carlo is powerful tool using Bayes' theorem which from the data, comparing with models and according to some a priori knowledge recreates what is called the posterior distribution in its true shape, from which we estimate how well our model is constrained.

A Markov Chain Monte Carlo is a process depending on two ideas: the randomness of the search - the Monte Carlo bit - and the property that a new solution only depends on the current state and on nothing else nor the past, nor the future - the Markov bit. The term *chain* gives the indication that this is a process with several steps.

Markov's property can be written as (Seneta 1996):

$$p(H_n = x_n | H_{n-1} = x_{n-1}, \dots H_0 = x_0) = p(H_n = x_n | H_{n-1} = x_{n-1}) \tag{2.18}$$

where the properties x_n of a new state H_n at time n, are estimated from the properties of present state H_{n-1} without taking into account what happened in the past (from $n-2 \rightarrow n = 0$ states). Each of our states is a set of parameters from which we derive a model which is compared with the data. Our aim is to vary those parameters and estimate their likelihood. The set of parameters we use is described next section. In practise Markov's property has been included into the code as:

$$P_{n,j} = P_{i-1,j} + f\sigma_{P_j} G(0,1) \tag{2.19}$$

where P is the set of parameters we search, j denotes each parameter in turn and i is the step increment. $P_{n,j}$ is thus a newly proposed j^{th} parameter. In the text and the papers that are included, we also call that set: the *jump parameters*, those for which the chain is varying (jumping about).

The present state is $i-1$ from which a new state n is estimated[2]. This new state will be tested and be accepted or rejected. $f\sigma_{P_j} G(0,1)$ is the step size: the amount by which a new state will be different from the new one. G(0,1) is a Gaussian random number of mean 0 and standard deviation 1. It is multiplied by σ_{P_j}, a standard deviation attached to each parameter, and f a general factor ensuring that about 25% of steps are accepted. This criterion was estimated in Tegmark et al. (2004). It ensures a good balance between the exploration of parameters space and efficiency in computation.

[1] although this is changing...

[2] we make a difference between n and i. i counts the number of *accepted* states, while n counts the number of *proposed* states.

An immediate question arises: which value of σ_{P_j} one should use. This topic is subject of a long debate (and referred to as an *art*[3] (Gregory 2005)) and linked to other questions regarding for example, the length each chain ought to be. This will be described later in the text (section 2.2.5).

We now use our new set of parameters P_n to estimate a model. We use a χ^2 statistics (thus assuming our data errors are following a normal distribution) as a means to estimate its *badness of fit*: quantitatively how data ν and model μ compare.

$$\chi^2_n = \sum_{k=1}^{l} \frac{(\nu_k - \mu_k)^2}{\sigma^2_{\nu_k}} \tag{2.20}$$

ν_k is a data point with a Gaussian error bar of σ_{ν_k} compared to what the model made with a P_n set of parameters predicts it ought to be: μ_k. This is summed over the total number of datapoints l. From this we define a new merit function including a set of priors on our parameters denoted as $P_{0,j} \pm \sigma_{P_{0,j}}$, with their Gaussian error bars. Those priors come, as their name suggest, from a prior idea of the end solution: it might be due to a physical model, or to previous observations. This new merit function is:

$$Q^2_n = \chi^2_n + \sum_j \frac{(P_{n,j} - P_{0,j})^2}{\sigma^2_{P_{0,j}}} \tag{2.21}$$

The aim of the MCMC is to recreate a probability density function (PDF) for each parameter: meaning a continuous function comprising the range of possible values for our set of parameters giving their relative likelihood. It essentially gives a measure of our ignorance on the values of our parameters. In order to recreate this function, we should now estimate how our new state P_n compares with our present state P_{i-1}:

We will now use the Metropolis-Hastings algorithm. This algorithm will make a choice between our two states P_n and P_{i-1} from the merit functions that we defined earlier. We accept the new state by computing the likelihood that P_n describes a closer fit to the data than P_{i-1} namely: $r = e^{-0.5\left(Q^2_n - Q^2_{i-1}\right)}$. In practise this amounts to:

1. if $r \geq 1$ (ie. $Q^2_n \leq Q^2_{i-1}$) we accept the step and denote it as $Q^2_i = Q^2_n$ with $P_i = P_n$. We then propose a new n and increment i. Q^2_i becomes our new Q^2_{i-1}, P_i our new P_{i-1}
2. if $r < 1$ (ie. $Q^2_n > Q^2_{i-1}$) we draw a uniformly distributed number between 0 and 1, called u.
   - if $r \geq u$ we accept the step and denote it as $Q^2_i = Q^2_n$ with $P_i = P_n$. We then propose a new n and increment i. Q^2_i becomes our new Q^2_{i-1}, P_i our new P_{i-1}
   - if $r < u$, we reject the step and denote it as: $Q^2_i = Q^2_{i-1}$ with $P_i = P_{i-1}$. We then propose a new n and increment i. Q^2_{i-1} and P_{i-1} are left unchanged.

Demonstrated in Gregory (2005), this algorithm will converge to a stationary distribution corresponding to the posterior distribution. In a manner of speaking, it reaches an equilibrium state. It will do so regardless of the step size, the only difference being the number of steps one need to compute to reach it. If the step size is too small, it will take a lot of steps to explore P_j far from the most likely value ($r \geq u$ is what we obtain most of the time: new states are always accepted). If the step size if too long, we obtain $r < u$ most of the time, new states are rarely accepted. Even in that case we can get an idea of the final distribution (with a poor resolution). This property comes from the fact that we keep the older state at each proposed state, so if a new state is not accepted, we still increment i though n would not. We thus have the information that the current state $i-1$ is much better than most of the proposed states n.

[3] I knew it! I am an artist!

This is where the factor f from equation 2.19 intervenes. After 100 accepted steps i, the number of proposed steps n is estimated. f is adjusted to try reach a 25 % acceptance rate, enough to explore the most likely solution as well as its surroundings. f essentially scales the step size so the exploration is done more efficiently.

During the initial steps, because we can at best, only start in the vicinity of the most likely solution (if we knew the solution there would be no need to estimate it), the first criterion in the Metropolis-Hastings algorithm plays an essential part drawing the P_j towards smaller and smaller Q^2. Initially too, f is let deliberately large: in this manner the step size is rather large and the solution wanders about exploring Q^2 space. Because the acceptance rate is bad, f is reduced and we progressively search on a smaller region around the best Q^2. This is called the *burn-in*. Eventually the chain settles and the second Metropolis-Hastings criterion becomes mostly used. By launching several chains it is possible to estimate if all chains converge to similar final distributions. Once the chain has settled we record the evolution of f and compute its mean. Then we start the chain that we will use to draw statistics from, where f is kept frozen for the rest of the computation.

σ_{P_j} are kept fixed during the entire chain. They can be guessed from the knowledge we have of the data and the error bars that are usually obtained from fitting it. They can also be estimated by doing a few preliminary chains. Those chains will give estimates of the dispersion for each P_j which can be used to set newer values of σ_{P_j} before a new chain is started.

All the beauty of this manner of adjusting models resides in the second criterion of the Metropolis-Hastings algorithm. Most other techniques focus on minimising χ^2 (which means finding the model that fits the data perfectly). This is not statistically right as a smaller χ^2 does not necessarily represent the true solution: after all χ^2 also has its intrinsic natural variance: we can observe a same physical reality but once have bad data, and another time data that fits too well. While other techniques can fall in the trap of a false signal in the data, the MCMC is less likely to do so since it describes how well (rather, how bad) the model compare with the data for varying parameters. The computation explores parameter space and recreates the χ^2 probability density function for j degrees of freedom (only the models are flexible, the data remains constant). The most likely solution is where the mode of the distribution is, in other words, where we have the largest density of accepted steps. and not where Q^2 has the smallest value.

The MCMC is a Bayesian fitting method. Bayes' Theorem is written as:

$$p(H|D,I) = \frac{p(D|H,I)\,p(H|I)}{p(D|I)} \tag{2.22}$$

where we multiply the probability of observing our data D, if our hypotheses H and priors I are true, to the prior probability of our hypothesis to give us the probability of this same hypothesis, $p(H|D,I)$, given the data and the prior. $p(D|I)$ is a normalisation factor. In the text above, we expressed our hypothesis H as a vector P with j dimensions: $p(D|H,I) \rightarrow p(D|P_j,I)$, which defined is by χ^2. The priors, also in a vector, $P_{0,j}$, are comprised in $p(H|I)$. The output from the MCMC is thus the posterior distribution $p(P_j|D,I)$. The Metropolis-Hastings algorithm checks $p(P_{n,j}|D,I)$ against $p(P_{i-1,j}|D,I)$ by computing r:

$$r = \frac{p(P_n|D,I)}{p(P_{i-1}|D,I)} \frac{q(P_{i-1}|P_n)}{q(P_n|P_{i-1})} \tag{2.23}$$

q is the description of how our parameter vector is chosen: the step size and notably, in our case, the Gaussian sampling. Because they are symmetric (one step in a direction is similar to one in another direction) they cancel out.

Thanks to this, the MCMC can output non Gaussian probability density distributions for each parameter. Because we obtained probability density distributions and not probability maps, we already have marginalised parameters and do not need to estimate covariances. Confidence intervals are given instead of a solution with error bars (for practical purposes, the mode of each distribution can be quoted as the solution and error bars estimated from the confidence intervals).

2.2.2 Adapting the models

We will use the models parametrised in the first chapter and in section 2.1. The parameters that describe them are the physical parameters of the effect, those for which we gain meaningful information about the nature of the objects we observed and those parameters that will be used to be compared with other objects. As often in Astronomy (and other sciences), what is measured is not always the physical parameter we seek. In addition following Bayes' theorem, the manner (the opinion, the prejudice) with which we adjust data can influence our results. We thus need to introduce which parameters are used and the reasons why they have been chosen.

Because the choice of parameters has evolved during the thesis and indeed will continue to evolve following the critics of our peers, this sections will describe what has been mostly used. The changes will be highlighted in the following sections, on the application of the code to various datasets and its mutations.

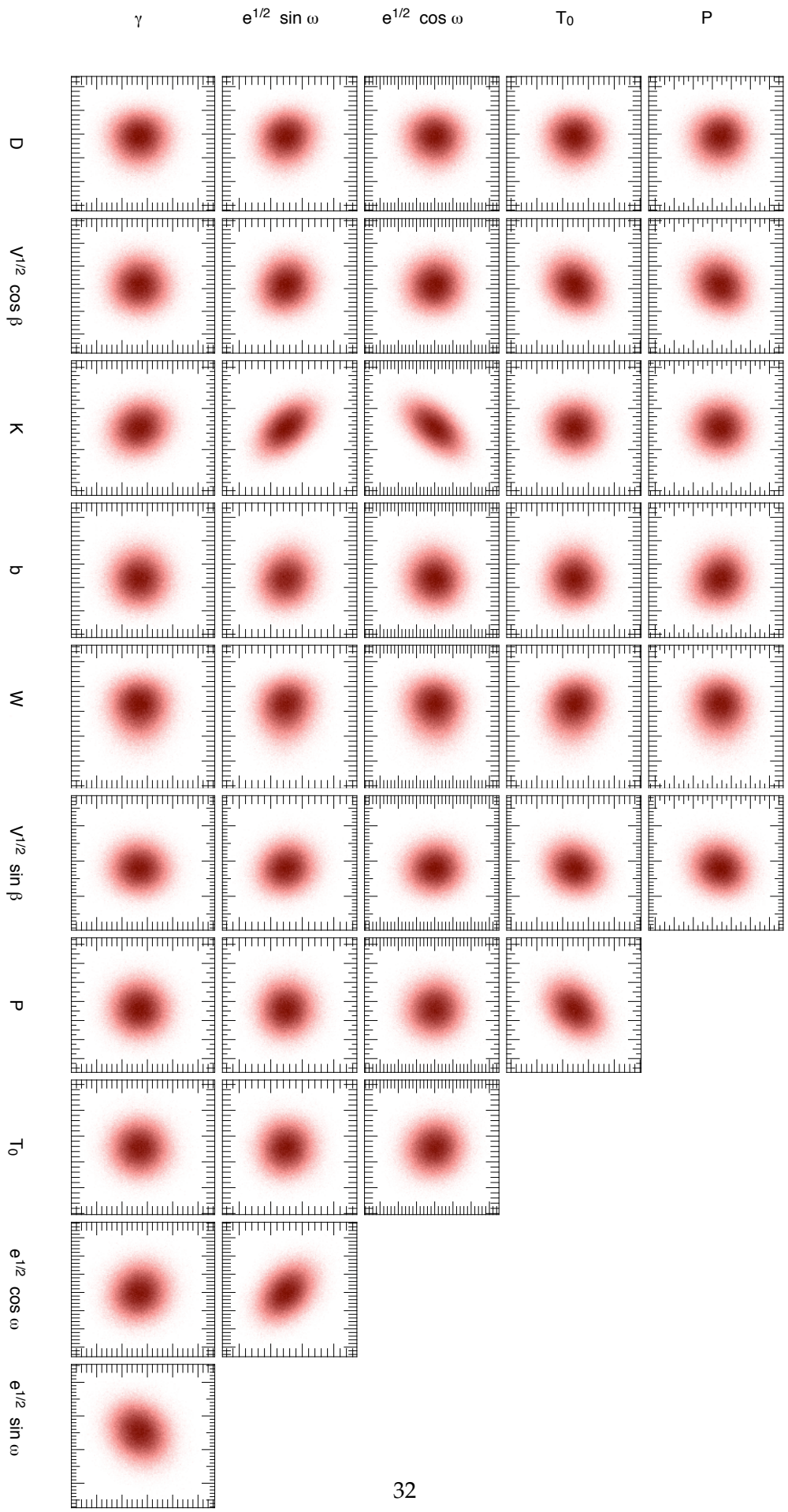
Whenever possible the observables, such as the transit's total width W and depth D, or the signal's period P and mid transit time T_0 were used. We also need the impact parameter b to adjust for the photometric signal of a transiting planet. To fit a Keplerian on the radial velocity measurements, P and T_0 are also used. In addition we fitted using $e\cos\omega$ and $e\sin\omega$ where e is the orbital eccentricity and w the longitude of the periastron. The reason for combining them is a practical one, first pointed out by Ford (2006). Using eq. 2.19, it is quasi impossible to have $e = 0$ as a possible solution, we thus bias our chain to non zero eccentricities. In addition, an eccentricity just above 0 will have a very undefined ω while for jumps at higher eccentricities, it becomes better determined. By linking both, we ensure the step size stays consistent. Similarly we will combine $V \sin I \cos\beta$ and $V \sin I \sin\beta$ to fit for the Rossiter-McLaughlin effect [4]. The combination of $V \sin I$ and β is made clear from equations 2.16 & 2.17. The other parameters needed to model the Rossiter-McLaughlin effect are the same than for a planetary transit.

In addition to those, we will also need to add correction parameters such as the systemic velocity γ. Because instruments are calibrated a little differently, this value will depend on the observation site. We need one per data set. The photometry is included as flux. We need to ensure the out-of-transit photometry is normalised. Those values are determined by an optimal scaling and thus are not *jump parameters* as the others are.

Cameron et al. (2007b) show that choosing W and D as jump parameters instead of using $R_\star/a$ and $R_\mathrm{p}/R_\star$ (as other authors in the literature) leads to posterior distributions that are less correlated with notably, b (compare figure 2.4 and 2.5). Correlated parameters make the MCMC sampling less efficient: because each step is drawn randomly, a large area of parameters space is sampled uselessly. I find that iterating on observable quantities rather than on physical parameters is always better as one can check visually if indeed the chain has converged to credible most likely solutions and confidence intervals.

As pointed out in section 2.1, in order to model the transit shape correctly, one needs to take into account the time taken during ingress and egress when the disc of the planet only partially

[4] The two pairs of paired parameters, $e\cos\omega$ & $e\sin\omega$ and $V \sin I \cos\beta$ & $V \sin I \sin\beta$ have since been replaced by $\sqrt{e}\cos\omega$ & $\sqrt{e}\sin\omega$ and $\sqrt{V \sin I}\cos\beta$ & $\sqrt{V \sin I}\sin\beta$. The reasons are explained later in section 2.4 and 3.4.4


γ
e^1/2 sin ω
e^1/2 cos ω
T0
P
D
V^1/2 cos β
K
b
W
V^1/2 sin β
P
T0
e^1/2 cos ω
e^1/2 sin ω

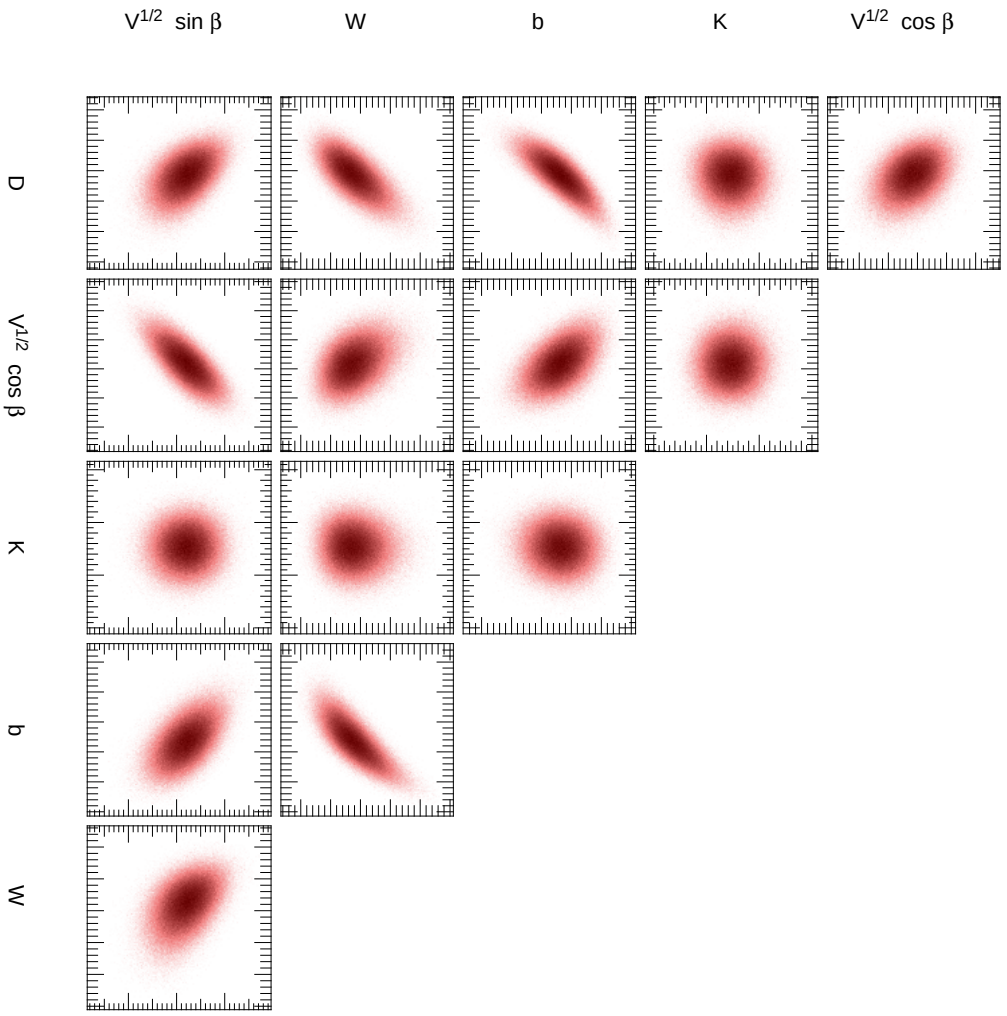


Figure 2.3: Example of an MCMC output showing the 11 jump parameters used in a fit for WASP-8 plotted against each others. Most show no correlation but some appear notably linked to b. There is a small conflict between the photometric transit and the Rossiter-McLaughlin effect. The scale are hidden as they would clog the graph. A blown-up version of W against b is shown in figure 2.4. A comparison with figure 2.5 shows that correlations could have been worse.

transit covers the star, as well as a variation in brightness over the stellar surface known as the limb darkening. A code from Mandel & Agol (2002) was used in order to determine the flux as a function of orbital phase. As input this code needs the ratio of the radii $R_{\rm p}/R_\star$, coefficients for limb darkening and the distance between the centre of the planet and centre of the star δ (given by equation 2.9). Using these, it will output the flux expected from the star for a planet at that phase. We do this for each individual data point. This code is used as much for the primary transit as well as for the secondary occultation. Alternatively, we can also choose to use a model developed by Giménez (2006a).

A code written by Giménez (2006b) will provide the model with which to fit the Rossiter-McLaughlin effect. This code is using a formalism notably published in Kopal (1942) and Hosokawa (1953) in the context of stellar binaries. Its input also requires limb darkening coefficients, the ratio of radii and δ as input, but also the sum of relative radii $R_{\rm p}/a + R_\star/a$. In output we obtain the radial velocity anomaly caused by the planet covering part of the velocity space of the star.

Limb darkening has been modelled by several laws, in most of cases, the quadratic law has been good enough. The two limb darkening coefficients are extracted using stellar parameters obtained from a spectral analysis[5] from tables compiled by Claret (2000, 2004) for the photometry. For the Rossiter-McLaughlin effect, we used new coefficient tables computed by Claret from HARPS's spectral response and first used in Triaud et al. (2009) (section 2.5.2).

Since we chose our iterative parameters as often as possible as direct observables, we need to convert those into values receivable by both codes (like in Seager & Mallén-Ornelas (2003)). The ratio of radii is taken as: $\sqrt{D}$ as exposed in eq. 1.15. In case of a grazing transit where the planet does not totally enter over the stellar disc, we can use a correction:

$$\frac{R_\mathrm{p}}{R_\star} = \frac{1}{2}\left((b-1) + \sqrt{(1-b)^2 + 8D}\right) \tag{2.24}$$

At each step both values are estimated the maximum of the two is taken as the ratio of radii. $R_\star/a$ is obtained from equation 2.8 but using substituting for $W = T/P$:

$$\frac{R_\star}{a} = W \frac{\pi}{\sqrt{\left(1+\frac{R_\mathrm{p}}{R_\star}\right)^2 - b^2}} \frac{1+e\sin\omega}{\sqrt{1-e^2}} \tag{2.25}$$

The phase ϕ is determined:

$$\phi = 2\pi \frac{(t-T_0)}{P} \tag{2.26}$$

where t designs the date of the observations, usually as a Barycentric Julian Date. From it a first guess at the eccentric anomaly E is made and iteratively we solve the Kepler Equation

$$E - e\sin E = \phi - \omega' \tag{2.27}$$

where ω' denotes a corrected longitude of periastron[6]. Using E we then determine a modified δ function (from eq. 2.9) as the separation between the centre of the planet and the centre of the star.

$$\delta = \frac{1-e^2}{1+e\cos\theta}\sqrt{1-\cos^2(\theta+\omega')\sin^2 i} \tag{2.28}$$

where θ corresponds to the true anomaly. So now, we have a flux estimate for every point. In the mean time, with the same parameters we estimate the radial velocity using eq. 1.9. Using the lightcurve and convolving it with Giménez's routine, we obtain the colour anomaly caused by the transiting planet and source of the Rossiter-McLaughlin effect. The proposed model is compared to the data and χ^2 is calculated. As χ^2 is estimated, we solve for the adjustment parameters (RV's γ velocities and photometric normalisation factors) thanks to an optimal scaling (Keith Horne's Astronomy Data Analysis lectures). This means those parameters do not influence the *jumping* of the model parameters (numerical proof for is displayed in section 2.2.5).

[5] usually realised by Barry Smalley at Keel University

[6] A note of caution here: convention in astronomy state that $\phi = 0$ is when the orbit passes at periastron. For transits, mid transit is always $\phi = 0$ which is when $\phi_\mathrm{RV} = \pi/2$ for a circular orbit, reason why ω' is used.

2.2.3 Inserting priors

Part of the interest of the MCMC and of the philosophy of combining different datasets is to also include as much information as possible about the physics we already know of this object to help affine our knowledge of it. It is also an occasion to help speed the fitting process as not necessarily all the proposed sets of parameters are physical. A quick example is the case of the impact parameter b. Being the shortest distance between the centres of the two bodies and expressed as units of stellar radii, this value cannot be negative. In order to make sure that solutions as close to 0 as possible are explored, when eq. 2.19 is used, negative values for b are produced. If those happen, they are immediately rejected. Similarly for the depth D and width W.

If one has prior information on say, the stellar radius, for example on a host star whose parallax has been detected, we can take this knowledge into account using eq. 2.21. In order to do that we need to compute which stellar radius the model we just estimated from observable corresponds to. In short, we need to estimate a host of physical parameters that can be deduced thanks to the proposed jump parameters.

As seen in section 2.1 apart from the stellar density, we need to assume the mass of the host star in order to derive most other physical parameters. From Kepler's law and geometrically:

$$a = \sqrt[3]{\frac{P^2 G M_\star}{4\pi^2}} \qquad \text{for } M_p \ll M_\star \tag{2.29}$$

$$i = \cos^{-1}\left(b \frac{R_\star}{a\left(\frac{1-e^2}{1+e\sin\omega}\right)}\right) \tag{2.30}$$

$$M_\mathrm{p} = \frac{K M_\star}{\sin i}\sqrt{\frac{a}{G M_\star}}\sqrt{1-e^2} \tag{2.31}$$

R_p is obtained from eq. 2.24 and a that we just found. Good care should be taken when using priors and a comparison between several such priors is recommended. One also should fit without prior and estimate by how much they influence the results. It is important to quote the observable quantities and their error bars as one can always find the physical quantities later. For instance, any error on $M_\star$ will be propagated to M_p, $R_\star$ and R_p.

2.2.4 Extracting statistics

For each object several chains are launched and only if they converge to a similar χ^2 posterior distribution can we proceed with a longer chain, this one aimed at exploring fully and refining our knowledge about the posterior. To obtain converging chains, the correlation step (the interval in takes for any P_j to come back to a similar value) needs to be small compared to the length of the chain. For practical reasons we do not want too long chains, as they take time to compute and thus need to reduce that correlation step. This is done by tweaking the step size. In essence initial runs are made and the root mean square is estimated for each parameter. This value is forwarded to σ_{P_j} iteratively until we arrive to a stable solution. That solution is then checked by taking different starting parameter values and see if we still converge.

All jump parameters and derived parameters, with the values of χ^2 for each dataset, at each step are kept. At the end of each chain, we can derive directly the marginalised distribution for each parameters (a feature of the Markov chains, see figures 2.4 and 2.5), get the mode of the distribution as our most likely solution and get confidence intervals at 1, 2 and 3 σ. If a distribution is a bimodal, only the highest mode is quoted, except in the case where two modes are clearly resolved and of similar significance.

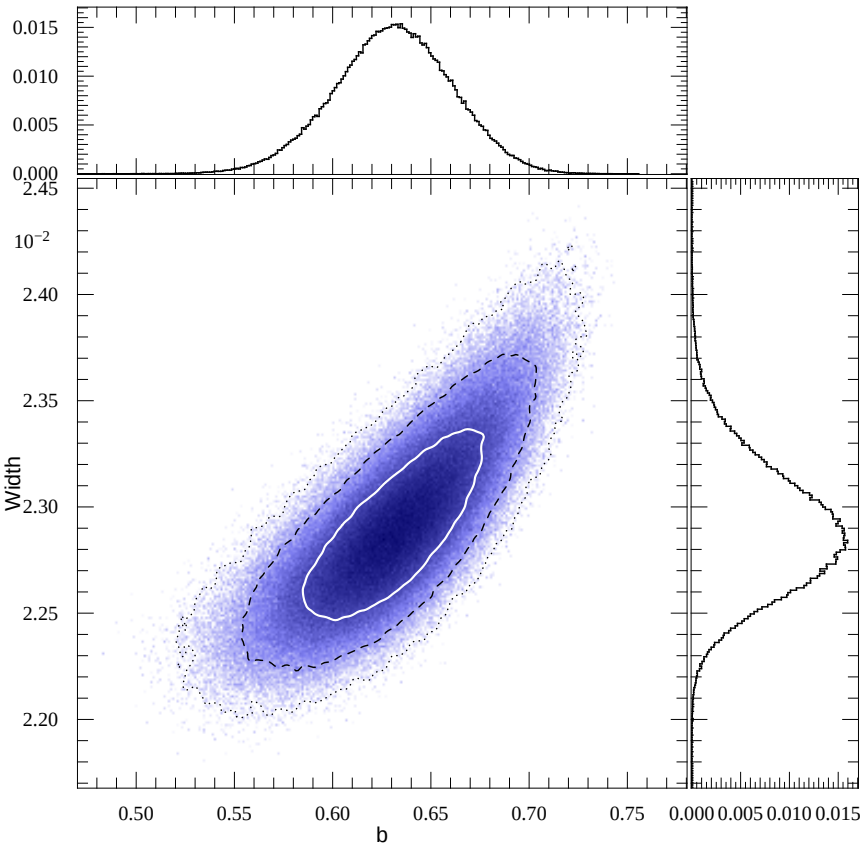


Figure 2.4: Zoom on the joint probability density function of the transit width W against impact parameter b and confidence intervals presented in figure 2.3. Marginalised probability density functions for each parameter are drawn in the side boxes.

Differing models are compared by means of the χ^2_{reduced}. Several chains are run, each with different hypotheses. For instance, one could assume a circular model, or an eccentric model. From the distribution in χ^2 for each dataset as a function of jump parameters, one can see that eccentricity is usually not constrained by photometry and that the radial velocities are the measurements that can act on the Metropolis-Hastings algorithm to choose eccentric solutions. Thus just the χ^2_{reduced} from the radial velocities are compared. If there is no significant improvement in χ^2 within its variance by having two extra parameters, using Ockham's razor, we choose the simpler, circular solution. This procedure comes as a simple version of a Bayes factor estimate. A more robust model selection is something that remains to be developed. The first steps are outlined next section.
A manner to have an effective model selection might be to use the Metropolis-Hastings algorithm between the two posterior distribution coming as output of two chains with different models, or even to run parallel chains with differing models, choosing at each step which of both is more likely.

2.2.5 A toy model

We here will describe a small toy model to illustrate the statements made since the start of this chapter and as a showcase on how the MCMC performs. We will take a simple polynomial model, create fake datasets around it and let them be adjusted by means of a Markov Chain, in every way similar to the one used for extracting planetary parameters. The model is:

$$y = ax^3 + bx^2 + cx + d \tag{2.32}$$

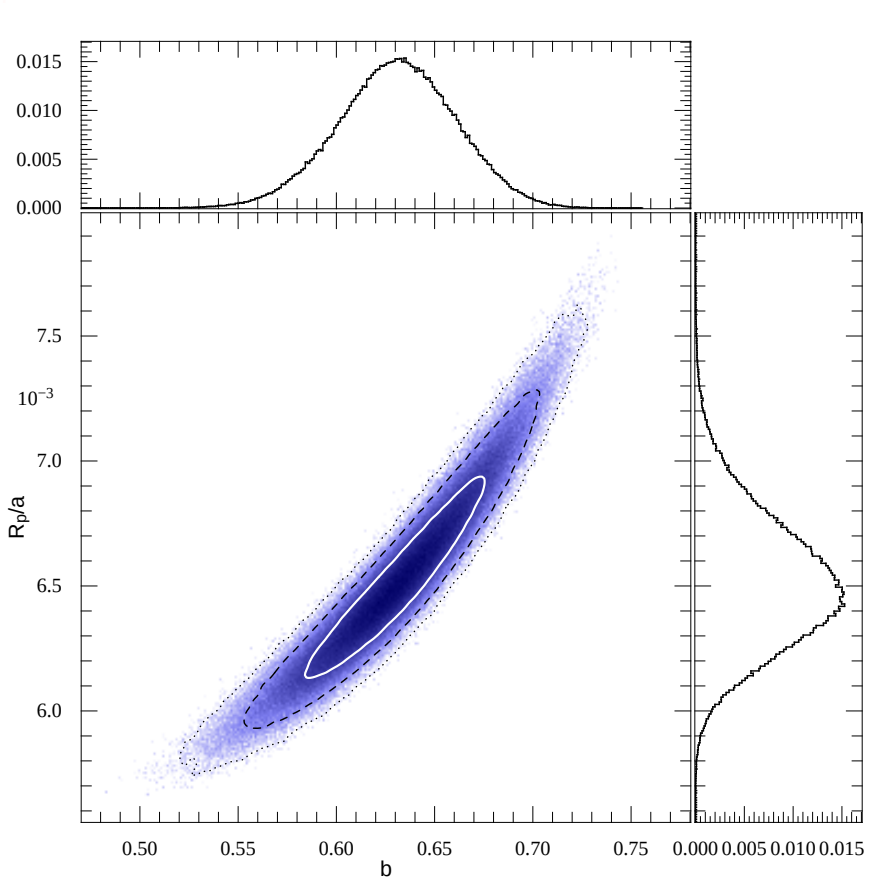


Figure 2.5: Joint probability density function of the scaled planetary radius R_p/a against impact parameter b and confidence intervals. Marginalised probability density functions for each parameter are drawn in the side boxes. The distribution shows a stronger correlation than in figure 2.3, validating the choice of W as a jump parameter instead of R_p/a.

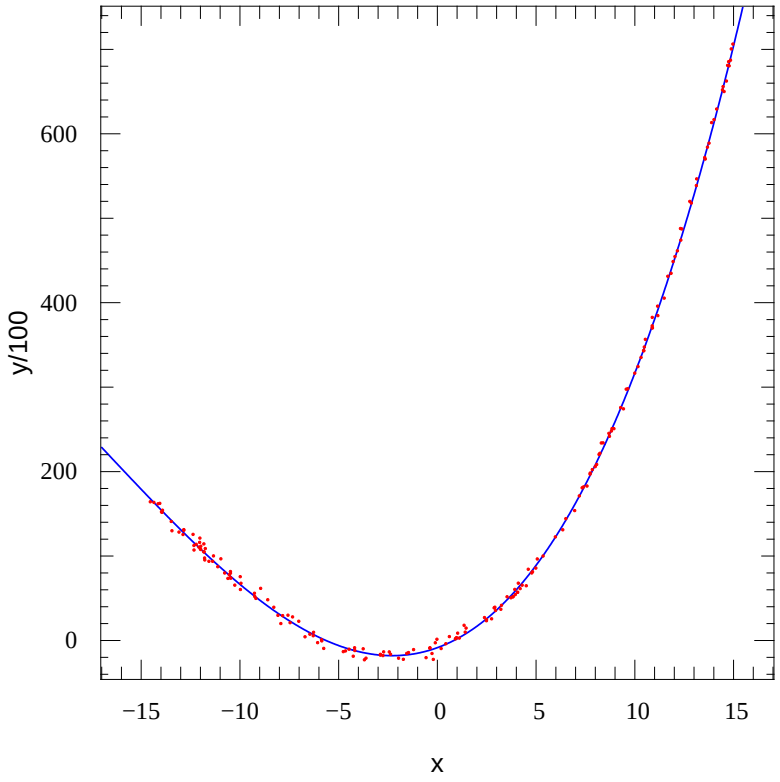


Figure 2.6: Cubic toy model with one example of 200 randomly selected points over it, as described in the text. Because values in y were very large, the axis has been scaled.

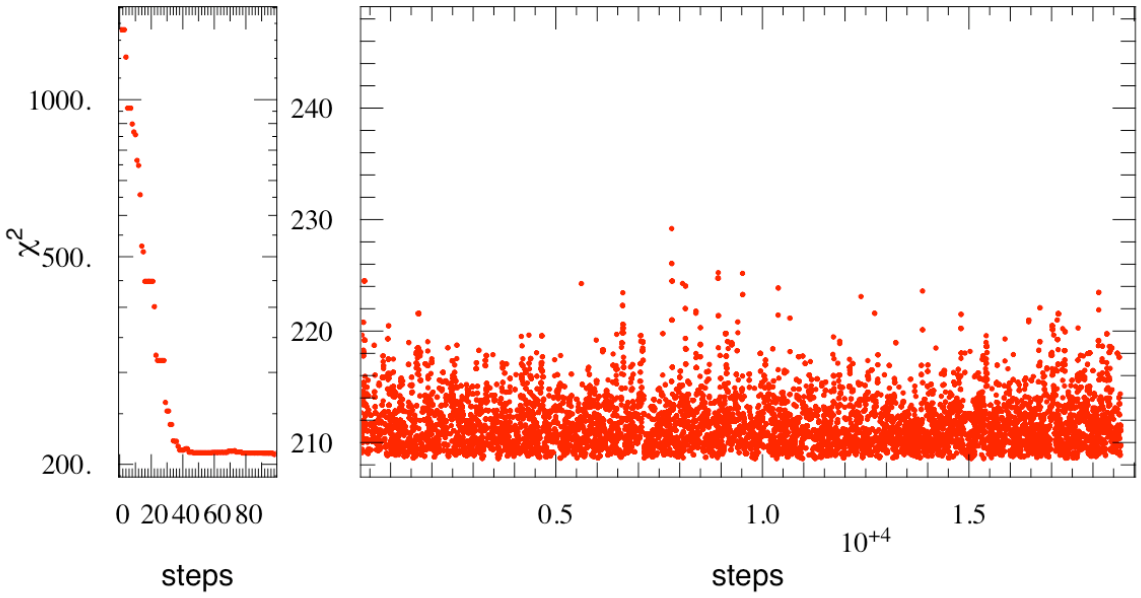


Figure 2.7: *left* evolution of χ^2 on the first 100 steps. *right*, evolution of χ^2 in the range of steps used for statistics. We clearly see the burn-in of the chain in the first few steps (check the scale). The chain then settles in a stationary state. One of the main features of the Metropolis-Hastings algorithm is also obvious: χ^2 jumps up and down, we are not doing a χ^2 minimisation. We can also observe that some steps are repeated: at about the 20^{th}, we see that χ^2 is constant for a little while. This happened because no proposed set of parameters had a χ^2 such that the new set would be accepted.

200 data points are created from a random uniform distribution in x on a range between -15 and $+15$. Values in y are computed randomly around the model in a Gaussian manner with mean corresponding to that calculated by the polynomial. Standard deviation is the same for every point (one could as easily create non Gaussian error bars, and variations in the size of error bars. Those simulation are not presented here).

testing the chain

A toy is made to play with. Before playing with our new little toy, let's test it and see if we can reproduce what we would expect from a Markov chain.

We use here, a, b and c as jump parameters, while d is estimated via optimal scaling as are the γ velocities (see section 2.2.2). The data covers enough range in x to distinguish between the quadratic and cubic models as shown in figure 2.6. A chain of 5 000 accepted step is launched. With a few iterations, it is possible to get good estimates on the step sizes by taking the final rms on individual parameters as described in section 2.2.4. To check convergence, ten chains are launched, all end up with the same posterior distribution showing good convergence. Figure 2.7 shows one such chain.

By accepted steps, one should understand, unique steps. Because of the Metropolis-Hastings algorithm and the 25% acceptance criterion, in average each step is repeated four times, for ex-

ample to a total of 18 977 steps for one particular chain we will now consider. Because of burn-in, (see figure 2.7) we leave out the 300 first steps and will draw statistics on the remaining steps. On figure 2.8 the resulting χ^2 distribution is shown. This is obtained by doing a histogram in the χ^2 direction on the data displayed in figure 2.7. The vertical axis is such that the area under the histogram is normalised.

Over, is plotted a χ^2 probability density function (equation 2.33 as given in Gregory (2005)) with $k = 3$ degrees of freedom and shifted to have both modes coincide. This is easily understandable since only the three jump parameters influence how χ^2 evolves thus only three degrees of freedom. The fourth parameter being estimated, does not participate. The good adjustment between $\chi^2_{\rm PDF}$ and the MCMC output demonstrates we are reproducing well the posterior distribution as one would expect it does.

Convergence of the chain can be checked thanks to this property: estimate the mode of the output χ^2 distribution from several separate chains. The root mean square of the modes should correspond to the standard deviation of $\chi^2_{\rm PDF}$ for k equal to the number of jump parameters.

$$\chi^2_{\rm PDF} = \frac{1}{2^{k/2}\Gamma(k/2)} x^{k/2-1} e^{-x/2} \tag{2.33}$$

This is an equation we will use several times in the text. As $k \to \infty$, $\chi^2_{\rm PDF}$ tends to a Gaussian. The variance of $\chi^2_{\rm PDF}$ is $2k$.

One can now extract the resulting distribution for each of the parameters and check them against the initial parameters. The mode of each distribution (and not the best χ^2) is chosen as the most likely solution. Confidence intervals can be estimated easily, here we will only quote the 68.3%. $a = -4.015^{+0.062}_{-0.062}$ instead of -4.0; $b = 200.48^{+0.57}_{-0.37}$ instead of 200.0539; $c = 850.9^{+7.6}_{-11.8}$ instead of 850.4309 and $d = -846^{+173}_{-161}$ instead of -850.694. The solution is found within 1σ in each case except for b which is a little above that. You can check on figure 2.9 where those solutions are located, compared to those from which the model is defined and the data derived.

We obtain a $\chi^2_{\rm mode} = 210$ (fig. 2.8) giving a $\chi^2_{\rm reduced} = 1.06$ indicating a good adjustment. But now we have to remember that χ^2 has a variance. We estimated it for the chain where the data was *fixed* and where parameters were *evolving*, but our data is only one realisation of a noise around a model. We thus also have a variance, this time attached on each value of χ^2 that the MCMC outputs. Variance is thus $\sim 2\chi^2$, hence the mode of the $\chi^2_{\rm PDF}$ we obtain in our case is at $\chi^2_{\rm mode} = 210 \pm 20$ and $\chi^2_{\rm reduced} = 1.06 \pm 0.10$. This natural variance on the data is important to keep in mind when trying to detect more complex models. Here we see that our result is entirely compatible with a $\chi^2_{\rm reduced} = 1.0$ leaving no room for a more complex model.

mis-estimated error bars

Error bars are sometimes mis-estimated. A typical example would be an extra source of noise, due to stellar activity for example, or bad weather affecting the data. How would that influence the fit? The same fake dataset was run in a new chain in every similar way, but the error bars on individual points were halved. In another run, those error bars were doubled. Because the shape of the output $\chi^2_{\rm PDF}$ depends only on the number of jump parameters, we would expect it to be entirely unaffected, which the simulation confirmed. Only the position of $\chi^2_{\rm mode}$ changed. The χ^2 posterior distribution is thus free from influence. What will be influenced are the marginalised posterior distributions of the parameters:

As one could expect from the way χ^2 is calculated: for a halving of error bars, $\chi^2_{\rm mode}$ is increased and the parameter space that the MCMC explored was halved. For a doubling of error bars on the

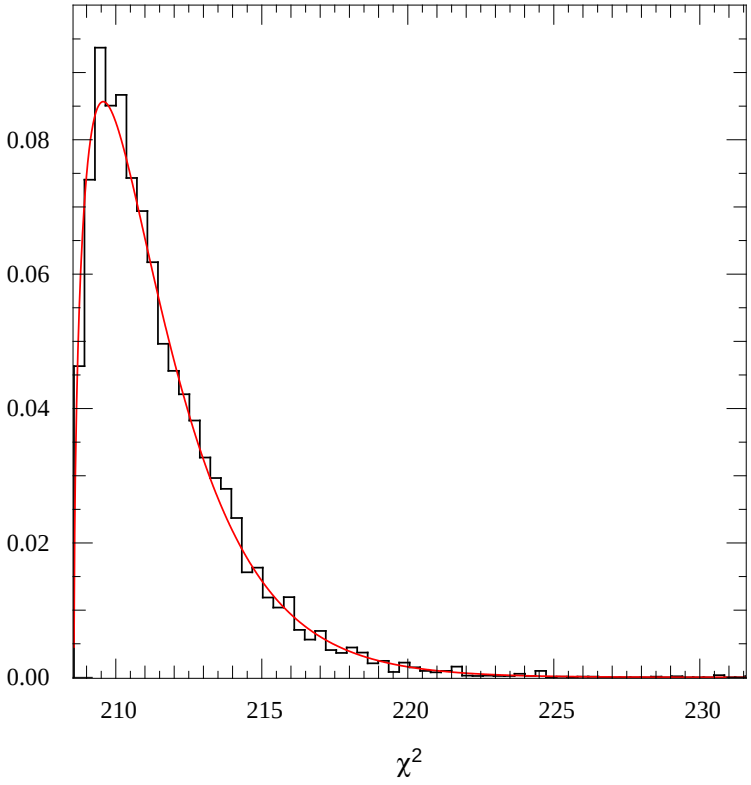


Figure 2.8: χ^2 probability density function outputed by the chain, in black. Overplotted in red, a smooth $\chi^2_{\rm PDF}$ with $k = 3$ degrees of freedom, corresponding to the number of jump parameters in the MCMC. The shape is only dependent on the number of jump parameters and not on the number of datapoints, thus not on the value of χ^2 at any moment. Mis-estimated error bar on the data would only affect where $\chi^2_{\rm mode}$ is located. Comparing the output with the expected $\chi^2_{\rm PDF}$ is a test that the chain is statistical.

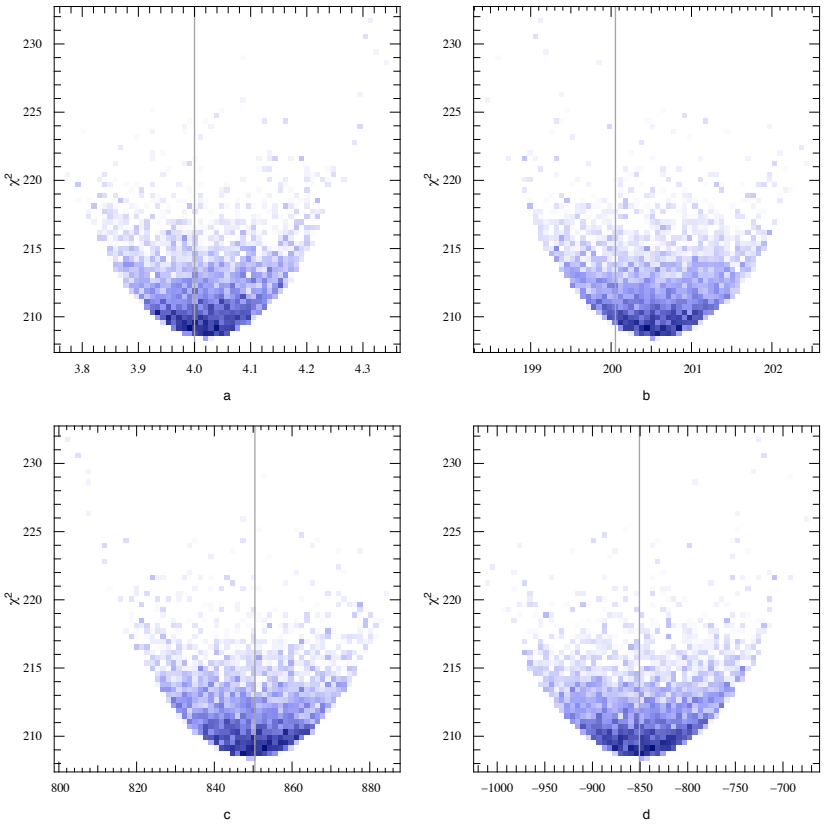


Figure 2.9: χ^2 distributions for each of the three jump parameter and the adjustment parameter. In grey, the initial solution. Running a chain for longer would smooth the distributions and explore parameter space a little further. Mis-estimated error bars on the data would give you the same range in χ^2 (vertical axis), but not on the horizontal axis, thus leading a wrong estimate of confidence intervals for each parameter.

data, that range was doubled. Thus, for underestimated error bars and $\chi^2_{\text{reduced}} > 1$, error bars on parameters are underestimated. This is in favour of increasing error bars when $\chi^2_{\text{reduced}} > 1$, but this should only be done once we are sure that the bad χ^2 is not due to another signal in the data, which we should then model so that its errors are propagated to all parameters.

data can naturally be good, or naturally be bad

People have been surprised when I started producing error bars on the χ^2 in the papers for which I had a role to play in the analysis. I was also surprised when I first saw Damien Ségransan use them (eg. Ségransan et al. (2010)). This paragraph aims to show why producing those errors is of interest. Underlying this paragraph is the intense will to avoid announcing fake signals. It is also a realisation that whatever we observe, is an incomplete image of reality.

Just previously I was making a distinction between the data being *fixed* during the chain but having to account that we only have one realisation of a noise around a model, of which we ignore the shape. So, let us make the data *change* and see what happens. For that, we will use our little toy which previous paragraph showed performs as expected:

Using the same set up, we will instead of running several chains on one dataset, run one chain on 10 000 different datasets of 200 points, each randomly drawn as described in the previous paragraph. This way we explore 10 000 different incomplete versions of a same reality. Each of the modes of the χ^2 distributions are kept. The probability density function of those 10 000 modes is shown in figure 2.10. For confirmation of the shape and the validity of the simulation, a χ^2_{PDF} with $k = 200 - 3$ degrees of freedom (200 datapoints - 3 fitted parameters) is plotted above the histogram of our simulation. That distribution shows that we have about 0.5% chance to obtain $\chi^2_{\text{PDF}} < 150$ and 0.5% chance to obtain $\chi^2_{\text{PDF}} > 250$. Thus, if we were to only obtain one dataset which $\chi^2_{\text{mode}} > 250$ from the MCMC's output, we have as much chance to have been unlucky in our data acquisition[7], than to have had a lucky draw, but missing an extra degree of complexity in our understanding of reality. Similarly, if we obtain $\chi^2_{\text{mode}} < 150$, we can't know for sure whether we had a lucky draw, or whether we have been over-fitting a bad dataset from a simpler reality. In this simulation we know which *reality* we have and its complexity, but when observing real astronomical object, we do not anymore.

Usually we have only one chance to get data and when getting more, we have no reason to separate it in many smaller sets. Is it a lucky or or unlucky draw? There is no way of knowing. What we can do is take that uncertainty into account: using the variance of χ^2. For example, taking the chain that was used to build figures 2.7 and 2.8, we will compute equation 2.33 for each value of χ^2 produced by the chain, taking $k = \chi^2 - 3$. We had 18 677 steps in that chain, thus we combine 18 677 individual χ^2_{PDF} into one, which is the offset blue curve on figure 2.10.

The two curves displayed on figure 2.10 represent the expected χ^2_{PDF} for a model of a complexity we have chosen to adjust for, and the distribution representing our measurements accounting for all uncertainties. Comparing both distributions as produced in figure 2.10 is a potentially good way to distinguish between two competing models. Here we see the overlap between both is large, thus, there is no room for a more complex model. This is the same conclusion we had obtained from looking at χ^2_{reduced} when its standard deviation had been estimated. Often in the refereed papers that I produced I compared χ^2_{reduced} with their error bar as an indicator for choosing a more complex model over a simpler one.

[7] just statistically, even if observational conditions were pristine (which is what is assumed in the current toy model)

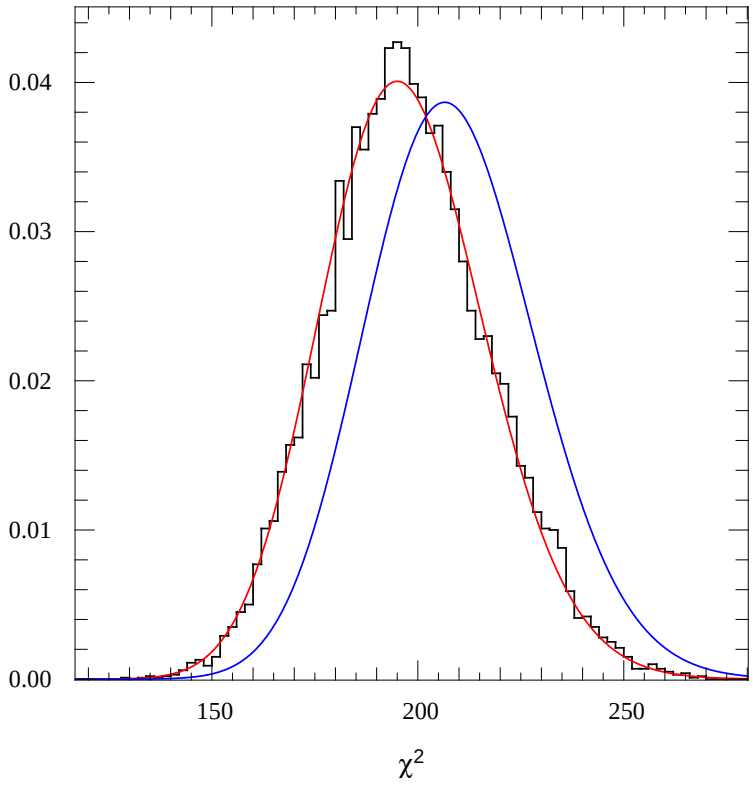


Figure 2.10: The black histogram represents the distribution of the modes of the 10 000 different χ^2_{PDF} resulting from MCMCs for 10 000 different datasets of 200 randomly selected points each. Overplotted in red is the χ^2_{PDF} with $k = 200 - 3$ degrees of freedom showing a match. In blue and shifted to the right, are the results extracted from the chain presented in figure 2.8, transformed as described in the text. The overlap between both curves indicates both are compatible.

detecting complexity

Let's continue playing with the toy model and try to make a choice between two models. Instead of the large range of data points displayed in figure 2.6, let us restrict ourselves to a part where the cubic parameter does not affect much the model's shape and try to estimate the detection of the cubic model (or M_3) over a simpler quadratic model (M_2). We will draw only 150 data points this time[8]. The data set that was randomly drawn is displayed in figure 2.11 along with the model from which it has been selected.

Two chains are run, one assuming the model is a quadratic polynomial (from eq. 2.32 $a = 0$), the other assuming a cubic polynomial (from eq. 2.32 a free). The resulting posterior distributions for χ^2 are shown in figure 2.12, both are well separated with the cubic distribution's mode at $\chi^2_{M_3} \sim 158$ and the quadratic model at $\chi^2_{M_2} \sim 197$ (note now that the shapes are very different, since for one chain we had three jump parameters while for the other, only two. Both distributions are reproducing what is expected statistically for $k = 3$ and $k = 2$). We then treat each of these as we have done earlier using the variance of χ^2 to obtain figure 2.13. Both distributions are now overlapping. To decide the likelihood of one model over another, we need to compare them with the distribution that would be expected: two χ^2_{PDF} with $k = 150 - 3$ and $k = 150 - 2$ respectively (dashed functions on figure 2.13).

Visually we can see that $\chi^2_{\mathrm{PDF,\,M_3}}$ and its expected distribution match well, but also, that because the peak of the $\chi^2_{\mathrm{PDF,\,M_2}}$ is within $3\,\sigma$ of its expected distribution, we won't be certain that we have a statistical bad luck draw from a quadratic model, or a rather good statistical draw from a cubic model.

[8] because estimating the χ^2 for large k is testing the limits of possible computation

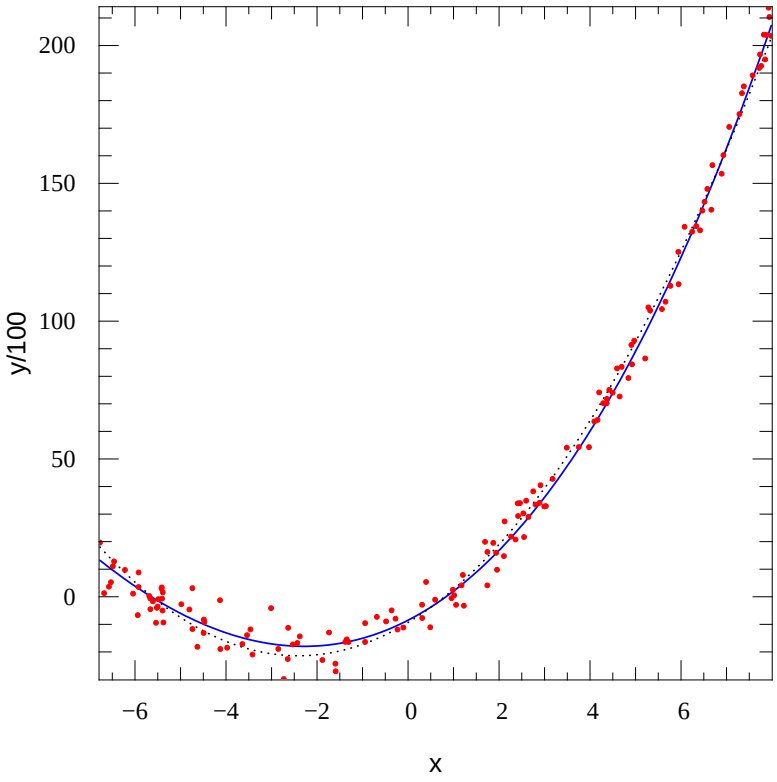


Figure 2.11: Second toy model with one example of 150 randomly selected points over it, zoomed in. Initial model is cubic (M_3) and represented as the plain blue line. The dotted black line is the best quadratic model (M_2) one can fit through the same data. Both models are buried within the data.

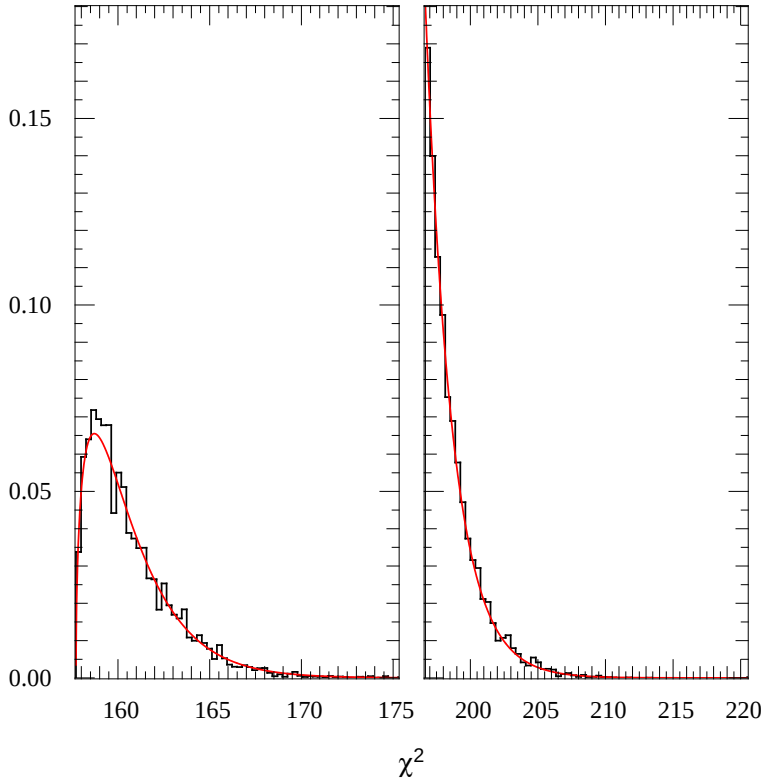


Figure 2.12: χ^2 probability density function outputed by two chains, in black. *left* with a cubic model (M_3). *right* with a quadratic model (M_2). Overplotted in red, a smooth χ^2_{PDF} with $k = 3$ and $k = 2$ degrees of freedom respectively, and corresponding to the number of jump parameters that were used.

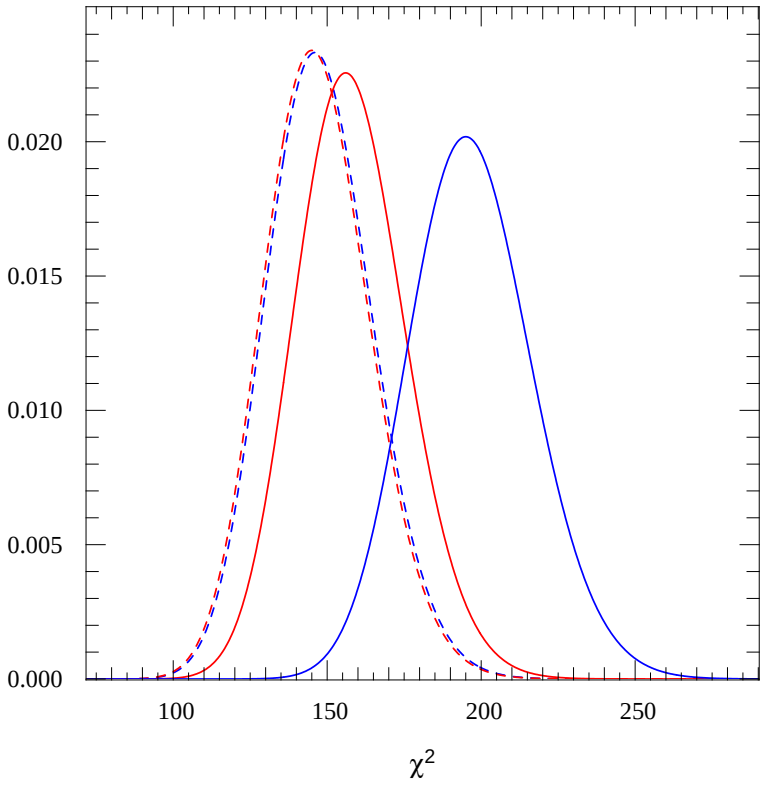


Figure 2.13: The red plain distribution (with a mode $\sim$ 158) shows $\chi^2_{\mathrm{PDF,\,M_3}}$ accounting for the variance of χ^2. The blue plain distribution (with a mode $\sim$ 197) shows the same but from fitting a quadratic model (M_2). Both dashed distributions are the expected χ^2_{PDF} from fitting 150 points with a cubic and a quadratic models respectively. The expected distribution for M_3 is a little shifted towards lower values.

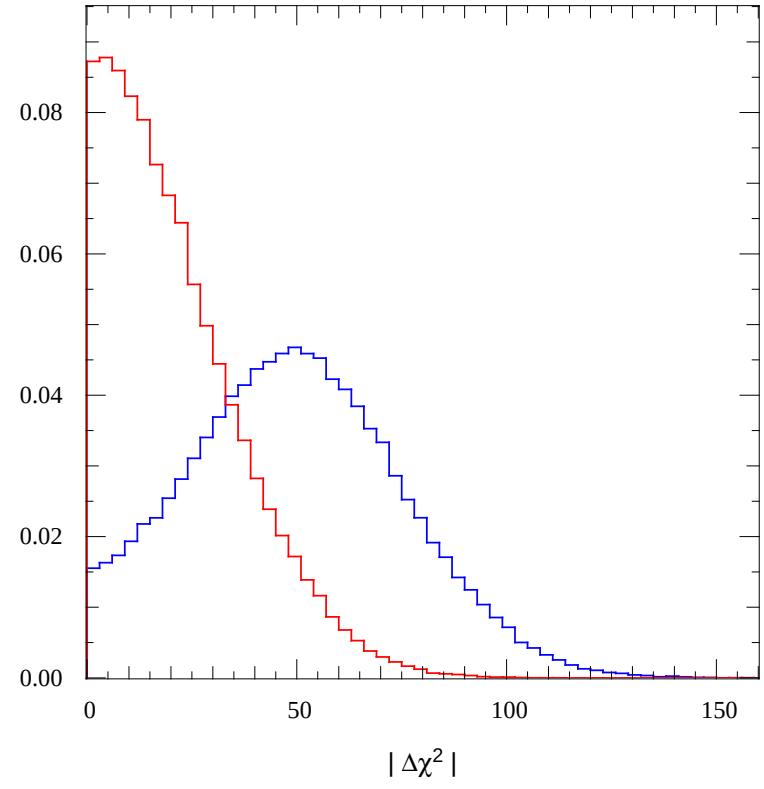


Figure 2.14: In red: the absolute difference in χ^2 between the expected and obtained χ^2 distributions, shown in figure 2.13, for the cubic model (M_3). Same in blue (shifted to higher values) but for the quadratic case (M_2). The overlap between both is large: 49.1 %. M_3 is thus only favoured over M_2 by 67 %.

Let's attempt to estimate the likelihood of M_3 (red curves) over M_2 (blue curves). We will do that by computing the difference between the obtained $\chi^2_{\mathrm{PDF,\,M}}$ and its expected distribution. Then, the overlap between both differences is a measure of how significant our models will be from each others.

Thus, we proceed by randomly drawing pairs of individually obtained χ^2 and expected χ^2 for M_3 (100 000 times), then for M_2 (100 000 times too) and doing the absolute difference between the $\chi^2_{\mathrm{PDF,\,M}}$ and expected χ^2_{PDF}(since we are as likely to get a dataset giving us a χ^2 better than expected than worse), we obtain figure 2.14. We observe that distributions for M_3 and M_2 moved a little closer to each other's (this is because the cubic model is penalised compared to the quadratic model for having an extra degree of complexity). The overlap between both distributions gives us the probability that both are similar: $49.1\,\%$, in other words, the cubic model is favoured, but only with a probability of $67\,\%$ over the quadratic model: barely above $1\,\sigma$.

Let's now see if we can use $\chi^2_{\mathrm{reduced}}$ as an approximation to such an approach: in the cubic case we have $\chi^2_{\mathrm{reduced,\,3}} = 1.07 \pm 0.12$ while the quadratic model has $\chi^2_{\mathrm{reduced,\,2}} = 1.33 \pm 0.13$ (the expected $\chi^2_{\mathrm{reduced}} = 1.00 \pm 0.12$). Both $1\,\sigma$ error bars are nearly touching each other, showing both posterior distributions are not significantly different. We can thus prefer the cubic model here but with absolutely no certainty over the quadratic model, reaching the same conclusion as the more thorough analysis.

To distinguish both models, one either needs more data into that range, increased precision, or obtain data on a larger range where the distinction between both models becomes easier to detect. One point at $x = -15$ would suffice.

It is worth noting that when fitting the cubic model, we obtain $a = 4.0^{+1.7}_{-1.9}$ within a $99.73\,\%$ confidence interval. This does not mean a is detected by about $6\,\sigma$ (twice the error bar on the $3\,\sigma$ interval) since we have not managed to detect the model. Such misconception are common when trying to detect extra parameters like, from our planetary experience: the orbital eccentricity.

applications on real data

Working on the shape of the posterior distribution for χ^2 is still an ongoing work and reflection. The idea that I am pushing relies on the property that χ^2 function can be summed; can we decompose the output χ^2_{PDF} in several components? We also see that the output from the MCMC depends on the number of jump parameters. The semi-amplitude of the radial velocity variation, K, is not affected by photometry, the period is mostly adjusted from photometry, thus, if I were to plot χ^2_{PDF} for a subset of the data (just for the radial velocity, say), would its shape change?

I will show early results on this matter for WASP-8 and WASP-23, two stars around which we have discovered planets (see section 3.4.3 and section 3.4.4). Those stars have also been used as benchmarks for testing the way model behaves when being adjusted (see section 2.6.1). The reason why those results are given here instead of in their respective section is that the topic is a little more *a propos* here, following the experimentation with the toy model. A series of graphs will illustrate the most of the results; as written, this is preliminary.

The χ^2_{PDF} distribution coming out of the MCMC are well behaved for both WASP-8 and 23 and follow the properties that have been shown earlier: the number of jump parameters affect the shape of the posterior. Namely, the normalisation factors and γ velocities do not affect the way χ^2 distributes (and quite a few of those were used in both cases).

Now, I tried to separate various components from those χ^2 distributions: the CORALIE sample, the HARPS sample, and the photometric sample. For WASP-23, the following graphs show

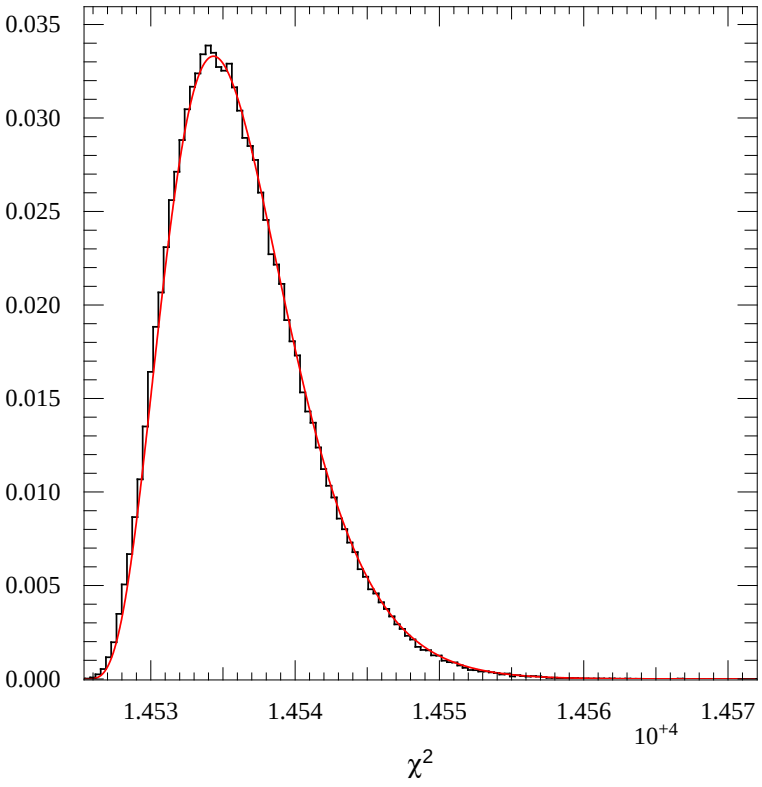


Figure 2.15: Marginalised χ^2_{PDF} from a chain fitting the WASP-8 data as presented in section 3.4.3. Overplotted, a χ^2_{PDF} function with $k = 11$ degrees of freedom, the number of jump parameters used in the MCMC.

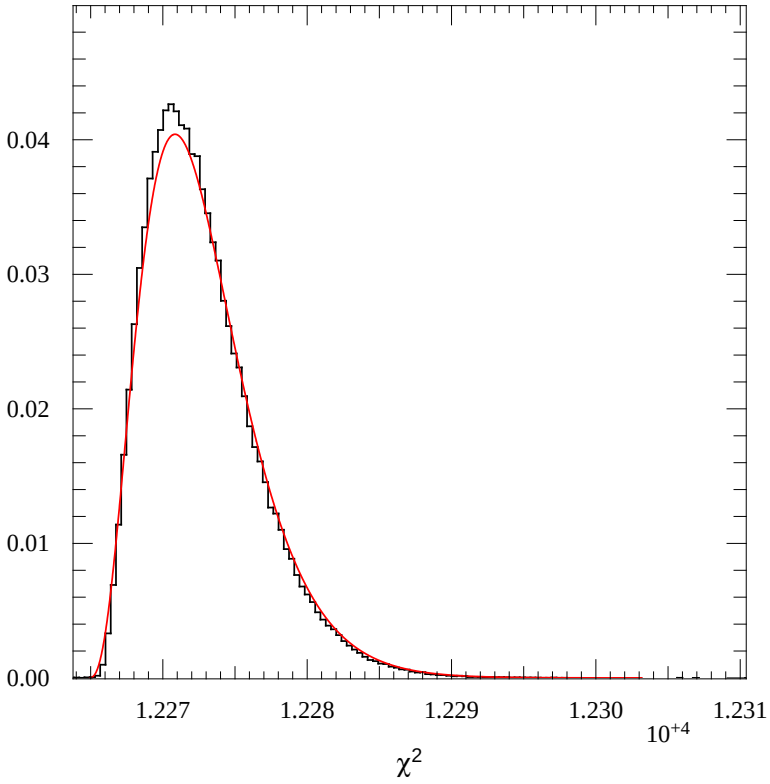


Figure 2.16: Marginalised χ^2_{PDF} from a chain fitting the WASP-23 data as presented in section 3.4.4. Overplotted, a χ^2_{PDF} function with $k = 8$ degrees of freedom, the number of parameters that were let free.

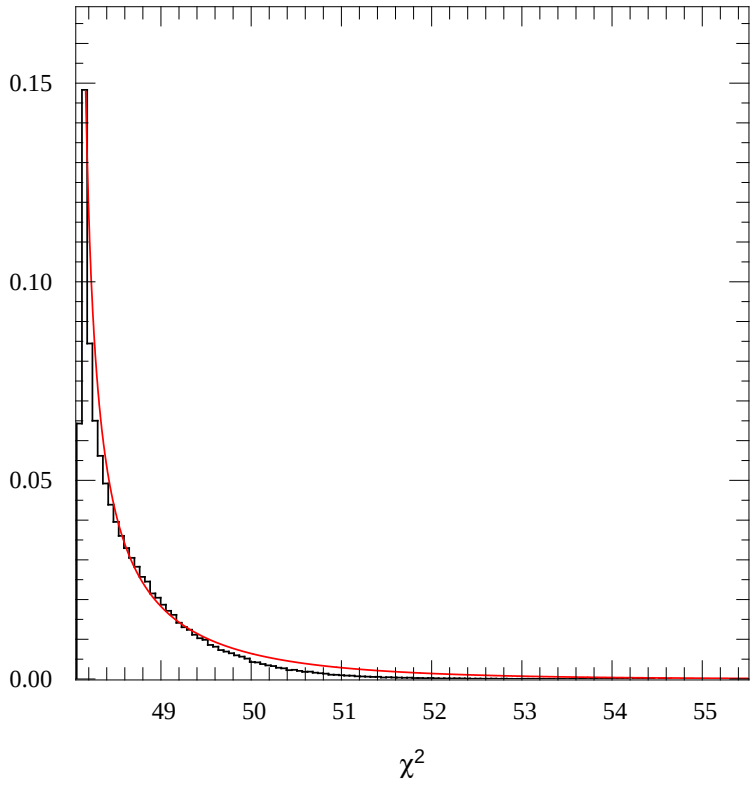


Figure 2.17: Marginalised $\chi^2_{\rm PDF}$ for the CORALIE data only from a chain fitting the WASP-23 data as presented in section 3.4.4. Overplotted, a $\chi^2_{\rm PDF}$ function with 0.5 degrees of freedom. The CORALIE data only affects the parameter K but does so jointly with the HARPS data.

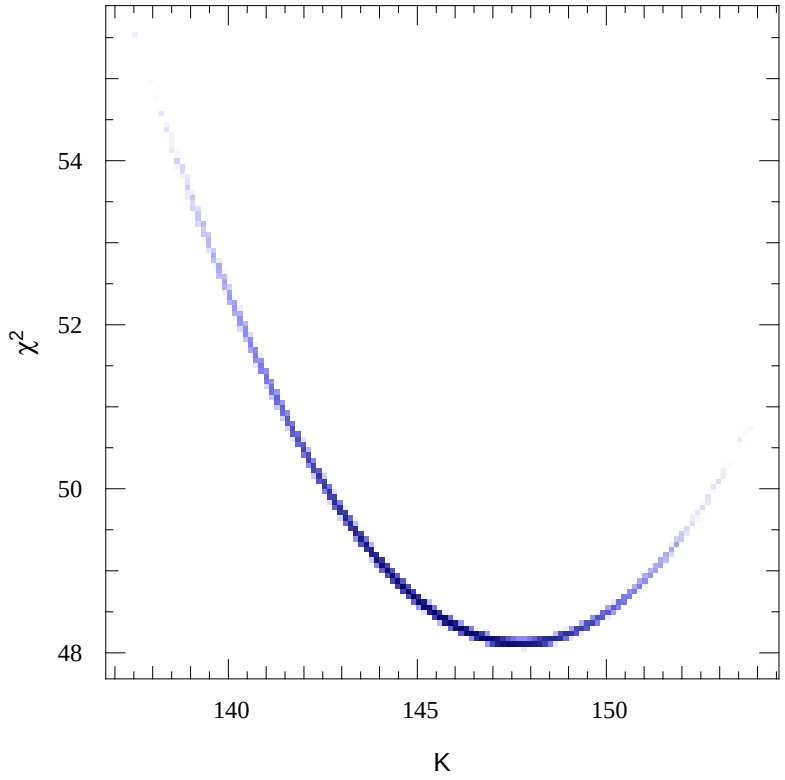


Figure 2.18: χ^2 distribution of the CORALIE data as a function of K from a chain fitting the WASP-23 data as presented in section 3.4.4. The CORALIE data only affects the parameter K but does so jointly with the HARPS data

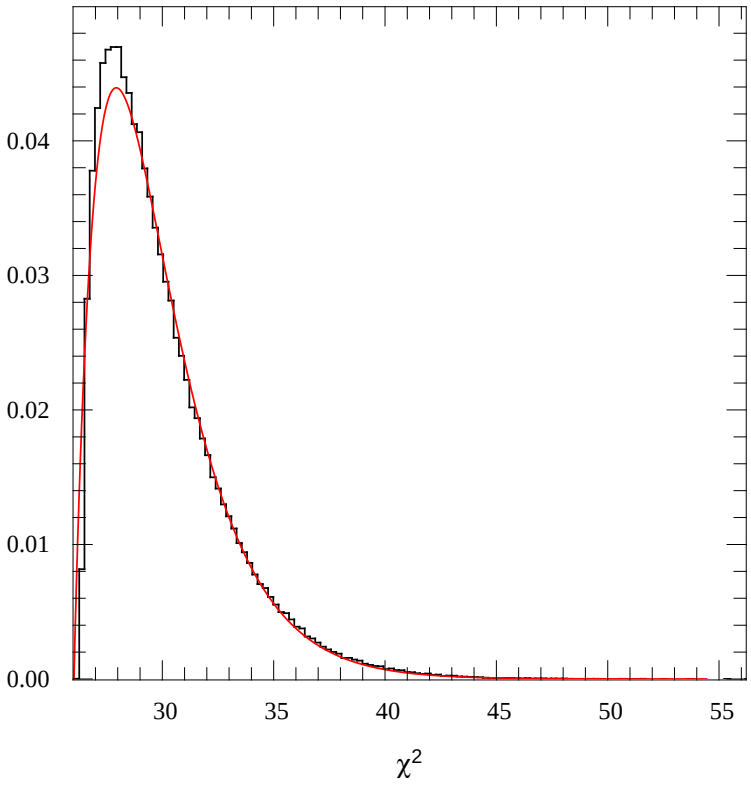


Figure 2.19: Marginalised χ^2 probability density function for the HARPS data only from a chain fitting the WASP-23 data as presented in section 3.4.4. Overplotted, a χ^2 function with 3.9 degrees of freedom. The HARPS data influences the parameter K but has also influence on other parameters, notably those controlling the Rossiter-McLaughlin effect.

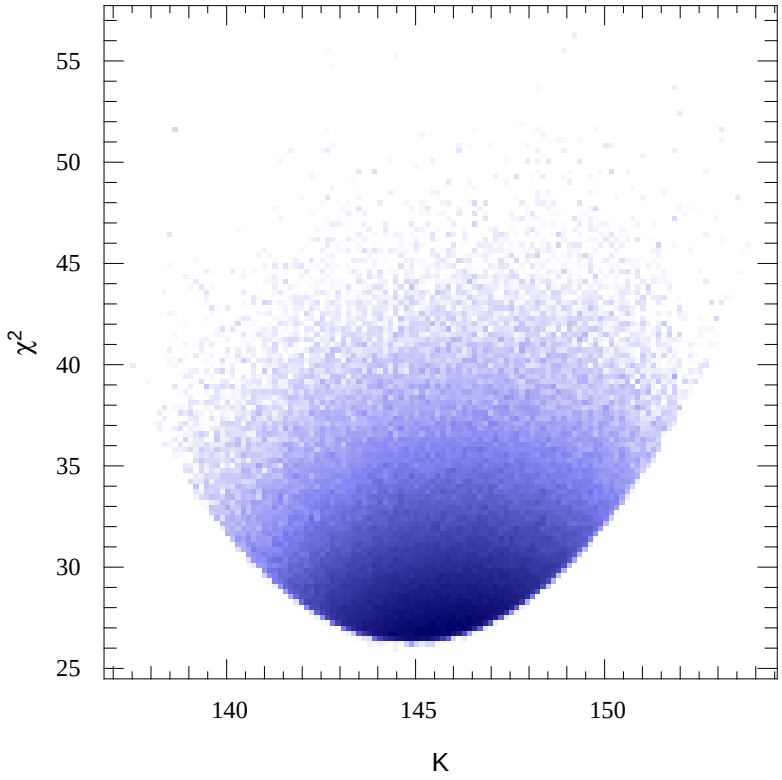


Figure 2.20: χ^2 distribution of the HARPS data as a function of K from a chain fitting the WASP-23 data as presented in section 3.4.4. The HARPS data influences the parameter K but has also influence on other parameters, notably those controlling the Rossiter-McLaughlin effect.

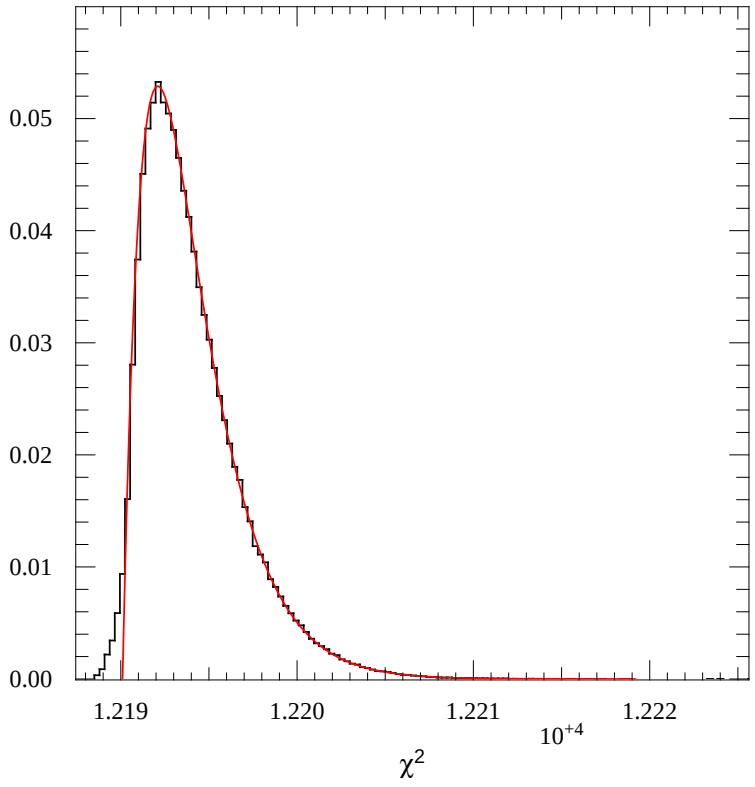


Figure 2.21: Marginalised $\chi^2_{\rm PDF}$ for the photometric data only from a chain fitting the WASP-23 data as presented in section 3.4.4. Overplotted, a χ^2 function with 4.0 degrees of freedom.

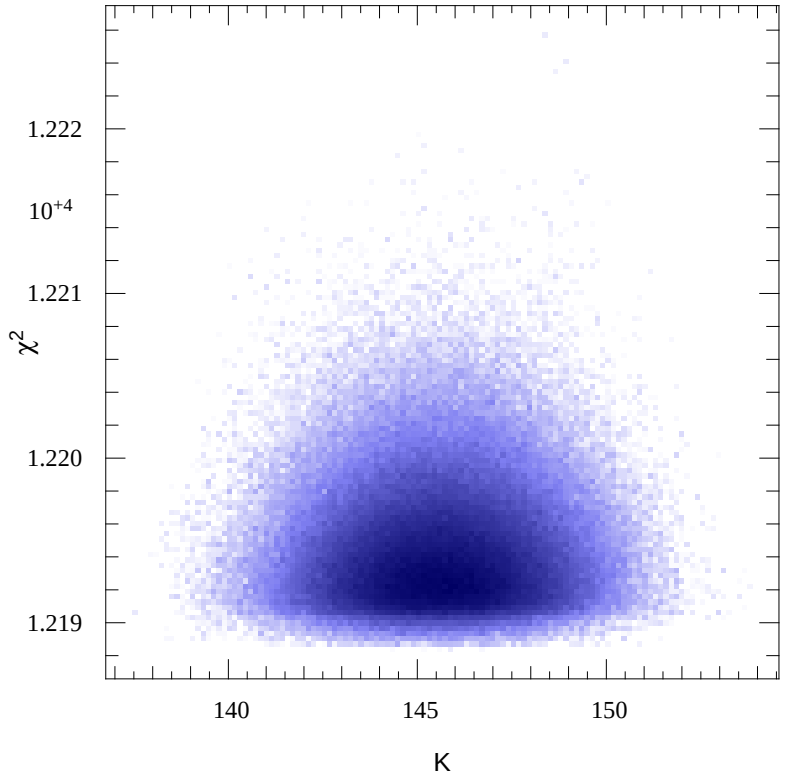


Figure 2.22: χ^2 distribution of the photometric data as a function of K from a chain fitting the WASP-23 data as presented in section 3.4.4. The photometric data does not influence the parameter K (hence the flat bottom in K) but has an influence on other parameters controlling the transit and the period (thus the high dispersion in the χ^2 axis).

that the different data sets are influencing parameters differently. I attempted to over plot χ^2 function, but the shape never shows a completely good adjustment showing this may be a wrong course of action. I also tried on WASP-8 where results are worse: the shape of subset $\chi^2_{\rm PDF}$ were also greatly affected by the size of error bars on data whereas the overall $\chi^2_{\rm PDF}$'s shape (figure 2.15) was unaffected with only a translation in the position of $\chi^2_{\rm mode}$.

The fact that the distribution shape differ between the CORALIE and HARPS sample in the case of WASP-23 should nevertheless be an incentive to understand what is happening more closely as it could give the possibility to estimate the number of effective free parameters that each sets has an influence on. Analysing the distribution's shape could also provide tests showing whether the chain is performing as it ought to.

2.3 First Applications on Photometry & Radial Velocities

I shall now show a couple of papers for which I conducted an analysis using the MCMC that was described earlier in this chapter. Those papers were the drivers behind improvements in the code. As for other papers presented in this thesis, I will give a short introduction to describe what part I had, which improvements to the code were made and what the historical context was.

2.3.1 Improved parameters for HD 17156 b

The following work became my first publication at Genève. The project began shortly after my arrival. Michaël Gillon then in a post-doctoral position at Genève had acquired a transit of HD 17156 b using the *Mercator* telescope at La Palma. That star had a known radial velocity planet around it, fairly massive and in a highly eccentric orbit. What also made that planet special was that it became for a while the planet with the longuest period known to transit. It also was among the brightest stars to show a transiting planet.

Using the available spectroscopy from the *Keck* and *Subaru* telescopes (Fischer et al. 2007) with the detection photometry (Barbieri et al. 2007) and the new photometry, it was possible to refine the orbital parameters by ensuring the period derived from the radial velocities was in accordance with the precise timing of the transits. Those ephemerides allowed us to estimate the probability that the star occults the planet. Unfortunately with 4 chances in 10 000 that probability is really low.

Above the scientific interest, this collaboration initiated a long working collaboration with Michaël which still goes on today in a variety of exciting projects. In addition, it was the perfect object with which to improve and test the MCMC that I had developed in St Andrews, see how well it behaved in a regime for which it had not been written for originally: a highly eccentric system, and offer a first analysis to the scrutiny of the scientific community.

Finally, several Rossiter-McLaughlin effects were observed on that star, the first of which, by Narita et al. (2008), claimed the orbit was misaligned. Having all the analysis done, it was an easy job to include the extra data and present a more conservative interpretation. This work was presented as a poster at the IAU Boston Symposium on transiting planets showing the interest of combining all possible data to obtain the best compromise between the radial velocities and the photometry.

Subsequent observations and analyses led to the conclusion that HD 17156 b has a coplanar orbit with the stellar equator (Narita et al. 2009a).

A&A 485, 871–875 (2008)
DOI: 10.1051/0004-6361:20079238
© ESO 2008

Astronomy & Astrophysics

Improved parameters for the transiting planet HD 17156b: a high-density giant planet with a very eccentric orbit⋆,⋆⋆

M. Gillon[1], A. H. M. J. Triaud[1], M. Mayor[1], D. Queloz[1], S. Udry[1], and P. North[2]

[1] Observatoire de Genève, Université de Genève, 51 Chemin des Maillettes, 1290 Sauverny, Switzerland
e-mail: michael.gillon@obs.unige.ch
[2] Laboratoire d'Astrophysique, École Polytechnique Fédérale de Lausanne (EPFL), Observatoire de Sauverny, 1290 Versoix, Switzerland

Received 12 December 2007 / Accepted 12 April 2008

ABSTRACT

We report high-precision transit photometry for the recently detected planet HD 17156b. Using these new data with previously published transit photometry and radial velocity measurements, we perform a combined analysis based on a Markov Chain Monte Carlo approach. The resulting mass $M_p = 3.09^{+0.22}_{-0.17}\ M_{Jup}$ and radius $R_p = 1.23^{+0.17}_{-0.20}\ R_{Jup}$ for the planet places it at the outer edge of the density distribution of known transiting planets with $\rho_p = 1.66^{+1.37}_{-0.60}\ \rho_{Jup}$. The obtained transit ephemeris is $T_{Tr} = 2\,454\,438.48271^{+0.00077}_{-0.00057} + N \times 21.21747^{+0.00070}_{-0.00067}$ BJD. The derived plausible tidal circularization time scales for HD 17156b are larger than the age of the host star. The measured high orbital eccentricity $e = 0.6719^{+0.0052}_{-0.0063}$ can thus not be interpreted as the clear sign of the presence of another body in the system.

Key words. binaries: eclipsing – planetary systems – stars: individual: HD 17156 – techniques: photometric

1. Introduction

Currently, exoplanets that transit their parent stars are undoubtedly the most important source of information about the physics and composition of the planetary objects outside our Solar System (see review by Charbonneau et al. 2007). The discovery rate of such transiting planets has increased recently thanks mainly to the excellent efficiency of ground-based wide-field surveys such as WASP (Pollaco et al. 2006) and HAT (Bakos et al. 2002). Also, a thorough characterization of the few transiting planets orbiting stars that are bright enough has brought very interesting results, most due to the high capabilites of the Spitzer Space Telescope (see e.g. Harrington et al. 2007; Knutson et al. 2007). With the space mission CoRoT that is now in operation (Baglin et al. 2006) and the future launch of Kepler (Borucki et al. 2007) and JWST (Gardner et al. 2007), we can expect that transiting planets will continue to play a major role in our understanding of extrasolar planets in the coming years.

Most of the known transiting planets are hot Jupiters, i.e. very short period (less than 5 days) tidally circularized planets with masses ranging from ∼0.5 to ∼2 M_{Jup} and densities spanning a rather large range with an upper limit close to that of Jupiter. Nevertheless, some planets very different from this description have been observed recently in transit. Among them are the very massive HD 147506b (Bakos et al. 2007), CoRoT-Exo-2b (Alonso et al. 2008) and XO-3b (Johns-Krull et al. 2008), and also the hot Neptune GJ 436b (Butler et al. 2004; Gillon et al. 2007a). Interestingly, three of these four planets have a non-null eccentricity despite their small periods.

Another exceptional transiting planet was announced recently: HD 17156b (Fisher et al. 2007; Barbieri et al. 2007). It orbits around a bright ($B = 8.8$, $V = 8.2$) G0V star. Its period $P \sim 21.2$ days is by far the longest one among the transiting planets. Furthermore, this massive planet ($M \sim 3.1\ M_{Jup}$) has a very eccentric orbit ($e \sim 0.67$). After GJ 436b, it is the second one for which the transiting status is detected after the announcement of the radial velocities (RV) orbit. This transit detection (Barbieri et al. 2007) was done under the auspices of the Transitsearch.org network (see e.g. Shankland et al. 2006) which is based on a collaboration between professional and amateur astronomers and aims to detect the possible transits of the planets detected by RV.

One transit of HD 17156b was observed by Barbieri et al. (2007). The quality of their photometry was high enough to detect the transit with a good level of confidence. Nevertheless, obtaining a more precise transit lightcurve at a different epoch was desirable to constrain more thoroughly the transit parameters and to obtain a more precise orbital period than the one deduced from RV measurements (21.2 ± 0.3 days). This motivated us to observe another transit of HD 17156b on December 3th 2007 from La Palma with the 1.2 m Mercator Belgian telescope. We present these observations in Sect. 2, and their reduction is described in Sect. 3. We analyzed this new photometry in combination with published transit photometry and RV measurements using a method based on a Markov Chain Monte Carlo (MCMC) approach described in Sect. 4. The results of our analysis are presented in Sect. 5 and discussed in Sect. 6.

⋆ Based on observations made with the Mercator Telescope, operated on the island of La Palma by the Flemish Community, at the Spanish Observatorio del Roque de los Muchachos of the Instituto de Astrofísica de Canarias.

⋆⋆ Photometric measurements are only available in electronic form at the CDS via anonymous ftp to
cdsarc.u-strasbg.fr (130.79.128.5) or via
http://cdsweb.u-strasbg.fr/cgi-bin/qcat?J/A+A/485/871

2. Observations

Based on the ephemeris presented in Barbieri et al. (2007), a transit of HD 17156b was expected to be clearly visible from Canary Islands during the night of December 3, 2007. We observed it with the 1.2 m Mercator Belgian telescope located at the Roque de los Muchachos Observatory on La Palma Island. The instrument used was the MEROPE CCD camera. It has a field of view (FOV) of 6.5′ by 6.5′ and a pixel scale of 0.19″. A set of 213 exposures were taken in the $B2$ filter ($\lambda_{\rm eff}$ = 447.8 nm, $\Delta\lambda$ = 13.9 nm) from 19h54 to 04h34 UT. The exposure time varied from 30 s to 60 s. A large defocus was applied to obtain a good trade-off between duty cycle, time sampling and scintillation mitigation. Transparency conditions during the night were good. The airmass decreased from 1.57 to 1.37 then increase to 2 at the end of the run.

During the first out-of-transit (OOT) part of the run, a problem of defocus adjustment caused a minority of the pixels of HD 17156b image to fall outside the linearity range for parts of the images. This problem was fixed just before the ingress. Another technical problem occured in the dome during the transit that led to a loss of ∼30 min of observation. Fortunately, this problem occured during the long bottom of the transit, not in the ingress or egress.

3. Data reduction

After a standard pre-reduction, all images were reduced with the IRAF/DAOPHOT aperture photometry software (Stetson 1987). As the defocus was not the same for the whole run, the reduction parameters were adapted to the FWHM of each image. Differential photometry was then performed using the flux of the nearby star BD+71 168 ($B = V = 9.6$) as the reference flux. The resulting lightcurve was finally decorrelated for airmass variations using its OOT parts. No correlation with the other external parameters was found.

The rms for the first OOT part is 2×10^{-3}. It is ∼2 times the theoretical error bar per point. As can be seen clearly in Fig. 1, this part of the curve is noisier and less populated than the rest of the curve. The cause is the too small defocus in the first part of the run and the resulting linearity problems. The rest of the curve is better. The rms of the residuals of the fit during the transit is 1.2×10^{-3}, while it is 1.7×10^{-3} for the second OOT part. The increase of the noise at the end of the run is due to the increase of the airmass and the resulting increase of the scintillation.

We estimated the level of red noise $\sigma_{\rm r}$ in our photometry using the equation (Gillon et al. 2006):

$$\sigma_{\rm r} = \left(\frac{N\sigma_N^2 - \sigma^2}{N-1} \right)^{1/2}, \quad (1)$$

where σ is the rms in the original OOT data and σ_N is the standard deviation after binning the OOT data into groups of N points. We used $N = 10$, corresponding to a bin duration similar to the ingress/egress timescale. The obtained value for $\sigma_{\rm r}$ is compatible with purely Gaussian noise.

4. Data analysis

In addition to our Mercator photometry, we used the "Almenara" transit photometry (Barbieri et al. 2007) and published Keck and Subaru RVs (Fischer et al. 2007) to determine the parameters of the system. The data were analysed with a program

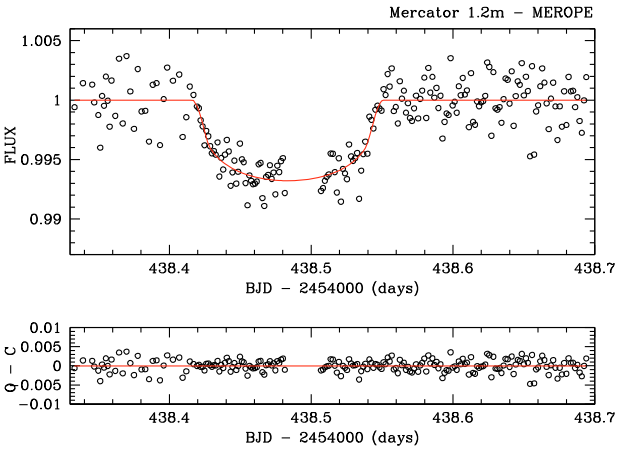


Fig. 1. *Top*: Mercator/MENOPE photometry for the transit of HD 17156b. The best fitting theoretical transit curve is superimposed in red. *Bottom*: residuals of the fit (rms = 1.6e−3).

called FullTransit. It carries out a combined multi-band photometry and spectroscopy fit based on a MCMC approach. The models used for the photometry are, that of Mandel & Agol (2002) and Giménez (2006a) with a quadratic limb darkening law, for the spectroscopy, a standard eccentric orbit model, and for the Rossiter-McLaughlin effect, Giménez (2006b) models. Since no spectroscopic measurements were taken during transit, the Rossiter effect is presented for information purposes.

4.1. Motivations

It seems normal to use all the available data in order to characterise a planet. By fitting at the same time different models in various datasets, the fit finds the best compromise between all of them and also reveals discrepancies between timings if they arise. It is also a way of remaining consistent in the model fitting of the data.

Our choice of MCMC is due to the now abundant literature on the subject (see Collier Cameron et al. 2007, and references thererein), but also because it seems the easiest way to have a single set of parameters common to each model for the fit. Also, the MCMC allows us to determine precise errors on the model from the simulations performed.

4.2. Method

The program currently fits 10 free parameters: the depth of the transit D, the rotational velocity of the star $V \sin I$, the RV semi-amplitude K, the impact parameter b, the width of the transit W, the angle between the equatorial plane of the star and the orbital plane of the planet β, the orbital period P, the middle of transit date $T_{\rm tr}$, the eccentricity e, and the angle to the periastron ω_0. Most of these parameters are directly observable or can be estimated from the data. This set has been choosen so as to minimize the correlation between parameters, which could lead to a non convergence or a biased result.

From these 10 parameters, physical parameters needed by the models are calculated. The model is created in phase for each point and χ^2 statistics is used to estimate the goodness of fit. A penalty on the χ^2 using Bayesian errors can be added if necessary.

In addition to these 10 parameters, there is also an optimal scaling for each set of data. In the current situation, we have 2 sets of radial velocity and 2 sets of photometry, hence 4 other parameters. These do not participate in the MCMC, they are rather the result of the χ^2 statistics.

Each of the parameters is calculated as follow:

$$\text{parameter}_2(j) = \text{parameter}_1(j)\,\sigma(j)\,G(0,1)\,f \quad (2)$$

where $\sigma(j)$ is the standard deviation of the parameter, $G(0,1)$ is a random Gaussian number, and f is a factor ensuring that 25% of the MCMC steps are being accepted. For each step in the MCMC a set of 10 parameters is created. This step is chosen to be accepted or not by a Metropolis-Hastings algorithm (see Collier Cameron et al. 2007).

At the start of the MCMC, some guessed parameters are inserted along with their respective σs. These have been fixed to make sure that each parameter explores randomly the parameter space around their best χ^2. The σs act as the error on the prior; $f\sigma(j)$ is the step size of the MCMC, f is estimated every 100 steps to make sure that 25% of the steps are accepted.

After n steps, the best χ^2 is found and its associated set of parameters becomes the best fit. The other sets are scrutinised and the 68.3% sets around the best fit give the error. It is not calculated using a $\Delta\chi^2$ because some of the distributions are not Gaussian.

It has been decided not to have limb darkening coefficients as free parameters so to not overload the MCMC as well as to avoid discrepancies in stellar parameters between individual photometric bands and a fitting of the Rossiter. Using Mandel & Agol (2002), this would add 4 more parameters, 4 in the case of fitting using the Giménez models, plus 2 others used for the Rossiter. As FullTransit is a characterization program, previoulsy independently fitted limb darkening coefficients can be inserted in the calculations of the models.

For a convergence, it is necessary to have a good idea of the period. We thus first fitted a theoretical transit on the Mercator photometry using the method described in Gillon et al. (2007b), then used the obtained timing and the one presented in Barbieri et al. (2007) to deduce a precise initial guess for the orbital period before starting the MCMC.

FullTransit is used to characterize the parameters of a planet, not to find them. Once the period is found, it is straightforward to find parameters approaching the best fit and to launch the MCMC. These, though, should not be too close to the final solution – if known in advance – so as to let the MCMC explore the χ^2 potential around the solution.

4.3. Analysis

A 2 $\mathrm{m\,s^{-1}}$ error was added to the existing error for the radial velocity measurements to allow for the jitter reported in Fischer et al. (2007).

The limb darkening coefficients were extracted for the two bands $B2$ and R from the table produced by Claret (2000) for the quadratic law. These were selected for a 6000 K star with $\log g$ = 4.5, [Fe/H] = 0.2, close to the physical parameters presented in Fischer et al. (2007). A stellar mass of $1.2 \pm 0.1\ M_\odot$ was used (Fischer et al. 2007); the mass was inserted randomly as $M_\star = 1.2 + 0.1\,G(0,1)$ and a Bayesian error was added to χ^2 to make a quality function $Q_j = \chi^2_j + \frac{(1.2-M_{\star,j})^2}{0.1^2}$ at each step j.

Two analyses could be done, one using the Mandel & Agol (2002) models, the other Giménez (2006a). Both were performed and being similar, only the Mandel & Agol (2002) was pursued, as it took much less time to run than the other. If there has been a radial velocity point during the transit, the whole analysis could have been conducted using Giménez (2006a,b) to remain consistent throughout the fitting process. For the same reason, because there is no Rossiter involved with this star, the two parameters $V \sin I$ and β are not effectively used in the fit.

Various starting parameters were tried on a range larger than the error bars on the final parameters calculated by each chain. All chains converged to within the error bars of each other. The chains allowed a large safety burn-in period of 15 000 steps, and a simulation of 100 000 steps each. The final results give an average over the chains that were calculated. The probability of a secondary transit was estimated by examining how many sets of parameters have a secondary eclipse impact parameter $b_{\rm sec} < 1 - \frac{R_p}{R_\star}$. For a grazing secondary transit, the probability is not much higher and would probably not be observable.

Table 1. Fitted and derived parameters for the HD 17156 system, host star and transiting planet. See Sect. 4.2. for a description of the fitted parameters.

MCMC fitted parameters	
D	$0.00605^{+0.00041}_{-0.00051}$
K [$\mathrm{m\,s^{-1}}$]	$272.6^{+4.5}_{-4.2}$
b	$0.591^{+0.088}_{-0.191}$
W [phase]	$0.00626^{+0.00015}_{-0.00016}$
P [days]	$21.21747^{+0.00070}_{-0.00067}$
$T_{\rm tr}$ [BJD]	$2\,454\,438.48271^{+0.00077}_{-0.00057}$
e	$0.6719^{+0.0052}_{-0.0063}$
ω_0 [°]	$121.14^{+0.76}_{-0.89}$
Deduced transit parameters	
$p = R_{\rm p}/R_\star$	$0.0777^{+0.0026}_{-0.0034}$
$r_\star = R_\star/a$	$0.0476^{+0.0045}_{-0.0058}$
$r_{\rm p} = R_{\rm p}/a$	$0.00371^{+0.00047}_{-0.00059}$
Deduced stellar radius*	
$R_\star$ [$R_\odot$]	$1.63^{+0.17}_{-0.20}$
Deduced planetary parameters	
$M_{\rm p}$ [$M_{\rm Jup}$]	$3.09^{+0.22}_{-0.17}$
$R_{\rm p}$ [$R_{\rm Jup}$]	$1.23^{+0.17}_{-0.20}$
$\rho_{\rm p}$ [$\rho_{\rm Jup}$]	$1.66^{+1.37}_{-0.60}$
Deduced orbital parameters	
a [AU]	$0.1589^{+0.0054}_{-0.0044}$
i [°]	$85.4^{+1.9}_{-1.2}$
Probability of secondary eclipse	0.04039%

* The value for the stellar mass was kept fixed to the one presented in Fischer et al. (2007): $1.2 \pm 0.1\ M_\odot$.

5. Results

Table 1 shows the 8 fitted parameters. For each set of parameters recorded by the simulations, a set of physical parameters – deduced transit parameters and stellar, planetary & orbital parameters – was calculated. The error on physical parameters was calculated the same way as the fitted parameters: by taking 68.3% of the sample around the best fit.

The impact parameter is the most volatile parameter in this fit, because of a lack of data at the bottom of the lightcurve trough.

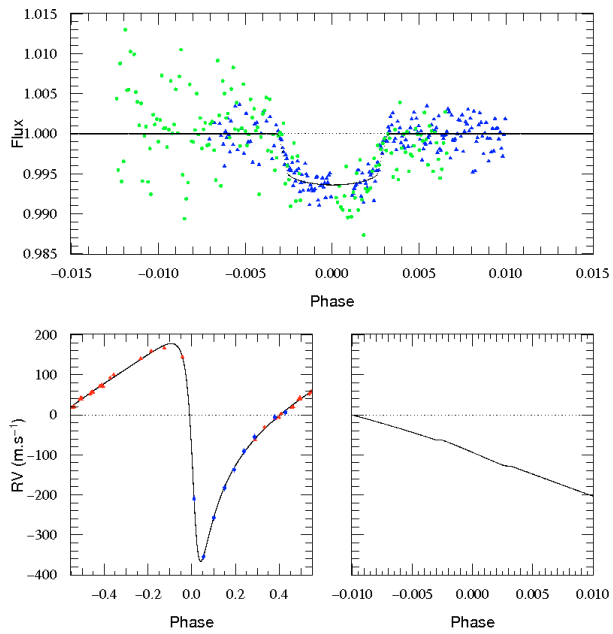


Fig. 2. Model fitted using FullTransit on the photometric (*top*) and RV (*bottom*) data. *Bottom left*: red triangles = Keck, blue circles = Subaru. *Bottom right*: zoom on the transit phase. *Top*: blue triangles = Mercator photometry, green circles = "Almenara" photometry.

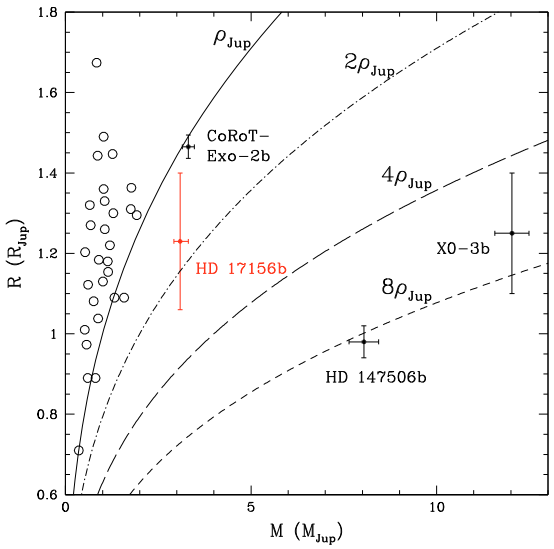


Fig. 3. Mass radius diagram for the known transiting planets with an error bar on the mass and radius smaller than 10% (except GJ 436b). While most of them (*open circles*) have a density comparable to or lower than the one of Jupiter, the three massive planets HD 17156b, HD 147506b and XO-3b are much denser, as predicted by theory, while CoRoT-Exo-2b appears to be "anomalously" large. The 1-sigma error bars are represented only for the 4 massive planets for clarity.

An average Q was estimated as 684.57 (25.99 on the spectroscopic data, 658.55 on the photometric data) giving an overal reduced Q = 1.63.

Figure 2 shows the global fit of the data, including the Rossiter-McLaughlin effect as it would occur for a $V \sin I$ of 2.8 km s^{-1}. Its amplitude is small due to the high slope of the eccentric orbit.

Optimal scaling for the Keck data is 93.8241 m s^{-1} while for the Subaru it is 93.1092 m s^{-1}. The optimal scaling for the Mercator photometry is a factor of 1.00005, while for the Almenara data, it is 1.0018.

6. Discussion

Irwin et al. (2008) presented new photometry for one transit of HD 17156b observed from three separate observatories. The agreement between their deduced parameters and ours is satisfactory. Our error bars on the planet radius are larger than theirs, and this comes from the fact that our photometry was good enough to independently determine the stellar radius, while Irwin et al. applied a Bayesian constraint on the stellar radius to keep its fitted value close to the one determined by spectroscopic analysis (Fischer et al. 2007). We notice that our error bars on the planet and star radius are larger than 10%, so the characterization of this system would benefit from further high-precision transit photometry.

Fortney et al. (2007) presented theoretical radius values for planets over a wide range of masses, using realistic atmospheric boundary conditions and equations of state for core materials. For a planet similar to HD 17156b, their theoretical radii range from 1.02 R_{Jup} for a 100 $M_{\oplus}$ core to 1.1 R_{Jup} if no core is present. The presence of a core has thus a very weak influence on the planetary radius in this planetary mass regime. Our measured radius seems to argue against a heavy core for HD 17156b, but the error bar is too large to constraint the core mass. As can be seen in Fig. 3, HD 17156b has the highest density among all transiting exoplanets except HD 147506b and XO-3b.

The very high orbital eccentricity of HD 17156b could indicate intense interaction with a still undetected third body. The circularization timescale τ_{circ} of a planet can be computed using (Goldreich & Sotter 1966):

$$\tau_{circ} = \left(\frac{2Q_p P}{63\pi}\right)\left(\frac{M_p}{M_*}\right)\left(\frac{a}{R_p}\right)^5 \quad (3)$$

where Q_p is the tidal quality factor. For Jupiter, Q_p is estimated to lie between 10^5 and 2×10^6 (Goldreich & Soter 1966; Peale & Greenberg 1980) Assuming the lowest of these values for the tidal quality factor of HD 17156b, the obtained value for τ_{circ} is 208 Gyr, largely exceeding the estimated stellar age of 5.7 Gyr (Fischer et al. 2007). Thus, the high eccentricity of HD 17156b does not necessarily indicate the presence of a third body in the system. If nevertheless such a perturber is present, it could be detected with more RV measurements or through the precise measurement of a large number of transits of HD 17156b, as was attempted for several other transiting planets by e.g. the TLC project (Holman & Winn 2006). In the case of a mean-motion resonance, the amplitude of the timing variations is proportional to the period of the perturbed body (see e.g. Holman & Murray 2005). As HD 17156b has the longest period among the known transiting planets, a dedicated monitoring of its transits should thus have a good sensitivity to any other planet in resonance with it.

HD 17156b is very different from all the other known transiting planets, and measuring its thermal emission would be very desirable to study its atmospheric heat distribution efficiency,

albedo and chemical composition, but the secondary eclipse probability we obtain is unfortunately very near to zero (0.04%).

Acknowledgements. The authors thank F. Courbin and G. Meylan for making possible the observations with the Belgian Mercator telescope. J.M. Almenara, R. Alonso and M. Barbieri are gratefully acknowledged for providing us with their photometric data. A.H.M.J. Triaud thanks A. Collier Cameron and A. Giménez for all their help and support. This work was supported by the Swiss National Fund for Scientific Research.

References

Alonso, R., Auvergne, M., Baglin, A., et al. 2008, A&A, 482, L21
Baglin, A., Auvergne, M., Boisnard, L., et al. 2006, 36th COSPAR Scientific Assembly, Held 16−23 July, in Beijing, China
Bakos, G. Á., Papp, I., Sári, P., & Green, E. M. 2002, PASP, 114, 974
Bakos, G. Á., Kovács, G., & Torres, G. 2007, ApJ, 670, 826
Barbieri, M., Alonso, R., Laughlin, G., et al. 2007, A&A, 476, L13
Bodenheimer, P., Laughlin, G., & Lin, D. N. C. 2003, ApJ, 592, 555
Borucki, W., Koch, D., & Lissauer, J. 2007, ASPC, 366, 309
Butler, P. R., Vogt, S. S., Marcy, G. W., et al. 2004, ApJ, 617, L580
Charbonneau, D., Brown, T. M., Burrows, A., & Laughlin, G. 2007, Protostars and Planets V, ed. B. Reipurth, D. Jewitt, & K. Keill (Tucson: University of Arizona Press), 701
Claret, A. 2000, A&A, 363, 1081
Collier Cameron, A., Wilson, D. M., West, R. G., et al. 2007, MNRAS, 380, 1230
Fischer, D. A., Vogt, S. S., Marcy, G. W., et al. 2007, ApJ, 669, 1336
Fortney, J. J., Marley, M. S., & Barnes, J. W. 2007, ApJ, 659, 1661
Gardner, J. P., Mather, J. C., Clampin, M., et al. 2006, SSRv, 123, 485
Gillon, M., Pont, F., Moutou, C., et al. 2006, A&A, 459, 249
Gillon, M., Pont, F., Demory, B.-O., et al. 2007a, A&A, 472, L13
Gillon, M., Demory, B.-O., Barman, T., et al. 2007b, A&A, 471, L51
Giménez, A. 2006a, A&A, 450, 1231
Giménez, A. 2006b, ApJ, 650, 408
Goldreich, P., & Soter, S. 1966, Icarus, 5, 375
Guillot, T., & Showman, A. P. 2002, 385, 156
Irwin, J., Charbonneau D., Nutzman P., et al. 2008, ApJ, accepted [arXiv:0801.1496]
Holman, M. J., & Murray, N. W. 2005, Science, 307, 1288
Holman, M. J., & Winn, J. N. 2006, A&AS, DPS meeting, 38, 862
Harrington, J., Luszcz, S., Seager, S., et al. 2007, Nature, 447, 691
Johns-Krull, C. M., McCullough, P. M., & Burke, C. J. 2008, ApJ, 677, 657
Knuston, H. A., Charbonneau, D., Allen, L. E., et al. 2007, Nature, 447, 183
Mandel, K., & Agol, E. 2002, ApJ, 580, L171
Peale, S. J., & Greenberg, R. J. 1980, in Lunar and Planetary Institute Conference Abstracts, 871
Pollaco, D. L., Skillen, I., Cameron, A. C., et al. 2006, PASP, 118, 1407
Rowe, J. F., Matthews, J. M., Seager, S., et al. 2006, ApJ, 646, 1241
Shankland, P. D., Rivera, E. J., Laughlin, G., et al. 2006, ApJ, 653, 700
Stetson, P. B. 1987, PASP, 99, 111

2.3.2 Improved parameters for WASP-4 b & WASP-5 b

The importance of discovering objects around bright targets is the ease with which one can start characterise them and learn more. If radial velocity planets, or the numerous candidates observed and released earlier this year by the space mission *Kepler* are of a definite interest, they mostly deal with the statistics of systems: the type and number of planets, their repartition in single or multiple systems, their orbital parameters. They give us a general outlook on the planet population and constraints on their formation.

Transit surveys on bright stars are of a different philosophy: one can start studying more in detail those planets and extend our knowledge on what physics goes on there. So far almost most known transiting planets around bright stars are hot Jupiters, because transit surveys suffer of a similar bias in nature of radial velocity surveys, but magnified due to the quick lowering of transit probabilities for orbits greater than a few 10s of days. Thus we started studying what was studyable: this special class of planets: the hot Jupiters. This lead to development in theoretical physics on the mechanisms which inflate those planets found with larger than expected radii, but also observationally with attempts of studying their atmospheric temperatures and compositions.

The following paper is just about that: it presents the finest lightcurve yet obtained from a ground telescope of a planetary transit. This allowed an exquisite determination of the system parameters and the realisation of something quite unexpected then: we are limited in our characterisation, not by the technology but by our knowledge on the host star. Because of equations 2.10, 1.15 and 1.13 we see that one determines very precisely the stellar density, the ratio of radii and ratio of masses from photometry and spectroscopy. In order to have useful physical parameters, one needs an assumption on the stellar mass. It is during the estimation of the stellar mass that we need our greatest improvement, something impaired at the moment by the lack of knowledge of those stars. If the targets WASP observes are considered bright (meaning: easy to do follow up observations), they are still faint when it comes to distance determination. This prevents knowing their absolute magnitude and thus an independent radius measurement. Even then, we still have uncertainties knowing their metallicity and $T_{\rm eff}$, something critical to improve the precision on stellar mass estimates.

We were also limited by technology too. The observations were obtained using the imager FORS2, on the the VLT. To achieve an interesting duty cycle as well as help produce precise photometry, it was necessary to heavily defocus the telescope. The point spread function of our main target, WASP-4, was around 12". The constraints proved too hard and enormous sytematics appeared on the lightcurves, fortunately out of transit for WASP-4, but during it for WASP-5. This became something of a proof that a larger telescope is not always better: our targets were too bright. A good, stable instrument on a smaller telescope might do better. This will have an impact for future follow-up, namely the characterisation of rocky planets' atmospheres around bright stars.

Nevertheless this paper was another occasion to progress and test the fitting algorithm in a high precision context, one where one can even adjust the limb darkening coefficients from the shape of the transit. It was also the start of a newer approach (as pioneered by Sozzetti et al. (2007)) to help in the estimation of stellar mass, using a modified Herztsprung-Russell diagram plotting stellar density (instead of the inaccurate $\log\, g$) versus effective temperature. This led further to a reflection on how to insert stellar parameters within the MCMC to determine the stellar mass, reducing a serious assumption, and a further step in combining most of the available information, which will be presented in section 2.6.

A&A 496, 259–267 (2009)
DOI: 10.1051/0004-6361:200810929
© ESO 2009

Astronomy & Astrophysics

Improved parameters for the transiting hot Jupiters WASP-4b and WASP-5b⋆

M. Gillon[1], B. Smalley[2], L. Hebb[3], D. R. Anderson[2], A. H. M. J. Triaud[1], C. Hellier[2], P. F. L. Maxted[2], D. Queloz[1], and D. M. Wilson[2]

[1] Observatoire de Genève, Université de Genève, 51 Chemin des Maillettes, 1290 Sauverny, Switzerland
e-mail: michael.gillon@obs.unige.ch
[2] Astrophysics Group, Keele University, Staffordshire, ST5 5BG, UK
[3] School of Physics and Astronomy, University of St. Andrews, North Haugh, Fife, KY16 9SS, UK

Received 7 September 2008 / Accepted 9 December 2008

ABSTRACT

The gaseous giant planets WASP-4b and WASP-5b are transiting 12-magnitude solar-type stars in the Southern hemisphere. The aim of the present work is to refine the parameters of these systems using high cadence VLT/FORS2 z-band transit photometry and high-resolution VLT/UVES spectroscopy. For WASP-4, the new estimates for the planet radius and mass from a combined analysis of our VLT data with previously published transit photometry and radial velocities are $R_{\rm p} = 1.30^{+0.05}_{-0.04}\ R_J$ and $M_{\rm p} = 1.21^{+0.13}_{-0.08}\ M_J$, resulting in a density $\rho_{\rm p} = 0.55^{+0.04}_{-0.02}\ \rho_J$. The radius and mass for the host star are $R_* = 0.87^{+0.04}_{-0.03}\ R_\odot$ and $M_* = 0.85^{+0.11}_{-0.07}\ M_\odot$. Our ground-based photometry reaches 550 ppm at time sampling of ~50 s. Nevertheless, we also report the presence of an instrumental effect on the VLT that degraded our photometry for the WASP-5 observations. This effect could be a major problem for similar programs. Our new estimates for the parameters of the WASP-5 system are $R_{\rm p} = 1.09 \pm 0.07\ R_J$, $M_{\rm p} = 1.58^{+0.13}_{-0.10}\ M_J$, $\rho_{\rm p} = 1.23^{+0.26}_{-0.16}\ \rho_J$, $R_* = 1.03^{+0.06}_{-0.07}\ R_\odot$, and $M_* = 0.96^{+0.13}_{-0.09}\ M_\odot$. The measured size of WASP-5b agrees well with the basic models of irradiated planets, while WASP-4b is clearly an "anomalously" large planet.

Key words. binaries: eclipsing – planetary systems – stars: individual: WASP-4 – stars: individual: WASP-5 – techniques: photometric – techniques: spectroscopic

1. Introduction

So far, the planets that transit their parent stars have undoubtedly brought the most important pieces of information about the physics and composition of the planetary objects outside our Solar System (see review by Charbonneau et al. 2007). Most of the transit detections are due to a few ground-based wide-field surveys targeting stars brighter than $V \sim 13$: HAT (Bakos et al. 2004), SuperWASP (Pollaco et al. 2006), TrES (O'Donovan et al. 2006), and XO (McCullough et al. 2005). Among these surveys, SuperWASP is the one showing the largest harvest so far. This efficiency is not only due to the constant optimization of the observational and follow-up strategy, reduction and data analysis (Cameron et al. 2007), but also to the recent starting of the Southern counterpart of the SuperWASP-North facility. Located at the Sutherland Station of the South African Astronomical Observatory, SuperWASP-South brings a second field of view of 482 square degrees to the survey, allowing it to search for transiting planets in a large portion of the sky.

The planets WASP-4b (Wilson et al. 2008, hereafter W08) and WASP-5b (Anderson et al. 2008, hereafter A08) were the first transiting planets detected by SuperWASP-South. They are both gas giants slightly heavier than Jupiter and orbiting very close (P = 1.338 and 1.628 days) to 12 mag solar-type stars. The analysis of the WASP and follow-up data led to radius values of about 1.4 and 1.1 R_J. With an estimated density ~0.4 ρ_J, WASP-4b appeared to belong to the subgroup of the planets with a radius larger than predicted by basic models of irradiated planets (Burrows et al. 2007a; Fortney et al. 2007) unlike WASP-5b ($\rho \sim 1.2\ \rho_J$). WASP-4b is slightly less massive than WASP-5b (1.2 vs. 1.6 M_J), while both planets have a similar irradiation (1.89 vs. 1.92×10^9 erg s^{-1} cm^{-2}), semi-major axis (0.023 vs. 0.027 AU) and host star spectral type (G7V vs. G4V).

Several hypotheses have been proposed to explain the radius anomaly shown by some highly irradiated planets such as WASP-4 b (see Guillot 2008), most importantly tides (Bodenheimer et al. 2001; Jackson et al. 2008), tides with atmospheric circulation (Guillot & Showman 2002) and enhanced opacities (Guillot et al. 2006; Burrows et al. 2007a). Receiving similar irradiation from their host stars while having significantly different radii, WASP-4b and WASP-5b represent a good test for theory and an interesting opportunity of progress on our understanding of the radius heterogeneity observed among the highly irradiated planets. It is thus desirable to obtain for these two planets the highest precision possible on the system parameters. This motivated us to use the VLT to obtain (1) a high cadence high precision transit light curve with the FORS2 camera; and (2) a high resolution spectrum of the host stars with the UVES spectrograph. We present respectively in Sects. 2 and 3

⋆ Based on data collected with the FORS2 imager at the VLT-UT4 telescope and with the UVES spectrograph at the VLT-UT2 telescope (Paranal Observatory, ESO, Chile) in the programme 280.C-5003.

Article published by EDP Sciences

these new VLT photometric and spectroscopic observations and their reduction. We analyze these new data in combination with former transit photometry and RV measurements in Sect. 4. The results of our analysis are discussed in Sect. 5.

2. VLT/FORS2 transit photometry

2.1. WASP-4

The photometry for WASP-4 was obtained on October 23, 2007. Altogether 339 exposures were acquired with the FORS2 camera on the VLT/UT4 telescope from 01h01 to 06h50 UT. To have enough reference flux to properly correct the photometry from atmospheric effects, the standard resolution mode was used, resulting in a $6.8' \times 6.8'$ field of view. To obtain a good time sampling of the light curve, a 2×2 binning of the pixels was performed, resulting in a pixel scale of $0.25''$/pixel. The exposure time was tuned by the ESO staff astronomer to 20 s while the mean read-out plus overhead time was 34 s. We chose to observe in the z-GUNN+78 filter ($\lambda_{\rm eff}$ = 910 nm, $FWHM$ = 130.5 nm) to minimize the impact of the stellar limb-darkening uncertainty on the deduced system parameters. A very large defocus was used to obtain a good duty cycle and to minimize the influence of flat-fielding errors: the mean characteristic profile width was 50 pixels = $12.5''$. Despite this large defocus, there was no PSF overlap for the target and the reference stars. The guiding system was turned on to make the stellar fluxes registered on nearly the same pixels during the run (centroid jitter ~3.5 pixels for the whole run). There was an interruption of 25 min in the sequence due to a technical problem with the secondary mirror setting, fortunately before the transit. The quality of the night was photometric. The moon illumination was 87%. It was at 44° at closest from the target. The airmass decreased from 1.08 to 1.05 then increased to 1.95 during the run (Fig. 1). The defocus was tuned several times to adapt it to atmospheric transparency variations due to the increase of airmass.

After a standard pre-reduction, the stellar fluxes were extracted for all the images with the `IRAF DAOPHOT` aperture photometry software (Stetson 1987). As the defocus was not the same for the whole run, the reduction parameters were adapted to the characteristic profile width of each image.

The transit is already very clear in the absolute flux curve of WASP-4. But as shown in Fig. 2, the absolute photometry of WASP-4 and of several other stars in the field suffer from an unexpected effect: while the shape of the largest part of these curves shows a nice airmass-flux correlation indicating that the night transparency conditions were very good, the first part seems to be affected by a large systematic dependent on the position on the chip. High-accuracy transit photometry has already been obtained with the FORS cameras (e.g. Gillon et al. 2007a; Pont et al. 2007), and this systematic was not detected in these former data. The main difference between these former observations and ours is the large defocus that we used. The explanation that we and the ESO staff favor is linked to the strange shape taken by the primary mirror M1 with respect to the secondary M2 in case of out-of-focus observations, with variations induced by the different amount of tangential component of the gravity as the dominant effect. Indeed, the active optics system of the telescope is supposed to compute for each exposure an optimal shape for the M1 so to correct for tangential gravity pull, and actuators perform micrometrical shifts of the M1 to obtain the computed shape, but here the active optics system was turned off at the beginning of the run to obtain the required huge defocus. Thus the needed correction for the tangential gravity pull

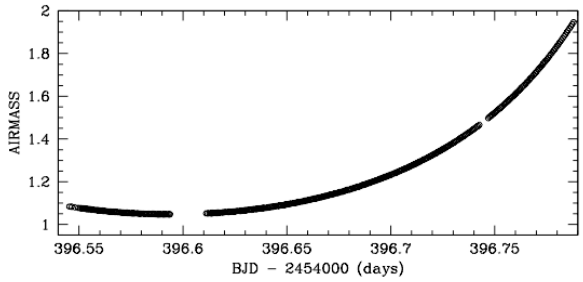


Fig. 1. Evolution of the airmass during the WASP-4 VLT/FORS2 run.

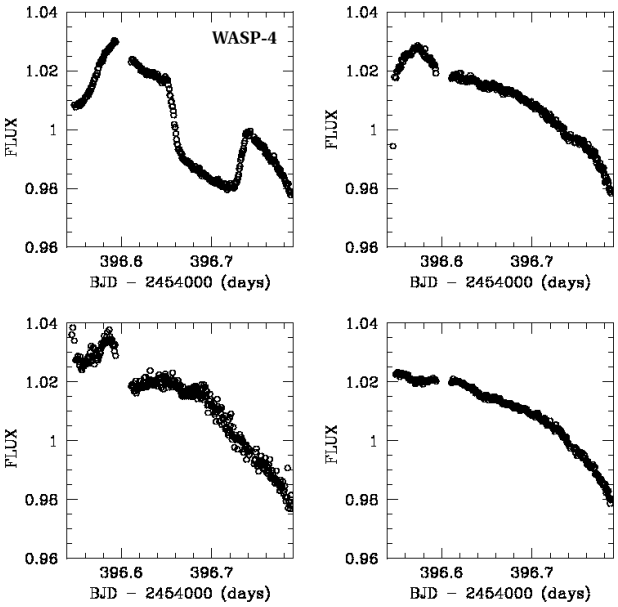


Fig. 2. *Top left*: normalized absolute VLT/FORS2 photometry for WASP-4. *Top right and bottom*: normalized absolute photometry for other stars of the field.

was not applied. The resulting spatial difference in illumination of the chip could then have been rather large at the beginning of the run, when the telescope was close to the meridian. As it moved away from meridian, the tangential correction became less important, and so did the effect.

Differential photometry was performed using the flux of several bright stable stars in the field, but the obtained curve is still plagued with a large systematic in its first part (see Fig. 3). Fortunately, the transit occured in the second part of the run for which the effect seems to be absent. We thus decided to use only the data after BJD = 2 454 396.625, for which the photometry seems to be reliable and accurate.

After a careful selection of the reference stars and the reduction parameters, we subtracted a linear fit for magnitude vs. airmass to correct the photometry for differential reddening using the out-of-transit (OOT) data. The corresponding fluxes were then normalized using the OOT part of the photometry. The

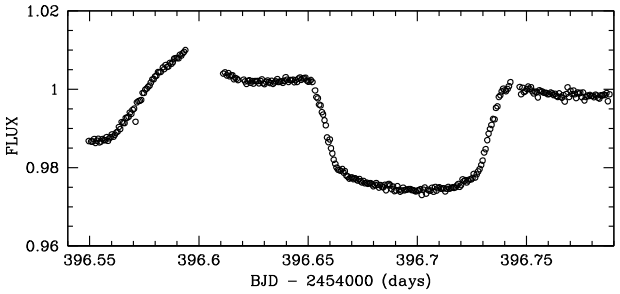


Fig. 3. Differential photometry for WASP-4 before rejection of the part of the curve damaged by the systematic and differential reddening correction.

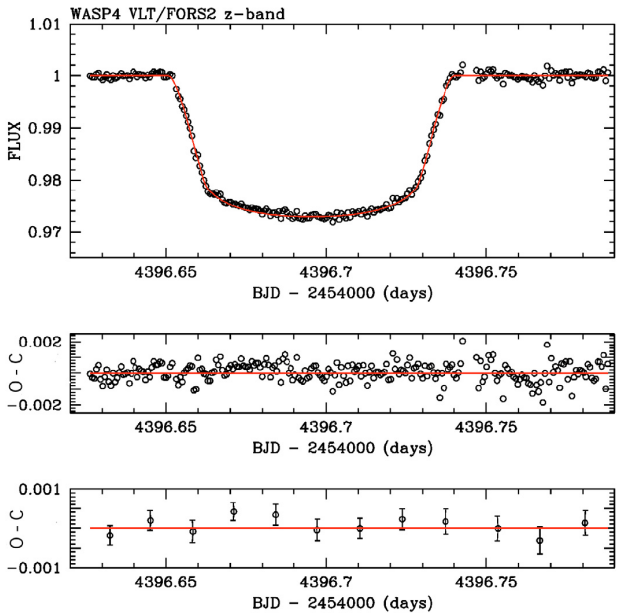


Fig. 4. *Top*: VLT/FORS2 z-band transit photometry for WASP-4. The best-fit transit curve is superimposed in red. *Middle*: residuals of the fit (rms = 570 ppm). *Bottom*: residuals of the fit after binning per 20 points (rms = 200 ppm).

resulting transit light curve is shown in Fig. 4, with the best-fit transit model (see Sect. 4) superimposed. The rms of the first OOT part is 420 ppm. This value is very close to the theoretical error per point obtained from the photon noise of the target and the reference stars, the sky background, read-out and scintillation noises (Gilliland et al. 1993): 400 ppm. For the second OOT part, the measured rms is 740 ppm while the median theoretical error is 510 ppm. This largest discrepancy between both values comes probably from the amplification of the effect of any transparency inhomogeneity across the field at high airmass. Indeed, the airmass ranges from 1.45 to 1.95 in the second OOT part.

The rms and the time sampling are not the only parameters needed to evaluate the quality of a photometric time series, the level of low-frequency noise (red noise) has also to be taken into account, especially for high SNRs (Pont et al. 2006). We

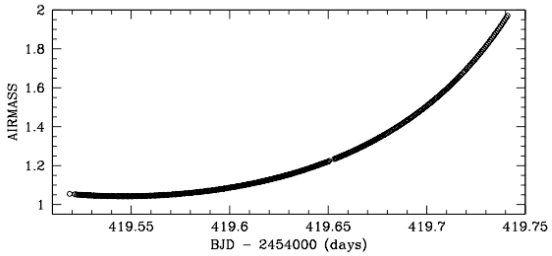


Fig. 5. Evolution of the airmass during the WASP-5 VLT/FORS2 run.

estimated the level of red noise σ_r in our photometry using the equation (Gillon et al. 2006):

$$\sigma_r = \left(\frac{N\sigma_N^2 - \sigma^2}{N-1} \right)^{1/2}, \quad (1)$$

where σ is the rms in the original OOT data and σ_N is the standard deviation after binning the OOT data into groups of N points. We used $N = 20$, corresponding to a bin duration similar to the ingress/egress timescale. The obtained value for σ_r is quite small: 110 ppm.

2.2. WASP-5

The photometry for WASP-5 was obtained on November 15, 2007. 337 exposures were acquired from 00h24 to 05h45 UT, again with the FORS2 camera. The same observational strategy as for WASP-4 was used. The quality of the night was photometric. The moon was in its first quarter (illumination = 24%), and its closest distance to the target was 48° at the end of the run. The airmass decreases from 1.06 to 1.04 then increased to 1.97 (Fig. 5).

The same reduction procedure as for WASP-4 was used. Here again, the photometry of the first part of the run shows the presence of a systematic at the percent level (Fig. 6). We notice that the amplitude of the effect depends here too on the position on the chip and appears to affect only the low-airmass photometry, it is thus probably the same effect than for WASP-4 (see above). Unfortunately, the transit happened at the beginning of the run and its photometry is too damaged to be useful. We thus decided to use only the UVES spectroscopy (see Sect. 3) and former data to characterize this system.

3. VLT/UVES spectroscopy

High-resolution spectra of WASP-4 and WASP-5 were obtained using the UVES spectrograph on the VLT/UT2 telescope on November 27, 2007. The red arm was used with standard setting 580, giving spectral coverage from 4780 to 6808 Å, except from 5758 to 5833 Å due to the gap between two CCD detectors. A 1-arcsec slit was used giving a spectral resolution of 40 000. Exposure times of 600 s were used yielding mean S/N of 94:1 and 102:1 for WASP-4 and WASP-5, respectively. The standard pipeline reduction products were used in the analysis.

The analysis was performed using the UCLSYN spectral synthesis package (Smith 1992; Smalley et al. 2001) and ATLAS9 models without convective overshooting (Castelli et al. 1997). The H_α line was used to determine the effective temperature ($T_{\rm eff}$), while the Na I D and Mg I lines were used as surface gravity ($\log g$) diagnostics. The parameters obtained from the analysis are listed in Table 1.

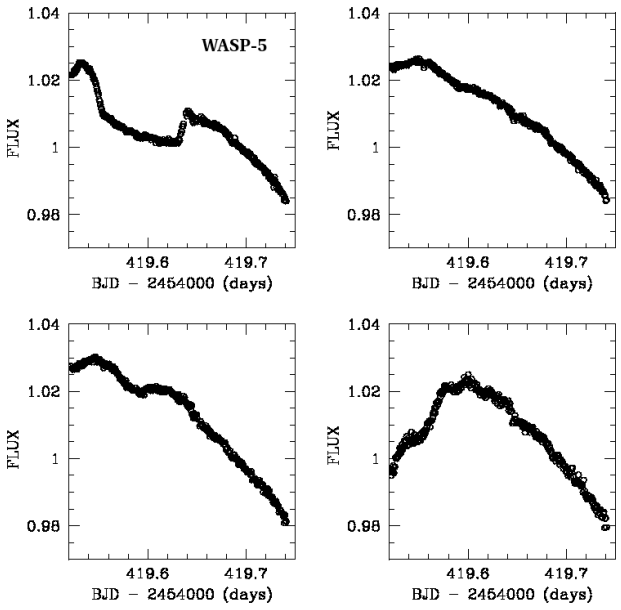


Fig. 6. *Top left*: normalized absolute VLT/FORS2 photometry for WASP-5. *Top right and bottom*: normalized absolute photometry for other stars in the field.

Table 1. Spectroscopic parameters obtained in this work for WASP-4 and WASP-5.

	WASP-4	WASP-5
$T_{\rm eff}$	5500 ± 100 K	5700 ± 100 K
$\log g$	4.5 ± 0.2	4.5 ± 0.2
$\xi_{\rm t}$	1.1 ± 0.2 km s^{-1}	1.2 ± 0.2 km s^{-1}
$v \sin i$	2.0 ± 1.0 km s^{-1}	3.5 ± 1.0 km s^{-1}
[Fe/H]	−0.03 ± 0.09	+0.09 ± 0.09
[Si/H]	+0.08 ± 0.05	+0.21 ± 0.06
[Ca/H]	+0.04 ± 0.14	+0.07 ± 0.14
[Sc/H]	+0.07 ± 0.13	+0.21 ± 0.10
[Ti/H]	+0.11 ± 0.12	+0.14 ± 0.08
[V/H]	+0.09 ± 0.07	+0.16 ± 0.07
[Cr/H]	+0.06 ± 0.08	+0.07 ± 0.10
[Co/H]	+0.07 ± 0.07	+0.20 ± 0.07
[Ni/H]	+0.02 ± 0.10	+0.15 ± 0.05
log N(Li)	<0.8	<0.5
$T_{\rm eff}$(IRFM)	5470 ± 130 K	5740 ± 130 K
θ(IRFM)	0.031 ± 0.002 mas	0.032 ± 0.002 mas

The equivalent widths of several clean and unblended lines were measured. Atomic line data was mainly taken from the Kurucz & Bell (1995) compilation, but with updated van der Waals broadening coefficients for lines in Barklem et al. (2000) and $\log gf$ values from Gonzalez & Laws (2000), Gonzalez et al. (2001) or Santos et al. (2004). A value for microturbulence ($\xi_{\rm t}$) was determined from Fe I using Magain's (1984) method. The ionization balance between Fe I and Fe II and the null-dependence of abundance on excitation potential were used as additional $T_{\rm eff}$ and $\log g$ diagnostics (Smalley 2005).

In addition to the spectral analysis, we have also used published broad-band photometry to estimate the total observed bolometric flux ($f_{\oplus}$). For WASP-4, TYCHO-2 (Høg et al. 2000), USNO-B1.0 R-mag. (Monet et al. 2003) and 2MASS (Cutri et al. 2003) were used, while for WASP-5 GALEX nuv flux (Morrissey et al. 2007), NOMAD (Zacharias et al. 2004), DENIS (Fouqué et al. 2000) and 2MASS were used, but no TYCHO photometry was available. The photometry was converted to fluxes and the best-fitting Kurucz (1993) model flux distribution found, which was integrated to determine $f_{\oplus}$. The Infrared Flux Method (Blackwell & Shallis 1977) was then used with 2MASS magnitudes to determine $T_{\rm eff}$ and stellar angular diameter (θ). The results are given in Table 1 and are consistent with those from the spectroscopic analysis.

We have determined the elemental abundances of several elements (listed in Table 1) from their measured equivalent widths. The quoted error estimates include those given by the uncertainties in $T_{\rm eff}$, $\log g$ and $\xi_{\rm t}$, as well as the scatter due to measurement and atomic data uncertainties. In our spectra the Li I 6708 Å line is not detected. Thus we can only give upper-limits on the Lithium abundances.

4. Data analysis

4.1. Determination of the system parameters

4.1.1. WASP-4

We derived stellar and planetary parameters for the system by fitting simultaneously our new VLT z-band transit light curve with the data presented in W08, i.e. (1) the WASP R-band photometry; (2) the FTS i-band transit light curve; (3) an EulerCAM R-band transit light curve and (4) 14 CORALIE radial velocity measurements.

The data were used as input into the Monte Carlo Markov Chain (MCMC) code described in Cameron et al. (2007) which was designed specifically to solve the multi-variate problem of transiting star-planet systems. Via the MCMC approach, the fitting code repeatedly adopts trial parameters until it converges on a set of values which produces the best model velocity curve and model light curves. In short, nine parameters were used to describe the light curves and radial velocity curve of the host star including the orbital period P, the time of minimum light T_0, the transit depth δ, the total transit duration t_T, the impact parameter b, the stellar mass M_*, the stellar velocity amplitude K_1, the systemic radial velocity γ, the orbital eccentricity e, and the longitude of periastron ω. These nine fitted parameters determine the physical properties of the star-planet system, including the masses and radii of the star and planet and the orbital inclination and separation. The goodness-of-fit statistic used to assess the best parameters is the sum of the χ^2 for all the data curves with respect to the models. Model light curves were derived according to the formalism outlined in Mandel & Agol (2002), adopting the small-planet approximation and using the non-linear limb darkening coefficients from Claret (2000, 2004) for the appropriate photometric filters. The code also has the option to apply a Bayesian main sequence prior on the stellar mass and radius which acts to keep the star on the main sequence. However, due to the exceptional quality of the follow-up photometry, we did not apply this constraint in the analysis of WASP-4.

We ran the MCMC code in an iterative fashion to derive the best overall solution for the properties of the star-planet system. We also combined the physical properties derived from the MCMC code with the stellar parameters from the spectral synthesis to determine the evolutionary status of the host star and to confirm that the stellar properties, including mass (which is not directly measured), were consistent with each other and with theoretical stellar evolution models.

In the initial run of the MCMC code, we adopted initial guesses for the light curve parameters from the results of the

box-least squares analysis of the WASP data. We also assumed a starting value for the eccentricity of 0.02, a systemic RV equal to the mean of the velocity data, and a velocity amplitude derived by fitting a sinusoidal velocity variation to the observed RVs by minimizing χ^2. The initial guess for the stellar mass was derived by interpolating the zero age main sequence, solar metallicity stellar evolution isochrone of Girardi et al. (2000) at the temperature of the host star. In addition, the input light curves had theoretically derived uncertainty values for each photometric measurement. The uncertainties were computed by considering shot noise, scintillation, read-out and background noises, but did not include correlated noise. For the RV measurements, the MCMC code adds quadratically an additional RV jitter to the theoretical uncertainties so that the reduced χ^2 of the RV data compared to the model curve is approximately equal to 1. Finally, we allowed the eccentricity to float freely.

The results of this initial run were used to inform the second and final run of the code in the following ways. First, the initial eccentricity result was well within 1σ of zero. Thus, for final run, we fixed the eccentricity to zero, assuming a circular orbit for the planet. Next, the best fitting model light curves from the initial run were used to make a correlated noise measurement for each photometric time-series. We employed the method described in Sect. 2.1 (Eq. (1)), but using the entire residual time-series, rather than just the OOT parts. Table 2 presents the red noise values obtained. For each photometric measurement, we added the appropriate correlated noise value in quadrature to the theoretical uncertainty. The resulting light curves were input into the final run of the MCMC code.

Finally, the first MCMC run produced a measurement of the mean stellar density ($\rho_s = M_s/R_s^3$) which we used to refine the initial guess of the stellar mass. We converted the derived stellar density to $R_s/M_s^{1/3}$ in solar units, and compared this property and the stellar temperature in a modified Hertzsprung-Russell (HR) to the Girardi solar metallicity models. The quantity, $R_s/M_s^{1/3}$, depends only on the observed transit properties (duration, depth, impact parameter, and orbital period) and is independent of the measured temperature. We generated the same property from the mass and log g values in the models, and then interpolated the models in the $R/M^{1/3} - T_{\rm eff}$ plane to determine a mass and age for WASP-4. We interpolated linearly along two consecutive mass tracks to generate an equal number of age points between the zero-age main sequence and the evolutionary state defined as Te-M which is the stage where the star reaches core Hydrogen exhaustion. We then interpolated between the mass tracks along equivalent evolutionary points to find the mass and age from the models that best match the stellar properties derived from the MCMC code (density) and the spectral synthesis (temperature). In this way, we obtained a new intital guess for the stellar mass of, $M_* = 0.93\ M_\odot$.

We then implemented a second and final run of the MCMC code, (1) fixing $e = 0$; (2) including correlated noise in the photometric uncertainties; (3) applying the results from the first MCMC run as the initial guesses for the fitted parameters; and (4) adopting a prior on the stellar mass of $M_* = 0.93\ M_\odot$. The results of this run are given in Table 3. The obtained value for the RV jitter is 7 m s^{-1}, identical to the value deduced in W08.

Lastly, we plotted the final stellar parameters on the modified HR diagram and interpolated the model tracks as described above to determine the age of the system. We derive an age of $5.2^{+3.8}_{-3.2}$ Gyr. We also confirmed that the final mass derived in the MCMC code was consistent with the observed temperature and the stellar evolution models (Fig. 7). The MCMC result gives a mass of $0.85^{+0.11}_{-0.07}\ M_\odot$ which is within the 1σ uncertainty on the mass determined from the theoretical tracks ($0.93 \pm 0.05\ M_\odot$).

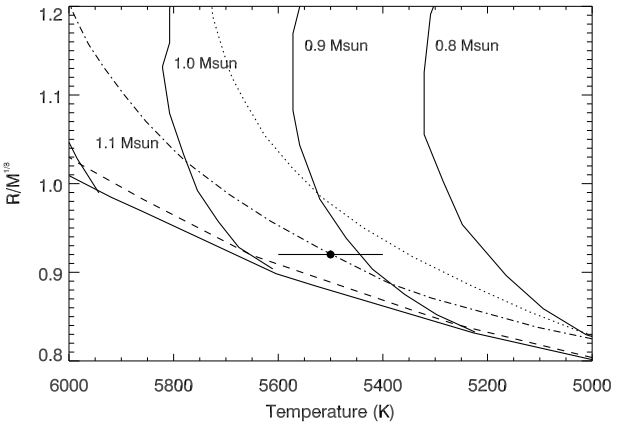


Fig. 7. Modified HR diagram showing $R/M^{1/3}$ in solar units versus effective temperature. The properties of the of WASP-4 are overplotted on the theoretical stellar evolutionary models of Girardi et al. (2000). The mass tracks are labeled and the isochrones are 100 Myr (solid), 1 Gyr (dotted), 5 Gyr (dot-dashed), 10 Gyr (dotted). According to the models, the host star has an age of $5.2^{+3.8}_{-3.2}$ Gyr. The y-axis error bars are smaller than the data point.

We also made an independent analysis aiming to test if the quality of our VLT z-band transit photometry is good enough to constraint reliably the limb-darkening of the star. In this analysis, we used as data our VLT transit light curve with only the WASP photometry and the CORALIE radial velocities. We assumed a quadratic limb-darkening law for the photometric models to minimize the number of free parameters and allowed the two limb-darkening coefficients u_1 and u_2 to float for the VLT photometry only, using as jump parameters not these coefficients themselves but the combinations $2 \times u_1 + u_2$ and $u_1 - 2 \times u_2$ to ensure that the obtained uncertainties are uncorrelated (Holman et al. 2006). We obtain values for the transit depth and duration that are slightly different from the values shown in Table 3, but all the deduced physical parameters are in good agreement with the previous values. The obtained values for the limb-darkening coefficients are $u_1 = 0.299^{+0.006}_{-0.026}$ and $u_2 = 0.248^{+0.016}_{-0.023}$. These values are physically plausible in the sense that they produce a monotonically decreasing intensity from the center of the star to the limb, but they are not consistent with the values interpolated from Claret's tables (2000, 2004): $u_1 = 0.266$ and $u_2 = 0.302$. This disagreement could be due to the fact that our VLT photometry has a small but significant level of correlated noise able to modify slightly the actual shape of the transit. The amplitude of this red noise is in fact similar to the difference between the models fitted with and without free limb-darkening coefficients. We thus prefer to consider the values for the system parameters obtained with a fixed non-linear limb-darkening law as our final ones.

4.1.2. WASP-5

An analysis similar to the one described above was performed for WASP-5 using data presented in A08: (1) the WASP photometry; (2) a FTS i-band transit light curve; (3) an EulerCAM R-band transit light curve and (4) 11 CORALIE radial velocities. As in A08, no additional RV jitter was needed to obtain a final reduced χ^2 close to 1 for the RV model. No Bayesian main

Table 2. Typical red noise values and mid-transit times evaluated for the photometric time-series used in this analysis.

Light curve	σ_r [ppm]	Mid-transit timing (MCMC) [BJD]	Mid-transit timing ("prayer bead") [BJD]
WASP-4 WASP06 *R*-band	3150	$2\,453\,963.10863^{+0.00074}_{-0.00081}$	$2\,453\,963.1086^{+0.0025}_{-0.0023}$
WASP-4 WASP07 *R*-band	4020	$2\,454\,364.57722^{+0.00068}_{-0.00075}$	$2\,454\,364.5757^{+0.0021}_{-0.0033}$
WASP-4 Euler *R*-band	0	$2\,454\,368.59244^{+0.00022}_{-0.00019}$	$2\,454\,368.59266^{+0.00025}_{-0.00027}$
WASP-4 FTS *i*-band	510	$2\,454\,371.26812^{+0.00033}_{-0.00028}$	$2\,454\,371.26738^{+0.00097}_{-0.00087}$
WASP-4 VLT *z*-band	190	$2\,454\,396.695410 \pm 0.000051$	$2\,454\,396.69548^{+0.00015}_{-0.00026}$
WASP-5 WASP06 *R*-band	3260	$2\,453\,945.71962^{+0.00091}_{-0.00093}$	$2\,453\,945.7187^{+0.0041}_{-0.0028}$
WASP-5 WASP07 *R*-band	1490	$2\,454\,364.2283^{+0.0012}_{-0.0013}$	$2\,454\,364.2285^{+0.0057}_{-0.0069}$
WASP-5 Euler *R*-band	360	$2\,454\,383.76684^{+0.00025}_{-0.00024}$	$2\,454\,383.76738^{+0.00031}_{-0.00032}$
WASP-5 FTS *i*-band	790	$2\,454\,387.02221^{+0.00034}_{-0.00037}$	$2\,454\,387.02197^{+0.00071}_{-0.00050}$

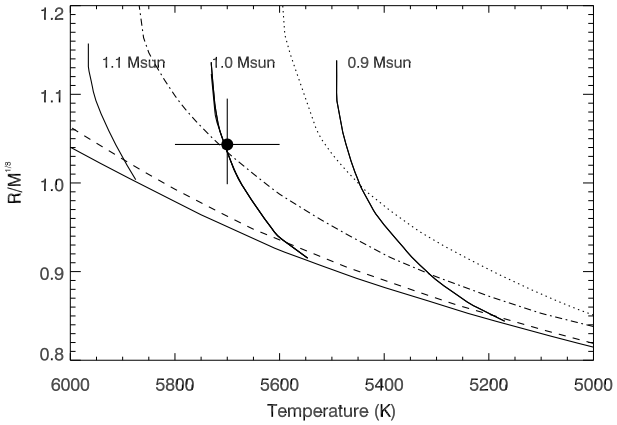


Fig. 8. Similar modified HR diagram than Fig. 7 but here for WASP-5. According to the models, the host star has an age of $5.4^{+4.4}_{-4.3}$ Gyr.

sequence prior was used as for WASP-4. The orbital eccentricity obtained in the first MCMC run was non-zero at the 2σ level, so it was kept as free parameter in the second run, leading to a final value of 0.04 ± 0.02 (see Table 3). Nevertheless, e and ω are not orthogonal parameters because e cannot be <0, and this asymmetry could lead to an overestimation of e for low eccentricity orbit. To check that our marginal detection of a non-null eccentricity is reliable, we made a new analysis using as jump parameters $e.\cos\omega$ and $e.\sin\omega$, which are orthogonal, and calculated e and ω afterwards. We obtained $e = 0.049^{+0.020}_{-0.017}$ and $\omega = 0.73^{+0.30}_{-0.45}$, in very good agreement with the values presented in Table 3. We thus claim the marginal detection of a non-null eccentricity for WASP-5b.

WASP-5 is slightly super solar metallicity with [Fe/H] = +0.09 ± 0.09 (see Table 1), so mass tracks of the Girardi models in metallicity at +0.09 were first linearly interpolated between the zero and +0.20 metallicity mass tracks before the obtained stellar parameters were plotted on the modified HR diagram and model tracks were interpolated (Fig. 8). From this final step, we derive an age of $5.4^{+4.4}_{-4.3}$ Gyr and a stellar mass of $1.00^{+0.07}_{-0.05}$ $M_\odot$, within the error bar of the MCMC value of $0.96^{+0.13}_{-0.09}$ $M_\odot$ (see Table 3).

4.2. Transit timings

Fixing all the system parameters except epoch to the ones deduced from the above analysis, we fitted with our MCMC code a transit profile to each transit to obtain individual timings. For the WASP data, the transits of the season 2006 and 2007 were folded together to obtain a timing per season. Table 2 gives the obtained timings and error bars. From these results, the VLT *z*-band photometry for WASP-4 appears to show a formal error of ~5 s on its deduced timing, comparable to the best precision obtained from space (see e.g. Knutson et al. 2007). Such a precision is doubtful for our ground-based data, because we know that despite their high quality they have a low but still significant level of covariant noise able to bring a systematic error on the deduced timing. To assess the influence of this covariant noise on our timing precision, we analyzed each transit with the method described in Gillon et al. (2007b), for which the estimation of the errors is based on the "prayer bead" procedure: after having determined the best-fitting eclipse model, a large number of fits are performed and for each of them the residuals of the initial fit are shifted sequentially about a random number and then added to the eclipse solution. This procedure allows to take into account the actual covariant noise of the data. At the end, the error bars of the fitted parameters are determined from the distribution of their derived values. Table 2 presents also the values and error bars obtained with this method. We notice that for the data showing the largest level of covariant noise, the WASP data, the error bars on the timing is ~4 times larger. For the Euler transits having a rather low level of covariant noise, the difference is much smaller. Interestingly, the error bars on the WASP-4 VLT transit timing is 3–4 times larger than the one obtained with the MCMC code and is only slightly better than the one of the Euler transits. This shows clearly that covariant noise has an important impact on the transit timing precision. While Table 2 presents the timings and errors obtained with both methods, we outline that our final results are the ones obtained with the "prayer bead" method: only these values should be used in future analysis.

Figure 9 shows for both planets the residuals from the subtraction to these timings of the calculated transit timings based on ephemeris presented in Table 3. The transits of WASP-4 show no clear sign of period variability. A linear fit to the transit timings as a function of the transit epoch results in a period of 1.3382319 ± 0.0000068 days, in excellent agreement with the period obtained from our combined MCMC analysis. The reduced χ^2 of the fit is 1.35, indicating that the epoch – timing relation is well modeled by a line. For WASP-5, the period deduced from a similar fit is 1.628430 ± 0.000013 days, in good agreement with the value obtained from the combined analysis, but here the reduced χ^2 is 5.7. At this stage, we cannot assign any firm significance to a possible period variability, because a shift of one of the two most precise timings (FTS or Euler) due to

Table 3. WASP-4 and WASP-5 system parameters and 1-σ error limits derived from MCMC analysis.

Parameter	Symbol	WASP-4	WASP-5	Units
Transit epoch (HJD)	T_0	$2\,454\,383.313070^{+0.000045}_{-0.000074}$	$2\,454\,373.99598^{+0.00025}_{-0.00019}$	days
Orbital period	P	$1.3382324^{+0.0000017}_{-0.0000029}$	$1.6284279^{+0.0000022}_{-0.0000049}$	days
Planet/star area ratio	$(R_p/R_s)^2$	$0.02357^{+0.00010}_{-0.00008}$	$0.01180^{+0.00022}_{-0.00029}$	
Transit duration	t_T	$0.08831^{+0.00016}_{-0.00021}$	$0.0987^{+0.0022}_{-0.0020}$	days
Impact parameter	b	$0.063^{+0.047}_{-0.062}$	$0.31^{+0.06}_{-0.28}$	R_*
Stellar reflex velocity	K_1	$0.2476^{+0.0139}_{-0.0068}$	$0.2797^{+0.0092}_{-0.0063}$	km s^{-1}
Centre-of-mass velocity	γ	$57.7387^{+0.0026}_{-0.0013}$	$20.0087^{+0.0032}_{-0.0025}$	km s^{-1}
Orbital semi-major axis	a	$0.02255^{+0.00095}_{-0.00065}$	$0.0267^{+0.0012}_{-0.0008}$	AU
Orbital inclination	I	$89.35^{+0.64}_{-0.49}$	$86.9^{+2.8}_{-0.7}$	degrees
Orbital eccentricity	e	0.0 (fixed)	$0.038^{+0.026}_{-0.018}$	
Longitude of periastron	ω	–	$0.60^{+0.47}_{-0.39}$	rad
Stellar mass	M_*	$0.85^{+0.11}_{-0.07}$	$0.96^{+0.13}_{-0.09}$	$M_\odot$
Stellar radius	R_*	$0.873^{+0.036}_{-0.027}$	$1.029^{+0.056}_{-0.069}$	$R_\odot$
Stellar surface gravity	$\log g_*$	$4.487^{+0.019}_{-0.015}$	$4.395^{+0.043}_{-0.040}$	[cgs]
Stellar density	ρ_*	$1.284^{+0.013}_{-0.019}$	0.88 ± 0.12	$\rho_\odot$
Planet radius	R_p	$1.304^{+0.054}_{-0.042}$	$1.087^{+0.068}_{-0.071}$	R_J
Planet mass	M_p	$1.21^{+0.13}_{-0.08}$	$1.58^{+0.13}_{-0.10}$	M_J
Planetary surface gravity	$\log g_p$	$3.212^{+0.025}_{-0.011}$	$3.485^{+0.054}_{-0.043}$	[cgs]
Planet density	ρ_p	$0.546^{+0.039}_{-0.025}$	$1.23^{+0.26}_{-0.16}$	ρ_{Jup}
Planet temperature ($A = 0$, $F = 1$)	T_{eq}	1650 ± 30	1706^{+52}_{-48}	K

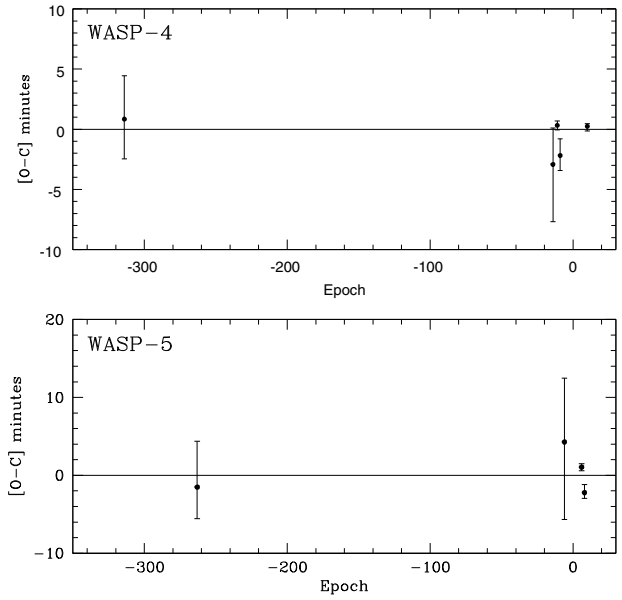


Fig. 9. Observed minus calculated (O−C) transit timings for the light curves included in this study. Table 2 lists the actual transit timings. The calculated timings were obtained from the ephemeris due to our combined MCMC analysis (see Table 3).

an unknown systematic effect could lead to a much bettered reduced χ^2, but obtaining more precise transit timings for WASP-5 is desirable.

5. Discussion

5.1. Ground-based photometry

Until recently, it was considered by many that ground-based photometry could not reach the high cadence sub-mmag regime because of the presence of the atmosphere. Indeed, high frequency atmospheric noises (mainly scintillation) limit the precision that high SNR photometry can reach within small time bins. If one is willing to compromise on the sampling of their photometric time-series, binning the data (or using longer exposures) allows for getting better errors, but the obtained precision will be finally limited by low frequency noises. To observe several times the same planetary eclipse and to fold the photometry with the orbital period is thus generally considered as the only option to get very well sampled and precise eclipse light curves from the ground. Nevertheless, we show here that reaching the sub-mmag sub-min regime for one eclipse is possible with a large aperture ground-based instrument. Photon noise and scintillation are not a concern even for small time bins when a rather bright transiting system like WASP-4 is monitored with a large aperture telescope like the VLT. The high standard quality of such a telescope and the excellent atmospheric conditions at Paranal lead furthermore to a very low level of covariant noise in the differential photometry.

Unfortunately, we report the presence of an instrumental effect on the VLT that damaged a part of our photometry and that could be a major problem for similar programs. It was unfortunately the case for WASP-5: the photometry is too damaged by the effect to be useful. As mentioned in Sect. 2, the effect is probably due to the fact that we had to turn off the active optics system of the VLT to obtain the required very large defocus. We emphasize that imaging in this manner is not at all a standard observational mode on the VLT. We suggest for similar programs a milder level of defocus combined with the use of the active optics system.

Recently, exquisite ground-based transit photometry for the hot Neptune GJ 436b was obtained by Alonso et al. (2008) using a different approach. They observed a transit in the H-band with the TCS telescope and its CAIN-II near-IR detector. As the red dwarf GJ 436 is very bright in the H-band ($H = 6.3$), the background variability is not a concern, so no dithering pattern was used and the images were severely defocused, i.e. the strategy was very similar to the one that we choose for our

VLT observations. The most surprising point is that no differential photometry was used by Alonso et al. to reach such a high photometric quality. These authors explain this by the much smoother behavior of the transparency variations in the H-band compared to the visible. It is very desirable to confirm this point by obtaining more high-quality eclipse light curves in the near-IR. Unfortunately, this method is limited to stars that are very bright in the near-IR, and only a few are known to harbor a transiting planet (e.g. HD 189733, HD 209458).

5.2. The hot Jupiters WASP-4b and WASP-5b

The high-quality of the WASP-4 VLT z-band transit photometry allows a significant improvement of the precision on the impact parameter ($0.063^{+0.047}_{-0.062}$ vs. $0.13^{+0.13}_{-0.12}$ in W08) that leads to a better precision on the orbital inclination ($89.35^{+0.64}_{-0.49}$ vs. $88.59^{+1.36}_{-1.50}$ degrees in W08), but our analysis fails to give a more precise value for the planetary mass ($1.21^{+0.13}_{-0.08}$ M_J vs. $1.215^{+0.09}_{-0.08}$ M_J in W08) and even for the planetary radius ($1.304^{+0.054}_{-0.042}$ R_J vs. $1.416^{+0.068}_{-0.043}$ R_J in W08) despite a significantly more precise determination of the planet/star area ratio ($0.02357^{+0.00010}_{-0.00008}$ vs. $0.0241^{+0.0005}_{-0.0002}$ R_J in W08). This is due to the fact that our new spectroscopy does not improve significantly our knowledge of the host star because it is now limited by the accuracy/validity of the stellar atmospheric and evolution models, and this uncertainty on the stellar parameters propagates to our final accuracy on the planet parameters. This fact is also illustrated with our results for WASP-5b: our new values for the planetary mass and radius agree well with the ones quoted in A08 ($1.58^{+0.13}_{-0.10}$ M_J and $1.087^{+0.068}_{-0.071}$ R_J vs. $1.58^{+0.13}_{-0.08}$ M_J and $1.090^{+0.024}_{-0.058}$ R_J in A08) but are not more accurate. This "stellar" accuracy limit relates to all transiting systems, except the putative systems (1) that could be studied by asteroseismology (see e.g. Christensen-Dalsgaard et al. 2007), allowing a more precise estimation of their age and radius; or (2) the systems that would be bright and nearby enough to allow a very precise direct determination of the stellar radius by long baseline interferometry (see e.g. Baines et al. 2008).

With a radius measurement $R_p = 1.30^{+0.05}_{-0.04}$ R_J, we confirm here that WASP-4b is larger than predicted by basic models of irradiated planets (Burrows et al. 2007a; Fortney et al. 2007). For instance, the theoretical value presented by Fortney et al. (2007) for an irradiated 1.46 M_J core-less planet of 4.5 Gyr orbiting a 0.02 AU from a sun-like star is only 1.17 R_J. WASP-4b is thus another case demonstrating that something is missing in basic models.

Fortney et al. (2008) proposed the theoretical division of hot Jupiters into two classes based on their level of irradiation. By analogy with M-dwarfs, the "pM" class would be composed of the planets warmer than required for condensation of Ti and V-bearing compounds, and these planets should show a stratospheric temperature inversion due to the absorption of most of the large incident flux by the high-opacity gaseous TiO and VO. The cooler planets would compose the "pL" class. Burrows et al. (2008) proposed a similar bifurcation into two groups, but without firmly identifying TiO and VO as the high opacity gaseous compounds causing the thermal inversion. Interestingly, recent *S pitzer* secondary eclipse measurements detected such temperature inversions for the highly irradiated planets HD 209458b and XO-1b (Burrows et al. 2007b; Knutson et al. 2008; Machalek et al. 2008). The updated estimation for the incident flux received by WASP-4b is now 1.7×10^9 erg s^{-1} cm^{-2}, classing it clearly in the theoretical pM planetary class proposed by Fortney et al. Figure 10 shows the location of WASP-4b in a mass-radius diagram. The location of the other transiting planets receiving an incident flux larger than 10^9 erg s^{-1} cm^{-2} (i.e. belonging clearly to Fortney's pM class) or smaller than 5×10^8 erg s^{-1} cm^{-2} (i.e. belonging clearly to Fortney's pL class) is also shown for comparison. We notice that the pL planets seem to have a smaller radius than their pM counterparts having a similar mass. WASP-4b follows this tendency. This is in favor of the proposition done by Burrows et al. (2007a) that the enhanced opacity of the highly irradiated giant planets could alter their cooling history and thus be part of the solution to their "anomalously" large radius. However, WASP-5b is even more irradiated then WASP-4b (2.0×10^9 erg s^{-1} cm^{-2}) but according to our result it is not extremely bloated ($R_p = 1.09 \pm 0.07$ R_J). As shown in Fig. 10, WASP-5b seems to be smaller than the other planets of similar mass that fall clearly in the pM class. This favors the fact that the size of highly irradiated gazeous planets is not only dependent on their level of stellar irradiation but also of other factors. The planetary core mass is probably one of them. In this context, it is interesting to notice that WASP-5 is more metal-rich than WASP-4. This goes in the right direction towards the existence of a correlation between the metallicity of the parent star and the core mass of the planet (Guillot et al. 2006; Burrows et al. 2007a; Guillot 2008).

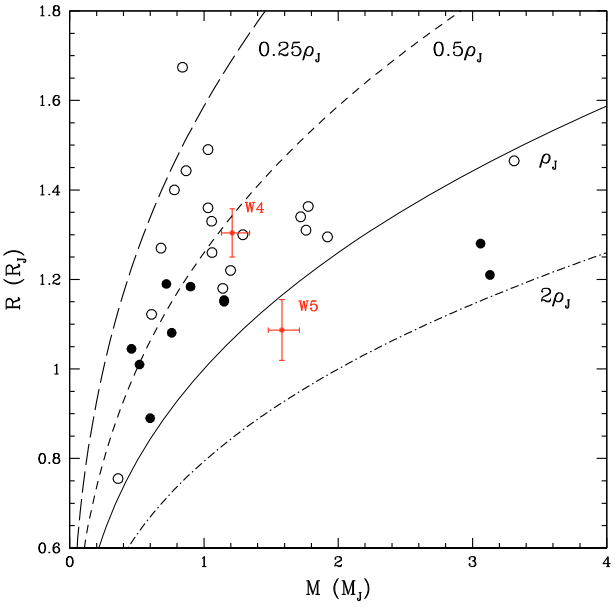


Fig. 10. Location of WASP-4b (W4) and WASP-5b (W5) in a mass-radius diagram. The location of the other transiting planets receiving an incident flux larger than 10^9 erg s^{-1} cm^{-2} (open circles) or smaller than 5×10^8 erg s^{-1} cm^{-2} (closed circles) is also shown.

More transit photometry for WASP-5 is needed to confirm the possible period variability shown by our transit timing measurements. Such an apparent period variability could be due to the presence of another close-in lighter planet in the system (see e.g. Holman & Murray 2005). A precise timing of the secondary eclipse of this planet is also desirable, because it could confirm the non-null eccentricity that we marginally deduce from our analysis. Such a non-null eccentricity could also be the sign of the presence of another planet around WASP-5.

Acknowledgements. The authors thank the ESO staff on the VLT for their diligent and competent execution of the observations. E. Pompei is particularly

gratefully acknowledged. We thank T. Guillot for very helpful suggestions. The anonymous referee is gratefully acknowledged for his valuable comments and suggestions.

References

Alonso, R., Barbieri, M., Rabus, M., et al. 2008, A&A, 487, L5
Anderson, D. R., Gillon, M., Hellier, C., et al. 2008, MNRAS, 387, L4
Baines, E. K., McAlister, H. A., ten Brummelaar, T. A., et al. 2008, ApJ, 680, 728
Barklem, P. S., Piskunov, N., & O'Mara, B. J. 2000, A&AS, 142, 467
Blackwell, D. E., & Shallis, M. J. 1977, MNRAS, 180, 177
Bakos, G. A., Noyes, R. W., Kovács, G., et al. 2004, PASP, 116, 266
Bodenheimer, P., Lin, D. N. C., & Mardling, R. A. 2001, ApJ, 548, 466
Burrows, A., Hubeny, I., Budaj, J., & Hubbard, W. B. 2007a, ApJ, 661, 502
Burrows, A., Hubeny, I., Budaj, J., et al. 2007b, ApJ, 668, L171
Burrows, A., Budaj, J., & Hubeny, I. 2008, ApJ, 678, 1436
Cameron, A. C., Wilson, D. M., West, R. G., et al. 2007, MNRAS, 380, 1230
Castelli, F., Gratton, R. G., & Kurucz, R. L. 1997, A&A, 318, 841
Charbonneau, D., Brown, T. M., Burrows, A., & Laughlin, G. 2007, Protostars and Planets V, ed. B. Reipurth, D. Jewitt, & K. Keill (Tucson: University of Arizona Press), 701
Christensen-Dalsgaard, J., Arentoft, T., Brown, T. M., et al. 2007, Commun. Asteroseismol., 150, 350
Claret, A. 2000, A&A, 363, 1081
Claret, A. 2004, A&A, 428, 1001
Cutri, R. M., Skrutskie, M. F., Van Dyk, S., et al. 2003, University of Massachusetts and Infrared Processing and Analysis Center (IPAC/California Institute of Technology)
Fortney, J. J., Marley, M. S., & Barnes, J. W. 2007, ApJ, 658, 1661
Fortney, J. J., Lodders, K., Marley, M. S., & Freedman, R. S. 2008, ApJ, 678, 1419
Fouqué, P., Chevallier, L., Cohen, M., et al. 2000, A&AS, 141, 313
Gilliland, R. L., Brown, T. M., Kjeldsen, H., et al. 1993, AJ, 106, 2441
Gillon, M., Pont, F., & Moutou, C. 2006, A&A, 459, 249
Gillon, M., Pont, F., Moutou, C., et al. 2007a, A&A, 466, 743
Gillon, M., Demory, B.-O., Barman, T., et al. 2007b, A&A, 471, L51
Girardi, L., Bressan, A., Bertelli, G., & Chiosi, C. 2000, A&AS, 141, 371
Gonzalez, G., & Laws, C. 2000, AJ, 119, 390
Gonzalez, G., Laws, C., Tyagi, S., & Reddy, B. E. 2001, AJ, 121, 432
Gray, D. F. 1992, The observation and analysis of stellar photospheres, CUP, 431
Guillot, T. 2008, PhST, 130, 4023
Guillot, T., & Showman, A. P. 2002, A&A, 385, 156
Guillot, T., Santos, N. C., Pont, F., et al. 2006, A&A, 453, L21
Høg, E., Fabricius, C., Makarov, V. V., et al. 2000, A&A, 355, L27
Holman, M. J., & Murray, N. W. 2005, Science, 307, 1288
Holman, M. J., Winn, J. N., Latham, D. W., et al. 2006, ApJ, 652, 1715
Jackson, B., Greenberg, R., & Barnes, R. 2008, ApJ, 681, 1631
Knutson, H. A., Charbonneau, D., Allen, L. E., et al. 2007, Nature, 447, 183
Knutson, H. A., Charbonneau, D., Allen, L. E., et al. 2008, ApJ, 673, 526
Kurucz, R. L. 1993, Kurucz CD-ROM 13: ATLAS9, SAO (USA: Cambridge)
Kurucz, R. L., & Bell, B. 1995, Kurucz CD-ROM 23: Atomic Line List, SAO (USA: Cambridge)
Machalek, P., McCullough, P. R., Burke, C. J., et al. 2008, ApJ, 684, 1427
Magain, P. 1984, A&A, 134, 189
Mandel, K., & Agol, E. 2002, ApJ, 580-2, L171
McCullough, P. R., Stys, J., Valenti, J., et al. 2005, PASP, 117, 783
Monet, D. G., Levine, S. E., Casian, B., et al. 2003, AJ, 125, 984
Morrissey, P., Conrow, T., Barlow, T. A., et al. 2007, ApJS, 173, 682
O'Donovan, F. T., Francis, T., Charbonneau, D., et al. 2006, ApJ, 651, L61
Pollacco, D. L., Skillen, I., Cameron, A. C., et al. 2006, PASP, 118, 1407
Pont, F., Zucker, S., & Queloz, D. 2006, MNRAS, 373, 231
Pont, F., Moutou, C., Gillon, M., et al. 2007, A&A, 465, 1069
Santos, N. C., Israelian, G., & Mayor, M. 2004, A&A, 415, 1153
Sestito, P., & Randich, S. 2005, A&A, 442, 615
Smalley, B. 2005, MSAIS, 8, 130
Smalley, B., Smith, K. C., & Dworetsky, M. M. 2001, UCLSYN Userguide
Smith, K. C. 1992, Ph.D. Thesis, University of London
Stetson, P. B. 1987, PASP, 99, 111
Wilson, D. M., Gillon, M., Hellier, C., et al. 2008, ApJ, 675, L113
Zacharias, N., Monet, D. G., Levine, S. E., et al. 2004, AAS, 205, 4815

2.4 Planetary Occultations

In the direct line to the estimation of a planetary occultation probability presented in section 2.3.1, fitting the capacity to adjust for an occultation was added to the code. In many ways it was one of the simplest additions, being but another transit shape model (without limb darkening) at phase 0.5 or around. A slight displacement in the occultation mid point $T_{0.5}$ gives information on the orbital eccentricity on the form of $e\,\cos\,\omega$. From Hilditch (2001) we have:

$$2\pi\frac{(T_{0.5}-T_0)}{P} = X - \sin X \tag{2.34}$$

where

$$X = \pi + 2\tan^{-1}\frac{e\cos\omega}{\sqrt{1-e^2}} \tag{2.35}$$

The width of the occultation can also be let to float in the MCMC thus potentially bringing information on the harder to estimate $e\,\sin\,\omega$:

$$e\sin\omega = \frac{W_{\rm occ}-W}{W_{\rm occ}+W} \tag{2.36}$$

The radial velocities also help in adjusting that parameter but thus far detecting a significant deviation from zero has proved a little elusive. Most measurements of occultations give eccentricities compatible with zero at the $3\,\sigma$ level. A reason for this is given in section 3.4.4.

The depth of the secondary transit is of prime interest here as it is dependant on the brightness temperature of planet. Having this depth in several bands amounts to build a low resolution spectrum of that planet. Many efforts have been undertaken by several members of the community, first using space-based observations then moving onto ground near-infrared instrumentation. These measurements are driving an intense theoretical and numerical work on modelling hot gas giant's atmospheres and participate to solving the problem of their larger than expected radii.

To find what type of signal to expect one needs to get the amount of flux reflected by the planet.

$$F_i(\lambda) = \frac{L_\star(\lambda)}{4\pi a^2} \tag{2.37}$$

where $F_i(\lambda)$ is the incident flux on the planet, as a function of wavelength and $L_\star$ is its luminosity. We need to define now the albedo as the ratio of reflected flux to incident flux when the planet is at its *fullest* phase ϕ:

$$A(\lambda) = \frac{F_r(\phi=0.5,\lambda)}{F_i(\lambda)} \tag{2.38}$$

The planet's flux arriving to Earth is at most:

$$f_{\rm p}(\lambda) = A(\lambda)F_i(\lambda)\frac{R_{\rm p}^2}{D^2} \tag{2.39}$$

with D the distance between the target and the Earth. The type of signal we seek is the contrast with the total flux approximated as the sole stellar flux $f_\star$:

$$\Delta f(\phi,i,\lambda) \sim \frac{f_{\rm p}(\phi,i,\lambda)}{f_\star(\lambda)} = A(\lambda)\frac{R_{\rm p}^2}{a^2}g(\phi,i) \tag{2.40}$$

where g is the phase function. This deficit in flux depends heavily on λ which depends on the opacity of the planet and its capacity to redistribute its incident flux into other wavelengths. By measuring in several bands we get an idea on the planet's spectrum.

A few observations like that of Knutson et al. (2009) have observed half an orbital phase and thus see the slow rise in flux as the planet progresses on its orbit and its reflected face becomes larger. By observing only at occultation we only measure Δf

A&A 506, 359–367 (2009)
DOI: 10.1051/0004-6361/200912231
© ESO 2009

The CoRoT space mission: early results

Astronomy & Astrophysics
Special feature

VLT transit and occultation photometry for the bloated planet CoRoT-1b⋆,⋆⋆

M. Gillon[1,2], B.-O. Demory[2], A. H. M. J. Triaud[2], T. Barman[3], L. Hebb[4], J. Montalbán[1], P. F. L. Maxted[5], D. Queloz[2], M. Deleuil[6], and P. Magain[1]

[1] Institut d'Astrophysique et de Géophysique, Université de Liège, Allée du 6 Août 17, Bât. B5C, Liège 1, Belgium
e-mail: michael.gillon@ulg.ac.be
[2] Observatoire de Genève, Université de Genève, 51 Chemin des Maillettes, 1290 Sauverny, Switzerland
[3] Lowell Observatory, 1400 West Mars Hill Road, Flagstaff, AZ 86001, USA
[4] School of Physics and Astronomy, University of St. Andrews, North Haugh, Fife, KY16 9SS, UK
[5] Astrophysics Group, Keele University, Staffordshire, ST5 5BG, UK
[6] Laboratoire d'Astrophysique de Marseille (UMR 6110), 38 rue Frédéric Joliot-Curie, 13388 Marseille, France

Received 30 March 2009 / Accepted 26 May 2009

ABSTRACT

We present VLT eclipse photometry for the giant planet CoRoT-1b. We observed a transit in the *R*-band filter and an occultation in a narrow filter centered on 2.09 μm. Our analysis of this new photometry and published radial velocities, in combination with stellar-evolutionary modeling, leads to a planetary mass and radius of $1.07^{+0.13}_{-0.18}$ $M_{\rm Jup}$ and $1.45^{+0.07}_{-0.13}$ $R_{\rm Jup}$, confirming the very low density previously deduced from CoRoT photometry. The large occultation depth that we measure at 2.09 μm ($0.278^{+0.043}_{-0.066}$%) is consistent with thermal emission and is better reproduced by an atmospheric model with no redistribution of the absorbed stellar flux to the night side of the planet.

Key words. binaries: eclipsing – planetary systems – stars: individual: CoRoT-1 – infrared: stars – techniques: photometric – techniques: radial velocities

1. Introduction

Transiting planets play an important role in the study of planetary objects outside our solar system. Not only can we infer their density and use it to constrain their composition, but several other interesting measurements are possible for these objects (see e.g. review by Charbonneau et al. 2007). In particular, their thermal emission can be measured during their occultation, allowing the study of their atmosphere without spatially resolving their light from that of the host star. The *Spitzer Space Telescope* (Werner et al. 2004) has produced a flurry of such planetary emission measurements, all at wavelengths longer than 3.5 μm. From the ground, several attempts to obtain occultation measurements at shorter wavelengths than the *Spitzer* spectral window were performed (Richardson et al. 2003a,b; Snellen 2005; Deming et al. 2007; Knutson et al. 2007; Snellen & Covino 2007; Winn et al. 2008). Very recently, two of them were successful: Sing & López-Morales (2009) obtained a ~4σ detection of the occultation of OGLE-TR-56b in the *z*-band (0.9 μm), while De Moiij & Snellen (2009) detected at ~6σ the thermal emission of TrES-3b in the *K*-band (2.2 μm). It is important to obtain more similar measurements to improve our understanding of the atmospheric properties of short-period extrasolar planets.

CoRoT-1b (Barge et al. 2008, hereafter B08) was the first planet detected by the CoRoT space transit survey (Baglin et al. 2006). With an orbital period of 1.5 days, this Jupiter-mass planet orbits at only ~5 stellar radii from its G0V host star. Thanks to this proximity, its stellar irradiation is clearly large enough (~ 3.9×10^9 erg s^{-1} cm^{-2}) to make it join OGLE-TR-56b, TrES-3b and a few other planets within the pM theoretical class proposed by Fortney et al. (2008). Under this theory, pM planets receive a stellar flux large enough to have high-opacity compounds like TiO and VO present in their gaseous form in the day-side atmosphere. These compounds should be responsible for a stratospheric thermal inversion, with re-emission on a very short time scale of a large fraction of the incoming stellar flux, resulting in a poor efficiency of the heat distribution from the day-side to the night-side and to enhanced infrared planetary fluxes at orbital phases close to the occultation. Like the other pM planets, CoRoT-1b is thus a good target for near-infrared occultation measurements. Furthermore, CoRoT-1b belongs to the subgroup of the planets with a radius larger than predicted by basic models of irradiated planets (e.g. Burrows et al. 2007; Fortney et al. 2007). Tidal heating has been proposed by several authors (e.g. Bodenheimer et al. 2001; Jackson et al. 2008b) as a possible extra source of energy able to explain the radius anomaly shown by these hyper-bloated planets. As shown by Jackson et al. (2008b) and Ibgui & Burrows (2009), even a tiny orbital eccentricity is able to produce an

⋆ Based on data collected with the VLT/FORS2 and VLT/HAWK-I instruments at ESO Paranal Observatory, Chile (programs 080.C-0661(B) and 382.C-0642(A)).

⋆⋆ The photometric time-series used in this work are only available in electronic form at the CDS via anonymous ftp to cdsarc.u-strasbg.fr (130.79.128.5) or via http://cdsweb.u-strasbg.fr/cgi-bin/qcat?J/A+A/506/359

intense tidal heating for very short-period planets. Occultation photometry does not only allow to measure the planetary thermal emission, but also strongly constrains the orbital eccentricity (see e.g. Charbonneau et al. 2005). Such an occultation measurement for CoRoT-1b could thus help for understanding its low density.

These reasons motivated us to measure an occultation of CoRoT-1b with the Very Large Telescope (VLT). We also decided to obtain a precise VLT transit light curve for this planet to better constrain its orbital elements. Furthermore, CoRoT transit photometry presented in B08 is exquisite, but it is important to obtain an independent measurement of similar quality to check its reliability and to assess the presence of any systematic effect in the CoRoT photometry.

We present in Sect. 2 our new VLT data and their reduction. Section 3 presents our analysis of the resulting photometry and our determination of the system parameters. Our results are discussed in Sect. 4, before giving our conclusion in Sect. 5.

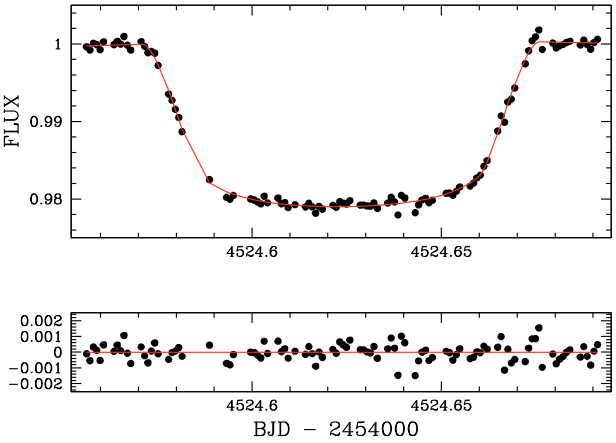


Fig. 1. *Top*: VLT/FORS2 *R*-band transit light curve with the best-fitting transit + trend model superimposed. *Bottom*: residuals of the fit.

2. Observations

2.1. VLT/FORS2 transit photometry

A transit of CoRoT-1b was observed on 2008 February 28 with the FORS2 camera (Appenzeller et al. 1998) installed at the VLT/UT1 (Antu). The FORS2 camera has a mosaic of two 2k × 4k MIT CCDs and is optimized for observations in the red with a very low level of fringes. It was used several times in the past to obtain high-precision transit photometry (e.g. Gillon et al. 2007a, 2008). The high-resolution mode was used to optimize the spatial sampling, resulting in a 4.6′ × 4.6′ field of view with a pixel scale of 0.063″/pixel. Airmass increased from 1.08 to 1.77 during the run that lasted from 1h16 to 4h30 UT. The quality of the night was photometric. Because of scheduling constraints, only a small amount of observations were performed before and after the transit, and the total out-of-transit (OOT) part of the run was only ∼50 min.

One hundred fourteen images were acquired in the R_SPECIAL filter ($\lambda_{\rm eff}$ = 655 nm, *FWHM* = 165 nm) with an exposure time of 15 s. After a standard prereduction, the stellar fluxes were extracted for all the images with the `IRAF`[1] `DAOPHOT` aperture photometry software (Stetson 1987). We noticed that CoRoT-1 was saturated in 11 images because of seeing and transparency variations, so we rejected these images from our analysis. Several sets of reduction parameters were tested, and we kept the one giving the most precise photometry for the stars of similar brightness to CoRoT-1. After a careful selection of reference stars, differential photometry was obtained. A linear fit for magnitude vs. airmass was performed to correct the photometry for differential reddening using the OOT data. The corresponding fluxes were then normalized using the OOT part of the photometry. The resulting transit light curve is shown in Fig. 1. After subtraction of the best-fit model (see next section), the obtained residuals show an rms of ∼520 ppm, very close to the photon noise limit (∼450 ppm).

2.2. VLT/HAWK-I occultation photometry

We observed an occultation of CoRoT-1b with HAWK-I (*High Acuity Wide-field K-band Imager*, Pirard et al. 2004; Casali et al. 2006), a cryogenic near-IR imager recently installed at the VLT/UT4 (Yepun). HAWK-I provides a relatively large field of view of 7.5′ × 7.5′. The detector is kept at 75 K and is composed of a mosaic of four Hawaii-2RG 2048 × 2048 pixels chips. The pixel scale is 0.106″/pixel, providing a good spatial sampling even for the excellent seeing conditions at Paranal (seeing down to 0.3 arcsec measured in *K*-band).

Instead of using a broad band *K* or $K_{\rm s}$ filter, we chose to observe with the narrow band filter NB2090 (central wavelength = 2.095 μm, width = 0.020 μm). This filter avoids absorption bands at the edge of the *K*-band, its small width minimizes the effect of differential extinction, and furthermore its bandpass shows much less sky emission than the one of the near Brγ filter (central wavelength = 2.165 μm, width = 0.030 μm), leading to a flux ratio background/star more than twice better than in Brγ or *K*-band filters. Because of the large aperture of the VLT and the relative brightness of CoRoT-1, the expected stellar count in this narrow filter is still good enough to allow theoretical noise of less than 0.15% for a 1 min integration.

Observations took place on 2009 January 06 from 1h54 to 7h56 UT. Atmospheric conditions were very good, while the mean seeing measured on the images was 0.47″. Airmass decreased from 1.36 to 1.08 then raised to 1.65. Each exposure was composed of 4 integrations of 11 s each. A random jitter pattern within a square 45″-sized box was applied to the telescope. This strategy aimed to obtain an accurate sky map from the neighboring for each image. Indeed, the near-IR background shows a strong spatial variability on different scales, and an accurate subtraction of this complex background is crucial, except when this background has a negligible amplitude when compared to the stellar count (see e.g. Alonso et al. 2008). In total, 318 images were obtained during the run.

After a standard pre-reduction (dark subtraction, flatfield division), a sky map was constructed and removed for each image using a median-filtered set of the ten adjacent images. The resulting sky-subtracted images were aligned and then compared on a per-pixel basis to the median of the 10 adjacent images in order to detect any spurious values due, e.g., to a cosmic hit or a pixel damage. The concerned pixels had their value replaced by the one obtained by linear interpolation using the 10 adjacent images.

Two different methods were tested to extract the stellar fluxes. Aperture photometry was obtained using the `IRAF`

[1] `IRAF` is distributed by the National Optical Astronomy Observatory, which is operated by the Association of Universities for Research in Astronomy, Inc., under cooperative agreement with the National Science Foundation.

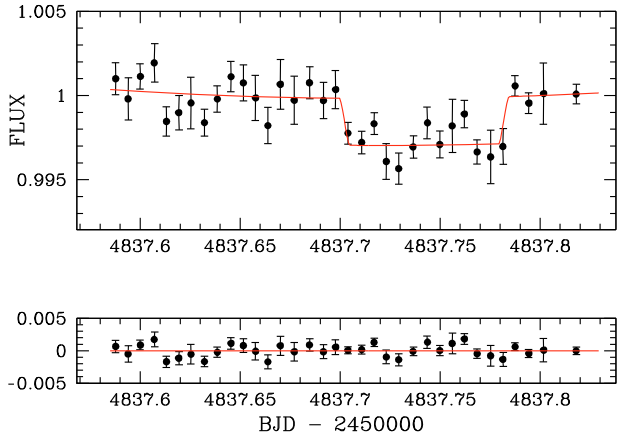


Fig. 2. *Top*: VLT/HAWK-I 2.09 μm occultation light curve binned per 10 min, with the best-fitting occultation + trend model superimposed. *Bottom*: residuals of the fit.

DAOPHOT software and compared to deconvolution photometry obtained with the algorithm DECPHOT (Gillon et al. 2006, 2007b; Magain et al. 2007). We obtained a significantly (~25%) better result with DECPHOT. We attribute this improvement to DECPHOT optimizing the separation of the stellar flux from the background contribution, while aperture photometry simply sums the counts within an aperture.

To avoid any systematic noise due to the different characteristics of the HAWK-I chips, we chose to use only reference stars located in the same chip than our target to obtain the differential photometry. As CoRoT-1 lies in a dense field of the Galactic plane, we have enough reference flux in one single chip to reach the desired photometric precision. After a careful selection of the reference stars, the obtained differential curve clearly shows an eclipse with the expected duration and timing (Fig. 2). We could not find any firm correlation of the OOT photometric values with the airmass or time, so we simply normalized the fluxes using the OOT part without any further correction. The OOT rms is 0.32%, much larger than the mean theoretical error: 0.13%. This difference implies an extra source of noise of ~0.3%. We attribute this noise to the sensitivity and cosmetic inhomogeneity of the detector combined with our jitter strategy. In the optical, one can avoid this noise by staring at the same exact position during the whole run, i.e. by keeping the stars on the same pixels. In the near-IR, dithering is needed to properly remove the large, complex, and variable background. This background varies in time at frequencies similar to the one of the transit, so any poor background removal is able to bring correlated noise in the resulting photometry. It is thus preferable to optimize the background subtraction by using a fast random jitter pattern even if this leads to extra noise, because this is dominated by frequencies much higher than the one of the searched signal and is thus unable to produce a fake detection or modify the eclipse shape.

3. Analysis

3.1. Data and model

To obtain an independent determination of the system parameters, we decided to use only our VLT R-band transit and 2.09 μm occultation photometry, in addition to the SOPHIE (Bouchy et al. 2006) radial velocities (RV) presented in B08 as data for our analysis.

These data were used as input into a Markov-Chain Monte-Carlo (MCMC; see e.g. Tegmark 2004; Gregory 2005; Ford 2006) code. MCMC is a Bayesian inference method based on stochastic simulations and provides the a posteriori probability distribution of adjusted parameters for a given model. Here the model is based on a star and a transiting planet on a Keplerian orbit about their center of mass. More specifically, we used a classical Keplerian model for the RV variations and fitted independent offsets for the two epochs of the SOPHIE observations to account for the drift between them mentioned in B08. To fit the VLT photometry, we used the photometric eclipse model of Mandel & Agol (2002) multiplied by a trend model. To obtain reliable error bars for our fitted parameters, it is indeed preferable to consider the possible presence of a low-amplitude time-dependent systematic in our photometry due, e.g. to an imperfect differential extinction correction or a low-amplitude low-frequency stellar variability. We chose to model this trend as a second-order time polynomial function for both FORS2 and HAWK-I photometry.

3.2. Limb-darkening

For the transit, a quadratic limb darkening law was assumed, with initial coefficients u_1 and u_2 interpolated from Claret's tables (2000, 2004) for the R-band photometric filter and for $T_{\rm eff}$ = 5950 ± 150 K, log g = 4.25 ± 0.30 and [Fe/H] = −0.30 ± 0.25 (B08). We used the partial derivatives of u_1 and u_2 as a function of the spectroscopic parameters in Claret's tables to obtain their errors σ_{u_1} and σ_{u_2} via

$$\sigma_{u_x} = \sqrt{\sum_{i=1}^{3} \left(\frac{\delta u_x}{\delta S_i} \sigma_{S_i} \right)^2}, \quad (1)$$

where x is 1 or 2, while S_i and σ_{S_i} are the ith ($i = 1, 3$) spectroscopic parameter and its error from B08. We obtained $u_1 = 0.279 \pm 0.033$ and $u_2 = 0.351 \pm 0.016$ as initial values. We allowed u_1 and u_2 to float in our MCMC analysis, using as jump parameters not these coefficients themselves but the combinations $c_1 = 2 \times u_1 + u_2$ and $c_2 = u_1 - 2 \times u_2$ to minimize the correlation of the obtained uncertainties (Holman et al. 2006). The following Bayesian penalty on c_1 and c_2 was added to our merit function:

$$BP_{\rm limb-darkening} = \sum_{i=1,2} \left(\frac{c_i - c_i'}{\sigma_{c_i'}} \right)^2, \quad (2)$$

where c_i' is the initial value deduced for the coefficient c_i and $\sigma_{c_i'}$ its error computed from σ_{u_1} and σ_{u_2}. We let c_1 and c_2 be free parameters under the control of a Bayesian penalty to propagate the uncertainty on the limb-darkening to the deduced transit parameters.

3.3. Jump parameters

The other jump parameters in our MCMC simulation were the transit timing (time of minimum light) T_0, the planet/star area ratio $(R_{\rm p}/R_{\rm s})^2$, the transit width (from first to last contact) W, the impact parameter $b' = a \cos i / R_*$, three coefficients per photometric time series for the low-frequency systematic, one systemic RV for each of the two SOPHIE epochs, and the two parameters $e \cos \omega$ and $e \sin \omega$, where e is the orbital eccentricity and ω the argument of periastron. The RV orbital

semi-amplitude K was not used as jump parameter, but instead we used the following parameter:

$$K_2 = K\sqrt{1-e^2}\,P^{1/3} = (2\pi G)^{1/3}\frac{M_{\rm p}\sin i}{(M_{\rm p}+M_*)^{2/3}}, \quad (3)$$

to minimize the correlation with the other jump parameters.

We notice that our used jump parameter b' is equal to the actual transit impact parameter b only for a circular orbit. For a non-zero eccentricity, it is related to the actual impact parameter b via

$$b = b'\,\frac{1-e^2}{1+e\sin\omega}\,. \quad (4)$$

Here too, the goal of using b' instead of b is to minimize the correlation between the jump parameters.

The orbital period P was let free in our analysis, constrained not only with the data presented above but also with the timings determined independently by Bean (2009) for each of the 35 CoRoT transits. Practically, we added the following Bayesian penalty $BP_{\rm timings}$ to our merit function:

$$BP_{\rm timings} = \sum_{i=1,35}\left(\frac{T_0+N_i\times P-T_i}{\sigma_{T_i}}\right)^2, \quad (5)$$

where T_i is the transit timing determined by Bean (2009) for the ith CoRoT transit, σ_{T_i} is its error and N_i is its differential epoch compared to our VLT transit. This procedure relies on the reasonable assumption that the timings determined by Bean (2009) are uncorrelated with the other transit parameters.

3.4. Photometric correlated noise and RV jitter noise

Our analysis was done in 4 steps. First, a single MCMC chain was performed. This chain was composed of 10^6 steps, the first 20% of each chain being considered as its burn-in phase and discarded. The best-fitting model found in the first chain was used to estimate the level of correlated noise in each photometric time-series and a jitter noise in the RV time series. For both photometric time series, the red noise was estimated as described in Gillon et al. (2006), by comparing the rms of the unbinned and binned residuals. We used a bin size corresponding to a duration of 20 min, similar to the timescale of the ingress/egress of the transit. The results were compatible with purely Gaussian noise for both time series. Still, it is possible that a low-amplitude correlated noise damaging only the eclipse part had been "swallowed" by our best-fitting model, so we preferred to be conservative and to quadratically add a red noise of 100 ppm to the theoretical uncertainties of each photometric time-series. The deduced RV jitter noise was high: 23 m s^{-1}. Nevertheless, we noticed that it goes down to zero if we discard the second RV measurement of the first SOPHIE epoch. Furthermore, this measurement has a significantly larger error bar than the others, so we decided to consider it as doubtful and to do not use it in our analysis. A theoretical jitter noise of 3.5 m s^{-1} was then added quadratically to the error bars of the other SOPHIE measurements, a typical value for a quiet solar-type star like CoRoT-1 (Wright 2005).

3.5. Determining the stellar density

Then, 10 new MCMC chains were performed using the updated measurement error bars. These 10 chains were then combined, using the Gelman & Rubin statistics (Gelman & Rubin 1992) to verify that they were converged and mixed enough, and the best-fitting values and error bars for each parameter were obtained from their distribution. The goal of this MCMC run was to provide us with an improved estimation of the stellar density ρ_* (see e.g. Torres 2007). The stellar density that we obtained was $\rho_* = 0.84^{+0.11}_{-0.07}\,\rho_\odot$.

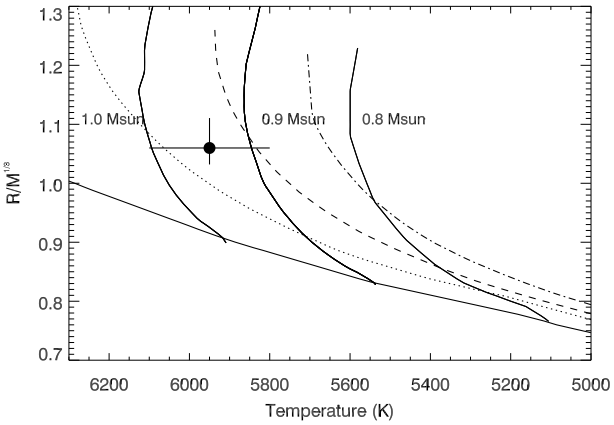


Fig. 3. $R/M^{1/3}$ (in solar units) versus effective temperature for CoRoT-1 compared to the theoretical stellar stellar evolutionary models of Girardi et al. (2000) interpolated at −0.3 metallicity. The labeled mass tracks are for 0.8, 0.9, and 1.0 $M_\odot$ and the isochrones are 100 Myr (solid), 5 Gyr (dotted), 10 Gyr (dashed), 16 Gyr (dot-dashed). We interpolated the tracks at −0.2 metallicity and included the uncertainty on the metallicity (±0.25) in the overall uncertainties on the mass and the age.

3.6. Stellar-evolutionary modeling

The deduced stellar density and the spectroscopic parameters were then used to better constrain the stellar mass and age via a comparison with theoretical stellar evolution models. Two independent stellar analysis were performed to assess the impact of the stellar evolution models used on the final system parameters.

– Our first analysis was based on Girardi's evolution models (Girardi et al. 2000), as follows. We first perform a linear interpolation between the solar (Z = 0.019) and subsolar (Z = 0.008) metallicity theoretical models to derive a set of mass tracks at the metallicity of the host star ([M/H] = −0.3). We then compare the effective temperature and the inverse cube root of the stellar density to the same values in the host star metallicity models. We interpolate linearly along the mass tracks to generate an equal number of age points between the zero age main sequence and the point corresponding to core hydrogen exhaustion. We then interpolate between the tracks along equivalent evolutionary points to find the mass, M = 0.94 $M_\odot$, and age, τ = 7.1 Gyr, of the host star that match the measured temperature and stellar density best. We repeat the above prescription using the extreme values of the observed parameters to determine the uncertainties on the derived mass and age. The large errors on the spectroscopic parameters, particularly the ±0.25 dex uncertainty on the metallicity, lead to a 15−20% error on the stellar mass ($M = 0.94^{+0.19}_{-0.16}\,M_\odot$) and an age for the system no more precise than older than 0.5 Gyr. Figure 3 presents the deduced position of CoRoT-1 in a $R/M^{1/3} - T_{\rm eff}$ diagram.

– In the second analysis, we applied the Levenberg-Marquard miniminization algorithm to derive the fundamental parameters of the host star. The merit function is defined by

$$\chi^2 = \sum_{i=1}^{3} \frac{(O_i^{\rm obs} - O_i^{\rm theo})^2}{(\sigma_i^{\rm obs})^2} \cdot \quad (6)$$

The observables ($O_i^{\rm obs}$) we take into consideration are effective temperature, surface metallicity, and mean density. The corresponding observational errors are $\sigma_i^{\rm obs}$. The theoretical values ($O_i^{\rm theo}$) are obtained from stellar evolution models computed with the code CLES (Code Liégois d'Evolution Stellaire, Scuflaire et al. 2008). Several fittings have been performed, in all of them we use the mixing-length theory (MLT) of convection (Böhm-Vitense 1958) and the most recent equation of state from OPAL (OPAL05, Rogers & Nayfonov 2002). Opacity tables are those from OPAL (Iglesias & Rogers 1996) for two different solar mixtures, the standard one from Grevesse & Noels (1993, GN93) and the recently revised solar mixture from Asplund et al. (2005, AGS05). In the first case $(Z/X)_\odot = 0.0245$, in the second one $(Z/X)_\odot = 0.0167$. These tables are extended at low temperatures with Ferguson et al. (2005) opacity values for the corresponding metal mixtures. The surface boundary conditions are given by grey atmospheres with an Eddington law. Microscopic diffusion (Thoul et al. 1994) is included in stellar model computation. The parameters of the stellar model are mass, initial hydrogen ($X_{\rm i}$), and metal ($Z_{\rm i}$) mass fractions, age, and the parameters of convection ($\alpha_{\rm MLT}$ and the overshooting parameter). Since we only have three observational constraints, we decided to fix the $\alpha_{\rm MLT}$ and $X_{\rm i}$ values to those derived from the solar calibration for the same input physics. Furthermore, given the low mass we expect for the host star, all the models are computed without overshooting. The values of stellar mass and age obtained for the two different solar mixtures are: $M = 0.90 \pm 0.21\ M_\odot$ with GN93 and $M = 0.92 \pm 0.18\ M_\odot$ with AGS05, and respectively $\tau = 7.5 \pm 6.0$ Gyr and $\tau = 6.9 \pm 5.4$ Gyr.

The result of our two independent stellar analyses are thus fully compatible, and the uncertainty due to the large errors on the spectroscopic parameters dominates the one coming from our imperfect knowledge of stellar physics. The large uncertainties affecting the stellar mass and age mainly come from the lack of accuracy in determining metallicity. We estimate from several tests that an improvement in determining the atmospheric parameters leading to an error in metallicity of 0.05 dex would translate in a reduction in uncertainty by a factor three for the stellar mass and a factor two for the stellar age. Moreover, decreasing the effective temperature error to 75 K would imply a subsequent reduction of stellar parameter errors by an additional factor two. Getting more high-SNR high-resolution spectroscopic data for the host star is thus very desirable.

3.7. Determining the system parameters

For the last part of our analysis, we decided to use $0.93 \pm 0.18\ M_\odot$, i.e. the average of the values obtained with the two different evolution models, as our starting value for the stellar mass. A new MCMC run was then performed. This run was identical to the first one, with the exception that M_* was also a jump parameter under the control of a Bayesian penalty based on $M_* = 0.93 \pm 0.18\ M_\odot$. At each step of the chains, the physical parameters $M_{\rm p}$, $R_{\rm p}$, and R_* were computed from the relevant jump parameters including the stellar mass. Table 1 shows the values deduced for the jump + physical parameters and compares them to the values presented in B08. It also shows the Bayesian penalties used in this second MCMC run.

4. Discussion

4.1. The density and eccentricity of CoRoT-1b

As can be seen in Table 1, the transit parameters that we obtain from our VLT/FORS-2 R-band photometry agree well with the ones presented in B08 and based on CoRoT photometry. Our value for the transit impact parameter is in good agreement with the one obtained by B08, and has a similar uncertainty. The planet/star area ratio that we deduce is within the error bar of the values obtained by B08, while our error bar is smaller. Our deduced physical parameters also agree very well with the ones presented in B08. Our analysis thus confirms the very low density of the planet (see Fig. 4) and its membership in the subgroup of short period planets too large for current models of irradiated planets (Burrows et al. 2007; Fortney et al. 2008).

In this context, it is worth noticing the marginal non-zero eccentricity that we deduce from our combined analysis: $e = 0.071^{+0.042}_{-0.028}$. As outlined in recent works (Jackson et al. 2008b; Ibgui & Burrows 2009), tidal heating could play a major role in the energy budget of very short period planets and help explain the very low density of some of them. Better constraining the orbital eccentricity of CoRoT-1b by obtaining more radial velocity measurements and occultation photometry is thus desirable. To test the amplitude of the constraint brought by the occultation on the orbital eccentricity, we made an analysis similar to the one presented in Sect. 3 but discarded the HAWK-I photometry. We obtained similar results for the transit parameters, but the eccentricity was poorly constrained, so we obtained much less precise values for $e\cos\omega$ and $e\sin\omega$, respectively, $0.020^{+0.024}_{-0.029}$ and $-0.170^{+0.062}_{-0.078}$. The HAWK-I occultation thus brings a strong constraint on these parameters, especially on $e\cos\omega$.

Table 1 shows that our analysis does not agree with B08 for one important parameter: the stellar density. Indeed, the value presented in B08 is significantly lower and more precise than ours. Still, B08 assumed a zero eccentricity in their analysis, while the stellar mean density deduced from transit observables depend on e and ω (see e.g. Winn 2009). To test the influence of the zero eccentricity assumption on the deduced stellar density, we made a new MCMC analysis assuming $e = 0$. This time we obtained $\rho_* = 0.695^{+0.043}_{-0.030}\ \rho_\odot$, in excellent agreement with the value $\rho_* = 0.698 \pm 0.033\ \rho_\odot$ presented by B08. This nicely shows that not only are VLT and CoRoT data fully compatible, but also that assuming a zero eccentricity can lead to an unreliable stellar density value and uncertainty. In our case, this has no significant impact on the deduced physical parameters because the large errors that we have on the stellar effective temperature and metallicity totally dominate the result of the stellar-evolutionary modeling (see Sect. 3.6). Still, this point is important. As shown by Jackson et al. (2008a), most published estimates of planetary tidal circularization timescales have used inappropriate assumptions that lead to unreliable values, and most close-in planets could probably keep a tiny but non-zero eccentricity during a major part of their lifetime. In this context, very precise transit photometry like the CoRoT one is not enough to reach the highest accurary on the physical parameters of the system, and a precise determination of e and ω is also needed. This strengthens the interest in getting complementary

Table 1. CoRoT-1 system parameters and 1-σ error limits derived from the MCMC analysis.

Parameter	Value	Bayesian penalty	B08	Unit
Jump parameters				
Transit epoch T_0	$2\,454\,524.62324^{+0.00009}_{-0.00013}$		$2\,454\,159.4532 \pm 0.0001$	BJD
Planet/star area ratio $(R_p/R_s)^2$	$0.01906^{+0.00020}_{-0.00040}$		0.01927 ± 0.00058	
Transit width W	0.10439 ± 0.00094			day
2.09 μm occultation depth	$0.00278^{+0.00043}_{-0.00066}$			
$b' = a \cos i/R_*$	$0.398^{+0.032}_{-0.043}$		0.420 ± 0.043	R_*
RV K_2	215^{+15}_{-16}		216 ± 13	
RV γ_1	$23.366^{+0.020}_{-0.017}$			km s^{-1}
RV γ_2	$23.350^{+0.012}_{-0.011}$			km s^{-1}
$e \cos \omega$	$0.0083^{+0.0038}_{-0.0025}$			
$e \sin \omega$	$-0.070^{+0.029}_{-0.042}$			
$A_{\rm transit}$	$0.99963^{+0.00028}_{-0.00009}$			
$B_{\rm transit}$	$0.017^{+0.003}_{-0.018}$			day^{-2}
$C_{\rm transit}$	$-0.10^{+0.12}_{-0.02}$			day^{-1}
$A_{\rm occultation}$	$1.00041^{+0.00096}_{-0.00052}$			
$B_{\rm occultation}$	$-0.008^{+0.007}_{-0.023}$			day^{-2}
$C_{\rm occultation}$	$0.029^{+0.079}_{-0.029}$			day^{-1}
Orbital period P	$1.5089686^{+0.0000005}_{-0.0000006}$	from timings in Bean (2009)	1.5089557 ± 0.0000064	day
Stellar mass M_*	$1.01^{+0.13}_{-0.22}$	0.93 ± 0.18	0.95 ± 0.15	$M_\odot$
R-filter c_1	$0.794^{+0.047}_{-0.048}$	0.909 ± 0.067		
R-filter c_2	$-0.444^{+0.054}_{-0.032}$	-0.423 ± 0.046		
Deduced parameters				
RV K	188 ± 14		188 ± 11	m s^{-1}
$b_{\rm transit}$	$0.426^{+0.035}_{-0.042}$		0.420 ± 0.043	R_*
$b_{\rm occultation}$	$0.370^{+0.037}_{-0.049}$		0.420 ± 0.043	R_*
Orbital semi-major axis a	$0.0259^{+0.0011}_{-0.0020}$		0.0254 ± 0.0014	AU
Orbital inclination i	$85.66^{+0.62}_{-0.48}$		85.1 ± 0.5	degree
Orbital eccentricity e	$0.071^{+0.042}_{-0.028}$		0 (fixed)	
Argument of periastron ω	$276.7^{+5.9}_{-4.3}$			degree
Stellar radius R_*	$1.057^{+0.055}_{-0.094}$		1.11 ± 0.05	$R_\odot$
Stellar density ρ_*	$0.86^{+0.13}_{-0.08}$		0.698 ± 0.033	$\rho_\odot$
R-filter u_1	$0.229^{+0.025}_{-0.022}$			
R-filter u_2	$0.336^{+0.012}_{-0.020}$			
Planet radius R_p	$1.45^{+0.07}_{-0.13}$		1.49 ± 0.08	R_J
Planet mass M_p	$1.07^{+0.13}_{-0.18}$		1.03 ± 0.12	M_J
Planet density ρ_p	$0.350^{+0.077}_{-0.042}$		0.31 ± 0.06	ρ_J

The parameters A, B, and C are the zero-, first- and second-order coefficients of the polynomial used to model the photometric trend. The values and error bars used in the Bayesian penalties are shown in the third column. Fourth column shows the values presented in B08.

occultation photometry in addition to high-precision radial velocities to improve the characterization of transiting planets.

4.2. The atmospheric properties of CoRoT-1b

The flux at 2.09 μm of this planet is slightly more than the one deduced from the (zero-albedo) equilibrium temperature, ~2660 K, obtained if the star's effective temperature is allowed to be as high as 6100 K (maximum within the 1-σ error-bars from B08). An irradiated planet atmosphere model (following Barman et al. 2005) for CoRoT-1b was computed by adopting the maximum observational allowed stellar effective temperature and radius and by assuming that zero energy is transported to the night side. Solar metallicity was assumed and all other parameters were taken from Table 1. This model (Fig. 5) falls short of matching the observations within 1-σ, while a black body with the same equilibrium temperature as the irradiated planet model is in better agreement. The atmosphere model is hot enough for a significant temperature inversion to form for $P < 0.1$ bar and is nearly isothermal from 0.1 down to ~100 bar. A model that uniformly redistributes the absorbed stellar flux across the entire planet surface (lower curve in Fig. 5) is far too cool to match the observations and is excluded at ~3σ. The flux at 2.09 μm alone is suggestive that very little energy is redistributed to the night side; however, additional observations at shorter and/or longer wavelengths are needed to better estimate the bolometric flux of the planet's day side. Occultation measurements in other bands will help provide limits on the day side bolometric flux and determine the depth of any possible temperature inversion and the extent of the isothermal zone.

Recently, Snellen et al. (2009) have measured the dayside planet-star flux ratio of CoRoT-1 in the optical (~0.7 μm) to be $1.26 \pm 0.33 \times 10^{-4}$. The hot, day-side only model shown in Fig. 5 predicts a value of $1.29 \pm 0.33 \times 10^{-4}$, which is fully consistent with the optical measurement. Consequently, it appears as

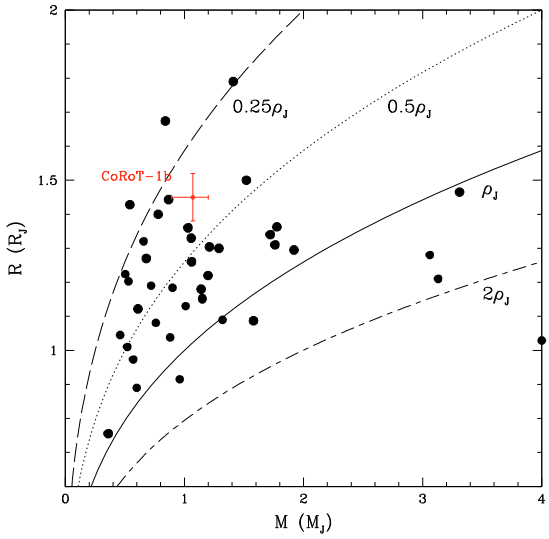


Fig. 4. Position of CoRoT-1b (in red) among the other transiting planets (black circles, values from http://exoplanet.eu) in a mass-radius diagram. The error bars are shown only for CoRoT-1b for the sake of clarity.

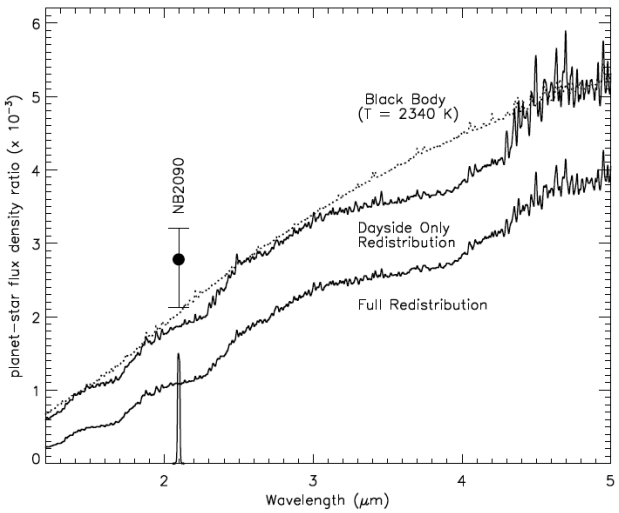


Fig. 5. Comparison of our 2.09 μm occultation depth measured for CoRoT-1 with models of planet-star flux density ratios assuming that the absorbed stellar flux is redistributed across the dayside only (top curve) and uniformly redistributed across the entire planetary atmosphere (lower curve). A black body model is also shown (dotted) for T = 2365 K.

though very little energy is being carried over to the night side of this planet.

4.3. Assessing the presence of another body in the system

As shown in Table 1, our deduced systemic RV for each SOPHIE epoch agrees with each other, so we do not confirm the RV drift mentioned in B08. Our combined analysis presented in Sect. 3 leads to a very precise determination of the orbital period: $1.5089686^{+0.0000005}_{-0.0000006}$ days, thanks to a lever arm of nearly one year between CoRoT transits and the VLT one. A simple linear

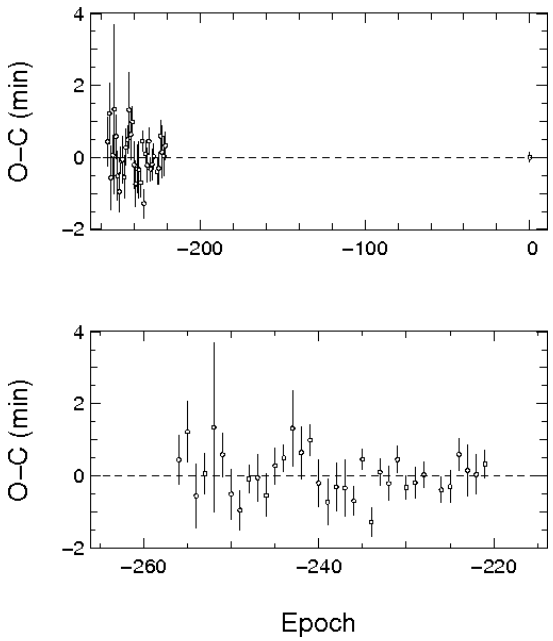


Fig. 6. *Top*: residuals of the linear fit timing vs. epoch for CoRoT-1b (see text for details). The rightmost point is our VLT/FORS2 timing. *Botttom*: zoom on the CoRoT residuals.

fit to timing versus epoch data based on the CoRoT and VLT transits lead to a similar level of precision, giving $P = 1.5089686^{+0.0000003}_{-0.0000005}$ days. This fit has a reduced χ^2 of 1.28, and the rms of its residuals (see Fig. 6) is 36 s. These values are fully consistent with those reported by Bean (2009) for CoRoT data alone. We also notice the same 3-σ discrepancy with transit #23 that, once removed, results in a reduced χ^2 of 1.00, hereby confirming the remarkable periodicity of the transit signal.

Limits on additional planetary companions in CoRoT-1 system were extensively discussed for transit timing variations (TTVs) by Bean (2009). Here we compare the approach proposed by Holman & Murray (2005) and the one from Agol et al. (2005). We have plotted the detection diagram related to the former in Fig. 7, where we represent the maximum successive transit timings interval as a function of mass and period of a putative perturbator.

Furthermore, Fig. 7 illustrates the domain where additional planets could be found through TTVs (white) and RV measurements (above colored curves). We focused on short period objects, since TTVs are more sensitive to nearby perturbators as compared to the known transiting planet. We assumed an eccentricity of 0.05 for a putative coplanar planet and used the MERCURY package described in Chambers (1999) to estimate the maximum TTV signal expected for CoRoT-1b by numerical integration. White is the domain with >3-σ detection by TTVs according to CoRoT data rms, while the black area is below the 1-σ detection threshold. Although approximate, this shows that, for a typical 3 m s^{-1} accuracy of radial velocities (dashed curve in Fig. 7) routinely obtained with HARPS spectrograph (Mayor et al. 2003), planetary companion detection is not possible by TTVs alone with this approach for this system.

Figure 8 shows the detection domain for Agol et al. (2005) approach, where the authors benefit from the TTV being cumulative in resonances yielding a larger amplitude signal. In this case, the minimum detectable mass in 2:1 resonance with available

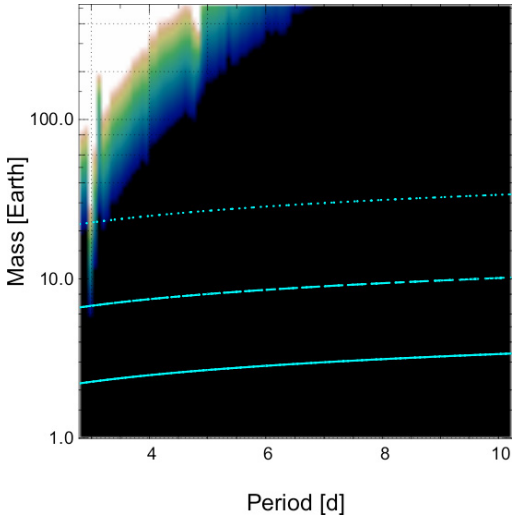


Fig. 7. Detectivity domain for a putative CoRoT-1c planet according to Holman & Murray (2005) approach, assuming $e_c = 0.05$. In white, the period-mass region where planets yield maximum TTV on CoRoT-1b above 100 s (5σ detection based on CoRoT data). Companions in the black area yield maximum TTV below the 1σ threshold. Solid, dashed and dotted curves shows RV detection limits for 1, 3 and 10 m/s rms.

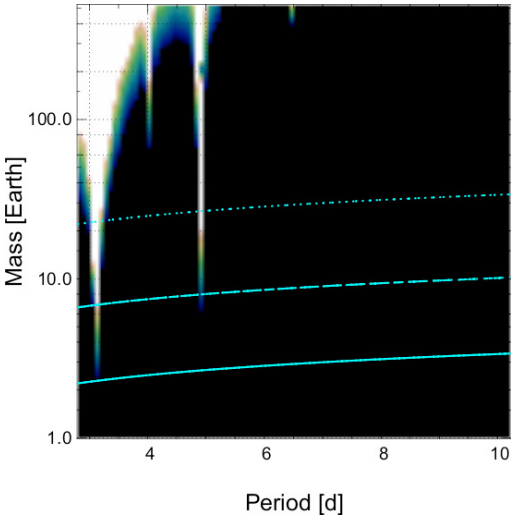


Fig. 8. Same as Fig. 7, but for the Agol et al. (2005) TTV approach. See text for details.

timings is about 2.5 Earth masses. In the case of planets near/in resonance, this approach provides an important gain in detection, provided observations on a long timescale are available. We evaluated our numerical integrations over a time scale corresponding to the interval between the first CoRoT-1b transit observation and our VLT transit, which spans 256 epochs. Those observations sample, only partly in most cases, the libration period of the putative planet, yielding an amplitude that is smaller than the one that would be obtained over a longer range. This approach does not require observation of successive transits in contrast to the Holman & Murray (2005) method.

The search for smaller temporal variations is more sensitive to noise. However, a comparison between Figs. 7 and 8 shows that for a short observation time span and outside resonances, observation of successive transits may be a fruitful strategy.

The TTV search method may be applied to active and/or stars for which RV measurements accuracy is limited, increasing a detectability area that RVs are not, or far less sensitive to. Each transit timing may be compared to a single RV measurement. The increased free parameters in a TTV orbital solution raise degeneracies that cannot be lifted by considering the same number of datapoints that would allow an orbital solution recovery with RVs. The determination of a large number of consecutive transits and their addition to occultation timings helps to determine a unique of the solution, as well as lowering constraints on timing accuracy (Nesvorný & Morbidelli 2008). This is thus a high-cost approach that is the most potentially rewarding for carefully determined target stars.

5. Conclusion

We have obtained new high-precision transit photometry for the planet CoRoT-1b. Our deduced system parameters are in very good agreement with the ones presented in B08, thus providing an independent verification of the validity of the CoRoT photometry. Thanks to the precision of the CoRoT and VLT transit photometry and the long baseline between them, the orbital period is now known to a precision better than 1/10th of a second. The precision on the planetary mass and radius is limited by the large errors on the stellar spectroscopic parameters, and a significant precision improvement should be made possible by getting new high-quality spectra of CoRoT-1.

We also successfully measured the occultation of the planet with HAWK-I, a new wide-field near-infrared imager mounted recently on the VLT. The large occultation depth that we measure is better reproduced by an atmospheric model with no redistribution of the absorbed stellar flux to the night side of the planet. This measurement firmly establishes the potential of the HAWK-I instrument for the study of exoplanetary atmospheres. At the time of writing, *Spitzer* cryogen is nearly depleted, and soon only its 3.6 μm and 4.5 μm will remain available for occultation measurements, while the eagerly awaited JWST (Gardner et al. 2006) is not scheduled for launch before 2013. It is thus reassuring to note that ground-based near-infrared photometry is now able to perform precise planetary occultation measurements, bringing new independent constraints on the orbital eccentricity and on the atmospheric physics and composition of highly irradiated extrasolar planets.

Acknowledgements. The authors thank the VLT staff for its support during the preparation and acquisition of the observations. In particular, J. Smoker and F. Selman are gratefully acknowledged for their help and support during the HAWK-I run. C. Moutou and F. Pont are acknowledged for their preparation of the FORS2 observations. F. Bouchy, PI of the ESO Program 080.C-0661(B), is also gratefully acknowledged. M. Gillon acknowledges support from the Belgian Science Policy Office in the form of a Return Grant, and thanks A. Collier Cameron for his help during the development of his MCMC analysis method. J. Montalbán thanks A. Miglio for his implementation of the optimization algorithm used in her stellar-evolutionary modeling. We thank the referee Scott Gaudi for a critical and constructive report. We are grateful to Eric Agol for providing insightful comments on this manuscript.

References

Agol, E., Steffen, J., Sari, R., & Clarkson, W. 2005, MNRAS, 359, 567
Alonso, R., Barbieri, M., Rabus, M., et al. 2008, A&A, 487, L5
Appenzeller, I., Fricke, K., Furtig, W., et al. 1998, The Messenger, 94, 1
Asplund, M., Grevesse, N., & Sauval, A. J. 2005, Cosmic Abundances as Records of Stellar Evolution and Nucleosynthesis, ASP Proc. Symp., 336, 25

Baglin, A., Auvergne, M., Boisnard, L., et al. 2006, 36th COSPAR Scientific Assembly, 36, 3749
Barge, P., Baglin, A., Auvergne, M., et al. 2008, A&A, 482, L17
Barman, T. S., Hauschildt, P., & Allard, F. 2005, ApJ, 632, 1132
Bean, J. L. 2009, A&A, 506, 369
Bodenheimer, P., Lin, D. N. C., & Mardling, R. A. 2001, ApJ, 548, 466
Böhm-Vitense, E. 1958, ZAp, 46, 108
Bouchy, F., The Sophie Team 2006, in Tenth Anniversary of 51 Peg-b, 319
Burrows, A., Hubeny, I., Budaj, J., & Hubbard, W. B. 2007, ApJ, 661, 502
Casali, M., Pirard, J.-F., Kissler-Patig, M., et al. 2006, SPIE, 6269, 29
Chambers, J. E. 1999, MNRAS, 304, 793
Charbonneau, D., Allen, L. E., Megeath, S. T., et al. 2005, ApJ, 626, 523
Charbonneau, D., Brown, T. M., Burrows, A., & Laughlin, G. 2007, Protostars and Planets V, ed. B. Reipurth, D. Jewitt, & K. Keill (Tucson: University of Arizona Press), 701
Claret, A. 2000, A&A, 363, 1081
Claret, A. 2004, A&A, 428, 1001
Deming, D., Richardson, L. J., & Harrington, J. 2007, MNRAS, 378, 148
De Mooij, E. J. W., & Snellen, I. A. G. 2009, A&A, 493, L35
Ferguson, J. W., Alexander, D. R., Allard, F., et al. 2005, ApJ, 623, 585
Ford, E. 2006, ApJ, 642, 505
Fortney, J. J., Marley, M. S., & Barnes, J. W. 2007, ApJ, 658, 1661
Fortney, J. J., Lodders, K., Marley, M. S., & Freedman, R. S. 2008, ApJ, 678, 1419
Gardner, J. P., Mather, J. C., Clampin, M., et al. 2006, Space Sci. Rev., 123, 485
Gillon, M., Pont, F., Moutou, C., et al. 2006, A&A, 459, 249
Gillon, M., Pont, F., Moutou, C., et al. 2007a, A&A, 466, 743
Gillon, M., Magain, P., Chantry, V., et al. 2007b, ASPC, 366, 113
Gillon, M., Smalley, B., Hebb, L., et al. 2009, A&A, 496, 259
Girardi, L., Bressan, A., Bertelli, G., & Chiosi, C. 2000, A&AS, 141, 371
Gelman, A., & Rubin, D. 1992, Stat. Sci., 7, 457
Gregory, P. C. 2005, ApJ, 631, 1198
Grevesse, N., & Noels, A. 1993, in La formation des éléments chimiques, AVCP, ed. B. Hauck, & S. R. D. Paltani
Holman, M. J., & Murray, N. W. 2005, Science, 307, 1288
Holman, M. J., Winn, J. N., Latham, D. W., et al. 2006, ApJ, 652, 1715
Ibgui, L., & Burrows, A. 2009, ApJ, 700, 1921
Iglesias, C. A., & Rogers, F. J. 1996, ApJ, 464, 943
Jackson, B., Greenberg, R., & Barnes, R. 2008a, ApJ, 681, 1631
Jackson, B., Greenberg, R., & Barnes, R. 2008b, ApJ, 681, 1631
Knutson, H. A., Charbonneau, D., Deming, D., & Richardson, L. J. 2007, PASP, 119, 616
Magain, P., Courbin, F., Gillon, M., et al. 2007, A&A, 461, 373
Mandel, K., & Agol, E. 2002, ApJ, 5802, L171
Mayor, M., Pepe, F., & Queloz, D. 2003, The Messenger, 114, 20
Nesvorný, D., & Morbidelli, A. 2008, ApJ, 688, 636
Pirard, J.-F., Kissler-Patig, M., Moorwood, A., et al. 2004, SPIE, 5492, 510
Richardson, L. J., Deming, D., & Seager, S. 2003a, ApJ, 597, 581
Richardson, L. J., Deming, D., Wiedemann, G., et al. 2003b, ApJ, 584, 1053
Rogers, F. J., & Nayfonov, A. 2002, ApJ, 576, 1064
Scuflaire, R., Théado, S., Montalbán, J., et al. 2008, APSS, 316, 83
Sing, D. K., & López-Morales, M. 2009, A&A, 493, L31
Snellen, I. A. G. 2005, MNRAS, 363, 211
Snellen, I. A. G., & Covino, E. 2007, MNRAS, 375, 307
Snellen, I. A. G., de Mooij, E. J. W., & Albrecht, S. 2009, Nature, 459, 543
Tegmark, M., Strauss, M. A., & Blanton, M. R. 2004, Phys. Rev. D., 69, 103501
Thoul, A., Bahcall, J. N., & Loeb, A. 1994, ApJ, 421, 828
Torres, G. 2007, ApJ, 671, L65
Werner, M. W., Roellig, T. L., & Low, F. J. 2004, ApJS, 154, 1
Winn, J. N. 2008, IAU 253, Transiting Planets, ed. F. Pont (Cambridge USA), 99
Winn, J. N., Holman, M. J., Shporer, A., et al. 2008, ApJ, 136, 267
Wrigth, J. T. 2005, PASP, 117, 657

2.5 Applications Using the Rossiter-McLaughlin Effect

So far, so good: it was possible to use the combined fitting tool in some extreme situations thus calling for a broader use. Originally it had been developed to adjust the Rossiter-McLaughlin effect over a photometric transit so as to reduce the total number of free parameters: each set would be controlling the other producing the best compromise possible.

A next step was therefore to continue testing the program and make it accepted in the literature and by the community has an accurate tool. The first test came by adjusting the newly published Rossiter-McLaughlin effect observed for HD 17156 b. The combined analysis allowed to present more conservative error bars on that tentative first detection of a misaligned effect (see section 2.3.1). Results were presented at the IAU symposium on transiting planets in Boston. Subsequent papers confirmed that the angle is not misaligned (Narita et al. 2009a) now something of a greater puzzle than if it was not aligned (see last chapter).

The first *real life* adjustment of a Rossiter-McLaughlin effect was made for CoRoT-2 b [9]:

2.5.1 The Rossiter-McLaughlin effect of CoRoT-2b

Shortly after my arrival in Genève, I was involved with the CoRoT space mission as well as the WASP follow-up. Because of the faintness of CoRoT targets it would be hard to obtain a Rossiter-McLaughlin effect out of them, except really for one target: CoRoT-2. CoRoT-2 b is a regular hot Jupiter orbiting a G7V star, but, unlike most solar type stars, this one rotates five to six times faster than the Sun, indicating a likely young age. The amplitude of the Rossiter-McLaughlin effect depends, on the ratio of radii $R_{\rm p}/R_\star$, but also scales roughly linearly with the $v_\star \sin I$ of the star. CoRoT-2's fast rotation made it a very interesting target to observe. Both the HARPS and SOPHIE spectrographs were used and both detected neatly a radial velocity anomaly at the time and with the shape expected of a Rossiter-McLaughlin effect.

My code being the only ready and able to fit with a single set of parameters the photometric transit, the radial velocity Doppler reflex motion and the Rossiter-McLaughlin effect, I was asked to make a fit which would be compared to another independent analysis. Within the $1\,\sigma$ error bar both analyses agreed.

This paper became my first related to the Rossiter-McLaughlin effect.

[9] then named CoRoT-Exo-2b

A&A 482, L25–L28 (2008)
DOI: 10.1051/0004-6361:200809433
© ESO 2008

Astronomy & Astrophysics

LETTER TO THE EDITOR

Transiting exoplanets from the CoRoT space mission

III. The spectroscopic transit of CoRoT-Exo-2b with SOPHIE and HARPS⋆

F. Bouchy[1], D. Queloz[2], M. Deleuil[3], B. Loeillet[1,3], A. P. Hatzes[4], S. Aigrain[5], R. Alonso[3], M. Auvergne[6], A. Baglin[6], P. Barge[3], W. Benz[7], P. Bordé[8], H. J. Deeg[9], R. De la Reza[10], R. Dvorak[11], A. Erikson[12], M. Fridlund[13], P. Gondoin[13], T. Guillot[14], G. Hébrard[1], L. Jorda[3], H. Lammer[15], A. Léger[8], A. Llebaria[3], P. Magain[16], M. Mayor[2], C. Moutou[3], M. Ollivier[8], M. Pätzold[17], F. Pepe[2], F. Pont[2], H. Rauer[12,19], D. Rouan[6], J. Schneider[18], A. H. M. J. Triaud[2], S. Udry[2], and G. Wuchterl[4]

(Affiliations can be found after the references)

Received 21 January 2008 / Accepted 6 March 2008

ABSTRACT

We report on the spectroscopic transit of the massive hot-Jupiter CoRoT-Exo-2b observed with the high-precision spectrographs SOPHIE and HARPS. By modeling the radial velocity anomaly occurring during the transit due to the Rossiter-McLaughlin (RM) effect, we determine the sky-projected angle between the stellar spin and the planetary orbital axis to be close to zero $\lambda = 7.2 \pm 4.5$ deg, and we secure the planetary nature of CoRoT-Exo-2b. We discuss the influence of the stellar activity on the RM modeling. Spectral analysis of the parent star from HARPS spectra are presented.

Key words. planetary systems – techniques: radial velocities

1. Introduction

Measurement of the spectroscopic signal during the transit of an exoplanet in front of its host star – known as the Rossiter-McLaughlin (RM) effect – provides an assessment the trajectory of the planet across the stellar disk and, more precisely, the sky-projected angle between the planetary orbital axis and the stellar rotation axis. This misalignment angle, denoted by λ, is a fundamental property of planetary systems that provides clues about the process of planet migration. Among the 30 transiting exoplanets known so far, λ has been reported for only 5 exoplanets (HD 209458b, Queloz et al. 2000; HD 189733b, Winn et al. 2006; HAT-P-2, Winn et al. 2007, Loeillet et al. 2008; HD 149026b, Wolf et al. 2007; and TrES-1, Narita et al. 2007). For all of these cases, λ is close to zero, as in the solar system, and the stellar rotation is prograde relative to the planet orbit. Such measurements should be extended to other transiting systems to understand whether this degree of alignment is typical.

The massive hot-Jupiter CoRoT-Exo-2b (Alonso et al. 2008) was revealed as planetary candidate by the CoRoT space mission (Baglin et al. 2003) and its planetary nature and mass was established thanks to ground-based facilities, including high-precision spectrographs SOPHIE (Bouchy et al. 2006) and HARPS (Mayor et al. 2003). This second CoRoT exoplanet is a 3.3 Jupiter-mass planet orbiting an active G7 dwarf star ($mv = 12.6$) every 1.743 days. We report here the measurements of the spectroscopic transit observed with both SOPHIE and HARPS spectrographs. These observations were made simultaneously with the space-based photometry with CoRoT. Such simultaneous monitoring is useful to assess anomalies in the transit parameters due to star spots or transient events.

Our data permits us to determine the sky-projected angle between the stellar spin and the planetary orbital axis, and it provids additional constraints on the orbital and physical parameters of the system. Furthermore, our data confirms and secures the planetary nature of the transiting body, excluding blending of an eclipsing binary with a third star as the cause of the observed shallow transits. We used HARPS spectra to perform the spectroscopic analysis of the parent star.

2. Observations

We performed high-precision radial velocity observations of CoRoT-Exo-2 ($mv = 12.6$) with the SOPHIE spectrograph, based on the 1.93-m OHP telescope (France), and the HARPS spectrograph, based on the 3.6-m ESO telescope (Chile). These two instruments are cross-dispersed, fiber-fed, echelle spectrographs dedicated to high-precision Doppler measurements based on the radial velocity techniques of simultaneous-thorium calibration. SOPHIE was used with its high efficiency mode (spectral resolution $R = 40\,000$). We reduced HARPS and SOPHIE data with the same pipeline based on the cross-correlation techniques (Baranne et al. 1996; Pepe et al. 2002). We observed CoRoT-Exo-2 with SOPHIE on 16 July 2007 and with HARPS on 1 September 2007. The exposure times were respectively 10 and 20 min on HARPS and SOPHIE corresponding to S/N per pixel at 550 nm of 16 and 25, respectively. We obtained the radial velocities by weighted cross-correlation with a numerical G2 mask constructed from the Sun spectrum atlas including up to 3645 lines. We eliminated the first 8 blue spectral orders

⋆ Observations made with SOPHIE spectrograph at Observatoire de Haute Provence, France (PNP.07A.MOUT) and HARPS spectrograph at ESO La Silla Observatory (079.C-0127(F)). The CoRoT space mission, launched on December 27th 2006, has been developed and is operated by CNES, with the contribution of Austria, Belgium, Brasil, ESA, Germany, and Spain.

Article published by EDP Sciences

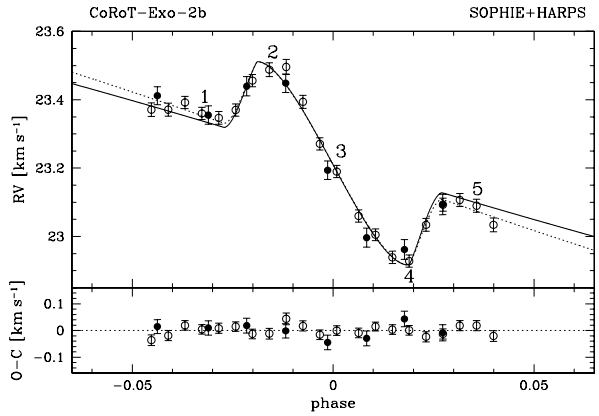


Fig. 1. Phase-folded radial velocity measurements of CoRoT-Exo-2 during the transit of the planet with SOPHIE (dark circle) and HARPS (open circle). The solid line corresponds to the Rossiter-McLaughlin model ajusted to these data assuming the semi-amplitude $K = 563$ m s^{-1} from Alonso et al. (2008). The dotted line corresponds to the Rossiter-McLaughlin model with K as free parameters.

containing only noise. Radial velocities are given in Table 1 and displayed in Fig. 1.

3. Rossiter-McLaughlin modeling

The RM effect corresponds to a distortion of the spectral lines observed during a planetary transit due to stellar rotation. The transiting body hides some of the velocity components that usually contribute to line broadening resulting in an Doppler-shift anomaly (see Otha et al. 2005; Giménez et al. 2006b; Gaudi & Winn 2007).

To model this RM effect, we used the analytical approach developed by Otha et al. (2005). The complete model has 12 parameters: the orbital period P; the mid-transit time T_c; the eccentricity e; the angle between the node and periastron ω; the RV semi-amplitude K; the velocity zero point V_0 (these first six are the standard orbital parameters); the radius ratio r_p/R_s; the orbital semi-major axis to stellar radius a/R_s (constrained by the transit duration); the sky-projected angle between the stellar spin axis and the planetary orbital axis λ; the sky-projected stellar rotational velocity $v \sin I$; the orbital inclination i; and the stellar limb-darkening coefficient ϵ. For our purpose, we started with the orbital parameters and photometric transit parameters as derived by Alonso et al. (2008). We fixed the linear limb-darkening coefficient $\epsilon = 0.78$, based on Claret (2004) tables for filter g' and for the stellar parameters derived in Sect. 4. Our free parameters are then λ and $v \sin I$. We introduced two additional parameters: the offset velocity of HARPS and SOPHIE, $\Delta_{\rm HARPS}$ and $\Delta_{\rm SOPHIE}$, which differ from V_0 due to the stellar activity. We determined the $v \sin I$ independently from SOPHIE cross-correlation functions (CCFs) to be 9.5 ± 1.0 km s^{-1} and from HARPS CCFs to be 10.7 ± 0.5 km s^{-1} with the calibration techniques described by Santos et al. (2002). However, we decided to leave it as free parameter in our fit.

The result of our fit, displayed in Fig. 1 and listed in Table 2, first shows that the stellar rotation is prograde relative to the planet orbit. During the first part of the transit the starlight is redshifted, indicating that the planet is in front of the approaching (blueshifted) half of the stellar disk. During the second part of transit, the sign is reversed as the planet moves to the receding (redshifted) half of the stellar disk. The sky-projected angle between the stellar spin axis and the planetary orbital axis λ is close to zero. The projected rotation velocity of the star $v \sin I$ determined by our RM fit (11.85 ± 0.5 km s^{-1}) seems slightly larger than our spectroscopic determination (2-σ greater). Previous studies by Winn et al. (2005) showed that the $v \sin I$ measured with Otha formulae was biased toward larger values by approximatively 10%. But, as already suggested by Loeillet et al. (2008), it may be due to the differential rotation of the star from equator to pole. Considering the exoplanet crosses the star near its equatorial plan, the fitted $v \sin I$ corresponds to the maximum value. Note that if we fix $v \sin I$ at the spectroscopic value, it does not change the value of the fitted λ angle.

We made the 2 epochs of RM observations at a minimum stellar flux (see Fig. 1 of Alonso et al. 2008), indicating that the stellar spots were at their maximum phase of visibility. Following the Saar & Donahue (1997) relation giving the expected RV jitter as a function of $v \sin I$ and spot filling factor, we found that CoRoT-Exo-2 is expected to present RV variations of up to 200 m s^{-1} peak-to-peak with a period of 4.5 days. The standard deviation of RV residuals (56 m s^{-1}) found by Alonso et al. (2008) is in agreement with this value. Such an activity-related RV variation should then change locally the apparent slope in the RV orbital curve. The maximum effect occurs at the maximum phase of stellar spot visibility, and should induce an apparent increase in the semi-amplitude K of up to 40 m s^{-1}. This explains why our fit in Fig. 1 is not perfect outside of the transit. If we increase K in our fit or leave it as a free parameter,

Table 1. Radial velocity measurements of CoRoT-Exo-2 obtained by HARPS and SOPHIE during the transit. BJD is the Barycentric Julian Date.

BJD −2 400 000	RV [km s^{-1}]	Uncertainty [km s^{-1}]
SOPHIE 2007-07-16		
54 298.4641	23.341	0.026
54 298.4862	23.285	0.027
54 298.5030	23.369	0.028
54 298.5198	23.378	0.027
54 298.5381	23.123	0.027
54 298.5550	22.926	0.028
54 298.5714	22.891	0.029
54 298.5879	23.023	0.030
HARPS 2007-09-01		
54 345.5225	23.371	0.020
54 345.5298	23.371	0.019
54 345.5371	23.392	0.018
54 345.5444	23.360	0.018
54 345.5517	23.347	0.019
54 345.5590	23.370	0.018
54 345.5663	23.456	0.018
54 345.5736	23.488	0.020
54 345.5809	23.496	0.022
54 345.5883	23.394	0.019
54 345.5956	23.271	0.018
54 345.6029	23.190	0.018
54 345.6124	23.060	0.018
54 345.6197	23.005	0.017
54 345.6270	22.939	0.018
54 345.6343	22.928	0.018
54 345.6417	23.034	0.019
54 345.6490	23.093	0.019
54 345.6563	23.107	0.019
54 345.6636	23.090	0.019
54 345.6709	23.034	0.020

Table 2. System parameters of CoRoT-Exo-2. The reduced χ^2 was computed assuming 24 degrees of freedom.

Fixed parameters from Alonso et al. (2008)	
P	1.7 429 964 days
T_c	54 237.53562
e	0.0
V_0	23.245 km s^{-1}
r_p/R_s	0.1667
a/R_s	6.70
i	87.84 deg
ϵ	0.78 (from Claret)
Adjusted parameters with K = 563 m s^{-1}	
$v \sin I$	11.85 ± 0.50 km s^{-1}
λ	7.2 ± 4.5 deg
Δ_{HARPS}	–21.5 ± 5 m s^{-1}
Δ_{SOPHIE}	+21.5 ± 12 m s^{-1}
reduced χ^2	1.43
Adjusted parameters with K as free parameter	
K	656 ± 27 m s^{-1}
$v \sin I$	11.25 ± 0.45 km s^{-1}
λ	5.0 ± 4.0 deg
Δ_{HARPS}	–25.0 ± 4.5 m s^{-1}
Δ_{SOPHIE}	+25.5 ± 11 m s^{-1}
reduced χ^2	1.01
Combined MCMC fit	
K	613 ± 14 m s^{-1}
$v \sin I$	$11.46^{+0.29}_{-0.44}$ km s^{-1}
λ	7.1 ± 5.0 deg
Δ_{HARPS}	–22.5 ± 4.5 m s^{-1}
Δ_{SOPHIE}	+23.5 ± 11 m s^{-1}
reduced χ^2	1.10

it significantly improves the fit and slightly decreases the value of $v \sin I$ and λ (see Table 2).

We also did a combined fitting of the photometry and the whole set of *RV* measurements. On each of the out-of-transit measurements, we inserted an additional error on the *RV* data to take the stellar activity into account. We chose this value as 56 m s^{-1}, corresponding to the standard deviation found by Alonso et al. (2008). This correction is justified since the action of activity on the points taken at random out-of-transit phases can be assumed as random for these points, while during transit we have sets of points with the same activity level throughout. The fitting was done using a Markov Chain Monte Carlo (MCMC) with a Metropolis-Hastings Algorithm for the decision process. We used the models of Giménez (2006a) and (2006b) for photometry and spectroscopic transits respectively. A quadratic law of limb darkening was used. For the photometry, we used the fitted parameters found by Alonso et al. (2008). For the spectroscopy parameters, we chose the *V*-band, from tables published by Claret (2000) for the stellar parameters derived in Sect. 4 ($u_+ = 0.748$, $u_- = 0.256$). The MCMC was performed over 20 000 accepted steps after 5000 steps of a burn-in period. The result of the combined fit is presented in Table 2, and is in full agreement with the other approachs.

The cross-correlation function (CCF) corresponds more or less to an average of all the spectral lines (see top of Fig. 2). In order to characterize the behavior of the spectral lines during the transit, we computed the difference between the HARPS CCFs corrected from the orbital velocity and a reference CCF taken out of the transit (more exactly an average of the 3 first exposures). This difference was computed at 5 epochs identified and labeled in Fig. 1 : (1) just before the ingress, (2) maximum of the *RM* effect, (3) mid-transit epoch, (4) minimum of the *RM* effect, (5) just after egress. These differences $\Delta CCF = CCF_{REF} - CCF_{\#}$

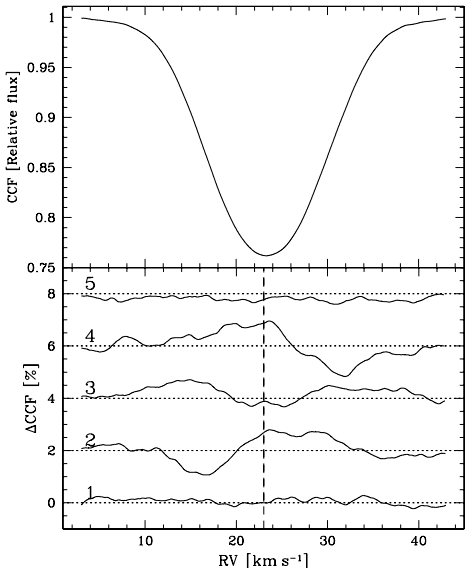


Fig. 2. (*Top*) Averaged cross-correlation function of CoRoT-Exo-2. (*Bottom*) Cross-correlation differences computed at 5 different epochs (see text) illustrating the behavior of the spectral lines during the transit.

are displayed in Fig. 2 and clearly show the spectroscopic anomaly shifting from the blue side (2) to the red side (4) of the CCF. During the transit, the depth or contrast of the CCFs is systematically larger, reflecting the renormalization effect of the CCF, which maintains a constant surface.

The observation of the spectroscopic transit of CoRoT-Exo-2b allows us to confirm definitively that the transiting candidate provided by CoRoT occurred at the central star (and not at a background star inside the CoRoT PSF). Furthermore, if we assume that the system is not diluted by an other star inside the HARPS or SOPHIE PSF, the RM anomaly reveals that the transiting body has a planetary size (from the RM anomaly amplitude) and planetary mass (from the *RV* slope outside the transit). In the case of an eclipsing binary whose light is diluted with a brighter third star, one should assume that the spectral lines of the fainter eclipsing binary move relative to the lines of the bright star and thus change the blended line-profiles. In such a configuration, one should consider not only the flux ratio but the $v \sin I$, velocity zero point, and spectral type of the two systems. In our present case, we did not find a configuration of a blended eclipsing binary that could simultaneously reproduce the *RV* anomaly and the photometric light curve. Furthermore, we computed *RV*s using different cross-correlation mask without significant changes in the shape and amplitude of the RM anomaly. We, thus, consider that the spectroscopic transit confirms and secures the planetary nature of the transiting body.

4. Spectroscopic analysis of CoRoT-Exo-2

We performed the spectroscopic analysis of the parent star using the HARPS spectra. We corrected individual spectra from the stellar velocity, rebinned to a constant wavelength step of 0.02 Å, and co-added spectral order per spectral order giving a S/N per pixel at 550 nm of about 80. We determined the effective temperature first from the analysis of the Hα line wings, providing a temperature of 5450 ± 120 K. In spite of the quite low S/N of the combined spectra, it appears that the star is at the border of the temperature domain in which the Hα line

wings are a good temperature indicator (from 5500 to 8500 K). We then checked this result with other methods. We performed synthetic spectra fitting using LTE MARCS atmosphere models (Gustafsson et al. 2005), which are well adapted for this range of temperature. We compared the synthetic spectra, previously convolved by the instrumental profile and a rotational profile with the $v \sin I$ value previously measured, to the observed one. The best-fit model yields a slightly higher temperature, but is still in agreement with the Hα estimate. Another analysis, using equivalent width measures of FeI and FeII lines, was also carried out and yields similar results. The adopted stellar parameters are $T_{\rm eff} = 5625 \pm 120$ K, $\log g = 4.3 \pm 0.2$ and [M/H] $= 0.0 \pm 0.1$, which correspond to a G7V type star with a solar metallicity. With these values, we derived the star's luminosity and mass with *StarEvolv* stellar evolution models (Siess 2006; Palacios, private communication). We combined these estimates of the star's mass to the $M_{\rm s}^{1/3}/R_{\rm s}$ value provided by the light curve analysis to derive the final star's mass and radius values in a consistent way between spectroscopic and photometric analyses. The method allows us to get rid of the large uncertainty that affects the estimate of the gravity and to take advantage of the excellent quality of the light curve. The method will be detailed in a forthcoming paper devoted to the fundamental parameters of the first CoRoT planet host stars, based on *UVES* spectra. The adopted stellar mass is $0.97 \pm 0.06\ M_{\odot}$ and the stellar radius is $0.90 \pm 0.02\ R_{\odot}$. Interestingly, the solar-like metallicity of the parent star and large radius of the planet is consistent with the trend that heavy element content in the planet and stellar metallicity are correlated (Guillot et al. 2006). According to stellar evolution models (Lebreton, private communication), the age of the star could be between 0.2 and 4 Gyr if the star is on the main sequence. However, the presence of the Li I absorption line and the strong emission line core in the CaII H and K lines, suggest that the star is still close the ZAMS and could be thus younger than 0.5 Gyr in full agreement with the observed stellar activity and the measured rotation period.

The knowledge of the main rotational period of CoRoT-Exo-2 determined from the light curve (4.54 days) and the spectroscopic $v \sin I$ determined from HARPS and SOPHIE CCFs (10.3 km s^{-1}) may be used to independently estimate the minimum radius of $R_s \sin I = 0.92\ R_{\odot}$ in very good agreement with our previous determination based on spectral classification. We note that this estimate, based on the well-determined stellar rotation thanks to the high-precision CoRoT light curve, does not depend on any spectral classification. On the other hand, if we assume the stellar radius from spectral analysis, we can deduce that $\sin I$ is close to 1, indicating a further constraint on the alignment of orbit and stellar spin.

5. Conclusions

In addition to the previous 5 transiting exoplanets where λ angle have been reported, CoRoT-Exo-2b presents a prograde orbit relative to the stellar rotation and an angle $\lambda = 7.2 \pm 4.5$ deg, close to zero. Our observations illustrate and demonstrate the capability of extending the reach of the RM technique to relatively-faint host stars ($mv \geq 12$) like the CoRoT targets even with a 2-m class telescope.

Acknowledgements. The authors wish to thank Xavier Bonfils and Gaspare Locurto for their precious help and support on HARPS observations. We are grateful for the OHP staff support at the 1.93-m telescope. The German CoRoT team (TLS and Univ. Cologne) acknowledges the support of DLR grants 50OW0603 and 50OW0204. F.B. acknowledges the support of PLS230371. H.J.D. acknowledges support by grants ESP2004-03855-C03-03 and ESP2007-65480-65480-C02-02 of the Spanish Education and Science ministry. The authors thank the referee for insightful comments and suggestions.

References

Alonso, R., Auvergne, M., Baglin, A., et al. 2008, A&A, 482, L21
Baglin, A., Auvergne, M., Boisnard, L., et al. 2006, in COSPAR, Plenary Meeting, 36th COSPAR Scientific Assembly, 36, 3749
Baranne, A., Queloz, D., Mayor, M., et al. 1994, A&AS, 119, 373
Bouchy, F., and the Sophie team 2006, in Tenth Anniversary of 51 Peg-b: Status of and prospects for hot Jupiter studies, ed. L. Arnold, F. Bouchy, & C. Moutou, 319
Claret, A. 2004, A&A, 428, 1001
Gaudi, B. S., & Winn, J. N. 2007, ApJ, 655, 550
Giménez, A. 2006a, A&A, 450, 1231
Giménez, A. 2006b, ApJ, 650, 408
Guillot, T., Santos, N. C., Pont, F., et al. 2006, A&A, 453, L21
Gustafsson, B., Asplund, M., Edvardsson, B., et al. 2005, IAU Symp. 228, ed. Francois & Primas (Cambridge University Press), 259
Loeillet, B., Shporer, A., Bouchy, F., et al. 2008, A&A, 481, 529
Mayor, M., Pepe, F., Queloz, D., et al. 2003, Messenger, 114, 20
Narita, N., Enya, K., Sato, B., et al. 2007, ApJ, 59, 763
Otha, Y., Taruya, A., & Suto, Y. 2005, ApJ, 622, 1118
Pepe, F., Mayor, M., Galland, F., et al. 2002, A&A, 388, 632
Queloz, D., Eggenberger, A., Mayor, M., et al. 2000, A&A, 359, L13
Saar, S. H., & Donahue, R. A. 1997, ApJ, 485, 319
Santos, N. C., Mayor, M., Naef, D., et al. 2002, A&A, 392, 215
Siess, L. 2006, A&A, 448, 717
Winn, J. N., Noyes, R. W., Holman, M. J., et al. 2005, ApJ, 631, 1215
Winn, J. N., Johnson, J. A., Marcy, G. W., et al. 2006, ApJ, 653, L69
Winn, J. N., Holman, M. J., Bakos, G. A., et al. 2007, ApJ, 665, L167
Wolf, A. S., Laughlin, G., Henry, G. W., et al. 2007, ApJ, 667, 549

[1] Institut d'Astrophysique de Paris, UMR7095 CNRS, Université Pierre & Marie Curie, 98bis Bd Arago, 75014 Paris, France
e-mail: bouchy@iap.fr
[2] Observatoire de Genève, Université de Genève, 51 Ch. des Maillettes, 1290 Sauverny, Switzerland
[3] Laboratoire d'Astrophysique de Marseille, CNRS UMR 6110, Traverse du Siphon, 13376 Marseille, France
[4] Thüringer Landessternwarte Tautenburg, Sternwarte 5, 07778 Tautenburg, Germany
[5] School of Physics, University of Exeter, Stocker Road, Exeter EX4 4QL, UK
[6] LESIA, CNRS UMR 8109, Observatoire de Paris, 5 place J. Janssen, 92195 Meudon Cedex, France
[7] Physikalisches Institut Universität Bern, Sidlerstrasse 5, 3012 Bern, Switzerland
[8] Institut d'Astrophysique Spatiale, Université Paris XI, 91405 Orsay, France
[9] Instituto de Astrofisica de Canarias, 38200 La Laguna, Tenerife, Spain
[10] Observatório Nacional, Rio de Janeiro, RJ, Brazil
[11] Institute for Astronomy, University of Vienna, Türkenschanzstr. 17, 1180 Vienna, Austria
[12] Institute of Planetary Research, DLR, Rutherfordstr. 2, 12489 Berlin, Germany
[13] Research and Scientific Support Department, European Space Agency, ESTEC, 2200 Noordwijk, The Netherlands
[14] Observatoire de la Côte d'Azur, Laboratoire Cassiopée, CNRS UMR 6202, BP 4229, 06304 Nice Cedex 4, France
[15] Space Research Institute, Austrian Academy of Sciences, Schmiedlstrasse 6, 8042 Graz, Austria
[16] Institut d'Astrophysique et de Géophysique, Université de Liège, Allée du 6 Août 17, Sart Tilman, Liège 1, Belgium
[17] Institute for Geophysics and Meteorology, Köln University, Albertus-Magnus-Platz, 50923 Cologne, Germany
[18] LUTH, Observatoire de Paris-Meudon, 5 place J. Janssen, 92195 Meudon Cedex, France
[19] Center for Astronomy and Astrophysics, TU Berlin, Hardenbergstr. 36, 10623 Berlin, Germany

2.5.2 Exploring the limits of fitting the Rossiter-McLaughlin effect

Testing on the code continued with the following paper. It presents two Rossiter-McLaughlin effects in two completely different regimes: on two stars: HD 189733 and CoRoT-3.

Three events had been observed for HD 189733 b and had remained unpublished. This star being the brightest transiting planet host, one could achieve high signal to noise measurements at a high cadence, both a requirement of a good observation of the Rossiter-McLaughlin effect. With this case we could test how the chain would be responding in a high precision environment.

One event had been observed for CoRoT-3 b. This object in one of those for which it is unclear whether they are a Brown Dwarf, or a very massive planet[10]. Observing spectroscopically the transit for this object was testing observations at a low signal to noise and low cadence, but also for an extreme object.

The results showed a slight misalignment in the case of CoRoT-3 b, something which ought to be checked by renewed observations. Later work on Brown Dwarfs and eclipsing M Dwarfs showed those massive bodies tend to be very rarely misaligned (Triaud et al, in prep). The lack of observations prior to the transit allows some freedom to the fit and makes the results sensitive to individual points. Furthermore, to reach a sufficient signal to noise, exposures were quite long and thus blurred the effect. My code does not take that blurring into account, something which I have been thinking about doing for a while now. This may bias the determination of β as an uneven sampling would appear as an asymmetry. The effect itself is well detected: the high rotation of the star makes it very large.

Results on HD 189733 were interesting as they showed a residual effect, reproduced for each of the observed events. After some work and the construction of a model, it was found out that the way the radial velocities are extracted (by comparing a Gaussian to the CCF) was showing its limits. With a planet hiding part of the stellar surface, some of the velocity space is missing in the CCF: we resolve the transiting planet in velocity space. The CCF no longer being a Gaussian, fitting with one is no longer appropriate. In addition to non flat residuals, it also forces the fit to overestimate $V \sin I$.

Pushing the analysis further it was estimated that only in the case of very high data precision and in the case of fast rotators would this effect be detectable. Also, we concluded that being a low order deviation from the model and symmetrical in shape, it would not affect estimates of the spin-orbit angle. This was confirmed analytically by Hirano et al. (2010).

This production became the first paper for which I conducted the analysis entirely.

[10] if there is a difference, the debate rages

A&A 506, 377–384 (2009)
DOI: 10.1051/0004-6361/200911897
© ESO 2009

The CoRoT space mission: early results

Astronomy & Astrophysics
Special feature

The Rossiter-McLaughlin effect of CoRoT-3b and HD 189733b⋆,⋆⋆

A. H. M. J. Triaud[1], D. Queloz[1], F. Bouchy[2,3], C. Moutou[4], A. C. Cameron[5], A. Claret[6], P. Barge[4], W. Benz[7], M. Deleuil[4], T. Guillot[8], G. Hébrard[2], A. Lecavelier des Étangs[2], C. Lovis[1], M. Mayor[1], F. Pepe[1], and S. Udry[1]

[1] Observatoire de l'Université de Genève, Chemin des Maillettes 51, 1290 Sauverny, Switzerland
e-mail: Amaury.Triaud@unige.ch
[2] Institut d'Astrophysique de Paris, CNRS UMR 7095, Université Pierre & Marie Curie, 98bis boulevard Arago, 75014 Paris, France
[3] Observatoire de Haute-Provence, CNRS USR 2207, 04879 St Michel de l'Observatoire, France
[4] Laboratoire d'Astrophysique de Marseille, CNRS UMR 6110, Traverse du Siphon, 13376 Marseille, France
[5] School of Physics & Astronomy, University of St Andrews, North Haugh, KY16 9SS, St Andrews, Fife, Scotland, UK
[6] Instituto de Astrofísica de Andalucía, CSIC, Apartado 3004, 18080 Granada, Spain
[7] Physikalisches Institut Universität Bern, Sidlerstrasse 5, 3012 Bern, Switzerland
[8] Observatoire de la Côte d'Azur, Laboratoire Cassiopée, CNRS UMR 6202, BP 4229, 06304 Nice Cedex 4, France

Received 20 February 2009 / Accepted 5 July 2009

ABSTRACT

We present radial-velocity sequences acquired during three transits of the exoplanet HD 189733b and one transit of CoRoT-3b. We applied a combined Markov-chain Monte-Carlo analysis of spectroscopic and photometric data on these stars, to determine a full set of system parameters including the projected spin-orbit misalignment angle of HD 189733b to an unprecedented precision via the Rossiter-McLaughlin effect: $\beta = 0.85^{\circ}{}^{+0.32}_{-0.28}$. This small but non-zero inclination of the planetary orbit is important to understand the origin of the system. On CoRoT-3b, results seem to point towards a non-zero inclination as well with $\beta = 37.6^{\circ}{}^{+10.0}_{-22.3}$, but this remains marginal. Systematic effects due to non-Gaussian cross-correlation functions appear to be the main cause of significant residuals that prevent an accurate determination of the projected stellar rotation velocity $V \sin(I)$ for both stars.

Key words. binaries: eclipsing – techniques: photometric – techniques: radial velocities – planetary systems – stars: individual: CoRoT-3b, HD 189733

1. Introduction

The spectroscopic transit, also known as the Rossiter-McLaughlin (RM) effect (Rossiter 1924; McLaughlin 1924), is a radial velocity (RV) anomaly superimposed on the radial-velocity curve arising from the Keplerian reflex orbit of the host star about its common centre of mass with a planet. As the planet transits, it covers – in the case of a prograde orbit – first the blue shifted part of the rotating star, shifting the overall spectrum slightly to the red. As the planet moves across the stellar disc, the radial velocity of the star's light centroid changes rapidly. The first RM effect caused by a transiting planet was observed on HD 209458 by Queloz et al. (2000). In addition to the standard information that a photometric transit brings us, the RM effect permits us to measure the $V \sin(I)$[1] of the star and is the only way to estimate the projected spin-orbit obliquity angle β (Giménez 2006b; Hosokawa 1953) (equal to $-\lambda$ Ohta et al. 2005). This angle reflects the history of the planet and can therefore be used to constrain models of planetary orbital evolution.

HD 189733 is a most interesting target due to its brightness and the possibility of observing it from both hemispheres fairly easily, while CoRoT-3b, orbiting a very fast rotating star and being itself in the middle of the Brown Dwarf desert (Deleuil et al. 2008) (D08), is a unique object to study. Also, HD 189733b has been extensively studied (Bouchy et al. 2005; Winn et al. 2006 (W06); Winn et al. 2007 (W07); Boisse et al. 2009 (B09)). The present paper is motivated by our recent acquisition of high-precision data - photometric for CoRoT-3, photometric and spectroscopic for HD 189733. Combining spectroscopic and photometric transits in one analysis allows us to refine the transit parameters, but also to ensure that the $V \sin(I)$ of the star and the spin-orbit angle β, which are solely extracted from the RM effect, are tightly constrained. This is especially effective when analysing high precision data ; thus we use the high precision obtained on HD 189733 and present this star as a test-case for combining data sets.

We describe the observations of these stars in Sect. 2, then move to a description of the fitting process and its results with Sect. 3 and explore a few reasons to explain the observed residuals that we obtained in Sect. 4. Finally we will discuss the results and conclude.

⋆ Using observations with the *Harps* spectrograph from the ESO 3.6 m installed at La Silla, Chile, under the allocated programmes 072.C-0488(E) and 079.C-0828(A). The data is publicly available in electronic form at the CDS.

⋆⋆ Tables 3 and 4 are only available in electronic form at http://www.aanda.org

[1] We used the Ohta et al. (2005) notation differentiating the $V \sin(i)$ to the $V \sin(I)$. i is the projected inclination of the planet's orbit on the sky, whereas I is the projected inclination of the stellar equator on the sky.

2. The observations

The observations were acquired using the High Resolution échelle spectrograph *Harps* mounted on the 3.6 m at the ESO observatory of La Silla, in Chile. The data were extracted using the Data Reduction Software present at the telescope. A reanalysis of the data was performed later in Geneva, using the latest version of the software as in Mayor et al. (2009).

One sequence of 11 *Harps* RV measurements in addition to those in the discovery paper (D08) was obtained on CoRoT-3 on August 26th 2008 as part of the spectroscopic follow-up (072.C-0488(E)); all are around the transit. On average the new data has an estimated photon noise of 28.4 m s^{-1} (Table 3).

Four sequences were taken of HD 189733 on July 30th, August 4th and September 8th 2006, and on August 29th 2007 under the allocated programme 079.C-0828(A) and as part of the GTO, three of which are during transit. One sequence was taken off-transit to act as a comparison sequence. Out of the three RM sequences, two were obtained using a low cadence (one point every 10.5 min). One of these suffered from bad weather and one was taken with a high cadence (one point every 5.5 min). In total we have 78 new RV measurements including 37 during transit. The mean estimated uncertainty in the radial velocities due to photon noise is 0.98 m s^{-1} (Table 4).

3. Fitting the data

Transiting planets have an important role to play in constraining planetary evolution models as well as atmosphere and interior models, therefore it is important that everything is done to ensure that information extracted from the data is accurate. Both spectroscopic and photometric effects can be observed on a star experiencing a planetary transit. The two types of observation constrain parameters differently but arise from the same cause. Hence it is logical to fit both types of data simultaneously to determine a single set of parameters for the planet and ensure full consistency between the models.

3.1. the modelling

A code was developed using full Bayesian statistics in a Markov Chain Monte-Carlo (MCMC). The code is similar to the one described in Collier Cameron et al. (2007) and has already been used (Gillon et al. 2008; Bouchy et al. 2008). The philosophy here is to combine everything that is known about each star into the fitting process to better constrain the final result. So far, the periodic Doppler shift caused by the planet, the RM effect and a drift can be fitted to the spectroscopy. For the photometry, requiring data stripped of instrumental or stellar effects, primary and secondary transits can be fitted. Limb darkening coefficients can also be allowed to float if data of very high photometric precision are available.

The present version of the code fits up to 12 free parameters: the depth of the primary transit D, the RV semi-amplitude K, the impact parameter b, the transit width W, the period P, the middle of transit T_0, $e\cos(\omega_0)$ and $e\sin(\omega_0)$ (with e being the eccentricity and ω_0 the angle between the line of sight and the periastron), $V\sin(I)\cos(\beta)$ and $V\sin(I)\sin(\beta)$, the RV drift Γ and the secondary transit depth D_2. If some parameters are irrelevant, they can be fixed. These parameters have been chosen to reduce correlations and increase the exploration of parameter space.

At each step i of the Markov chain, one set of j parameters is calculated from the previously accepted value $(i-1)$ following:

$$P_{i,j} = P_{i-1,j} + f\sigma_{P_j} G(0,1) \quad (1)$$

where P_j is a parameter, σ_{P_j} is the 1σ uncertainty, f is a factor ensuring 25% of steps are being accepted (see Tegmark et al. 2004) and $G(0,1)$ is a random Gaussian number centred on zero with a standard deviation equal to 1. From these parameters a large variety of other – more physical – values can be inferred such as the stellar density $\rho_\star$ (see Table 1).

The parameters are then used to calculate three different models. Both primary and secondary transit are calculated by using either codes developed by Mandel & Agol (2002), or by Giménez (2006a). The RV curve is modelled by the standard orbital equations (Mayor & Queloz 1995; Hilditch 2001) and by the code presented in Giménez (2006b) for the RM effect. To model the stellar limb darkening, we use the quadratic law (Claret 2000). The model and the data are compared using a χ^2 statistics.

χ^2 from the photometry is added to the value found for the spectroscopy. On that value Bayesian penalties are added. These can be estimated for every parameter for which we have independent prior knowledge of their value and error. The stellar mass $M_\star$ is allowed to vary subject to a Bayesian penalty on a value and its 1σ error bar. All added, it creates a merit function:

$$Q_i = \chi^2_i + \frac{(M_{\star_i} - M_{\star_0})^2}{\sigma^2_{M_\star}} + \sum_{j=1}^{P} \frac{(P_{i,j} - P_{0,j})^2}{\sigma^2_{P_j}} \quad (2)$$

where here, P_j can be any parameter, fitted or physical and $P_{0,j}$ is the value of the prior as $M_\star$ is the floating parameter for stellar mass and $M_{\star_0}$ is the prior on the mass.

This Q_i is compared to the Q_{i-1}, value calculated from the previous set of parameters, with the Metropolis-Hasting algorithm. This is repeated as many times as is necessary to ensure that the fitting has converged and that the exploration of parameter space around the best value is truly random (meaning that the correlation length for each parameter is small compared to the number of accepted steps) and gives credible error bars.

Obviously in addition to all these parameters, we also have to add one γ velocity for each RV set and one normalisation constant for each photometric set; they are estimated by optimal averaging and optimal scaling in χ^2 calculations. The γ velocity reflects the mean radial velocity due to the motion of the star in comparison to the Sun; its measured value varies with activity levels and between instruments by a small offset. The normalisation factors re-estimate the normalisation of the lightcurves. The best fit parameters are chosen to be the set with the lowest χ^2 and the error bars are calculated by taking the 68.3% lowest values of χ^2 and finding their extremes.

3.2. the results

One chain of 500 000 accepted steps was calculated for each star. Results for both stars appear in Table 1. The corresponding fits are displayed in Figs. 1 and 2.

3.2.1. CoRoT-3b

Nine free parameters, four γ velocities and one photometric normalisation factor were used for CoRoT-3b to fit four RV sequences totalling 29 measurements and one sequence of photometry – the binned and phase folded data from D08 – with

Table 1. Fitted and physical parameters found after fitting photometric and spectroscopic data of CoRoT-3b and of HD 189733b.

Parameters (units)	CoRoT-3b	HD 189733b
Fitted parameters		
D	$0.004398^{+0.000084}_{-0.000091}$	$0.0200^{+0.00015}_{-0.00017}$
K (m s^{-1})	$2169.9^{+35.1}_{-22.7}$	$201.96^{+1.07}_{-0.63}$
b ($R_\star$)	$0.54^{+0.041}_{-0.081}$	$0.6873^{+0.0047}_{-0.0078}$
W (days)	$0.1566^{+0.0012}_{-0.0014}$	$0.07527^{+0.00020}_{-0.00037}$
P (days)	$4.2567994^{+0.0000039}_{-0.0000031}$	$2.21857312^{+0.00000036}_{-0.00000076}$
T_0 (bjd)	$54283.13388^{+0.00026}_{-0.00022}$	$53988.80339^{+0.000072}_{-0.000039}$
$e\ \cos(\omega_0)$	$-0.0083^{+0.0054}_{-0.0041}$	$0.0038^{+0.0020}_{-0.0020}$
$e\ \sin(\omega_0)$	$0.000^{+0.021}_{-0.020}$	$-0.0017^{+0.0024}_{-0.0034}$
$V\ \sin(I)\ \cos(\beta)$	$28.4^{+6.5}_{-5.6}$	$3.316^{+0.017}_{-0.068}$
$V\ \sin(I)\ \sin(\beta)$	$21.9^{+8.3}_{-14.1}$	$0.049^{+0.018}_{-0.017}$
Γ (m s^{-1} yr^{-1})	–	$-0.2^{+2.7}_{-3.9}$
Derived parameters		
$R_p/R_\star$	$0.06632^{+0.00063}_{-0.00069}$	$0.15812^{+0.00046}_{-0.00052}$
$R_\star/a$	$0.1257^{+0.0057}_{-0.0064}$	$0.1142^{+0.0006}_{-0.0012}$
$\rho_\star$ ($\rho_\odot$)	$0.372^{+0.064}_{-0.047}$	$1.831^{+0.059}_{-0.029}$
$R_\star$ ($R_\odot$)	$1.540^{0.083}_{0.078}$	$0.766^{+0.007}_{-0.013}$
$M_\star$ ($M_\odot$)	$1.359^{+0.059}_{-0.043}$	$0.823^{+0.022}_{-0.029}$
$V\ \sin(I)$ (km s^{-1})	$35.8^{+8.2}_{-8.3}$	$3.316^{+0.017}_{-0.067}$
R_p/a	$0.00834^{+0.00042}_{-0.00050}$	$0.01805^{+0.00011}_{-0.00025}$
R_p (R_J)	$0.9934^{+0.058}_{-0.058}$	$1.178^{+0.016}_{-0.023}$
M_p (M_J)	$21.23^{+0.82}_{-0.59}$	$1.138^{+0.022}_{-0.025}$
a (AU)	$0.05694^{+0.00096}_{-0.00079}$	$0.03120^{+0.00027}_{-0.00037}$
i (°)	$86.10^{+0.73}_{-0.52}$	$85.508^{+0.10}_{-0.05}$
e	$0.008^{+0.015}_{-0.005}$	$0.0041^{+0.0025}_{-0.0020}$
ω_0 (°)	179^{+170}_{-170}	$-24.1^{+33.9}_{-34.5}$
β (°)	$37.6^{+10.0}_{-22.3}$	$0.85^{+0.28}_{-0.32}$
γ *Velocities* (m s^{-1})		
Sophie	–56182.46	–2273.59
TLS	–56652.08	
Keck	–	–15.84
Harps	–56156.08	–2161.14
Harps (RM)	–56160.84	–2191.92
	–	–2225.44
	–	–2204.07
Normalisation factors		
CoRoT	0.9999998	–
FLWO 1.2 m z-band	–	0.99974
T10 (b + y)/2 band	–	0.99977
MAGNUM 2 m V-band	–	0.99979
Wise 1 m I-band	–	0.99977
$\chi^2_{\rm reduced}$	1.17 ± 0.08	1.21 ± 0.03

The reduced χ^2 were calculated with 414 degrees of freedom for CoRoT-3b and 2890 for HD 189773b.
Nota Bene: $\beta = -\lambda$; β is used since the first reference of a projected spin-orbit angle was named thus, in Hosokawa (1953). $V\ \sin(I)$s are probably overestimated, see Sect. 4 for details.

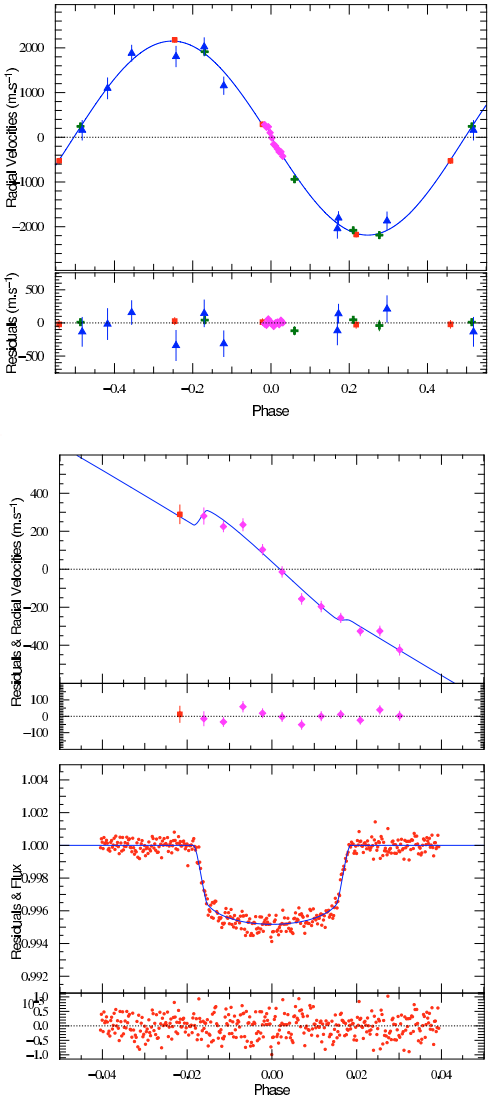


Fig. 1. *Top*: overall Keplerian fit of the RV data for CoRoT-3b. *Bottom*: composite plot showing both the spectroscopic and the photometric transit for CoRoT-3b. *(red) squares* are *Harps* measurement which are not part of the RM sequence, *(green) crosses* are *Sophie* measurements, *(blue) triangles* show *TLS* data and *(magenta) diamonds* indicate the RM *Harps* sequence; *(red) circles* are for the CoRoT photometry.

400 points in it. This amounts to 414 degrees of freedom. Results between this last paper and the present analysis are not very different. The transit spectroscopic sequence covers little outside the RV anomaly of the RM effect and due to the faintness of the star and poor sampling during the transit, $V\ \sin(I)$ and β are not well defined. $V\ \sin(I)$ is found abnormally large at 35 ± 8 km s^{-1} (see Sect. 4.3); β is different from zero only at the 2σ level.

Bayesian penalties were imposed for priors on the stellar mass $M_{\star_0} = 1.37 \pm 0.09\,M_\odot$ and also for the period $P_0 = 4.25680 \pm 0.000005$ days because we made use of an already folded lightcurve as the data from D08 was released, rather than individual transits; the RM effect was not strong enough to constrain P. T_0 was allowed to float and is found to differ from the published value of 54 283.1383 ± 0.0003. This is possibly an

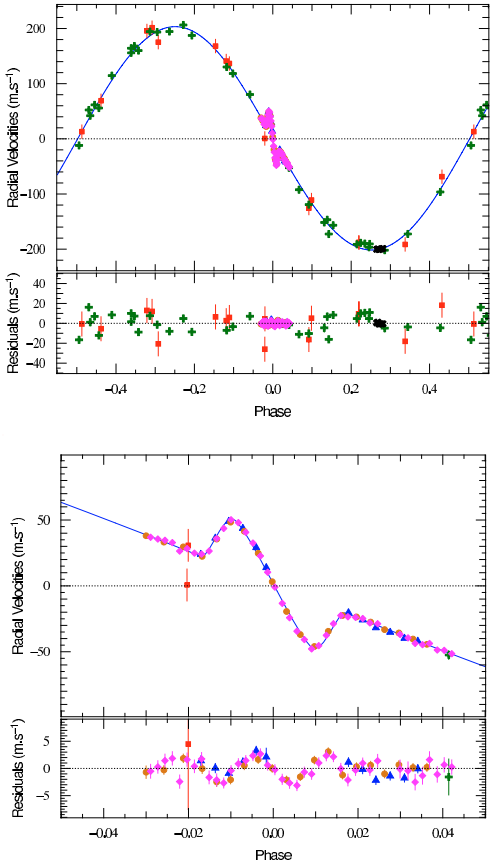


Fig. 2. *Top*: Overall Keplerian fit of the RV data for HD 189733b. *Bottom*: RM effect on HD 189733. *(red) squares* shows *Keck* data from W06, *(green) crosses* are *Sophie* data from B09, *(blue) triangles*, *(orange) circles*, *(magenta) diamonds* are the new three *Harps* sequences on the RM effect and *(black) oblique crosses* show the off transit *Harps* sequence. Residuals are displayed below and show a clear correlated signal during the transit.

artefact due to using a folded lightcurve. The RM sequence also suffers from a lack of *continuum* on either side of the transit. We employed the same limb darkening coefficients as D08.

Our initial fit had a Bayesian penalty on the $V \sin(I)$ for the value of $17 \pm 1\,\mathrm{km\,s^{-1}}$ published in D08. Removing the penalty allowed us to find the current value of $35 \pm 8\,\mathrm{km\,s^{-1}}$ and permitted a minimisation of χ^2 on the spectroscopy. See Table 2 where we show that having a $V \sin(I) = 35\,\mathrm{km\,s^{-1}}$ and a $\beta = 37.6°$ is a significant improvement of the model compared to an aligned system with the spectral analysis value of $V \sin(I) = 17\,\mathrm{km\,s^{-1}}$ (because of a difference in P and T_0 we also show results using parameters found by D08).

We have 11 RV data points and three free parameters here (one γ velocity, $V \sin(I)$ and β) making the total number of degrees of freedom eight. Thanks to the photometry, we have a secured detection of the planetary transit and of the Keplerian orbit and hence have a 100% chance that the RM effect will occur. It is only a matter of $V \sin(I)$ being different from zero. We obtain a $\chi^2_{\mathrm{reduced}} = 1.575$ just for the RM effect which has to be compared with a $\chi^2_{\mathrm{reduced}} = 5.962$ if we adjust with a $V \sin(I) = 0$. Hence, there is a clear detection of an RV deviation from the Keplerian orbit at the location of the RM effect.

Table 2. Comparing χ^2 for various solutions proposed for CoRoT-3b.

χ^2	P, T_0	$V \sin(I)\,(\mathrm{km\,s^{-1}})$	$\beta\,(°)$
12.6 ± 5.0	this paper	35	37.6
24.1 ± 6.9	this paper	17	0
47.7 ± 9.8	this paper	0	0
14.0 ± 5.3	D08	35	37.6
23.2 ± 6.8	D08	17	0
47.7 ± 9.8	D08	0	0

3.2.2. HD 189733b

A total of 127 RV measurements were used for the fit including those published in B09 and W06 outside of the RM region. The RM effect in W06 is not used here. The RV data were fitted along with 2735 photometric points representing data from four transits in the z, $(b+y)/2$, V and I bands from W07. Compared to CoRoT-3b, 11 parameters were allowed to float, adding a drift Γ and P, plus two γ velocities and three photometric normalisation factors more. This gives 2890 degrees of freedom.

We applied a Bayesian penalty on $M_\star$ alone, with the value $0.82 \pm 0.03\,M_\odot$ (Bouchy et al. 2005), i.e. using a Q_i from Eq. (2) with the two first terms only. We obtain very good constraints on P and T_0 to a similar order of magnitude compared to Agol et al. (2008) who used five *Spitzer* transits and four secondary transits. Most notable is the precision on the spin-orbit angle $\beta = 0.85^{\circ\,+0.32}_{-0.28}$, a 99.92% ($3\sigma$) confident detection (W06 had found $\beta = 1.4° \pm 1.1$). This value is found by comparing χ^2 with the value obtained by fixing $\beta = 0$ and calculating the probability that indeed χ^2 was improved.

HD 189733 is known to be active (Bouchy et al. 2005), and stellar activity (stellar spots) causes changes in RV. Because the activity is acting on a timescale of the order of the rotational period, each of the four *Harps* sequences are expected to have no jitter related to stellar activity. But, the sequences were taken at different epochs, therefore at different activity levels. This is why each of the four sequences is fitted with its own γ velocity. The change in γ velocity of $33.5\,\mathrm{m\,s^{-1}}$ is consistent with activity levels found by W06 and by B09.

The results on HD 189733 confirm it is an exceptional target against which to test the models, fitting techniques and data extraction.

4. Residual analysis

It is clear when looking at the residuals of HD 189733b's RM effect that a systematic error is present. The rms of points within transit is 57% larger than outside and their dispersion is correlated the same way for all three sequences. We also note that the residuals have a form very similar to those found by W06 (see Fig. 1 of that paper).

On CoRoT-3 the rms is comparable to the mean error bar outside and inside the transit indicating a good fit of the RV anomaly caused by the RM effect.

For both stars we find $V \sin(I)$ values larger than those present in the literature and found by an analysis of the spectral lines. For HD 189733, we have a 10% difference (or 2σ from the accepted value); for CoRoT-3, the value found is twice that which is inferred from spectral line analysis. We considered several possible causes of the effect observed in the residuals of HD 189733b and the large $V \sin(I)$ found on both stars.

4.1. limb darkening

We assumed that *Harps* was centred on the V band and limb darkening coefficients were chosen accordingly. The *Harps* spectral response was used to determine a new table of coefficients in the manner described in Claret (2000). The difference between those newly found coefficients was small: $u_a = 0.6454$ instead of 0.6355 and $u_b = 0.1375$ instead of 0.1488. χ^2, for just the three HD 189773b RM *Harps* sequences, passed from 213 to 206 ± 20, consistent with no change at all. The shape in the residuals was not altered; this difference in limb darkening coefficients cannot explain the problem.

Limb darkening being less well constrained near the limbs than at centre of the star, we omitted observations taken during ingress and egress, and re-fitted the RM effect. This tested whether the limb-darkening law itself could be causing the problem. The fit was no better, the shape in the residuals was still present, ruling out this possibility as well.

4.2. differential rotation

The Sun exhibits surface differential rotation as a function of latitude. It is reasonable to assume that other solar like stars rotate differentially. The change in apparent rotational velocity for HD 189733b, thanks to a misaligned orbital angle and by taking a value of differential rotation to be 10% between the stellar poles and the equator, affects the amplitude of the RM effect very little:

$$\Delta V \sin(I) = 0.3\,\mathrm{km\,s^{-1}} . \Delta R_\star \tag{3}$$

$$\delta h \simeq |2 . \sqrt{1 - (b . \cos \beta)^2} . \tan \beta | = 0.0218\, R_\star \tag{4}$$

$$\delta V \sin(I) = \Delta V \sin(I) . \delta h = 0.0065\,\mathrm{km\,s^{-1}} \tag{5}$$

with h the altitude of the planet's path above the stellar equator, projected onto the star (see Fig. 3). The value is an order of magnitude lower than our error bars.

It would also be expected to have an effect similar to a non zero spin-orbit angle: a difference in the amplitude on either side. Here the residuals are symmetric with respect to the centre of the transit. This said, with the level of precision now obtained on the spin-orbit angle of HD 189733b, it would be interesting to see how much of the β value is due to differential rotation, but this analysis goes beyond the scope of this paper. It can be emphasised here that thanks to misaligned planets and in conjonction with more precise observations the Rossiter-McLaughlin effect will allow to detect differential rotation on stars without needing the spots that are used at the moment by Doppler tomography on stars like AB Dor.

4.3. a systematic effect in the data reduction

Winn et al. (2005) (W05) pointed out that by fitting a symmetric Gaussian to a – by definition – non symmetric and varying cross correlation function (CCF) of the spectra in order to find the RVs and comparing these with a model which takes the centroid of the velocity weighted by the light emitted, we introduce a systematic error. The RV amplitude based on the symmetric Gaussian fit would be larger than that which a model with the same parameters would create. W05 tried to correct this effect by adding a polynomial on the RM model. This action was repeated on W06 and subsequent papers.

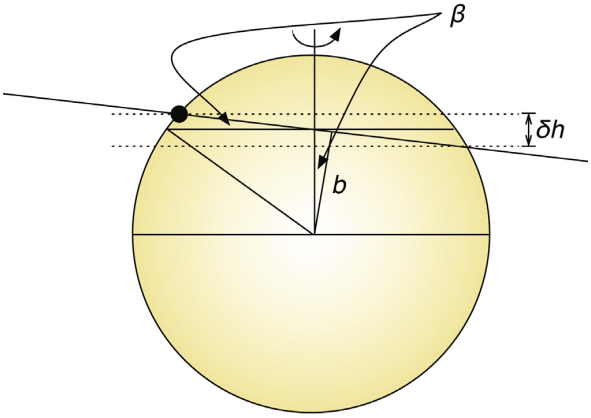


Fig. 3. Problem geometry and parameters used in equations present in Sect. 4.2.

In W05, it was not shown what effect such a misuse of the model would have on the fit. Thus, we created two models: one would act as the theoretical RM model does (Ohta's or Gimenez's), the other recreates the way the spectroscopic data is affected by the transiting planet, and the way the RVs composing the RM sequences are extracted.

We created a grid on a star. Each element of the grid had two pieces of information on it: its intensity (taking limb darkening into account) and its apparent velocity on the line of sight. For the theoretical model, a planet was passed with similar characteristics as the two planets studied in this paper and the centroid of velocity weighted by the light was found for each position thereby recreating the RM effect. For the simulated data, a planet was also passed and a CCF of the star minus the contribution hidden by the planet was generated for each position assuming a Gaussian spectral line for each point on the star. A Gaussian function was fitted to that CCF and its minimum was taken as the simulated RV measurement.

A comparison of the simulated data and the theoretical model showed what W05 had demonstrated: that the simulated data, using the same parameters, has a higher amplitude than the model predicts (see Fig. 4). Now, we want to see what a fit of that data would create. All transit parameters are heavily constrained by the photometry save the spin-orbit angle and the $V \sin(I)$. Assuming a β of zero we determined what would happen if only $V \sin(I)$ was varying.

On HD 189733, our test-case, by changing the $V \sin(I)$ value of the simulated data and comparing it to a model using the found value of $3.30\,\mathrm{km\,s^{-1}}$ (see Table 1), we achieved a very good agreement when $V \sin(I) = 3.05\,\mathrm{km\,s^{-1}}$. By subtracting one from the other, we obtained the theoretical residuals expected for a fit such as that produced by the MCMC. The observed residuals from Fig. 2 were added on the graph (Fig. 4) and showed a match, therefore indicating that a likely reason was found for these residuals.

The error bars presented in Table 1 seem to exclude such a large difference on $V \sin(I)$ at first sight, but it must be remembered that error bars depend on the model used; if the a priori is wrong, then the a posteriori must be too. The presence of similar residuals in Fig. 1 of W06 shows that not everything is corrected with their method. Nevertheless, the value of $V \sin(I)$ ($2.97 \pm 0.20\,\mathrm{km\,s^{-1}}$) is similar to what this study infers showing the method developed by W06 is a good tool to estimate $V \sin(I)$.

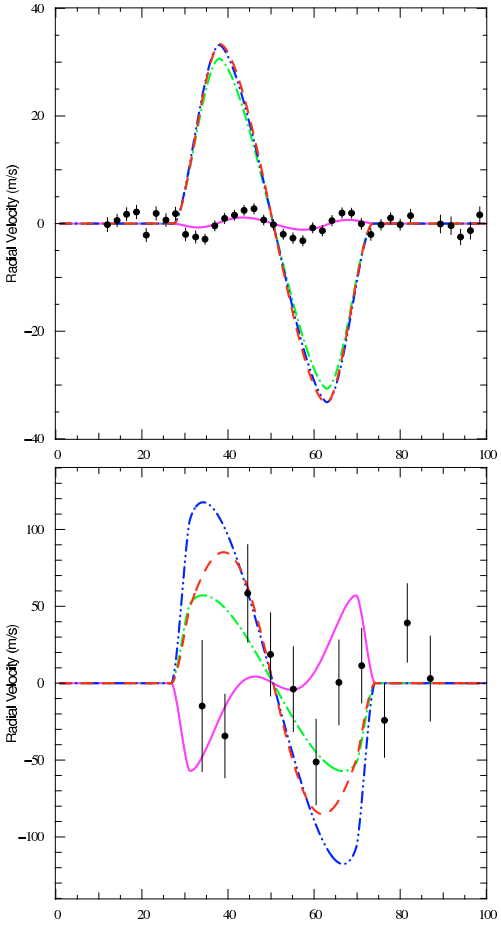


Fig. 4. *Top*: For HD 189733: *dash (red)* is the simulated spectroscopic data with $V\sin(I) = 3.05\,\mathrm{km\,s^{-1}}$; *dash double dot (blue)* is a RM model with $V\sin(I) = 3.30\,\mathrm{km\,s^{-1}}$; *dash dot (green)* is the same model for a $V\sin(I) = 3.05\,\mathrm{km\,s^{-1}}$; *solid (magenta)* is representing the residuals expected by subtracting the RM model by the simulated data; in *(black) points*, a sequence of residuals from Fig. 2 with *Harps*. These residuals are reproduced! *Bottom*: For CoRoT-3b: *dash (red)* is the simulated spectroscopic data with $V\sin(I) = 17\,\mathrm{km\,s^{-1}}$; *dash double dot (blue)* is a RM model with $V\sin(I) = 35\,\mathrm{km\,s^{-1}}$; *dash dot (green)* is the same model for a $V\sin(I) = 17\,\mathrm{km\,s^{-1}}$; *solid (magenta)* is representing the residuals expected by subtracting the RM model by the simulated data; with the *(black) points*, a sequence of residuals from Fig. 1 with *Harps*.

The data for HD 189733b were good enough to allow an adjustment. In the case of CoRoT-3b, where the sizes of error bars are large, such an adjustment was not possible. Instead we compared a theoretical model with the $V\sin(I)$ value found in Table 1 to simulated data with the value found by spectral analysis: $17 \pm 1\,\mathrm{km\,s^{-1}}$ (D08). The expected residuals and the residuals of the *Harps* sequence were added on top (see Fig. 4). Were it not for the abnormally large value of $V\sin(I)$ found by the fit, which gave clues that something might be going wrong, little information would have been extracted to support the idea the model is not adapted to the data because of error bars of the same order of magnitude as the RM effect itself, let alone the residuals! The absence of a clear signal due to a misfit of the model in the residuals is not enough to rule out the conclusions found with the case of HD 189733b that indeed the correlated residuals are caused by the imposition of a model not adapted to the data, or vice-versa that the data is not extracted with the same assumptions taken in the model.

Two main paths are now being investigated to rectify the discovered problem: altering the models to take the effect into account, which is the path already taken by W05 (but incomplete as the same residuals are observed), or finding alternative ways of looking at the data to extract it properly. It may be worth noting than tackling asymmetries in the CCF is underway in various areas, be it to understand stellar spots or classical cepheids stars (Nardetto et al. 2006). The RM effect is gaining popularity as a new powerful tool to estimate the rotation of stars. Potentially, on misaligned objects like XO-3b (Hébrard et al. 2008; Winn et al. 2009) HD 80606b (Moutou et al. 2009) and CoRoT-3b, if confirmed, we could study differential rotation of stars other than the Sun. Before this can be achieved, however, we have to make sure that the RM effect is properly fitted.

5. Discussion and conclusions

The results that we find are in accordance with previously published results, $V\sin(I)$s aside.

A spin-orbit angle is obtained for an exoplanet with unprecedented precision with the value $\beta = 0.85^{\circ\,+0.32}_{-0.28}$ and is a 3σ detection of an angle different from zero for HD 189733b's orbit. We confirm a marginal eccentricity which has been strengthened by the addition of the *Harps* data. It remains consistent with values found in Agol et al. (2008) and B09. Both values are important to constrain planetary formation and evolution models. Results are consistent with the star having no radial velocity drift with time with $\Gamma = 0.2^{+2.7}_{-3.9}\,\mathrm{m\,s^{-1}\,yr^{-1}}$. A comparison with a fit fixing Γ to zero showed that the variation in χ^2 was not significant: $\Delta\chi^2 = 10$ for an error on χ^2 of 30. The $V\sin(I)$ value found by the fit is spurious, as demonstrated in Sect. 4.3. The real value is probably closer to $3.05\,\mathrm{km\,s^{-1}}$, value found for the simulated data to explain the theoretical models.

On CoRoT-3b, the fit yields an implausibly high $V\sin(I)$ at $35 \pm 8\,\mathrm{km\,s^{-1}}$, a two fold increase compared to the spectral analysis value, which is only explainable because of a discrepancy of assumptions between the model and the extraction of the data. This overestimation of $V\sin(I)$ can also be read in the literature: in Loeillet et al. (2008) a $V\sin(I)$ of $29.5 \pm 3\,\mathrm{km\,s^{-1}}$ is found for Hat-P-2 by fitting the RM effect without a prior. This value has to be compared to the value of $21 \pm 1\,\mathrm{km\,s^{-1}}$ found with an analysis of the spectral lines and of the photometry. Similarly for CoRoT-2b, in Bouchy et al. (2008), a $V\sin(I)$ extracted from the RM model is found to be larger than its spectral and photometric analyses counterparts. The discrepancy between the data and the model has for the moment mostly been observed in the case of fast stellar rotators. Yet, this effect is also dependent on the $R_\mathrm{p}/R_\star$ ratio. This means that in the case where the RM effect is fitted independently of photometry leaving every parameter free, this mismatch between the centre of a fitted Gaussian and the true velocity of the star's light centroid could lead to incorrect fitting of RM effects on slowly-rotating host stars of planets with high $R_\mathrm{p}/R_\star$ ratios, and be mistaken for a $V\sin(I)$ problem.

On CoRoT-3b we also get a marginal 97% probability detection (equivalent to 2σ) of an asymmetry in the current RM data. This result, if confirmed could shed a light into the debated origins and the uncertain nature of CoRoT-3b, a Brown Dwarf according to its mass and the presence of Deuterium burning, but a planet if created by accretion. A tormented history, reflected by a misaligned orbit, could point towards a more planetary origin

for this body, notably via coalescence of large planetary bodies as outlined in Baraffe et al. (2008), who also point out the confusion of having Deuterium burning as the only limit between Brown Dwarfs and planets. The measure of β could become a way of segregating Brown Dwarfs from planets.

Our study of HD 189733b began as a test-case for combining two different data sets. It also tested the RM model. CoRoT-3b came as an application of the analysis developed for HD 189733b and validates that a problem exists between the current models and the way the RV data is extracted.

This paper shows the significance of fitting the various data sets in a combined way. In conclusion this combined analysis, (1) helps reduce the number of free parameters applied to fitting all the data; (2) breaks correlations between some parameters as they are fitted differently, hence exploring parameter space better and (3) insures a consistency on the transit parameters between the models and helps reveal model inconsistencies, as it did here with the case of the Rossiter-McLaughlin effect, therefore ensuring that systematics are not mistaken for physics.

Acknowledgements. The authors would like to acknowledge the use of the ESO archive, ADS, *Simbad* and *Vizier* but mostly the help and the kind attention of the ESO staff at La Silla. The work is supported by the Swiss Fond National de Recherche. A. Triaud would like to acknowledge that he owes a beer to D. Queloz and two to A. Collier Cameron. We also thank the referee for the useful suggestions provided.

References

Agol, E., Cowan, N. B., Bushong, J., et al. 2008, Proc. IAU Symp., 253 [arXiv:0807.2434]
Baraffe, I., Chabrier, G., & Barman, T. 2008, A&A, 482, 315
Boisse, I., Moutou, C., Vidal-Madjar, A., et al. 2009, A&A, 495, 959
Bouchy, F., Udry, S., Mayor, M., et al. 2005, A&A, 444, L15
Bouchy, F., Queloz, D., Deleuil, M., et al. 2008, A&A, 482, L25
Cameron, A. C., Wilson, D. M., West, R. G., et al. 2007, MNRAS, 380, 1230
Claret, A. 2000, A&A, 363, 1081
Deleuil, M., Deeg, H. J., Alonso, R., et al. 2008, A&A, 491, 889
Gillon, M., Triaud, A. H. M. J., Mayor, M., et al. 2008, A&A, 485, 871
Giménez, A. 2006a, A&A, 450, 1231
Giménez, A. 2006b, ApJ, 650, 408
Hébrard, G., Bouchy, F., Pont, F., et al. 2008, A&A, 488, 763
Hilditch, R. W. 2001, An Introduction to Close Binary Stars, p773
Hosokawa, Y. 1953, Pub. Astron. Soc. Jap., 5, 88
Loeillet, B., Shporer, A., Bouchy, F., et al. 2008, A&A, 481, 529
Mandel, K., & Agol, E. 2002, ApJ, 580, L171
Mayor, M., & Queloz, D. 1995, Nature, 378, 355
Mayor, M., Udry, S., Lovis, C., et al. 2009, A&A, 493, 639
McLaughlin, D. B. 1924, ApJ, 60, 22
Moutou, C., Hebrard, G., Bouchy, F., et al. 2009, A&A, 498, L5
Nardetto, N., Mourard, D., Kervella, P., et al. 2006, A&A, 453, 309
Ohta, Y., Taruya, A., & Suto, Y. 2005, ApJ, 622, 1118
Queloz, D., Eggenberger, A., Mayor, M., et al. 2000, A&A, 359, L13
Rossiter, R. A. 1924, ApJ, 60, 15
Tegmark, M., Strauss, M. A., Blanton, M. R., et al. 2004, PhRvD, 69, 103501
Winn, J. N., Noyes, R. W., Holman, M. J., et al. 2005, ApJ, 631, 1215
Winn, J. N., Johnson, J. A., Marcy, G. W., et al. 2006, ApJ, 653, L69
Winn, J. N., Holman, M. J., Henry, G. W., et al. 2007, AJ, 133, 1828
Winn, J. N., Johnson, J. A., Fabrycky, D., et al. 2009, ApJ, submitted

Page 384 (Tables 3 and 4) is available in the electronic edition of the journal at http://www.aanda.org

2.6 Adding Stellar Isochrones

This is as yet unpublished work, but the first application should come out quite soon. As already written earlier, we depend on an estimate of the stellar mass in order to get to other interesting physical parameters such as the stellar radius, planet radius and planet mass. Early on (eg. Wilson et al. (2008)) the mass estimate could crudely be estimated from the effective temperature and stellar gravity ($\log g$). The WASP-4 b paper (section 2.3.2) shows clearly that the limitations we had were not the photometric precision but the knowledge we have of the star, or rather - and this is what this section will try dealing with - how and what information we use.

Sozzetti et al. (2007) remarked that under the reasonable assumption that the planet's mass is much smaller than the stars, we obtain directly from the transit, the stellar density (see equation 2.10). While $\log g$ is poorly and unaccurately determined from spectral analysis, stellar density could help determine stellar mass. Fairly easily one could run a first chain and obtain the density, which interpolated along with the effective temperature and metallicity within stellar evolutionary tracks could give an estimate of the stellar mass with error bars which could then be forwarded into a second chain. Some WASP papers (see next chapter) have been using such a technique of which Hebb et al. (2009) is a good example.

Other possibilities exist such as using a so-called Main-Sequence prior (Cameron et al. 2007a). Such a prior is known to influence the parameters extracted from a fit (eg. Anderson et al. (2010), Brown et al. in prep.). It is used only when photometry is too poor to determine the impact parameter (and thus bring a good constraint on stellar density). One can also use an empirical calibration for stellar mass obtained from detached eclipsing binaries (Torres et al. 2010), refined by Enoch et al. (2010). Its use it very similar to the procedure described lower, with the difference that they do not extract stellar age.

Ultimately, it would be nice to explore the ($T_{\rm eff}$, $\rho_\star$, $[M/H]$) space in the MCMC itself. All non physical stars (falling beyond the main sequence) could be discarded and help refine the measure on stellar density to keep within the bounds of what is physically possible, and thus help refine all other physical parameters. It would also show a less ad hoc manner to providing a stellar mass in the fit and obtain, in the spirit of fitting combined datasets, the most consistent model for all data we have acquired.

At Genève, there is a stellar evolution group producing stellar evolution models that act as reference in many fields of astrophysics. I took the opportunity to have the possibility to talk to those experts, to access the newer, refined models (using the adjusted solar abundances and stellar rotation into account), as well as an improved interpolation between the tracks (Mowlavi et al. in prep), to start working on the matter. Key aspects describing the models can be found in Maeder & Meynet (1989), Schaller et al. (1992), Charbonnel et al. (1999) and Eggenberger et al. (2008, 2010a,b). The first application was on WASP-23, for which I had just finished a thorough analysis. This work will now be presented. I also made an attempt on WASP-8.

2.6.1 Description of the method

First and foremost, I took the assumption that the $[Fe/H]$ provided by spectral line analysis is similar to $[M/H]$ the content in metals. In addition, the models provide the stellar content in metals Z which can be a little different from the observed surface metallicity. This has been neglected as current error bars are large enough. Harder to deal with are the new Asplund solar abundances: the Geneva models use the revised abundance of $Z_\odot = 0.014$ instead of the more widely used $Z_\odot = 0.019$ that Barry Smalley [11] uses in his spectral analyses (Smalley et al. 2010).

[11] (Keele University) the collaborator within WASP that provides the spectral analysis

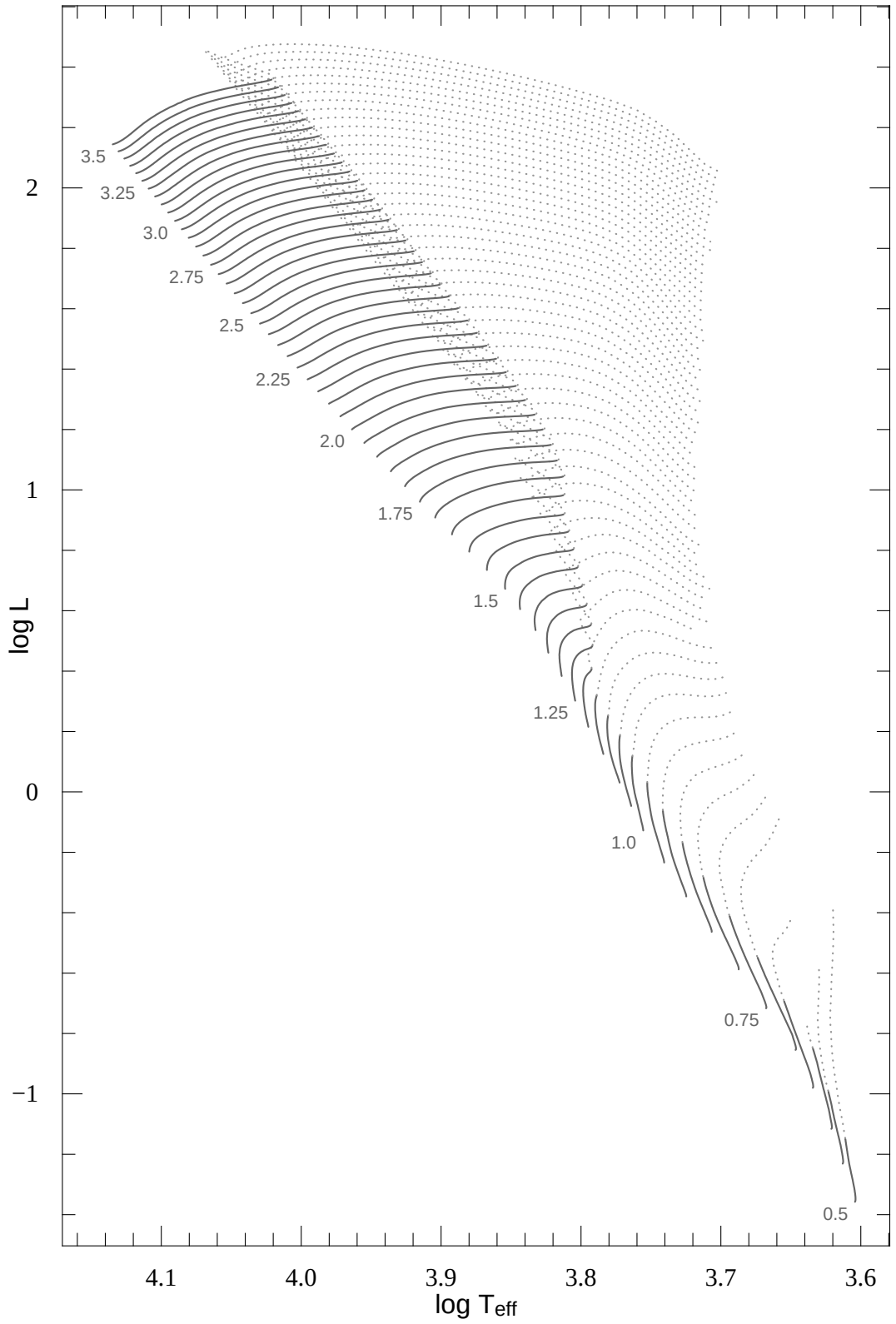


Figure 2.23: Traditional representation of the Herzsprung-Russell diagram with the Geneva stellar tracks at interval of 0.05 $M_{\odot}$, from 0.5 to 3.5 $M_{\odot}$. In plain is the main sequence. The dotted part starts when Hydrogen-core burning stops and goes into the start of Helium-core burning. Tracks are still incomplete at the lower mass range, because the evolution takes a very long time (but complete for the range that interest us). These are at solar metallicity.

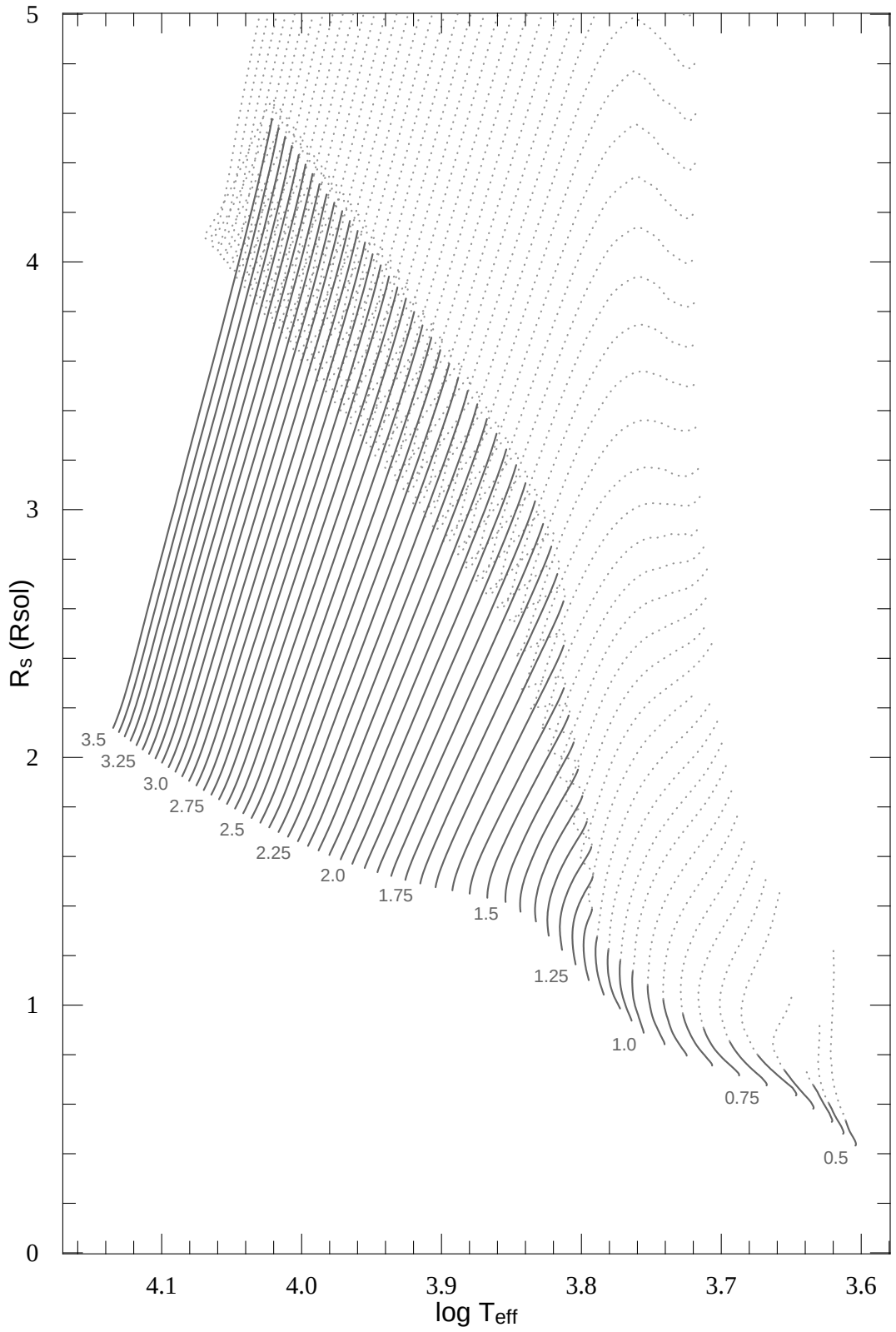


Figure 2.24: Same as previous figure, but having the stellar radius instead of luminosity. We are less likely to find evolved stars with transiting planets because of their larger radii diluting the transit, and the shorter time they spend in that region. For masses < 0.8 $M_{\odot}$, the plain tracks are longer than a Hubble time. These are at solar metallicity.

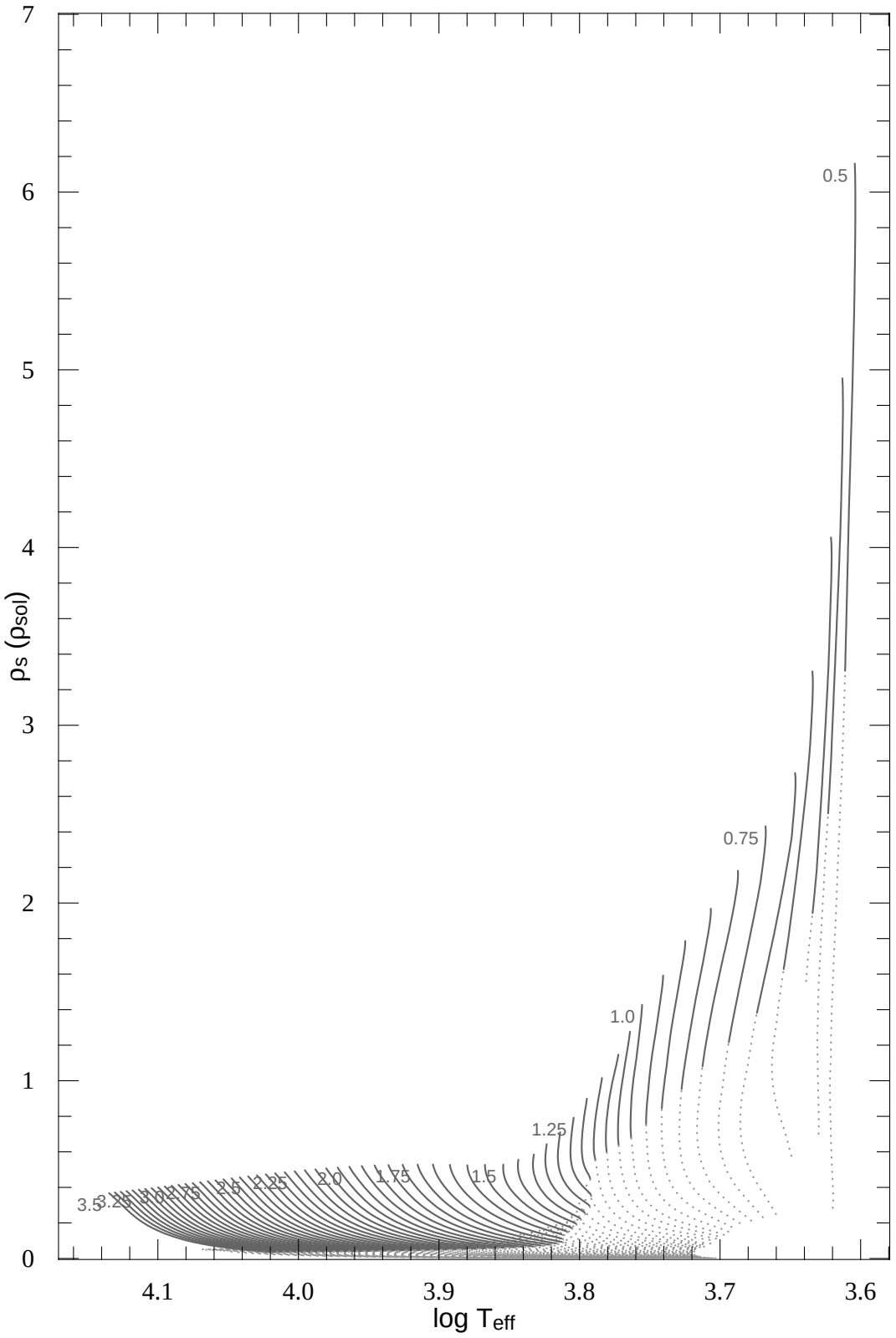


Figure 2.25: Again the same, this time using stellar density $\rho_\star$. We see an enormous variation and sharp slopes towards the lower masses, not so practical for interpolation. These are at solar metallicity.

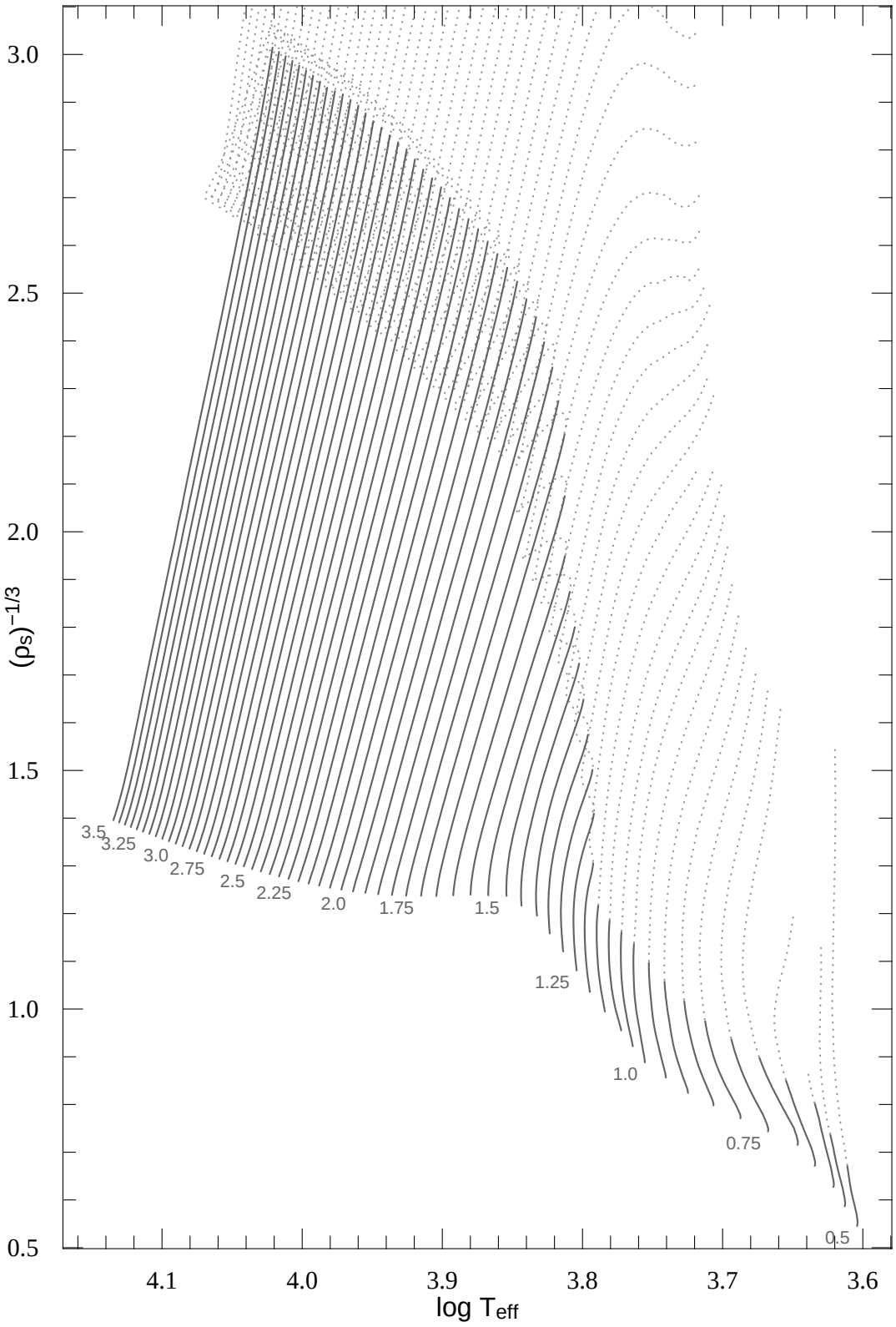


Figure 2.26: Modified HR diagram showing the relevant parts of the Geneva stellar tracks as a function of $\rho_\star^{-1/3}$. Because of our detection limits at the moment we effectively have a range from 0.5 to 1.5 in $\rho_\star^{-1/3}$. These are at solar metallicity.

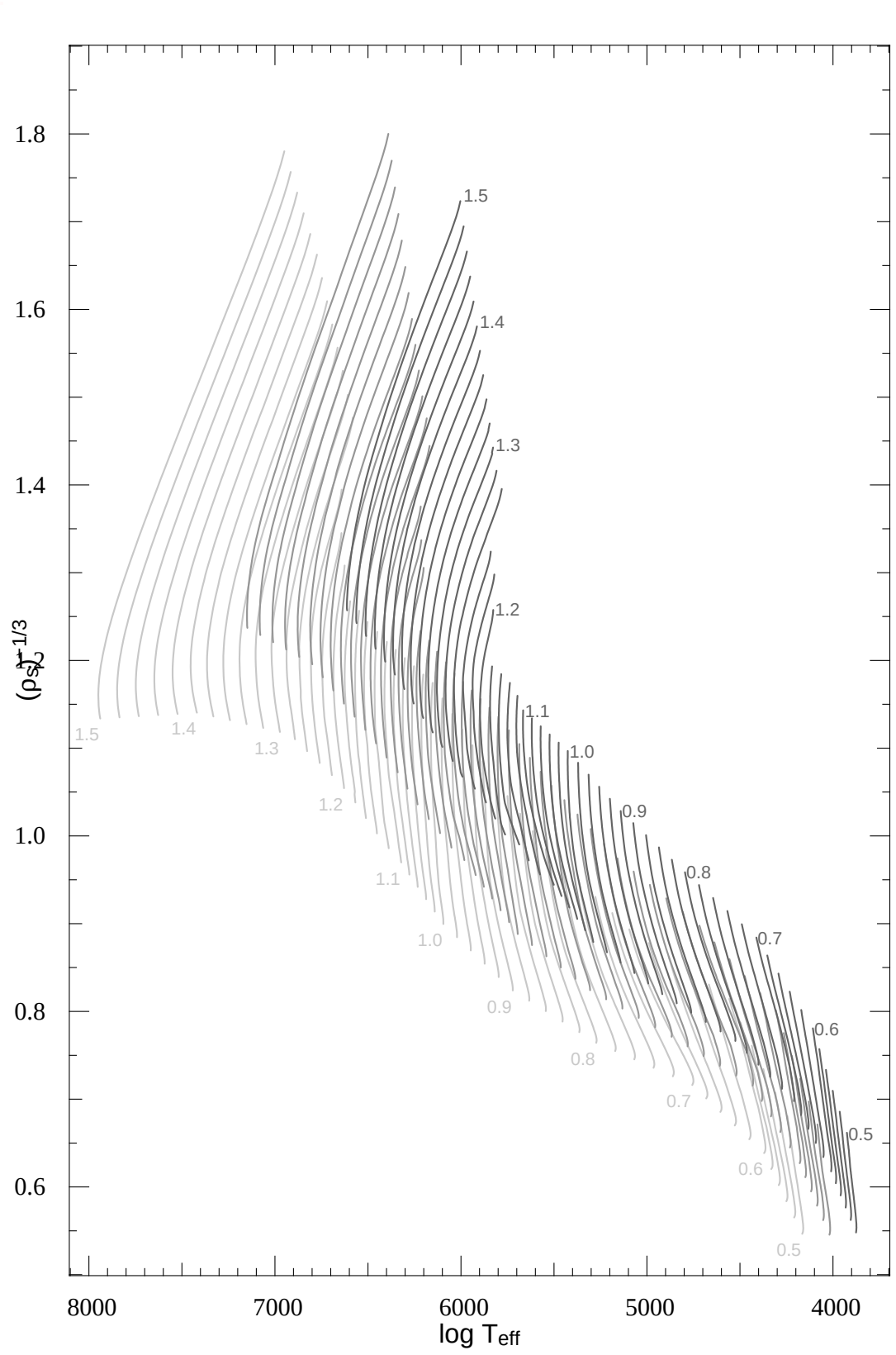


Figure 2.27: Only the main sequence between 0.5 and 1.5 $M_\odot$ for solar metallicity (grey), half solar metallicity (lighter grey) and twice solar metallicity (darker grey)

Interpolating within the stellar tracks become degenerate once stars evolve to from H-core burning to H-shell burning due to a *kink* in the tracks (see figure 2.23 and 2.26). Another assumption is that we only find hot Jupiters around main-sequence stars. The chance to catch a star in the region between H-core burning and H-shell burning is negligible. Once in H-shell burning, a star has a relatively fast increasing radius making it much harder to detect a transit in front of them (but being brighter those objects will be over-represented in a magnitude limited survey such as WASP). Only a handful of object may have been detected around stars in the Hertzprung gap. We thus restrict ourselves between the Zero Age Main Sequence and the end of H-core burning at the moment. Work is on progress to include tracks so that evolved objects be studied too.

Instead of using the stellar density $\rho_\star$, $(\rho_\star/\rho_\odot)^{-1/3}$ was used instead. $(\rho_\star/\rho_\odot)^{-1/3}$ is linked to R_p/a one of the major parameters extracted from a lightcurve. The main reason is computational: it was easier to use as the range over which $(\rho_\star/\rho_\odot)^{-1/3}$ varies for the majority of star around which we can detect hot Jupiters is less extended than for $\rho_\star$. The Main Sequence has also a shallower slope, making the simple interpolation that I conduct to supplement the good one, more accurate and faster. The choice of $(\rho_\star/\rho_\odot)^{-1/3}$, or other parameters linked to that value is not settled yet.

The principle on which the inclusion in the MCMC is simple: the tracks have a regular mesh at constant evolutionary stages produced from a complex interpolation between calculated tracks (see Mowlavi et al. in prep), notably using equivalent evolutionary points. An additional interpolation is conducted along the tracks along $(\rho_\star/\rho_\odot)^{-1/3}$ so as to obtain a very fine grid. Those numbers are transformed into integers, corresponding to indices in a large matrix.

The stellar density is estimated from the jump parameters using in the MCMC (see section 2.2.2), and made to correspond to one particular index. A random value for T_eff and $[Fe/H]$ is drawn assuming Gaussianity and using the values and error bars from spectral analysis. $[Fe/H]$ is transformed into $Z_\star$. The tracks are read at the right (density) index, between the two nearest T_eff for the two nearest $Z_\star$ (each of those four points bears a certain stellar mass at a certain age). Then the real position in (T_eff, $Z_\star$) is triangulated. The mass and the age are estimated similarly. If the proposed ($(\rho_\star/\rho_\odot)^{-1/3}$, T_eff, $Z_\star$) falls outside the tracks' range (below the main sequence), the step is not accepted and a new set of parameters is drawn. This insures we only keep "physically possible" stars. In that line, I have to point that currently, each step for which an age > 12 Gyr is found, is rejected as the likelihood to find them is small, especially if the proposed step ($(\rho_\star/\rho_\odot)^{-1/3}$, T_eff, $Z_\star$) is not metal poor. A prior on metal enrichment could replace this ad hoc barrier.

Because the models can also disagree between each others (Southworth 2009), the stellar mass distribution is convolved, at each step, with an additional random error which final value remains to be determined. The method just described is only computationally intensive at the beginning. One could think of adding tracks from several groups within the MCMC and derive parameters from the best compromise.

In short, they are not directly affecting χ^2 as one is never estimated: there is no better or worse stellar track to be on. χ^2 will nevertheless be affected if the distribution, as shown on figure 2.28 goes beyond what the stellar models describe. This will mostly affect object for which we have a poor determination of $\rho_\star$, the models will give a prior restricting parameter space and help produce only physically realistic values. For star with great precision in $((\rho_\star/\rho_\odot)^{-1/3}, T_\mathrm{eff}, [Fe/H])$, the tracks provide a direct estimate for stellar mass, taking in account the true probability distribution and departures from Gaussian distribution.

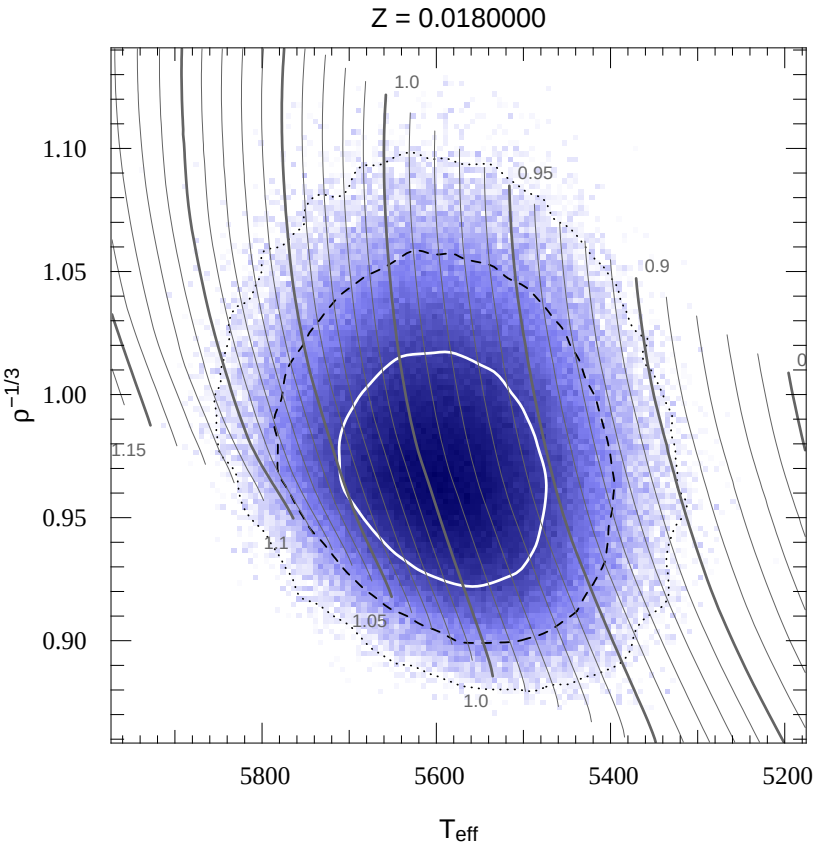


Figure 2.28: WASP-8: Output from the MCMC and stellar evolution tracks in $((\rho_\star/\rho_\odot)^{-1/3}, T_{\rm eff}, Z)$ space for the most likely value of $Z_\star = 0.018$. Bold tracks are every 0.05 $M_\odot$. 1, 2 and 3 σ confidence intervals are shown. We see that the distribution is truncated because of the proximity of the Zero Age Main Sequence.

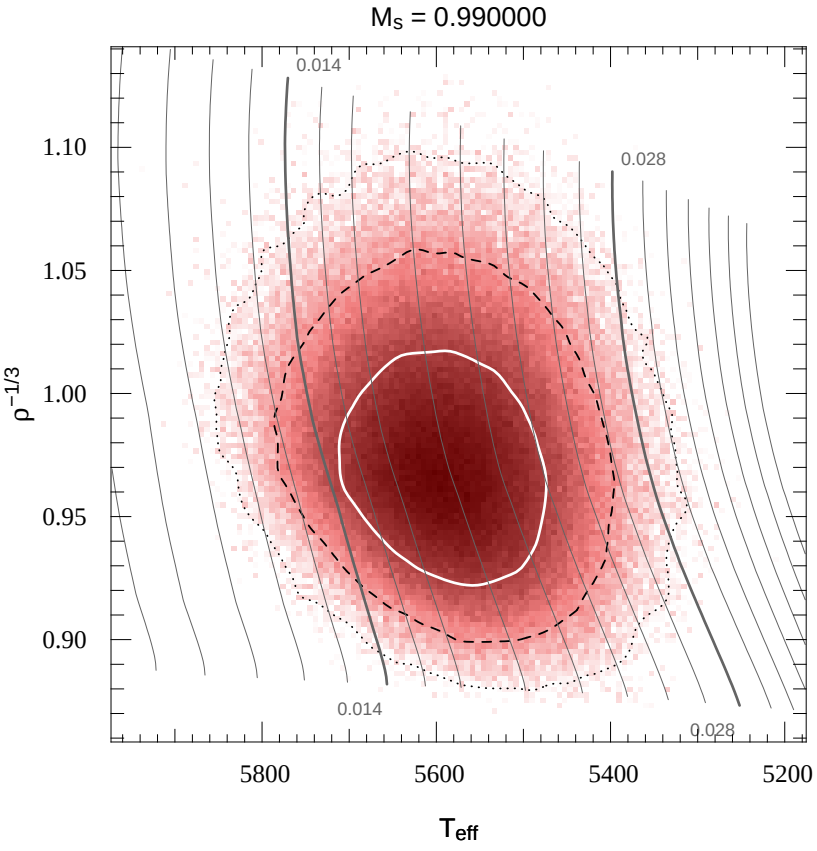


Figure 2.29: WASP-8: Output from the MCMC and stellar evolution tracks in $((\rho_\star/\rho_\odot)^{-1/3}, T_{\rm eff}, Z)$ space for the most likely value of $M_\star = 0.99 M_\odot$. Bold tracks show solar metallicity and twice solar metallicity. 1, 2 and 3 σ confidence intervals are shown.

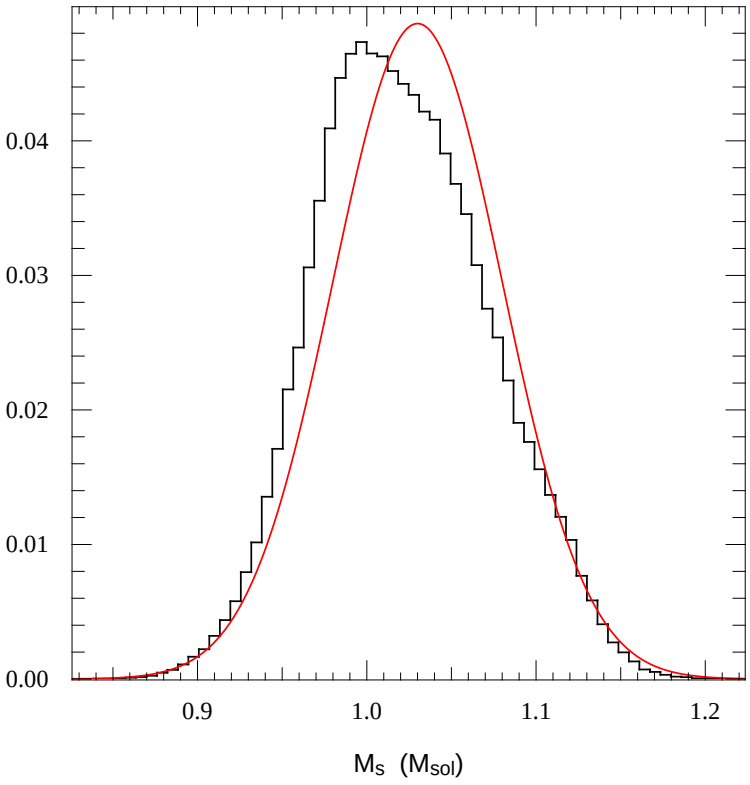


Figure 2.30: WASP-8: Histogram of the marginalised probability density function for the stellar mass as estimated by the MCMC interpolating in the stellar tracks. The plain curve is the Gaussian with mean and variance estimated in the paper. That value was an estimate based on a Gaussian density result from an earlier chain, interpolated in the Girardi tracks. The cut due to the Zero Age Main Sequence biases our result towards lower stellar masses.

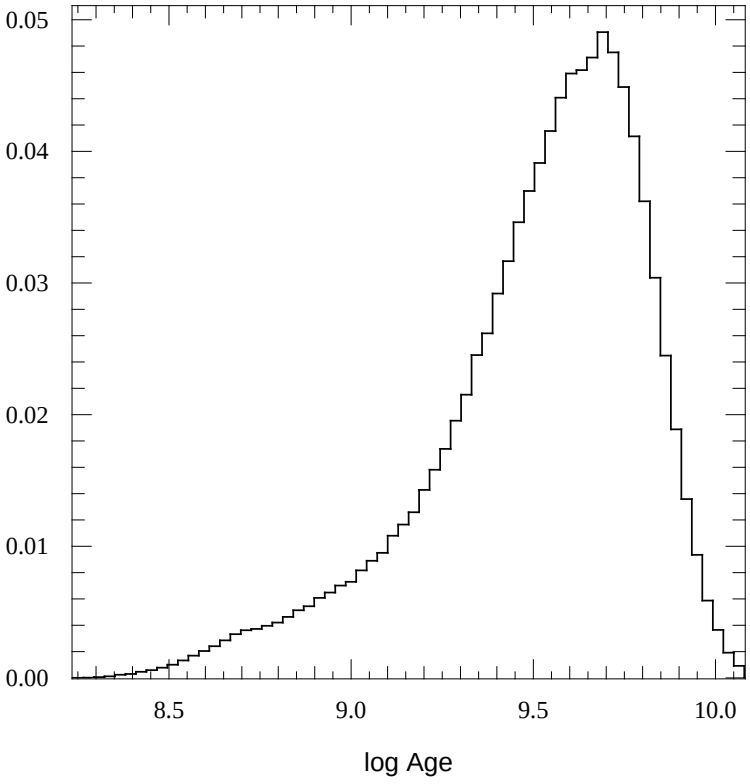


Figure 2.31: WASP-8: Histogram of the marginalised probability density function for the stellar age as estimated by the MCMC interpolating in the stellar tracks .

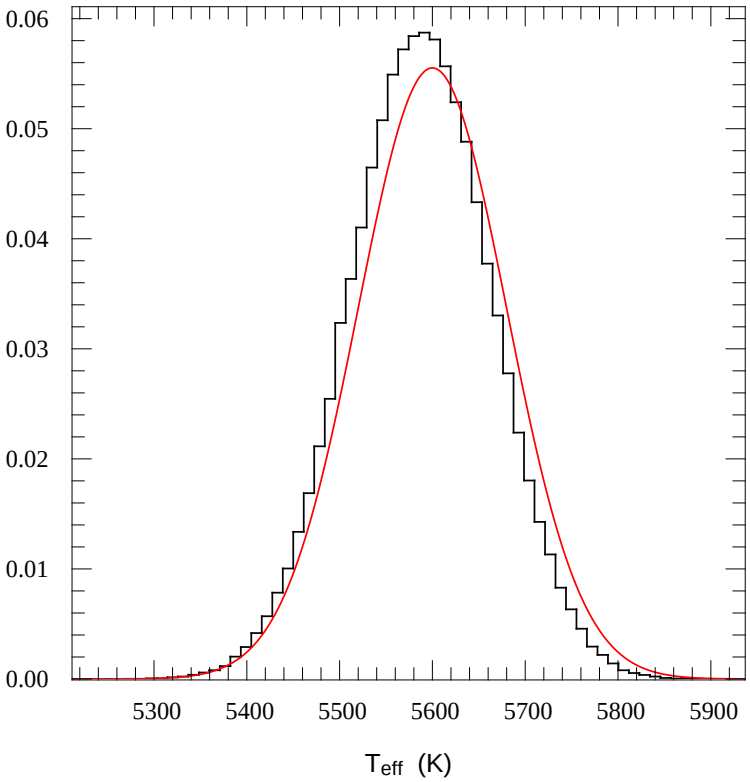


Figure 2.32: WASP-8: Histogram of the marginalised probability density function for the stellar effective temperature as estimated by the MCMC interpolating in the stellar tracks. The plain curve is the Gaussian with mean and variance estimated via spectral analysis in the paper.

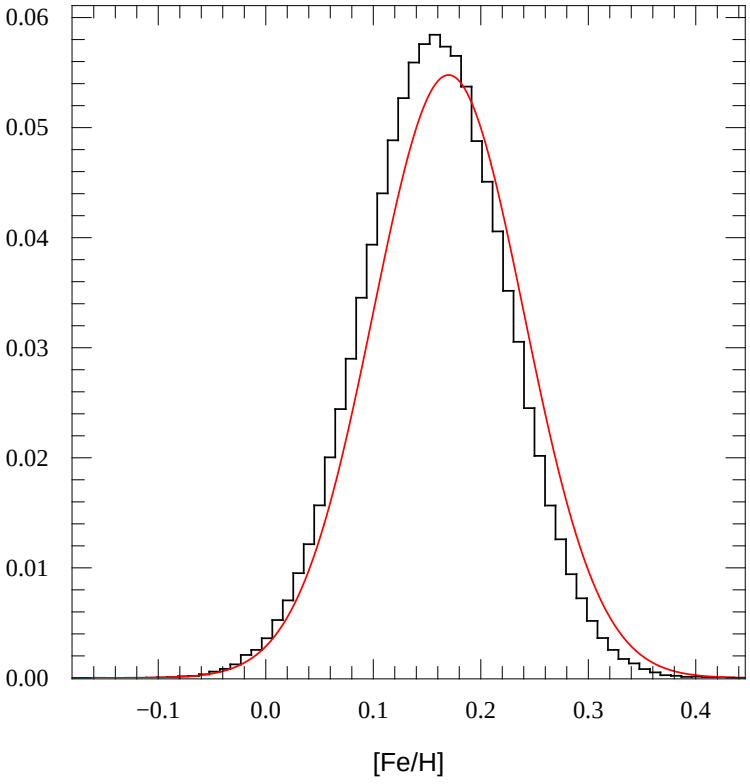


Figure 2.33: WASP-8: Histogram of the marginalised probability density function for the stellar metallicity as estimated by the MCMC interpolating in the stellar tracks. The plain curve is the Gaussian with mean and variance estimated via spectral analysis in the paper.

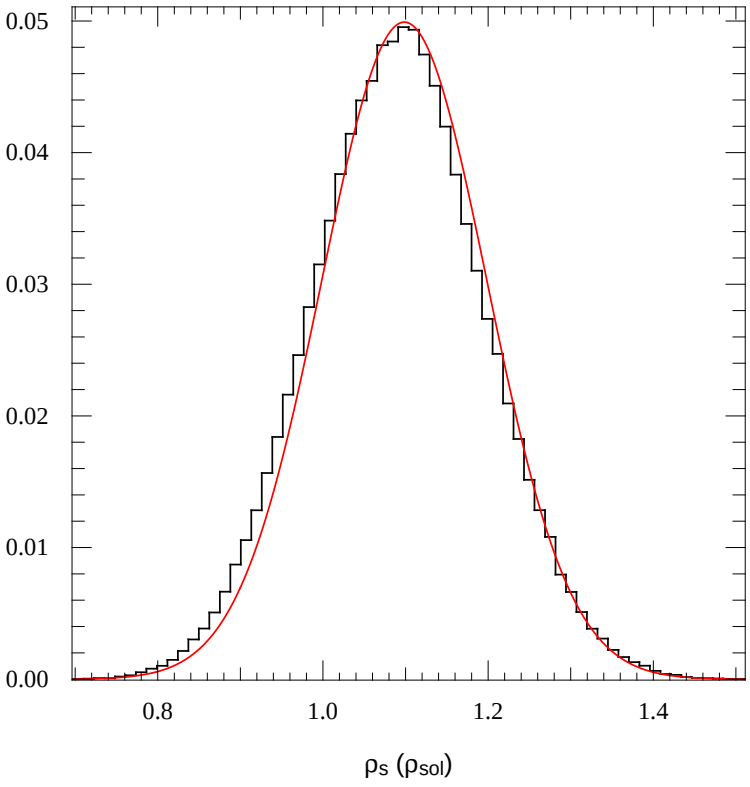


Figure 2.34: WASP-8: Histogram of the marginalised probability density function for the stellar density as estimated by the MCMC while interpolating in the stellar tracks. The plain curve is a Gaussian model with mean and variance estimated from the distribution.

2.6.2 Case study on WASP-8 & WASP-23

In the case of WASP-8, the transit and the Rossiter-McLaughlin effect constrain $\rho_\star$ sufficiently well that its distribution is close to Gaussian (see figure 2.34). This means that the mass determination is also close to what other methods would derive by more traditional means, using an assumed Gaussian distribution for $\rho_\star$ (figure 2.30). The values of $[Fe/H]$ and $T_{\rm eff}$ obtained from spectral line analyses place the star in the middle of the main sequence and are small enough not to be affected much by its edges. We can place an age (figure 2.31), albeit low precision on it, of about 5 Gyr.

Because the final $\rho_\star$ probability distribution function is symmetrical figures 2.28 & 2.29, to obtain a better estimate on $M_\star$ one has therefore to improve mostly its precision in $T_{\rm eff}$ and $[Fe/H]$ as the tracks are almost vertical. Increasing the precision in photometry will make the $\rho_\star^{-1/3}$ distribution narrower, which will mostly refine the age of the star.

In the case of WASP-23, the transit does not well constrain the impact parameter, and this affects the distribution in $\rho_\star$ which is far from Gaussian (figure 2.41). Thus, it was a hard distribution to interpolate into the Girardi tracks when the analysis for the paper was done, and this led to a rather wide estimate for the mass as $M_\star = 0.79 \pm 0.13\, M_\odot$. The same graphs as for WASP-8 are given. One can see the mass is better determined now, with the interpolation in the MCMC of the tracks giving $M_\star = 0.84 \pm 0.04\, M_\odot$. An approximate Gaussian distribution is also given and shows an improvement of a factor three in precision! The age distribution peaks around 8.5 Gyr, showing the star is probably quite old. The temperature distribution is well reproduced, the $[Fe/H]$ comes out thinner from the MCMC than when it entered it.

Checks were done on the well observed and studied planet hosting stars, HD 17156, HD 189733

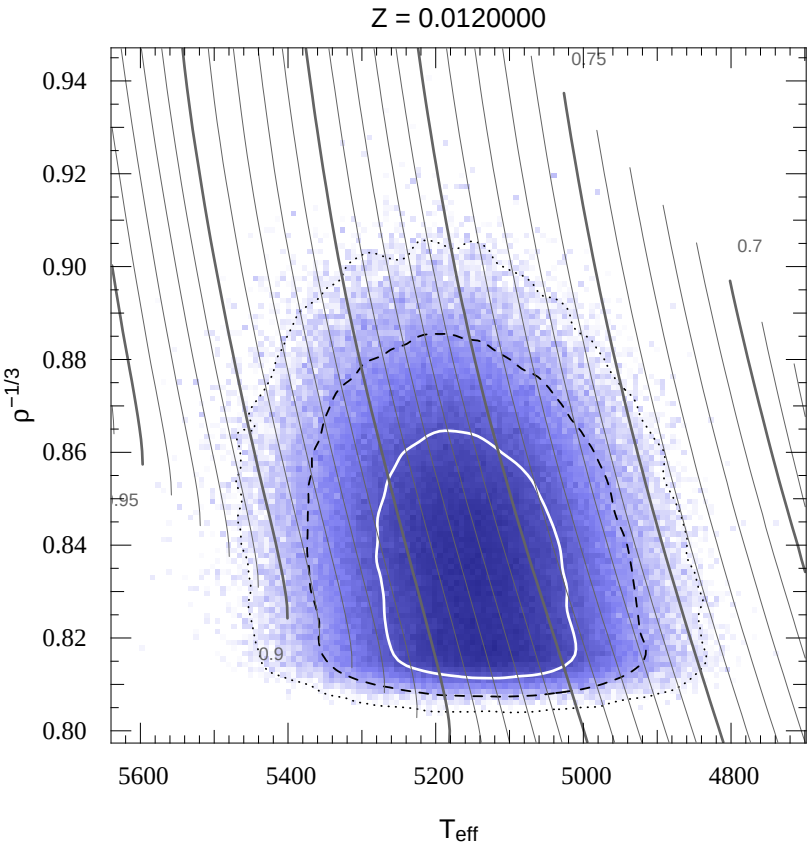


Figure 2.35: WASP-23: Output from the MCMC and stellar evolution tracks in $((\rho_\star/\rho_\odot)^{-1/3}, T_{\rm eff}, Z)$ space for the most likely value of $Z_\star = 0.012$. Bold tracks are every 0.05 $M_\odot$. 1, 2 and 3 σ confidence intervals are shown.

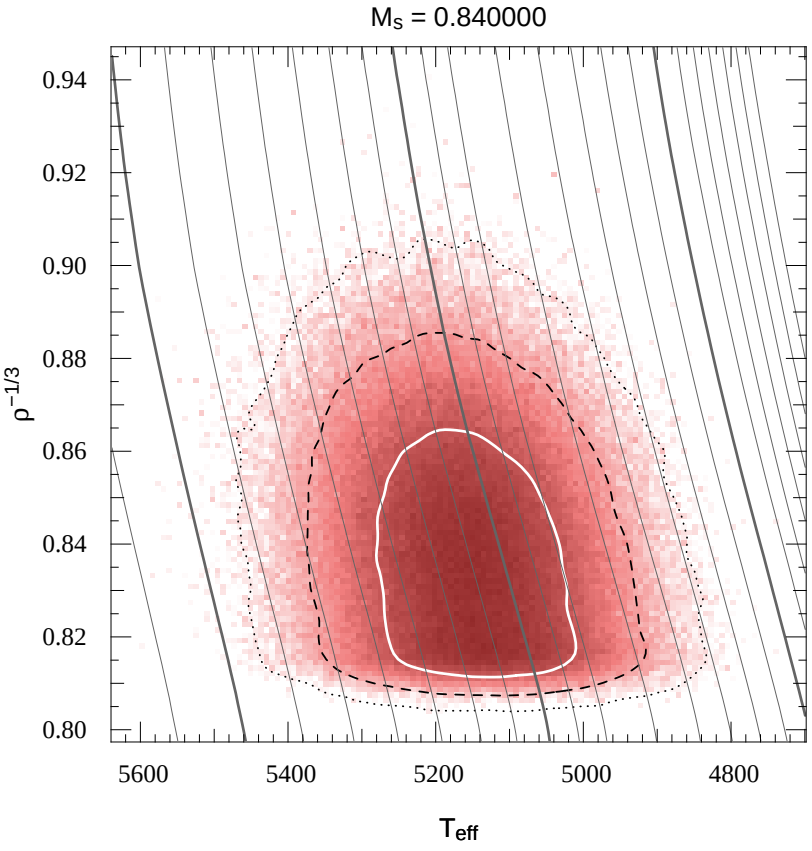


Figure 2.36: WASP-23: Output from the MCMC and stellar evolution tracks in $((\rho_\star/\rho_\odot)^{-1/3}, T_{\rm eff}, Z)$ space for the most likely value of $M_\star = 0.84\,M_\odot$. Bold tracks show half solar metallicity, solar metallicity and twice solar metallicity. 1, 2 and 3 σ confidence intervals are shown.

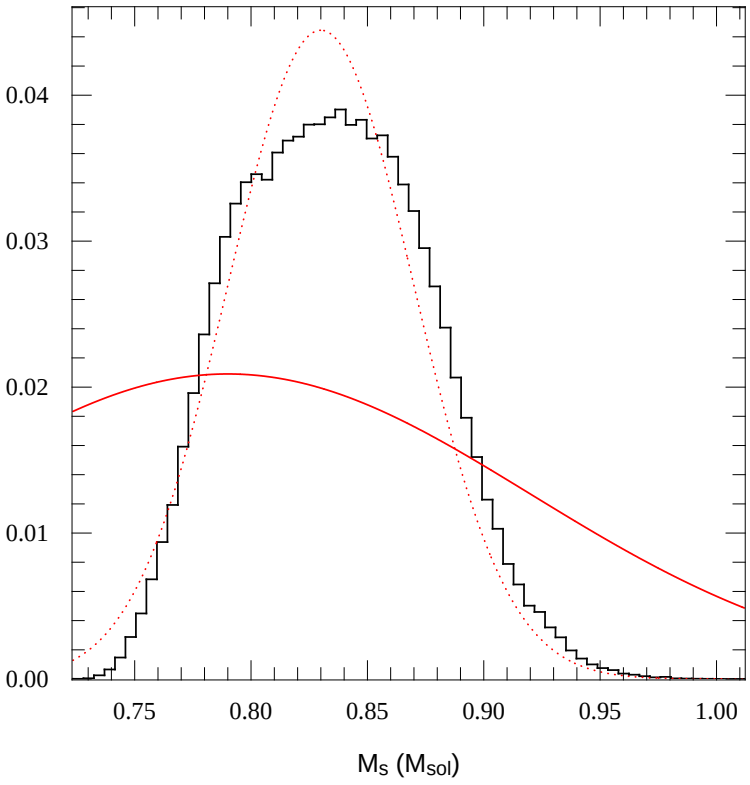


Figure 2.37: WASP-23: Histogram of the marginalised probability density function for the stellar mass as estimated by the MCMC interpolating in the stellar tracks. The plain curve is the Gaussian with mean and variance estimated in the paper. That value was an estimate based on a Gaussian density result from an earlier chain, interpolated in the Girardi tracks. The dotted curve is a Gaussian with approximate mean and variance as the histogram, for comparison.

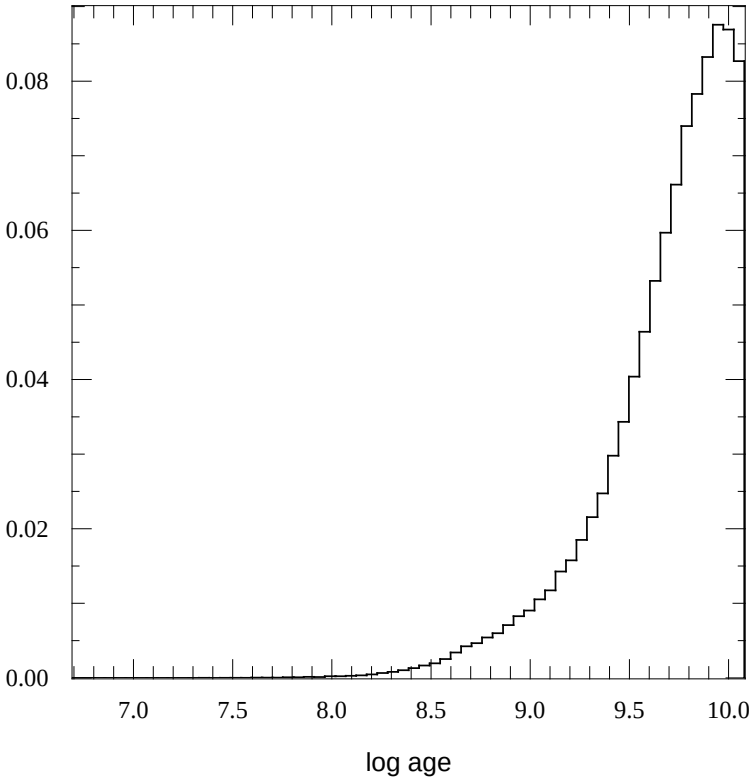


Figure 2.38: WASP-23: Histogram of the marginalised probability density function for the stellar age as estimated by the MCMC interpolating in the stellar tracks .

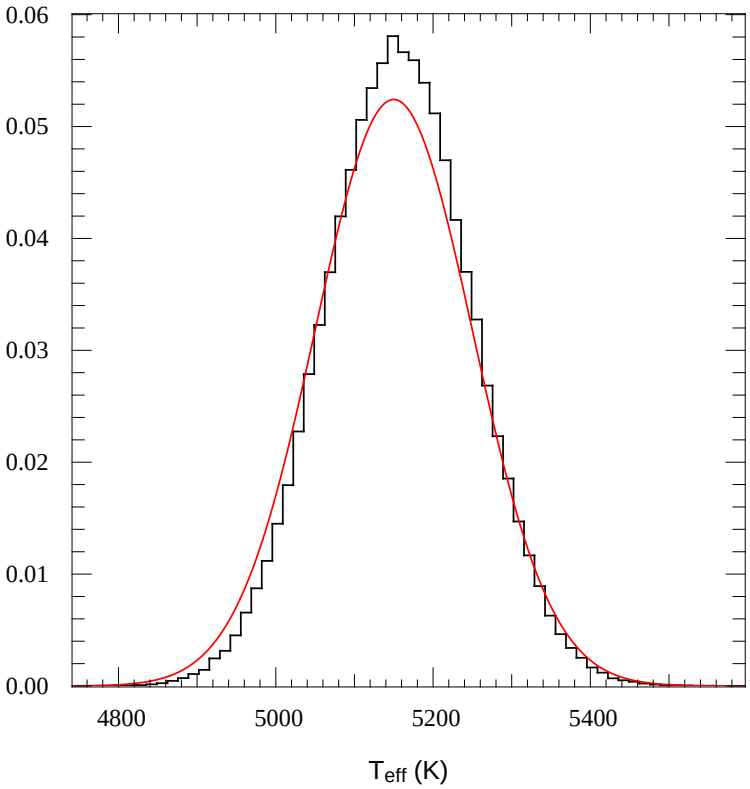


Figure 2.39: WASP-23: Histogram of the marginalised probability density function for the stellar effective temperature as estimated by the MCMC interpolating in the stellar tracks. The plain curve is the Gaussian with mean and variance estimated via spectral analysis in the paper.

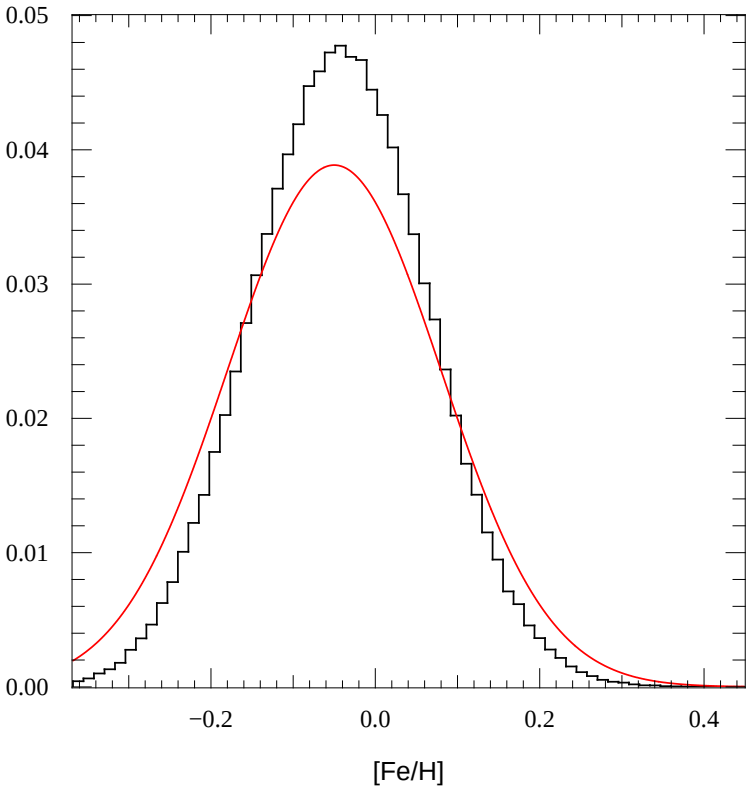


Figure 2.40: WASP-23: Histogram of the marginalised probability density function for the stellar metallicity as estimated by the MCMC interpolating in the stellar tracks. The plain curve is the Gaussian with mean and variance estimated via spectral analysis in the paper.

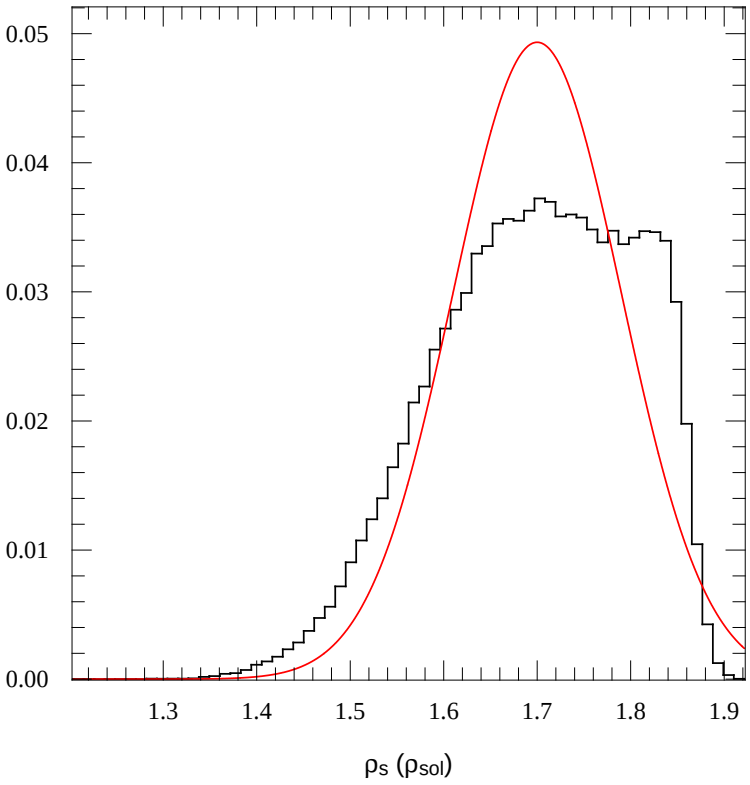


Figure 2.41: WASP-23: Histogram of the marginalised probability density function for the stellar density as estimated by the MCMC while interpolating in the stellar tracks. The plain curve is a Gaussian model with mean and variance approximated from the distribution.

and WASP-4. Each has exquisite lightcurves, giving good estimates for $\rho_\star$. HD 17156 also has asteroseismologic measurements. From the values in the literature, and placing them in the tracks, the mass estimates were close to those using other models. A full analysis is needed on these objects and should constitute a forthcoming work.

High precision in $\rho_\star$, combined with a high precision in the determination of stellar parameters like $T_{\rm eff}$ and $[Fe/H]$ can give us a tool to measure the age of stars for singleton. This is of interest as one could then plot $\rho_{\rm p}$ against age, or β against age and see if any relation appears. High precision unfortunately does not necessarily mean high accuracy.

In the case of measuring $\rho_\star$, a varying stellar spot coverage, even out of the transit chord will affect ΔF from which $\rho_\star$ is determined. A variation in transit depth should warn us and one can imagine always taking the deepest transits as a better indication of the true ratio of radii. Worse cases would be for stars with constant spot coverage at latitudes never crossed by the planet. We would thus stay oblivious to their presence and obtain a systematically wrong $\rho_\star$ (this of course would also mean all other parameters, for the star and the planet are also wrong).

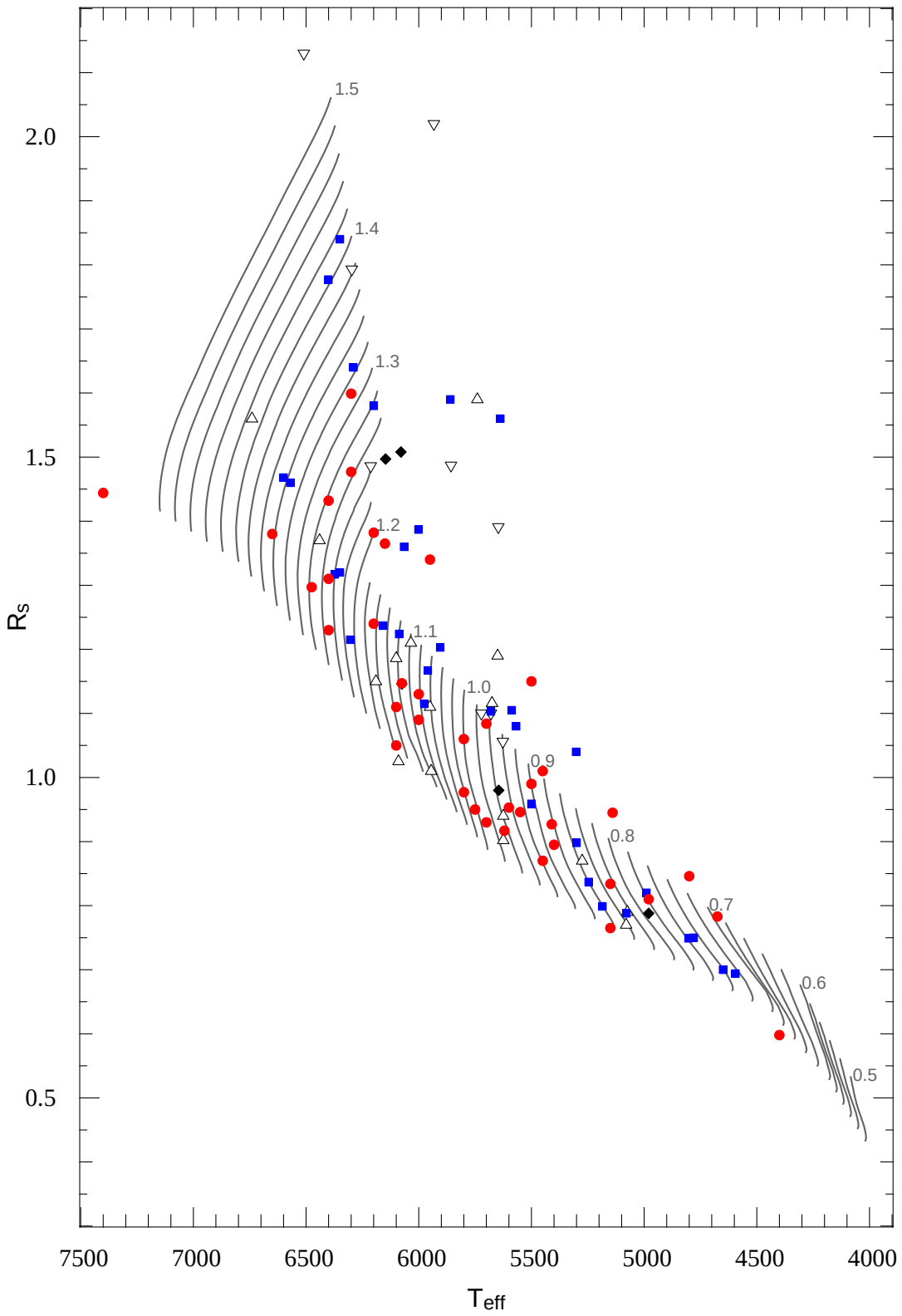


Figure 2.42: Transit planet host stars in the HR diagram. Diamonds: RV surveys. Open triangles: CoRoT; open inverted triangles: *Kepler*, blue squares: Hat; red discs: WASP. WASP tend to find planets on smaller star than HAT. Tracks have solar metallicities. Most objects appearing above the Main Sequence are around more metal rich stars. Higher metallicities would move the tracks sideways to the right.

Chapter 3

Discovering Transiting Extrasolar Planets

We have thus far learned much about how to analyse the signal caused by a transiting planets with the trove of information that can be extracted. Because Astronomy is a science where the experiment is impossible, in order to guess at physical processes and their evolution, it is necessary to gather data from as many objects as possible and check if theoretical predictions hold.

This chapter will focus on how to find a great number of transiting planets that are relatively easy to follow-up and characterise to learn about the physics of these other worlds.

Shortly after my arrival in Genève I was placed in charge of the confirmation of WASP planet candidates. This work has been an exciting one and still, after dozens of planets found, it is still a pleasure to discover a new one. It also taught me a great lesson: being at the source of the data is of utmost importance as then one can choose what to focus on and still work on many other topics in collaboration with others.

3.1 The WASP Survey

The WASP survey (Wide Angle Search for Planets) is a consortium of British Universities, among them, Queen's University Belfast, the University of St Andrews, of Leicester, of Keele and the Open University (Pollacco et al. 2006). The consortium built two instruments, SuperWASP-North and SuperWASP-South, located at La Palma, Canary Islands, and in Sutherland in South Africa. It is the only survey operating in both hemispheres (a contender, the HAT network (Bakos et al. 2004) has installed a few telescopes[1]).

Both WASP sites have the same set-up: eight 11.1 cm refractive telescopes[2] on one mount. Each has a 2048 x 2048 pixel CCD with a field of view of 7.8° x 7.8°. Observations are done using a broad band filter with a defined passband from 400 to 700 nm.

Both sites operate in the same manner. Seven to eight fields at one hour in right ascension are selected and followed during the night. Every hour when one field sets it is dropped and another picked-up. No new field is observed that is not observable for at least four hours. The instruments return to the same field every 8 minutes. SuperWASP-North has been operating since 2004. The South started in 2006. 30 237 250 individual stars from 7 126 480 images have been observed over most of the sky with only the poles and the galactic plane left out, this over 1654 individual nights[3].

[1] rumors about their first southern planet have reached my hears, but still nothing on astro-ph.

[2] Canon zoom lenses

[3] numbers given by Pierre Maxted and estimated at mid May 2011

The data needs to come back to the UK and is stored at Leicester[4]. The frames are treated following a traditional approach of flat fielding and debiasing. The stellar fields are recognised and aperture photometry done on all stars but typically between V magnitude 9 and 13. The *Hunter* algorithm (Cameron et al. 2006) is used to search transit signals on a range of periods between 0.5 and 10 days. Periodograms are produced with estimates of transit depth, width and impact parameter. Stellar masses are estimated from all sky survey colours indices; possible stellar and planetary radii are computed.

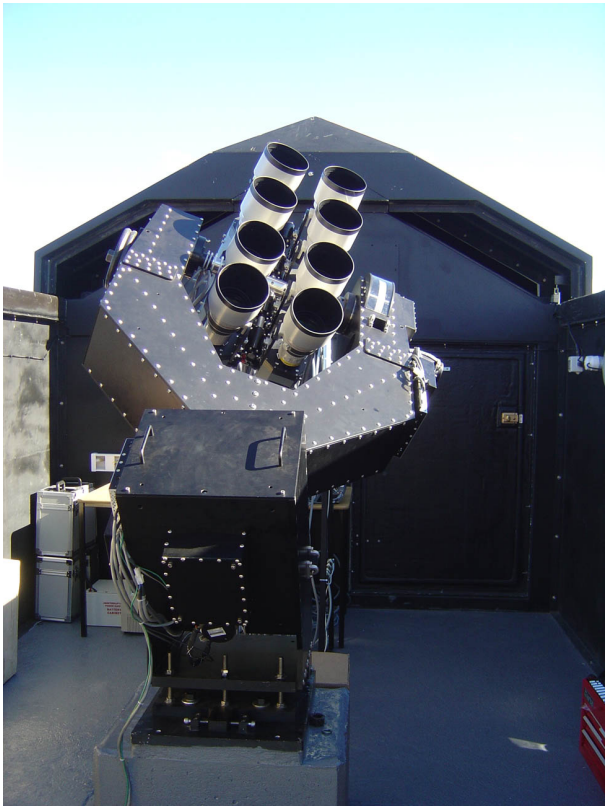


Figure 3.1: Photo showing the SuperWASP instrument, its robototic mount supports eight 11.1 cm refractive telescopes. We also see the roof which automatically opens and closes. Photo courtesy www.superwasp.org.

Then comes a process of verifying by eye each candidate's lightcurve. The smallest photometric aperture used by SuperWASP is quite large ($\sim$ 34") and the light from nearby stars can fall in, altering the photometry on the desired target. Some tools have been devised to help spot those cases. The transits' shapes are also verified and their occurence. A planetary transit is expected to have a fairly flat bottom. Candidates are classified in terms of the quality of the lightcurve, the robustness of their period and the lack of nearby sources of contamination. The position of the star in a colour proper-motion diagram also helps diagnose giants, very likely to be false positives[5]. From experience, a minimum of five complete transits are needed before a candidate can be reliably detected from the archive. This places quite strong constraints on the detection of objects with period longer than 10 days, as the number of transits in one season is not enough (not counting in weather, technical difficulties and Moon brightness) for immediate detection. One would need to observe several seasons. The selection process is described in Cameron et al. (2007a) and the impact of correlated noise in Smith et al. (2006).

Once vetted, the candidates are placed in a list. The confirmation and follow-up can now start. A total of 689 candidates[6] have been sent to Genève for confirmation using the spectrograph CORALIE, mounted on the *Euler* 1.2 m Swiss Telescope, at La Silla, Chile.

Information between WASP and Genève is organised around a website nicknamed *The Hunter page*. Though this site one can access the candidate lists produced by the entire consortium (3.3). Each of the candidates has its own page, automatically created and containing all relevant information. The photometry is present, per field, per season, per reduction or combined. Each of

[4] a public archive is now reacheable at the following address: http://www.wasp.le.ac.uk/public/
[5] as giants have larger radii than the orbital periods that we seek
[6] numbers until mid spring 2011, since we have received more

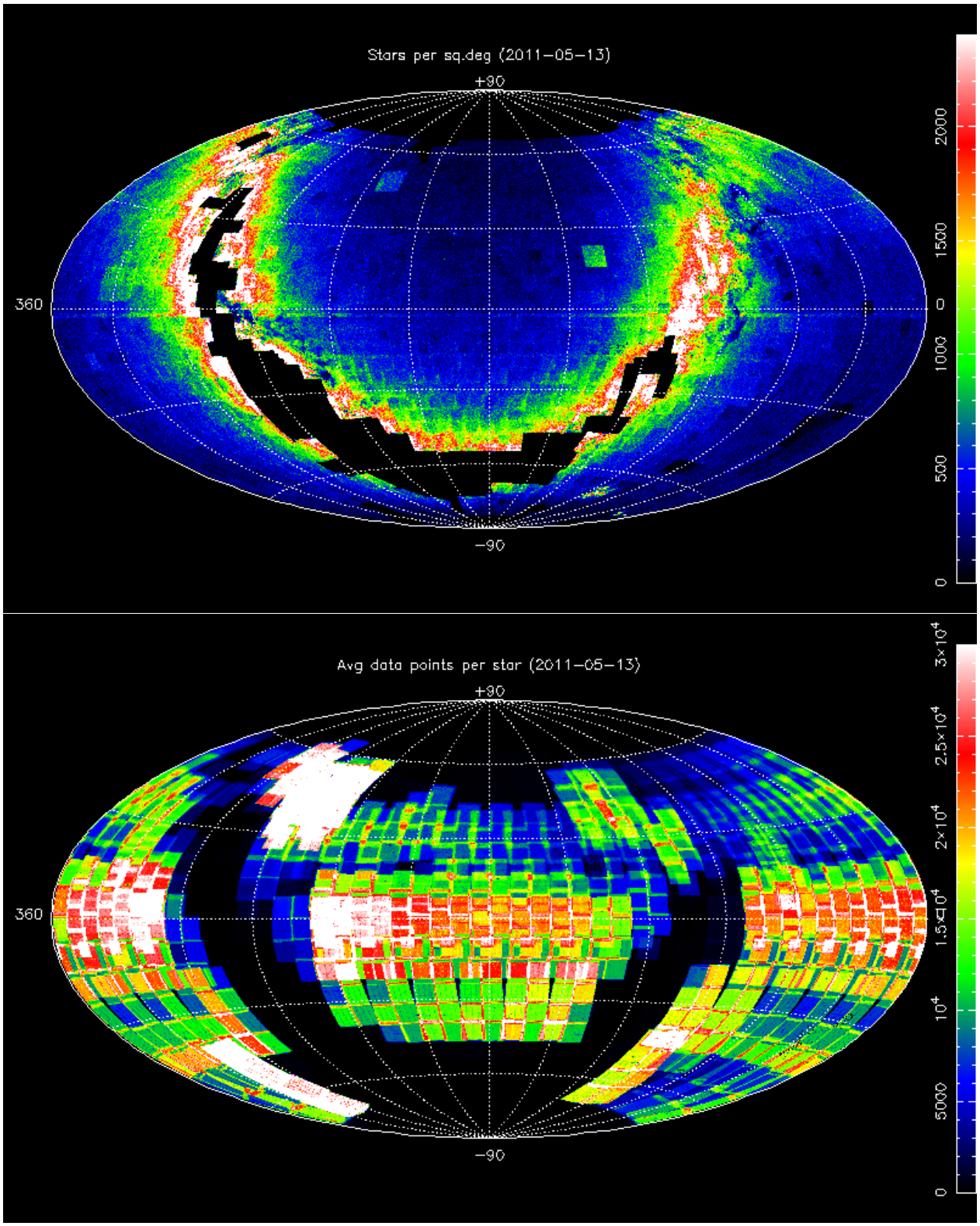


Figure 3.2: All sky images from WASP. *top* location of individually detected objects. *bottom* number of data points per individual source. Courtesy Pierre Maxted.

these has a periodogram and folded lightcurve on the most likely period. Other periods can be accessed easily (figure 3.4). Finding charts are available and show the proximity of other stars and likely sources of contamination (figure 3.5). One can also do its own periodogram choosing which datasets and which period range, as well as bin the data to help visual confirmation of the transit and checking the presence ellipsoidal variation or occultations, indicative of eclipsing binaries. First estimates of physical parameters such as the stellar mass, stellar radius, and planet radius are available. One can check easily at which orbital phase a planet is at any moment with predictions of coming transits.

Not least in the interesting features is a comment box where people can leave their impression about the data, the observations they conducted, what is in need to do next and flags, for observing but also for classifying false positives. Files can be uploaded for other colleagues to download or check the presented evidence. The photometric data can be downloaded from the website; Ephemeris can be updated. All in all, the *Hunter* page is a great communication and data sharing tool for our collaboration spanning many people in several institutions. It also means that when observations are conducted, all relevant information is readily available.

3.2 Using *Euler* to Confirm Transiting Hot Jupiters

In the last few years, about half the time given to the exoplanet's group on the *Euler* telescope has been dedicated to the confirmation of WASP planet candidates. This includes follow-up photometry as much as spectroscopic follow-up. I am mostly involved with the latter.

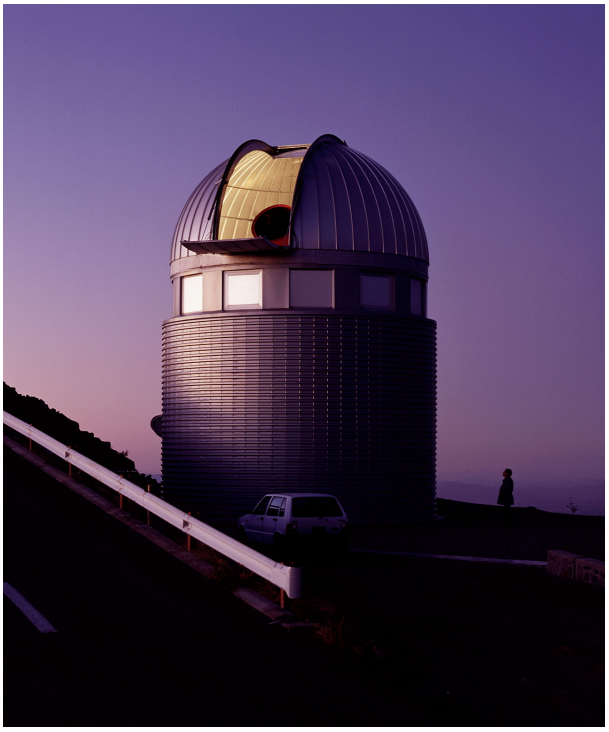


Figure 3.8: Photo showing the 1.2 m *Euler* Telescope, at La Silla, Chile. The échelle spectrograph CORALIE is connected at the Nasmyth focus via optical fibre. An imager is located at the secondary focus. Photo courtesy www.eso.org.

CORALIE is a high resolution fibre-bed échelle spectrograph, mounted on the *Euler* telescope as soon as the telescope was built, in 1998. Since it has surveyed a sample of stars limited in volume for periodic radial velocity shifts, indicative of a perturbing body and found about 50 planets on a variety of orbits (cf. forthcoming PhD thesis by Maxime Marmier). In 2007, the instrument received a major upgrade which saw its throughput increased by a factor six while keeping the much sought after stability, precision and accuracy. This upgrade allowed to observe fainter targets and reach about 25 $\mathrm{m\,s^{-1}}$ in a 30 minute exposure on a quiet $V = 13$ star while achieving regularly below 5 $\mathrm{m\,s^{-1}}$ on the brighter targets. Without this upgrade, the work on the WASP follow-up would not have been near as successful as it became. Details of the operations can be found in the discovery paper for the first CORALIE/WASP planet: WASP-4 (Wilson et al. 2008).

Coralie list 31 (CH 23/11/10)

ASCII Input List

1	1SWASPJ002328.03-022914.5	J002328	Vmag = 9.545	A
2	1SWASPJ015703.20+004531.9	J015703	Vmag = 10.568	A
3	1SWASPJ025349.11-111307.6	J025349	Vmag =	Blend
4	1SWASPJ050256.00-221341.2	J050256	Vmag = 12.94	EB
5	1SWASPJ051745.59-103930.0	J051745	Vmag = 11.22	EB
6	1SWASPJ053035.09-274017.2	J053035	Vmag = 11.859	RAF
7	1SWASPJ053353.31-544842.4	J053353	Vmag = 13.11	Blend
8	1SWASPJ055532.69-571726.0	J055532	Vmag = 10.038	A
9	1SWASPJ060316.90-191023.3	J060316	Vmag = 11.917	A
10	1SWASPJ091007.27-434656.1	J091007	Vmag = 11.093	Blend
11	1SWASPJ091819.03-341026.4	J091819	Vmag = 11.947	A
12	1SWASPJ093209.37-451132.4	J093209	Vmag = 11.292	Blend
13	1SWASPJ110917.04-285353.0	J110917	Vmag = 10.537	RAF
14	1SWASPJ111644.43-015207.5	J111644	Vmag = 12.77	EBLM
15	1SWASPJ111747.30+022721.6	J111747	Vmag = 11.09	A
16	1SWASPJ112849.00-071346.9	J112849	Vmag = 11.464	EB
17	1SWASPJ122742.79-371258.3	J122742	Vmag = 10.732	A
18	1SWASPJ123317.01-205033.7	J123317	Vmag = 12.423	EBLM
19	1SWASPJ123332.84-100846.1	J123332	Vmag = 11.592	A
20	1SWASPJ124036.51-191703.4	J124036	Vmag = 12.869	A
21	1SWASPJ124404.30-132011.9	J124404	Vmag = 11.039	EB
22	1SWASPJ133440.30-123134.0	J133440	Vmag = 11.742	A
23	1SWASPJ133501.94-173012.7	J133501	Vmag = 11.76	P
24	1SWASPJ142325.29-160429.1	J142325	Vmag = 12.64	EB
25	1SWASPJ143152.15-111840.4	J143152	Vmag = 12.75	EBLM
26	1SWASPJ145516.84-020327.5	J145516	Vmag =	A
27	1SWASPJ201844.06-184545.1	J201844	Vmag = 11.96	A
28	1SWASPJ204804.59-184017.5	J204804	Vmag = 12.28	A
29	1SWASPJ212710.58-542025.5	J212710	Vmag = 10.972	A

Candidate Lists index page

Figure 3.3: Page for the CORALIE List 31. We notably see links towards each of the individual planet candidates and the current observing flag. We are usually only provided A-class candidates. Sometimes some are downgraded to B, after further scrutiny, or additional data. RAF stands for *Rejected After Follow-up*, EB for *Eclipsing Binary*, EBLM for Eclipsing Binary of Low Mass, Blend, for false positive due to a nearby EB or EBLM, P for planets

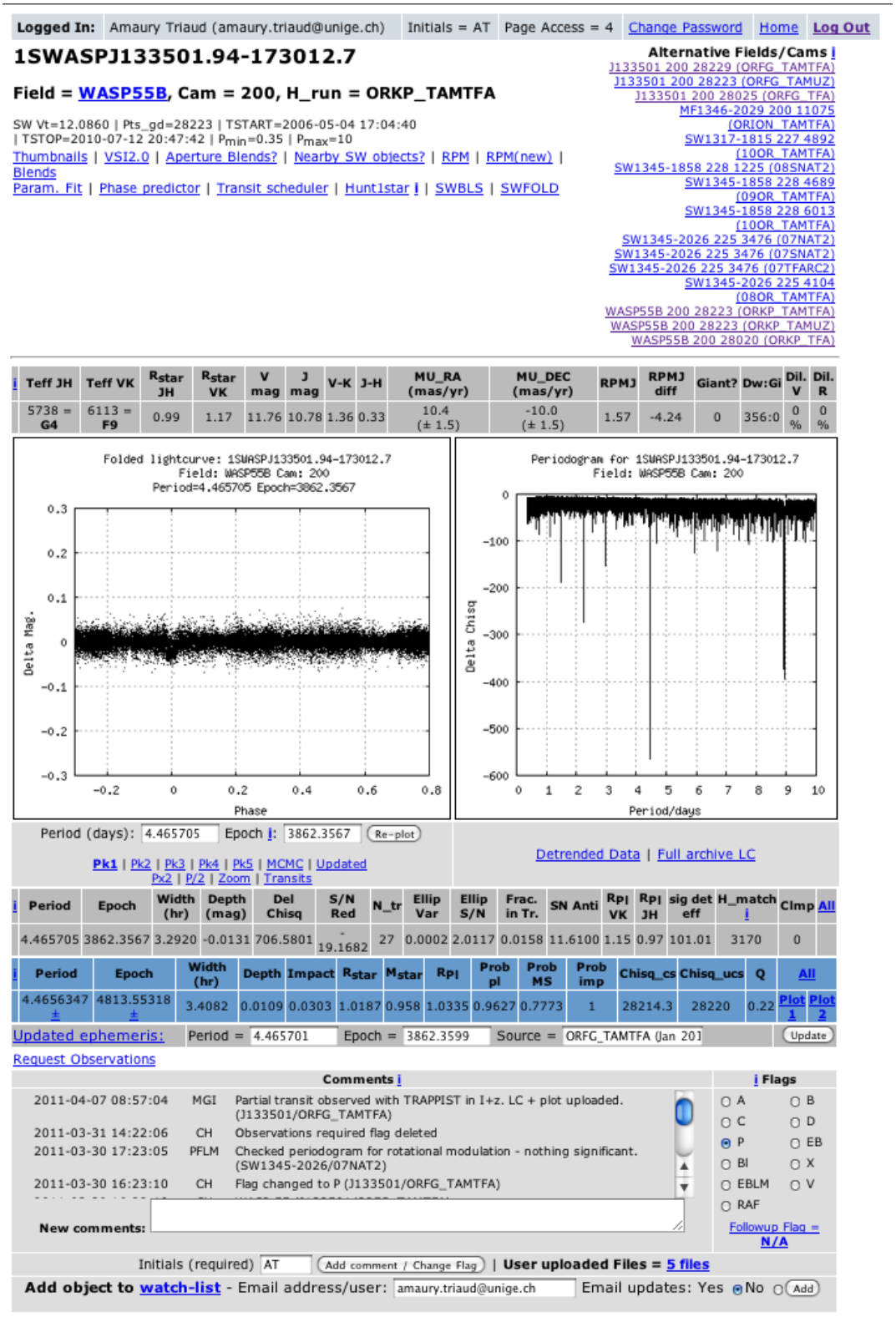
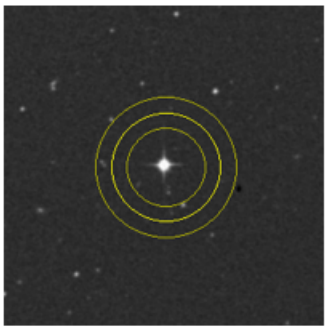


Figure 3.4: Candidate page for an object that was confirmed as a planet by CORALIE. Links on top right lead to similar pages the difference being the data reduction or individual cameras and observing seasons or combinations of. Each gives a different periodogram with a different phase folded lightcurve. Most interesting links are *Nearby SW objects?*, *Transit Scheduler* and *RPM(new)*. At the bottom we see the comments' and observing flags' section, with the possibility to upload files.

SuperWASP objects within 140" of 1SWASP J133501.94-173012.7

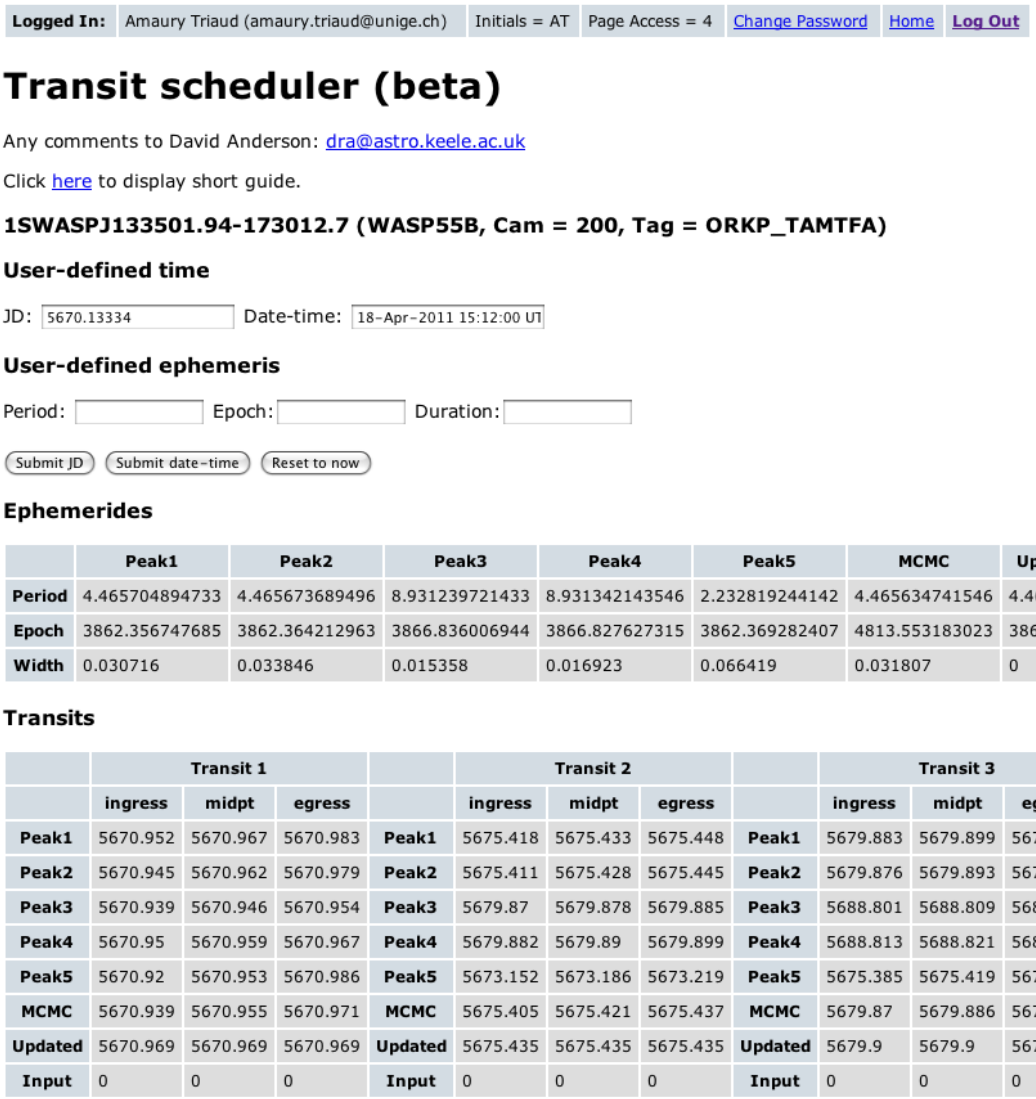
SW ID	USNO R1	Dist.	Hunter match?	Hunter Period	Lightcurve	LCFOLD
1SWASP J133501.94-173012.7	11.24	0"	SW1345-1858 228 08SNAT2	0.7873	Folded LC (P=4.4657)	Binned LC (P=4.4657)
1SWASP J133501.94-173012.7	11.24	0"	SW1345-2026 225 07SNAT2	0.8127	Folded LC (P=4.4657)	Binned LC (P=4.4657)
1SWASP J133501.94-173012.7	11.24	0"	SW1345-2026 225 07NAT2	4.4611	Folded LC (P=4.4657)	Binned LC (P=4.4657)
1SWASP J133501.94-173012.7	11.24	0"	SW1345-2026 225 07TFARC2	4.4613	Folded LC (P=4.4657)	Binned LC (P=4.4657)
1SWASP J133501.94-173012.7	11.24	0"	SW1345-1858 228 10OR_TAMTFA	4.4656	Folded LC (P=4.4657)	Binned LC (P=4.4657)
1SWASP J133501.94-173012.7	11.24	0"	J133501 200 ORFG_TFA	4.4656	Folded LC (P=4.4657)	Binned LC (P=4.4657)
1SWASP J133501.94-173012.7	11.24	0"	J133501 200 ORFG_TAMTFA	4.4657	Folded LC (P=4.4657)	Binned LC (P=4.4657)
1SWASP J133501.94-173012.7	11.24	0"	WASP55B 200 ORKP_TAMTFA	4.4657	Folded LC (P=4.4657)	Binned LC (P=4.4657)
1SWASP J133501.94-173012.7	11.24	0"	J133501 200 ORFG_TAMUZ	4.4657	Folded LC (P=4.4657)	Binned LC (P=4.4657)
1SWASP J133501.94-173012.7	11.24	0"	WASP55B 200 ORKP_TAMUZ	4.4657	Folded LC (P=4.4657)	Binned LC (P=4.4657)
1SWASP J133501.94-173012.7	11.24	0"	WASP55B 200 ORKP_TFA	4.4657	Folded LC (P=4.4657)	Binned LC (P=4.4657)
1SWASP J133501.94-173012.7	11.24	0"	SW1317-1815 227 10OR_TAMTFA	4.4667	Folded LC (P=4.4657)	Binned LC (P=4.4657)
1SWASP J133501.94-173012.7	11.24	0"	SW1345-2026 225 08OR_TAMTFA	4.4689	Folded LC (P=4.4657)	Binned LC (P=4.4657)
1SWASP J133501.94-173012.7	11.24	0"	MF1346-2029 200 ORION_TAMTFA	8.9317	Folded LC (P=4.4657)	Binned LC (P=4.4657)
1SWASP J133501.94-173012.7	11.24	0"	SW1345-1858 228 09OR_TAMTFA	8.9326	Folded LC (P=4.4657)	Binned LC (P=4.4657)



280"x280" DSS Image (Hover mouse over stars to identify corresponding SW objects)

The circles indicate the photometry extraction aperture size: Flux 1: 2.5 pixels, Flux2: 3.5 pixels and Flux3: 4.5 pixels. 1 pixel is 13.7" on the sky.

Figure 3.5: By clicking on the link *Nearby SW objects?*, on the top of the page shown on figure 3.4, we obtain a small finding chart with showing the three beams used by WASP to conduct aperture photometry. This is star is alone in the field. In the case where other stars are detected, we get, in the list above the chart, the possibility to check the photometry on nearby stars folded on best period and see if the transit is deeper or fainter. Deeper meaning usually that that other star is the transited and we have a blend scenario. The number of additional sources within the different beams also prompts the need for an *On/Off* to check which star has a transit.



Logged In: Amaury Triaud (amaury.triaud@unige.ch) | Initials = AT | Page Access = 4 | Change Password | Home | Log Out

Transit scheduler (beta)

Any comments to David Anderson: dra@astro.keele.ac.uk

Click here to display short guide.

1SWASPJ133501.94-173012.7 (WASP55B, Cam = 200, Tag = ORKP_TAMTFA)

User-defined time

JD: 5670.13334 Date-time: 18-Apr-2011 15:12:00 UT

User-defined ephemeris

Period: Epoch: Duration:

Submit JD | Submit date-time | Reset to now

Ephemerides

	Peak1	Peak2	Peak3	Peak4	Peak5	MCMC	Updated	Input
Period	4.465704894733	4.465673689496	8.931239721433	8.931342143546	2.232819244142	4.465634741546	4.465701	
Epoch	3862.356747685	3862.364212963	3866.836006944	3866.827627315	3862.369282407	4813.553183023	3862.3599	
Width	0.030716	0.033846	0.015358	0.016923	0.066419	0.031807	0	

Transits

	Transit 1				Transit 2				Transit 3			
	ingress	midpt	egress		ingress	midpt	egress		ingress	midpt	egress	
Peak1	5670.952	5670.967	5670.983	**Peak1**	5675.418	5675.433	5675.448	**Peak1**	5679.883	5679.899	5679.914	**Peak1**
Peak2	5670.945	5670.962	5670.979	**Peak2**	5675.411	5675.428	5675.445	**Peak2**	5679.876	5679.893	5679.91	**Peak2**
Peak3	5670.939	5670.946	5670.954	**Peak3**	5679.87	5679.878	5679.885	**Peak3**	5688.801	5688.809	5688.817	**Peak3**
Peak4	5670.95	5670.959	5670.967	**Peak4**	5679.882	5679.89	5679.899	**Peak4**	5688.813	5688.821	5688.83	**Peak4**
Peak5	5670.92	5670.953	5670.986	**Peak5**	5673.152	5673.186	5673.219	**Peak5**	5675.385	5675.419	5675.452	**Peak5**
MCMC	5670.939	5670.955	5670.971	**MCMC**	5675.405	5675.421	5675.437	**MCMC**	5679.87	5679.886	5679.902	**MCMC**
Updated	5670.969	5670.969	5670.969	**Updated**	5675.435	5675.435	5675.435	**Updated**	5679.9	5679.9	5679.9	**Updated**
Input	0	0	0	**Input**	0	0	0	**Input**	0	0	0	**Input**

Figure 3.6: Following the link *Transit Scheduler* on figure 3.4 we have a way to compare the transit time predictions given by the five most important peaks detected in the periodogram. One can also input its own information and updated ephemeris.

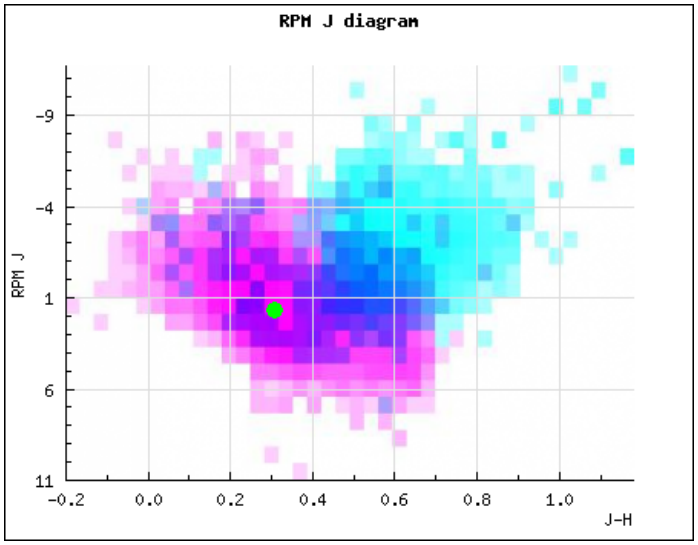


Figure 3.7: Proper Motion-Colour diagram for the candidate shown in figure 3.4. It is well inside the main sequence. (in magenta: the main sequence; in cyan: the giant branch. Compiled by Pierre Maxted and Heather Cegla from the RAVE survey (Steinmetz et al. 2006))

The inner workings of CORALIE are similar to other instruments such as ELODIE and HARPS, which are described in several thesis and papers realised at Genève, amongst those I can point to Didier Queloz's, Claudio Melo's, Dominique Naef's and Christophe Lovis's theses, as well as to Baranne et al. (1996). In short the stellar light comes through the fiber and is dispersed. The spectrum is cut by the échelle into several orders which are all illuminated onto one CCD. On a parallel fiber, a Thorium-Argon lamp's spectrum is obtained and through the same optical path as the stellar spectrum, is shone on the same CCD, in between the different stellar orders. The position of the Th-Ar emission lines is known to a high degree of precision (Lovis & Pepe 2007). They are used to calibrate the instrument insuring a constant zero point in time. CORALIE has systematic error bars and a long term stability < 6 m s^{-1}.

An optimised binary[7] mask (or template) with holes at the location of expected stellar absorption cross correlates the stellar spectrum and recreates a function (the CCF) that we can see as the mean absorption line, which shape is close to a Gaussian (Pepe et al. 2002). A Gaussian is adjusted to it and its mean gives the radial velocity, by comparison with the Th-Ar lamp. The height of the CCF is called contrast. The full width at half maximum (FWHM) of the Gaussian is a convolution between the instrument's resolving power, the atmospheric broadening of the photosphere and the rotational broadening caused by the rotation of the star. The profile stays close to Gaussian up to FWHM 20 km s^{-1}, after which the shape approaches a rotation profile. The reduction of the data into precise radial velocity measurement is done as soon as the exposure is finished. This quick and automated process (called DRS, for Data Reduction Software) has proven to be important in our rejection of false positives (see next section). As they can be identified right away, we suffered no loss of time. Two masks were used: one matching the expected stellar spectrum of a K5V star and one matching a G2V.

When a list is published on the *Hunter* page, I check every candidate WASP is proposing and insert all relevant information in a spreadsheet[8] which will help observers confirm planets with high efficiency. Those candidates that have a nearby source of contamination are flagged for *On/Off*, a few photometric observations during transit and out of transit to check on which star and what depth the transit really is. Likely orbital periods and ephemeris are entered into the spreadsheet. The phase at every hour of the night is calculated guiding to the observer to acquire data at the

[7] not a binary star, but binary as in 1s and 0s
[8] the famous spreadsheet, loved by so many observers!

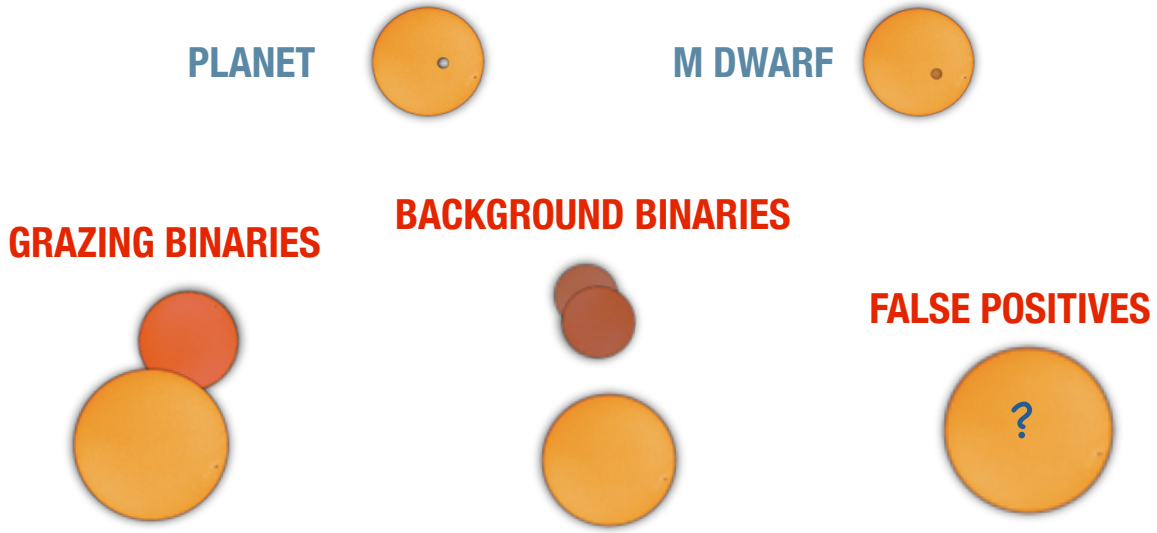


Figure 3.9: Diagram showing a few scenarios through which a 1 to 2 % periodic drop in flux can be observed. Most are astrophysical false positives, while some can be instrumental.

orbital phases where confirmation is fastest. Internet communication proved extremely useful as the acquired data could be repatriated to Genève at the end of the night where I could compared it with previous observations and send back updated instructions to the observer before the start of the night. This allowed to keep a fast pace of false positive rejection and planet confirmation.

When dealing with detecting weak signals on faint stars, one is sensitive to all sorts of noise sources. One of the major sources of that noise is the reflected sunlight on the Moon which imprints a second spectrum on the CCD and creates a second peak in the CCF. Other teams place a fibre on the sky to estimate the Moon contamination and remove it from their data. More or less free of scheduling constraints, we tackled the problem altogether differently: we only observe in dark time and when our stars are more than 90° from the Moon.

3.3 From a Candidate to a Confirmed Planet

Many objects can mimic the signal caused by a planet. Amongst others, a grazing eclipsing binary, or a diluted eclipsing binary (either a background object, or physically linked to a third star) can show depth of order of 1%. Usually their shape is recognisable as a being triangular instead of being box like. The low photometric precision of WASP does not always allow for such a distinction. Another traditional source of false positives are low mass eclipsing binaries, where the transiter is a M dwarf of size roughly similar to that of a planet (1 to 2 $R_{\rm Jup}$). Although many authors consider them as such, here, those are not here considered as false positives but more as *other object of interest*: they were followed up and provide a unique comparison sample for our planet survey (see section 3.6). For a review of what type of objects can resemble a planetary transit please refer to Brown (2003) and Torres et al. (2011). The aim of this section is to show the process of verification and confirmation of candidates produced by WASP. The results from this verification process are given later, in table 3.1.

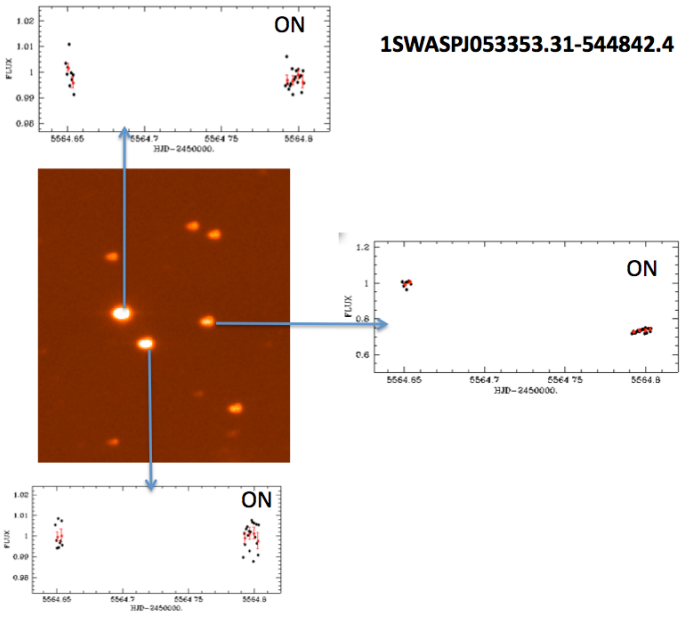


Figure 3.10: This WASP candidate had two bright star within the smallest aperture and seven altogether within the largest aperture. Michaël Gillon used the 70 cm TRAPPIST robotic telescope to observe in transit (*On*) and out of transit (*Off*) and determine which of the star was being transited. In this case a faint nearby star shows a 20 % depth eclipse. Not a planet. Plot & analysis by Michaël Gillon.

Observations usually starts with spectroscopy with the observer's first job is to first acquire a couple of spectra using CORALIE at $\phi = 0.25$ and $\phi = 0.75$ location of the expected quadrature points of the Doppler motion. If no variation is observed, another alternative period from the *Hunter* page can be tried. If that fails too, an *On/Off* is asked to check if the transit really exists.

3.3.1 *On/Off* photometry

The *On/Off* is usually done by Michaël Gillon (now also by Monika Lendl), first using the *Euler* telescope, then also his 70 cm robotic telescope called TRAPPIST and located in La Silla, Chile[9] (Gillon et al. 2011). The aim is to obtain a quick photometric timeseries in (*On*) and out (*Off*) of transit to check the reality of the signal announced by WASP while saving telescope time. This is also done for distinguishing a candidate within a crowded stellar field, or for verifying an ephemeris when several possible options are provided.

To produce transit lightcurves such as those presented in this document, one needs notably to correct for the airmass of the star, which light will cross different atmospheric width with time. On a long timeseries this is an obvious effect which is easily corrected. It is harder for short timeseries. If one observes the *On* and the *Off* at the same airmass, the problem is evaded. This is certainly enough to distinguish which star in a crowded field is the transited, and certainly if that transit is larger than that expected for a planet (see figure 3.10).

It is also possible to obtain measurements on two nights, one with an *On* and an *Off*, and one with two *Off*s. This allows to correct better for atmospheric variation and allows a confirmation of when a transit is, and update its ephemeris. This has been used to disentangle periods which the *Hunter* algorithm had had wrong because only few transits were detected, or because it locked onto an alias of the period. The *On/Off* can also be used to attempt the detection of an occultation at $\phi = 0.5$, invisible for WASP but a sure sign of a eclipsing binary when observing in the visible at our precision. *On/Off* sequences at different wavelengths can also distinguish between a planet transiting a star, or a star eclipsing another.

[9] this is a project jointly run with his colleague Emmanuel Jehin from the Université de Liège, and Genève

Typically those sequences last about 10 minutes. An *On/Off* thus last between 25 and 50 minutes of telescope time. Thanks to large availability of time that TRAPPIST enjoys, recently Michaël has taken full transits, confirming the shape of the signal and allowing us to exclude blending scenarios in triple systems more easily.

A lack of radial velocity variation and a negative result from *On/Off* point to a true false positive - different from astrophysical false positives - where the signal in WASP is artificially caused by the instrument, the data reduction or period searching algorithms.

3.3.2 Checking the spectrum

After the first spectrum has been obtained (and often before the second is) a number of diagnostics can be carried out, triggering different responses:

is it a binary?

In the regular radial velocity survey that CORALIE is used for, the targets have been selected in a certain volume of space as single peak and slow rotators. The stars we observe with WASP are generally unstudied; we get all kind of things. It is the observer's job to run the automated cross correlation on a larger window (typically $\pm$ 200 km s^{-1} instead of the traditional $\pm$ 30 km s^{-1}) to search for a second peak in the CCF indicative of a double line binary (SB2). Having two peaks reduces seriously the probability for the candidate to be planetary. The first argument is that there are two stars so the effective transit depth should be larger. Other arguments come as follow:

If both peaks are several 10s of km s^{-1} apart there is a good chance both objects orbit around each others on a short period. One would expect two stars on a short orbit to be synchronised therefore having large FWHM, if both peaks are thin (<15 km s^{-1}), another spectrum is obtained at a later date to verify if any of the peaks has moved. If a planet was around one of them, we should not expect one to move by more than the expected planetary signal. If both peaks are wide, no more observations are conducted and the candidate is flagged as an eclipsing binary.

If both peaks are thin and blended, or not too far away from each others, it indicates that their orbital period is probably long and a planet may exist around one of the components. Another spectrum is therefore taken. If one of both is a fast rotator, it is assumed something make it rotate fast; the candidate is flagged as an eclipsing binary, although the lack of a third spectrum may indicate this is in fact a low mass eclipsing binary. A number of cases are represented in figures 3.11 to 3.15.

So far all SB2s have been rejected. If three or more (not happened yet) peaks are observed, the candidate is immediately rejected and flagged as eclipsing binary.

If no SB2 is detected and after the observer has acquired a second spectrum we can quickly see if there are variations in the radial velocity. If those variations are of order 10 to 100 km s^{-1}, the candidate is flagged a likely low mass eclipsing binary, an astrophysical false positive, but also interesting in their own right. Subsequent lower precision spectra have been acquired on a number of objects to check their period and their orbital parameters.

maybe a giant?

After observing the first spectrum and if the contrast of the CCF is close or exceeds 50%, the object we observe is a cold slow rotating star, quite typical of giants (see Didier Queloz's thesis). If the candidate's position in the colour magnitude diagram is also close to the giants' branch,

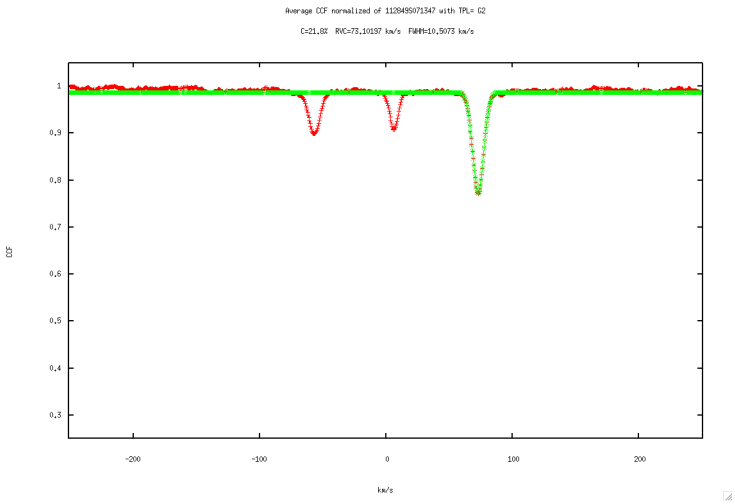


Figure 3.11: Cross Correlation function and Gaussian fit as outputed from the Coralie Data Reduction Software. Here the very clear case of a triple line binary (SB3). The transit can be caused by a paire of either peak, or due to a fourth undetected companion.

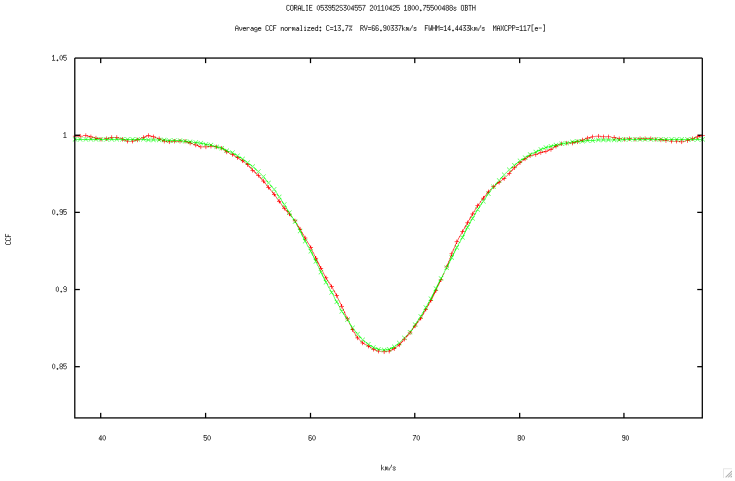


Figure 3.12: CCF and Gaussian fit as outputed from the DRS Here the case of a blended double line binary (SB2). We observe an assymetry on left hand side of the CCF, indicating a second component. This is a fairly long period binary ($\sim$100 day period). The transit WASP detected can be on either companion, or on another unseen component but is probably on the secondary which is seen emerging.

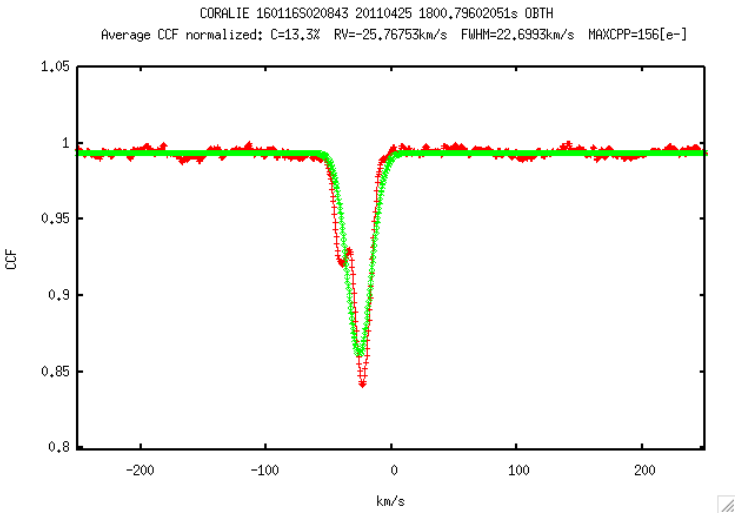


Figure 3.13: CCF and Gaussian fit as outputed from the DRS. Here the case of a blended double line binary (SB2). A second peak is clearly resolved. The deeper CCF (the primary) is seen moving from another epoch by several km s^{-1}. This system is probably an fairly short period binary (20 day period). The transit WASP detected is most probably on the primary.

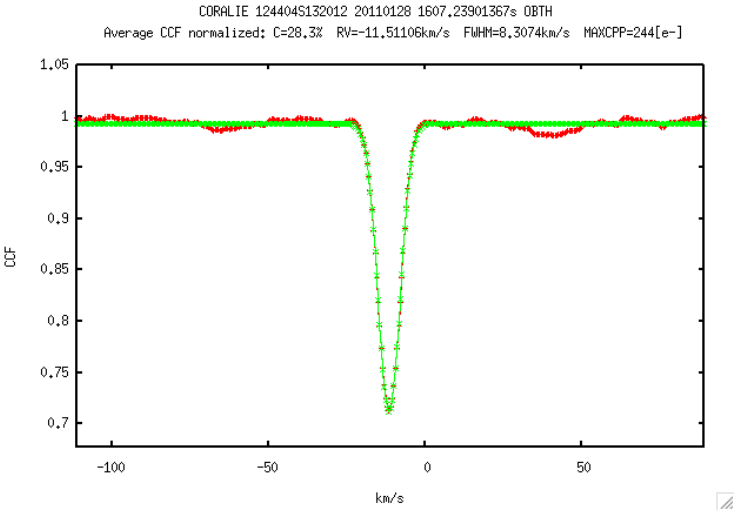


Figure 3.14: CCF and Gaussian fit as outputed from the DRS. Here the case of a triple line binary (SB3). Around the main peak, we can see two much shallower peaks moving. On the top picture the deeper of the two in on the left at $\sim$ 40 km s^{-1} while on the bottom picture we see it around -60 km s^{-1}. Those two are very likely responsible for the transit signal, and could well be in orbit around the primary.

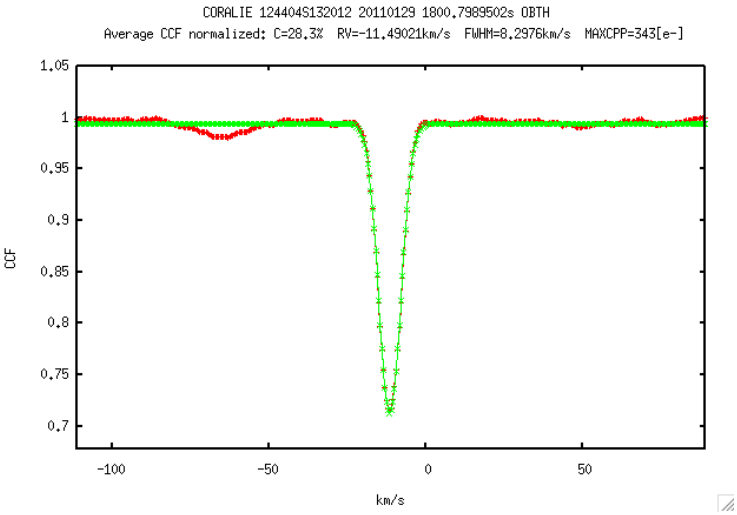


Figure 3.15: CCF and Gaussian fit as outputed from the DRS. Here the case of the same triple line binary (SB3) as above. Now the deeper of the two shallow peaks in on the left of the main one at $\sim$ -60 km s^{-1} instead of 40 km s^{-1} above. Those two are very likely responsible for the transit signal, and are in orbit around the primary.

the spectrum is sent to Barry Smalley who performing a spectral analysis determines at which evolutionary stage it is. If a dwarf, observations are resumed.

It can also happen that we have variations in RV which do not phase with the photometry. If many solar type stars have stellar activity able to produce such variations, so do giants. In that case the spectra are sent and analysed.

fast rotators...

Alternatively, the DRS might return what appears like a straight line. A correlation on a larger window might show that instead of the usual 8 to 9 km s^{-1} expected usually for the FWHM, this object has a 30, 50, 150 km s^{-1} wide CCF: a hot, fast rotating star. If they are SB1s, there are re-observed. If the peak does not move more than 10 km s^{-1}, it is re-observed and placed for photometric follow-up. Then, one can use the same technique as used for the discovery and confirmation of WASP-33 b (Cameron et al. 2010b) where Doppler imaging during transit confirmed the presence of a transiting body around that star (on a retrograde orbit), and placed upper limits to the transiter's mass. A couple of such candidates remain, but no firm detection has happened yet with CORALIE using this technique.

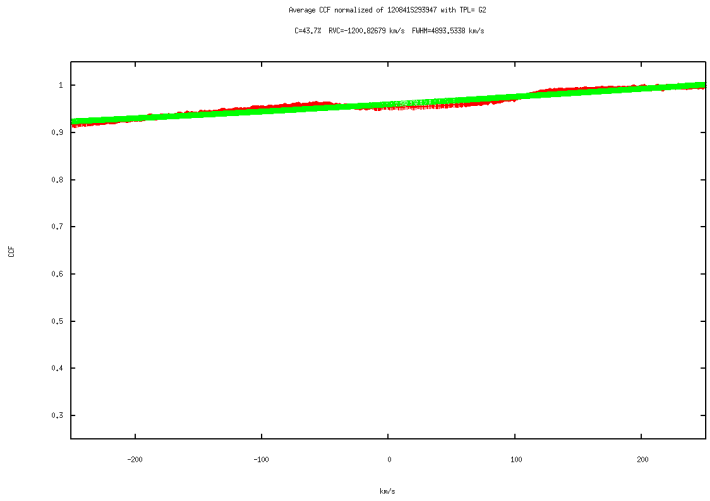


Figure 3.16: CCF and Gaussian fit as outputed from the Coralie DRS online at the telescope, without blaze correction. We barely see the peak in the ccf, and the software could not adjust a solution to it.

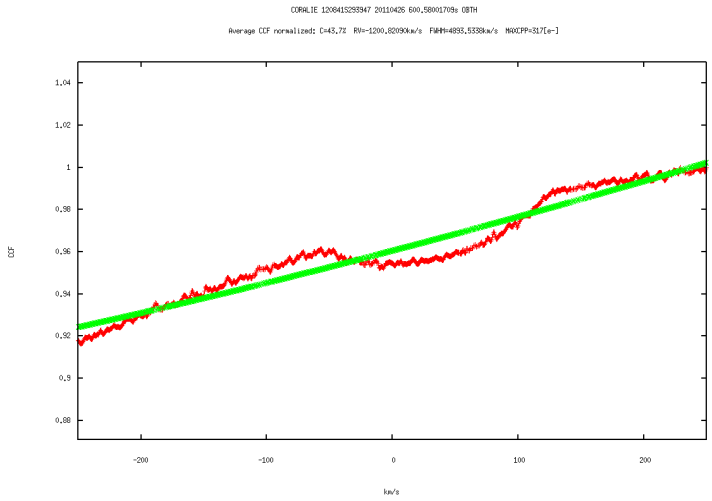


Figure 3.17: Same as above but zoomed in.

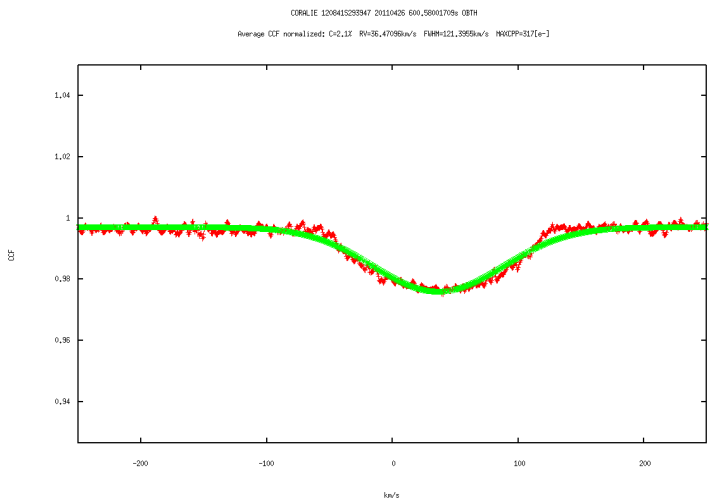


Figure 3.18: same as above but with blaze correction. A Gaussian model is adjusted and an estimate of the radial velocity can be made. Because the CCF is no longer approximated by Gaussian at this width and because of the low depth of it, we suffer systematics effect of order 1 km/s. Enough for characterising low mass eclipsing binaries if present and if not: enough precision to detect reliably that there is no motion making a planet still a valid solution. In this case more spectra are taken, and a series during transit to attempt detecting it using the Doppler shadow method.

Prior to the WASP program starting on CORALIE, the DRS was not correcting for the blaze function of the spectrograph. This was not an issue for the CORALIE RV survey because using small correlation windows for slow rotators, it was unnoticeable. Because some of our target are faster rotators or hotter stars than the targets selected for the CORALIE RV survey, we needed to increase the size of the correlation window by about an order of magnitude, making a clear slope appear. Correcting for the blaze allowed the extracting of radial velocities on fast rotators (see figure 3.16 to 3.18).

3.3.3 No variations, or another period

We have cases where the star is single peaked and shows no variation in radial velocity. *On/Off* shows the transit is on target and confirms the period. We reobserve, still see nothing. Increase exposure time and still see nothing. This is very likely at least a binary star (gravitationally linked or not). The transiter could be a planet, or a third star, orbiting around the secondary that we do not resolve. Not resolving it in the spectrum means it is either a cold star, or that it rotates fast and the width and shallow depth of the second CCF peak went unnoticed (or both). Those are classified as false positives.

Alternatively we could start observing a slope in the RV, with time, or a quadratic motion, this confirms that we are very likely in the case of a binary system whose secondary is being eclipsed. A few points now and then can help confirm the outer period. Similarly to the previous case, we won't be able to confirm if it is a planet or not and thus those are progressively dropped.

3.3.4 Bissector, FWHM & mask variations

Imagine now that we have observed a single line star, at $\phi = 0.25$ and $\phi = 0.75$ and obtain a variation compatible with that expected for a planet with the period that WASP has given. We need to do the same checks than those that are done for discovering planets with the Doppler method: check if the variation in radial velocity can be explained by another physical phenomenon.

A true Gaussian would have a vertical bissector. The motion of a planet around a stars causes a translation of the line and thus a translation of the bissector with time. Its slope does not change. If the radial velocity measured by the DRS is due to a misfit of the Gaussian on a CCF which shape is changing, this will appear as a change in the slope of the bissector. The estimate we use is the *bissector-span*, the difference in the slope at the top of the bissector with the the slope at its bottom. Queloz et al. (2001) show the definition of the span of the bissector, as a measure of the line's shape.

The bissector span will be anti-correlated to the radial velocities if those are caused by presence of stellar spots (Queloz et al. 2001). We are quite immune to such a a configuration: we decided to observe that particular star because it presented a periodic transit-like signal. The photometric signal caused by activity is very different[10]. This bissector diagnosis only becomes important to understand the residuals from fitting a Keplerian. If those are anti-correlated with the bissector, they are likely caused by stellar activity.

What we are quite likely to see is a correlation between the bissector span and the radial velocity, as described in Santos et al. (2002). This is caused by the motion of a second peak over the primary peak in a blended SB2 scenario. This secondary can be within the primary peak: reason why we have not noticed it earlier, or can be very wide and shallow and thus has been unnoticed

[10] Actually observing a weak slope could be indicative of stellar activity induced by the planet

too. Both cases occurred in our survey. Another way to check this is to plot the FWHM with radial velocity and see if a structure there also appears. Santos et al. (2002), modelling the line concluded that the radial velocity signal they observed was caused by a brown dwarf orbiting the secondary component of a K+M binary.

There is a relative occurrence of this effect: this is because the stars we observe are not preselected: we can have visual binaries too close for *Euler* to resolve, and thus the light of two stars falling into the fibre, or the simple scenario of a background eclipsing binary whose systemic velocity matches that of the foreground star[11].

A final test can be conducted: cross correlating the spectra using both the G2 and K5 mask. A planetary signal is achromatic while a signal caused by another star, or the parasite signal produced by stellar activity will have an RV amplitude changing with the mask used. Good examples are provided in Santos et al. (2002) and Huélamo et al. (2008).

3.3.5 Doppler imaging for odd cases

Until now, those were fairly obvious cases, others, more treacherous, lurk in the darker recesses of data and require great attention to be spotted. Some were close calls; hopefully no such false positive has been published as a planet[12].

A good example of what can happen is the case of WASP-9 which should become a paper (Ségransan et al., in prep). Since, another similar system was spotted, showing their relative frequency and our sensitivity to them. The *Hunter* page announced that we had a transit signal close to a 2.00 day period. We observed in radial velocity and saw a variation. That variation was not correlated to the bissector slope and was similar to that of a planet. At a later date we observed a fast drop in the radial velocity caused by an object that we now know, has a period above 1 000 days and a minimum mass compatible with an M dwarf. We continued following it with CORALIE while obtaining a Rossiter-McLaughlin effect with HARPS. Something odd appeared: the Rossiter-McLaughlin effect did not have the same width as the photometric signal. A second effect was observed and matched the first one completely. When using the HARPS data one could start observing a correlation with the bissector and the FWHM. Photometric transits in several band were observed, and we realised the orbit was 0.666 days. Transit depths appeared consistent with each others. That change of orbital period meant we had never obtained radial velocity on our target at the expected quadrature. Observing again the correlations became more evident: a blend scenario.

To be sure the CCFs were sent to be analysed by Andrew Collier Cameron, who using Doppler imaging techniques reached the conclusion that we have a hierarchical quadruple system composed of a star which we see as the single peak in the CCF around which an M dwarf orbits, with another pair of stars eclipsing each other. Of this second pair we can observe a very wide and shallow CCF that eluded me when looking at single CCFs but appeared clear after Andrew's treatment (check Hilditch (2001) for examples of that technique). Furthermore we could see the Doppler shadow of the transiter clearly showing that it was not around the star creating the strongest peak in the CCF (with a similar treatment to Cameron et al. (2010b)). A wicked case!

[11] unlikely, but we are biased to detect some
[12] I really dread this!

3.4 Using the Tool for Discovery & Immediate Characterisation

The interest of having a MCMC ready is to use it as soon as data (magically) lands on your desk. Now coming are a few example of planet discovery papers for which I had a prime role in the analysis of the signal.

3.4.1 WASP-6 b

This paper marks quite an important step as it was one of my first, but above else, the first planet to which I had a hand in discovering, analysing and characterising. It is one of many papers done in close collaboration with Michaël Gillon.

This star also carries a funny story: after two photometric transits observed 10 days apart with *Euler* showed another feature. For one transit it was during during egress, on the second it was before ingress. We immediately thought we had a second planet in the system, smaller (depth was compatible with something round about a Neptune size). After a long search, in RV and photometry we could not find it. The feature finally turned out to be instrumental and caused by the meridian passage. That interlude gave the time to gather more data and produce a paper which is quite complete showing good photometry (without those embarrassing features), radial velocities on a few epochs and even a Rossiter-McLaughlin effect, the first published from the HARPS program (chapter 4). This is becoming progressively the standard type of paper for planet discovery.

A&A 501, 785–792 (2009)
DOI: 10.1051/0004-6361/200911749
© ESO 2009

Astronomy & Astrophysics

Discovery and characterization of WASP-6b, an inflated sub-Jupiter mass planet transiting a solar-type star⋆,⋆⋆

M. Gillon[1,2], D. R. Anderson[3], A. H. M. J. Triaud[2], C. Hellier[3], P. F. L. Maxted[3], D. Pollaco[4], D. Queloz[2], B. Smalley[3], R. G. West[5], D. M. Wilson[3], S. J. Bentley[3], A. Collier Cameron[6], B. Enoch[6], L. Hebb[6], K. Horne[6], J. Irwin[7], Y. C. Joshi[4], T. A. Lister[8], M. Mayor[2], F. Pepe[2], N. Parley[5], D. Segransan[2], S. Udry[2], and P. J. Wheatley[9]

[1] Institut d'Astrophysique et de Géophysique, Université de Liège, Allée du 6 Août 17, Bât. B5C, Liège 1, Belgium
e-mail: michael.gillon@obs.unige.ch
[2] Observatoire de Genève, Université de Genève, 51 Chemin des Maillettes, 1290 Sauverny, Switzerland
[3] Astrophysics Group, Keele University, Staffordshire, ST5 5BG, UK
[4] Astrophysics Research Centre, School of Mathematics & Physics, Queen's University, University Road, Belfast, BT7 1NN, UK
[5] Department of Physics and Astronomy, University of Leicester, Leicester, LE1 7RH, UK
[6] School of Physics and Astronomy, University of St. Andrews, North Haugh, Fife, KY16 9SS, UK
[7] Department of Astronomy, Harvard University, 60 Garden Street, MS 10, Cambridge, Massachusetts 02138, USA
[8] Las Cumbres Observatory, 6740 Cortona Dr. Suite 102, Santa Barbara, CA 93117, USA
[9] Department of Physics, University of Warwick, Coventry, CV4 7AL, UK

Received 29 January 2009 / Accepted 4 May 2009

ABSTRACT

We report the discovery of WASP-6b, an inflated sub-Jupiter mass planet transiting every $3.3610060^{+0.0000022}_{-0.0000035}$ days a mildly metal-poor solar-type star of magnitude $V = 11.9$. A combined analysis of the WASP photometry, high-precision followup transit photometry and radial velocities yield a planetary mass $M_p = 0.503^{+0.019}_{-0.038}\ M_J$ and radius $R_p = 1.224^{+0.051}_{-0.052}\ R_J$, resulting in a density $\rho_p = 0.27 \pm 0.05\ \rho_J$. The mass and radius for the host star are $M_* = 0.88^{+0.05}_{-0.08}\ M_\odot$ and $R_* = 0.870^{+0.025}_{-0.036}\ R_\odot$. The non-zero orbital eccentricity $e = 0.054^{+0.018}_{-0.015}$ that we measure suggests that the planet underwent a massive tidal heating ~1 Gyr ago that could have contributed to its inflated radius. High-precision radial velocities obtained during a transit allow us to measure a sky-projected angle between the stellar spin and orbital axis $\beta = 11^{+14}_{-18}$ deg. In addition to similar published measurements, this result favors a dominant migration mechanism based on tidal interactions with a protoplanetary disk.

Key words. binaries: eclipsing – stars: individual: WASP-6 – planetary systems – techniques: photometric – techniques: radial velocities – techniques: spectroscopic

1. Introduction

Transiting planets play an important role in our understanding of the nature of the extrasolar planetary objects. They are the only exoplanets for which an accurate measurement of the mass and radius is available. The deduced density is a key parameter to constrain theoretical models for the formation, evolution and structure of planets (e.g. Fortney et al. 2007; Liu et al. 2008). For the brightest transiting systems, a study of the atmospheric composition and physics is possible, even with existing instruments like *HST* or *Spitzer* (e.g. Charbonneau et al. 2008; Swain et al. 2008). The discovery rate of transiting planets has increased recently thanks mainly to the efficiency of the CoRoT space-based survey (Baglin et al. 2006) and of a handful of ground-based wide-field surveys targeting rather bright stars ($V < 13$): HATNet (Bakos et al. 2004), WASP (Pollaco et al. 2006), TrES (O'Donovan et al. 2006), and XO (McCullough et al. 2005).

The ~50 transiting planets known at the time of writing show a broad range of mass and radius. Their masses go from 23 $M_\oplus$ for the hot Neptune GJ 436b (Butler et al. 2004; Gillon et al. 2007) to more than 10 M_J for XO-3 (Johns-Krull et al. 2008). Many planets have a size in agreement with basic models of irradiated planets (e.g. Burrows et al. 2007; Fortney et al. 2007), some of them like HD 149026 b (Sato et al. 2005) appearing to be very rich in heavy elements. Nevertheless, a few planets like HD 209458 b (Charbonneau et al. 2000; Henry et al. 2000) are "anomalously" large. Several hypothesis have been proposed to explain this radius anomaly, most importantly tides (Bodenheimer et al. 2001; Jackson et al. 2008b), tides with atmospheric circulation (Guillot & Showman 2002) and enhanced opacities (Guillot et al. 2006; Burrows et al. 2007). The existence of several correlations between parameters of transiting systems has been proposed, for instance between the planet mass and the orbital period (Mazeh et al. 2005; Gaudi et al. 2005) and between the heavy-element content of the planet and the stellar metallicity (Guillot et al. 2006; Burrows et al. 2007). The astrophysics supporting these correlations has still to be fully understood.

It is highly desirable to detect and characterize thoroughly many more bright short period transiting systems to improve our understanding of the highly irradiated gaseous planets and to constrain the structure and evolution models for these objects.

⋆ Based on data collected with the HARPS spectrograph at ESO La Silla Observatory in the programs 082.C-0040(E) and 082.C-0608.
⋆⋆ The photometric time-series and radial velocities (Tables 4, 5) used in this work are only available in electronic form at the CDS via anonymous ftp to cdsarc.u-strasbg.fr (130.79.128.5) or via http://cdsweb.u-strasbg.fr/cgi-bin/qcat?J/A+A/501/785

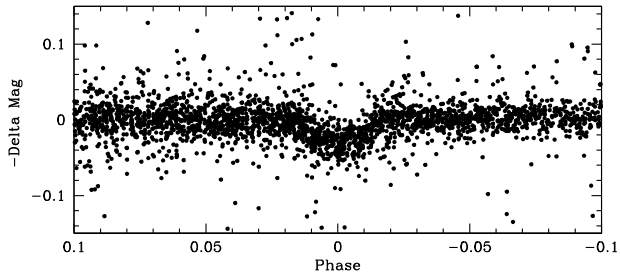


Fig. 1. WASP photometry of WASP-6 phase-folded with the best-fit period from the transit search algorithm presented in Collier Cameron et al. (2006).

With its very high detection efficiency, the WASP transit survey is making a large contribution to this goal. It is the only transit survey operating in both hemispheres: it uses an instrument named WASP-North and located at La Palma to search for planets from the Northern hemisphere and a twin instrument named WASP-South and located at Sutherland to do the same from the Southern hemisphere. Each of these instruments covers a huge field of view of 482 square degrees per pointing, allowing them to search for transiting planets in a large portion of the sky. Due to the brightness of the host stars, planets detected by WASP are very good targets for high-precision followup observations. For instance, it is possible to measure for most of them the alignment between the stellar rotation axis and the planetary orbital axis via the observation of the Rossiter-McLaughlin effect (RM; Queloz et al. 2000). The measured value for this spin-orbit angle is a strong constraint for inward planetary migration models (see Winn 2008, and references therein).

We report here the discovery and characterization of WASP-6b, a new sub-Jupiter mass planet transiting a mildly metal-poor solar-type star of magnitude $V = 11.9$. We present in Sect. 2 the WASP discovery photometry plus high precision followup transit photometry and radial velocity measurements confirming the planetary nature of WASP-6b and including the observation of a spectroscopic transit. Section 3 presents the determination of the host star parameters. Our determination of the system parameters is presented in Sect. 4. These parameters are discussed in Sect. 5.

2. Observations

2.1. WASP photometry

The host star 1SWASP J231237.75-224026.1 (=USNO-B1.0 0673-1077008 = 2MASS 23123773-2240261; hereafter WASP-6) was observed by WASP-South during the 2006 and 2007 observing seasons, covering the intervals 2006 May 07 to 2006 November 12 and 2007 July 05 to 2007 November 13 respectively. The 9630 pipeline-processed photometric measurements were de-trended and searched for transits using the methods described in Collier Cameron et al. (2006). The selection process (Collier Cameron et al. 2007) elected WASP-6 as a high priority candidate presenting a periodic transit-like signature with a period of 3.361 days. A total of 18 transits are observed in the data. Figure 1 presents the WASP photometry folded with the best-fit period.

2.2. High-S/N transit photometry

Followup transit photometry was obtained on 2007 October 13 using the 2048 × 2048 pixels camera HawkCam2 (Wilson et al. 2008; Anderson et al. 2008) on the 2.0-m Faulkes Telescope South (FTS) at Siding Spring Observatory . The camera has a scale of 0.135 arcsec/pixel and a field of view of ∼4.6 × 4.6 arcmin^2. We observed the target field using the SDSS i' band in the 2 × 2 bin mode to improve the duty cycle. We acquired 247 frames of 60 s exposure during the run. The telescope was sufficiently defocussed to keep the stellar flux within the linear range of the CCD. The images were bias subtracted and flat-field corrected with a master bias and twilight flat field images using `IRAF`[1]. `DAOPHOT` aperture photometry (Stetson 1987) was performed around the target and comparison stars. We substracted a linear fit from the differential magnitudes as a function of airmass to correct for the different colour dependance of the extinction for the target and comparison stars. The linear fit was calculated from the out-of-transit (OOT) data and applied to all the data. The corresponding fluxes were then normalized using the OOT part of the photometry. We discarded the first 17 measurements because they were obtained during twilight. Figure 2 shows the resulting lightcurve folded on the best-fit orbital period and the residuals obtained after removing the best-fit transit model (see Sect. 4). Their rms is 1.67×10^{-3}. This can be compared to 9.54×10^{-4}, the mean theoretical error bar taking into account photon, read-out, scintillation and background noises.

High precision transit observations of WASP-6 were also carried out using the 1024 × 1024 pixels thermoelectrically cooled frame transfer CCD camera RISE mounted on the 2-m Liverpool Telescope (LT) in La Palma (Steele et al. 2008). The camera has a scale of 0.55 arcsec/pixel and a total field of view of ∼9.4 × 9.4 arcmin^2. We observed the target field using a single broad band $V + R$ filter in the 2 × 2 bin mode. We acquired 4200 frames of 3 s exposure on the night of 2008 July 25 and 2880 frames of 5 s exposure on the night of 2008 August 11. The telescope was, here too, defocussed. A similar reduction procedure as for the FTS photometry was used. The resulting normalized light curves of WASP-6 folded with the best-fit orbital period are shown in Fig. 2. The rms of the residuals is respectively 0.54% and 0.5% for the first and second run, while their mean theoretical error bar are 0.51% and 0.40%.

As can be seen in Fig. 2, our three high-S/N transit photometric time-series, and especially the FTS one, show a significant level of correlated noise. We could not identify the origin of this noise, but we take it into account in our derivation of the system parameters (see Sect. 4).

2.3. Spectroscopy

As soon as WASP-6 was identified as a high priority target, spectroscopic measurements were obtained using the CORALIE spectrograph mounted on the Euler Swiss telescope (La Silla, Chile) to confirm the planetary nature of the eclipsing body and measure its mass. WASP-6 was observed from 2007 September 16 to 2007 October 26 and from 2008 September 11 to 2008 September 25. Radial velocities (RV) were computed by weighted cross-correlation (Baranne et al. 1996; Pepe et al. 2005) with a numerical G2-spectral template. RV variations of semi-amplitude ∼75 m s^{-1} were detected consistent with a

[1] `IRAF` is distributed by the National Optical Astronomy Observatory, which is operated by the Association of Universities for Research in Astronomy, Inc., under cooperative agreement with the National Science Foundation.

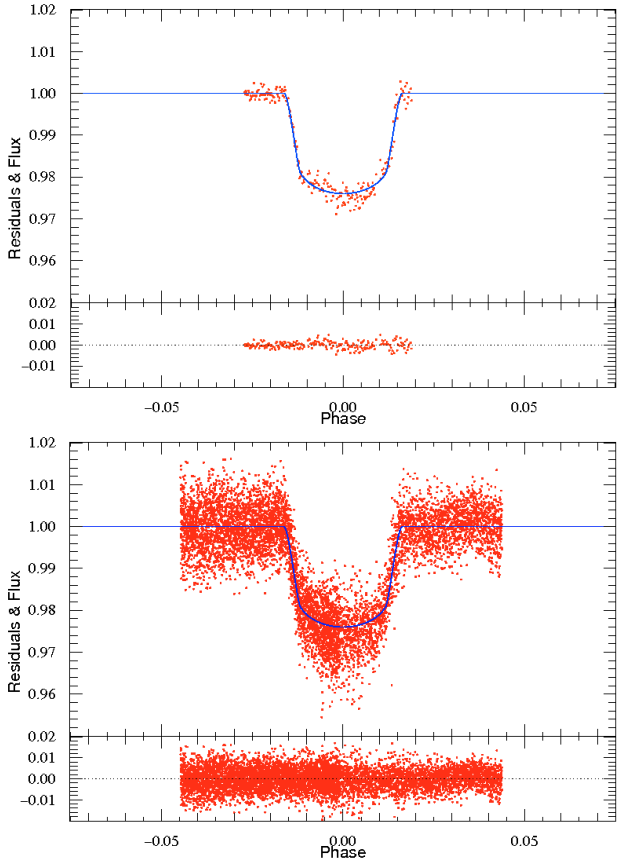


Fig. 2. FTS i'-band (*top*) and LT/RISE $V+R$ (*bottom*) transit photometry for WASP-6 and residuals after subtraction of the best-fit transit curve (superimposed in blue).

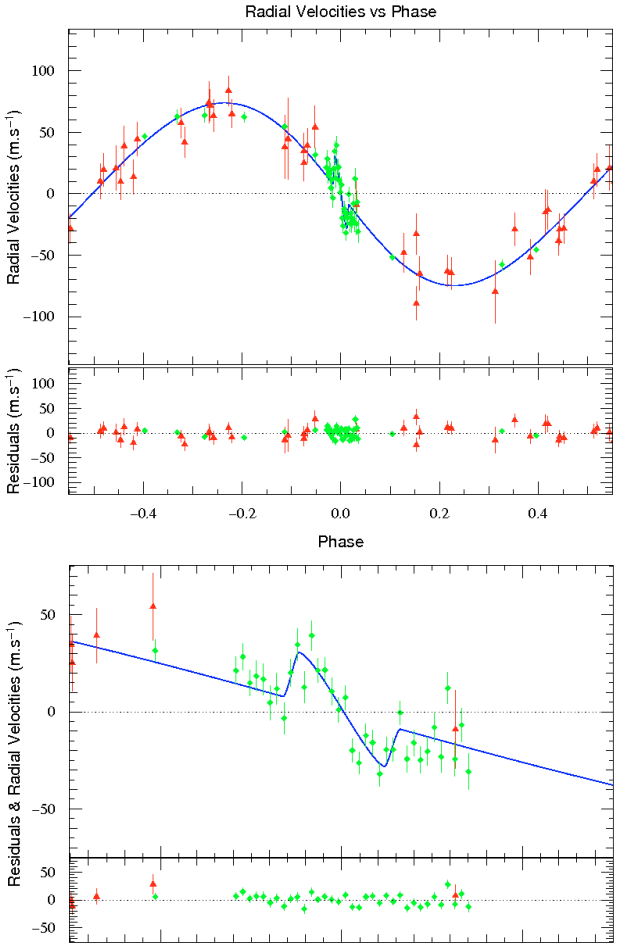


Fig. 3. *Top*: the RV measurements of WASP-6 obtained with CORALIE (red triangles) and HARPS (green squares). The systematic velocity has been subtracted. The solid line is the MCMC solution (see Sect. 4); it includes the RM effect. *Bottom*: zoom on the transit phase showing the RM effect.

planetary-mass companion whose period closely matches that from the WASP transit detections.

44 additional spectroscopic measurements were obtained with the HARPS spectrograph (Mayor et al. 2003) based on the 3.6-m ESO telescope (La Silla, Chile) in the context of the programs 082.C-0040(E) and 082.C-0608(E). These programs aim to improve the characterization of WASP transiting planets. As CORALIE, HARPS is a cross-dispersed, fiber-fed, echelle spectrograph dedicated to high-precision Doppler measurements. HARPS data were reduced with a pipeline very similar to the CORALIE one. In addition to several measurements covering the whole orbital phase, high-cadence measurements of a spectroscopic transit were obtained with HARPS on 2008 October 08 in order to determine the sky-projected angle between the planetary orbital axis and the stellar rotation axis and included two points taken the night before, a point as far as possible from the transit on the transit night and a point the night after. This strategy aims to determine the systematic RV with greater accuracy than if the RM effect was taken on its own, assuming that stellar activity is the same over the three nights.

Our RV measurements are shown phase-folded and overplotted with the best-fitting orbital+RM model in Fig. 3.

To exclude that the RV signal shown in Fig. 3 is due to spectral line distortions caused by a blended eclipsing binary, the CORALIE and HARPS cross-correlation functions were analyzed using the line-bisector technique described in Queloz et al. (2001). No evidence for a correlation between the bisector spans and the RV variations was found (Fig. 4). The most likely cause for the periodic signal observed in photometry and RV measurements and for the RM effect observed on 2008 October 08 is thus the presence of a giant planet transiting the star WASP-6 every 3.36 days.

3. WASP-6 stellar parameters

The individual CORALIE and HARPS spectra are relatively low signal-to-noise, but when co-added into 0.01 Å steps they give a S/N of in excess of 100:1 which is suitable for a photospheric analysis of WASP-6. The standard pipeline reduction products were used in the analysis.

The analysis was performed using the UCLSYN spectral synthesis package (Smith 1992; Smalley et al. 2001) and ATLAS9 models without convective overshooting (Castelli et al. 1997). The H_α line was used to determine the effective temperature ($T_{\rm eff}$), while the Na I D and Mg I b lines were used as surface gravity ($\log g$) diagnostics. The parameters obtained from the analysis are listed in Table 1.

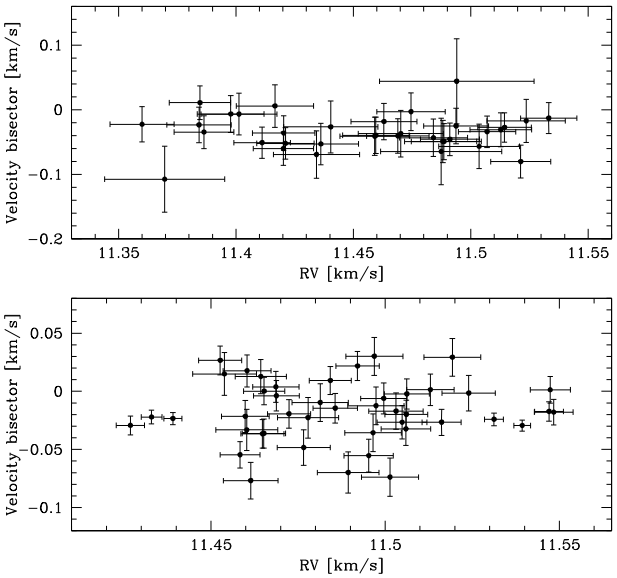


Fig. 4. Bisector versus RV measured from all the observed CORALIE (*top*) and HARPS (*bottom*) spectra. We adopt uncertainties of twice the RV uncertainty for all bisector measurements. There is no correlation between these two parameters indicating the RV variations are not caused by stellar activity or line-of-sight binarity.

Table 1. Stellar parameters derived for WASP-6.

Parameter	Value
RA (J2000)	$23^h12^m37.74^s$
Dec (J2000)	$-22°40'26.''2$
V	11.9
$T_{\rm eff}$	5450 ± 100 K
$\log g$	4.6 ± 0.2
ξ_t	1.0 ± 0.2 km s^{-1}
$V_{\rm rot} \sin I$	1.4 ± 1.0 km s^{-1}
[Fe/H]	−0.20 ± 0.09
[Na/H]	−0.17 ± 0.06
[Mg/H]	−0.13 ± 0.07
[Al/H]	−0.15 ± 0.10
[Si/H]	−0.12 ± 0.08
[Ca/H]	−0.09 ± 0.10
[Sc/H]	−0.22 ± 0.15
[Ti/H]	−0.05 ± 0.09
[V/H]	−0.02 ± 0.08
[Cr/H]	−0.17 ± 0.09
[Mn/H]	−0.20 ± 0.13
[Co/H]	−0.16 ± 0.14
[Ni/H]	−0.21 ± 0.08
$\log N$(Li)	<0.5
$T_{\rm eff}$(IRFM)	5470 ± 130 K
θ(IRFM)	0.037 ± 0.002 mas

The equivalent widths of several clean and unblended lines were measured. Atomic line data was mainly taken from the Kurucz & Bell (1995) compilation, but with updated van der Waals broadening coefficients for lines in Barklem et al. (2000) and $\log gf$ values from Gonzalez & Laws (2000), Gonzalez et al. (2001) or Santos et al. (2004). A value for microturbulence (ξ_t) was determined from Fe I using Magain's (1984) method. The ionization balance between Fe I and Fe II and the null-dependence of abundance on excitation potential were used as an additional the $T_{\rm eff}$ and $\log g$ diagnostics (Smalley 2005).

We have determined the elemental abundances of several elements (listed in Table 1) from their measured equivalent widths. The quoted error estimates include that given by the uncertainties in $T_{\rm eff}$, $\log g$ and ξ_t, as well as the scatter due to measurement and atomic data uncertainties. In our spectra the Li I 6708 Å line is not detected ($EW < 2$ mÅ), allowing us to derive an upper-limit on the Lithium abundance of $\log n$(Li/H) + 12 < 0.5. The lack of lithium implies an age in excess of ∼3 Gyr (Sestito & Randich 2005).

Projected stellar rotation velocity ($V_{\rm rot} \sin I$) was determined by fitting the profiles of several unblended Fe I lines in the HARPS spectra. We used a value for macroturbulence ($v_{\rm mac}$, see Gray 2008) of 2 km s^{-1} and an instrumental *FWHM* of 0.060 ± 0.005 Å, determined from the telluric lines around 6300 Å. A best fitting value of $V_{\rm rot} \sin I = 1.4 \pm 1.0$ km s^{-1} was obtained. If, however, mactroturbulence is lower, then higher rotation values are found, with $V_{\rm rot} \sin I = 3.0 \pm 0.5$ km s^{-1} obtained for $v_{\rm mac} = 0$ km s^{-1}. If, on the other hand, $v_{\rm mac}$ is slightly higher than 2 km s^{-1}, then $V_{\rm rot} \sin I$ could be undetectable.

In addition to the spectral analysis, we have also used broad-band photometry from TYCHO-2, USNO-B1.0 *R*-mag, CMC14 r', DENIS and 2MASS to estimate the total observed bolometric flux. The Infrared Flux Method (Blackwell & Shallis 1977) was then used with 2MASS magnitudes to determine $T_{\rm eff}$ and stellar angular diameter (θ). This gives $T_{\rm eff}$= 5470 ± 130 K, which is in close agreement with that obtained from the spectroscopic analysis and implies a spectral type of G8V (Gray 2008).

4. Derivation of the system parameters

We derived stellar and planetary parameters for the system by fitting simultaneously the WASP, FTS and LT/RISE photometry with the CORALIE and HARPS RVs. These data were used as input into the Markov Chain Monte Carlo (MCMC, Ford 2006) code described in Gillon et al. (2008) and Triaud et al. (in prep.). MCMC is a Bayesian inference method based on stochastic simulations and provides the a posteriori probability distribution of adjusted parameters for a given model. Here the model is based on a star and a transiting planet on a keplerian orbit about their center of mass. Specifically, we used the photometric transit model of Mandel & Agol (2002) and the spectroscopic transit model of Giménez (2006) in addition to a classical Keplerian model for the orbital part of the RV variations. To model the transit lightcurves, a quadratic limb darkening law was assumed, with coefficients interpolated from Claret's tables (2000, 2004) for the appropriate photometric filters. For the RISE broad band filter, the average from V and R bands was taken to be our theoretical limb darkening parameters.

We used 16 jump parameters in our MCMC simulations: the orbital period P, the time of minimum light T_0, the transit depth D, the total transit width W, the impact parameter b, the stellar mass M_*, the orbital RV semi-amplitude K, a systematic radial velocity γ for each spectroscopic instrument (HARPS and CORALIE), the parameters $e \cos \omega$ and $e \sin \omega$ where e is the orbital eccentricity and ω is the argument of periastron, the products $V_{\rm rot} \sin I \cos \beta$ and $V_{\rm rot} \sin I \sin \beta$ where $V_{\rm rot} \sin I$ is the projected stellar rotational velocity and β is the spin-orbit angle (see Giménez 2006), and a normalization factor for each of the 4 light curves (assuming the same normalization for the whole SW photometry). As explained in the now abundant literature on the application of MCMC to perform Bayesian inference for transiting planets (see e.g. Collier Cameron et al. 2007, and references therein), each MCMC simulation is composed of a large

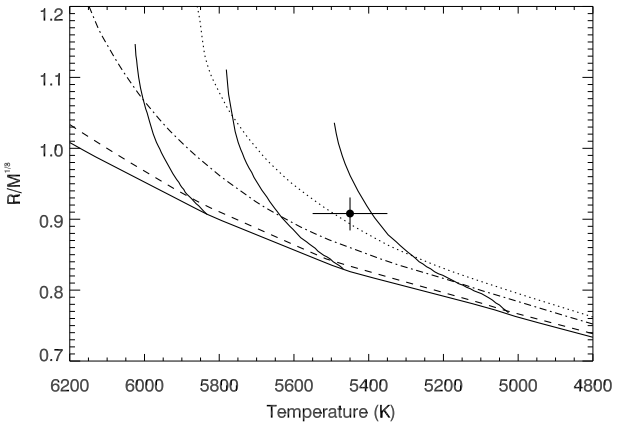


Fig. 5. $R/M^{1/3}$ (in solar units) versus effective temperature for WASP-6 compared to the theoretical stellar stellar evolutionary models of Girardi et al. (2000). The labeled mass tracks are for 0.8, 0.9 and 1.0 $M_{\odot}$ and the isochrones are 100 Myr (solid), 1 Gyr (dashed), 5 Gyr (dot-dashed), 10 Gyr (dotted). We have interpolated the tracks at −0.2 metallicity and have included the uncertainty on the metallicity (+−0.1) in the overall uncertainties on the mass and the age. According to the models, the host star has an age of 11 ± 7 Gyr.

number of consecutive steps for which the jump parameters are randomly modified or not depending of the result of a test on the merit function (MF). The MF used here is the sum of the χ^2 for all the data with respect to the models added to a Bayesian prior on $V_{\rm rot}\sin I$ and M_* representing our constraints on these parameters from spectroscopy:

$$MF = \chi^2 + \frac{(V_{\rm rot}\sin I - (V_{\rm rot}\sin I)_0)^2}{\sigma^2_{V_{\rm rot}\sin I}} + \frac{(M_* - (M_*)_0)^2}{\sigma^2_{M_*}} \quad (1)$$

where $(V_{\rm rot}\sin I)_0 = 1.4$ km s^{-1}, $\sigma_{V_{\rm rot}\sin I} = 1$ km s^{-1}, $M_* = 0.87$ and $\sigma_{M_*} = 0.08$. These last two values were obtained by interpolation of Girardi stellar evolution models (Girardi et al. 2000) in order to find the mass and age that best match the spectroscopic parameters. We notice that our data do not constrain strongly M_* and that it is a free parameter under the control of a Bayesian prior in our simulations only to propagate its uncertainty to the other physical parameters.

A first MCMC run was performed and led to a refined value for the stellar density. We converted it to $R_*/M_*^{1/3}$ in solar units, and compared this property and the stellar temperature to the Girardi models interpolated at −0.2 metallicity. The quantity, $R_*/M_*^{1/3}$, depends only on the observed transit properties (duration, depth, impact parameter, and orbital period) and is independent of the measured temperature. We generated the same property from the mass and log g values in the models, and then interpolated the models in the $R/M^{1/3}$-$T_{\rm eff}$ plane to determine a mass and age for WASP-6. We interpolated linearly along two consecutive mass tracks to generate an equal number of age points between the zero-age main sequence and the evolutionary state where the star reaches the end of core hydrogen burning. We then interpolated between the mass tracks along equivalent evolutionary points to find the mass and age from the models that best match the stellar density derived from the MCMC and the effective temperature. In this way, we obtained a value for the stellar mass of, $M_* = 0.83^{+0.07}_{-0.09}$ $M_{\odot}$ and a derived age for the system of 11 ± 7 Gyr (see Fig. 5).

The best-fitting model found in the first MCMC run was used to estimate the level of correlated noise in each photometric time-series and a jitter noise in the RV time series. For each photometric time-series, the red noise was estimated as described in Gillon et al. (2006), by comparing the rms of the unbinned and binned residuals. We used a bin size corresponding to a duration of 25 min, similar to the timescale of the ingress/egress of the transit. For the SW data, the red noise was estimated to be negligible when compared to the theoretical error bar of the measurements and it was thus neglected. The deduced red noise values (Table 2) were added quadratically to the theoretical uncertainties of each corresponding time-series. No jitter is detected in the CORALIE data. For the HARPS data, a significant jitter is obtained, but it seems to be originating mostly from the residuals of the RM effect and is probably more due to lower-than-usual S/N on the spectra and a worsening of airmass (reaching 1.8 at the end of the sequence) than stellar activity. For this reason, no jitter noise was added to the RV uncertainties.

Table 2. Deduced values for the photometric red noise (*top*), and the RV jitter and systematic velocities (*bottom*).

Photometric time-series	Red noise [ppm]	
FTS	545	
RISE-1	317	
RISE-2	770	
RV time-series	**Jitter [m s^{-1}]**	**systematic RV [km s^{-1}]**
CORALIE	0	11.449
HARPS	6.4	11.485

Using the updated value of the stellar mass as initial value, a second MCMC run was then performed. This chain allowed a large safety burn-in period of discarded 50 000 steps followed by a simulation of 500 000 steps allowing a robust determination of the a posteriori probability distributions for the jumped parameters. The parameter set (jump + deduced parameters) corresponding to the lowest MF was considered as the best solution, and for each parameter upper and lower 1-σ error bars were obtained from respectively the 68.3% larger and smaller values. Best-fitting jump + physical parameters are shown in Table 3. The reduced χ^2 of the best-fitting solution is 0.86.

5. Discussion

With half of the mass of Jupiter and a radius significantly larger, WASP-6b appears too large for basic models of irradiated planets (Burrows et al. 2007a; Fortney et al. 2007), even if an absence of core is assumed. For instance, tables presented in Fortney et al. (2007) predict a maximum radius of ∼1.1 $R_{\rm J}$ for a 0.5 Jupiter-mass planet orbiting at 0.045 AU of a 4.5 Gyr solar-type star. WASP-6 is smaller, cooler and probably older than the Sun, so 1.2 $R_{\rm J}$ is clearly too large for these models. In this context, it is worth noticing the non-null eccentricity that we infer for its orbit ($e = 0.054^{+0.018}_{-0.015}$). The fact that the planetary orbit is still not circularized despite the large age of the system indicates that the tidal evolution of WASP-6b probably played an important role in its energy budget. As outlined by Jackson et al. (2008b), tidal heating could have been large enough for many close-in planets to explain at least partially the large radius of some of them. To assess the past and future tidal evolution of WASP-6b, we integrated the equations for da/dt and de/dt presented in Jackson et al. (2008a) and computed at each step the tidal heating rate H using the formula presented in Jackson et al. (2008b). We assumed values of $Q'_{\rm p} = 10^{6.5}$ and $Q'_* = 10^{5.5}$ for respectively the

Table 3. Values and 1-σ error limits derived in this work for the jump and physical parameters of the WASP-6 system.

Parameter	Value	Units
Transit epoch T_0	$2\,454\,596.43267^{+0.00015}_{-0.00010}$	HJD
Orbital period P	$3.3610060^{+0.0000022}_{-0.0000035}$	days
Planet/star area ratio $(R_p/R_s)^2$	$0.02092^{+0.00019}_{-0.00025}$	
Transit duration t_T	$0.10860^{+0.00073}_{-0.00067}$	days
Impact parameter b	$0.26^{+0.07}_{-0.11}$	R_*
RV semi-amplitude K	$74.3^{+1.7}_{-1.4}$	m s^{-1}
$e \cos \omega$	$-0.007^{+0.011}_{-0.008}$	
$e \sin \omega$	$0.054^{+0.018}_{-0.017}$	
$V_{rot} \sin I \cos \beta$	$1.57^{+0.28}_{-0.10}$	
$V_{rot} \sin I \sin \beta$	$0.32^{+0.49}_{-0.50}$	
Orbital semi-major axis a	$0.0421^{+0.0008}_{-0.0013}$	AU
Orbital inclination i	$88.47^{+0.65}_{-0.47}$	degrees
Orbital eccentricity e	$0.054^{+0.018}_{-0.015}$	
Argument of periastron ω	$1.70^{+0.12}_{-0.23}$	rad
Spin-orbit angle β	$0.20^{+0.25}_{-0.32}$	rad
Stellar mass M_*	$0.880^{+0.050}_{-0.080}$	$M_\odot$
Stellar radius R_*	$0.870^{+0.025}_{-0.036}$	$R_\odot$
Stellar surface gravity $\log g_*$	4.50 ± 0.06	[cgs]
Stellar density ρ_*	$1.34^{+0.11}_{-0.10}$	$\rho_\odot$
Projected rotational velocity $V_{rot} \sin I$	$1.60^{+0.27}_{-0.17}$	km s^{-1}
Planet radius R_p	$1.224^{+0.051}_{-0.052}$	R_J
Planet mass M_p	$0.503^{+0.019}_{-0.038}$	M_J
Planetary surface gravity $\log g_p$	2.940 ± 0.063	[cgs]
Planet density ρ_p	0.27 ± 0.05	ρ_J
Planet temperature $(A = 0, f = 1/4)$ T_{eff}	1194^{+58}_{-57}	K

planetary and stellar tidal dissipation parameters[2]. These values were found by Jackson et al. (2008a) to conciliate the eccentricity distribution of close-in planets before their tidal evolution to the one of the planets detected further from their star. We also took into account the evolution of the stellar rotation period due to the tide raised by the planet using (Goldreich & Soter 1966):

$$\frac{d\Omega_*}{dt} = -\mathrm{sign}(\Omega_* - n)\frac{9}{4} G \frac{R_*^3}{\alpha_* M_* Q'_*} \frac{M_p^2}{a^6}, \quad (2)$$

where G is the gravitational constant, n is the mean orbital motion, Ω_* is the stellar spin angular rate and $\alpha_* = I_*/(M_* R_*^2)$ with I_* being the moment of inertia though the spin axis of the star. For α_*, we assumed a value of 0.07 (Pätzold et al. 2004). To assess the reliability limits of the model, we also computed the evolution of the total angular momentum of the system (assuming a negligible contribution of the planet rotation):

$$L_{tot} = \frac{M_* M_p}{M_* + M_p} n a^2 \sqrt{1 - e^2} + \alpha_* M_* R_*^2 \Omega_*. \quad (3)$$

Neglecting the possible decrease due stellar wind (Dobbs-Dixon et al. 2004), L_{tot} should be a conserved quantity during the whole tidal evolution of the system.

[2] We use here the same convention as Jackson et al. (2008a): the coefficients Q'_p and Q'_* used here are equal to the actual tidal dissipation parameters Q_p and Q_* multiplied by the ratio $3/2k$ where k is the Love number.

Figure 6 shows the obtained evolution for a, e, H, L_{tot} and the orbital and stellar rotation period from 2 Gyr ago to 5 Gyr in the future. Interestingly, the model predicts (1) that the eccentricity and semi-major axis of WASP-6b were significantly larger in the past; (2) that the orbit will be fully circularized 1 Gyr from now; and (3) that the planet will continue to slowly approach the star until finally reaching its Roche limit. This last results agrees well with the fact that the ratio L_{tot}/L_c, where L_c is critical angular momentum (see Levrard et al. 2009), has a value of ~0.6, implying that the system is tidally unstable and will ultimately merge. Levrard et al. (2009) showed that all the other transiting systems, except HAT-P-2, are in the same case.

Under this tidal evolution model, WASP-6b was brought to a distance >0.05 AU of its host star in the very early life of the system, then its orbital evolution has been totally dominated by tides until now. This evolution does not consider the possible influence of one or more other planets able to pump the eccentricity of WASP-6b (Mardling 2007), but our RV data do not reveal the presence of another planet so it seems reasonable at this stage to assume that the orbital evolution of WASP-6b was not dominated by planet-planet interactions. The model assumes also a constant radius for the planet during the whole tidal evolution, which is not very likely (Liu et al. 2008). Furthermore, Fig. 6 shows that it does not conserve L_{tot} for $e >\sim 0.3$ and during the final runaway merging of the planet with the star. Considering as valid only the part of the tidal evolution for which L_{tot} is conserved at the 1-% level, we can nevertheless conclude from Fig. 6 that WASP-6b experienced 0.6–1.2 Gyr ago a large tidal

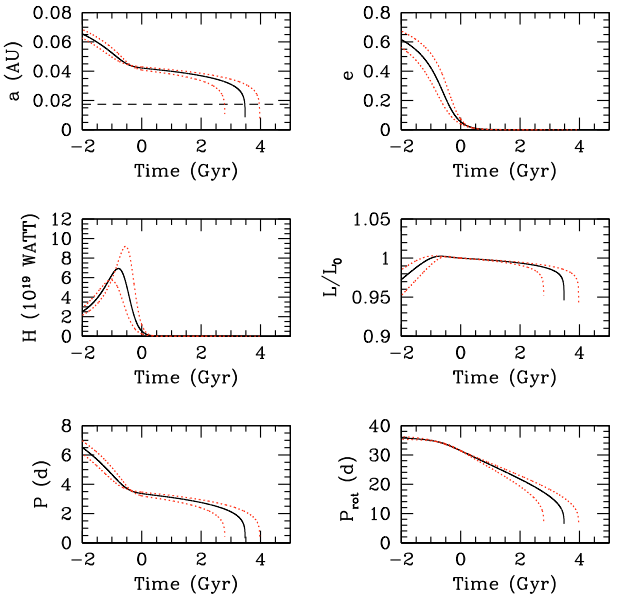


Fig. 6. Tidal evolution for WASP-6b computed using the method described in Jackson et al. (2008b) . *Top left*: evolution of the semi-major axis. The dashed line shows the Roche limit of the system. *Top right*: evolution of the eccentricity. *Middle left*: evolution of the tidal heating rate. *Middle right*: evolution of the total angular momentum. *Bottom*: evolution of the orbital (*left*) and star rotational (*right*) period. For each parameter, the solid line shows the evolution computed with the best-fitting present eccentricity and semi-major axis while the red dotted lines assume the maximum and minimum tidal heating consistent with their 1-σ error bars.

heating rate of 5–10 $\times$ 10^{19} W. Such a large heating rate in the past should have modified drastically the thermal history of the planet and could have contributed significantly to the measured inflated radius.

It is worth exploring the influence of the assumed values of Q'_p and Q'_* on the future tidal evolution of the planet. Q'_p is found to be of order 10^5–10^6 for Jupiter (Golreich & Soter 1966; Yoder & Peale 1981). It is unknown for extrasolar planets, but the theoretical analysis of Ogilvie & Lin (2004) suggests that its most probable value should be of order 5×10^6. WASP-6b is not a good case to constrain this parameter, because its small mass makes negligible the tides that it raises on the star: the tidal history that we compute does not change for any value of Q'_p ranging from 10^5–10^9. Most studies assume Q'_* to be around 10^5–10^6, but values up to 10^9 are still considered as plausible (Eggleton et al. 1998). We computed the tidal evolution of the system for Q'_* values ranging from 10^5 to 10^9. As can be seen in Fig. 7, we cannot constrain Q'_* either: even with a value for Q'_* of 10^5, the future lifetime of the planet would still remain a significant fraction of its age and its detection would not have been an extremely improbable event. We can only conclude from Fig. 7 that for the smallest Q_* values WASP-6b could fall on its host star before this latter leaves the main sequence.

The large radius of WASP-6b (~1.2 R_J) and the metal deficiency of its host star seem to strengthen the existence of a correlation between the heavy-element content of giant planets and the stellar metallicity (Guillot et al. 2006; Burrows et al. 2007). Still, this proposed correlation is not obvious at all in a planetary mass-radius diagram presenting separately the planets for which the host star has a sub-solar metallicity (see Fig. 8, top

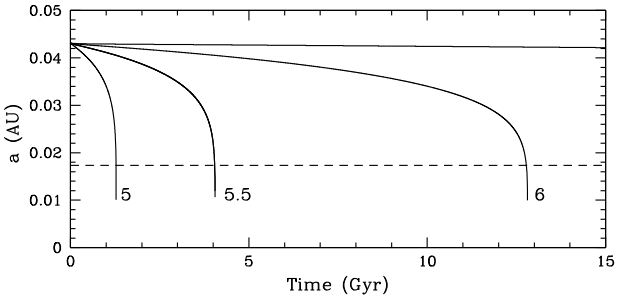


Fig. 7. Future tidal evolutions for WASP-6b computed with different values for Q'_* (see text for details). The labeled evolutions correspond to $Q'_* = 10^5$, $10^{5.5}$ and 10^6.

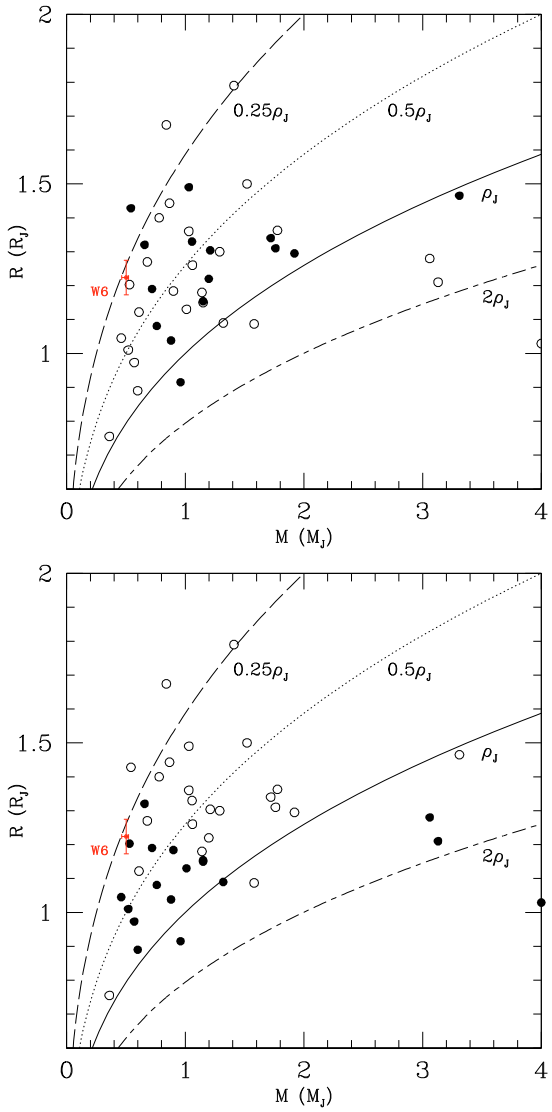


Fig. 8. Mass-radius diagrams for the transiting gaseous giant planets less massive than 4 M_J. The error bars are shown only for WASP-6 (red dot) for the sake of clarity. In *the top panel*, the filled circles indicate the planets for which the host-star metallicity is sub-solar, while in *the bottom panel* they indicate the planets receiving a stellar insolation $<10^9$ erg s^{-1} cm^{-2}.

panel): both populations seem well mixed without any hint of a smaller density for planets orbiting around metal-poor stars. On the other side, the division of transiting planets into two well separated groups in the mass-radius diagram seems clearer when the level of irradiation is considered (Fig. 8, bottom panel). This apparent correlation density-irradiation does not necessarily indicate a direct influence of the incoming stellar flux on the planet size, it could also be explained by a more indirect action. For instance, the most irradiated planets are the ones being the closest to their host star, so the ones for which tidal heating should be the largest.

With a stellar irradiation $\sim 4.7 \times 10^8$ erg s^{-1} cm^{-2}, WASP-6b belongs to the theoretical pL planetary class proposed by Fortney et al. (2008; see also Burrows et al. 2008). Under this theory, Ti and V-bearing compounds should mostly be condensed in the planetary atmosphere and occultation measurements at different wavelengths should not reveal any stratospheric thermal inversion. Such occultation observations would not only constrain atmospheric models of giant close-in planets, they would also constrain the eccentricity of the orbit and thus the tidal thermal history of the planet.

The value that we determine for the sky-projected angle between the stellar spin and the planetary orbital axis is compatible with zero ($\beta = 11^{+14}_{-18}$ deg). This good alignment was observed for ten other close-in giant planets (see Winn 2008, and references therein), while a misalignment was observed only for the planet XO-3 (Hébrard et al. 2008; Winn et al. 2009). Together, these results favor migration via tidal interactions with a protoplanetary disk (Lin et al. 1996) as the dominant mechanism of planetary migration, because it should preserve spin-orbit alignement (Ward & Hahn 1994) contrary to migration via planet-planet scattering (Rasio & Ford 1996) or Kozai cycles (Fabrycky & Tremaine 2007).

Acknowledgements. We thank the ESO La Silla staff for their support during the CORALIE and HARPS observations. The HARPS consortium is gratefully acknowledged for contributing to some of the observations presented here.

References

Anderson, D. R., Gillon, M., Hellier, C., et al. 2008, MNRAS, 387, L4
Baglin, A., Auvergne, M., Boisnard, L., et al. 2006, in COSPAR, Plenary Meeting, 36th COSPAR Scientific Assembly, 36, 3749
Bakos, G. A., Noyes, R. W., Kovács, G., et al. 2004, PASP, 116, 266
Baranne, A., Queloz, D., Mayor, M., et al. 1996, A&AS, 119, 373
Barklem, P. S., Piskunov, N., & O'Mara, B. J. 2000, A&AS, 142, 467
Blackwell, D. E., & Shallis, M. J. 1977, MNRAS, 180, 177
Bodenheimer, P., Lin, D. N. C., & Mardling, R. A. 2001, ApJ, 548, 466
Butler, R. P., Marcy, G. W., & Fischer, D. A. 2004, ApJ, 617, 580
Burrows, A., Hubeny, I., Budaj, J., & Hubbard, W. B. 2007, ApJ, 661, 502
Burrows, A., Budaj, J., & Hubeny, I. 2008, ApJ, 678, 1436
Castelli, F., Gratton, R. G., & Kurucz, R. L. 1997, A&A 318, 841
Charbonneau, D., Brown, T. M., Latham, D. W., & Mayor, M. 2000, ApJ, 529, L45
Charbonneau, D., Knutson, H. A., & Barman, T. 2008, ApJ, 686, 1341
Claret, A. 2000, A&A, 363, 1081
Claret, A. 2004, A&A, 428, 1001
Collier Cameron, A., Pollacco, D., Street, R. A., et al. 2006, MNRAS, 373, 799
Collier Cameron, A., Wilson, D. M., West, R. G., et al. 2007, MNRAS, 380, 1230
Dobbs-Dixon, I., Lin, D. N. C., & Mardling, R. A. 2004, ApJ, 610, 464
Eggleton, P. P., Kiseleva, L. G., & Hut, P. 1998, ApJ, 499, 853
Fabrycky, D., & Tremaine, S. 2007, ApJ, 669, 1298
Ford, E. 2006, ApJ, 642, 505
Fortney, J. J., Marley, M. S., & Barnes, J. W. 2007, ApJ, 659, 1661
Fortney, J. J., Lodders, K., Marley, M. S., & Freedman, R. S. 2008, ApJ, 678, 1419
Gaudi, B. S., Seager, S., & Mallén-Ornelas, G. 2005, ApJ, 623, 472
Gillon, M., Pont, F., & Moutou, C. 2006, A&A, 459, 249
Gillon, M., Demory, B.-O., Barman, T., et al. 2007, A&A, 471, L51
Gillon, M., Triaud, A. H. M. J., Mayor, M., et al. 2008, A&A, 485, 871
Giménez 2006, ApJ, 650, 408
Girardi, L., Bressan, A., Bertelli, G., & Chiosi, C. 2000, A&AS, 141, 371
Goldreich, P., & Soter, S. 1966, Icarus, 5, 375
Gonzalez, G., & Laws, C. 2000, AJ 119, 390
Gonzalez, G., Laws, C., Tyagi, S., & Reddy, B. E. 2001, AJ, 121, 432
Gray, D. F. 2008, The Observation and Analysis of Stellar Photospheres, 3rd edition (CUP), 507
Guillot, T., & Showman, A. P. 2002, A&A, 385, 156
Guillot, T., Santos, N. C., Pont, F., et al. 2006, A&A, 453, L21
Hébrard, G., Bouchy, F., Pont, F., et al. 2008, A&A, 488, 763
Henry, G. W., Marcy, G. W., Butler, R. P., & Vogt, S. S. 2000, ApJ, 529, L41
Jackson, B., Greenberg, R., & Barnes, R. 2008a, ApJ, 678, 1396
Jackson, B., Greenberg, R., & Barnes, R. 2008b, ApJ, 681, 1631
Johns-Krull, Christopher, M., & McCullough, P. R. 2008, ApJ, 677, 657
Kurucz, R. L., & Bell, B. 1995, Kurucz CD-ROM 23: Atomic Line List, SAO, Cambridge, USA
Levrard, B., Winidoerffer, C., & Chabrier, G. 2009, to appear in ApJ [arXiv:0901.2048]
Lin, D. N. C., Bodenheimer, P., & Richardson, D. C. 1996, Nature, 380, 606
Liu, X., Burrows, A., & Abgui, L. 2008, ApJ, 687, 1191
Magain, P. 1984, A&A, 134, 189
Mandel, K., & Agol., E. 2002, ApJ, 5802, L171
Mardling, R. A. 2007, MNRAS, 382, 1768
Mayor, M., Pepe, F., & Queloz, D. 2003, The Messenger, 114, 20
Mazeh, T., Zucker, S., & Pont, F. 2005, MNRAS, 356, 955
McCullough, P. R., Stys, J., Valenti, J., et al. 2005, PASP, 117, 783
O'Donovan, F. T., Francis, T., Charbonneau, D., et al. 2006, ApJ, 651, L61
Ogilvie, G., & Lin, D. N. C. 2004, ApJ, 610, 477
Pätzold, M., Carone, L., & Rauer, H. 2004, A&A, 427, 1075
Pepe, F., Queloz, D., Mayor, M., et al. 2005, The Messenger, 120, 22
Pollacco, D. L., Skillen, I., Cameron, A. C., et al. 2006, PASP, 118, 1407
Queloz, D., Eggenberger, A., Mayor, M., et al. 2000, A&A, 359, L13
Queloz, D., Henry, G. W., Sivan, J. P., et al. 2001, A&A, 379, 279
Rasio, F. A., & Ford, E. B. 1996, Science, 274, 954
Santos, N. C., Israelian, G., & Mayor, M. 2004, A&A, 415, 1153
Sato, B., Fischer, D. A., & Henry, G. W. 2005, ApJ, 633, 465
Sestito, P., & Randich, S. 2005, A&A, 442, 615
Smalley, B. 2005, MSAIS, 8, 130
Smalley, B., Smith, K. C., & Dworetsky, M. M. 2001, UCLSYN Userguide
Smith, K. C. 1992, Ph.D. Thesis, University of London
Steele, I. A., Bates, S. D., Gibson, N., et al. 2008, Proc. SPIE, 7014, 70146
Stetson, P. B. 1987, PASP, 99, 111
Swain, M. R., Vasisht, G., Tinetti, G., et al. 2009, ApJL, 690, 114
Ward, W. R., & Hahn, J. M. 1994, Icarus, 110, 95
Winn, J. N. 2008, IAU 253 Transiting Planets, ed. F. Pont, Cambridge, USA, [arXiv:0807.4929]
Winn, J. N., Johnson, J. A., Fabrycky, D., et al. 2009, ApJ, submitted, [arXiv:0902.3461]
Wilson, D. M., Gillon, M., Hellier, C., et al. 2008, ApJ, 675, L113
Yoder, C. F., & Peale, S. J. 1981, Icarus, 47, 1

3.4.2 Discovery of CoRoT-5 b

This work, in collaboration with the CoRoT science team could a priori be presented as yet another hot Jupiter discovery. My contribution to that paper was to delay it[13]. Space based photometry and HARPS & SOPHIE radial velocities had been collected and I was charged to check with a Markov chain the results that had been adjusted by other means. I kept getting an eccentric orbital solution fitted to the RVs instead of a circular one. Forcing the eccentricity to zero I was confirming their results. Although it was unlikely that the orbit was as eccentric as I was fitting it - it would be the first hot Jupiter to have one on a 4 day orbit - what the fit was showing was a possibility and the non uniqueness of the circular solution. Two reasons can be found to explain the fit: the orbit was not well covered in phase because of a period close to an integer number of days: only three epochs had data, notably at the quadrature points, leaving a lot of freedom for the fits. In addition there is a little bit of scatter in the data, probably due to the faintness of the host star.

More data was obtained at phases which could constrain the orbit better. The orbit was published circular.

This benign episode was an illustration of a constant attention to check about other explanations and see whether our solutions are unique or not: is there not another way to explain the same observations? To discover planets for WASP and avoid missing too many I had to adopt a course of action where every variation is considered a potential planet[14]. This also showed how often one can have a wrong impression about reality when having only partial information.

This paper also marked the end of my collaboration with the CoRoT team which was a little too large already and onto which I could only have little impact. In addition, operations with WASP we very well underway and were keeping me very busy.

[13] should I be proud of that?

[14] observers can probably testify of my excitement at any variation in radial velocities, even after two RV measurements

A&A 506, 281–286 (2009)
DOI: 10.1051/0004-6361/200911902
© ESO 2009

The CoRoT space mission: early results

Astronomy & Astrophysics
Special feature

Transiting exoplanets from the CoRoT space mission⋆

VII. The "hot-Jupiter"-type planet CoRoT-5b

H. Rauer[1,2], D. Queloz[3], Sz. Csizmadia[1], M. Deleuil[4], R. Alonso[4], S. Aigrain[5], J. M. Almenara[6], M. Auvergne[7], A. Baglin[7], P. Barge[4], P. Bordé[16], F. Bouchy[8], H. Bruntt[9], J. Cabrera[1], L. Carone[10], S. Carpano[11], R. De la Reza[19], H. J. Deeg[6], R. Dvorak[12], A. Erikson[1], M. Fridlund[11], D. Gandolfi[14], M. Gillon[3,18], T. Guillot[13], E. Guenther[14], A. Hatzes[14], G. Hébrard[8], P. Kabath[1], L. Jorda[4], H. Lammer[15], A. Léger[16], A. Llebaria[4], P. Magain[18], T. Mazeh[20], C. Moutou[4], M. Ollivier[16], M. Pätzold[10], F. Pont[5], M. Rabus[6], S. Renner[1], D. Rouan[7], A. Shporer[20], B. Samuel[16], J. Schneider[17], A. H. M. J. Triaud[3], and G. Wuchterl[14]

(Affiliations can be found after the references)

Received 20 February 2009 / Accepted 23 July 2009

ABSTRACT

Aims. The CoRoT space mission continues to photometrically monitor about 12 000 stars in its field-of-view for a series of target fields to search for transiting extrasolar planets ever since 2007. Deep transit signals can be detected quickly in the "alarm-mode" in parallel to the ongoing target field monitoring. CoRoT's first planets have been detected in this mode.

Methods. The CoRoT raw lightcurves are filtered for orbital residuals, outliers, and low-frequency stellar signals. The phase folded lightcurve is used to fit the transit signal and derive the main planetary parameters. Radial velocity follow-up observations were initiated to secure the detection and to derive the planet mass.

Results. We report the detection of CoRoT-5b, detected during observations of the LRa01 field, the first long-duration field in the galactic anti-center direction. CoRoT-5b is a "hot Jupiter-type" planet with a radius of $1.388^{+0.046}_{-0.047}$ $R_{\rm Jup}$, a mass of $0.467^{+0.047}_{-0.024}$ $M_{\rm Jup}$, and therefore, a mean density of $0.217^{+0.031}_{-0.025}$ g cm^{-3}. The planet orbits an F9V star of 14.0 mag in 4.0378962 ± 0.0000019 days at an orbital distance of $0.04947^{+0.00026}_{-0.00029}$ AU.

Key words. planets and satellites: general – techniques: photometric – techniques: radial velocities

1. Introduction

CoRoT searches for the photometric signal of transiting extrasolar planets. Radial-velocity follow-up measurements help us understand the nature of the transiting body and allow us to derive its mass.

The nominal lightcurve analysis for small transiting signals has to await the completion of an observing run and detailed signal analysis. The mission "alarm-mode" (Quentin et al. 2006; Surace et al. 2008), however, can be used to quickly trigger follow-up measurements during ongoing observations of a target field. The "alarm-mode" is used to increase the transmitted time-sampling for individual stellar lightcurves in the CoRoT exoplanet channel. The sampling is increased from 512 s to 32 s if a transit-like signal is detected during the observations. It therefore provides planetary candidates early during an observing run, which are, however, biased towards relatively large planetary candidates because of the limited data set available at this point.

CoRoT-5b is the fifth secured transiting planet detected by CoRoT. As CoRoT-1b to CoRoT-4b (Alonso et al. 2008; Barge et al. 2008; Deleuil et al. 2008; Moutou et al. 2008; Aigrain et al. 2008), it was first detected by the alarm-mode. Here, we present the photometric detection of CoRoT-5b by the satellite based on pre-processed alarm-mode data, the accompanying radial-velocity observations confirming its planetary nature, and the resulting planet parameters.

2. Observations and data reduction

CoRoT-5b was detected in the LRa01-field, the second long-run field of CoRoT. The field is located near the anti-center direction of the galaxy at RA(2000): $06^{\rm h}46^{\rm m}53^{\rm s}$ and Dec(2000): –00°12′00″ (Michel et al. 2006). The observing sequence started on October 24, 2007 and finished after 112 days duration. CoRoT observations usually have a very high duty cycle since data gaps are mainly caused by the regular crossings of the South Atlantic Anomaly (SAA), which typically last for about 10 min. During the observations of the LRa01 field, however, two longer interruptions occurred. An intermediate interruption of about 12 hours occurred eight days after the beginning of the observing run, and a longer data gap of about 3.5 days started on January 18, 2008, after a DPU reset. Finally, a duty cycle of 93% was achieved.

⋆ Observations made with SOPHIE spectrograph at the Observatoire de Haute Provence (07B.PNP.MOUT), France, and HARPS spectrograph at ESO La Silla Observatory (072.C-0488(E), 082.C-0312(A)), and partly based on observations made at the Anglo-Australian Telescope. The CoRoT space mission, launched on December 27, 2006, was developed and is operated by CNES, with the contribution of Austria, Belgium, Brasil, ESA, Germany, and Spain.

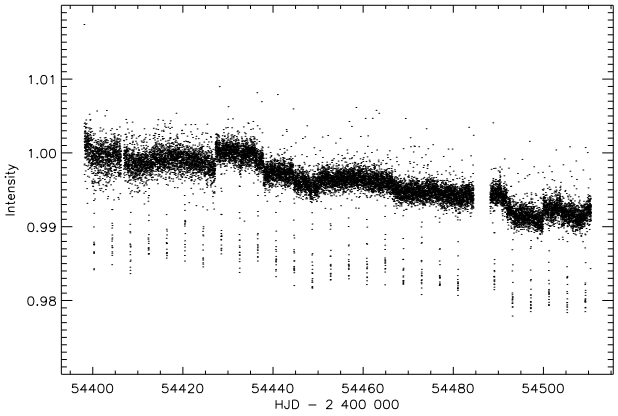


Fig. 1. Lightcurve of CoRoT-5 re-sampled to 512 s time resolution. No corrections for data jumps due to "hot pixels" have been applied in this figure to show the raw data quality.

The alarm-mode was triggered after 29 days of observations. When seven transit-like signals were detected, the time sampling was switched to 32 s. The alarm-mode data for CoRoT-5 are based on the analysis of "white light" lightcurves, without using the color information of the CoRoT prism. In total 219 711 data points were obtained, 214 938 of it in oversampling mode. The data pipeline flags data points taken during the SAA crossing or affected by other events decreasing the data quality. When taking only unflagged data into account, the number of data points reduced to 204,092 in total and 199,917 as highly sampled.

The alarm-mode data were processed with a first version of the data reduction pipeline (Auvergne et al. 2009). The pipeline corrects for the CCD zero offsets and gain, the sky background intensity and the telescope jitter. In addition, "hot pixels" (Pinheiro da Silva et al. 2008) affect the lightcurves, causing sudden jumps in intensity of varying duration. The lightcurve of CoRoT-5 was, however, only moderately affected by such jumps, as can be seen in Fig. 1, which shows the full lightcurve. The oversampled part of the data set was re-binned to display the whole lightcurve with a 512 s time sampling. The measured intensity decreases during the observing run, as observed for all stars in the fields. Overall, CoRoT-5 only shows a minor level of variability, without clear periodicity.

CoRoT measures stellar intensities by aperture photometry using optimized masks (Llebaria et al. 2003) that encompass the shape of the stellar point-spread-functions (PSFs). The bi-prism introduced in the light path of the exoplanet channel (Auvergne et al. 2009) causes relatively wide PSFs of unusual shapes that vary with e.g. stellar magnitude. Contaminating eclipsing binary stars within the PSF could mimic a planetary transit-like signal. Based on the pre-launch observations of the target field included in the *Exo-Dat* data base (Deleuil et al. 2009), the contamination of the mask of CoRoT-Exo5 is estimated to 8.4%. Refinement of this value will be performed in a more detailed future analysis using the dedicated windowing mask for this target star. We subtracted this flux level from the lightcurve before normalization to take low level contamination into account.

The overall intensity trend and smaller scale variability of the lightcurve were removed. To do this, we resampled the lightcurve to 512 s sampling rate first and convolved this lightcurve with a fourth order Savitzky-Golay filter (similar to the treatment for CoRoT-2b, Alonso et al. 2008). Then median averages were calculated for 24 h segments of the lightcurve (excluding the transit points and the data jumps), which was fitted by a spline-curve. The original lightcurve was then divided by the spline fit. The filtered lightcurve was used for normalization and further analysis. The out-of-eclipse scatter of CoRoT-5 was determined from the standard deviation of data points in the phase-folded lightcurve. It was found to be 0.0017 mag.

Table 1. Radial velocity measurements of the star CoRoT-5 obtained by SOPHIE and HARPS spectrographs from December 2007 to December 2008.

BJD −2 400 000	RV km s^{-1}	Error km s^{-1}
SOPHIE		
54463.4939000	48.947	0.017
54465.5247100	48.816	0.028
54506.3770000	48.767	0.016
54525.3478500	48.860	0.020
54528.2886100	48.933	0.031
54544.3463300	48.925	0.026
HARPS		
54548.583775	48.933	0.014
54550.577783	48.792	0.021
54551.584161	48.865	0.013
54553.525234	48.883	0.010
54554.546158	48.819	0.012
54556.554191	48.929	0.010
54768.852140	48.820	0.009
54769.848137	48.900	0.008
54771.850953	48.851	0.009
54772.841289	48.827	0.010
54773.847921	48.900	0.008
54802.777527	48.929	0.009
54805.748602	48.852	0.012

3. Photometric follow-up observation

Photometric follow-up observations with higher spatial resolution than CoRoT's (of ≈20″× 6″) are used to exclude the presence of nearby contaminating eclipsing binaries (Deeg et al., this volume). Such observations of CoRoT-5 were performed at the IAC 80 cm telescope at Teide Observatory, Tenerife, on the January 12, and March 11, 2008 at a spatial resolution of about 1.5″. These data showed only one star bright enough to cause a potential false alarm, about 8″ southwest of the target. Observations obtained during and out of a transit ("on/off photometry") showed, however, that this contaminating star varies by less than 0.08 mag. This is far below the variation of about 0.55 mag that is required by this star in order to explain the observed signal in the CoRoT data.

4. Radial velocity follow-up observations

In January 2008, after the identification of a transit signal by the alarm-mode, CoRoT-5 was observed with the SOPHIE spectrograph installed on the 193 cm telescope at the Haute Provence Observatory. Two radial velocity measurements were taken at opposite quadrature phases of the radial velocity variation expected from the transit ephemerides assuming a circular orbit. At this time the data were found to be compatible with a radial velocity amplitude suggesting a Jupiter mass planet. Additional measurements were obtained later in the season to confirm the reality of the signal but not enough to obtain a precise measurement of the orbit eccentricity. One year later, a new series of measurements was obtained with the HARPS spectrograph installed on the 3.6 m ESO telescope at La Silla in Chile

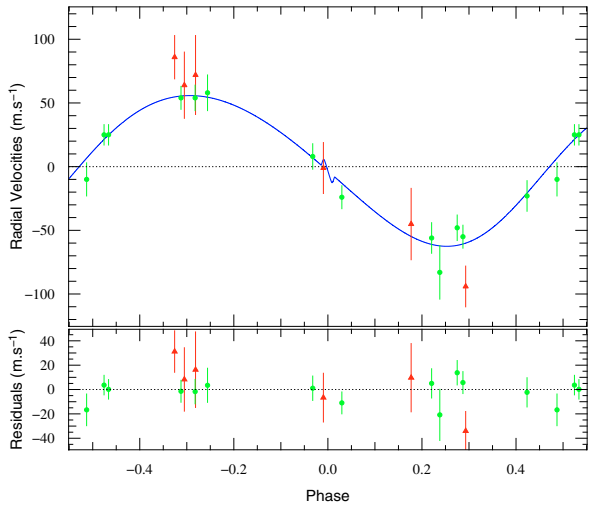


Fig. 2. Radial velocity measurements and Keplerian fit to the data including the Rossiter effect. Red: SOPHIE, green: HARPS.

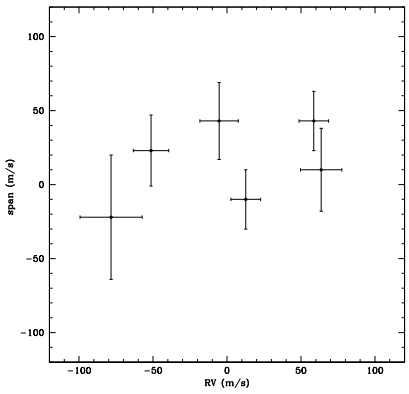


Fig. 3. Bisector analysis of CoRoT-5.

(Mayor et al. 2003). Both sets of data (SOPHIE and HARPS) have been processed as in Bouchy et al. (2008). Radial velocities (RV) were computed by weighted cross-correlation (Baranne et al. 1996; Pepe et al. 2005) with a numerical G2-spectral template excluding spectral orders below 4200 Å. Radial velocity values are listed in Table 1 and plotted in Fig. 2.

We analyzed the cross-correlation function computed from the HARPS spectra using the line-bisector technique according to the description in Queloz et al. (2001) to detect possible spectral distortions caused by a faint background eclipsing binary mimicking a small RV amplitude signal. No correlation between the RV data and the bisector span was found at the level of the uncertainty on the data (Fig. 3).

The stability of the bisector, combined both with the amplitude of the radial velocity and the accuracy of transit of the lightcurve, is enough to discard an alternate background eclipsing binary scenario. In the case of a hypothetical background eclipsing binary, obtaining a sine-shaped radial-velocity signal would require a superimposed spectrum moving with the same systemic velocity as the brightest component, and on an RV range corresponding to the sum of the width of both CCF line profiles. This prerequisite constrains both on the mass of the potential eclipsing component and its companion. The example of HD41004 provides us with an interesting benchmark (Santos et al. 2002). This system was detected with a similar radial velocity amplitude but with a strong bisector correlation, and could be explained by a superimposed spectrum with 3% flux of the bright star. If one scales down this result to CoRoT-5, which has no bisector correlation, one finds that the contrast ratio between the brightest star and the hypothetical eclipsing binary is such that the eclipse must be very deep and the radius of the eclipsing stars much smaller than CoRoT-5. Considering the quality of the CoRoT lightcurve such a binary scenario does not match the transit ingress and egress timing and the detailed shape of the curve.

5. Properties of the central star

We determined the fundamental parameters of the host star carrying out a spectral analysis of the set of HARPS spectra acquired for radial velocity measurements. The individual spectra were reduced with the HARPS standard pipeline. The extracted spectra were corrected for cosmics impacts, for the Earth and the stars velocity, and then corrected for the blaze function and normalized, order by order, to increase the signal-to-noise (S/N). The S/N level in the continuum is around 40 in the range 5000–6500 Å and it decreases to 15 towards the blue at 4000 Å.

Spectroscopic observations of the central star have also been performed in January 2008 with the AAOmega multi-object facility at the Anglo-Australian Observatory. By comparing the low-resolution (R = 1300) AAOmega spectrum of the target with a grid of stellar templates, as described in Frasca et al. (2003) and Gandolfi et al. (2008), we derived the spectral type and luminosity class of the star (F9 V).

As for the previous planet host stars, we used different methods to derive Corot-5 atmospheric parameters: line profile fitting with the SME (Valenti & Piskunov 1996) and the VWA packages (Bruntt et al. 2002, 2008). We find general agreement and here we quote the results from VWA. The star has a very low projected rotational velocity, $v \sin i$ = 1 ± 1 km s^{-1}. More than 600 mostly non-blended lines were selected for analysis in the wavelength range 3990–6810 Å. VWA uses atmosphere models from the grid by Heiter et al. (2002) and atomic parameters from the VALD database (Kupka et al. 1999). The abundance determined for each line is computed relative to the result for the same line in the solar spectrum from Hinkle et al. (2000), following the approach of Bruntt et al. (2008). The results for CoRoT-5 are shown in Table 2. Using these parameters for the atmospheric model, we determined the abundances of 21 individual elements. The uncertainty on the abundances includes a contribution of 0.04 dex due to the uncertainty on the fundamental parameters. The abundance pattern is shown in Fig. 4. The overall metallicity is found as the mean abundance of the elements with at least 20 lines (Si, Ca, Ti, Cr, Fe, Ni) giving [M/H] = −0.25 ± 0.04. We did not include Mn, as this has a significantly lower abundance. The metallicity and the 1-σ error bar is indicated by the horizontal bar in Fig. 4. There is no evidence of the host star being chemically peculiar, except Mn.

The fundamental parameters of the parent star, its mass and radius were subsequently derived using stellar evolutionary tracks as presented in Deleuil et al. (2008) plotted in a $M^{(1/3)}$/R – $T_{\rm eff}$ HR diagram. The stellar density parameter was

Table 2. Parameters of the parent star CoRoT-5.

parameter	value	source
RA	$06^h45^m07^s$	*Exo-Dat*
Dec	00° 48′ 55″	*Exo-Dat*
epoch	2000.0	
type	F9V	*Exo-Dat, AAOmega*
V	14.0	*Exo-Dat*
GSC2.3 ID	N82O011953	
2MASS ID	06450653+0048548	
$v \sin i$ [km s^{-1}]	1 ± 1	VWA
ξ_t [km s^{-1}]	0.91 ± 0.09	VWA
$T_{\rm eff}$ [K]	6100 ± 65	VWA
$\log g$	4.19 ± 0.03	VWA
[M/H]	−0.25 ± 0.06	VWA
$M_{\rm star}$ [$M_\odot$]	1.00 ± 0.02	Evolut. tracks
$R_{\rm star}$ [$R_\odot$]	1.186 ± 0.04	Evolut. tracks
$M^{(1/3)}/R$ [$M_\odot^{1/3}/R_\odot$]	0.843 ± 0.024	lightcurve
age [Gyr]	5.5–8.3	photometry +Evolut. tracks

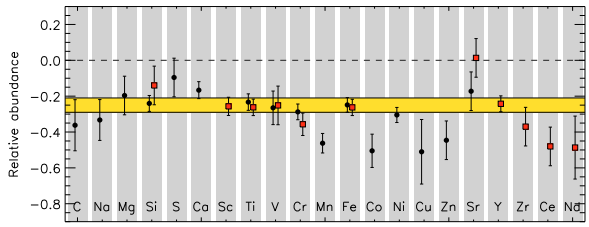


Fig. 4. Stellar abundances of CoRoT-5. Abundances found from neutral lines are marked by circles, for ionized lines box symbols are used.

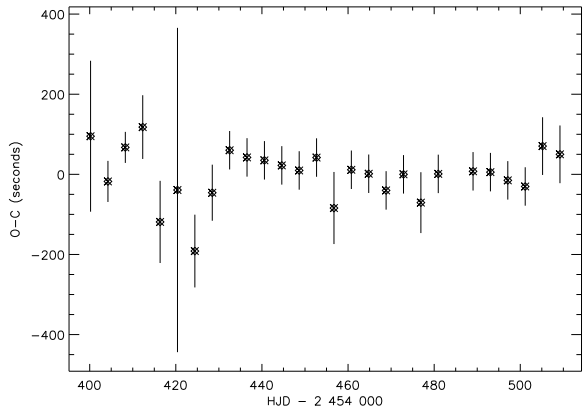


Fig. 5. The O − C diagram of the CoRoT-5b system. No clear period variation can be seen.

derived from the lightcurve fitting (see Sect. 7). We determined the mass and radius of the star to: $M_{\rm star} = 1.00 \pm 0.02\ M_\odot$ and $R_{\rm star} = 1.186 \pm 0.04\ R_\odot$. As a final check, we calculated the corresponding surface gravity $\log g = 4.311 \pm 0.033$ while the spectroscopic value is 4.19 ± 0.03. These two values of $\log g$ are comparable with each other at the 3σ level. Based on our photometric analysis, we estimate the age of the star to 5.5–8.3 Gyr. The spectra show no sign of Ca II emission or of a strong Li I absorption line, which is consistent with a relatively evolved star.

Table 3. Parameters of the CoRoT-5 system derived from the combined MCMC analysis.

Fitted parameters	Value	Units
$(R_{\rm p}/R_{\rm star})^2$	$0.01461^{+0.00030}_{-0.00032}$	
t_T	$0.0290^{+0.00038}_{-0.00053}$	
b	$0.755^{+0.017}_{-0.022}$	
K	$59.1^{+6.2}_{-3.1}$	m s^{-1}
$e \cos \omega$	$-0.057^{+0.048}_{-0.020}$	
$e \sin \omega$	$-0.071^{+0.147}_{-0.130}$	

t_T denotes the transit duration given in fraction of phase; b the impact parameter and K the RV semi-amplitude.

6. Period determination and transit timing variations

In total, 27 individual transit events are clearly seen, separated by an orbital period of about 4.03 days. One event was lost in a data gap.

First, we estimated the mid-times of each transit by applying the so-called Kwee-van Woerden method (Kwee & van Woerden 1956). This method mirrors the lightcurve around a pre-selected time-point, T, computes the differences of original and mirrored lightcurves and then searches for an optimum T. The O − C diagram of the system was constructed, based on the resulting transit times and an initial guess of the period. A linear fit of this diagram yielded an improved estimate of the period. This period value was then refined with the following procedure. The lightcurve was phase-folded using this previously determined period and then averaged. The size of the bin used was 0.001 in phase (or to 5.81 min, using the final period). Then, this lightcurve was fitted (see the next section) by a theoretical transit lightcurve. The transit mid-times were then determined again by cross-correlating the observed and the theoretical lightcurve. This resulted in more precise mid-times of the transit and a new O − C curve. Another linear fit to this O − C diagram yielded a better period value, and the whole procedure was repeated. The final O − C diagram can be seen in Fig. 5. The resulting ephemeris is given in Table 4.

There is no obvious period variation present in the O − C diagram. The first part of the lightcurve was obtained with the 512 s sampling rate, so the first seven minima typically consist of only 20 data points. Thus, they have larger scatter and uncertainties. The next twenty minima were obtained with the high sampling rate (32 s) and typically consist of a few hundred data points, leading to much higher accuracy. If one takes only these high-resolution minima into account, the constancy of the period is clearer. However, we cannot exclude that small period variations are present in the system. The upper limit of such a period variation was estimated by a quadratic fit to the data, which showed that it should be less than 0.42 s/cycle.

7. Analysis of parameters of CoRoT-5b

The final phase-folded lightcurve of the transit event is seen in Fig. 6. The transit signal shows a depth of about 1.4% and lasts for about 2.7 h. We derived the planetary parameters by fitting simultaneously the lightcurve of CoRoT-5 with the SOPHIE and HARPS radial velocities. A planetary model on a Keplerian orbit in the formalism of Giménez (2006a) and Giménez (2006b) was fitted to the data using a Markov Chain Monte-Carlo (MCMC)

Table 4. The derived planet parameters.

Derived physical parameters	Value	Units
Transit epoch T_0	2454400.19885 ± 0.0002	HJD
Orbital period P	4.0378962 ± 0.0000019	days
Orbital semi-major axis a	$0.04947^{+0.00026}_{-0.00029}$	AU
Orbital inclination i	$85.83^{+0.99}_{-1.38}$	degrees
Orbital eccentricity e	$0.09^{+0.09}_{-0.04}$	
Argument of periastron ω	$-2.24^{+5.05}_{-0.84}$	rad
Planet radius R_p	$1.388^{+0.046}_{-0.047}$	R_J
Planet mass M_p	$0.467^{+0.047}_{-0.024}$	M_J
Mean planet density ρ_p	$0.217^{+0.031}_{-0.025}$	g cm^{-3}
Planetary surface gravity log g_p	$7.77^{+0.14}_{-0.08}$	cgs
Zero albedo equilibrium temperature T_{eq}	1438 ± 39	K

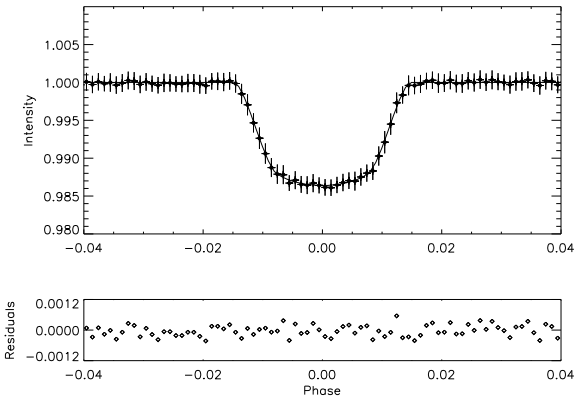


Fig. 6. *Top*: phase-folded lightcurve of CoRoT-5b. *Bottom*: residuals of fitted transit curve.

code described in Triaud et al. (in prep.) but using $e.\cos\omega$ and $e.\sin\omega$ instead of e and w as free parameters for better error estimation. In the fit a quadratic limb-darkening law was assumed at $u_+ = 0.616$ and $u_- = 0$. In the initial *burn-in* phase of the MCMC adjustment, 15 000 steps were chosen to allow the fit to converge. A further 50 000 steps were used to derive the best parameters and their errors. In the fit, there are eight fitted parameters plus two γ velocities and a normalization factor, totalling 11 free parameters. In addition, the fit assumed the presence of a Rossiter-McLaughlin effect with the two fixed parameters $v\sin i = 1.0$ km s^{-1} and $\lambda = 0$ (λ: angle between stellar rotation axis and normal vector of the orbital plane). A Bayesian penalty is added to the χ^2 creating a prior for $M_\star = 0.99 \pm 0.02$. The fit to the rv measurements is shown in Fig. 2, and the derived fitting parameters are shown in Table 3.

In addition, a model transit curve (Mandel & Agol 2002) was fitted to the photometric phase folded transit curve separately. The parameters fitted are the center of transit, the planet radius expressed in stellar radii, the semi-major axis in stellar radii and the orbital inclination. In this fit the limb-darkening coefficients (u_1 and u_2) were free parameters, assuming a quadratic limb-darkening law. The fitting method follows a Metropolis-Hastings algorithm, which is a kind of Markov Chain Monte-Carlo procedure. The fitting procedure was performed ten times with different starting values to find the global minimum in χ^2. The errors of the fit were estimated from the standard deviations of the points in the chain. In addition to the transit curve, a third light component is included as a free parameter in the fit. In this way, we could check whether another contaminant is present, which remained unresolved in the photometric follow-up. However, no such additional source of light was found. The transformation between contamination factor c and the third light l_3 is $c = l_3/(1 - l_3)$. We had $c = 0.005 \pm 0.024$. Since we already removed the known contaminant factor from the lightcurve (see Sect. 2), we could therefore conclude that no further observable contaminant is present in the lightcurve of CoRoT-5. The planet parameters derived from this fit agree with the simultaneous fitting within the error bars, so we do not report them again here.

The resulting planetary parameters based on the MCMC approach with fixed limb-darkening coefficients and without any third light are summarized in Table 4. The major uncertainties on the planet are, as usual, introduced mainly from the uncertainty of the stellar parameters.

8. Summary

We report the discovery of a "hot-Jupiter-type" planet, CoRoT-5b, orbiting a type F9V star of 14.0 mag. The planet mass and radius were derived to $0.467^{+0.047}_{-0.024}$ M_{Jup} and $1.388^{+0.046}_{-0.047}$ R_{Jup}, respectively. It orbits its central star at $0.04947^{+0.00026}_{-0.00029}$ AU orbital distance. The determined eccentricity is low (see Table 4), but further radial velocity measurements would be needed for a more accurate determination.

CoRoT-5b has a density of $0.217^{+0.031}_{-0.025}$ g cm^{-3}, similar to the planets WASP-12b and WASP-15b (Hebb et al. 2009; West et al. 2009), implying that it belongs to the planets with the lowest mean density found so far. As such, it is found to be larger by 20% than standard evolution models (Guillot et al. 2006) would predict. Standard recipes that account for missing physics (kinetic energy transport or increased opacities) can explain this large size, and predict that the planet is mostly made of hydrogen-helium, with at most 28 $M_\oplus$ of heavy elements (maximum value obtained in the kinetic energy model, assuming 0.5% of the incoming energy is dissipated at the planet center). Thus, CoRoT-5b supports the proposed link between the metallicity of planets and of their host star.

Acknowledgements. H.J.D. and J.M.A. acknowledge support from grant ESP2007-65480-C02-02 of the Spanish Education and Science Ministry. Some

of the data published in this article were acquired with the IAC80 telescope operated by the Instituto de Astrofísica de Tenerife at the Observatorio del Teide. The German CoRoT Team (TLS and Univ. Cologne) acknowledges DLR grants 50OW0204, 50OW0603, 50QP07011. R.A. acknowledges support by grant CNES-COROT-070879. The building of the input *CoRoT*/Exoplanet catalog was made possible by observations collected for years at the Isaac Newton Telescope (INT), operated on the island of La Palma by the Isaac Newton group in the Spanish Observatorio del Roque de Los Muchachos of the Instituto de Astrofisica de Canarias.

References

Aigrain, S., Collier Cameron, A., Ollivier, M., et al. 2008, A&A, 488, L43
Alonso, R., Auvergne, M., Baglin, A., et al. 2008, A&A, 482, L21
Auvergne, M., Bodin, P., Boisnard, L., et al. 2009, A&A, 506, 411
Baranne, A., Queloz, D., Mayor, M., et al. 1996, A&AS, 119, 373
Barge, P., Baglin, A., Auvergne, M., et al. 2008, A&A, 482, L17
Bouchy, F., Queloz, D., Deleuil, M., et al. 2008, A&A, 482, L25
Bruntt, H., Catala, C., Garrido, R., et al. 2002, A&A, 389, 345
Bruntt, H., De Cat, P., & Aerts, C. 2008, A&A, 478, 487
Deleuil, M., Deeg, H. J., Alonso, R., et al. 2008, A&A, 491, 889
Deleuil, M., Meunier, J. C., Moutou, C., et al. 2009, AJ, 138, 649
Frasca, A., Alcalá, J. M., Covino, E., et al. 2003, A&A, 405, 149
Gandolfi, D., Alcalá, J. M., Leccia, S., et al. 2008, ApJ, 687, 1303
Giménez, A. 2006a, A&A, 450, 1231
Giménez, A. 2006b, ApJ, 650, 408
Guillot, T., Santos, N. C., Pont, F., et al. 2006, A&A, 453, L21
Hebb, L., Collier-Cameron, A., Loeillet, B., et al. 2009, ApJ, 693, 1920
Heiter, U., Kupka, F., van't Veer-Menneret, C., et al. 2002, A&A, 392, 619
Hinkle, K., Wallace, L., Valenti, J., et al. 2000, Visible and Near Infrared Atlas of the Arcturus Spectrum 3727-9300 A (San Francisco: ASP)
Kupka, F., Piskunov, N., Ryabchikova, T. A., Stempels, H. C., & Weiss, W. W. 1999, A&AS, 138, 119
Kwee, K. K., & van Woerden, H. 1956, Bull. Astron. Inst. Netherlands, 12, 327
Llebaria, A., Guterman, P., & Ollivier, M. 2003, in Techniques and Instrumentation for Detection of Exoplanets, ed. by D. R. Coulter, Proc. SPIE, 5170, 155
Mandel, K. & Agol, E. 2002, ApJ, 580, L171
Mayor, M., Pepe, F., Queloz, D., et al. 2003, The Messenger, 114, 20
Michel, E., Deleuil, M., & Baglin, A. 2006, in ESA SP 1306, ed. M. Fridlund, A. Baglin, J. Lochard, & L. Conroy, 473
Moutou, C., Bruntt, H., Guillot, T., et al. 2008, A&A, 488, L47
Pepe, F., Mayor, M., Queloz, D., et al. 2005, The Messenger, 120, 22
Pinheiro da Silva, L., Rolland, G., Lapeyrere, V., et al. 2008, MNRAS, 384, 1337
Queloz, D., Henry, G. W., Sivan, J. P., et al. 2001, A&A, 379, 279
Quentin, C., Barge, P., Cautain, R., et al. 2006, in ESA SP 1306, 409
Santos, N. C., Mayor, M., Naef, D., et al. 2002, A&A, 392, 215
Surace, C., Alonso, R., Barge, P., et al. 2008, in SPIE Conf. Ser., 7019
Valenti, J. A., & Piskunov, N. 1996, A&AS, 118, 595
West, R. G., Anderson, D. R., Gillon, M., et al. 2009, AJ, 137, 4834

[1] Institute of Planetary Research, DLR, Rutherfordstr. 2, 12489 Berlin, Germany
e-mail: heike.rauer@dlr.de
[2] Center for Astronomy and Astrophysics, TU Berlin, Hardenbergstr. 36, 10623 Berlin, Germany
[3] Observatoire de Genève, Université de Genève, 51 Ch. des Maillettes, 1290 Sauverny, Switzerland
[4] Laboratoire d'Astrophysique de Marseille, CNRS UMR 6110, Traverse du Siphon, 13376 Marseille, France
[5] School of Physics, University of Exeter, Stocker Road, Exeter EX4 4QL, UK
[6] Instituto de Astrofýsica de Canarias, 38205 La Laguna, Tenerife, Spain
[7] LESIA, CNRS UMR 8109, Observatoire de Paris, 5 place J. Janssen, 92195 Meudon, France
[8] Institut d'Astrophysique de Paris, UMR7095 CNRS, Université Pierre & Marie Curie, 98bis Bd Arago, 75014 Paris, France
[9] Sydney Institute for Astronomy, School of Physics, University of Sydney, NSW 2006, Australia
[10] Rheinisches Institut für Umweltforschung an der Universität zu Köln, Abt. Planetenforschung, Aachener Str. 209, 50931 Köln, Germany
[11] Research and Scientific Support Department, European Space Agency, ESTEC, 2200 Noordwijk, The Netherlands
[12] Institute for Astronomy, University of Vienna, Türkenschanzstrasse 17, 1180 Vienna, Austria
[13] Observatoire de la Côte d'Azur, Laboratoire Cassiopée, CNRS UMR 6202, BP 4229, 06304 Nice Cedex 4, France
[14] Thüringer Landessternwarte Tautenburg, Sternwarte 5, 07778 Tautenburg, Germany
[15] Space Research Institute, Austrian Academy of Sciences, Schmiedlstrasse 6, 8042 Graz, Austria
[16] Institut d'Astrophysique Spatiale, Université Paris XI, 91405 Orsay, France
[17] LUTH, Observatoire de Paris-Meudon, 5 place J. Janssen, 92195 Meudon, France
[18] Institut d'Astrophysique et de Géophysique, Université de Liège, Allée du 6 août 17, Sart Tilman, Liège 1, Belgium
[19] Observatorio Nacional, Rio de Janeiro, RJ, Brazil
[20] School of Physics and Astronomy, Raymond and Beverly Sackler Faculty of Exact Sciences, Tel Aviv University, Tel Aviv 69978, Israel

3.4.3 The WASP-8 triple star system

This planet was found quite early in the project, its high amplitude signal was easy to spot but an error in the estimation of the period by WASP was showing the radial velocities were not in phase. Quickly Didier (who observed then[15]) realised that we were at three times the period announced and that this candidate was on a fairly long orbit for a transiting object. With an orbit of about 8 days and an eccentricity of 0.3 (its periastron distance is similar to that of a typical hot Jupiter), WASP-8 turned out to be a very interesting catch.

Observations resumed on this object the following year and immediately it became clear the points were not covering the expected orbit. With a few more observations we could reliably adjust a linear drift in radial velocity, an additional acceleration caused by another body in that system. Immediately suspicions fell on a tiny dot near the star observed from the CORALIE guiding camera. Photometric observations at good seeing and deconvolved confirmed a star four arcseconds away, on a common proper motion with the primary compared with 70 year old observations.

An estimation of the probable orbital separation was found around 600 AU. With its observed brightness temperature and position, this body cannot be responsible for the additional acceleration seen in the radial velocities computed about 60 times larger than one would expect otherwise. We could only conclude there is yet a second unseen body in this system, mayber stellar, maybe substellar.

Furthermore, its Rossiter-McLaughlin effect was measured and detected to be retrograde. This was the first such measurement (other observations on WASP-17 b (Anderson et al. 2010) and Hat-P-7 b (Narita et al. 2009b; Winn et al. 2009b) published earlier were in fact observed later) and in fact the first fully confirmed misaligned planet as then, there was still a doubt on XO-3 b spin/orbit angle (Hébrard et al. 2008). WASP-8 is a very good example of system which could be dynamically active. All this information was gathered in a letter written by Didier, presented next page and for which I produced the analysis .

To date the drift continues with only a hint of a departure from linearity which may be confirmed when it will reappear in the sky in Summer 2011. A current adjustment indicates a minimum mass of 4 $M_{\rm Jup}$ on a 1 300 day orbit for that second unseen companion.

This paper led to an adjustment of the MCMC in order to include that drift (you can see it as part of the other jump parameters in figure 2.3).

[15] this was, if I recall well, my first mission in Chile and Didier was teaching the tricks of planet hunting and being a decent observer

A&A 517, L1 (2010)
DOI: 10.1051/0004-6361/201014768
© ESO 2010

Astronomy & Astrophysics

Letter to the Editor

WASP-8b: a retrograde transiting planet in a multiple system⋆,⋆⋆

D. Queloz[1], D. Anderson[2], A. Collier Cameron[3], M. Gillon[4], L. Hebb[3], C. Hellier[2], P. Maxted[2], F. Pepe[1], D. Pollacco[5], D. Ségransan[1], B. Smalley[2], A. H. M. J. Triaud[1], S. Udry[1], and R. West[6]

[1] Observatoire Astronomique de l'Université de Genève, Chemin des Maillettes 51, 1290 Sauverny, Switzerland
e-mail: Didier.Queloz@unige.ch
[2] Astrophysics Group, Keele University, Staffordshire, ST55BG, UK
[3] School of Physics & Astronomy, University of St Andrews, North Haugh, KY16 9SS, St Andrews, Fife, Scotland, UK
[4] Institut d'Astrophysique et de Géophysique, Université de Liège, Allée du 6 Août, 17, Bat. B5C, Liège 1, Belgium
[5] Astrophysics Research Centre, School of Mathematics & Physics, Queens University, University Road, Belfast, BT71NN, UK
[6] Department of Physics and Astronomy, University of Leicester, Leicester, LE17RH, UK

Received 12 April 2010 / Accepted 21 June 2010

ABSTRACT

We report the discovery of *WASP-8b*, a transiting planet of 2.25 ± 0.08 $M_{\rm Jup}$ on a strongly inclined eccentric 8.15-day orbit, moving in a retrograde direction to the rotation of its late-G host star. Evidence is found that the star is in a multiple stellar system with two other companions. The dynamical complexity of the system indicates that it may have experienced secular interactions such as the Kozai mechanism or a formation that differs from the "classical" disc-migration theory.

Key words. stars: individual: *WASP-8* – techniques: photometric – techniques: spectroscopic – planet-star interactions – planetary systems – techniques: radial velocities

1. Introduction

Transiting planets provide a wealth of information on the structure and formation of planets. The measurement of planet radius combined with its mass has found a surprising diversity in the mean densities and in particular "inflated" hot Jupiters. Spectroscopic measurement of the Rossiter-McLaughlin effect on the radial velocity during transits indicates that some of these planets may not be aligned with the rotation axes of their stars (see references in Winn 2010). The diversity in the observed spin-orbit misalignments is somewhat similar to that seen earlier in period and eccentricity distribution of planets detected by radial velocity surveys (see references in Udry & Santos 2007, and references therein). The recent sharp rise in the detections of transiting planets is the outcome of successful ground-based wide transit searches surveys among which WASP (Pollacco et al. 2006) is the most prolific.

These discoveries have stimulated theoretical investigations of alternative formation scenarios to the migration theory (Lin et al. 1996; Wu & Murray 2003). These alternative theories account for the discoveries of eccentric hot Jupiters on orbits not aligned with the rotation equator of their star (Wu & Murray 2003; Fabrycky & Winn 2009; Nagasawa et al. 2008; Barker & Ogilvie 2009).

⋆ Based on observations made with HARPS spectrograph on the 3.6-m ESO telescope and the EULER Swiss telescope at La Silla Observatory, Chile.

⋆⋆ Radial velocity data are only available in electronic form at the CDS via anonymous ftp to cdsarc.u-strasbg.fr (130.79.128.5) or via http://cdsweb.u-strasbg.fr/cgi-bin/qcat?J/A+A/517/L1

2. Observations

2.1. The WASP-8 multiple stellar system

The star *WASP-8* (TYC2 7522-505-1) at α(2000): $23^{\rm h}59^{\rm m}36.07^{\rm s}$, δ(2000): $-35°1'52.9''$, was observed in 2006 and 2007 by the WASP-south telescope (Pollacco et al. 2006). It is a V = 9.79 mag star with a Tycho $(B-V)$ color of 0.73 which is indicative of a G8 spectral type. The Infra-red Flux Method (IRFM) (Blackwell & Shallis 1977), using GALEX, TYCHO-2, USNO-B1.0 R-magnitude, and 2MASS broad-band photometry, yields a distance of 87 ± 7 pc.

WASP-8 is identified in the CCDM catalogue (CCDM 23596-3502) as the A component of a system of three stars. The B component is a 15th magnitude red star, 4 arcsec south of A, and the third component C is a 10th magnitude star (HIP 118299, HD 224664) 142 arcsec north of A. The radial velocity of HD 224664 is 4.7 km s^{-1} and stable over two years (Mayor, priv. com.) but differs from the *WASP-8* value of −1.5 km s^{-1}. The proper motions of the components also differs. It is therefore unlikely that C and A are physically associated.

We measured the photometry and position of *WASP-8* and its nearby star (B component) with the Euler CCD camera of the 1.2 m swiss Euler telescope at La Silla (see Fig. 1). By comparing with nearby stars, we obtained a magnitude difference Δm_V = 4.7, Δm_I = 3.5. A separation and a projected angle was measured on the deconvolved images (Gillon et al. 2007) and we obtained 4.83 ± 0.01″ and PA = 170.7 ± 0.1° (only internal errors being considered). Assuming that *WASP-8* and its B component are part of a multiple system, the color indices would represent those of an M star. A similar photometric analysis of the individual 2MASS archive images indicates that Δm_J = 2.7, Δm_H = 2.2, and Δm_K = 2.1, which are also

A&A 517, L1 (2010)

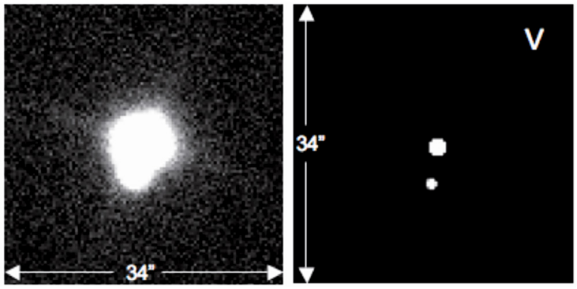


Fig. 1. Original (*left*) and deconvolved (*right*) *V*-band image from the Euler telescope of the A and B component of *WASP-8*.

indicative of an M star. The value mentioned in the Washington Visual Double Star Catalog measured 70 years ago indicates 4.0″ and PA = 170° (Mason et al. 2001). This suggests little, if any, relative motion of the two stars over the 70-year time span between these observations. When compared with the proper motion in right ascension of *WASP-8*, about 100 mas/yr (Zacharias et al. 2004), this indicates a common proper motion pair. Given the distance of *WASP-8* the sky-projected separation of the pair is about 440 AU. Using available differential photometry, we estimate the temperature of the B component to be about 3700 K.

2.2. Photometric and radial-velocity observations

WASP-8 was recorded simultaneously by two cameras of the WASP-south telescope during two seasons (2006 and 2007). Altogether 11 224 independent photometric points were recorded with a typical sampling of 8 min. Transit events were detected in data from the first observation season. This triggered radial velocity follow-up observations of *WASP-8* in November 2007 with the *Coralie* spectrograph mounted at the Swiss Euler telescope (Baranne et al. 1996; Queloz et al. 2000; Pepe et al. 2002). With a combined analysis of the radial-velocity data and the photometry including additional WASP data from the 2007 season, a transit period of 8.15 days was found. No changes to the spectroscopic profile were detected, ruling out a blended eclipsing binary or starspots as the cause of the radial-velocity variation (Queloz et al. 2001) (see bottom diagram in Fig. 2). In the next season, observations with *CORALIE* were continued, revealing an additional drift in the γ velocity of the system (Fig. 3). No second-order curvature term was detected.

On 25 August 2008, following up on the confirmation of the planet, a complete and densely sampled transit event was recorded in *R* band with the Euler telescope to improve the determination of the transit parameters (Fig. 4). On 4 October 2008, a spectroscopic transit was measured with the *HARPS* spectrograph installed on the 3.6 m telescope at La Silla. During the sequence, 75 spectra (44 in the transit) were measured with an exposure time of 300 s, corresponding to a typical signal-to-noise ratio per pixel of 50. The radial velocity measurement from these spectra shows an obvious Rossiter-McLaughlin effect with a shape suggesting a non-coplanar orbit (Fig. 4). In addition, four spectra were measured on the same night before and after the transit to help us to determine the rate of change in the radial velocity outside the transit. Three measurements were obtained later at other phases of the system to improve the matching and zero point correction between *CORALIE* and *HARPS* data.

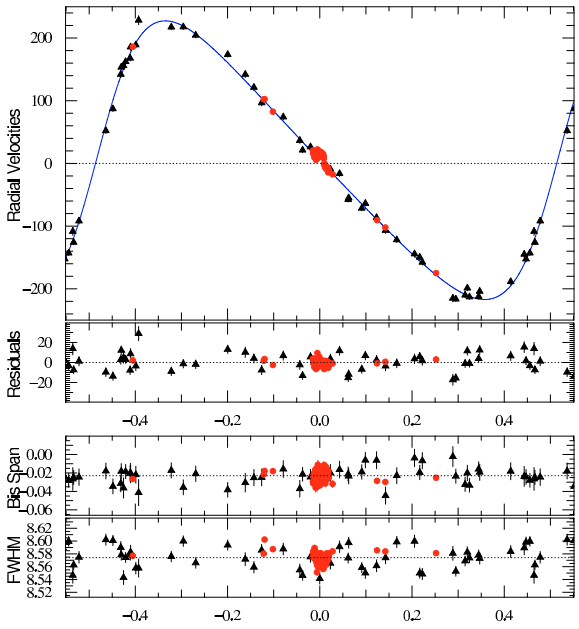


Fig. 2. *Top*: overall Keplerian fit to the RV data for *Wasp-8b*. Black triangles indicates *Coralie* data and red dots the *Harps* data. The long-term drift was removed to plot the velocity in phase (the zero is set at the time of the transit). *Bottom*: bissector span and *FWHM* (in km s^{-1} unit) plotted with the phase of the orbit. The *HARPS* radial velocity data were shifted to correct from the γ velocity difference with *CORALIE*.

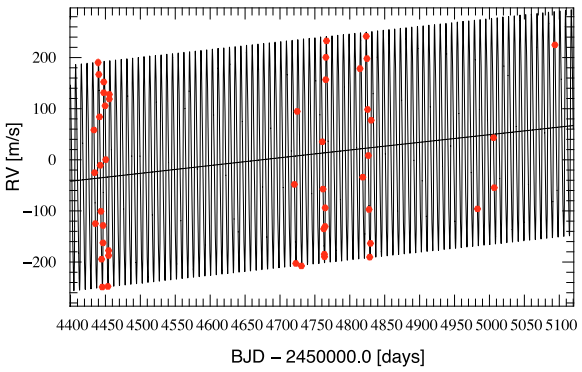


Fig. 3. *CORALIE* radial velocity measurements (red dots) of *WASP-8* superimposed on the best-fit solution (solid line).

During the measurement of the transit sequence, a significant change in telescope focus happened at JD 54 744.592, improving the flux entering the fiber by a factor of 2.

3. Determination of system parameters

3.1. Spectral analysis

The individual *HARPS* spectra were coadded and used for a detailed spectroscopic analysis of *WASP-8*. The results are displayed in Table 1. As in previous WASP-papers (Cameron et al. 2007), the analysis was performed using the UCLSYN spectral synthesis package and ATLAS9 models without convective overshooting with H_α and H_β Na I D and Mg I b lines as diagnostics for $T_{\rm eff}$ and (log g). The abundances and the microturbulence

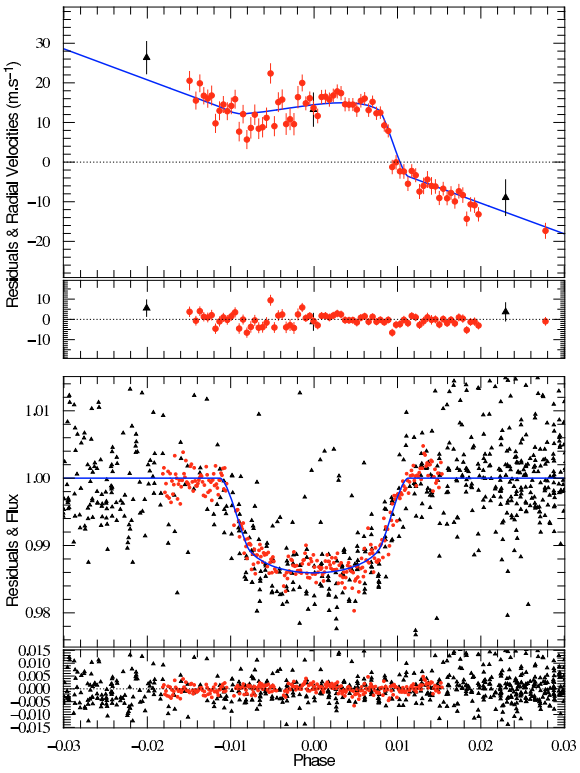


Fig. 4. *Top*: radial velocity measurement phased with the transit (mid-transit is at 0). Black triangles are *CORALIE* data and red dots *HARPS* data. *Bottom*: normalized transit photometry measurement of *WASP-8*. Black triangles indicates SuperWASP data and red dots the *R*-band Euler photometry data. The best-fit model is superimposed in blue.

Table 1. Stellar parameters of *WASP-8* derived from spectroscopic analysis.

$T_{\rm eff}$	5600 ± 80 K	[Na/H]	+0.22 ± 0.07
log g	4.5 ± 0.1	[Mg/H]	+0.21 ± 0.04
$\xi_{\rm t}$	1.1 ± 0.1 km s^{-1}	[Si/H]	+0.29 ± 0.09
$v \sin i$	2.0 ± 0.6 km s^{-1}	[Ca/H]	+0.24 ± 0.12
[Fe/H]	+0.17 ± 0.07	[Sc/H]	+0.23 ± 0.05
log A(Li/H)+12	1.5 ± 0.1	[Ti/H]	+0.24 ± 0.08
		[V/H]	+0.30 ± 0.08
dist	87 ± 7 pc	[Cr/H]	+0.17 ± 0.09
age	3−5 Gyr	[Co/H]	+0.29 ± 0.07
		[Ni/H]	+0.23 ± 0.07

Notes. The quoted error estimates include those given by the uncertainties in $T_{\rm eff}$, log g, and $\xi_{\rm t}$, as well as atomic data uncertainties.

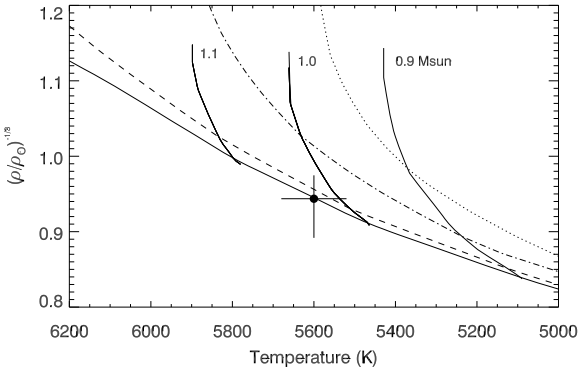


Fig. 5. Comparison of the best-fitting stellar parameters from the transit profile and spectroscopic analysis with evolutionary models interpolated at [Fe/H] = 0.17. The isochrones are 100 Myr, 1 Gyr, 5 Gyr and 10 Gyr. The evolutionary tracks are indicated for 0.9, 1.0 and 1.1 $M_{\rm sun}$.

were determined in a similarly way to the work of Gillon et al. (2009) and used as additional $T_{\rm eff}$ and log g diagnostics (Smalley 2005).

The Li I 6708 Å line is detected in the spectra indicating an abundance of log A(Li/H) + 12 = 1.5 ± 0.1, which implies an age of 3−5 Gyr according to Sestito & Randich (2005). However, Israelian et al. (2009) noted that stars with planets have lower lithium abundances than normal solar-type stars, so the lithium abundance may not be a good age indicator for them.

The rotational broadening $v \sin i$ was measured by fitting the observed HARPS profiles of several unblended Fe I lines. A typical value of macroturbulence $v_{\rm mac}$ = 2 km s^{-1} was adopted and an instrumental profile determined from telluric absorption lines. We found that $v \sin i$ = 2.0 ± 0.6 km s^{-1}, which is typical of a G dwarf of intermediate age.

3.2. Analysis of the planetary system

This whole data set was found to detect without doubt a planet transiting the star *WASP-8*. We analyzed together the photometric (WASP and Euler data) and the radial velocity data, including the spectroscopic transit sequence in this context. Our model was based on the transit modeling by Mandel & Agol (2002) and the radial velocity description by Giménez (2006). The best-fit model parameters and their error bars were computed using a MCMC convergence scheme that solves all parameters together. For details of the code and fitting techniques, we refer to Triaud et al. (2009); Collier Cameron et al. (2007). To obtain a coherent solution, we determined the mass of the star by comparing the spectroscopically-determined effective temperature and the stellar density outcome of the MCMC adjustment, with evolutionary tracks and isochrones of the observed metallicity from the stellar evolution model of Girardi et al. (2000). We converged iteratively on a stellar mass of 1.04(+0.02 −0.09) $M_\odot$ and an age younger than 6 Gyr (see in Fig. 5).

The free parameters of our model were the depth of transit D, the width of transit W, the impact parameter b, the period P, the epoch of transit centre T_0, the RV semi-amplitude K, $e \cos \omega$ and $e \sin \omega$ (e being the eccentricity and ω the angle of the periastron), and $V \sin I \cos \beta$ and $V \sin I \sin \beta$, with $V \sin I$ being the projection of the stellar equatorial rotation, and β the projection of the angle between the stellar spin axis and the planetary orbit axis. In addition, we employed free normalization factors for each lightcurve (WASP and Euler) and each set of radial velocity ($\gamma_{\rm H}$ for *HARPS* and $\gamma_{\rm C}$ for *CORALIE*), which enabled variations to be made in instrumental zero points. From these parameters, *physical* parameters were derived to characterise the planetary system. The best-fit set of parameters that minimize the $\chi^2_{\rm r}$ (reduced χ^2 is 0.86) are listed in Table 2 as well as their related computed physical parameters. With this best-fit solution one computes for the *CORALIE* data χ^2 = 204 with 48 measurements, and for HARPS data χ^2 = 188 with 82 measurements which implies that additional jittering is present that is not accounted for by the fitted model. Since the main deviation is related to the *CORALIE* data, the uncertainties in the orbital

Table 2. Fitted and physical parameters of the *WASP-8* planetary system.

D	0.01276	(+0.00033 − 0.00030)
W (days)	0.1832	(+0.0030 − 0.0024)
b ($R_\star$)	0.604	(+0.043 − 0.040)
P (days)	8.158715	(+0.000016 − 0.000015)
T_0 (BJD-2 450 000)	4679.33394	(+0.00050 − 0.00043)
K (m s^{-1})	222.23	(+0.84 − 0.60)
dγ/dt (m s^{-1} yr^{-1})	58.1	(+1.2 − 1.3)
e cos ω	0.02307	(+0.0010 − 0.0010)
e sin ω	−0.3092	(+0.0024 − 0.0029)
V sin I cos β	−0.873	(+0.059 − 0.064)
γ_C[a] (m s^{-1})	−1565.76	(+0.16 − 0.21)
γ_H[a] (m s^{-1})	−1548.10	(+0.60 − 0.13)
V sin I sin β	1.59	(+0.08 − 0.09)
$R_p/R_\star$	0.1130	(+0.0015 − 0.0013)
$R_\star/a$	0.0549	(+0.0024 − 0.0024)
$\rho_\star$ ($\rho_\odot$)	1.22	(+0.17 − 0.15)
$R_\star$ ($R_\odot$)	0.945	(+0.051 − 0.036)
$M_\star$ ($M_\odot$)	1.030	(+0.054 − 0.061)
V sin I (km s^{-1})	1.59	(+0.08 − 0.09)
R_p/a	0.00620	(+0.00036 − 0.00033)
R_p (R_J)	1.038	(+0.007 − 0.047)
M_p (M_J)	2.244	(+0.079 − 0.093)
a (AU)	0.0801	(+0.0014 − 0.0016)
i (°)	88.55	(+0.15 − 0.17)
e	0.3100	(+0.0029 − 0.0024)
ω (°)	−85.73	(+0.17 − 0.18)
β (°)	123.3	(+4.4 − 3.4)

Notes. The error bars are calculated at 68% of the statistical distributions.
[a] Computed at JDB = 2 454 691.15781.

solutions are most likely underestimated. However, the error bars in the Rossiter parameters are driven mostly by the HARPS on-transit data, and one can assume that they are almost correct.

Our best-fit solution corresponds to a giant planet with an eccentric (e = 0.3) 8.16-day orbit and an additional long-term radial-velocity drift of 58 m s^{-1} yr^{-1}. The planet is dense with 2.25 M_j and a radius of 1.04 R_j, in contrast to the substantial fraction of "inflated" hot Jupiters. Surprisingly, the projected angle between the orbital and stellar spin axes is found to be β = 123.3°, indicative of a retrograde orbit. We note that V sin I = 1.59 km s^{-1} is in accordance with the line rotation broadening v sin i (in Table 1) derived by the spectral analysis.

We checked whether the partial defocusing of HARPS during the transit spectroscopic sequence had any effect on our result. We divided the series into two subsets and considered for each of them an independent offset (γ). We obtain a solution with a marginal improvement in the χ^2. By comparing the solution obtained from these two sets with that for the complete set, the angle β was changed by 1.5σ. The defocusing problem does not affect the results of this paper.

4. Discussion

The detection of a hot Jupiter on an eccentric orbit that is misaligned with the stellar rotation axis and moving in a retrograde direction raises many questions about the origins of this system. Although the answer is beyond the scope of this paper, the visual faint companion and the drifting γ velocity of the system are key components of the puzzle. From the observed separation between the A and B components, one can derive a most likely orbital semi-major axis (a = 1.35ρ ≈ 600 AU) (Duquennoy & Mayor 1991). The observed radial-velocity drift is therefore unlikely to be related to the B component of the binary ($\dot{\gamma} < GMa^{-2} < 1$ m s^{-1} yr^{-1}), suggesting that these is an additional closer companion of both unknown mass and period. The lack of curvature indicates that the companion is more massive than the transiting planet. This intermediate body is very likely to play a significant dynamical role in the system.

Apart from the complex dynamics of the whole system, the planet *WASP-8b* is a "standard" hot Jupiter. It orbits a metal-rich star, which accounts for the observed increase in the incidences of hot Jupiters with the metallicity of the host star (Udry & Santos 2007). The period of *WASP-8b* is longer than the 3–4 days typical value, but considering the eccentricity of its orbit, its periastron distance is typical of hot Jupiters.

The orbit misalignment of the planet with the stellar rotation axis of *WASP-8* is measured with the β parameter. The true angle between the axes of the stellar and planetary orbits is usually called ψ and is statistically related to β through sin I (unknown) and the orbital inclination (i) (see Fabrycky & Winn 2009, for details). When β deviates significantly from zero, this provides us with a lower limit to the ψ. When β is beyond 90°, the orbital spin has the opposite direction to the stellar rotation provided that the orbit does not transit the star between its pole and its limb. According to Eq. (9) from Fabrycky & Winn (2009), this condition is met when I > 3.6 degree. By combining V sin I, with the estimated age of the star, one can exclude such a small I angle. Interpreted with the large β value, we can conclude that a true retrograde orbit is the most likely scenario for *WASP-8b*.

The origin of the unusual shape and orientation of the orbit of *WASP-8b* is possibly related to the Kozai mechanism (Kozai 1962; Wu & Murray 2003) or the outcome of a violent dynamical interaction history. The evidence of two other bodies and a possible series of secular effects (Takeda et al. 2008) make the *WASP-8* system unique and interesting for additional dynamical studies and a test case for formation scenarios of hot Jupiters that constitute an alternative to the disc-migration mechanism.

References

Baranne, A., Queloz, D., Mayor, M., et al. 1996, A&AS, 119, 373
Barker, A. J., & Ogilvie, G. I. 2009, MNRAS, 395, 2268
Blackwell, D. E., & Shallis, M. J. 1977, MNRAS, 180, 177
Cameron, A. C., Bouchy, F., Hébrard, G., et al. 2007, MNRAS, 375, 951
Collier Cameron, A., et al. 2007, MNRAS, 380, 1230
Duquennoy, A., & Mayor, M. 1991, A&A, 248, 485
Fabrycky, D. C., & Winn, J. N. 2009, ApJ, 696, 1230
Gillon, M., Magain, P., Chantry, V., et al. 2007, ASP Conf. Ser., 366, 113
Gillon, M., Smalley, B., Hebb, L., et al. 2009, A&A, 496, 259
Giménez, A. 2006, ApJ, 650, 408
Girardi, L., Bressan, A., Bertelli, G., & Chiosi, C. 2000, A&AS, 141, 371
Israelian, G., Delgado Mena, E., Santos, N. C., et al. 2009, Nature, 462, 189
Kozai, Y. 1962, AJ, 67, 591
Lin, D. N. C., Bodenheimer, P., & Richardson, D. C. 1996, Nature, 380, 606
Mandel, K., & Agol, E. 2002, ApJ, 580, L171
Mason, B. D., Wycoff, G. L., Hartkopf, W. I., et al. 2001, AJ, 122, 3466
Nagasawa, M., Ida, S., & Bessho, T. 2008, ApJ, 678, 498
Pepe, F., Mayor, M., Galland, F., et al. 2002, A&A, 388, 632
Pollacco, D. L., Skillen, I., Cameron, A. C., et al. 2006, PASP, 118, 1407
Queloz, D., Mayor, M., Weber, L., et al. 2000, A&A, 354, 99
Queloz, D., Henry, G. W., Sivan, J. P., et al. 2001, A&A, 379, 279
Smalley, B. 2005, Mem. Soc. Astron. It. Suppl., 8, 130
Sestito, P., & Randich, S. 2005, A&A, 442, 615
Takeda, G., Kita, R., & Rasio, F. A. 2008, ApJ, 683, 1063
Triaud, A. H. M. J., Queloz, D., Bouchy, F., et al. 2009, A&A, 506, 377
Udry, S., & Santos, N. C. 2007, ARA&A, 45, 397
Winn, J. N. 2010 [arXiv:1001.2010]
Wu, Y., & Murray, N. 2003, ApJ, 589, 605
Zacharias, N., Monet, D. G., Levine, S. E., et al. 2004, BAAS, 36, 1418

3.4.4 Analysing WASP-23 b

As part of the effort that I give for WASP, the discovery paper for WASP-23 was awarded to me. Although a pretty straight forward analysis, it took a long while before being submitted because of the many other results regarding the Rossiter-McLaughlin effect that will be exposed next chapter. This allowed to gather more data, add transit lightcurves, add additional CORALIE data; we even observed it with HARPS and got a Rossiter-McLaughlin. I don't know if this was a curse or an opportunity. A curse since its analysis, because of the slow rotation of its host star, was made more harduous, which delayed the paper further. An opportunity since it gave the occasion to explore a little more the jump parameters for the MCMC and the role of priors in fitting for the Rossiter-McLaughlin model.

In this paper were explained the reasons for using $\sqrt{e}\,\cos\omega$ and $\sqrt{e}\,\sin\omega$ instead of $e\,\cos\omega$ and $e\,\sin\omega$ as jump parameters. The latter pair is equivalent to have a prior proportional to e. Using the new pair avoids biasing the chain towards finding higher, apparently significantly detected values for the eccentricity. Similarly was introduced the pair for $\sqrt{V\,\sin I}\,\cos\beta$ and $\sqrt{V\,\sin I}\,\sin\beta$ to fit the Rossiter-McLaughlin effect. These two changes might have led us to slightly different results in earlier paper (especially think about the Rossiter-McLaughlin effect of WASP-2 (see next chapter) (and actually confirmed by Albrecht et al. (2011)).

As can be seen in the following paper, a degeneracy develops between $V\,\sin I$, β and b when b, the impact parameter goes to zero. In fact, using equations 2.16 and 2.17 (and Albrecht et al. (2011)), one sees that only $V\,\sin I\cos\beta$ can be detected. $V\,\sin I\sin\beta$ being meaningless, we loose information about any asymmetry making it impossible to distinguish an angle. We can only decide whether the system is prograde or retrograde. In WASP-23's case the matter is made worse because the photometry does not constrain b well enough, thus the RVs push the chain towards the most flexible solution, where $b = 0$. This shows the Rossiter-McLaughlin effect in our case is very symmetric. Any slight asymmetry would help adjust b rather than hamper it.

In principle, if one has prior knowledge about either of $V\,\sin I$ or β, one could solve the degeneracy. We thus hunted for values of $v_\star\,\sin I$, which can be determined from spectral line broadening. Imposing that prior, forces the solution to highly inclined orbits. In order to test the robustness of it, we hunted for another value, and attempted an old dream. Using the $\log R'_{\rm HK}$, an index for stellar activity based Calcium emission in the H and K bands, one can draw from empirical relationship, an estimate for the stellar period. Having the stellar radius as output of the MCMC, it is an easy task to get a stellar rotation velocity. We now have I and β. Assuming $I = 90°$, we get the highest value possible for an estimate of $v_\star\,\sin I$. Although technically an upper limit, we found that value quite lower from the previous. Imposing it on the chain as a prior gives out a less inclined orbit. Playing with the priors was a stark reminder that those depend heavily on our own biases, and that any fit with a prior is meaningless without a fit not using it, to allow comparison.

Getting to the stellar rotation $v_\star$ accurately (from the $\log R'_{\rm HK}$ for example) and to reliable $v_\star\,\sin I$ can be of enormous use, as this, would help us find the real obliquity ψ instead of its projection on the sky β. This has also other uses for example in the recent astrometric paper by Sahlmann et al. (2011a) where it is possible to determine the planet's orbital inclination i, then to determine the star spin inclination I for non transiting systems and get to the obliquity ψ.

Doppler imaging , is also a way to lift the degeneracy, as β can be measured from the location in velocity space at which the planet enters, and exits. This chord also gives a very precise measure on b (Cameron et al. 2010a).

A&A 531, A24 (2011)
DOI: 10.1051/0004-6361/201016367
© ESO 2011

Astronomy & Astrophysics

WASP-23b: a transiting hot Jupiter around a K dwarf and its Rossiter-McLaughlin effect⋆,⋆⋆,⋆⋆⋆

A. H. M. J. Triaud[1], D. Queloz[1], C. Hellier[2], M. Gillon[3], B. Smalley[2], L. Hebb[4], A. Collier Cameron[5], D. Anderson[2], I. Boisse[6,7], G. Hébrard[7,8], E. Jehin[3], T. Lister[9], C. Lovis[1], P. F. L. Maxted[2], F. Pepe[1], D. Pollacco[10], D. Ségransan[1], E. Simpson[10], S. Udry[1], and R. West[11]

[1] Observatoire Astronomique de l'Université de Genève, Chemin des Maillettes 51, 1290 Sauverny, Switzerland
e-mail: Amaury.Triaud@unige.ch
[2] Astrophysics Group, Keele University, Staffordshire, ST55BG, UK
[3] Institut d'Astrophysique et de Géophysique, Université de Liège, Allée du 6 Août, 17, Bât. B5C, Liège 1, Belgium
[4] Department of Physics and Astronomy, Vanderbilt University, Nashville, TN37235, USA
[5] SUPA, School of Physics & Astronomy, University of St Andrews, North Haugh, KY16 9SS, St Andrews, Fife, Scotland, UK
[6] Centro de Astrofísica, Universidade do Porto, Rua das Estrelas, 4150-762 Porto, Portugal
[7] Institut d'Astrophysique de Paris, CNRS (UMR 7095), Université Pierre & Marie Curie, 98bis bd. Arago, 75014 Paris, France
[8] Observatoire de Haute-Provence, CNRS/OAMP, 04870 St Michel l'Observatoire, France
[9] Las Cumbres Observatory, 6740 Cortona Dr. Suite 102, Santa Barbara, CA 93117, USA
[10] Astrophysics Research Centre, School of Mathematics & Physics, Queens University, University Road, Belfast, BT71NN, UK
[11] Department of Physics and Astronomy, Universityof Leicester, Leicester, LE17RH, UK

Received 20 December 2010 / Accepted 13 March 2011

ABSTRACT

We report the discovery of a new transiting planet in the southern hemisphere. It was found by the WASP-south transit survey and confirmed photometrically and spectroscopically by the 1.2 m Swiss *Euler* telescope, LCOGT 2m Faulkes South Telescope, the 60 cm TRAPPIST telescope, and the ESO 3.6 m telescope. The orbital period of the planet is 2.94 days. We find that it is a gas giant with a mass of $0.88 \pm 0.10\,M_J$ and an estimated radius of $0.96 \pm 0.05\,R_J$. We obtained spectra during transit with the HARPS spectrograph and detect the Rossiter-McLaughlin effect despite its small amplitude. Because of the low signal-to-noise ratio of the effect and a small impact parameter, we cannot place a strong constraint on the projected spin-orbit angle. We find two conflicting values for the stellar rotation. We find, via spectral line broadening, that $v \sin I = 2.2 \pm 0.3$ km s^{-1}, while applying another method, based on the activity level using the index $\log R'_{HK}$, gives an equatorial rotation velocity of only $v = 1.35 \pm 0.20$ km s^{-1}. Using these as priors in our analysis, the planet might be either misaligned or aligned. This result raises doubts about the use of such priors. There is evidence of neither eccentricity nor any radial velocity drift with time.

Key words. binaries: eclipsing – planetary systems – stars: individual: WASP-23 – techniques: spectroscopic – techniques: photometric – stars: rotation

1. Introduction

Finding planets by detecting their transit has proven to be very successful there having been detections past the hundred mark. After the discovery that HD 209458b was transiting (Charbonneau et al. 2000), a plethora of ground-based small aperture wide-angle photometric surveys have been put in place to find similar bodies, such as WASP (Pollacco et al. 2006), the HAT network (Bakos et al. 2004), XO (McCullough et al. 2005), TrES (O'Donovan et al. 2006), or the OGLE search (Udalski et al. 1997; Snellen et al. 2007). WASP is the only survey currently operating in both hemispheres. About 20% of extrasolar planets discovered so far are currently known to transit their host stars, the vast majority of which are the so-called *hot Jupiters*, planets similar in mass to Jupiter but on orbits with periods <5 days.

Transiting planets provide a treasure trove of observables allowing the study of a special class of planets that is absent from our Solar System. A transiting system, observed with photometry and radial velocities, allows us to measure the planet's mass ratio with the star, and both the stellar density and ratio of radii. Through observations at the time of occultation, it is possible measure the temperature of the planet. Careful analysis during transit and occultation can provide insight into its atmospherical composition.

Another observable that has been under intense scrutiny recently is the spin-orbit angle. As the planet transits, it covers a part of the approaching or receding hemisphere of the star, therefore red-shifting or blue-shifting the spectrum. This appears as a radial velocity anomaly in the main reflex Doppler motion curve. It is called the Rossiter-McLaughlin effect (Holt 1893; Rossiter 1924; McLaughlin 1924) and was first measured for

⋆ Using WASP-South photometric observations confirmed with LCOGT Faulkes South Telescope, the 60 cm TRAPPIST telescope, the *CORALIE* spectrograph and the camera from the Swiss 1.2 m *Euler* Telescope placed at La Silla, Chile, as well as with the HARPS spectrograph, mounted on the ESO 3.6 m, also at La Silla, under proposal 084.C-0185. The data is publicly available at the *CDS* Strasbourg and on demand to the main author.
⋆⋆ RV data is only available at the CDS via anonymous ftp to cdsarc.u-strasbg.fr (130.79.128.5) or via http://cdsarc.u-strasbg.fr/viz-bin/qcat?J/A+A/531/A24
⋆⋆⋆ Appendix is available in electronic form at http://www.aanda.org

A&A 531, A24 (2011)

a planet by Queloz et al. (2000) and modelled by Ohta et al. (2005), Giménez (2006), and Hirano et al. (2010). Recently it was found that hot Jupiters are located on a vast range of orbital planes with respect to the stellar rotation, some even on retrograde orbits (Hébrard et al. 2008; Winn et al. 2009; Narita et al. 2009; Anderson et al. 2010; Queloz et al. 2010). The study of this angle's distribution is being used to distinguish the processes through which hot Jupiters have arrived at their current orbits (Triaud et al. 2010; Winn et al. 2010a; Morton & Johnson 2011).

All this gathered data helps developments in theoretical physics in regimes beforehand out of reach: intense heat transfer between hot and cold hemispheres (Guillot & Showman 2002) and on supersonic winds (Dobbs-Dixon et al. 2010) to name only two. The few detections of multi-planet systems in which at least one component is transiting can also provide insight into the interior structure (Batygin et al. 2009). Obviously the study of these special exoplanets is also shedding light on how planets form as well as on the evolution of their orbits with time. The hot Jupiters are thought to have experienced a migration to the star after their formation beyond the ice-line, be it through some angular momentum exchange with the primordial protoplanetary disc (Lin et al. 1996), or via dynamical interactions and subsequent tidal friction (Fabrycky & Tremaine 2007; Nagasawa et al. 2008; Malmberg et al. 2011), an explanation now preferred to the previous one. The history of that post formation evolution might hold a key to the understanding of the various processes that planetary systems are likely to experience thus shed light on the events surrounding the origin of our own Solar System.

In this light, we announce the discovery of a new transiting gas giant by the WASP consortium, in close proximity to its host star, which participates in providing a deeper understanding of these objects.

2. Observations

The object, WASP-23, (1SWASP J064430.59-424542.5) is a K1V star with $V = 12.68$ that was observed during two seasons of the WASP-South survey, located in Sutherland, South Africa, in a single camera field from 2006 October 13 to 2007 March 11 and from 2007 October 11 to 2008 March 11 representing 10 846 photometric measurements. The WASP-South instrument, part of the WASP survey is amply described in Pollacco et al. (2006). The *Hunter* algorithm (Collier Cameron et al. 2007b) searched the data and found 11 partial transits with a period of 2.94 days and a depth of 1.7% in both seasons (Fig. 1). It was selected for spectroscopic follow-up. No rotational variability could be found in the photometric data, which is indicative of slow rotation and few stellar spots.

The 1.2 m *Euler* Swiss telescope, in La Silla, Chile, established the planetary nature of the object by detecting a Doppler variation of semi-amplitude 145 m s^{-1} with the same period and epoch as the WASP-South photometry. Observations started on 2008 August 31 and were pursued until 2010 April 08 totalling 38 radial velocity measurements (Fig. 2), each a 30 min exposure.

A photometric timeseries was acquired with the camera mounted on the *Euler* telescope, in the z-band on 2008 December 13. We gathered 254 measurements and confirmed the reality of the photometric signal discovered by WASP-South (Fig. 3). In addition we gathered another 215 measurements in the z band during transit with the Faulkes South Telescope on 2009 September 27. We observed a third transit on 2010 February 7, with *Euler*, collecting 193 datapoints in the R-band filter (Fig. 3). Two further transits were observed during December 2010 using the newly built 60 cm TRAPPIST robotic telescope (Gillon et al. 2011), also located in La Silla, were finally added to this analysis (Fig. 4).

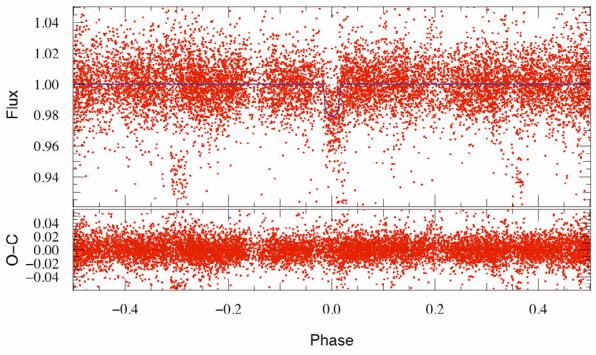


Fig. 1. Phased WASP-South photometry, of two seasons, and residuals. R band model superimposed.

Under ESO proposal 084.C-0185, we observed with the spectrograph HARPS, mounted on the ESO 3.6 m telescope, at La Silla, Chile, obtaining 35 spectra between 2009 December 18 and 2010 February 9. Twenty-eight spectra at a mean cadence of roughly 600 s were acquired on the first night, 14 of which are positioned as the planet transits (Figs. 2 and 3). The others were observed a few months later because of scheduling contraints and have exposure times of 1200 s.

3. Data analysis

3.1. The Euler z-band transit

The transit was observed in the z-band, on 2008 December 12, from 2h15 to 7h35 UTC using the *Euler* camera. The z-band filter was used to minimise the impact of stellar limb-darkening on the deduced system parameters. The images were 2×2 binned to improve the duty cycle of the observations, resulting in a pixel scale of 0.7 arcsec. We acquired 254 exposures during the run, of exposure times ranging from 45 s to 60 s. Two outliers were removed from our analysis. To keep a good spatial sampling while minimising the impact of interpixel sensitivity inhomogeneities and seeing variations, the telescope was heavily defocused and produced a mean profile width of 4.8 ± 0.2 arcsec. The airmass decreased from 1.43 to 1.03 then increased to 1.09.

After a standard pre-reduction, stellar fluxes were extracted using the IRAF[1] version of the DAOPHOT aperture photometry software (Stetson 1987). After a careful selection of reference stars, we subtracted a linear fit from the differential magnitudes as a function of airmass to correct for the different colour dependance of the extinction for the target and comparison stars. The linear fit was calculated from the out-of-transit (OOT) data and applied to all the data. The corresponding fluxes were then normalised using the OOT part of the photometry. Figure 3 shows the resulting timeseries. The OOT rms is 2.2 mmag for a mean time sampling of 75 s. Comparing this OOT rms to the one

[1] IRAF is distributed by the National Optical Astronomy Observatory, which is operated by the Association of Universities for Research in Astronomy, Inc., under cooperative agreement with the National Science Foundation.

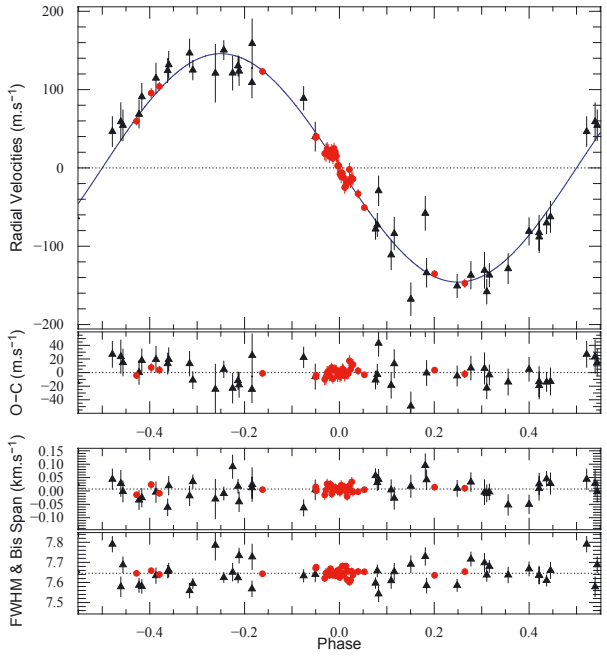


Fig. 2. Black triangles: CORALIE data; red discs: HARPS data. *Top*: radial velocities with model superimposed, and residuals (both in m s^{-1}), as a function of orbital phase. Added are the 1σ error bars. *Bottom*: phased bisector span and *FWHM* (both in km s^{-1}). The HARPS data has been translated to have its mean correspond to the CORALIE data.

obtained after binning the data in units of 25 min (a duration comparable to that of ingress/egress) as described by Gillon et al. (2006) indicates that a correlated noise of ~600 ppm is present in the photometry.

3.2. The Euler *R*-band transit

A similar reduction was performed for the transit of 2010 February 7. After outlier rejection, we were left with 183 images of a mean sampling time of 63 s. In this instance the telescope was not defocused, the mean profile width being 2.3 arcsec. Transparency was good and airmass ranged from 1.03 to 2.22. Five stars were used as reference totalling a comparative flux 4.2 times that of the target. We also observe some correlated noise, of ~600 ppm in the photometry. The photometry is shown in Fig. 3.

3.3. The FTS *z*-band transit

An additional transit of WASP-23b was obtained with the LCOGT[2] 2.0 m Faulkes Telescope South (FTS) at Siding Spring Observatory, Australia on the night of 2009 September 27. Observations took place between 15:30 UTC and 19:00 UTC and the airmass decreased throughout the night from 1.9 at the start of the night to 1.1. The em03 Merope camera was used with a 2×2 binning mode giving a field of view of $5' \times 5'$ and a pixel scale of 0.278 arcsec/pixel. The data were taken through a Pan-STARRS-z filter and the telescope was defocussed to prevent saturation and allow longer 35 s exposure times to be used.

[2] http://lcogt.net

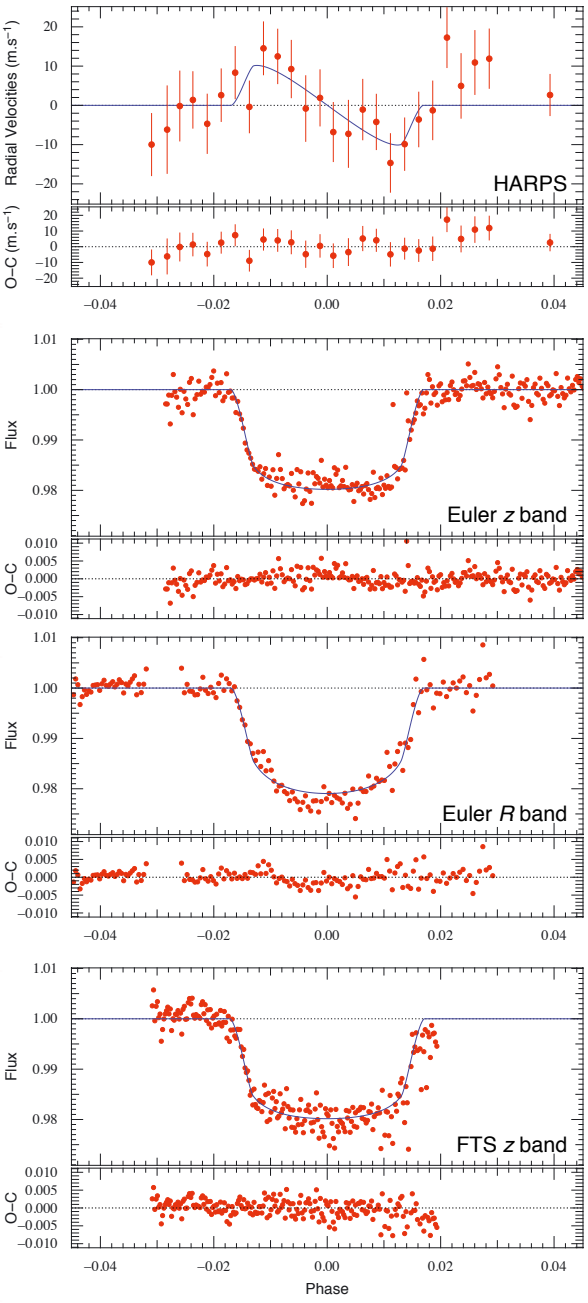


Fig. 3. HARPS radial velocity data corrected for the reflex Doppler motion due to the planet and model of the Rossiter-McLaughlin effect with residuals. Below: three photometric transits (instruments are indicated), the best-fit model and residuals. All are presented as a function of the orbital phase.

The data were pre-processed in the standard manner to perform the debiassing, dark subtraction, and flatfielding steps. Aperture photometry was performed using DAOPHOT within the IRAF environment using a 10 pixel radius aperture and the differential photometry was performed relative to 14 comparison stars that were within the FTN field of view.

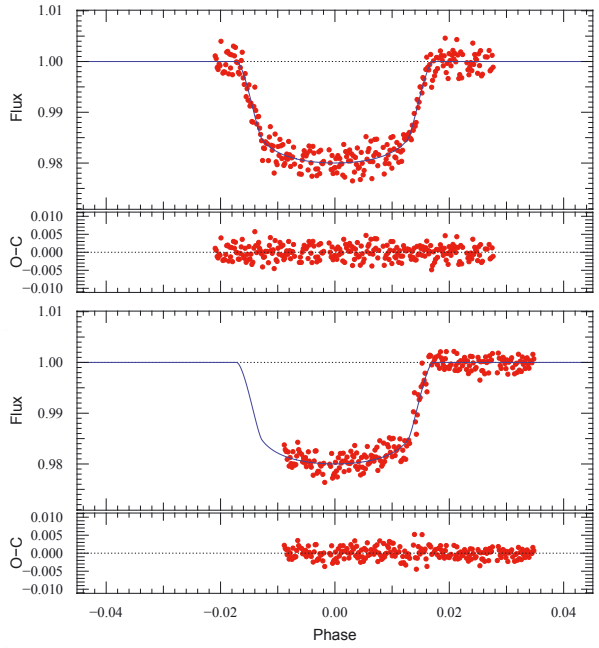


Fig. 4. The two $I+z$ band timeseries observed by TRAPPIST, with best-fit model being overplotted.

During the course of the FTS observations, we detected a $\gtrsim$0.55 mag deep flat-bottomed partial eclipse on a nearby (∼109 arcsec) star (USNO-B1.0 0472-0093932, α = 06h44′37.63″ $\delta = -42°45'13.5''$) which appears to be an eclipsing binary. A cursory search of the WASP archive indicates that it is has an ephemeris of HJD(Min I) = 2 454 021.573377E + 1.421933 days with an eclipse depth of ∼0.75 mag.

3.4. The TRAPPIST $I+z$ band transits

A complete and a partial transit of WASP-23 was also observed with the robotic 60 cm telescope TRAPPIST[3]) (Gillon et al. 2011). Located at La Silla ESO observatory (Chile), TRAPPIST is equipped with a 2K × 2K Fairchild 3041 CCD camera that has a 22′ × 22′ field of view (pixel scale = 0.64″/pixel). The transits of WASP-23 were observed on the nights of 2010 December 21 and 30. The sky conditions were clear. We used the 1 × 2 MHz read-out mode with 1 × 1 binning, resulting in a typical read-out + overhead time and read noise of 8.2 s and 13.5 e^-, respectively. The integration time was 35 s for both nights. We observed through a special "$I+z$" filter that has a transmittance of zero below 700 nm, and >90% from 750 nm to beyond 1100 nm. The telescope was defocused to average pixel-to-pixel sensitivity variations and to optimize the duty cycle, resulting in a typical full width at half-maximum of the stellar images of ∼5.2 pixels (∼3.3″). The positions of the stars on the chip were maintained to within a few pixels over the course of the two runs, thanks to the "software guiding" system that regularly derives an astrometric solution from the most recently acquired image and sends pointing corrections to the mount if needed. After a standard pre-reduction (bias, dark, flatfield), the stellar fluxes were extracted from the images using the `IRAF/DAOPHOT` aperture photometry software (Stetson 1987). Several sets of reduction parameters were tested, and we kept the one giving the most precise photometry for the stars of brightness similar to WASP-23. After a careful selection of reference stars, differential photometry was obtained. The data is shows in Fig. 4.

[3] http://arachnos.astro.ulg.ac.be/Sci/Trappist

Table 1. Stellar parameters of WASP-23 from spectroscopic analysis.

$T_{\rm eff}$	5150 ± 100 K	[Fe/H]	−0.05 ± 0.13
$\log g$	4.4 ± 0.2	[Mg/H]	+0.15 ± 0.15
$\xi_{\rm t}$	0.8 ± 0.2 km s^{-1}	[Si/H]	+0.03 ± 0.08
$v_{\rm mac}$	0.8 ± 0.3 km s^{-1}	[Ca/H]	+0.17 ± 0.16
$v \sin I$	2.2 ± 0.3 km s^{-1}	[Sc/H]	+0.03 ± 0.12
		[Ti/H]	+0.18 ± 0.13
$B-V$	0.88 ± 0.05	[V/H]	+0.34 ± 0.13
$\log R'_{\rm HK}$	−4.68 ± 0.07	[Cr/H]	+0.04 ± 0.10
$S_{\rm MW}$	0.32 ± 0.04	[Mn/H]	+0.05 ± 0.15
		[Co/H]	+0.11 ± 0.15
$\log A$(Li)	<1.0	[Ni/H]	−0.03 ± 0.12

3.5. The spectral analysis

A total of 26 individual CORALIE spectra of WASP-23 were coadded to produce a single spectrum with a typical signal-to-noise ratio of around 50:1. The standard pipeline reduction products were used in the analysis.

The analysis was performed using the methods given in Gillon et al. (2009). The H_α line was used to determine the effective temperature ($T_{\rm eff}$), while the Na I D and Mg I b lines were used as surface gravity ($\log g$) diagnostics. The parameters obtained from the analysis are listed in Table 1. The elemental abundances were determined from equivalent width measurements of several clean and unblended lines. A value for microturbulence ($\xi_{\rm t}$) of 0.8 km s^{-1} was determined from Fe I using the Magain (1984) method. The quoted error estimates include those given by the uncertainties in $T_{\rm eff}$, $\log g$ and $\xi_{\rm t}$, as well as the scatter due to measurement and atomic data uncertainties.

The projected stellar rotation velocity ($v \sin I$)[4] was determined by fitting the profiles of several unblended Fe I lines. Because the value of $v \sin I$ was paramount to the model fitting, we used the combined HARPS spectra. A value for macroturbulence ($v_{\rm mac}$) of 0.8 ± 0.3 km s^{-1} was assumed, based on work by Bruntt et al. (2010) and an instrumental *FWHM* of 0.060 Å, determined from the telluric lines around 6300 Å. A best-fitting value of $v \sin I$ = 2.2 ± 0.3 km s^{-1} was obtained. Using a macroturbulence based on the tabulation by Gray (2008) of 1.2 km s^{-1}; we obtain the same result for $v \sin I$ showing its robustness.

The HARPS spectra show that there is weak emission in the cores of the calcium H & K lines. Activity levels on the star are estimated by means of the $\log R'_{\rm HK}$ (Noyes et al. 1984; Santos et al. 2000; Boisse et al. 2009) and obtained using a $B-V$ = 0.88 ± 0.05 estimated from the effective temperature. The Mount Wilson index, $S_{\rm MW}$ is also given.

3.6. The RV extraction

The spectroscopic data were reduced using the online Data Reduction Software (DRS) for the HARPS instrument. The radial velocity information was obtained by removing the

[4] We make a distinction between $v \sin I$ and $V \sin I$. The latter is a result of the Rossiter-McLaughlin fit. i traditionally being the planet's orbital inclination, we denote by I, the inclination of the stellar spin axis.

instrumental blaze function and cross-correlating each spectrum with a K5 mask. This correlation was compared with the Th-Ar spectrum used as a wavelength-calibration reference (see Baranne et al. 1996; Pepe et al. 2002, for details). The DRS was shown to achieve remarkable precision (Mayor et al. 2009) thanks to a revision of the reference lines for thorium and argon by Lovis & Pepe (2007). A similar software package was used the prepare the CORALIE data. A resolving power $R = 110\,000$ for HARPS provided a cross-correlation function (CCF) binned in 0.25 km s^{-1} increments, while for the CORALIE data, with a lower resolution of 50 000, we used 0.5 km s^{-1}. The CCF window was adapted to be three times the size of the full width at half maximum (*FWHM*) of the CCF.

1σ error bars on individual data points were estimated from photon noise alone. HARPS is stable in the long term to within 1 m s^{-1} and CORALIE to better than 5 m s^{-1}. These are smaller than our individual error bars, thus were not taken into account.

The absence of any variation in bisector span correlated with the phase, or any variation in the *FWHM*, indicate that the photometric and spectroscopic signals are indeed those of a planet. For comparison, we invite the reader to read Santos et al. (2002), studying HD 41004 for which it has been proven that a blend by a star and its brown dwarf companion produced a spectroscopic Doppler shift similar to that of a planet on a foreground object.

4. Modelling the data

The data was fitted using a Markov Chain Monte-Carlo (MCMC) method in a code allowing us to combine both photometry and spectroscopy. It has been used in several occasions (Bouchy et al. 2008; Gillon et al. 2008) and is described at length in Triaud et al. (2009). It is similar to those presented in Collier Cameron et al. (2007a). The code uses a common set of free parameters from which physical parameters can be derived to construct models for the photometric and spectroscopic signals.

4.1. Parameter choice

We used the following free (or jump) parameters: P for the period of the object, T_0 the mid-transit time, D the depth of the transit, W its width, b the impact parameter, and K the semi-amplitude of the Doppler reflex motion by the star. To fit the Rossiter-McLaughlin effect, we use $\sqrt{V \sin I}\cos\beta$ and $\sqrt{V \sin I}\sin\beta$ where $V \sin I$ is the projected stellar rotation and β the projected spin-orbit angle. To estimate whether the orbit is eccentric, we used $\sqrt{e}\cos\omega$ and $\sqrt{e}\sin\omega$ where e is the eccentricity and ω is the argument of the periastron. In addition, we added at times $\dot{\gamma}$, a radial-velocity drift with time, to assess the presence of an additional body in the system. We also fitted one normalisation factor for each photometric dataset (five in our case) and two γ velocities for the radial velocities, one for each set. We used Gaussian priors to randomly draw each parameter.

We decided to use $\sqrt{e}\cos\omega$ and $\sqrt{e}\sin\omega$ as free parameters instead of the more traditional $e\cos\omega$ and $e\sin\omega$ because this would amount to imposing a prior proportional to e^2 as noted in Ford (2006). Figure 5 shows the difference between both runs. Considering $\sqrt{e}\cos\omega$ & $\sqrt{e}\sin\omega$ ensures that the eccentricity is less biased towards high values. We therefore made a similar change to another pair of variables, defining $\sqrt{V \sin I}\cos\beta$ and $\sqrt{V \sin I}\sin\beta$ as free parameters rather than using $V \sin I \cos\beta$ and $V \sin I \sin\beta$. We conducted checks of these parameters to validate our choice of jump parameters.

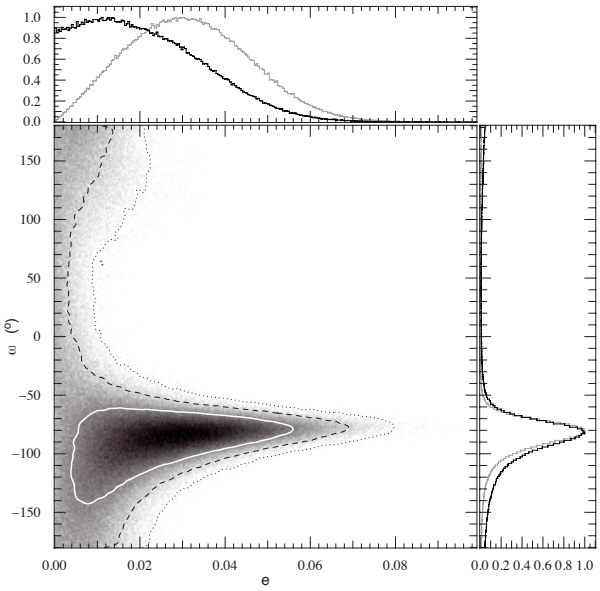


Fig. 5. In the central box we show the a posteriori probability density function for e and ω, resulting from a chain using $\sqrt{e}\cos\omega$ and $\sqrt{e}\sin\omega$ as free parameters (from which e and ω were computed to fit an eccentric model to the data). The white contour marks the 68.27% confidence region. The black dashed contour shows the 95.45%, and the black dotted contour is the 99.73% confidence region. Marginalised distributions are also shown as black histograms in side boxes, which have been normalised to the mode. Grey histograms in the side boxes show the same fit but instead having $e\cos\omega$ and $e\sin\omega$ as jump parameters.

Table 2. Limb darkening coefficients used (quadratic law).

Band	u_a	u_b	Band	u_a	u_b
$V_{\rm HARPS}$	0.576	0.191	z	0.284	0.289
R	0.450	0.260	$I+z$	0.325	0.275

4.2. Models and hypotheses

We used the models of Mandel & Agol (2002) to fit the photometric transit and of Giménez (2006) to adjust the Rossiter-McLaughlin effect as well as a classical Keplerian model for the orbital variation in the radial velocities. Limb darkening coefficients for the quadratic law were extracted from Claret (2000, 2004) for the photometry. To fit the Rossiter-McLaughlin effect, we used coefficients specially inferred from HARPS's spectral response, which were presented in Triaud et al. (2009). Table 2 shows the values we adopted.

These models are compared to the data using a χ^2 statistics. A first series of four chains was performed to derive a stellar density estimate. This values were used to determine a stellar mass from the evolutionary models of Girardi et al. (2000) as described in Hebb et al. (2009) using the metallicity and temperature determined in the spectral analysis and the stellar density from fitting the photometric transit. By interpolating between the tracks, we found that $M_\star = 0.79^{+0.13}_{-0.12}\,M_\odot$ (Fig. 6). This stellar mass was inserted as a prior in a new series of chains. The stellar age could not be constrained but is likely to be old; the star sits above the 10 Gyr isochrone. This first series of chains also allowed the quantification of the correlated noise in the data, which is accounted for in the following chains by increasing the

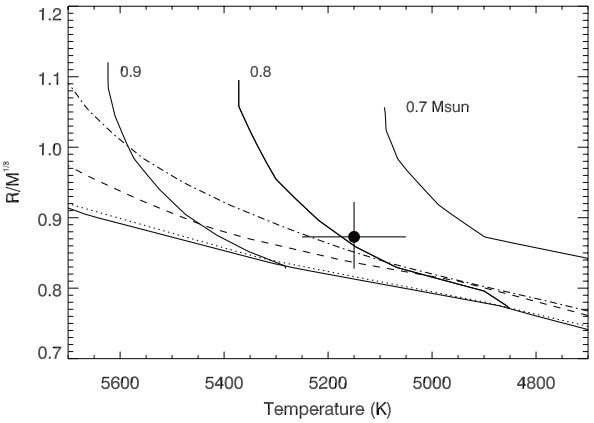


Fig. 6. Modified Hertzprung-Russell diagram comparing the stellar density and temperature of WASP-23 to theoretical stellar evolutionary tracks interpolated for a metallicity of [M/H] = −0.05. The star sits just above the 10 Gyr tracks (dashdotted line). Other tracks are 0.1 Gyr (solid), 1 Gyr (dotted), and 5 Gyr (dashed). Models are those of Girardi et al. (2000).

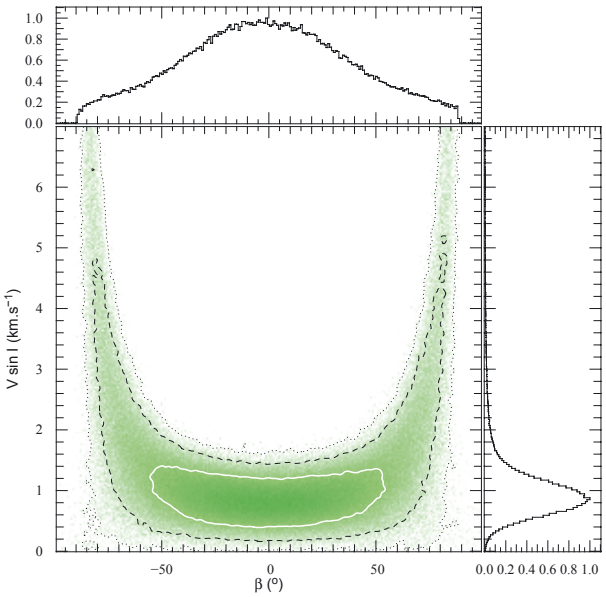


Fig. 7. Same legend as in Fig. 5 but here showing V sin I and β, for a circular, non-drifting orbital solution using no prior on V sin I.

individual error bars. This allows us to place evaluate credible error bars for parameters determined by the photometry.

Two families of chains, each with 2 000 000 random steps, were run. A family consists of four chains based on different hypotheses:

- eccentricity and RV drift are allowed to vary freely;
- no eccentricity but RV drift varie freely;
- no RV drift but eccentricity varies freely;
- no eccentricity and no RV drift.

We considered two families, one where the Rossiter-McLaughlin effect is allowed to vary freely and another that neglects this effect, our null hypothesis. Hence from these eight chains we tested for the presence of a linear trend in the radial velocities, for the detection of eccentricity, and for the detection of the Rossiter-McLaughlin effect.

5. Results

We have computed eight different chains, each based on different hypotheses. All chains agree in their results within each others' error bars in their common parameters, giving strong evidence that they have indeed converged to the solution. Results were extracted from each chain and their comparison with each others led to the final results presented here. This comparison, the most salient points of which are presented in Appendix, made us choose a circular, non-drifting model for the radial velocity. WASP-23b's parameters were extracted by taking the mode of the marginalised distributions computed by the Markov chains. When two clearly separated mode appeared, each was estimated and its errors bars calculated (see Fig. 8). Error bars are computed by taking the 68.27%, 95.45%, and 99.73% marginalised confidence regions in the a posteriori probability density distribution. Models using eccentricity and a drift as free floating parameters are useful for placing upper constraints on these parameters. Results are presented in Table 3. The final reduced χ^2 for the radial velocities, for both CORALIE and HARPS observations, is consistent with one. We therefore saw no need to add any additional terms to our error bars.

Hence, WASP-23b is a 0.88 M_J planet with a 0.96 R_J radius on a 2.94 day orbit, placing it among the normally sized hot Jupiter planets. We can reasonably estimate upper limits to the eccentricity and RV trend at the 99% exclusion level, from the chains that had these as free parameters. Thus, we find that $e < 0.062$ & $|\dot{\gamma}| < 30$ m s^{-1} yr^{-1}.

Using no prior, we detected a radial velocity anomaly compatible with the expected location and shape of the Rossiter-McLaughlin (χ^2 changes from 19.6 ± 6.2 to 6.4 ± 3.6 for the 14 data points positioned during transit and one on either side). We detected this effect to a confidence of 3.2 σ from a simple Keplerian model. We see a degeneracy arising between β, V sin I, and b, the impact parameter: V sin I increases to extremely large values (up to 60 km s^{-1}, Fig. 7) by forcing β to a severely misaligned solution and b to becloser to an equatorial transit.

Because of the non-physicality of this result for V sin I we had to resort to using some prior in order to constrain the space within which the MCMC can explore. We do this by imposing a Bayesian penalty on χ^2. This additional analysis is presented in the discussion.

Our chains indicate that the effect is mostly symmetrical with respect to the centre of transit (see Fig. 7), and that we can exclude a retrograde orbit.

6. Discussion

Figure 7 unambiguously shows that we have a strong degeneracy between β and V sin I. This is a well-known problem that was reported in particular in Narita et al. (2010) & Triaud et al. (2010). The spectral line analysis (Sect. 3.5) showed that the projected stellar rotation velocity $v \sin I = 2.2 \pm 0.3$ km s^{-1}. From Fig. 7, we observe that a V sin I at such a value would lead to a severely misaligned orbit. This is confirmed when running the MCMC for an additional family of chains using this value of $v \sin I$ as a prior on V sin I.

Table 3. Fitted and derived parameters for WASP-23 & WASP-23b with their error bars for confidence intervals of 68.27%, 95.45%, and 99.73%. For asterisked parameters, please refer to the text. Underscripted 1 and 2 indicate two distinct solutions for the same parameter.

Parameters (*units*)		1σ	2σ	3σ
Fitted parameters				
P (days)	2.9444256	$^{+0.0000011}_{-0.0000013}$	$^{+0.0000024}_{-0.0000024}$	$^{+0.0000036}_{-0.0000036}$
T_0 (bjd-2 450 000)	5320.12363	$^{+0.00012}_{-0.00013}$	$^{+0.00023}_{-0.00026}$	$^{+0.00036}_{-0.00039}$
D	0.01691	$^{+0.00010}_{-0.00011}$	$^{+0.00024}_{-0.00024}$	$^{+0.00053}_{-0.00034}$
W (days)	0.09976	$^{+0.00031}_{-0.00039}$	$^{+0.00081}_{-0.00077}$	$^{+0.00188}_{-0.00116}$
b_1 ($R_\star$) *	0.04	$^{+0.05}_{-0.04}$	$^{+0.17}_{-0.04}$	$^{+0.33}_{-0.04}$
b_2 ($R_\star$) *	0.05	$^{+0.23}_{-0.05}$	$^{+0.31}_{-0.05}$	$^{+0.37}_{-0.05}$
K (m s^{-1})	145.8	$^{+1.5}_{-2.1}$	$^{+3.4}_{-4.0}$	$^{+5.3}_{-5.6}$
$\sqrt{V \sin I_1} \cos \beta_1$ *	0.57	$^{+0.18}_{-0.16}$	$^{+0.42}_{-0.34}$	$^{+0.66}_{-0.46}$
$\sqrt{V \sin I_1} \sin \beta_1$ *	−1.4	$^{+2.8}_{-0.1}$	$^{+3.0}_{-0.3}$	$^{+3.0}_{-0.4}$
$\sqrt{V \sin I_1} \cos \beta_2$ *	1.00	$^{+0.09}_{-0.29}$	$^{+0.16}_{-0.56}$	$^{+0.23}_{-0.79}$
$\sqrt{V \sin I_1} \sin \beta_2$ *	−0.9	$^{+1.9}_{-0.2}$	$^{+1.9}_{-0.2}$	$^{+2.1}_{-0.4}$
Derived parameters				
$R_p/R_\star$	0.13004	$^{+0.00040}_{-0.00045}$	$^{+0.00095}_{-0.00091}$	$^{+0.00203}_{-0.00132}$
$R_\star/a$	0.09429	$^{+0.00041}_{-0.00047}$	$^{+0.00212}_{-0.00091}$	$^{+0.00675}_{-0.00124}$
$\rho_\star$ ($\rho_\odot$)	1.843	$^{+0.025}_{-0.027}$	$^{+0.054}_{-0.119}$	$^{+0.069}_{-0.347}$
$R_\star$ ($R_\odot$)	0.765	$^{+0.033}_{-0.049}$	$^{+0.068}_{-0.098}$	$^{+0.102}_{-0.164}$
$M_\star$ ($M_\odot$)	0.78	$^{+0.13}_{-0.12}$		
R_p/a	0.012260	$^{+0.000077}_{-0.000077}$	$^{+0.000340}_{-0.000168}$	$^{+0.001093}_{-0.000222}$
R_p (R_J)	0.962	$^{+0.047}_{-0.056}$	$^{+0.095}_{-0.118}$	$^{+0.139}_{-0.199}$
M_p (M_J)	0.884	$^{+0.088}_{-0.099}$	$^{+0.178}_{-0.203}$	$^{+0.262}_{-0.321}$
a (AU)	0.0376	$^{+0.0016}_{-0.0024}$	$^{+0.0034}_{-0.0046}$	$^{+0.0049}_{-0.0078}$
i (°)	88.39	$^{+0.79}_{-0.45}$	$^{+1.50}_{-0.69}$	$^{+1.56}_{-1.03}$
$V \sin I_1$ (km s^{-1}) *	2.03	$^{+0.37}_{-0.35}$	$^{+0.70}_{-0.70}$	$^{+0.99}_{-1.00}$
$\lvert\beta_1\rvert$ (°) *	69	$^{+6}_{-9}$	$^{+14}_{-24}$	$^{+18}_{-65}$
$V \sin I_2$ (km s^{-1}) *	1.21	$^{+0.17}_{-0.23}$	$^{+0.42}_{-0.39}$	$^{+0.64}_{-0.52}$
β_2 (°) *	−43	$^{+99}_{-17}$	$^{+109}_{-22}$	$^{+122}_{-35}$
e				<0.062
$\lvert\dot{\gamma}\rvert$ (m s^{-1} yr^{-1})				<30
γ *velocity* (m s^{-1})				
CORALIE	5674.403	$^{+0.040}_{-0.046}$	$^{+0.085}_{-0.088}$	$^{+0.130}_{-0.136}$
HARPS	5691.60	$^{+0.33}_{-0.84}$	$^{+0.90}_{-1.38}$	$^{+1.44}_{-1.97}$
Normalisation factors				
WASP-South	1.00068	$^{+0.000011}_{-0.000011}$	$^{+0.000021}_{-0.000022}$	$^{+0.000032}_{-0.000033}$
-	1.000272	$^{+0.0000020}_{-0.0000021}$	$^{+0.0000041}_{-0.0000041}$	$^{+0.0000060}_{-0.0000062}$
Euler z-band	1.00013	$^{+0.000052}_{-0.000086}$	$^{+0.000125}_{-0.000159}$	$^{+0.000190}_{-0.000232}$
Euler R-band	0.99998	$^{+0.000064}_{-0.000052}$	$^{+0.000122}_{-0.000112}$	$^{+0.000178}_{-0.000176}$
FTS z-band	1.01110	$^{+0.00011}_{-0.00010}$	$^{+0.00022}_{-0.00021}$	$^{+0.00032}_{-0.00033}$
TRAPPIST I + z-band	1.000117	$^{+0.000078}_{-0.000078}$	$^{+0.000163}_{-0.000160}$	$^{+0.000239}_{-0.000239}$
	1.000150	$^{+0.000059}_{-0.000068}$	$^{+0.000125}_{-0.000130}$	$^{+0.000192}_{-0.000195}$

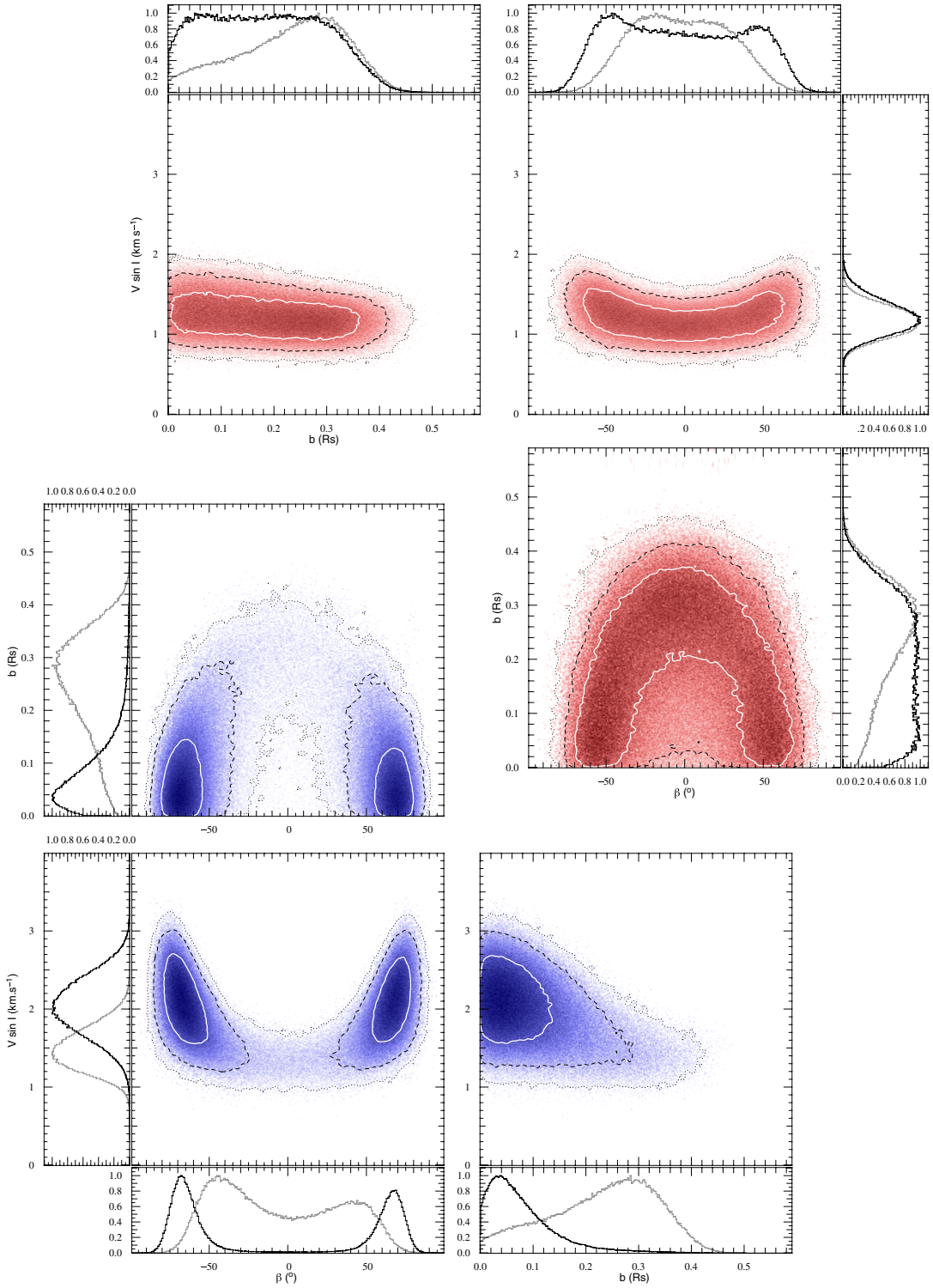


Fig. 8. Square boxes present the a posteriori probability density functions for $V \sin I, \beta$ and impact parameter b, from which we extract our results. The white contour marks the 68.27% confidence region. The black dashed contour shows the 95.45%, and the black dotted contour the 99.73% confidence regions. Marginalised distributions are also shown as black histograms in side boxes, normalised to the mode. At the top right, in red, we have the results for a circular, non drifting solution with use of a prior of $v = 1.35 \pm 0.20$ km s^{-1}. On *bottom left*, in blue, we show a circular, non-drifting solution with the application of a prior of $v \sin I = 2.2 \pm 0.3$ km s^{-1}. Grey histograms in $V \sin I$ and β show results in the photometry limited runs; for b, we plotted the resulting distribution by fitting the photometry alone without the Rossiter-McLaughlin effect.

We call this our solution 1: we obtain two modes for β symmetrically opposite each other (see Fig. 8, bottom left corner). We therefore choose to denote this result by its absolute value as $|\beta_1| = 69^{\circ}{}^{+6}_{-9}$ $V \sin I_1 = 2.03^{+0.37}_{-0.35}$ km s^{-1}, and the impact parameter $b_1 = 0.04 \pm 0.05\,R_\star$. This prior choice makes the detection of the Rossiter-McLaughlin effect close to 7.5σ.

Before claiming that an additional misaligned planet is present, one around a cool star (thus a strong exception according to Winn et al. 2010a), we searched for another independent estimate of the stellar rotation.

From spectral analysis, we obtained a value quantifying the emission in the calcium II lines expressed in the form of $\log R'_{\rm HK} = -4.68 \pm 0.07$. This value can be used as an indirect measurement of the true stellar rotation period. We used two methods, developed by Noyes et al. (1984), finding $28.6^{+5.3}_{-5.3}$ days and a more recent estimate by Mamajek & Hillenbrand (2008) and got the value $28.2^{+4.4}_{-5.3}$ days in very good agreement with the previous value. Using the distribution of $R_\star$ computed from our MCMC chains, we transformed these values into the equatorial rotation v obtaining $1.30^{+0.24}_{-0.19}$ and $1.35^{+0.28}_{-0.20}$ km s^{-1} respectively. Combining both, we have our new prior that we included as 1.35 ± 0.20 km s^{-1} into a new series of four chains. The results of these indicate that the planet is most likely on an aligned orbit, but error bars remain large.

We refer to these results as our solution 2. We only have one large range of values for the projected spin-orbit angle $\beta_2 = -43^{\circ}{}^{+99}_{-17}$. $V \sin I_2 = 1.21^{+0.17}_{-0.23}$ km s^{-1} and $b_2 = 0.05^{+0.23}_{-0.05}\,R_\star$. The detection of the Rossiter-McLaughlin effect is more secure in this case as well, increasing to a value close to 7σ.

To test our results, we simulated whether an infinitely precise photometry would help us discriminate between our different solutions for β since the parameter b, for example, is influenced by the adjustment of the Rossiter-McLaughlin model. We therefore removed the Rossiter-McLaughlin effect before running a chain using only photometry to adjust for the transit parameters keeping the non-drifting, non eccentric model. Having photometry as the sole influence on the impact parameter, one finds that $b = 0.28^{+0.08}_{-0.14}\,R_\star$. The value found for b_1 and b_2 are not at odds with this value. We fixed the parameters controlled by photometry to the most likely values (i.e. $b = 0.28$) and ran an additional three chains. Those three "photometry limited" chains had the following characteristics:

- no imposed prior;
- a prior of 2.2 ± 0.3 km s^{-1};
- a prior of 1.35 ± 0.20 km s^{-1}.

We refer to Fig. 8 for the resulting probability distributions (grey histograms). By fixing all parameters to the values that can be determined by photometry alone and again allowing all remaining parameters to be free, we see some changes in the posterior probability distributions (see grey histograms in Fig. 8). The distribution of $V \sin I_1$ is shifted to lower values, while that of β_1, although still bimodal, is offset to a far smaller extent. $V \sin I_2$ is left almost unchanged, but β_2 is more closely confined to zero. This illustrates the effect of our poorly constrained impact parameter on our fit, but this also indicates that, unless a new transit lead us to a higher value of b, even an infinitely precise photometry would not enable us to break entirely the degeneracy between β and $V \sin I$ for $b < 0.28\,R_\star$.

The measurement of the projected spin-orbit angle β is mostly affected by the small amplitude of the signal and in part by the poorly determined impact parameter, which, floating to small values, creates a degeneracy between small β, small $V \sin I$ and high β, high $V \sin I$.

7. Conclusions

After analysing more than four years of photometric and spectroscopic data, we are able to confidently conclude that we have detected a typical hot Jupiter around the K1V star called WASP-23. The analysis was a bit more arduous than anticipated because of a degeneracy that arose when fitting the Rossiter-McLaughlin effect. A total of 19 Markov chains were used to derive our conclusions.

Despite the slow rotation and likely old age of the star, we have managed to detect the Rossiter-McLaughlin effect, which is of similar amplitude to that of WASP-2b (Triaud et al. 2010) and of a similar signal-to-noise as detections such as that on Hat-P-11b (Winn et al. 2010b; Hirano et al. 2011). Imposing priors on $V \sin I$ increases our detection level but seriously affects the posterior probability distribution (see Figs. 7 and 8) and thus our results and possible interpretations. This is mostly because of the difference between our two priors, which are 2.7σ away from each other, although our value of $v \sin I = 2.2 \pm 0.3$ km s^{-1} (solution 1) should be seen as a lower value, while $v = 1.35 \pm 0.20$ km s^{-1} (solution 2) is more of an upper value.

There is strong evidence that for stars colder than 6250 K, planets tend to have a high a priori probability of being aligned with the stellar spin (Winn et al. 2010a). This would then be consistent with our solution 2 , thus imply that the spectral line broadening method is not accurate enough to determine $v \sin I$. This would demonstrate that there is a potential difficulty in estimating $v \sin I$ and its use as a prior. However solution 2 is not without its problems either because the determination of the stellar rotation from activity indices could be altered by the presence of a nearby hot Jupiter as well as by long term magnetic cycles.

To resolve WASP-23b's spin orbit angle, one has several options. One could acquire additional and higher quality photometry. If b were found to be small, then the degeneracy would not be lifted, but the larger its value is found to be, the more likely the system is to be aligned. In addition, further observations of the Rossiter-McLaughlin effect might be needed. There is also a possibility that the current data is enough as one could use the *Doppler shadow* method pioneered in Collier Cameron et al. (2010) and Miller et al. (2010). This method provides precise determinations of $V \sin I$, β, and b but is most effective best for fast rotators and bright targets.

Either way, the solution to the degeneracy of our results is interesting. If solution 1 (prior on $V \sin I = 2.2 \pm 0.3$ km s^{-1}) were confirmed, we would have a misaligned system around a cold star and a need to rectify the determination of stellar rotation based on activity levels. If solution 2 (prior on $V \sin I = 1.35 \pm 0.20$ km s^{-1}) were instead the most likely one, then we are observing probably an aligned system and one will need to be careful when using $v \sin I$ prior infered by spectral line broadening.

We therefore recommend extreme caution when using priors, as final results can depend entirely on those and a small initial systematic error can lead to dramatic changes in interpretation.

Nota Bene. We used the UTC time standard and Barycentric Julian Dates in our analysis. Our results are based on the equatorial solar and jovian radii and masses taken from Allen's Astrophysical Quantities.

Acknowledgements. The authors would like to acknowledge the use of ADS and of *Simbad* but mostly the help and the kind attention of the ESO staff at La Silla which with its (now gone and much regretted) *completos* insured a good and stable supply of energy during the long observing nights. The work is supported by the Swiss Fond National de Recherche Scientifique. TRAPPIST is a project

funded by the Belgian Fund for Scientific Research (FNRS) with the participation of the Swiss National Science Fundation (SNF). M. Gillon and E. Jehin are FNRS Research Associates. We also thank R. Heller for providing a copy of Holt's 1893 paper.

References

Anderson, D. R., Hellier, C., Gillon, M., et al. 2010, ApJ, 709, 159
Bakos, G., Noyes, R. W., Kovács, G., et al. 2004, PASP, 116, 266
Baranne, A., Queloz, D., Mayor, M., et al. 1996, A&A, 119, 373
Batygin, K., Bodenheimer, P., & Laughlin, G. 2009, ApJ, 704, L49
Boisse, I., Moutou, C., Vidal-Madjar, A., et al. 2009, A&A, 495, 959
Bouchy, F., Queloz, D., Deleuil, M., et al. 2008, A&A, 482, L25
Bruntt, H., Bedding, T. R., Quirion, P.-O., et al. 2010, MNRAS, 405, 1907
Charbonneau, D., Brown, T. M., Latham, D. W., & Mayor, M. 2000, ApJ, 529, L45
Claret, A. 2000, A&A, 363, 1081
Claret, A. 2004, A&A, 428, 1001
Collier Cameron, A. C., Bouchy, F., Hébrard, G., et al. 2007a, MNRAS, 375, 951
Collier Cameron, A. C., Wilson, D. M., West, R. G., et al. 2007b, MNRAS, 380, 1230
Collier Cameron, A. C., Bruce, V. A., Miller, G. R. M., Triaud, A. H. M. J., & Queloz, D. 2010, MNRAS, 403, 151
Dobbs-Dixon, I., Cumming, A., & Lin, D. N. C. 2010, ApJ, 710, 1395
Fabrycky, D., & Tremaine, S. 2007, ApJ, 669, 1298
Ford, E. B. 2006, ApJ, 642, 505
Gillon, M., Pont, F., Moutou, C., et al. 2006, A&A, 459, 249
Gillon, M., Triaud, A. H. M. J., Mayor, M., et al. 2008, A&A, 485, 871
Gillon, M., Anderson, D. R., Triaud, A. H. M. J., et al. 2009, A&A, 501, 785
Gillon, M., Jehin, E., Magain, P., et al. 2011, EPJ Web Conf., 11, 06002
Giménez, A. 2006, ApJ, 650, 408
Girardi, L., Bressan, A., Bertelli, G., & Chiosi, C. 2000, A&AS, 141, 371
Gray, D. F. 2008, The Observation and Analysis of Stellar Photospheres
Guillot, T., & Showman, A. P. 2002, A&A, 385, 156
Hebb, L., Cameron, A. C., Loeillet, B., et al. 2009, ApJ, 693, 1920
Hébrard, G., Bouchy, F., Pont, F., et al. 2008, A&A, 488, 763
Hirano, T., Suto, Y., Taruya, A., et al. 2010, ApJ, 709, 458
Hirano, T., Narita, N., Shporer, A., et al. 2011, PASJ, 63, 531
Holt, J. 1893, A&A, XII, 646
Lin, D. N. C., Bodenheimer, P., & Richardson, D. C. 1996, Nature, 380, 606
Lovis, C., & Pepe, F. 2007, A&A, 468, 1115
Magain, P. 1984, A&A, 134, 189
Malmberg, D., Davies, M. B., & Heggie, D. C. 2011, MNRAS, 411, 859
Mamajek, E. E., & Hillenbrand, L. A. 2008, ApJ, 687, 1264
Mandel, K., & Agol, E. 2002, ApJ, 580, L171
Mayor, M., Udry, S., Lovis, C., et al. 2009, A&A, 493, 639
McCullough, P. R., Stys, J. E., Valenti, J. A., et al. 2005, PASP, 117, 783
McLaughlin, D. B. 1924, ApJ, 60, 22
Miller, G. R. M., Collier Cameron, A. C., Simpson, E. K., et al. 2010, A&A, 523, A52
Morton, T. D., & Johnson, J. A. 2011, ApJ, 729, 138
Nagasawa, M., Ida, S., & Bessho, T. 2008, ApJ, 678, 498
Narita, N., Sato, B., Hirano, T., & Tamura, M. 2009, PASJ, 61, L35
Narita, N., Hirano, T., Sanchis-Ojeda, R., et al. 2010, PASJ, 62, L61
Noyes, R. W., Weiss, N. O., & Vaughan, A. H. 1984, ApJ, 287, 769
O'Donovan, F. T., Charbonneau, D., & Hillenbrand, L. 2006, 2007 AAS/AAPT Joint Meeting, 209, 1212
Ohta, Y., Taruya, A., & Suto, Y. 2005, ApJ, 622, 1118
Pepe, F., Mayor, M., Galland, F., et al. 2002, A&A, 388, 632
Pollacco, D. L., Skillen, I., Cameron, A. C., et al. 2006, PASP, 118, 1407
Queloz, D., Eggenberger, A., Mayor, M., et al. 2000, A&A, 359, L13
Queloz, D., Anderson, D., Cameron, A. C., et al. 2010, A&A, 517, L1
Rossiter, R. A. 1924, ApJ, 60, 15
Santos, N. C., Mayor, M., Naef, D., et al. 2000, A&A, 361, 265
Santos, N. C., Mayor, M., Naef, D., et al. 2002, A&A, 392, 215
Snellen, I. A. G., van der Burg, R. F. J., de Hoon, M. D. J., & Vuijsje, F. N. 2007, A&A, 476, 1357
Stetson, P. B. 1987, PASP, 99, 191
Triaud, A. H. M. J., Queloz, D., Bouchy, F., et al. 2009, A&A, 506, 377
Triaud, A. H. M. J., Cameron, A. C., Queloz, D., et al. 2010, A&A, 524, A25
Udalski, A., Kubiak, M., & Szymanski, M. 1997, Acta Astron., 47, 319
Winn, J. N., Johnson, J. A., Albrecht, S., et al. 2009, ApJ, 703, L99
Winn, J. N., Fabrycky, D., Albrecht, S., & Johnson, J. A. 2010a, ApJ, 718, L145
Winn, J. N., Johnson, J. A., Howard, A. W., et al. 2010b, ApJ, 723, L223

Pages 11 to 12 are available in the electronic edition of the journal at http://www.aanda.org

Appendix A: Comparisons between different chains.

In order to lighten the text, here are placed the results of the Markov Chains using various starting hypotheses and from which we estimated upper limits on eccentricity and long term radial velocity trends.

Table A.1 compares the results in χ^2 by instrument and during the Rossiter-McLaughlin effect for eights chains. From this we concluded that the eccentric orbit model is compatible with the circular, that a drift that can be fitted is statistically indistinguishable from zero, but that we detect an anomaly in the reflex Doppler motion, corresponding to the location where the Rossiter-McLaughlin effect is expected.

Table A.2 explores the parameters issued from chains where the Rossiter-McLaughlin effect was fitted in order to make sense of the results and see their dependency on initial hypotheses.

Table A.1. Comparison of the results in χ^2 by instrument and during the Rossiter-McLaughlin effect 2 different families of chains: having no prior on $V \sin I$, and not fitting the Rossiter-McLaughlin effect.

$(e, \lvert\dot{\gamma}\rvert)$	(Free, free)	(Free, fixed)	(Fixed, free)	(Fixed, fixed)
Rossiter-McLaughlin effect fitted, no Prior				
$\chi^2_{\rm CORALIE,\,38\,RVs}$	38.1 ± 8.7	45.9 ± 9.6	41.3 ± 9.1	48.5 ± 9.8
$N_{\rm param}$	7	6	5	4
$\chi^2_{\rm reduced}$	1.23 ± 0.28	1.44 ± 0.30	1.25 ± 0.28	1.43 ± 0.29
$\chi^2_{\rm HARPS,\,35\,RVs}$	25.2 ± 7.1	23.8 ± 7.0	27.1 ± 7.4	26.2 ± 7.2
$N_{\rm param}$	12	11	10	9
$\chi^2_{\rm reduced}$	1.10 ± 0.31	1.00 ± 0.29	1.08 ± 0.29	1.01 ± 0.28
$\chi^2_{\rm in\,RM,\,16\,RVs}$	6.8 ± 3.7	6.8 ± 3.7	6.3 ± 3.6	6.4 ± 3.6
all 73 RVs, 2 sets				
$\chi^2_{\rm RV}$	63.4 ± 11.3	69.7 ± 11.8	68.4 ± 11.7	74.7 ± 12.2
$N_{\rm param}$	13	12	11	10
$\chi^2_{\rm reduced}$	1.06 ± 0.19	1.14 ± 0.19	1.10 ± 0.19	1.19 ± 0.19
Rossiter-McLaughlin effect absent				
$\chi^2_{\rm CORALIE,\,38\,RVs}$	38.1 ± 8.7	45.1 ± 9.5	40.7 ± 9.0	48.4 ± 9.8
$N_{\rm param}$	7	6	5	4
$\chi^2_{\rm reduced}$	1.23 ± 0.28	1.41 ± 0.30	1.23 ± 0.27	1.42 ± 0.29
$\chi^2_{\rm HARPS,\,35\,RVs}$	39.7 ± 8.9	38.9 ± 8.8	40.8 ± 9.0	39.5 ± 8.9
$N_{\rm param}$	7	6	5	4
$\chi^2_{\rm reduced}$	1.42 ± 0.32	1.34 ± 0.30	1.36 ± 0.30	1.27 ± 0.29
$\chi^2_{\rm in\,RM,\,16\,RVs}$	21.2 ± 6.5	21.2 ± 6.5	19.6 ± 6.3	19.6 ± 6.2
all 73 RVs, 2 sets				
$\chi^2_{\rm RV}$	77.9 ± 12.5	84.1 ± 13.0	81.5 ± 12.8	87.9 ± 13.3
$N_{\rm param}$	8	7	6	5
$\chi^2_{\rm reduced}$	1.20 ± 0.19	1.27 ± 0.20	1.22 ± 0.19	1.29 ± 0.20

A&A 531, A24 (2011)

Table A.2. Results from various Markov chains of the three parameters which control the shape of the Rossiter-McLaughlin effect.

	$V \sin I$ (km s^{-1}) ±				β (°) ±				b ($R_\star$) ±			
		1σ	2σ	3σ		1σ	2σ	3σ		1σ	2σ	3σ
$V \sin I$ *Prior off*	0.82	$^{+0.11}_{-0.35}$	$^{+1.98}_{-0.82}$	$^{+9.45}_{-0.82}$	-1	$^{+38}_{-41}$	$^{+76}_{-76}$	$^{+89}_{-86}$	0.27	$^{+0.05}_{-0.27}$	$^{+0.10}_{-0.27}$	$^{+0.15}_{-0.27}$
$V \sin I$ *Prior on, 1.35 km s*$^{-1}$	1.21	$^{+0.17}_{-0.23}$	$^{+0.42}_{-0.39}$	$^{+0.64}_{-0.52}$	-43	$^{+99}_{-17}$	$^{+109}_{-22}$	$^{+122}_{-35}$	0.05	$^{+0.23}_{-0.02}$	$^{+0.31}_{-0.05}$	$^{+0.37}_{-0.05}$
$V \sin I$ *Prior on, 2.2 km s*$^{-1}$	2.03	$^{+0.37}_{-0.35}$	$^{+0.70}_{-0.70}$	$^{+0.99}_{-1.00}$	68 -69	$^{+7}_{-8}$ $^{+8}_{-7}$	$^{+14}_{-23}$ $^{+25}_{-14}$	$^{+18}_{-155}$ $^{+155}_{-18}$	0.04	$^{+0.05}_{-0.04}$	$^{+0.17}_{-0.04}$	$^{+0.33}_{-0.04}$
Rossiter-McLaughlin effect not fitted												
	0		(fixed)		0		(fixed)		0.28	$^{+0.08}_{-0.14}$	$^{+0.11}_{-0.26}$	$^{+0.15}_{-0.28}$
Photometry Limited runs												
$V \sin I$ *Prior off*	0.87	$^{+0.28}_{-0.28}$	$^{+0.57}_{-0.53}$	$^{+0.87}_{-0.80}$	4	$^{+23}_{-36}$	$^{+46}_{-57}$	$^{+70}_{-77}$	0.28		(fixed)	
$V \sin I$ *Prior on, 1.35 km s*$^{-1}$	1.15	$^{+0.19}_{-0.17}$	$^{+0.37}_{-0.33}$	$^{+0.54}_{-0.49}$	-15	$^{+42}_{-21}$	$^{+67}_{-40}$	$^{+84}_{-55}$	0.28		(fixed)	
$V \sin I$ *Prior on, 2.2 km s*$^{-1}$	1.37	$^{+0.35}_{-0.17}$	$^{+0.66}_{-0.35}$	$^{+0.95}_{-0.55}$	-44	$^{+98}_{-14}$	$^{+106}_{-19}$	$^{+120}_{-30}$	0.28		(fixed)	

Notes. These are for circular non drifting orbital solutions.

3.5 The Southern WASP Planet Collection

The candidates come, and the planets go.

Being responsible for the transmutation of a nameless candidate into a fully fledge transiting planet (section 3.2) inside our collaboration between WASP and Genève, I am at the bottleneck of the data flow and get a ride as a co-author on most WASP discovery papers. This is the main source the high paper rate throughout my thesis. Although having a crucial role for the planet-hood determination, I have only a small role in the write up and analysis of those papers. I tried to read each as they got submitted to the collaboration, making comments when I felt necessary. Because most of them are fairly similar, and similar to the WASP-6, 8 and 23 papers, only the 1st pages are now shown. It should give an idea about the high success that WASP and Genève enjoyed.

The papers (only those that have been released publically) are in order of WASP numbering, and not of publication date (when possible, since recently the planets got bundled with numbers not necessarily following each others)[16].

Some objects are more special than others because they were harder to find, or around atypical stars, or even just with a funny[17] coordinate number. One of the objects I am most proud of having found is WASP-30, which, strangely enough is probably not a planet[18] (see Sahlmann et al. (2011b)).

For bodies below about 4 $M_{\rm Jup}$ the radius rises sharply, it then transforms into a slow downward slope up to masses of round about 80 $M_{\rm Jup}$ before rising again sharply (see figure 3.23). Few low M dwarves have had a radius measured to constrain that fast rising slope. But fewer than that were the Brown Dwarfs for which no direct radius measurements existed until very recently.

Ever since I saw this gap in the mass/radius diagram for bodies between 15 and 100 $M_{\rm Jup}$ during Brice-Olivier Demory's PhD defence, the so-called Brown Dwarf desert, have I yearned to find an object there. Thus I changed the instructions sent to the observers who started obtaining more data on candidates classified as fast rotators and stars for which we had a variation of order 10 km/s, all of which had been discarded. Needless to say that newer contemporaneous candidates with such characteristics were also included. On the previously observed star: nothing was found, indicating Brown Dwarfs are indeed much rarer than planets. Many eclipsing M-dwarfs (SB1) were detected and now have characterised orbits thanks to that process.

But finally the search yielded results: CoRoT had found one candidate, around a hotter star than traditionally observed by RV surveys (Deleuil et al. 2008). Its photometric precision made the transit clear, but was of a depth which with WASP is hard to detect. The confirmation with radial velocities was easier than for planets: the signal is larger.

Not too long after, CORALIE finally confirmed one such object from the WASP survey: WASP-30 (Anderson et al. 2011). It is to date the smallest transit depth that has been detected by the instrument. It is around a hot star too. About the same time, CoRoT announced another such object (Bouchy et al. 2011). A fourth detection was found by *Kepler*: a brown dwarf around an M dwarf in what may be a more traditional binary with a small mass ratio (Johnson et al. 2011a).

One of the main interest in finding those objects, especially on a bright target, is to determine accurately their radius and compare it with theoretical predictions such as Chabrier et al. (2000a,b).

[16] There is only one gap in the numbering: WASP-9 (see 3.3.5). Other missing numbers indicate planets found in the North, or for which the paper is not ready yet (such as WASP-20 (Collier Cameron, in prep))

[17] the definition of *funny* being very culturally dependent, I won't define what a funny coordinate number is.

[18] again problems of definition, what is a planet, what is a brown dwarf, what is a low mass star? Is there any difference? I won't enter the debate.

The Astrophysical Journal, 690:L89–L91, 2009 January 1 doi:10.1088/0004-637X/690/1/L89
© 2009. The American Astronomical Society. All rights reserved. Printed in the U.S.A.

WASP-7: A BRIGHT TRANSITING-EXOPLANET SYSTEM IN THE SOUTHERN HEMISPHERE

Coel Hellier[1], D. R. Anderson[1], M. Gillon[2], T. A. Lister[1,3], P. F. L. Maxted[1], D. Queloz[2], B. Smalley[1], A. H. M. J. Triaud[2], R. G. West[4], D. M. Wilson[1], K. Alsubai[5], S. J. Bentley[1], A. Collier Cameron[5], L. Hebb[5], K. Horne[5], J. Irwin[6], S. R. Kane[7], M. Mayor[2], F. Pepe[2], D. Pollacco[8], I. Skillen[9], S. Udry[2], P. J. Wheatley[10], D. J. Christian[8], R. Enoch[11,5], C. A. Haswell[11], Y. C. Joshi[8], A. J. Norton[11], N. Parley[11], R. Ryans[8], R. A. Street[3,8], and I. Todd[8]
[1] Astrophysics Group, Keele University, Staffordshire, ST5 5BG, UK
[2] Observatoire de Genève, 51 ch. des Maillettes, 1290 Sauverny, Switzerland
[3] Las Cumbres Observatory, 6740 Cortona Dr. Suite 102, Santa Barbara, CA 93117, USA
[4] Department of Physics and Astronomy, University of Leicester, Leicester, LE1 7RH, UK
[5] School of Physics and Astronomy, University of St. Andrews, North Haugh, Fife, KY16 9SS, UK
[6] Department of Astronomy, Harvard University, 60 Garden Street, MS 10, Cambridge, Massachusetts 02138, USA
[7] Michelson Science Center, Caltech, MS 100-22, 770 South Wilson Avenue, Pasadena, CA 91125, USA
[8] Astrophysics Research Centre, School of Mathematics & Physics, Queen's University, University Road, Belfast, BT7 1NN, UK
[9] Isaac Newton Group of Telescopes, Apartado de Correos 321, E-38700 Santa Cruz de la Palma, Tenerife, Spain
[10] Department of Physics, University of Warwick, Coventry, CV4 7AL, UK
[11] Department of Physics and Astronomy, The Open University, Milton Keynes, MK7 6AA, UK
Received 2008 May 17; accepted 2008 November 17; published 2008 December 11

ABSTRACT

We report that a Jupiter-mass planet, WASP-7b, transits the $V = 9.5$ star HD 197286 every 4.95 d. This is the brightest discovery from the WASP-South transit survey so far and is currently the brightest transiting-exoplanet system in the southern hemisphere. WASP-7b is among the densest of the known Jupiter-mass planets, suggesting that it has a massive core. The planet mass is $0.96^{+0.12}_{-0.18}\ M_{\rm Jup}$, the radius is $0.915^{+0.046}_{-0.040}\ R_{\rm Jup}$, and the density is $1.26^{+0.25}_{-0.21}\ \rho_{\rm Jup}$ $\left(1.67^{+0.33}_{-0.28}\ {\rm g\,cm^{-3}}\right)$.

Key words: stars: individual (WASP-7, HD 197286) – planetary systems

1. INTRODUCTION

Transiting exoplanets are valuable discoveries since they offer the most opportunities for parameterization and study. The WASP project (Pollacco et al. 2006) is one of the number of wide-area surveys, along with HAT (Bakos et al. 2002), TrES (O'Donovan et al. 2006), and XO (McCullough et al. 2005), all aimed at finding exoplanets transiting relatively bright stars, where they are easiest to observe. A prime aim is to fill out diagrams such as the exoplanet mass–radius plot, which has the potential to be a diagnostic tool for exoplanets comparable to the Hertzsprung–Russell diagram for stars, possibly leading to an understanding of the large disparity in the parameters of known hot Jupiters.

WASP is the only one of the above surveys operating in both hemispheres. We report here on WASP-7 (= HD 197286), a new discovery from WASP-South that, at magnitude 9.5, is currently the brightest transiting-exoplanet system in the southern hemisphere, being three magnitudes brighter than the previously announced WASP-4 (Wilson et al. 2008) and WASP-5 (Anderson et al. 2008). WASP-7b is also among the densest known Jupiter-mass exoplanets, extending the populated region of the mass–radius plot.

2. OBSERVATIONS

The WASP-South survey is described in Pollacco et al. (2006) and Wilson et al. (2008), while a discussion of our candidate selection methods can be found in Collier Cameron et al. (2007a), Pollacco et al. (2007), and references therein.

WASP-7 (= HD 197286) is a $V = 9.5$ F5V star in Microscopium. It was observed by WASP-South from May to mid-October in both 2006 and 2007, being recorded in two overlapping cameras, each having an 11.1 cm aperture Canon 200 mm f/1.8 lens backed by a 2k × 2k *e2V* CCD. Exposure times were 30 s, with a typical cadence of 8 minute. We obtained 5800 photometric data points from each camera in 2006, and a further 5700 data points from each in 2007.

The WASP-South lightcurves revealed dips with a depth of 0.007 magnitudes recurring with a 4.95 day period (Figure 1). Spectroscopic observations were then obtained using the CORALIE spectrograph on the Euler 1.2m telescope. Eleven radial-velocity measurements were obtained during 2007 September 15–October 12 (Figure 2; Table 1), establishing WASP-7b as a Jupiter-mass companion.

We used a line-bisector analysis to look for asymmetries in the spectral line profiles, as could be caused by contamination from an unresolved eclipsing binary (Queloz et al. 2001). Such a binary would produce bisector spans that vary in phase with the photometric period with an amplitude comparable to the radial-velocity amplitude. This is not seen in our data, supporting the conclusion that the radial-velocity variations are caused by a planet.

3. WASP-7 PARAMETERS

The CORALIE spectra, when co-added, give a signal-to-noise ratio of ∼ 50 in 0.01 Å bins, which is suitable for a preliminary photospheric analysis of WASP-7.

We analyzed the spectra using the UCLSYN package and ATLAS9 models, without convective overshooting (Castelli et al. 1997), leading to the parameters in Table 2. The effective temperature ($T_{\rm eff}$) comes from an analysis of the Hα line, while the surface gravity ($\log g$) comes from the Na I D and Mg I b lines. An estimate of the microturbulence ($\xi_{\rm t}$) comes from several clean and unblended Fe I and Fe II lines, while the ionization balance between Fe I and Fe II was used as an additional diagnostic of $T_{\rm eff}$ and $\log g$.

In addition to the spectral analysis, we have also used TYCHO, DENIS, and 2MASS magnitudes to estimate the

The Astronomical Journal, 137:4834–4836, 2009 June doi:10.1088/0004-6256/137/6/4834
© 2009. The American Astronomical Society. All rights reserved. Printed in the U.S.A.

THE LOW DENSITY TRANSITING EXOPLANET WASP-15b

R. G. West[1], D. R. Anderson[2], M. Gillon[3,4], L. Hebb[5], C. Hellier[2], P. F. L. Maxted[2], D. Queloz[3], B. Smalley[2], A. H. M. J. Triaud[3], D. M. Wilson[2], S. J. Bentley[2], A. Collier Cameron[5], B. Enoch[5], K. Horne[5], J. Irwin[6], T. A. Lister[7], M. Mayor[3], N. Parley[5], F. Pepe[3], D. Pollacco[8], D. Segransan[3], M. Spano[3], S. Udry[3], and P. J. Wheatley[9]
[1] Department of Physics and Astronomy, University of Leicester, Leicester LE1 7RH, UK
[2] Astrophysics Group, Keele University, Staffordshire ST5 5BG, UK
[3] Observatoire de Genève, Université de Genève, 51 Chemin des Maillettes, 1290 Sauverny, Switzerland
[4] Institut d'Astrophysique et de Géophysique, Université de Liège, Allée du 6 Août, 17, Bat. B5C, Liège 1, Belgium
[5] School of Physics and Astronomy, University of St. Andrews, North Haugh, Fife KY16 9SS, UK
[6] Department of Astronomy, Harvard University, 60 Garden Street, MS 10, Cambridge, MA 02138, USA
[7] Las Cumbres Observatory, 6740 Cortona Dr. Suite 102, Santa Barbara, CA 93117, USA
[8] Astrophysics Research Centre, School of Mathematics & Physics, Queen's University, University Road, Belfast BT7 1NN, UK
[9] Department of Physics, University of Warwick, Coventry CV4 7AL, UK
Received 2009 February 11; accepted 2009 March 16; published 2009 April 29

ABSTRACT

We report the discovery of a low-density exoplanet transiting an 11th magnitude star in the Southern hemisphere. WASP-15b, which orbits its host star with a period $P = 3.7520656 \pm 0.0000028$ d, has a mass $M_p = 0.542 \pm 0.050\,M_J$ and radius $R_p = 1.428 \pm 0.077\,R_J$, and is therefore one of the least dense transiting exoplanets so far discovered ($\rho_p = 0.247 \pm 0.035$ g cm^{-3}). An analysis of the spectrum of the host star shows it to be of spectral type around F5, with an effective temperature $T_{\rm eff} = 6300 \pm 100$ K and [Fe/H] $= -0.17 \pm 0.11$.

Key words: binaries: eclipsing – planetary systems – stars: individual (WASP-15) – techniques: photometric – techniques: radial velocities – techniques: spectroscopic

1. INTRODUCTION

Transiting exoplanets represent the best current opportunity to test theoretical models of the internal structure of such planets, and the formation and evolution of planetary systems. At the time of this writing the discovery of approaching 60 transiting systems had been announced in the literature by numerous well-established survey projects, such as HATnet (Bakos et al. 2004), XO (McCullough et al. 2005), TrES (O'Donovan et al. 2006), and WASP (Pollacco et al. 2006).

The WASP project operates two identical observatories, one at La Palma in the Canary Islands, and the other at Sutherland in South Africa. Each telescope has a field of view of approximately 500 square degrees. The WASP survey is capable of detecting planetary transit signatures in the light curves of hosts in the magnitude range $V \sim 9$–13. A full description of the telescope hardware, observing strategy and pipeline data analysis is given in Pollacco et al. (2006).

2. OBSERVATIONS

The host star WASP-15 (= 1SWASP J135542.70-320934.6 = 2MASS 13554269-3209347 = USNO-B1.0 0578-0402627 = NOMAD1 0578-0409366 = TYCH2 7283-01162-1) is cataloged as a star of magnitude $V = 11.0$ and coordinates $\alpha = 13^h55^m42\overset{s}{.}71$, $\delta = -32°09'34\overset{''}{.}6$. WASP-15 was observed by the WASP-South observatory in a single camera field from 2006 May 4 to 2006 July 17, and in two overlapping camera fields from 2007 January 31 to 2007 July 17 and from 2008 January 31 to 2008 May 29.

The data were processed using the project's routine analysis pipeline, de-trending, and transit-detection tools as described in Pollacco et al. (2006) and Collier Cameron et al. (2006, 2007). A total of 24,943 data points were acquired, in which a recurrent transit signature with a period of 3.7520 days and a depth of 0.011 ± 0.001 mag was detected (Figure 1, top panel). In total, some 11 full or partial transits were observed by WASP-South.

Follow-up photometric observations were made using the EulerCAM photometer on the 1.2 m Euler telescope in the *I*-band on 2008 March 29 and the *R*-band on 2008 May 13 (Figure 1, middle and lower panel), which confirmed the presence of a flat-bottomed dip expected from the transit of an exoplanet. Both transit light-curves from EulerCAM exhibit excess variability likely due to systematic noise.

Subsequent observations using the CORALIE spectrograph on the Euler telescope between 2008 March 6 and 2008 July 17 yielded 21 radial velocity measurements (Table 1; Figure 2, upper panel) which show a sinusoidal variation with a semi-amplitude of around 65 m s^{-1} on the same period as the transit signature. An analysis of the bisector spans (Figure 2, lower panel) shows no correlation with the measured radial velocity, which rules out the possibility that the RV variations were due to a blended eclipsing binary system.

3. EVOLUTIONARY STATUS OF THE HOST STAR

The individual CORALIE spectra have a relatively low signal-to-noise ratio (S/N), but when co-added into 0.01 Å steps they give an S/N of around 80:1 which is suitable for a photospheric analysis of WASP-15. In addition, a single HARPS spectrum was used to complement the CORALIE analysis, but this spectrum had a relatively modest S/N of around 50:1.

An analysis of the available spectral data was performed using the UCLSYN spectral synthesis package (Smith 1992; Smalley et al. 2001) and ATLAS9 models without convective overshooting (Castelli et al. 1997). The Hα and Hβ lines were used to determine the effective temperature ($T_{\rm eff}$), while the Na I D and Mg I b lines were used as surface gravity ($\log g$) diagnostics. Additionally, the Ca H and K lines provide a further check on the derived $T_{\rm eff}$ and $\log g$. This fit yielded a $T_{\rm eff} = 6300 \pm 100$ K and $\log g = 4.35 \pm 0.15$ (Table 2).

The Astrophysical Journal, 703:752–756, 2009 September 20 doi:10.1088/0004-637X/703/1/752
© 2009. The American Astronomical Society. All rights reserved. Printed in the U.S.A.

WASP-16b: A NEW JUPITER-LIKE PLANET TRANSITING A SOUTHERN SOLAR ANALOG

T. A. Lister[1], D. R. Anderson[2], M. Gillon[3,4], L. Hebb[5], B. S. Smalley[2], A. H. M. J. Triaud[3], A. Collier Cameron[5], D. M. Wilson[2,6], R. G. West[7], S. J. Bentley[2], D. J. Christian[8,9], R. Enoch[5,10], C. A. Haswell[10], C. Hellier[2], K. Horne[5], J. Irwin[11], Y. C. Joshi[8], S. R. Kane[12], M. Mayor[3], P. F. L. Maxted[2], A. J. Norton[10], N. Parley[5,10], F. Pepe[3], D. Pollacco[8], D. Queloz[3], R. Ryans[8], D. Segransan[3], I. Skillen[13], R. A. Street[1], I. Todd[8], S. Udry[3], and P. J. Wheatley[14]

[1] Las Cumbres Observatory, 6740 Cortona Drive Suite 102, Goleta, CA 93117, USA; tlister@lcogt.net
[2] Astrophysics Group, Keele University, Staffordshire, ST5 5BG, UK
[3] Observatoire de Genève, Universit' de Genève, 51 Ch. des Maillettes, 1290 Sauverny, Switzerland
[4] Institut d'Astrophysique et de Géophysique, Université de Liège, Allée du 6 Août, 17, Bat. B5C, Liège 1, Belgium
[5] SUPA, School of Physics and Astronomy, University of St Andrews, North Haugh, St Andrews, Fife KY16 9SS, UK
[6] Centre for Astrophysics & Planetary Science, School of Physical Sciences, University of Kent, Canterbury, Kent, CT2 7NH, UK
[7] Department of Physics and Astronomy, University of Leicester, Leicester, LE1 7RH, UK
[8] Astrophysics Research Centre, School of Mathematics & Physics, Queen's University, University Road, Belfast, BT7 1NN, UK
[9] California State University, 18111 Nordhoff Street, Northridge, CA 91330-8268, USA
[10] Department of Physics and Astronomy, The Open University, Milton Keynes, MK7 6AA, UK
[11] Harvard-Smithsonian Center for Astrophysics, 60 Garden Street, Cambridge, MA 02138, USA
[12] NASA Exoplanet Science Institute, Caltech, MS 100-22, 770 South Wilson Avenue, Pasadena, CA 91125, USA
[13] Isaac Newton Group of Telescopes, Apartado de Correos 321, E-38700 Santa Cruz de la Palma, Tenerife, Spain
[14] Department of Physics, University of Warwick, Coventry, CV4 7AL, UK
Received 2009 April 24; accepted 2009 August 4; published 2009 September 1

ABSTRACT

We report the discovery from WASP-South of a new Jupiter-like extrasolar planet, WASP-16b, which transits its solar analog host star every 3.12 days. Analysis of the transit photometry and radial velocity spectroscopic data leads to a planet with $R_p = 1.008 \pm 0.071\ R_{Jup}$ and $M_p = 0.855 \pm 0.059\ M_{Jup}$, orbiting a host star with $R_* = 0.946 \pm 0.054\ R_\odot$ and $M_* = 1.022 \pm 0.101\ M_\odot$. Comparison of the high resolution stellar spectrum with synthetic spectra and stellar evolution models indicates the host star is a near-solar metallicity ($[Fe/H] = 0.01 \pm 0.10$) solar analog ($T_{eff} = 5700 \pm 150$ K and $\log g = 4.5 \pm 0.2$) of intermediate age ($\tau = 2.3^{+5.8}_{-2.2}$ Gyr).

Key words: planetary systems – stars: abundances – stars: individual (WASP-16b)

1. INTRODUCTION

There are currently over 300 known exoplanets[15] with the majority of them discovered through the radial velocity (RV) technique. A growing number of exoplanets in recent years have been discovered through the transit method. Transiting exoplanets are particularly valuable as they allow parameters such as the mass, radius, and density to be accurately determined and further studies such as transmission spectroscopy, secondary eclipse measurements, and transit timing variations to be carried out.

There are several wide angle surveys that have been successful in finding transiting exoplanets around bright stars, namely HAT (Bakos et al. 2002), TrES (Alonso et al. 2004), XO (McCullough et al. 2005), and WASP (Pollacco et al. 2006). The WASP Consortium conducts the only exoplanet search currently operating in both hemispheres although HATnet is planning a southern extension and several groups are planning searches from Antarctica (e.g., Strassmeier et al. 2007; Crouzet et al. 2009).

We report the discovery from the WASP-South observatory of a $\sim 0.86\ M_{Jup}$ mass companion orbiting a $V \sim 11.3$ close solar analog WASP-16 (=TYC 6147-229-1, USNO-B1.0 0697-0298329).

2. OBSERVATIONS

2.1. Photometric Observations

WASP-South, located at SAAO, South Africa, is one of two SuperWASP instruments and comprises eight cameras on a robotic mount. Each camera consists of a Canon 200mm $f/1.8$ lens with an Andor 2048×2048 e2v CCD camera giving a field of view of $7.^\circ8 \times 7.^\circ8$ and a pixel scale of $13.''7$. Exposure times were 30 s and the same field is returned to and reimaged every 8–10 minutes. Further details of the instrument, survey, and data reduction pipelines are given in Pollacco et al. (2006); and the candidate selection procedure is described in Collier Cameron et al. (2007), Pollacco et al. (2008), and references therein.

WASP-16 was observed for a partial season in 2006, a full season in 2007, and a further partial season in 2008 with the distribution of data points as 3324 points (2006), 6013 (2007), and 4084 (2008). The 2007 light curve revealed the presence of a $\sim$ 1.3% dip with a period of $\sim$ 3.11 days. The transit coverage in the other two seasons was very sparse, particularly in 2006, and there is only evidence for two partial transits in the 2008 data. WASP-16 was a fairly strong candidate for follow up despite the small number of transits, passing the filtering tests of Collier Cameron et al. (2006) with a signal to red noise ratio, $S_{red} = 9.38$ (with $S_{red} > 5$ required for selection), "transit to antitransit ratio" $\Delta\chi^2/\Delta\chi^2_- = 2.5(\Delta\chi^2/\Delta\chi^2_- \geqslant 1.5$ required for selection) and no measurable ellipsoidal variation.

The SuperWASP light curve showing a zoom of the transit region, along with the model transit fit, is shown in Figure 1. In order to better constrain the transit parameters, follow-up high precision photometric observations with the Swiss 1.2m+EULERCAM on La Silla, were obtained in the I_c band on the night of 2008 May 4 and are shown in Figure 2.

2.2. Spectroscopic Observations

In order to confirm the planetary nature of the transit signal, we obtained follow-up spectroscopic observation with the

[15] http://exoplanet.eu

The Astrophysical Journal, 709:159–167, 2010 January 20 doi:10.1088/0004-637X/709/1/159
© 2010. The American Astronomical Society. All rights reserved. Printed in the U.S.A.

WASP-17b: AN ULTRA-LOW DENSITY PLANET IN A PROBABLE RETROGRADE ORBIT*

D. R. Anderson[1], C. Hellier[1], M. Gillon[2,3], A. H. M. J. Triaud[2], B. Smalley[1], L. Hebb[4], A. Collier Cameron[4], P. F. L. Maxted[1], D. Queloz[2], R. G. West[5], S. J. Bentley[1], B. Enoch[4], K. Horne[4], T. A. Lister[6], M. Mayor[2], N. R. Parley[4], F. Pepe[2], D. Pollacco[7], D. Ségransan[2], S. Udry[2], and D. M. Wilson[1,8]
[1] Astrophysics Group, Keele University, Staffordshire, ST5 5BG, UK; dra@astro.keele.ac.uk
[2] Observatoire de Genève, Université de Genève, 51 Chemin des Maillettes, 1290 Sauverny, Switzerland
[3] Institut d'Astrophysique et de Géophysique, Université de Liège, Allée du 6 Août, 17, Bat. B5C, Liège 1, Belgium
[4] School of Physics and Astronomy, University of St. Andrews, North Haugh, Fife, KY16 9SS, UK
[5] Department of Physics and Astronomy, University of Leicester, Leicester, LE1 7RH, UK
[6] Las Cumbres Observatory, 6740 Cortona Dr. Suite 102, Santa Barbara, CA 93117, USA
[7] Astrophysics Research Centre, School of Mathematics & Physics, Queen's University, University Road, Belfast, BT7 1NN, UK
Received 2009 August 11; accepted 2009 November 30; published 2009 December 29

ABSTRACT

We report the discovery of the transiting giant planet WASP-17b, the least-dense planet currently known. It is 1.6 Saturn masses, but 1.5–2 Jupiter radii, giving a density of 6%–14% that of Jupiter. WASP-17b is in a 3.7 day orbit around a sub-solar metallicity, $V = 11.6$, F6 star. Preliminary detection of the Rossiter–McLaughlin effect suggests that WASP-17b is in a retrograde orbit ($\lambda \approx -150^\circ$), indicative of a violent history involving planet–planet or star–planet scattering. WASP-17b's bloated radius could be due to tidal heating resulting from recent or ongoing tidal circularization of an eccentric orbit, such as the highly eccentric orbits that typically result from scattering interactions. It will thus be important to determine more precisely the current orbital eccentricity by further high-precision radial velocity measurements or by timing the secondary eclipse, both to reduce the uncertainty on the planet's radius and to test tidal-heating models. Owing to its low surface gravity, WASP-17b's atmosphere has the largest scale height of any known planet, making it a good target for transmission spectroscopy.

Key words: planetary systems – stars: individual (WASP-17)

Online-only material: color figures, machine-readable table

1. INTRODUCTION

The first measurement of the radius and density of an extrasolar planet was made when HD 209458b was seen to transit its parent star (Charbonneau et al. 2000; Henry et al. 2000). The large radius (1.32 $R_{\rm Jup}$) of HD 209458b, confirmed by later observations (e.g., Knutson et al. 2007), could not be explained by standard models of planet evolution (Guillot & Showman 2002). Since the discovery of HD 209458b, other bloated planets have been found, including TrES-4 (Mandushev et al. 2007), WASP-12b (Hebb et al. 2008), WASP-4b (Wilson et al. 2008; Gillon et al. 2009a, Winn et al. 2009a, Southworth et al. 2009), WASP-6b (Gillon et al. 2009b), XO-3b (Johns-Krull et al. 2008; Winn et al. 2008), and HAT-P-1b (Bakos et al. 2007; Winn et al. 2007; Johnson et al. 2008). Of these, TrES-4 is the most bloated, with a density 15% that of Jupiter, and a radius larger by a factor 1.78 (Sozzetti et al. 2009).

The mass, composition, and evolution history of a planet determines its current radius (e.g., Burrows et al. 2007; Fortney et al. 2007). Recently, numerous theoretical studies have attempted to discover the reasons why some short-orbit, giant planets are bloated. A small fraction of stellar insolation energy would be sufficient to account for bloating, but no known mechanism is able to transport the insolation energy deep enough within a planet to significantly affect the planet's evolution (Guillot & Showman 2002; Burrows et al. 2007). Enhanced atmospheric opacity would cause internal heat to be lost more slowly, causing a planet's radius to be larger than otherwise at a given age (Burrows et al. 2007). Indeed, the more highly irradiated planets are thought to have enhanced opacity due to species such as gas-phase TiO/VO, tholins or polyacetylenes (Burrows et al. 2008; Fortney et al. 2008). These upper-atmosphere absorbers result in detectable stratospheres (e.g., Knutson et al. 2009) and prevent incident flux from reaching deep into the atmosphere, causing a large day–night temperature contrast, which leads to faster cooling (Guillot & Showman 2002). That some planets are not bloated, though they are in similar irradiation environments and have otherwise similar properties to bloated planets, may be due to differences in evolution history or in core mass (Guillot et al. 2006; Burrows et al. 2007).

Currently, the most promising explanation for the large radii of some planets is that they were inflated when the tidal circularization of eccentric orbits caused energy to be dissipated as heat within the planets (Bodenheimer et al. 2001; Gu et al. 2003; Jackson et al. 2008a; Ibgui & Burrows 2009). Indeed, Jackson et al. (2008b) found that the distribution of the eccentricities of short-orbit ($a < 0.2$ AU) planets could have evolved, via tidal circularization, from a distribution identical to that of the farther-out planets.

The angular momenta of a star and its planets derive from that of their parent molecular cloud, so close alignment is expected between the stellar spin and planetary orbit axes. When a planet obscures a portion of its parent star, we observe an apparent spectroscopic redshift or blueshift, which we see depends on whether the area obscured is approaching or receding relative to the star's bulk motion. This manifests as an "anomalous" radial velocity (RV) and is known as the Rossiter–McLaughlin (RM) effect (e.g., Queloz et al. 2000a; Gaudi & Winn 2007).

* Based in part on data collected with the HARPS spectrograph at ESO La Silla Observatory under programme ID 081.C-0388(A).
[8] Current address: Centre for Astrophysics & Planetary Science, University of Kent, Canterbury, Kent, CT2 7NH, UK.

nature Vol 460|27 August 2009|doi:10.1038/nature08245

LETTERS

An orbital period of 0.94 days for the hot-Jupiter planet WASP-18b

Coel Hellier[1], D. R. Anderson[1], A. Collier Cameron[2], M. Gillon[3,4], L. Hebb[2], P. F. L. Maxted[1], D. Queloz[3], B. Smalley[1], A. H. M. J. Triaud[3], R. G. West[5], D. M. Wilson[1], S. J. Bentley[1], B. Enoch[2], K. Horne[2], J. Irwin[6], T. A. Lister[7], M. Mayor[3], N. Parley[2], F. Pepe[3], D. L. Pollacco[8], D. Segransan[3], S. Udry[3] & P. J. Wheatley[9]

The 'hot Jupiters' that abound in lists of known extrasolar planets are thought to have formed far from their host stars, but migrate inwards through interactions with the proto-planetary disk from which they were born[1,2], or by an alternative mechanism such as planet–planet scattering[3]. The hot Jupiters closest to their parent stars, at orbital distances of only ~0.02 astronomical units, have strong tidal interactions[4,5], and systems such as OGLE-TR-56 have been suggested as tests of tidal dissipation theory[6,7]. Here we report the discovery of planet WASP-18b with an orbital period of 0.94 days and a mass of ten Jupiter masses (10 $M_{\rm Jup}$), resulting in a tidal interaction an order of magnitude stronger than that of planet OGLE-TR-56b. Under the assumption that the tidal-dissipation parameter Q of the host star is of the order of 10^6, as measured for Solar System bodies and binary stars and as often applied to extrasolar planets, WASP-18b will be spiralling inwards on a timescale less than a thousandth that of the lifetime of its host star. Therefore either WASP-18 is in a rare, exceptionally short-lived state, or the tidal dissipation in this system (and possibly other hot-Jupiter systems) must be much weaker than in the Solar System.

Through monitoring by the WASP-South transit survey[8], coupled with radial-velocity observations from the Coralie spectrograph, we have discovered a 10-$M_{\rm Jup}$ planet transiting the star WASP-18 (= HD 10069) every 0.94 days (Fig. 1). WASP-18b is the first confirmed hot-Jupiter planet that has a period of less than one day (candidates with periods of less than a day have previously been announced based on photometry alone[9], though experience shows that less than 10% of such candidates are actual planets[10]).

From comparison of the host star to stellar evolutionary tracks[11,12] (see the Supplementary Information) we find a stellar mass of 1.24 ± 0.04 solar masses, $M_{\odot}$, and an age of 630^{+950}_{-530} Myr, which is short compared to the approximately 5-Gyr main-sequence lifetime of a star of this mass. A further age constraint is that the observed lithium abundance of WASP-18 is below that typical of F6 stars in the Pleiades (age 120 Myr) but comparable to that in the Hyades[13] (age 600 Myr). Thus we conclude that WASP-18 has an age of 0.5–1.5 Gyr, making it one of the youngest known planet-hosting stars.

The theory of tidal interaction for hot Jupiters in close orbits[4,5,14] predicts that the tidal bulge on the star, raised by the planet, exerts a torque that drains angular momentum from the planet's orbit, causing it to spiral inwards (this arises when the planetary orbit is shorter than the stellar rotation, and contrasts with the Earth–Moon system where the longer orbit of the Moon compared to Earth's spin causes it to move away over time). The spiral infall timescale is determined by the mass and orbital distance of the planet, and by the tidal dissipation parameter of the host star, Q. This quality factor is the ratio of the

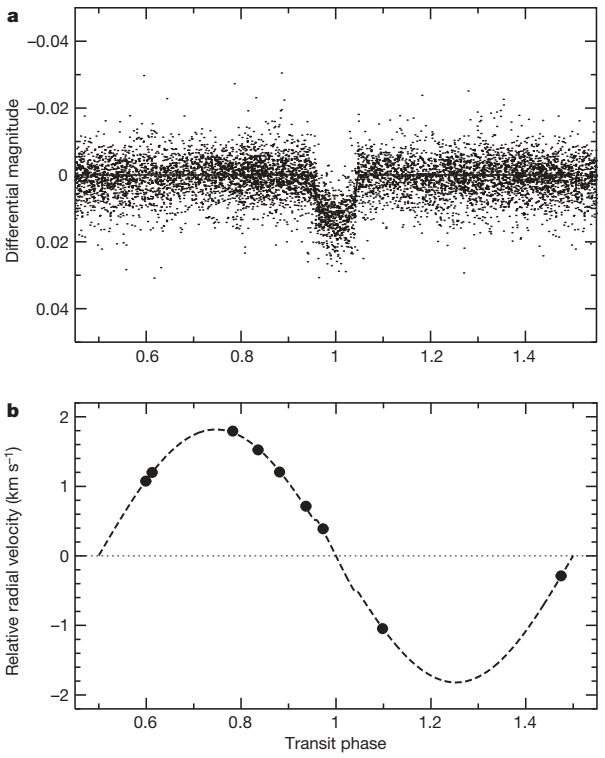


Figure 1 | Discovery data for WASP-18b. a, The WASP-South lightcurve folded on the 0.94-day transit period, together with the model curve from the parameters of Table 1. Monitoring from May–December in 2006 and 2007 resulted in 8,235 photometric data points. **b**, Coralie radial-velocity measurements, again with the best-fitting model. The parameters of the system, derived from[26] the radial-velocity data, the WASP photometry, and additional transit photometry from the Euler telescope, are given in Table 1. The parameters of the host star in Table 2 were derived independently[27] from the stellar spectra. The stellar rotation rate ($v \sin i$) is 11.0 ± 1.5 km s^{-1}, which (assuming that the spin and orbit are aligned) implies a rotation period of 5.6 days, typical for a young F star.

[1]Astrophysics Group, Keele University, Staffordshire, ST5 5BG, UK. [2]School of Physics and Astronomy, University of St Andrews, North Haugh, Fife, KY16 9SS, UK. [3]Observatoire de Genève, Université de Genève, 51 ch. des Maillettes, 1290 Sauverny, Switzerland. [4]Institut d'Astrophysique et de Géophysique, Université de Liège, 17 Allée du 6 Août, Batiment B5C, Liège 1, Belgium. [5]Department of Physics and Astronomy, University of Leicester, Leicester, LE1 7RH, UK. [6]Department of Astronomy, Harvard University, 60 Garden Street, MS 10, Cambridge, Massachusetts 02138, USA. [7]Las Cumbres Observatory, 6740 Cortona Dr. Suite 102, Santa Barbara, California 93117, USA. [8]Astrophysics Research Centre, School of Mathematics and Physics, Queen's University, University Road, Belfast, BT7 1NN, UK. [9]Department of Physics, University of Warwick, Coventry, CV4 7AL, UK.

©2009 Macmillan Publishers Limited. All rights reserved

The Astrophysical Journal, 708:224–231, 2010 January 1 doi:10.1088/0004-637X/708/1/224
© 2010. The American Astronomical Society. All rights reserved. Printed in the U.S.A.

WASP-19b: THE SHORTEST PERIOD TRANSITING EXOPLANET YET DISCOVERED

L. Hebb[1], A. Collier-Cameron[1], A.H.M.J. Triaud[2], T.A. Lister[3], B. Smalley[4], P.F.L. Maxted[4], C. Hellier[4], D.R. Anderson[4], D. Pollacco[5], M.Gillon[2,6], D. Queloz[2], R.G. West[7], S.Bentley[4], B. Enoch[1], C.A. Haswell[8], K. Horne[1], M. Mayor[2], F. Pepe[2], D. Segransan[2], I. Skillen[9], S. Udry[2], and P.J. Wheatley[10]
[1] School of Physics and Astronomy, University of St. Andrews, North Haugh, St. Andrews, Fife KY16 9SS, UK
[2] Observatoire de Genève, Université de Genève, 51 Ch. des Maillettes, 1290 Sauverny, Switzerland
[3] Las Cumbres Observatory, 6740 Cortona Dr. Suite 102, Santa Barbara, CA 93117, USA
[4] Astrophysics Group, Keele University, Staffordshire, ST5 5BG, UK
[5] Astrophysics Research Centre, School of Mathematics & Physics, Queen's University, University Road, Belfast, BT7 1NN, UK
[6] Institut d'Astrophysique et de Géophysique, Université de Liège, Allée du 6 Août, 17, Bat. B5C, Liège 1, Belgium
[7] Department of Physics and Astronomy, University of Leicester, Leicester, LE1 7RH, UK
[8] Department of Physics and Astronomy, The Open University, Milton Keynes, MK7 6AA, UK
[9] Isaac Newton Group of Telescopes, Apartado de Correos 321, E-38700 Santa Cruz de la Palma, Tenerife, Spain
[10] Department of Physics, University of Warwick, Coventry CV4 7AL, UK
Received 2009 June 19; accepted 2009 November 9; published 2009 December 9

ABSTRACT

We report on the discovery of a new extremely short period transiting extrasolar planet, WASP-19b. The planet has mass $M_{\rm pl} = 1.15 \pm 0.08\ M_J$, radius $R_{\rm pl} = 1.31 \pm 0.06\ R_J$, and orbital period $P = 0.7888399 \pm 0.0000008$ days. Through spectroscopic analysis, we determine the host star to be a slightly super-solar metallicity ($[{\rm M/H}] = 0.1 \pm 0.1$ dex) G-dwarf with $T_{\rm eff} = 5500 \pm 100$ K. In addition, we detect periodic, sinusoidal flux variations in the light curve which are used to derive a rotation period for the star of $P_{\rm rot} = 10.5 \pm 0.2$ days. The relatively short stellar rotation period suggests that either WASP-19 is somewhat young ($\sim$600 Myr old) or tidal interactions between the two bodies have caused the planet to spiral inward over its lifetime resulting in the spin-up of the star. Due to the detection of the rotation period, this system has the potential to place strong constraints on the stellar tidal quality factor, Q'_s, if a more precise age is determined.

Key words: planetary systems – techniques: photometric – techniques: radial velocities

Online-only material: color figure

1. INTRODUCTION

Since the unexpected discovery of the first "hot Jupiter," 51 Peg b (Mayor & Queloz 1995), exoplanets with an exceptionally wide variety of properties have been detected which have dramatically changed our understanding of planetary physics. In particular, through the discovery of various transiting planets, we have learned that extrasolar planets can have radii much larger (e.g., Hebb et al. 2009) or densities much higher (Sato et al. 2005) than Jupiter. Many, but not all, "hot Jupiters" have temperature inversions in their atmospheres (e.g., Knutson et al. 2008), and they can have very low optical albedos (Rowe et al. 2008). Despite their short periods, not all transiting exoplanets have been tidally circularized (Gillon et al. 2009a), and both rocky (e.g., CoRoT-Exo-7, $P \sim 0.85$ days) and gas giant (e.g., WASP-12b, $P \sim 1.09$ days) planets can exist in extremely short period orbits. Here, we report on the discovery of a new extreme transiting extrasolar planet with the shortest orbital period yet detected which is on the verge of spiraling into its host star. This transiting planet not only can inform us about the properties and evolution of close-in planets, but also has the potential to provide information about the characteristics of its host star.

In this paper, we first describe all the observations that were obtained to detect and analyze the transiting star–planet system (Section 2). We describe the data analysis in Section 3 where we present the planet and its host star. Finally, in Section 4, we discuss the implications of the planet's short period and its future evolution.

2. OBSERVATIONS

2MASS J09534008-4539330 (hereafter WASP-19) is an apparently unremarkable 12th magnitude ($V = 12.59$), G8V star in the southern hemisphere located at $\alpha = 09{:}53{:}40.08$, $\delta = -45{:}39{:}33.0$ (J2000). The target was observed with the WASP-South telescope and instrumentation (Pollacco et al. 2006; Wilson et al. 2008) in the winter and spring observing seasons from 2006 to 2008. Between 2006 May 4–June 20, 1496 photometric data points were obtained, 6695 measurements were made between 2006 December 18–2007 May 18, and 8968 observations were taken from 2007 December 18–2008 May 22. All data sets were processed independently with the standard WASP data reduction pipeline and photometry package (Collier Cameron et al. 2006). The individual data points have typical uncertainties of $\sim$0.02 mag including Poisson noise and systematic noise. The resulting light curves were then run through our implementation of the box least squares algorithm (Kovács et al. 2002) designed to detect periodic transit-shaped dips in brightness.

The target was initially flagged as a transiting planet candidate because a strong periodic signal was detected in the 2007 data. The phase-folded light curve showed a square-shaped dip in brightness with a depth $\delta \sim 25$ mmag and duration $\tau \sim 1.2$ hr, consistent with a planet-sized object around a main-sequence star. Further, a periodic transit was also apparent in the 2006 data when phase folded with the 2007 ephemeris, and a transit was subsequently detected in the 2008 season of data. Therefore, we classified the object as needing follow-up photometry and

A&A 519, A98 (2010)
DOI: 10.1051/0004-6361/201014817
© ESO 2010

Astronomy & Astrophysics

WASP-21b: a hot-Saturn exoplanet transiting a thick disc star⋆,⋆⋆

F. Bouchy[1,2], L. Hebb[3,5], I. Skillen[4], A. Collier Cameron[5], B. Smalley[6], S. Udry[7], D. R. Anderson[6], I. Boisse[1], B. Enoch[5], C. A. Haswell[8], G. Hébrard[1], C. Hellier[6], Y. Joshi[9], S. R. Kane[10], P. F. L. Maxted[6], M. Mayor[7], C. Moutou[11], F. Pepe[7], D. Pollacco[9], D. Queloz[7], D. Ségransan[7], E. K. Simpson[9], A. M. S. Smith[6], H. C. Stempels[12], R. Street[13], A. H. M. J. Triaud[7], R. G. West[14], and P. J. Wheatley[15]

[1] Institut d'Astrophysique de Paris, UMR7095 CNRS, Université Pierre & Marie Curie, 98bis Bd Arago, 75014 Paris, France
e-mail: bouchy@iap.fr
[2] Observatoire de Haute-Provence, CNRS/OAMP, 04870 St. Michel l'Observatoire, France
[3] Department of Physics and Astronomy, Vanderbilt University, Nashville, TN 37235, USA
[4] Isaac Newton Group of Telescopes, Apartado de Correos 321, 38700 Santa Cruz de la Palma, Tenerife, Spain
[5] SUPA, School of Physics and Astronomy, University of St. Andrews, North Haugh, St. Andrews, Fife KY16 9SS, UK
[6] Astrophysics Group, Keele University, Staffordshire, ST5 5BG, UK
[7] Observatoire de Genève, Université de Genève, 51 Ch. des Maillettes, 1290 Sauverny, Switzerland
[8] Department of Physics and Astronomy, The Open University, Milton Keynes, MK7 6AA, UK
[9] Astrophysics Research Centre, School of Mathematics and Physics, Queen's University, University Road, Belfast, BT7 1NN, UK
[10] NASA Exoplanet Science Institute, Caltech, MS 100-22, 770 South Wilson Avenue, Pasadena, CA 91125, USA
[11] Laboratoire d'Astrophysique de Marseille, 38 rue Frédéric Joliot-Curie, 13388 Marseille Cedex 13, France
[12] Department of Physics and Astronomy, Uppsala University, Box 516, 75120 Uppsala, Sweden
[13] Las Cumbres Observatory, 6740 Cortona Drive Suite 102, Goleta, CA 93117, USA
[14] Department of Physics and Astronomy, University of Leicester, Leicester, LE1 7RH, UK
[15] Department of Physics, University of Warwick, Coventry CV4 7AL, UK

Received 19 April 2010 / Accepted 13 May 2010

ABSTRACT

We report the discovery of WASP-21b, a new transiting exoplanet discovered by the Wide Angle Search for Planets (WASP) Consortium and established and characterized with the FIES, SOPHIE, CORALIE and HARPS fiber-fed echelle spectrographs. A 4.3-d period, 1.1% transit depth and 3.4-h duration are derived for WASP-21b using SuperWASP-North and high precision photometric observations at the Liverpool Telescope. Simultaneous fitting to the photometric and radial velocity data with a Markov Chain Monte Carlo procedure leads to a planet in the mass regime of Saturn. With a radius of 1.07 $R_{\rm Jup}$ and mass of 0.30 $M_{\rm Jup}$, WASP-21b has a density close to 0.24 $\rho_{\rm Jup}$ corresponding to the distribution peak at low density of transiting gaseous giant planets. With a host star metallicity [Fe/H] of –0.46, WASP-21b strengthens the correlation between planetary density and host star metallicity for the five known Saturn-like transiting planets. Furthermore there are clear indications that WASP-21b is the first transiting planet belonging to the thick disc.

Key words. planetary systems – techniques: photometric – techniques: radial velocities

1. Introduction

Observations of planets that transit their host star represent currently the best opportunity to test models of exoplanet structure and evolution. These last ten years, the photometric surveys have led to an increasing list of transiting planets. More than seventy transiting planetary systems have been identified from Super-Earth to Jupiter-like planets. The WASP project operates two identical instruments, at La Palma in the Northern hemisphere, and at Sutherland in South Africa in the Southern hemisphere and led recently to the detection of about 30% of known transiting planets. Each WASP telescope has a field of view of just under 500 square degrees. The WASP survey is sensitive to planetary transit signatures in the light curves of stars in the magnitude range $V \sim 9$–13. A detailed description of the telescope hardware, observing strategy and pipeline data analysis is given in Pollacco et al. (2006).

Here we present the WASP photometry of SWASPJ230958.23+182346.0, high-precision photometric follow-up observations with the RISE instrument on the Liverpool Telescope and high-precision radial velocity (RV) observations with the FIES (2.6-m NOT), SOPHIE (1.93-m OHP), CORALIE (1.2-m Euler) and HARPS (3.6-m ESO) fiber-fed echelle spectrographs. These observations lead to the discovery of WASP-21b, a hot-Saturn transiting exoplanet.

⋆ Based on observations made with the SuperWASP-North camera hosted by the Isaac Newton Group on La Palma, the FIES spectrograph on the Nordic Optical Telescope, the CORALIE spectrograph on the 1.2-m Euler Swiss telescope on La Silla Observatory, the SOPHIE spectrograph on the 1.93-m telescope on Haute Provence Observatory and the HARPS spectrograph on the 3.6-m ESO telescope at La Silla Observatory under programs 081.C-0388, 082.C-0040, 084.C-0185.

⋆⋆ Tables of photometric data are only available in electronic form at the CDS via anonymous ftp to cdsarc.u-strasbg.fr (130.79.128.5) or via http://cdsarc.u-strasbg.fr/viz-bin/qcat?J/A+A/519/A98

The Astronomical Journal, 140:2007–2012, 2010 December doi:10.1088/0004-6256/140/6/2007
© 2010. The American Astronomical Society. All rights reserved. Printed in the U.S.A.

WASP-22 b: A TRANSITING "HOT JUPITER" PLANET IN A HIERARCHICAL TRIPLE SYSTEM

P. F. L. Maxted[1], D. R. Anderson[1], M. Gillon[2,3], C. Hellier[1], D. Queloz[2], B. Smalley[1], A. H. M. J. Triaud[2], R. G. West[4], D. M. Wilson[1], S. J. Bentley[1], H. Cegla[1,5,6], A. Collier Cameron[7], B. Enoch[7], L. Hebb[7], K. Horne[7], J. Irwin[8], T. A. Lister[9], M. Mayor[2], N. Parley[7], F. Pepe[2], D. Pollacco[6], D. Segransan[2], S. Udry[2], and P. J. Wheatley[10]
[1] Astrophysics Group, Keele University, Staffordshire, ST5 5BG, UK
[2] Observatoire de Genève, Université de Genève, 51 Chemin des Maillettes, 1290 Sauverny, Switzerland
[3] Institut d'Astrophysique et de Géophysique, Université de Liège, Allée du 6 Août, 17, Bat. B5C, Liège 1, Belgium
[4] Department of Physics and Astronomy, University of Leicester, Leicester, LE1 7RH, UK
[5] Physics and Astronomy Department, Vanderbilt University, 6301 Stevenson Center, Nashville, TN 37235, USA
[6] Astrophysics Research Centre, School of Mathematics and Physics, Queen's University, University Road, Belfast, BT7 1NN, UK
[7] School of Physics and Astronomy, University of St. Andrews, North Haugh, Fife, KY16 9SS, UK
[8] Department of Astronomy, Harvard University, 60 Garden Street, MS 10, Cambridge, MA 02138, USA
[9] Las Cumbres Observatory, 6740 Cortona Drive, Suite 102, Santa Barbara, CA 93117, USA
[10] Department of Physics, University of Warwick, Coventry, CV4 7AL, UK
Received 2010 April 8; accepted 2010 October 12; published 2010 November 10

ABSTRACT

We report the discovery of a transiting planet orbiting the star TYC 6446-326-1. The star, WASP-22, is a moderately bright ($V = 12.0$) solar-type star ($T_{\rm eff} = 6000 \pm 100$ K, [Fe/H]$= -0.05 \pm 0.08$). The light curve of the star obtained with the WASP-South instrument shows periodic transit-like features with a depth of about 1% and a duration of 0.14 days. The presence of a transit-like feature in the light curve is confirmed using z-band photometry obtained with Faulkes Telescope South. High-resolution spectroscopy obtained with the CORALIE and HARPS spectrographs confirms the presence of a planetary mass companion with an orbital period of 3.533 days in a near-circular orbit. From a combined analysis of the spectroscopic and photometric data assuming that the star is a typical main-sequence star we estimate that the planet has a mass $M_{\rm p} = 0.56 \pm 0.02 M_{\rm Jup}$ and a radius $R_{\rm p} = 1.12 \pm 0.04 R_{\rm Jup}$. In addition, there is a linear trend of 40 m s^{-1} yr^{-1} in the radial velocities measured over 16 months, from which we infer the presence of a third body with a long-period orbit in this system. The companion may be a low mass M-dwarf, a white dwarf, or a second planet.

Key words: planetary systems

Online-only material: color figure

1. INTRODUCTION

The WASP project (Pollacco et al. 2006) is currently one of the most successful wide-area surveys designed to find exoplanets transiting bright stars ($V < 12.5$). Other successful surveys include HATnet (Bakos et al. 2004), XO (McCullough et al. 2005), and TrES (O'Donovan et al. 2006). There is continued interest in finding transiting exoplanets because they can be accurately characterized and studied in some detail, e.g., the mass and radius of the planet can be accurately measured. This gives us the opportunity to explore the relationships between the density of the planet and other properties of the planetary system, e.g., the semimajor axis, the spectral type of the star, the eccentricity of the orbit. Given the wide variety of transiting planets being discovered and the large number of parameters that characterize them, statistical studies will require a large sample of systems to identify and quantify the relationships between these parameters. These relationships can be used to test models of the formation, structure, and evolution of short period exoplanets.

A particular puzzle related to the properties of hot Jupiters is the wide range in their densities. Very dense hot Jupiters such as HD 149026 are thought to contain a dense, metallic core (Sato et al. 2005). There is currently no generally agreed explanation for the existence of hot Jupiters with densities 5–10 times lower than the density of Jupiter, e.g., WASP-17 b (Anderson et al. 2010), TrES-4 b (Mandushev et al. 2007), and WASP-12 b (Hebb et al. 2009). One possibility is that the planets are heated by tidal forces and that these are driven by the presence of a third body in the system (Mardling 2007). Other possibilities include enhanced opacity in the atmosphere (Burrows et al. 2007), the distribution of heavy elements in the core (Baraffe et al. 2008), and kinetic heating from the irradiated atmosphere into the interior (Showman & Guillot 2002).

Here, we report the discovery of a hot Jupiter system, WASP-22, identified using the WASP-South instrument and present evidence that it is a member of a hierarchical triple system.

2. OBSERVATIONS

The WASP survey is described in Pollacco et al. (2006) and Wilson et al. (2008) while a discussion of our candidate selection methods can be found in Collier Cameron et al. (2007), Pollacco et al. (2008), and references therein.

The WASP-South instrument consists of eight cameras, each with a Canon 200 mm $f/1.8$ lens and a 2k × 2k e2V CCD detector resulting in an image scale of approximately 14 arcsec pixel^{-1}. The star TYC 6446-326-1 (=1SWASP J033116.32 − 234911.0) was observed 3133 times by one camera on the WASP-South instrument from 2006 August to 2007 January. A further 6282 observations were obtained with the same camera from 2007 August to 2008 January. The star also appeared in the images obtained with a second camera during the second observing season, so further 5889 observations were obtained with this camera during that interval.

The WASP-South light curves of WASP-22 show transit-like features with a depth of approximately 0.012 mag recurring

The Astrophysical Journal, 720:337–343, 2010 September 1 doi:10.1088/0004-637X/720/1/337
© 2010. The American Astronomical Society. All rights reserved. Printed in the U.S.A.

WASP-24 b: A NEW TRANSITING CLOSE-IN HOT JUPITER ORBITING A LATE F-STAR

R. A. Street[1], E. Simpson[2], S. C. C. Barros[2], D. Pollacco[2], Y. Joshi[2], I. Todd[2], A. Collier Cameron[3], B. Enoch[3], N. Parley[3], E. Stempels[4], L. Hebb[5], A. H. M. J. Triaud[6], D. Queloz[6], D. Segransan[6], F. Pepe[6], S. Udry[6], T. A. Lister[1], É. Depagne[1], R. G. West[7], A. J. Norton[8], B. Smalley[9], C. Hellier[9], D. R. Anderson[9], P. F. L. Maxted[9], S. J. Bentley[9], I. Skillen[10], M. Gillon[11], P. Wheatley[12], J. Bento[12], P. Cathaway-Kjontvedt[13], and D. J. Christian[2,13]
[1] Las Cumbres Observatory Global Telescope Network, 6740 Cortona Drive, Suite 102, Goleta, CA 93117, USA
[2] Astrophysics Research Centre, Physics Building, Queen's University, Belfast, County Antrim, BT7 1NN, UK
[3] SUPA, School of Physics and Astronomy, University of St. Andrews, North Haugh, St. Andrews, KY16 9SS, UK
[4] Department of Physics and Astronomy, P.O. Box 516, SE-751 20 Uppsala, Sweden
[5] Physics & Astronomy Department, Vanderbilt University, 1807 Station B, Nashville, TN 37235, USA
[6] Observatoire Astronomique de l'Université de Genève, 51 Chemin des Maillettes, 1290 Sauverny, Switzerland
[7] Department of Physics & Astronomy, University of Leicester, University Road, Leicester, LE1 7RH, UK
[8] Department of Physics & Astronomy, The Open University, N2041, Venables Building, Milton Keynes, MK7 6AA, UK
[9] Astrophysics Group, Keele University, Staffordshire, ST5 5BG, UK
[10] Isaac Newton Group of Telescopes, Apartado de correos 321, E-38700 Santa Cruz de la Palma, Canary Islands, Spain
[11] Institut d'Astrophysique et de Géophysique, Université de Liège, Allée du 6 Août 17, Bât. B5C, 4000 Liège, Belgium
[12] Department of Physics, University of Warwick, Gibbet Hill Road, Coventry, CV4 7AL, UK
[13] Department of Physics and Astronomy, California State University Northridge, 18111 Nordhoff Street, Northridge, CA 91330, USA
Received 2010 March 12; accepted 2010 July 3; published 2010 August 10

ABSTRACT

We report the discovery of a new transiting close-in giant planet, WASP-24 b, in a 2.341 day orbit, 0.037 AU from its F8-9 type host star. By matching the star's spectrum with theoretical models, we infer an effective temperature $T_{\rm eff} = 6075 \pm 100$ K and a surface gravity of $\log g = 4.15 \pm 0.10$. A comparison of these parameters with theoretical isochrones and evolutionary mass tracks places only weak constraints on the age of the host star, which we estimate to be $3.8^{+1.3}_{-1.2}$ Gyr. The planetary nature of the companion was confirmed by radial velocity measurements and additional photometric observations. These data were fit simultaneously in order to determine the most probable parameter set for the system, from which we infer a planetary mass of $1.071^{+0.036}_{-0.038}$ $M_{\rm Jup}$ and radius $1.3^{+0.039}_{-0.037}$ $R_{\rm Jup}$.

Key words: planetary systems

Online-only material: color figures

1. INTRODUCTION

Large-scale, ground-based surveys for transiting planets are yielding a surprisingly diverse set of close-in giant planets. The last few years have seen the discovery of a number of so-called bloated close-in Jovian planets, for example, WASP-17 b (Anderson et al. 2010) and Kepler-7 b (Latham et al. 2010). The very low densities of these objects present an ongoing challenge to theories of planet formation and evolution (Fortney et al. 2008; Guillot et al. 2006; Burrows et al. 2007). Ultra-short period planets such as WASP-19 b (Hebb et al. 2010) offer a testbed for the physics of the dissipation of tidal energy, thought to both bolster the planetary radius (Fortney et al. 2007; Burrows et al. 2007) and perhaps cause the planet's orbits to decay (Jackson et al. 2009), ultimately leading them to spiral into their host stars. Each new wave of planets discovered has produced new surprises. As the surveys searching for new systems reach maturity, and are complemented by targeted space-based missions, we are populating a wider range of the planetary orbital and physical parameter space. A more complete picture of the planetary menagerie will lead to a better understanding of the formation and evolutionary forces at work.

There is a particular value in completing a census of the transiting planets of bright stars, which is evident from the extraordinary insights offered by follow-up work into the composition, structure, and even weather of their atmospheres and exospheres (e.g., Désert et al. 2009; Knutson et al. 2009; Burrows et al. 2009, and references therein). We may even be able to detect changes in weather patterns over the course of an orbit for the long period and eccentric planets (Iro & Deming 2010). Ground-based instruments survey large numbers of bright stars spanning spectral types F–M and produce targets well suited for further study.

We report the discovery of a new close-in giant planet orbiting an 11.3 mag, F8-9 type host star. Our observations are described in Section 2, including both our discovery data and follow-up work. In Section 3, we present the fitting procedure from which we determine the overall system parameters. We discuss the new system in the context of the current sample of known planets in Section 4.

2. OBSERVATIONS

2.1. SuperWASP Discovery Data

The WASP Consortium[14] operates two fully robotic, dedicated observatories: WASP-North, sited at the Observatorio del Roque de los Muchachos (ORM), La Palma, Canary Islands, Spain, and WASP-South, hosted by the South African Astronomical Observatory at Sutherland, South Africa. Both stations support eight cameras, each consisting of a Canon 200 mm, f/1.8 lens, and an Andor 2048 × 2048 pixel thinned e2v CCD. Each camera has a 7.°8 × 7.°8 field of view and a pixel scale of 13.″7 pixel^{-1}. Every clear night the stations execute pre-set observing programs, repeatedly imaging a sequence of 6–12 planet fields every ∼8 minutes for as long as they are visible. Full details of the hardware and data reduction procedures are

[14] www.superwasp.org

Monthly Notices of the ROYAL ASTRONOMICAL SOCIETY

Mon. Not. R. Astron. Soc. **410,** 1631–1636 (2011) doi:10.1111/j.1365-2966.2010.17550.x

WASP-25b: a 0.6$M_{\rm J}$ planet in the Southern hemisphere

B. Enoch,[1⋆] A. Collier Cameron,[1] D. R. Anderson,[2] T. A. Lister,[3] C. Hellier,[2] P. F. L. Maxted,[2] D. Queloz,[4] B. Smalley,[2] A. H. M. J. Triaud,[4] R. G. West,[5] D. J. A. Brown,[1] M. Gillon,[4,6] L. Hebb,[7] M. Lendl,[4] N. Parley,[1] F. Pepe,[4] D. Pollacco,[8] D. Segransan,[4] E. Simpson,[8] R. A. Street[3] and S. Udry[4]

[1]*School of Physics and Astronomy, University of St Andrews, North Haugh, St Andrews KY16 9SS*
[2]*Astrophysics Group, Keele University, Staffordshire ST5 5BG*
[3]*Las Cumbres Observatory, 6740 Cortona Drive Suite 102, Goleta, CA 93117, USA*
[4]*Observatoire astronomique de l'Universitén de Genéve, 51 Chemin des Maillettes, 1290 Sauverny, Switzerland*
[5]*Department of Physics and Astronomy, University of Leicester, Leicester LE1 7RH*
[6]*Institut d'Astrophysique et de Géophysique, Université de Liége, Allée de 6 Août, 17, Bat B5C, Liége 1, Belgium*
[7]*Vanderbilt University, Department of Physics and Astronomy, Nashville, TN 37235, USA*
[8]*Astrophysics Research Centre, School of Mathematics & Physics, Queen's University, University Road, Belfast BT7 1NN*

Accepted 2010 August 16. Received 2010 July 22; in original form 2010 April 13

ABSTRACT

We report the detection of a 0.6 $M_{\rm J}$ extrasolar planet by WASP-South, WASP-25b, transiting its solar-type host star every 3.76 d. A simultaneous analysis of the WASP, FTS and Euler photometry and CORALIE spectroscopy yields a planet of $R_{\rm p} = 1.22 R_{\rm J}$ and $M_{\rm p} = 0.58 M_{\rm J}$ around a slightly metal-poor solar-type host star, [Fe/H] $= -0.05 \pm 0.10$, of $R_* = 0.92\,{\rm R}_\odot$ and $M_* = 1.00\,{\rm M}_\odot$. WASP-25b is found to have a density of $\rho_{\rm p} = 0.32\,\rho_{\rm J}$, a low value for a sub-Jupiter mass planet. We investigate the relationship of planetary radius to planetary equilibrium temperature and host star metallicity for transiting exoplanets with a similar mass to WASP-25b, finding that these two parameters explain the radii of most low-mass planets well.

Key words: planetary systems.

1 INTRODUCTION

To date, over 440 exoplanets have been discovered, including more than 70 detected by the transit method.[1] The transit method together with follow-up radial velocity observations allow measurement of both the mass and radius of the planet, leading to a value for the planet's bulk density (Charbonneau et al. 2000). The atmospheric composition of transiting exoplanets can also be investigated through high-precision photometric and spectroscopic measurements, see e.g. Charbonneau et al. (2002).

A wide range of transiting exoplanets radii has been found and there has been much investigation into the factors that may influence a planet's radius. For example, Guillot et al. (2006) propose a negative relationship between the metallicity of a host star and the radius of an orbiting planet, caused by an increase in the amount of heavy elements in the planet, leading to a more massive core and hence smaller radius for a given mass. Alternatively, Burrows et al. (2007) consider that increasing the metallicity may increase the opacity of an exoplanet's atmosphere, retarding cooling and leading to a larger radius for a given mass. Another influence on a planet's radius may be the equilibrium temperature of the planet (Guillot & Showman 2002), determined by the stellar irradiation and the planet's distance from its host star. Tidal heating due to the circularization of the orbits of close-in exoplanets may also play a role in inflating the planetary radius (Bodenheimer, Laughlin & Lin 2003; Jackson, Greenberg & Barnes 2008). One motivation of the SuperWASP project is to detect enough transiting exoplanets, with a wide range of orbital and compositional parameters, to allow analyses that may distinguish between such differing models.

In this paper, we report the discovery of a 0.6$M_{\rm J}$ planet orbiting a solar mass star, WASP-25 (TYC6706-861-1, 1SWASP J130126.36-273120.0), in the Southern hemisphere. Analysis of photometric and spectroscopic data reveals WASP-25b to be another low-density planet, comparable to HD 209458b (Charbonneau et al. 2000). We also analyse the dependence of the radii of low-mass planets on host star metallicity and planetary equilibrium temperature, including WASP-25b and 18 other transiting planets, finding a relationship using singular value decomposition (SVD) analysis that gives an excellent agreement between observed and calibrated radii.

In Section 2 we describe the photometric and spectroscopic observations and data reduction procedures. In Section 3 we present the stellar and planetary parameters extracted from these data. Finally,

⋆E-mail: becky.enoch@st-andrews.ac.uk
[1] www.exoplanet.eu

© 2010 The Authors. Journal compilation © 2010 RAS

A&A 520, A56 (2010)
DOI: 10.1051/0004-6361/201014705
© ESO 2010

Astronomy & Astrophysics

WASP-26b: a 1-Jupiter-mass planet around an early-G-type star⋆

B. Smalley[1], D. R. Anderson[1], A. Collier Cameron[2], M. Gillon[3,4], C. Hellier[1], T. A. Lister[5], P. F. L. Maxted[1], D. Queloz[4], A. H. M. J. Triaud[4], R. G. West[6], S. J. Bentley[1], B. Enoch[2], F. Pepe[4], D. L. Pollacco[7], D. Segransan[4], A. M. S. Smith[1], J. Southworth[1], S. Udry[4], P. J. Wheatley[8], P. L. Wood[1], and J. Bento[8]

[1] Astrophysics Group, Keele University, Staffordshire, ST5 5BG, UK
e-mail: bs@astro.keele.ac.uk
[2] School of Physics and Astronomy, University of St. Andrews, North Haugh, Fife, KY16 9SS, UK
[3] Institut d'Astrophysique et de Géophysique, Université de Liège, 17 Allée du 6 Août, Bât. B5C, Liège 1, Belgium
[4] Observatoire de Genève, Université de Genève, 51 Chemin des Maillettes, 1290 Sauverny, Switzerland
[5] Las Cumbres Observatory, 6740 Cortona Dr. Suite 102, Santa Barbara, CA 93117, USA
[6] Department of Physics and Astronomy, University of Leicester, Leicester, LE1 7RH, UK
[7] Astrophysics Research Centre, School of Mathematics & Physics, Queen's University, University Road, Belfast, BT7 1NN, UK
[8] Department of Physics, University of Warwick, Coventry CV4 7AL, UK

Received 1 April 2010 / Accepted 24 June 2010

ABSTRACT

We report the discovery of WASP-26b, a moderately over-sized Jupiter-mass exoplanet transiting its 11.3-mag early-G-type host star (1SWASP J001824.70-151602.3; TYC 5839-876-1) every 2.7566 days. A simultaneous fit to transit photometry and radial-velocity measurements yields a planetary mass of 1.02 ± 0.03 $M_{\rm Jup}$ and radius of 1.32 ± 0.08 $R_{\rm Jup}$. The host star, WASP-26, has a mass of 1.12 ± 0.03 $M_{\odot}$ and a radius of 1.34 ± 0.06 $R_{\odot}$ and is in a visual double with a fainter K-type star. The two stars are at least a common-proper motion pair with a common distance of around 250 ± 15 pc and an age of 6 ± 2 Gy.

Key words. planets and satellites: general – stars: individual: WASP-26 – binaries: visual – techniques: photometric – techniques: spectroscopic – techniques: radial velocities

1. Introduction

Most of the known exoplanets have been discovered using the radial velocity technique (Mayor & Queloz 1995). However, in recent years an increasing number have been discovered using the transit technique, via ground-based and space-based survey projects. Transiting exoplanets allow parameters such as the mass, radius, and density to be accurately determined, as well as their atmospheric properties to be studied during their transits and occultations (Charbonneau et al. 2005; Southworth 2009; Winn 2009).

The SuperWASP project has a robotic observatory on La Palma in the Canary Islands and another in Sutherland in South Africa. The wide angle survey is designed to find planets around relatively bright stars in the V-magnitude range 9−13. A detailed description is given in Pollacco et al. (2006).

In this paper we report the discovery of WASP-26b, a Jupiter-mass planet in orbit around its V = 11.3 mag host star 1SWASP J001824.70-151602.3 in the constellation Cetus. We present the SuperWASP-South discovery photometry, together with follow-up optical photometry and radial velocity measurements.

2. Observations

2.1. SuperWASP photometry

The host star WASP-26 (1SWASP J001824.70-151602.3; TYC 5839-876-1) was within two fields observed by SuperWASP-South during the 2008 and 2009 observing seasons, covering the intervals 2008 June 30 to November 17 and 2009 June 28 to November 17. A total of 18 807 data points were obtained. The pipeline-processed data were de-trended and searched for transits using the methods described in Collier Cameron et al. (2006), yielding a detection of a periodic, transit-like signature with a period of 2.7566 days and a depth of 0.009 mag (Fig. 1).

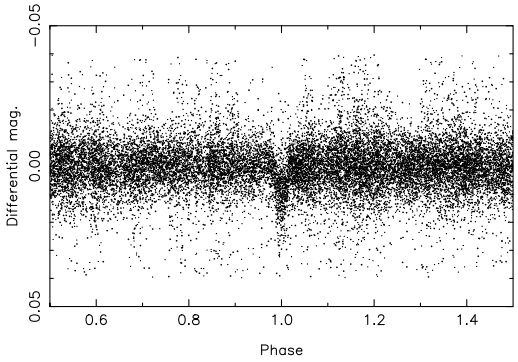


Fig. 1. SuperWASP photometry of WASP-26 folded on the orbital of period of 2.7566 days.

There is a second star (1SWASP J001825.25-151613.8; USNO-B1 0747-0003869), ~2.5 mag fainter, 15″ from WASP-26. Both stars are contained within the 3.5-pixel (≡48″) reduction aperture. Hence, from the SuperWASP photometry alone, we could not be totally sure that WASP-26 was the star varying and not the fainter one in deep eclipse. Targeted photometry was

⋆ RV and photometric data are only available in electronic form at the CDS via anonymous ftp to cdsarc.u-strasbg.fr (130.79.128.5) or via http://cdsarc.u-strasbg.fr/viz-bin/qcat?J/A+A/520/A56

The Astrophysical Journal Letters, 723:L60–L63, 2010 November 1 doi:10.1088/2041-8205/723/1/L60
© 2010. The American Astronomical Society. All rights reserved. Printed in the U.S.A.

WASP-29b: A SATURN-SIZED TRANSITING EXOPLANET

Coel Hellier[1], D. R. Anderson[1], A. Collier Cameron[2], M. Gillon[3], M. Lendl[4], P. F. L. Maxted[1], D. Queloz[4], B. Smalley[1], A. H. M. J. Triaud[4], R. G. West[5], D. J. A. Brown[2], B. Enoch[2], T. A. Lister[6], F. Pepe[4], D. Pollacco[7], D. Ségransan[4], and S. Udry[4]
[1] Astrophysics Group, Keele University, Staffordshire, ST5 5BG, UK
[2] SUPA, School of Physics and Astronomy, University of St. Andrews, North Haugh, Fife, KY16 9SS, UK
[3] Institut d'Astrophysique et de Géophysique, Université de Liège, Allée du 6 Août, 17, Bat. B5C, Liège 1, Belgium
[4] Observatoire astronomique de l'Université de Genève 51 ch. des Maillettes, 1290 Sauverny, Switzerland
[5] Department of Physics and Astronomy, University of Leicester, Leicester, LE1 7RH, UK
[6] Las Cumbres Observatory, 6740 Cortona Dr. Suite 102, Santa Barbara, CA 93117, USA
[7] Astrophysics Research Centre, School of Mathematics & Physics, Queen's University, University Road, Belfast, BT7 1NN, UK
Received 2010 March 25; accepted 2010 September 29; published 2010 October 12

ABSTRACT

We report the discovery of a Saturn-sized planet transiting a $V = 11.3$, K4 dwarf star every 3.9 days. WASP-29b has a mass of $0.24 \pm 0.02\ M_{\rm Jup}$ and a radius of $0.79 \pm 0.05\ R_{\rm Jup}$, making it the smallest planet so far discovered by the WASP survey, and the exoplanet most similar in mass and radius to Saturn. The host star WASP-29 has an above-solar metallicity and fits a possible correlation for Saturn-mass planets such that planets with higher-metallicity host stars have higher core masses and thus smaller radii.

Key words: stars: individual (WASP-29) – planetary systems

Online-only material: color figures

1. INTRODUCTION

Searches for transiting exoplanets have now found more than 50 "hot Jupiters" with masses of ∼0.5–3 Jupiters. At much smaller masses there are several transiting "Neptunes" (GJ 436b, Gillon et al. 2007; HAT-P-11b, Bakos et al. 2010; & Kepler-4b, Borucki et al. 2010) and "super-Earths" (GJ1214b, Charbonneau et al. 2009; CoRoT-7b, Léger et al. 2009).

By 2009 there were only two known transiting planets of Saturn-mass (∼0.3 $M_{\rm Jup}$), namely, HD 149026b (Sato et al. 2005) and HAT-P-12b (Hartman et al. 2009). In 2010 this number is growing fast, with near simultaneous announcements of WASP-29b (this Letter), CoRoT-8b (Bordé et al. 2010), WASP-21b (Bouchy et al. 2010), and HAT-P-18b and HAT-P-19b (Hartman et al. 2010), giving rapidly increasing insight into planets of this mass range.

2. OBSERVATIONS

WASP-South is an array of cameras based on 11.1 cm, $f/1.8$ lenses which cover a total of 450 deg^2 of sky. The typical observing pattern tiles 30 s exposures of several fields with a cadence of 8 minutes, recording stars in the range $V = 8$–15. The WASP-South survey is described in Pollacco et al. (2006) while a discussion of our planet-hunting methods can be found in Collier Cameron et al. (2007a), Pollacco et al. (2008), and references therein.

WASP-29 is a $V = 11.3$, K4V star in the constellation Phoenix. It was observed by WASP-South from May to November in both 2006 and 2007, accumulating 9161 data points. These data show periodic transits with a 3.9 day period (Figure 1). There are no other significant sources within the 48″ extraction aperture (3.5 14″ pixels) to dilute the transit depth.

We used the CORALIE spectrograph on the Euler 1.2 m telescope at La Silla to obtain fourteen radial-velocity measurements over 2009 August–December (Table 1). These show that the transiting body is a Saturn-mass planet. On 2010 September 6, we obtained a transit light curve with Euler's CCD camera, using 20 s, *R*-band exposures, resulting in a mean error of 1.5 mmag (Figure 1).

The CORALIE radial-velocity measurements were combined with the Euler and WASP-South photometry in a simultaneous Markov chain Monte Carlo (MCMC) analysis to find the parameters of the WASP-29 system (Table 2). For details of our methods see Collier Cameron et al. (2007b) and Pollacco et al. (2008). For limb darkening, we used the four parameter non-linear law of Claret (2000) with parameters fixed to the values noted in Table 2. The eccentricity was a free parameter but the data are compatible with a circular orbit.

One departure from early WASP practice is the way we determine the stellar mass. The stellar effective temperature and metallicity are treated as jump parameters in the Markov chain, and controlled by Gaussian priors derived from their spectroscopically determined values and uncertainties. At each step in the chain the stellar density is determined from the transit duration and impact parameter. The stellar mass is then determined at each step as a polynomial function of $T_{\rm eff}$, [Fe/H], and $\log \rho/\rho_\odot$, as determined by Enoch et al. (2010a). This calibration is derived from the compilation of 40 stars in eclipsing binaries with well-determined masses, radii, effective temperatures, and metallicities, published by Torres et al. (2010).

3. WASP-29 STELLAR PARAMETERS

The 14 CORALIE spectra of WASP-29 were co-added to produce a spectrum with a typical S/N of 80:1, which we analyzed using the methods described in Gillon et al. (2009). We used the Hα line to determine the effective temperature ($T_{\rm eff}$), and the Na I D and Mg I b lines as diagnostics of the surface gravity ($\log g$). The parameters obtained are listed in Table 2. The elemental abundances were determined from equivalent-width measurements of several clean and unblended lines. A value for microturbulence ($\xi_{\rm t}$) was determined from Fe I using

The Astrophysical Journal Letters, 726:L19 (5pp), 2011 January 10 doi:10.1088/2041-8205/726/2/L19
© 2011. The American Astronomical Society. All rights reserved. Printed in the U.S.A.

WASP-30b: A 61 $M_{\rm Jup}$ BROWN DWARF TRANSITING A $V = 12$, F8 STAR

D. R. Anderson[1], A. Collier Cameron[2], C. Hellier[1], M. Lendl[3], P. F. L. Maxted[1], D. Pollacco[4], D. Queloz[3], B. Smalley[1], A. M. S. Smith[1], I. Todd[4], A. H. M. J. Triaud[3], R. G. West[5], S. C. C. Barros[4], B. Enoch[2], M. Gillon[6], T. A. Lister[7], F. Pepe[3], D. Ségransan[3], R. A. Street[7], and S. Udry[3]
[1] Astrophysics Group, Keele University, Staffordshire, ST5 5BG, UK; dra@astro.keele.ac.uk
[2] SUPA, School of Physics and Astronomy, University of St. Andrews, North Haugh, Fife, KY16 9SS, UK
[3] Observatoire de Genève, Université de Genève, 51 Chemin des Maillettes, 1290 Sauverny, Switzerland
[4] Astrophysics Research Centre, School of Mathematics & Physics, Queen's University, University Road, Belfast, BT7 1NN, UK
[5] Department of Physics and Astronomy, University of Leicester, Leicester, LE1 7RH, UK
[6] Institut d'Astrophysique et de Géophysique, Université de Liège, Allée du 6 Août, 17, Bat. B5C, Liège 1, Belgium
[7] Las Cumbres Observatory, 6740 Cortona Dr. Suite 102, Santa Barbara, CA 93117, USA
Received 2010 October 14; accepted 2010 November 30; published 2010 December 17

ABSTRACT

We report the discovery of a 61-Jupiter-mass brown dwarf (BD), which transits its F8V host star, WASP-30, every 4.16 days. From a range of age indicators we estimate the system age to be 1–2 Gyr. We derive a radius ($0.89 \pm 0.02\ R_{\rm Jup}$) for the companion that is consistent with that predicted ($0.914\ R_{\rm Jup}$) by a model of a 1 Gyr old, non-irradiated BD with a dusty atmosphere. The location of WASP-30b in the minimum of the mass–radius relation is consistent with the quantitative prediction of Chabrier & Baraffe, thus confirming the theory.

Key words: binaries: eclipsing – brown dwarfs – stars: individual (WASP-30)

Online-only material: color figures, machine-readable table

1. INTRODUCTION

A brown dwarf (BD) is traditionally defined as an object with a mass above the deuterium-burning limit ($13\ M_{\rm Jup}$; e.g., Chabrier et al. 2000a) and below the hydrogen-burning limit ($0.07\ M_{\odot}$; e.g., Chabrier et al. 2000b). However, an alternative suggestion is that the manner in which an object forms should determine whether it is a planet or a BD. Thus, if an object formed by core accretion of dust and ices in a protoplanetary disk then it would be a planet, and if it formed by gravoturbulent collapse of a molecular cloud, as do stars, then it would be a BD.

Studies such as the Caballero et al. (2007) observations of a young open cluster core find a continuous mass function down to $\sim 6\ M_{\rm Jup}$, indicating that the star formation mechanism can produce objects with planetary masses. This is supported by theoretical studies (Padoan & Nordlund 2004; Hennebelle & Chabrier 2008) which suggest that gravoturbulent fragmentation of molecular clouds produces stars and BDs down to a few Jupiter masses in numbers comparable to the observationally determined distribution. In contrast, when taking into account planetary migration through the protoplanetary disk, the core accretion process might result in giant planets with masses of up to $10\ M_{\rm Jup}$ (Alibert et al. 2005) or even $25\ M_{\rm Jup}$ (Mordasini et al. 2008). Sahlmann et al. (2010) see evidence for a bimodal distribution in BD masses, with the less-massive group presumably representing the high-mass tail of the planetary distribution.

An accurate, precise measurement of an object's radius is therefore required to probe for the existence of a core and thus discriminate between the two formation mechanisms. For example, the radius of the $8\ M_{\rm Jup}$ body, HAT-P-2b, is consistent with an irradiated planet incorporating a 340-Earth-mass core, but is smaller than if it were coreless (Leconte et al. 2009). The $22\ M_{\rm Jup}$ CoRoT-3b (Deleuil et al. 2008) is sufficiently massive to qualify as a BD under the traditional definition, but the radius of this object is uncertain at the 7% level. This is higher than the 3% required to discriminate between the absence or the presence of a core and thus determine how it formed (Leconte et al. 2009). Irwin et al. (2010) found a $\sim 30\ M_{\rm Jup}$ BD, NLTT 41135C, which transits one member of an M-dwarf binary system. However, as the transits are grazing, it is not currently possible to accurately measure its radius.

There is less ambiguity around the upper end of the BD mass regime: if a body is sufficiently massive to fuse hydrogen then it is a star, otherwise it is a BD. High-mass BDs with precise radius measurements are useful for testing BD evolution models, as it is in the high-mass regime that models predict the greatest changes in radius with age (e.g., Baraffe et al. 2003). Stassun et al. (2006) discovered a BD eclipsing binary system in the Orion Nebula star-forming region, with masses of $57 \pm 5\ M_{\rm Jup}$ and $36 \pm 3\ M_{\rm Jup}$. With very large radii of $0.699 \pm 0.034\ R_{\odot}$ and $0.511 \pm 0.026\ R_{\odot}$, it seems that these objects are in the earliest stages of gravitational contraction. Similar to the NLTT 41135 system, LHS 6343 C (Johnson et al. 2010; J. A. Johnson 2010, private communication) is a $63\ M_{\rm Jup}$ BD that transits one member of an M-dwarf binary system. In this case, the transits are full and so the radius ($0.825 \pm 0.023\ R_{\rm Jup}$) of this object is precisely determined. CoRoT-15b (Bouchy et al. 2010) is a $63\ M_{\rm Jup}$ mass BD in a 3 day orbit around an F7V star. Due to the faintness of the host star ($V \sim 16$), the BD radius ($1.12^{+0.30}_{-0.15}\ R_{\rm Jup}$) is not yet well determined.

To test and refine models of BD formation and evolution, a population of well-characterized objects is required. In this Letter, we present the discovery of WASP-30b, a $61\ M_{\rm Jup}$ BD that transits its moderately bright host star.

2. OBSERVATIONS

WASP-30 is a $V = 11.9$, F8V star located in Aquarius, on the border with Cetus. A transit search (Collier Cameron et al. 2006) of WASP-South data from 2008 July to November found a strong, 4.16 day periodicity. Further observations in 2009 with

A&A 531, A60 (2011)
DOI: 10.1051/0004-6361/201016208
© ESO 2011

Astronomy & Astrophysics

WASP-31b: a low-density planet transiting a metal-poor, late-F-type dwarf star⋆,⋆⋆

D. R. Anderson[1], A. Collier Cameron[2], C. Hellier[1], M. Lendl[3], T. A. Lister[4], P. F. L. Maxted[1], D. Queloz[3], B. Smalley[1], A. M. S. Smith[1], A. H. M. J. Triaud[3], R. G. West[5], D. J. A. Brown[2], M. Gillon[6], F. Pepe[3], D. Pollacco[7], D. Ségransan[3], R. A. Street[4], and S. Udry[3]

[1] Astrophysics Group, Keele University, Staffordshire ST5 5BG, UK
e-mail: dra@astro.keele.ac.uk
[2] SUPA, School of Physics and Astronomy, University of St. Andrews, North Haugh, Fife KY16 9SS, UK
[3] Observatoire de Genève, Université de Genève, 51 Chemin des Maillettes, 1290 Sauverny, Switzerland
[4] Las Cumbres Observatory, 6740 Cortona Dr. Suite 102, Santa Barbara, CA 93117, USA
[5] Department of Physics and Astronomy, University of Leicester, Leicester LE1 7RH, UK
[6] Institut d'Astrophysique et de Géophysique, Université de Liège, Allée du 6 Août 17, Bat. B5C, Liège 1, Belgium
[7] Astrophysics Research Centre, School of Mathematics & Physics, Queen's University, University Road, Belfast BT7 1NN, UK

Received 25 November 2010 / Accepted 18 May 2011

ABSTRACT

We report the discovery of the low-density, transiting giant planet WASP-31b. The planet is 0.48 Jupiter masses and 1.55 Jupiter radii. It is in a 3.4-day orbit around a metal-poor, late-F-type, $V = 11.7$ dwarf star, which is a member of a common proper motion pair. In terms of its low density, WASP-31b is second only to WASP-17b, which is a more highly irradiated planet of similar mass.

Key words. binaries: eclipsing – planetary systems – stars: individual: WASP-31

1. Introduction

To date, 107 transiting extrasolar planets have been discovered[1], the majority of which are gas giants in short orbits. The radii of a subset of these exoplanets are larger than predicted by standard models of irradiated gas giants (e.g., Burrows et al. 2007; Fortney et al. 2007), including TrES-4b (Mandushev et al. 2007; Sozzetti et al. 2009), WASP-12b (Hebb et al. 2009), and WASP-17b (Anderson et al. 2010, 2011b). A number of mechanisms have been proposed as potential solutions to the radius anomaly (see Fortney et al. 2010, for a review), each of which involves either injecting heat into the planet from an external source or slowing heat loss from the planet.

One such mechanism is the dissipation of energy within a planet as heat during the tidal circularisation of an eccentric orbit (Bodenheimer et al. 2001; Gu et al. 2003; Jackson et al. 2008; Ibgui & Burrows 2009). Such studies suggest that tidal heating may be sufficient to explain the large radii of even the most bloated exoplanets, though we would have to be observing some systems at very special times. A high heating rate, as suggested by Leconte et al. (2010), would mean most tidal energy is radiated away by the age typical of the very most bloated planets (a few Gyr) and so could not have played a significant role in their observed bloating. However, the current uncertainty in tidal theory allows for a wide range of heating rates (e.g. Ibgui et al. 2011). Though most studies have considered a transient phase of tidal heating, ongoing tidal heating (e.g. Ibgui et al. 2010) would occur if an additional companion continues to excite the orbital eccentricity of the bloated planet (e.g. Mardling 2007).

Burrows et al. (2007) proposed that enhanced opacities would retard the loss of internal heat and thus slow contraction of bloated planets. They suggested that enhanced opacities may arise due to the strong optical and UV irradiation of short-orbit, gas giants that could alter their atmospheres, producing thick hazes, absorbing clouds and non-equilibrium chemical species (e.g. tholins or polyacetylenes).

The bloated planets are all very strongly irradiated by their host stars, and a small fraction of stellar insolation energy would be sufficient to account for the observed degrees of bloating. Guillot & Showman (2002) suggested that the kinetic energy of strong winds, induced in the atmosphere by the large day-night temperature contrasts that result from tidal locking, may be transported downward and deposited as thermal energy in the deep interior. However, a mechanism to convert the kinetic energy into thermal energy would still be required. Li & Goodman (2010) and Youdin & Mitchell (2010) found that turbulence is efficient at dissipating kinetic energy. Magnetic drag on weakly ionized winds (Perna et al. 2010) and Ohmic heating (Batygin & Stevenson 2010) are alternative mechanisms. The non-bloated planets are also highly irradiated. Hence, such a mechanism would either have to act more efficiently on the bloated planets, or some other property must counteract its effect. One such possibility is the presence of a massive core.

⋆ Based in part on observations made with the HARPS spectrograph on the 3.6-m ESO telescope (proposal 085.C-0393) and with the CORALIE spectrograph and the Euler camera on the 1.2-m Euler Swiss telescope, both at the ESO La Silla Observatory, Chile.
⋆⋆ The photometric time-series and radial-velocity data used in this work are available at the CDS via anonymous ftp to cdsarc.u-strasbg.fr (130.79.128.5) or via http://cdsarc.u-strasbg.fr/viz-bin/qcat?J/A+A/531/A60
[1] 2010 Nov. 25, http://exoplanet.eu

PUBLICATIONS OF THE ASTRONOMICAL SOCIETY OF THE PACIFIC, **122**:1465–1470, 2010 December
© 2010. The Astronomical Society of the Pacific. All rights reserved. Printed in U.S.A.

WASP-32b: A Transiting Hot Jupiter Planet Orbiting a Lithium-Poor, Solar-Type Star

P. F. L. MAXTED,[1] D. R. ANDERSON,[1] A. COLLIER CAMERON,[2] M. GILLON,[3] C. HELLIER,[1] D. QUELOZ,[4]
B. SMALLEY,[1] A. H. M. J. TRIAUD,[4] R. G. WEST,[5] R. ENOCH,[2] T. A. LISTER,[6] F. PEPE,[4]
D. L. POLLACCO,[7] D. SÉGRANSAN,[4] I. SKILLEN,[8] AND S. UDRY[4]

Received 2010 July 19; accepted 2010 October 8; published 2010 November 3

ABSTRACT. We report the discovery of a transiting planet orbiting the star TYC 2-1155-1. The star, WASP-32, is a moderately bright ($V = 11.3$) solar-type star ($T_{\rm eff} = 6100 \pm 100$ K, $[{\rm Fe/H}] = -0.13 \pm 0.10$). The light curve of the star obtained with the WASP-South and WASP-North instruments shows periodic transitlike features with a depth of about 1% and a duration of 0.10 day every 2.72 days. The presence of a transitlike feature in the light curve is confirmed using z-band photometry obtained with Faulkes Telescope North. High-resolution spectroscopy obtained with the Coralie spectrograph confirms the presence of a planetary mass companion. From a combined analysis of the spectroscopic and photometric data, assuming that the star is a typical main-sequence star, we estimate that the planet has a mass $M_{\rm p}$ of $3.60 \pm 0.07\ M_{\rm Jup}$ and a radius $R_{\rm p} = 1.19 \pm 0.06\ R_{\rm Jup}$. WASP-32 is one of a small group of hot Jupiters with masses greater than $3\ M_{\rm Jup}$. We find that some stars with hot Jupiter companions and with masses $M_\star \approx 1.2\ M_\odot$, including WASP-32, are depleted in lithium and that the majority of these stars have lithium abundances similar to field stars.

1. INTRODUCTION

The Wide Angle Search for Planets (WASP) project (Pollacco et al. 2006) is currently one of the most successful wide-area surveys designed to find exoplanets transiting relatively bright stars. Other successful surveys include Hungarian-made Automated Telescope Network (HATnet; Bakos et al. 2004), XO (McCullough et al. 2005), and Trans-Atlantic Exoplanet Survey (TrES; O'Donovan et al. 2006). The Kepler satellite is now also starting to find many transiting exoplanets (Borucki et al. 2010). There is continued interest in finding transiting exoplanets, because they can be accurately characterized and studied in some detail; e.g., the mass and radius of the planet can be accurately measured. This gives us the opportunity to explore the relationships between the density of the planet and other properties of the planetary system: e.g., the semimajor axis, the composition and spectral type of the star, etc. Given the wide variety of transiting planets being discovered and the large number of parameters that characterize them, statistical studies will require a large sample of systems to identify and quantify the relationships between these parameters. These relationships can be used to test models of the formation, structure, and evolution of short-period exoplanets. Here, we report the discovery of a hot Jupiter companion to the star WASP-32 and show that this star is lithium-poor, compared with other stars of similar mass.

2. OBSERVATIONS

The two WASP instruments each consist of an array of eight cameras with Canon 200 mm f/1.8 lenses and 2048×2048 e2v CCD detectors providing images with a field of view of $7.8° \times 7.8°$ at an image scale of $13.7''\,{\rm pixel}^{-1}$ (Pollacco et al. 2006; Wilson et al. 2008). The star TYC 2-1155-1 ($=1$ SWASP J$001550.81 + 011201.5$) was observed 5906 times in one camera of the WASP-South instrument in Sutherland, South Africa, during the interval from 2008 June 30 to 2008 November 17. Our transit detection algorithm (Collier Cameron et al. 2007) identified a periodic feature with a depth of approximately 0.01 magnitudes recurring with a 2.72 day period in these data. The width and depth of the transit are consistent with the hypothesis that it is due to a planet with a radius of approximately $1\ R_{\rm Jup}$ orbiting a solar-type star. The proper motion and catalog photometry available for TYC 2-1155-1

[1] Astrophysics Group, Keele University, Staffordshire, ST5 5BG, UK.
[2] School of Physics and Astronomy, University of St. Andrews, North Haugh, Fife, KY16 9SS, UK.
[3] Institut d'Astrophysique et de Géophysique, Université de Liège, Allée du 6 Août, 17, Bat. B5C, Liège 1, Belgium.
[4] Observatoire de Genève, Université de Genève, 51 Chemin des Maillettes, 1290 Sauverny, Switzerland.
[5] Department of Physics and Astronomy, University of Leicester, Leicester, LE1 7RH, UK.
[6] Las Cumbres Observatory, 6740 Cortona Dr. Suite 102, Santa Barbara, CA 93117, USA
[7] Astrophysics Research Center, School of Mathematics & Physics, Queen's University, University Road, Belfast, BT7 1NN, UK.
[8] Isaac Newton Group of Telescopes, Apartado de Correos 321, E-38700 Santa Cruz de la Palma, Tenerife, Spain.

A&A 526, A130 (2011)
DOI: 10.1051/0004-6361/201015992
© ESO 2011

Astronomy & Astrophysics

WASP-34b: a near-grazing transiting sub-Jupiter-mass exoplanet in a hierarchical triple system⋆

B. Smalley[1], D. R. Anderson[1], A. Collier Cameron[2], C. Hellier[1], M. Lendl[3], P. F. L. Maxted[1], D. Queloz[3], A. H. M. J. Triaud[3], R. G. West[4], S. J. Bentley[1], B. Enoch[2], M. Gillon[5,3], T. A. Lister[6], F. Pepe[3], D. Pollacco[7], D. Segransan[3], A. M. S. Smith[1], J. Southworth[1], S. Udry[3], P. J. Wheatley[8], P. L. Wood[1], and J. Bento[8]

[1] Astrophysics Group, Keele University, Staffordshire, ST5 5BG, UK
e-mail: bs@astro.keele.ac.uk
[2] SUPA, School of Physics and Astronomy, University of St. Andrews, North Haugh, Fife, KY16 9SS, UK
[3] Observatoire de Genève, Université de Genève, 51 chemin des Maillettes, 1290 Sauverny, Switzerland
[4] Department of Physics and Astronomy, University of Leicester, Leicester, LE1 7RH, UK
[5] Institut d'Astrophysique et de Géophysique, Université de Liège, Allée du 6 Août, 17, Bât. B5C, Liège 1, Belgium
[6] Las Cumbres Observatory, 6740 Cortona Dr. Suite 102, Santa Barbara, CA 93117, USA
[7] Astrophysics Research Centre, School of Mathematics & Physics, Queen's University, University Road, Belfast, BT7 1NN, UK
[8] Department of Physics, University of Warwick, Coventry CV4 7AL, UK

Received 25 October 2010 / Accepted 9 December 2010

ABSTRACT

We report the discovery of WASP-34b, a sub-Jupiter-mass exoplanet transiting its 10.4-magnitude solar-type host star (1SWASP J110135.89-235138.4; TYC 6636-540-1) every 4.3177 days in a slightly eccentric orbit ($e = 0.038 \pm 0.012$). We find a planetary mass of $0.59 \pm 0.01\ M_{\rm Jup}$ and radius of $1.22^{+0.11}_{-0.08}\ R_{\rm Jup}$. There is a linear trend in the radial velocities of $55 \pm 4\ {\rm m\,s^{-1}\,y^{-1}}$ indicating the presence of a long-period third body in the system with a mass $\gtrsim 0.45\ M_{\rm Jup}$ at a distance of $\gtrsim 1.2$ AU from the host star. This third-body is either a low-mass star, a white dwarf, or another planet. The transit depth ($(R_{\rm P}/R_*)^2 = 0.0126$) and high impact parameter ($b = 0.90$) suggest that this could be the first known transiting exoplanet expected to undergo grazing transits, but with a confidence of only ~80%.

Key words. planets and satellites: general – stars: individual: WASP-34 – techniques: photometric – techniques: spectroscopic – techniques: radial velocities

1. Introduction

The majority of the known exoplanets have been discovered using the radial velocity technique (Mayor & Queloz 1995). In recent years, however, an ever increasing number have been discovered as a result of group-based and space-based transit search survey projects. Transiting exoplanets allow parameters such as the mass, radius, and density to be accurately determined, as well as their atmospheric properties to be studied during their transits and occultations (Charbonneau et al. 2005; Southworth 2009; Winn 2009).

The SuperWASP project has robotic observatories in the Canary Islands and South Africa. The wide angle survey is designed to find exoplanets around relatively bright stars in the V-magnitude range $9 \sim 13$. A detailed description of the SuperWASP project is given in Pollacco et al. (2006).

In this paper we report the discovery of WASP-34b, an exoplanet in orbit around its $V = 10.4$ mag. host star 1SWASP J110135.89-235138.4 in the constellation Crater. We present the WASP-South discovery photometry, together with Euler Telescope photometry and CORALIE radial velocity measurements.

⋆ Radial velocity and photometric data are only available in electronic form at the CDS via anonymous ftp to cdsarc.u-strasbg.fr (130.79.128.5) or via http://cdsarc.u-strasbg.fr/viz-bin/qcat?J/A+A/526/A130

2. Observations

2.1. WASP-South photometry

The host star WASP-34 (1SWASP J110135.89-235138.4; CD-23 9677; TYC 6636-540-1; GSC 06636-00540) was observed within two WASP-South camera fields during the periods 2006 May 4 to June 20 and 2007 January 4 to June 1, and in 3 fields during the period 2008 January 1 to May 28. A total of 35 351 data points were obtained. The pipeline-processed data were de-trended and searched for transits using the methods described in Collier Cameron et al. (2006), yielding a detection of a periodic, transit-like signature with a period of 4.3177 days and a depth of 0.011 mag (Fig. 1).

2.2. Spectroscopic observations with CORALIE

Spectroscopic observations were obtained with the CORALIE spectrograph on the Swiss 1.2 m telescope. The data were processed using the standard pipeline (Baranne et al. 1996; Queloz et al. 2000; Pepe et al. 2002). A total of 24 radial velocity (RV) and line bisector span ($V_{\rm span}$) measurements were made between 2009 December 1 and August 1 (Table 1). The bisector spans are a measure of the asymmetry of the cross-correlation function and, based on our experience, have standard errors of $\approx 2\sigma_{\rm RV}$.

The RV measurements show velocity variations with the same period as the transit light curve, but with a relatively

arXiv:1104.2827v1 [astro-ph.EP] 14 Apr 2011

WASP-35b, WASP-48b and WASP-51b: Two new planets and an independent discovery of HAT-P-30b.

B.Enoch[1], D.R.Anderson[2], S.C.C.Barros[3], D.J.A.Brown[1], A.Collier Cameron[1], F.Faedi[3], M.Gillon[4], G.Hébrard[5,6], T.A.Lister[7], D.Queloz[8], A.Santerne[9], B.Smalley[2], R.A.Street[7], A.H.M.J.Triaud[8], R.G.West[10], F.Bouchy[5,6], J.Bento[11], O.Butters[10], L.Fossati[12], C.A.Haswell[12], C.Hellier[2], S.Holmes[12], E.Jehen[4], M.Lendl[8], P.F.L.Maxted[2], J.McCormac[3], G.R.M.Miller[1], V.Moulds[3], C.Moutou[9], A.J.Norton[12], N.Parley[1], F.Pepe[8], D.Pollacco[3], D.Segransan[8], E.Simpson[3], I.Skillen[13], A.M.S.Smith[2], S.Udry[8] and P.J.Wheatley[11]

ABSTRACT

We report the detection of WASP-35b, a planet transiting a metal-poor ([Fe/H] = −0.15) star in the Southern hemisphere, WASP-48b, an inflated planet which may have spun-up its slightly evolved host star of $1.75R_{\odot}$ in the Northern hemisphere, and the independent discovery of HAT-P-30b / WASP-51b, a new planet in the Northern hemisphere. Using WASP, RISE, FTS and TRAPPIST photometry, with CORALIE, SOPHIE and NOT spectroscopy, we determine that WASP-35b has a mass of $0.72 \pm 0.06M_J$ and radius of $1.32 \pm 0.03R_J$, and orbits with a period of 3.16 days, WASP-48b has a mass of $0.98 \pm 0.09M_J$, radius of $1.67 \pm 0.08R_J$ and orbits in 2.14 days, while WASP-51b, with an orbital period of 2.81 days, is found to have a mass of $0.76 \pm 0.05M_J$ and radius of $1.42 \pm 0.04R_J$, agreeing with values of $0.71 \pm 0.03M_J$ and $1.34 \pm 0.07R_J$ reported for HAT-P-30b.

[1]SUPA, School of Physics and Astronomy, University of St. Andrews, North Haugh, St Andrews, KY16 9SS.

[2]Astrophysics Group, Keele University, Staffordshire, ST5 5BG, UK.

[3]Astrophysics Research Centre, School of Mathematics & Physics, Queen's University Belfast, University Road, Belfast, BT7 1NN, UK.

[4]Institut d'Astrophysique et de Géophysique, Université de Liége, Allée de 6 Août, 17, Bat B5C, Liége 1, Belgium.

[5]Institut d'Astrophysique de Paris, UMR7095 CNRS, Université Pierre & Marie Curie, France.

[6]Observatoire de Haute-Provence, CNRS/OAMP, 04870 St Michel l'Observatoire, France

[7]Las Cumbres Observatory, 6740 Cortona Drive Suite 102, Goleta, CA 93117, USA.

[8]Observatoire astronomique de l'Université de Genéve, 51 Chemin des Maillettes, 1290 Sauverny, Switzerland.

[9]Laboratoire d'Astrophysique de Marseille, Université d'Aix-Marseille & CNRS, 38 rue Frédéric Joliot-Curie, 13388 Marseille cedex 13, France

[10]Department of Physics and Astronomy, University of Leicester, Leicester, LE1 7RH, UK.

[11]Department of Physics, University of Warwick, Coventry, CV4 7AL, UK

[12]Department of Physics and Astronomy, The Open University, Milton Keynes, MK7 6AA, UK

[13]Isaac Newton Group of Telescopes, Apartado de Correos 321, E-38700 Santa Cruz de Palma, Spain

The Astronomical Journal, 141:8 (7pp), 2011 January doi:10.1088/0004-6256/141/1/8
© 2011. The American Astronomical Society. All rights reserved. Printed in the U.S.A.

WASP-37b: A 1.8 M_J EXOPLANET TRANSITING A METAL-POOR STAR

E. K. Simpson[1], F. Faedi[1], S. C. C. Barros[1], D. J. A. Brown[2], A. Collier Cameron[2], L. Hebb[3], D. Pollacco[1], B. Smalley[4], I. Todd[1], O. W. Butters[5], G. Hébrard[6], J. McCormac[1], G. R. M. Miller[2], A. Santerne[7], R. A. Street[8], I. Skillen[9], A. H. M. J. Triaud[10], D. R. Anderson[4], J. Bento[11], I. Boisse[6], F. Bouchy[6,12], B. Enoch[2], C. A. Haswell[13], C. Hellier[4], S. Holmes[13], K. Horne[2], F. P. Keenan[1], T. A. Lister[8], P. F. L. Maxted[4], V. Moulds[1], C. Moutou[7], A. J. Norton[13], N. Parley[2], F. Pepe[10], D. Queloz[10], D. Segransan[10], A. M. S. Smith[4], H. C. Stempels[14], S. Udry[10], C. A. Watson[1], R. G. West[5], and P. J. Wheatley[11]

[1] Astrophysics Research Centre, School of Mathematics and Physics, Queen's University, Belfast BT7 1NN, UK
[2] School of Physics and Astronomy, University of St Andrews, North Haugh, St Andrews, Fife KY16 9SS, UK
[3] Department of Physics and Astronomy, Vanderbilt University, Nashville, TN 37235, USA
[4] Astrophysics Group, Keele University, Staffordshire ST5 5BG, UK
[5] Department of Physics and Astronomy, University of Leicester, Leicester LE1 7RH, UK
[6] Institut d'Astrophysique de Paris, UMR7095 CNRS, Université Pierre & Marie Curie, F-75014 Paris, France
[7] Laboratoire d'Astrophysique de Marseille, 38 rue Frédéric Joliot-Curie, F-13388 Marseille cedex 13, France
[8] Las Cumbres Observatory Global Telescope Network, 6740 Cortona Drive Suite 102, Goleta, CA 93117, USA
[9] Isaac Newton Group of Telescopes, Apartado de Correos 321, E-38700 Santa Cruz de la Palma, Tenerife, Spain
[10] Observatoire de Genève, Université de Genève, 51 Ch. des Maillettes, CH-1290 Sauverny, Switzerland
[11] Department of Physics, University of Warwick, Coventry CV4 7AL, UK
[12] Observatoire de Haute-Provence, CNRS/OAMP, F-04870 St Michel l'Observatoire, France
[13] Department of Physics and Astronomy, The Open University, Milton Keynes MK7 6AA, UK
[14] Department of Physics and Astronomy, Uppsala University, Box 516, SE-751 20 Uppsala, Sweden
Received 2010 August 17; accepted 2010 September 30; published 2010 December 7

ABSTRACT

We report on the discovery of WASP-37b, a transiting hot Jupiter orbiting an $m_v = 12.7$ G2-type dwarf, with a period of 3.577469 ± 0.000011 d, transit epoch $T_0 = 2455338.6188 \pm 0.0006$ (HJD; dates throughout the paper are given in Coordinated Universal Time (UTC)), and a transit duration $0.1304^{+0.0018}_{-0.0017}$ d. The planetary companion has a mass $M_p = 1.80 \pm 0.17\ M_J$ and radius $R_p = 1.16^{+0.07}_{-0.06}\ R_J$, yielding a mean density of $1.15^{+0.12}_{-0.15}\ \rho_J$. From a spectral analysis, we find that the host star has $M_\star = 0.925 \pm 0.120\ M_\odot$, $R_\star = 1.003 \pm 0.053\ R_\odot$, $T_{\rm eff} = 5800 \pm 150$ K, and [Fe/H] $= -0.40 \pm 0.12$. WASP-37 is therefore one of the lowest metallicity stars to host a transiting planet.

Key words: planetary systems – stars: individual (WASP-37, GSC 00326-00658) – techniques: photometric – techniques: spectroscopic

1. INTRODUCTION

Extrasolar planets show a huge diversity in their properties and this has important implications for theories of planet formation, structure, and evolution. Systems with high orbital inclinations, in which the planet transits across the face of the host star as seen from Earth, are extremely valuable as they allow us to precisely measure many fundamental planetary properties, including radius, mass, and density, which can be used to test these theories (Haswell 2010).

The parameter space which we are able to explore with transiting planets is biased by instrumental and observational limitations. However, many challenges faced by the current surveys are being overcome by the ability to decrease systematic noise and optimize follow-up strategies. Although the majority of the ~100 transiting planets thus far discovered are short-period, Jupiter-sized objects, they show a remarkable variety in their physical and dynamical characteristics, such as the extreme eccentricity of HD 80606b (Naef et al. 2001; Laughlin et al. 2009; Moutou et al. 2009; Fossey et al. 2009; Garcia-Melendo & McCullough 2009), the ultra-short period of WASP-19b (Hebb et al. 2010), and the puzzlingly low densities of WASP-17b (Anderson et al. 2010) and Kepler-7b (Latham et al. 2010).

Here we describe the properties of a new transiting planet discovered by the SuperWASP survey, WASP-37b. SuperWASP has been a major contributor to the discovery of bright ($9 < m_v < 13$) transiting planets since it began operation in 2004 (Pollacco et al. 2006). The project runs two stations, SuperWASP on La Palma, Canary Islands, and WASP-S at SAAO in South Africa, each with a field of view of almost 500 deg^2. A number of recent upgrades have been implemented to reduce systematic noise and improve photometric precision. These include reducing temperature fluctuations, which cause changes in the camera focus, by installing heating tubes, air conditioning, and improving dome insulation. As a consequence, the variation in the stellar FWHM during the course of a night has been halved. For more details, see Barros (2010).

The planet host star WASP-37 resides in an equatorial region of the sky which is monitored by both WASP instruments, significantly increasing the amount of data collected on the target. It is accessible to observatories in both hemispheres and we present follow-up photometric and spectroscopic observations taken to establish the planetary nature of the transiting object and characterize it using the RISE (Liverpool Telescope), Spectral (Faulkes Telescope South), SOPHIE (1.93 m OHP), and CORALIE (Swiss 1.2 m) instruments.

This paper is structured as follows: Section 2 describes the observations, including the discovery data and photometric and spectroscopic follow-up. The results of the derived system parameters are presented in Section 3, including the stellar and planetary properties. Finally, we discuss our findings in Section 4.

A&A 525, A54 (2011)
DOI: 10.1051/0004-6361/201015800
© ESO 2010

Astronomy & Astrophysics

WASP-38b: a transiting exoplanet in an eccentric, 6.87d period orbit⋆

S. C. C. Barros[1], F. Faedi[1], A. Collier Cameron[2], T. A. Lister[3], J. McCormac[1], D. Pollacco[1], E. K. Simpson[1], B. Smalley[4], R. A. Street[3], I. Todd[1], A. H. M. J. Triaud[5], I. Boisse[6], F. Bouchy[6,7], G. Hébrard[6,7], C. Moutou[8], F. Pepe[6], D. Queloz[6], A. Santerne[8], D. Segransan[6], S. Udry[6], J. Bento[9], O. W. Butters[10], B. Enoch[2], C. A. Haswell[11], C. Hellier[4], F. P. Keenan[1], G. R. M. Miller[2], V. Moulds[1], A. J. Norton[11], N. Parley[2], I. Skillen[12], C. A. Watson[1], R. G. West[10], and P. J. Wheatley[9]

[1] Astrophysics Research Centre, School of Mathematics & Physics, Queen's University Belfast, University Road, Belfast, BT7 1NN, UK
e-mail: s.barros@qub.ac.uk
[2] SUPA, School of Physics & Astronomy, University of St Andrews, North Haugh, St Andrews KY16 9SS, UK
[3] Las Cumbres Observatory, 6740 Cortona Drive Suite 102, Goleta, CA 93117, USA
[4] Astrophysics Group, Keele University, Staffordshire, ST5 5BG, UK
[5] Observatoire de Geneve, Université de Geneve, 51 Ch. des Maillettes, 1290 Sauverny, Switzerland
[6] Institut d'Astrophysique de Paris, UMR7095 CNRS, Université Pierre & Marie Curie, 75014 Paris, France
[7] Observatoire de Haute-Provence, CNRS/OAMP, 04870 Saint-Michel l'Observatoire, France
[8] Laboratoire d'Astrophysique de Marseille, Université d'Aix-Marseille & CNRS, 38 rue Frédéric Joliot-Curie, 13388 Marseille Cedex 13, France
[9] Department of Physics, University of Warwick, Coventry CV4 7AL, UK
[10] Department of Physics and Astronomy, University of Leicester, Leicester LE1 7RH, UK
[11] Department of Physics and Astronomy, The Open University, Milton Keynes MK7 6AA, UK
[12] Isaac Newton Group of Telescopes, Apartado de Correos 321, 38700 Santa Cruz de la Palma, Tenerife, Spain

Received 21 September 2010 / Accepted 21 October 2010

ABSTRACT

Aims. We report the discovery of WASP-38b, a long period transiting planet in an eccentric 6.871815 day orbit. The transit epoch is 2 455 335.92050 ± 0.00074 (HJD) and the transit duration is 4.663 h.
Methods. WASP-38b's discovery was enabled due to an upgrade to the SuperWASP-North cameras. We performed a spectral analysis of the host star HD 146389/BD+10 2980 that yielded $T_{\rm eff}$ = 6150 ± 80 K, $\log g$ = 4.3 ± 0.1, $v \sin i$ = 8.6 ± 0.4 km s^{-1}, M_* = 1.16 ± 0.04 $M_\odot$ and R_* = 1.33 ± 0.03 $R_\odot$, consistent with a dwarf of spectral type F8. Assuming a main-sequence mass-radius relation for the star, we fitted simultaneously the radial velocity variations and the transit light curves to estimate the orbital and planetary parameters.
Results. The planet has a mass of 2.69 ± 0.06 $M_{\rm Jup}$ and a radius of 1.09 ± 0.03 $R_{\rm Jup}$ giving a density, $\rho_{\rm p}$ = 2.1 ± 0.1 $\rho_{\rm J}$. The high precision of the eccentricity e = 0.0314 ± 0.0044 is due to the relative transit timing from the light curves and the RV shape. The planet equilibrium temperature is estimated at 1292 ± 33 K. WASP-38b is the longest period planet found by SuperWASP-North and with a bright host star (V = 9.4 mag), is a good candidate for followup atmospheric studies.

Key words. planets and satellites: detection – stars: individual: WASP-38 – techniques: photometric – techniques: radial velocities

1. Introduction

Transiting planets are important because the geometry of these systems gives us a wealth of information. Photometry during transit allows us to derive the inclination of the orbit and the radii of both the host star and planet. Combining this information with radial velocity variations allows us to derive the absolute mass of the planet and, hence, the density. Even just an estimation of the bulk density gives us an insight into the composition of the planet (Guillot 2005; Fortney et al. 2007) and can be used to put constraints on planetary structure and formation models. These systems also offer a potential for measuring planetary emission spectra through occultation observations (e.g. Charbonneau et al. 2008) and we can gain an insight into the composition of planetary atmospheres using transit spectroscopy (Charbonneau et al. 2002; Vidal-Madjar et al. 2003; Swain et al. 2009).

For these reasons, there are several ground-based surveys searching for transiting exoplanets, such as HATNet (Bakos et al. 2004), TrES (Alonso et al. 2004), XO (McCullough et al. 2005) and WASP (Pollacco et al. 2006). Currently, there are also two space-based surveys: CoRoT (Baglin et al. 2006) and Kepler (Borucki et al. 2010). WASP is the most prolific of these surveys having discovered 38 of the 106 known transiting exoplanets. The WASP project consists of two robotic observatories: one in the Observatorio del Roque de los Muchachos, La Palma, Canary Islands, Spain and the other in the South African Astronomical Observatory of Sutherland, South Africa.

In this paper, we report the discovery of WASP-38b, an eccentric giant planet in a 6.87 day orbit. The candidate was identified in February 2010 in SuperWASP-North data. Radial velocity followup started at the end of March with *FIES* (2.6 m NOT).

⋆ Photometry and RV data are only available in electronic form at the CDS via anonymous ftp to cdsarc.u-strasbg.fr (130.79.128.5) or via http://cdsarc.u-strasbg.fr/viz-bin/qcat?J/A+A/525/A54

A&A 531, A40 (2011)
DOI: 10.1051/0004-6361/201116671
© ESO 2011

Astronomy & Astrophysics

WASP-39b: a highly inflated Saturn-mass planet orbiting a late G-type star⋆

F. Faedi[1], S. C. C. Barros[1], D. R. Anderson[2], D. J. A. Brown[3], A. Collier Cameron[3], D. Pollacco[1], I. Boisse[4,5], G. Hébrard[4,6], M. Lendl[7], T. A. Lister[8], B. Smalley[2], R. A. Street[8], A. H. M. J. Triaud[7], J. Bento[9], F. Bouchy[4,6], O. W. Butters[10], B. Enoch[3], C. A. Haswell[11], C. Hellier[2], F. P. Keenan[1], G. R. M. Miller[3], V. Moulds[1], C. Moutou[12], A. J. Norton[11], D. Queloz[7], A. Santerne[4,6], E. K. Simpson[1], I. Skillen[13], A. M. S. Smith[2], S. Udry[7], C. A. Watson[1], R. G. West[10], and P. J. Wheatley[9]

[1] Astrophysics Research Centre, School of Mathematics and Physics, Queen's University Belfast, University Road, Belfast BT7 1NN, UK
e-mail: f.faedi@qub.ac.uk
[2] Astrophysics Group, Keele University, Staffordshire, ST5 5BG, UK
[3] School of Physics and Astronomy, University of St Andrews, St Andrews, Fife KY16 9SS, UK
[4] Institut d'Astrophysique de Paris, UMR 7095 CNRS, Université Pierre & Marie Curie, France
[5] Centro de Astrofísica, Universidade do Porto, Rua das Estrelas, 4150-762 Porto, Portugal
[6] Observatoire de Haute-Provence, CNRS/OAMP, 04870 St Michel l'Observatoire, France
[7] Observatoire astronomique de l'Université de Genève, 51 Ch. des Maillettes, 1290 Sauverny, Switzerland
[8] Las Cumbres Observatory Global Telescope Network, 6740 Cortona Drive Suite 102, CA 93117, USA
[9] Department of Physics, University of Warwick, Coventry CV4 7AL, UK
[10] Department of Physics and Astronomy, University of Leicester, Leicester, LE1 7RH, UK
[11] Department of Physics and Astronomy, The Open University, Milton Keynes, MK7 6AA, UK
[12] Laboratoire d'Astrophysique de Marseille, 38 rue Frédéric Joliot-Curie, 13388 Marseille Cedex 13, France
[13] Isaac Newton Group of Telescopes, Apartado de Correos 321, 38700 Santa Cruz de Palma, Spain

Received 7 February 2011 / Accepted 21 April 2011

ABSTRACT

We present the discovery of WASP-39b, a highly inflated transiting Saturn-mass planet orbiting a late G-type dwarf star with a period of 4.055259 ± 0.000008 d, Transit Epoch T_0 = 2 455 342.9688 ± 0.0002 (HJD), of duration 0.1168 ± 0.0008 d. A combined analysis of the WASP photometry, high-precision follow-up transit photometry, and radial velocities yield a planetary mass of $M_{\rm pl}$ = 0.28 ± 0.03 $M_{\rm J}$ and a radius of $R_{\rm pl}$ = 1.27 ± 0.04 $R_{\rm J}$, resulting in a mean density of 0.14 ± 0.02 $\rho_{\rm J}$. The stellar parameters are mass $M_\star$ = 0.93 ± 0.03 $M_\odot$, radius $R_\star$ = 0.895 ± 0.23 $R_\odot$, and age 9^{+3}_{-4} Gyr. Only WASP-17b and WASP-31b have lower densities than WASP-39b, although they are slightly more massive and highly irradiated planets. From our spectral analysis, the metallicity of WASP-39 is measured to be [Fe/H] = −0.12 ± 0.1 dex, and we find the planet to have an equilibrium temperature of 1116^{+33}_{-32} K. Both values strengthen the observed empirical correlation between these parameters and the planetary radius for the known transiting Saturn-mass planets.

Key words. stars: individual: WASP-39 – techniques: photometric – techniques: radial velocities – planetary systems

1. Introduction

The importance of transiting extrasolar planets is related to their geometrical configuration (Sackett 1999). Transit geometry severely constrains the orbital inclination of the planet, allowing accurate measurements of its mass and radius to be derived. The inferred planet's density provides information on the system's bulk physical properties, and thus is a fundamental parameter for constraining theoretical models of planetary formation, structure, and evolution (e.g. Guillot 2005; Fortney et al. 2007; Liu et al. 2008).

To date, more than 100 transiting planets have been discovered, which show a huge range of diversity in their physical and dynamical properties. For example, their mass ranges from ~5 $M_\oplus$ (Kepler-10b, Batalha et al. 2011) to about 12 $M_{\rm J}$ (XO-3b, Johns-Krull et al. 2008; Hébrard et al. 2008). Some planets have radii that agree with models of irradiated planets (Burrows et al. 2007; Fortney et al. 2007), while others are found to be anomalously large (e.g. WASP-12b, Hebb et al. 2009, and TrES-4b, Southworth 2010; Torres et al. 2008; Mandushev et al. 2007). The diversity in exoplanet densities, hence in their internal compositions, is particularly noticeable at sub-Jupiter masses. For example, some exoplanets have very high densities and are thought to have a rocky/ice core (e.g. HD 149026b, $\rho_{\rm pl} \simeq 1\,\rho_{\rm J}$, Sato et al. 2005), while systems such as TrES-4b ($\rho_{\rm pl} = 0.17\,\rho_{\rm J}$, Mandushev et al. 2007), WASP-17b ($\rho_{\rm pl} = 0.06\,\rho_{\rm J}$, Anderson et al. 2010b, 2011b), WASP-31b ($\rho_{\rm pl} = 0.132\ \rho_{\rm J}$, Anderson et al. 2010a), and Kepler-7b ($\rho_{\rm pl} = 0.13\ \rho_{\rm J}$, Latham et al. 2010) are examples of planets with puzzlingly low densities that challenge standard evolutionary theories in reproducing their radii (Fortney et al. 2007; Burrows et al. 2007). To assess the inflation status of a system, generally planetary radii are compared to

⋆ Spectroscopic and photometric data are only available at the CDS via anonymous ftp to
cdsarc.u-strasbg.fr (130.79.128.5) or via
http://cdsarc.u-strasbg.fr/viz-bin/qcat?J/A+A/531/A40

PUBLICATIONS OF THE ASTRONOMICAL SOCIETY OF THE PACIFIC, **123**:555–560, 2011 May
© 2011. The Astronomical Society of the Pacific. All rights reserved. Printed in U.S.A.

WASP-40b: Independent Discovery of the 0.6 $M_{\rm Jup}$ Transiting Exoplanet HAT-P-27b

D. R. ANDERSON,[1] S. C. C. BARROS,[2] I. BOISSE,[3,4] F. BOUCHY,[3,5] A. COLLIER CAMERON,[6] F. FAEDI,[2] G. HEBRARD,[3,5] C. HELLIER,[1] M. LENDL,[7] C. MOUTOU,[8] D. POLLACCO,[2] A. SANTERNE,[8] B. SMALLEY,[1] A. M. S. SMITH,[1] I. TODD,[2] A. H. M. J. TRIAUD,[7] R. G. WEST,[9] P. J. WHEATLEY,[10] J. BENTO,[10] B. ENOCH,[6] M. GILLON,[11] P. F. L. MAXTED,[1] J. MCCORMAC,[2] D. QUELOZ,[7] E. K. SIMPSON,[2] AND I. SKILLEN[12]

Received 2011 January 24; accepted 2011 March 21; published 2011 April 13

ABSTRACT. From WASP photometry and SOPHIE radial velocities we report the discovery of WASP-40b (HAT-P-27b), a $0.6\ M_{\rm Jup}$ planet that transits its 12th magnitude host star every 3.04 days. The host star is of late G-type or early K-type and likely has a metallicity greater than solar ($[{\rm Fe/H}] = 0.14 \pm 0.11$). The planet's mass and radius are typical of the known hot Jupiters, thus adding another system to the apparent pileup of transiting planets with periods near 3–4 days. Our parameters match those of the recent HATnet announcement of the same planet, thus giving confidence in the techniques used. We report a possible indication of stellar activity in the host star.

Online material: color figures

1. INTRODUCTION

While the Kepler mission is currently producing the most candidates for transiting extrasolar planets (e.g., Borucki et al. 2010), the ground-based transit-search programs continue to find more planets around stars at brighter magnitudes than those found in the space missions. Of these, Hungarian Automated Telescope Network (HATnet; Bakos et al. 2004) and Wide Angle Search for Planets (WASP; Pollacco et al. 2006) have been the most successful. Both projects are based on arrays of 200 mm f/1.8 lenses backed by CCDs, with the biggest difference being that HATnet operates at several longitudes, while WASP consists of one station in each hemisphere. The two projects look at overlapping regions of sky, which has led to some near-simultaneous discoveries, such as the planet WASP-11b (West et al. 2009) also being HAT-P-10b (Bakos et al. 2009). Reporting of such independent discoveries gives important information on the reliability of the respective techniques and on the completeness of the transit surveys.

Recently, HATnet announced the planet HAT-P-27b (Béky et al. 2011), a hot Jupiter in a 3 day orbit around a $m_V = 12.2$ star. This planet had been independently discovered by the WASP project and assigned the name WASP-40b (Hellier et al. 2011). We report here on the discovery of WASP-40b made using data from SuperWASP-North and WASP-South combined, together with radial velocities from the SOPHIE spectrograph at the Observatoire de Haute-Provence (OHP) observatory.

2. OBSERVATIONS

We observed WASP-40, an ~K0-type star located in Virgo, with the SuperWASP-North and WASP-South cameras during the three seasons of 2008–2010. A transit search (Collier Cameron et al. 2006) of the resulting 30,260 photometric measurements found a strong 3.04 day periodicity. The discovery light curve is displayed in Figure 1a, folded on this period.

Using the SOPHIE spectrograph mounted on the 1.93 m OHP telescope (Perruchot et al. 2008; Bouchy et al. 2009), we obtained eight spectra of WASP-40 during 2010 April and May. The high-efficiency mode and slow readout were

[1] Astrophysics Group, Keele University, Staffordshire, ST5 5BG, UK; dra@astro.keele.ac.uk.
[2] Astrophysics Research Centre, School of Mathematics & Physics, Queen's University, University Road, Belfast, BT7 1NN, UK.
[3] Institut d'Astrophysique de Paris, UMR7095 CNRS, Universite Pierre & Marie Curie, 75014 Paris, France.
[4] Centro de Astrofísica, Universidade do Porto, Rua das Estrelas, 4150-762 Porto, Portugal.
[5] Observatoire de Haute-Provence, CNRS/OAMP, 04870 Saint-Michel l'Observatoire, France.
[6] SUPA, School of Physics and Astronomy, University of St. Andrews, North Haugh, Fife, KY16 9SS, UK.
[7] Observatoire Astronomique de l'Université de Genève 51 ch. des Maillettes, 1290 Sauverny, Switzerland.
[8] Laboratoire d'Astrophysique de Marseille, 38 rue Fréderic Joliot-Curie, 13388 Marseille Cedex 13, France.
[9] Department of Physics and Astronomy, University of Leicester, Leicester, LE1 7RH, UK.
[10] Department of Physics, University of Warwick, Coventry CV4 7AL, UK.
[11] Institut d'Astrophysique et de Géophysique, Université de Liège, Allée du 6 Août, 17, Bat. B5C, Liège 1, Belgium.
[12] Isaac Newton Group of Telescopes, Apartado de Correos 321, E-38700 Santa Cruz de la Palma, Tenerife, Spain.

PUBLICATIONS OF THE ASTRONOMICAL SOCIETY OF THE PACIFIC, **123**:547–554, 2011 May
© 2011. The Astronomical Society of the Pacific. All rights reserved. Printed in U.S.A.

WASP-41b: A Transiting Hot Jupiter Planet Orbiting a Magnetically Active G8V Star

P. F. L. MAXTED,[1] D. R. ANDERSON,[1] A. COLLIER CAMERON,[2] C. HELLIER,[1] D. QUELOZ,[3] B. SMALLEY,[1]
R. A. STREET,[4] A. H. M. J. TRIAUD,[3] R. G. WEST,[5] M. GILLON,[6] T. A. LISTER,[4] F. PEPE,[3]
D. POLLACCO,[7] D. SÉGRANSAN,[3] A. M. S. SMITH,[1] AND S. UDRY[3]

Received 2010 December 6; accepted 2011 March 3; published 2011 April 19

ABSTRACT. We report the discovery of a transiting planet with an orbital period of 3.05 days orbiting the star TYC 7247-587-1. The star, WASP-41, is a moderately bright G8 V star ($V = 11.6$) with a metallicity close to solar ($[\mathrm{Fe/H}] = -0.08 \pm 0.09$). The star shows evidence of moderate chromospheric activity, both from emission in the cores of the Ca II H and K ines and photometric variability with a period of 18.4 days and an amplitude of about 1%. We use a new method to show quantitatively that this periodic signal has a low false-alarm probability. The rotation period of the star implies a gyrochronological age for WASP-41 of 1.8 Gyr with an error of about 15%. We have used a combined analysis of the available photometric and spectroscopic data to derive the mass and radius of the planet ($0.92 \pm 0.06\ M_{\mathrm{Jup}}$, $1.20 \pm 0.06\ R_{\mathrm{Jup}}$). Further observations of WASP-41 can be used to explore the connections between the properties of hot Jupiter planets and the level of chromospheric activity in their host stars.

1. INTRODUCTION

There is continued interest in finding bright stars that host transiting exoplanets, because they can be accurately characterized and studied in some detail; e.g., the mass and radius of the planet can be accurately measured. This gives us the opportunity to explore the relationships between the properties of the planet and its host star: e.g., the orbital eccentricity, the composition and spectral type of the star, the age of the system, etc. Given the wide variety of transiting planets being discovered and the large number of parameters that characterize them, statistical studies will require a large sample of systems to identify and quantify the relationships between these parameters. These relationships can be used to test models of the formation, structure, and evolution of short-period exoplanets.

Here, we report the discovery by the Wide Angle Search for Planets (WASP) survey of a planetary mass companion to the star TYC 7247-587-1. We find that the star is a G8 V star showing moderate chromospheric activity. The planet, WASP-41b, is a typical hot Jupiter planet with an orbital period of 3.05 days.

[1] Astrophysics Group, Keele University, Staffordshire, ST5 5BG, UK.
[2] SUPA, School of Physics and Astronomy, University of St. Andrews, North Haugh, Fife, KY16 9SS, UK.
[3] Observatoire astronomique de l'Université de Genève 51 ch. des Maillettes, 1290 Sauverny, Switzerland.
[4] Las Cumbres Observatory, 6740 Cortona Dr. Suite 102, Santa Barbara, CA 93117, USA.
[5] Department of Physics and Astronomy, University of Leicester, Leicester, LE1 7RH, UK.
[6] Institut d'Astrophysique et de Géophysique, Université de Liège, Allée du 6 Août, 17, Bat. B5C, Liège 1, Belgium.
[7] Astrophysics Research Centre, School of Mathematics & Physics, Queen's University, University Road, Belfast, BT7 1NN, UK.

2. OBSERVATIONS

The WASP survey is described in Pollacco et al. (2006) and Wilson et al. (2008), while a discussion of our candidate selection methods can be found in Collier Cameron et al. (2007), Pollacco et al. (2008), and references therein.

The star TYC 7247-587-1 (WASP-41, 1SWASP J124228 .50-303823.5) was observed 6767 times by one camera on the WASP-South instrument from 2007 January 20 to 2007 June 22. A further 5637 observations were obtained with the same camera from 2008 January 17 to 2008 May 28.

The WASP-South light curves of WASP-41 show transitlike features, with a depth of approximately 0.02 mag recurring with a 3.05 day period (Fig. 1). These were independently detected in the WASP-South photometry from the two seasons using the detrending and transit detection methods described in Collier Cameron et al. (2007), which was taken as good evidence that the periodic transit signal was real. The spectral type of the star was estimated to be approximately G8, based on the catalog photometry available for this star at the time. The duration and depth of the transit are consistent with the hypothesis that they are due to the transit of a planetlike companion to a main-sequence G8 star, and the WASP-South light curves show no indication of any ellipsoidal variation due to the distortion of the star by a massive companion.

We obtained 22 radial velocity measurements during the interval of 2010 January 3 to 2010 August 5 with the fiber-fed

Astronomy & Astrophysics manuscript no. w43
April 15, 2011
© ESO 2011

L E

WASP-43b: The closest-orbiting hot Jupiter

Coel Hellier[1], D.R. Anderson[1], A. Collier Cameron[2], M. Gillon[3], E. Jehin[3], M. Lendl[4], P.F.L. Maxted[1], F. Pepe[4], D. Pollacco[5], D. Queloz[4], D. Ségransan[4], B. Smalley[1], A.M.S. Smith[1], J. Southworth[1], A.H.M.J. Triaud[4], S. Udry[4] & R.G. West[6]

[1] Astrophysics Group, Keele University, Staffordshire, ST5 5BG, UK
[2] SUPA, School of Physics and Astronomy, University of St. Andrews, North Haugh, Fife, KY16 9SS, UK
[3] Institut d'Astrophysique et de Géophysique, Université de Liège, Allée du 6 Août, 17, Bat. B5C, Liège 1, Belgium
[4] Observatoire astronomique de l'Université de Genève 51 ch. des Maillettes, 1290 Sauverny, Switzerland
[5] Astrophysics Research Centre, School of Mathematics & Physics, Queen's University, University Road, Belfast, BT7 1NN, UK
[6] Department of Physics and Astronomy, University of Leicester, Leicester, LE1 7RH, UK

Preprint online version: April 15, 2011

arXiv:1104.2823v1 [astro-ph.EP] 14 Apr 2011

ABSTRACT

We report the discovery of WASP-43b, a hot Jupiter transiting a K7V star every 0.81 d. At 0.6-$M_\odot$ the host star has the lowest mass of any star hosting a hot Jupiter. It also shows a 15.6-d rotation period. The planet has a mass of 1.8 M_{Jup}, a radius of 0.9 R_{Jup}, and with a semi-major axis of only 0.014 AU has the smallest orbital distance of any known hot Jupiter. The discovery of such a planet around a K7V star shows that planets with apparently small remaining lifetimes owing to tidal decay of the orbit are also found around stars with deep convection zones.

Key words. stars: individual (WASP-43) — planetary systems

1. Introduction

As planet discoveries increase we begin to see patterns in their distribution, and to find the rarer systems that mark the edges of the envelope. The ground-based transit searches such as WASP (Pollacco et al. 2006) and HAT (Bakos et al. 2002) are particularly suitable for finding the systems that delineate the cut-off of hot Jupiters as orbital radius decreases. This distribution is expected to tell us about several processes, including disk migration and possible 'stopping mechanisms' (e.g. Matsumura, Pudritz & Thommes 2007), third-body processes, such as scattering and the Kozai mechanism, that can move planets onto eccentric orbits that circularize at short periods (e.g. Guillochon et al. 2010), and the effect of tidal interactions with the host star (e.g. Matsumura, Peale & Rasio 2010).

The WASP-South camera array has been monitoring stars of magnitude 9–13 since 2006, and, in conjunction with radial-velocities from the Euler/CORALIE spectrograph, is now responsible for the majority of transiting hot Jupiters currently known in the Southern hemisphere (see Hellier et al. 2011a). Here we report the discovery of WASP-43b, which has the smallest semi-major axis of any known hot Jupiter.

Table 1. CORALIE radial velocities of WASP-43.

BJD – 2400 000	RV (km s^{-1})	σ_{RV} (km s^{-1})	Bisector (km s^{-1})
55205.7594	–3.058	0.013	0.052
55325.6232	–4.041	0.021	0.055
55327.5745	–3.430	0.026	0.050
55328.5441	–3.067	0.014	0.033
55334.5030	–3.821	0.018	0.023
55359.4824	–3.026	0.022	–0.098
55362.5333	–3.522	0.031	0.050
55364.4596	–3.262	0.017	0.110
55375.4741	–3.830	0.018	0.048
55376.4911	–3.036	0.045	0.097
55378.4837	–3.994	0.018	–0.035
55379.5246	–3.904	0.021	–0.003
55380.4904	–3.282	0.021	0.017
55391.4617	–3.869	0.028	0.036
55392.4602	–4.086	0.021	0.072

Bisector errors are twice RV errors

2. Observations

The WASP project uses 8-camera arrays that cover 450 square degrees of sky with a typical cadence of 8 mins. The WASP surveys are described in Pollacco et al. (2006) while a discussion of our planet-hunting methods can be found in Collier-Cameron et al. (2007a) and Pollacco et al. (2007).

WASP-43 is a V = 12.4, K7V star in the constellation Sextans. It was flagged as a planet candidate based on WASP-South data obtained during 2009 January–May, and has been further observed by both WASP-South and SuperWASP-North over 2010 January–May, leading to a total of 13 768 data points. A putative 0.81-d transit period led to radial-velocity followup with the CORALIE spectrograph on the Euler 1.2-m telescope at La Silla. Fourteen radial-velocity measurements over 2010 January–July (Table 1) showed that the transiting body is a 1.8-M_{Jup} planet. On 2010 December 07 we obtained a transit lightcurve with the TRAPPIST 0.6-m telescope in a passband of I+z, while on 2010 December 29 we obtained a further transit lightcurve with EulerCAM in a Gunn r passband (Fig. 1).

Mon. Not. R. Astron. Soc. **000**, 1–12 (2011) Printed 17 May 2011 (MN LATEX style file v2.2)

WASP-44b, WASP-45b and WASP-46b: three short-period, transiting extrasolar planets

D. R. Anderson,[1⋆] A. Collier Cameron,[2] M. Gillon,[3] C. Hellier,[1] E. Jehin,[3] M. Lendl,[4] P. F. L. Maxted,[1] D. Queloz,[4] B. Smalley,[1] A. M. S. Smith,[1] A. H. M. J. Triaud,[4] R. G. West,[5] F. Pepe,[4] D. Pollacco,[6] D. Ségransan,[4] I. Todd[6] and S. Udry[4]

[1] *Astrophysics Group, Keele University, Staffordshire ST5 5BG, UK*
[2] *SUPA, School of Physics and Astronomy, University of St. Andrews, North Haugh, Fife, KY16 9SS, UK*
[3] *Institut d'Astrophysique et de Géophysique, Université de Liège, Allée du 6 Août, 17, Bat. B5C, Liège 1, Belgium*
[4] *Observatoire de Genève, Université de Genève, 51 Chemin des Maillettes, 1290 Sauverny, Switzerland*
[5] *Department of Physics and Astronomy, University of Leicester, Leicester, LE1 7RH, UK*
[6] *Astrophysics Research Centre, School of Mathematics & Physics, Queen's University, University Road, Belfast, BT7 1NN, UK*

arXiv:1105.3179v1 [astro-ph.EP] 16 May 2011

17 May 2011

ABSTRACT

We report the discovery of three extrasolar planets that transit their moderately bright (m_V = 12–13) host stars. WASP-44b is a 0.89-$M_{\rm Jup}$ planet in a 2.42-day orbit around a G8V star. WASP-45b is a 1.03-$M_{\rm Jup}$ planet which passes in front of the limb of its K2V host star every 3.13 days. Weak Ca H+K emission seen in the spectra of WASP-45 suggests the star is chromospherically active. WASP-46b is a 2.10-$M_{\rm Jup}$ planet in a 1.43-day orbit around a G6V star. Rotational modulation of the light curves of WASP-46 and weak Ca H+K emission in its spectra show the star to be photospherically and chromospherically active.

We imposed circular orbits in our analyses as the radial velocity data are consistent with (near-)circular orbits, as could be expected from both empirical and tidal-theory perspectives for such short-period, Jupiter-mass planets. We discuss the impact of fitting for eccentric orbits for these type of planets when not supported by the data. The derived planetary and stellar radii depend on the fitted eccentricity and further studies use these quantities in attempts to understand planet structure, the interdependence of parameters and the relevant physics for extrasolar planets. As such, we recommend exercising caution in fitting the orbits of short period, Jupiter-mass planets with an eccentric orbital model when there is no evidence of non-circularity.

Key words: planetary systems – planets and satellites: individual: WASP-44b, WASP-45b, WASP-46b – stars: individual: WASP-44, WASP-45, WASP-46

1 INTRODUCTION

The ensemble of well-characterised transiting extrasolar planets is growing at pace, with over one hundred known to date. It is important to determine the system parameters accurately so that the inferrences on which they are based are reliable. For example, to determine the bulk composition of a planet it is necessary to accurately measure its radius (e.g. Fortney, Marley & Barnes 2007). Many short-period, giant planets (e.g. WASP-17b, Anderson et al. 2010b, 2011) are larger than predicted by standard cooling theory of irradiated, gas-giant planets (e.g. Fortney, Marley & Barnes 2007). One potential explanation is that energy from the tidal circularisation of eccentric orbits was dissipated within the planets' interiors, causing them to bloat (e.g. Bodenheimer, Lin & Mardling 2001). To evaluate the likelihood that a planet was inflated by such tidal heating, it is necessary to have an accurate determination of both its radius and its orbital eccentricity (e.g. Ibgui, Spiegel & Burrows 2011).

A planet's orbital eccentricity can be determined by measuring the radial motion of its host star across an orbit (e.g. Queloz et al. 2010), or by observing an occultation of a planet by its host star (e.g. Anderson et al. 2011), or from a combination of the two. By combining this eccentricity measurement with high-quality transit light curves, we can measure a star's density (Seager & Mallén-Ornelas 2003). The stellar mass can be estimated using stellar evolu-

⋆ dra@astro.keele.ac.uk

3.6 Summary of the WASP/CORALIE Survey

Writing this thesis was a good occasion to have a look back at the intense work done with CORALIE to confirm WASP planet candidates. The partnership between WASP and Genève started in Summer 2007 when the first CORALIE data got acquired. I arrived in Genève at the beginning of Septembre, WASP-4 and 5 had just been confirmed, WASP-6 was underway. I remember clearly the discovery of WASP-8, observing with Didier Queloz, at La Silla as he was teaching me how to be an observer. At that time Didier and Michaël Gillon were organising the Genevan side of the survey. I took progressively over during List 7 (see section 3.1) and was fully operationnal when List 8 was published, in April 2008.

3.6.1 WASP results in numbers

How best to capture WASP's results but to show the shear number of results we obtain in a number of tables and graphs.

Next table, (3.1) summarises in a few quick numbers the broadline of the work done for WASP (up to date for mid spring 2011). A table showing the status of the 689 candidates provided by WASP between 2007 and mid spring 2011 could have been presented, but would not have been that interesting on top of the fact that some of the objects are still being confirmed. In table 3.1 you will see several categories defined defined following in broad lines from the description of various objects described in section 3.2:

- P (for *planet*): WASP candidate observed by CORALIE and confirmed as a planet (the one brown dwarf we found, WASP-30, is also included in this category while WASP-2, which was not in any of our Southern candidate list is not);
- M (for *M dwarf*): WASP candidate which after some CORALIE follow-up and a Keplerian fit gives a stellar body < 0.5 $M_{\odot}$ transiting -eclipsing- a K, G, F or A primary;
- M? (for *maybe M dwarf*): WASP candidate with a variation in radial velocity $\Delta RV < 100\,\mathrm{km\,s^{-1}}$ and/or that could correspond to stellar body < 0.5 $M_{\odot}$ transiting a K, G, F or A primary;
- LP (for *long period binary*): candidates for which we have a period or long term radial velocity drift without a hint of another orbital frequency linked to that found by WASP. Potential triple, quadruple+ systems;
- SB2: double line spectral binary
- SB3: triple line spectral binary (no SB4 has been found)
- EB (for *eclipsing binaries*): candidates with a variation in radial velocity $\Delta RV > 100\,\mathrm{km\,s^{-1}}$, candidates having a transit too deep to be produced by a planet, and candidates with an observed occultation (secondary eclipse in this case);
- Blend: a star near the candidate selected by WASP is the actual transited star. This is not linked at all to the nature of the object. It simply points out to a confusion on the target. Some of the blending star can have a transiting planet, although this is unlikely (we had only one recent such case); most are EBs, or LPs;
- G (for *giant*): spectral analyses of reconnaissance spectra show this is a giant star, thus a blend or a false positive;

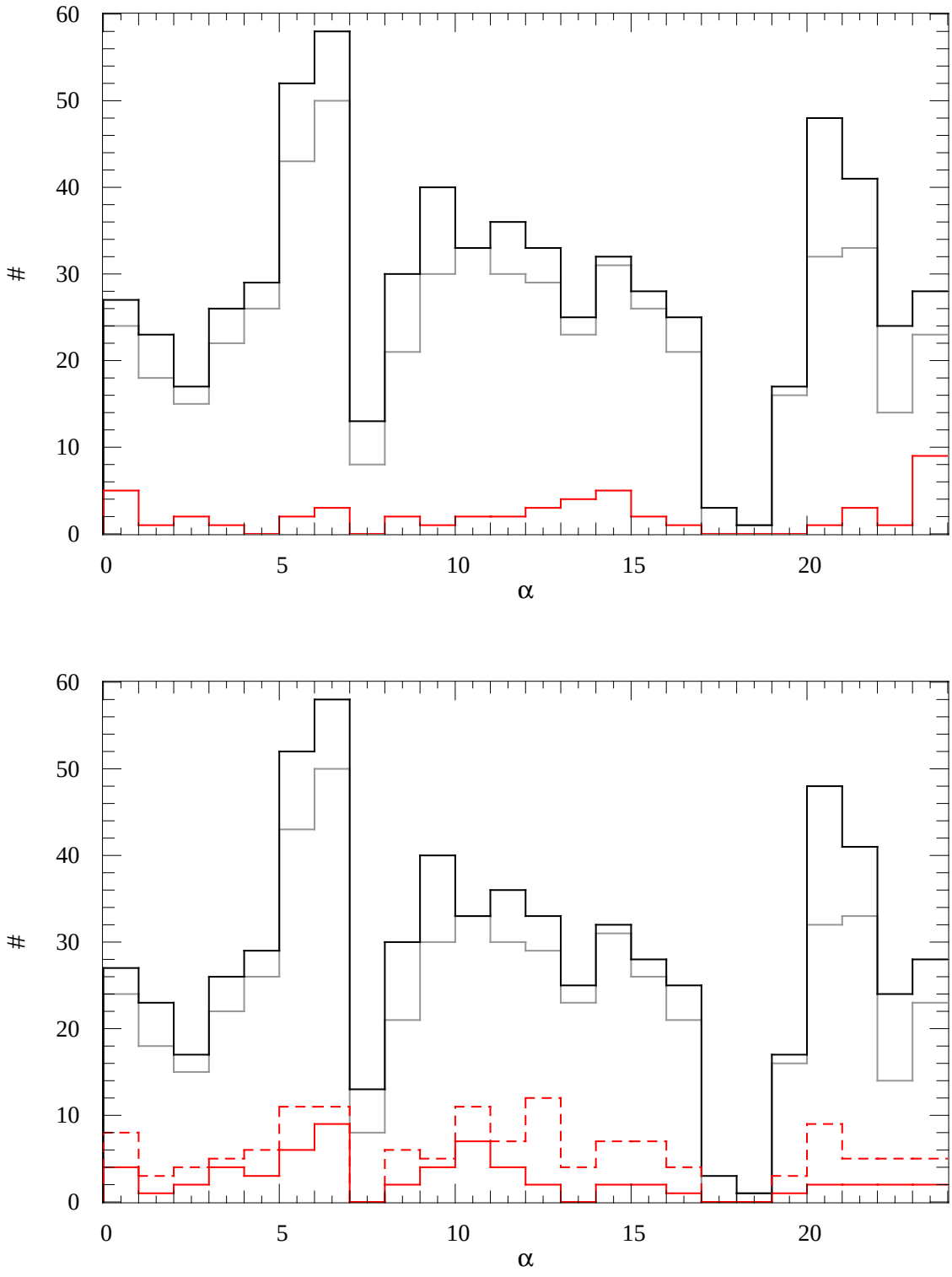


Figure 3.19: *Black*: histogram in right ascension of the WASP candidates. *Grey*: all those candidates for which we have a status, of which in *red*: *top*: the planets (P); *bottom*: (plain), the transiting M dwarfs (M), (dashed), the potential transiting M dwarfs (M?) and long period non transiting objects (LP). The "holes" at 6h and 18h show the location of the galactic plane.

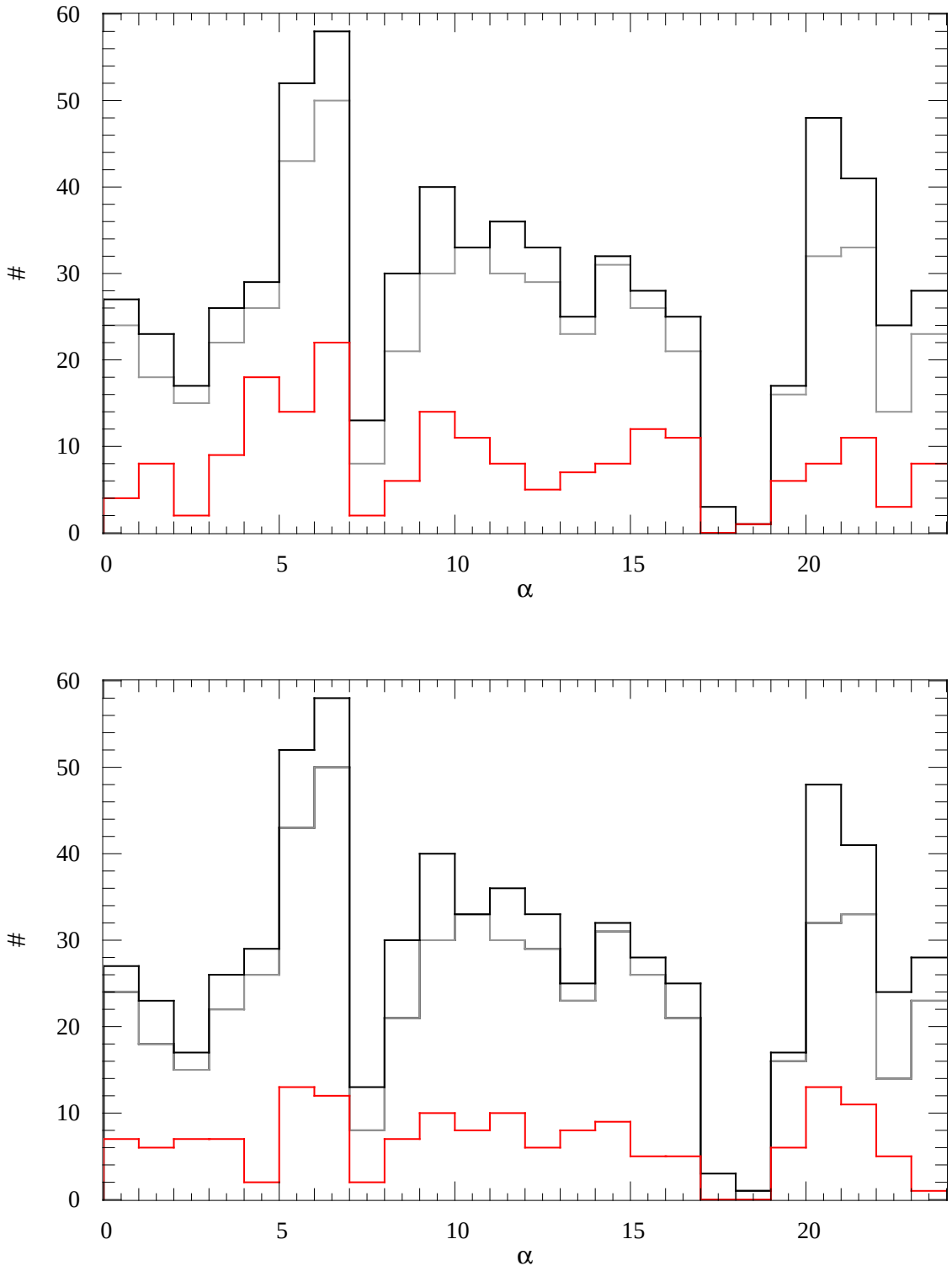


Figure 3.20: *Black*: histogram in right ascension of the WASP candidates. *Grey*: all those candidates for which we have a status, of which in *red*: *top*: the binaries (SB2, SB3, and EB) and *bottom*: the false positives (Blend, G, H, FP).The "holes" at 6h and 18h show the location of the galactic plane.

Table 3.1: WASP Statistics

category	number	frequency
P	50	$8.8 \pm 1.2\%$
M	62	$10.9 \pm 1.4\%$
M? + LP	76	$13.4 \pm 1.5\%$
SB2 + SB3 + EB	221	$38.8 \pm 2.6\%$
Blend + G	102	$17.9 \pm 1.8\%$
FP + H	58	$10.2 \pm 1.3\%$
subtotal	569	
n/a	120	
total	689	

NB: frequencies estimated from subtotal

- FP (for *false positive*): for some reason the *Hunter* algorithm found a period but it is spurious, or caused by instrumental defects;
- H (for *stars that are too hot*): or rotating too fast that we can't extract meaningful RVs; this meaning has changed a little in the course of the past years;
- n/a (for *non available*): candidates still under scrutiny, not yet observed, not fully confirmed, waiting for photometric *On/Off*...;

One has to remember some candidates might belong to several categories physically (see for example Brown (2003)). The classification was chosen to correspond to what is causing the signal found in WASP and triggering their presence in the candidate lists. Some changes might occur with new observations coming in. In Table 3.1, these categories are linked into broader categories:

- planets;
- transiting M dwarfs;
- M? & LP: potentially interesting;
- SB2, SB3 & EB: binaries, detected object for which we are not much interested in;
- Blend & G: both are blend really, demonstrates a capacity for detection, despite being wrong detections;
- FP & H: not much to learn from those;

In a little under four years we thus have discovered 48 planets[19] (two of the 50 were actual detection by SOPHIE that because they were in our candidate lists, we later picked up and followed, but would probably have been found independently, thus justifying being in that statistics), a number close to the number of planets found by the CORALIE RV survey which has been ongoing since 1998. I am going to be very quick to point that the comparison is unfair as the type of planets found is radically different and thus what we learn about them. The WASP/CORALIE survey is, at the end, a study of a special class of planets, the hot Jupiters, planets that are quite rare and thus underrepresented in the CORALIE RV survey.

[19] since more have been discovered :o)

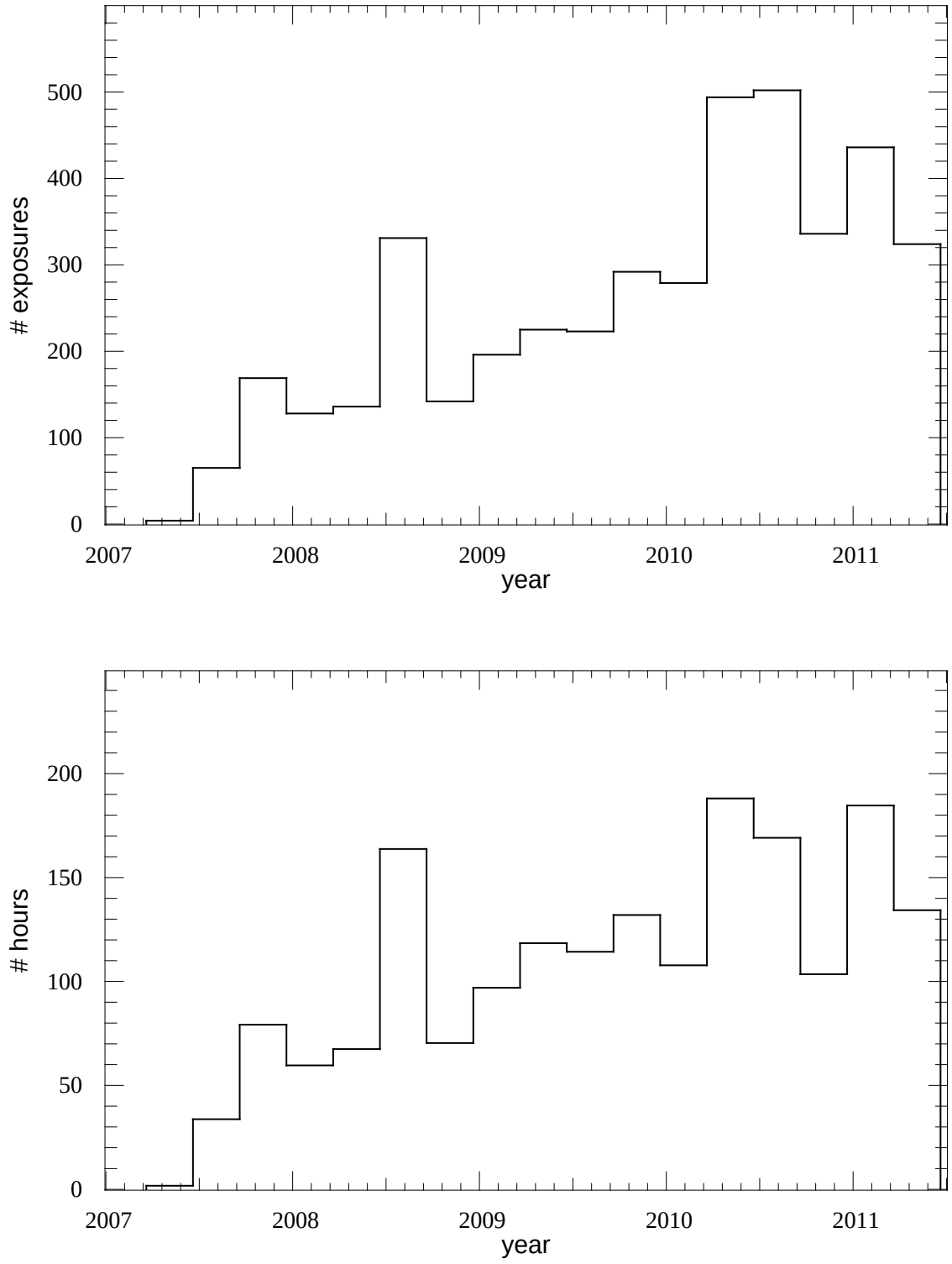


Figure 3.21: *top*: Number of exposures as a function of time, binned per trimester. *bottom*: Number of hours observed with time, binned in trimester from Spring equinox 2007. Data incomplete for the last bin.

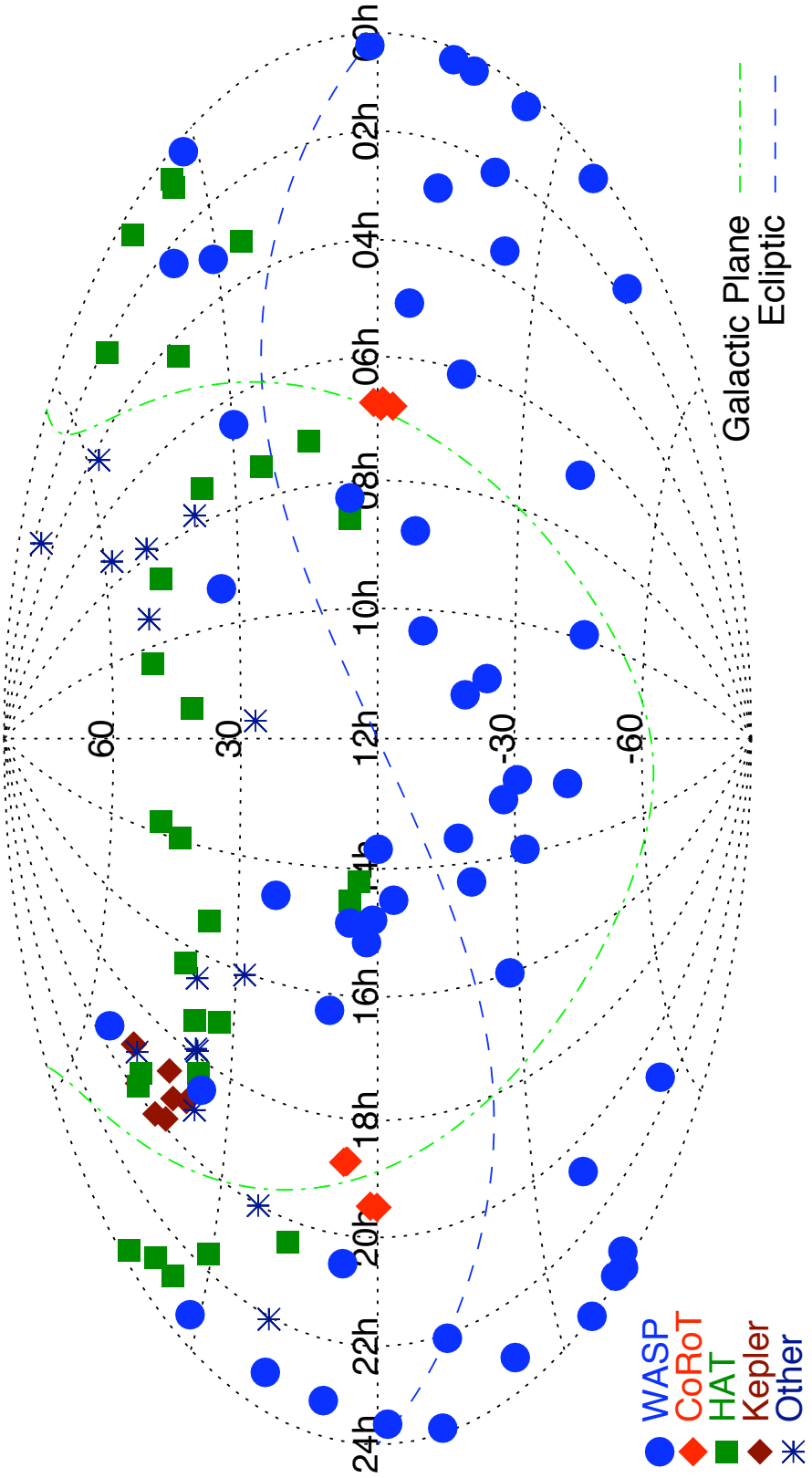


Figure 3.22: Position of known transiting planets including WASP, our main competitors, the HAT network, and the two space missions, CoRoT and *Kepler*. Courtesy Pierre Maxted.

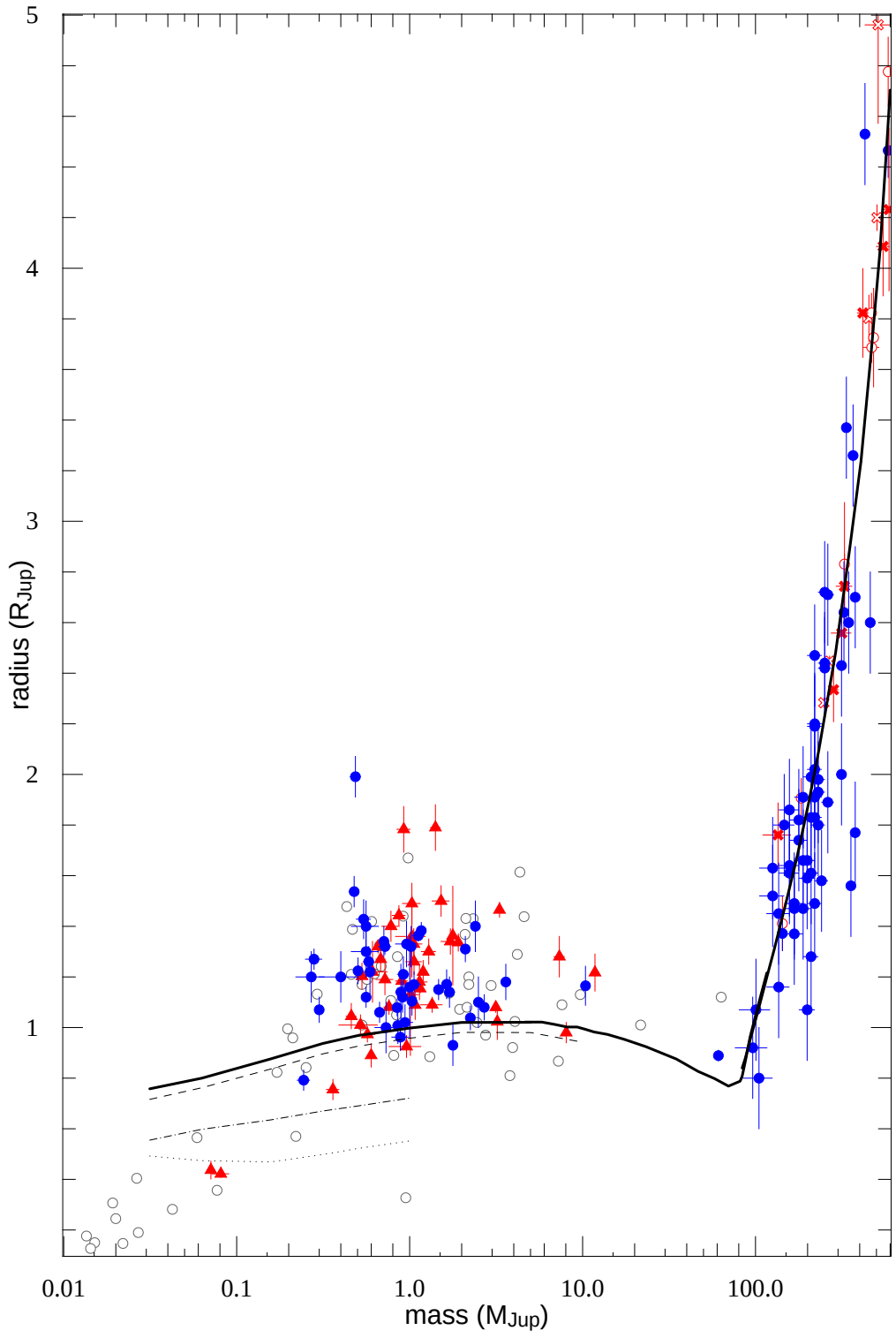


Figure 3.23: Updated graph from the thesis by B-O Demory (red symbols, literature in mid 2009) with results from WASP-South and CORALIE (bleu circles), and other groups (open grey circles). Overplotted, models by Baraffe et al. (1998). Plain model are 5 Gyr models for solar metallicity. Other models allow for larger amounts of metals for the planets: 10%, 50% and 90% in content. (data from B-O Demory, `www.exoplanets.eu` and this thesis). Caution: data for low mass stars is preliminary.

To find those planets, we observed for about 1800 hours in integration time, meaning the work end to end of roughly 200 nights of observing[20] (see figure 3.21). We observed data during more than 650 individual nights spanning over the 1400 nights since the joint survey started; the survey is still ongoing. In addition to these observations one would also have to count the time spent for photometry, for *On/Off* and for the confirmation and characterisation transit observations.

Roughly estimated, a planet thus costs an effort of about 40h of observing time, or a bit more than four nights. One such planet is discovered in average every 30 days but that pace is increasing slightly.

Figure 3.23 illustrates well WASP and CORALIE's achievements. When a similar plot was presented at Brice-Olivier Demory's thesis, only the red non circular symbols were populating this graph. WASP-8 was the last discovered southern planet. Since CoRoT and *Kepler* have populated the low mass, low radius end, CoRoT and WASP added objects in the Brown Dwarf desert, and WASP in the low mass eclipsing binaries[21]. This graph clearly shows that the radii of hot Jupiters are larger than expected by theory for *isolated* planets (like our Jupiter is).

A note of caution. The masses and radii for the low mass M dwarfs are preliminary estimates, very likely to change. The mass was estimated from assuming the primary's mass is much larger than the secondary's (like in the planet's case) which is not entirely just. The radii were obtained from the *Hunter* page and do not take into account the fact that those are self luminescent objects. Additionally some of those transits are probably grazing leading to a wrong radius estimation at the moment. Determining those radii is an undergoing effort with Leslie Hebb and Yilen Gomez. Occultations will be taken to completely solve the system and get accurate radii.

3.6.2 Evolution of results and detection capacity

Some areas in the sky appear to have a higher probability for discovering planets. This might sound a little strange but looking at the two bins between right ascensions $\alpha = 23$h and $\alpha = 1$h (top panel of figure 3.19) we confirmed 14 planets. Assuming we have discovered all possible planets (which is hopefully wrong) and averaging over this area, when we propagate the same probability for planet detection over the whole sky, we reach a total number of at least 170 ± 40 planets. This is a simplified argument but shows how much left can be done, but also of how much we have achieved: a third of the total number! Of course some areas are harder to probe than others, notably the poles and the galactic plane.

WASP has given a fairly constant stream of candidates of similar transit depth which median is close to 1.5 % (figure 3.24). We can remark that there has not been much improvement in the announced depth for confirmed WASP candidates. More shallower transits could probably be found as WASP-7 and WASP-30 were both advertised as having transit depth $< 0.5\%$. Certainly a survey over the same fields with only a slight improvement in precision would yield many more objects. Let's also point out that both WASP-7 and WASP-30 are around hotter stars, object of great interest for the Rossiter-McLaughlin observations (see next chapter).

The lower panel (figure 3.24) shows the conversion of the advertised transit depths into the published radii. Outliers do not correlate. WASP-43 is the deepest transit we confirmed, but its planet's size is perfectly in the norm (the star is small). WASP-17 had an advertised depth no different from other candidates, while it is a clear outlier when it comes to its radius[22]. Finally WASP-29 is our smallest planet, but its depth, again was lost among that of other candidates.

[20] this is about as much time as a pregnancy!
[21] those results should come out fairly soon
[22] were it not on a retrograde orbit I would have a hard time believing it is a planet

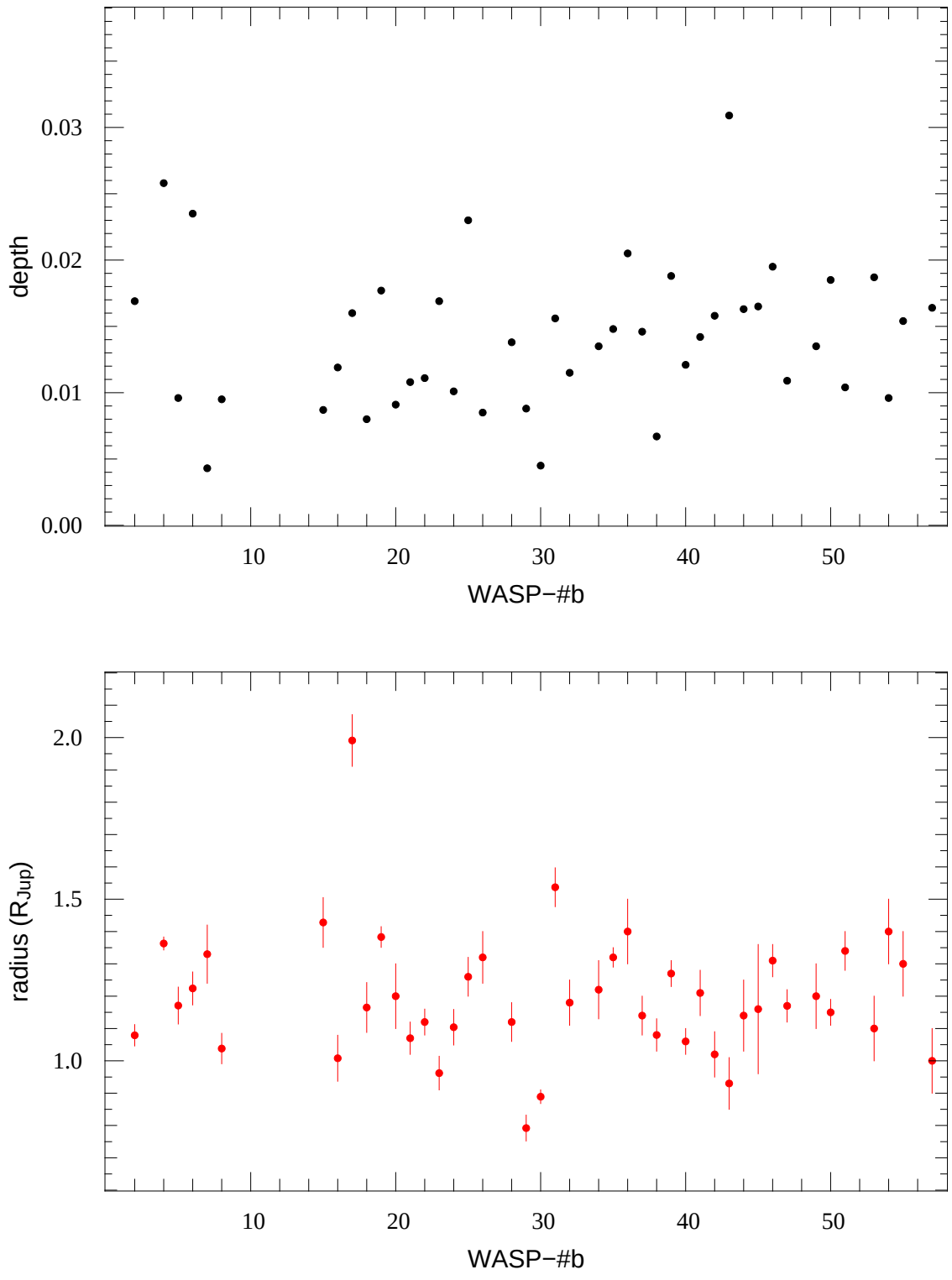


Figure 3.24: *top*: depth as advertised on the *Hunter* page as a function of the WASP planet numbering system. *bottom*: radius after careful analysis as a function of the WASP planet numbering system. WASP-17b is a clear outlier for radius, but not in depth. Inversely, WASP-43b has a very deep transit, but is a normal planet in size. This means we probably have missed more WASP-43b type planets than WASP-17b.

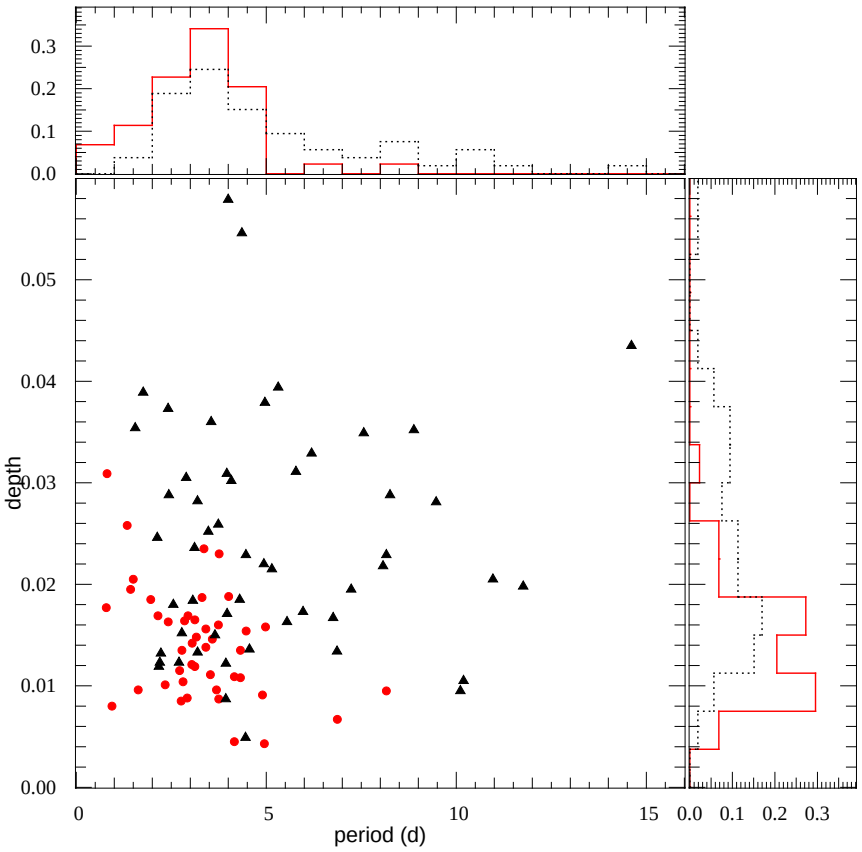


Figure 3.25: Red dots: planets. Black triangles: transiting M dwarfs, and histograms (black and dotted for transiting M-dwarfs, red and plain for transiting planets). They have different period distribution. We find M dwarfs at longer period though with a similar transit depth. We also do not find as many low depth transit in the M dwarfs as for the planets, pointing to a deficit of low mass transiting M dwarfs

WASP-29's Doppler signal is quite clear, so I do not think we would have missed similar candidates if they were as present as other hot Jupiters. Similarly I think we are quite complete regarding the typical hot Jupiters around solar type stars. Other WASP-17s should have been found without too much trouble by either WASP or Genève and thus are probably very rare objects, WASP-30s might have been missed by WASP more than Genève because of the small transit depth, and so would WASP-43s whose large transit depth is quite unusual and might have been censored at candidate selection. On our side we might have missed a few WASP-7 and WASP-31 which orbital Doppler amplitude is of order of error bars on individual measurements[23]. The reason is mostly because those stars are hotter and faster rotators, degrading the FWHM of their CCF peak and thus our precision on individual measurements. Apart from WASP-8 and WASP-38, all our objects have period < 6 days, while our main competitors, the HAT network, have found a few transiting planets out at 10 day orbits, like Hat-P-15 and 17 b (Kovács et al. 2010; Howard et al. 2010). Did we miss any of these? This is where we can use the transiting M-dwarfs that we have also confirmed as a comparison sample to our planet detection.

Figure 3.25 compares the distribution of the advertised transit depths (a proxy for our detection capacity) on the *Hunter* page with respect to orbital period. Four out of the five M dwarfs at orbits > 10 days that were found, have transit depths which are similar to confirmed planets. I thus see no reason why we should not have been able to find planets at such orbital periods, except of course if they are less frequent than M dwarfs. Similarly, for orbital periods > 6 days, we have found ten M dwarfs which depth are planet-like, but only two planets. The main disadvantage WASP has compared to HAT is that we observe only from one longitude making it harder to detect longer

[23] but hopefully not too many. Those candidate would be those for which we have an *On/Off* confirmation of the transit and no visible RV motion

period planet which only have few visible transits every year. Taking an astronomical night as a third of an Earth rotation, we can only catch three times less transits than HAT for similar objects. Since our detection depends on repeated observations, we are well penalised. Thus, observing the same fields anew with increased precision would yield more easily long period candidates as we would require a lesser number of events for a detection. In addition, comparing this new data with the one already acquired to increase the timespan would help in having precise ephemeris.

3.7 The Rossiter-McLaughlin Effect as a Detection Tool

Besides trying to find more planets, it is also most interesting to detect the transit of known radial velocity planets. The brightness of their host star makes them brilliant objects to characterise, as HD 189733 b (Bouchy et al. 2005), GJ 436 b (Gillon et al. 2007) and 55 Cancri e (Winn et al. 2011b; Demory et al. 2011) are perfect examples of. Three projects come to mind: the TRANSITSEARCH.ORG, run by Greg Laughlin, using amateurs to check the transit windows of bright stars; the TERMS project by Stephen Kane, refining the ephemerids of known highly eccentric planet presenting a higher chance of transit despite being on longer periods (Kane et al. 2009); and Michaël Gillon's Spitzer program on the HARPS's small planet candidates (Gillon et al. 2010)[24].

One of the most spectacular recent result was the detection of the occultation of HD 80606 b, a planet on a 0.93 eccentric orbit of 111 days (Laughlin et al. 2009). The chance of occultation was large enough to be tempted. Once known to occult, the transit probability increased dramatically. The main issue to catching it was that this object was expected to have a transit longer than a night, making it very hard to be sure one has observed an ingress or an egress. There comes the Rossiter-McLaughlin effect. The beauty of it, is that using spectroscopic measurements, we know the zero point of the instrument and the position and slope in the radial velocity (according to the Doppler reflex motion) that the star ought to have. It was observed by Moutou et al. (2009) combining photometry and spectroscopy. Fossey et al. (2009) and Garcia-Melendo & McCullough (2009) also observed the transit photometrically.

HD 156846 has a planet around it (Tamuz et al. 2008). It was observed by CORALIE and *Keck* with some very recent observations produced by the TERMS project (Kane et al. 2011). Its 360 day orbit is very eccentric, bringing the planet from beyond the orbit of Mars to well within Mercury's. Its probability of transit is of order 5 %. Among the interesting features of that planet, is the length of its orbit, making it a cold Jupiter. Also of great interest is the distance at periastron (Kane et al. 2011), leaving a Hill sphere around the planet large enough for satellites to stay dynamically stable.

Realising the interest of that target, on 2009 September 3rd we attempted catching the Rossiter-McLaughlin effect, expected if the planet is transiting, using CORALIE. The results will now be presented and should be taken with all the caution necessary: visually there is a radial velocity anomaly at the time and of the shape expected for the Rossiter-McLaughlin effect, but statistically, it is not detected: we have *marginal evidence*. Other worrying factors come into play: the night was not the best, being partially cloudy in La Silla (weather was apparently worse at Cerro Tololo, despite their relative proximity, where Kane et al. (2011) attempted a photometric transit the same night[25]). Nevertheless, this is a perfect example to work with and show how a Rossiter-McLaughlin effect detection can be carried out, in the absence of photometric data.

[24] yielding a transit detection on a planet not found using HARPS, oh joy, sweet irony! (Demory et al. 2011)

[25] to continue rambling on bad luck, we attempted catching photometrically the transit from La Palma, which was also clouded over. That ain't funny!

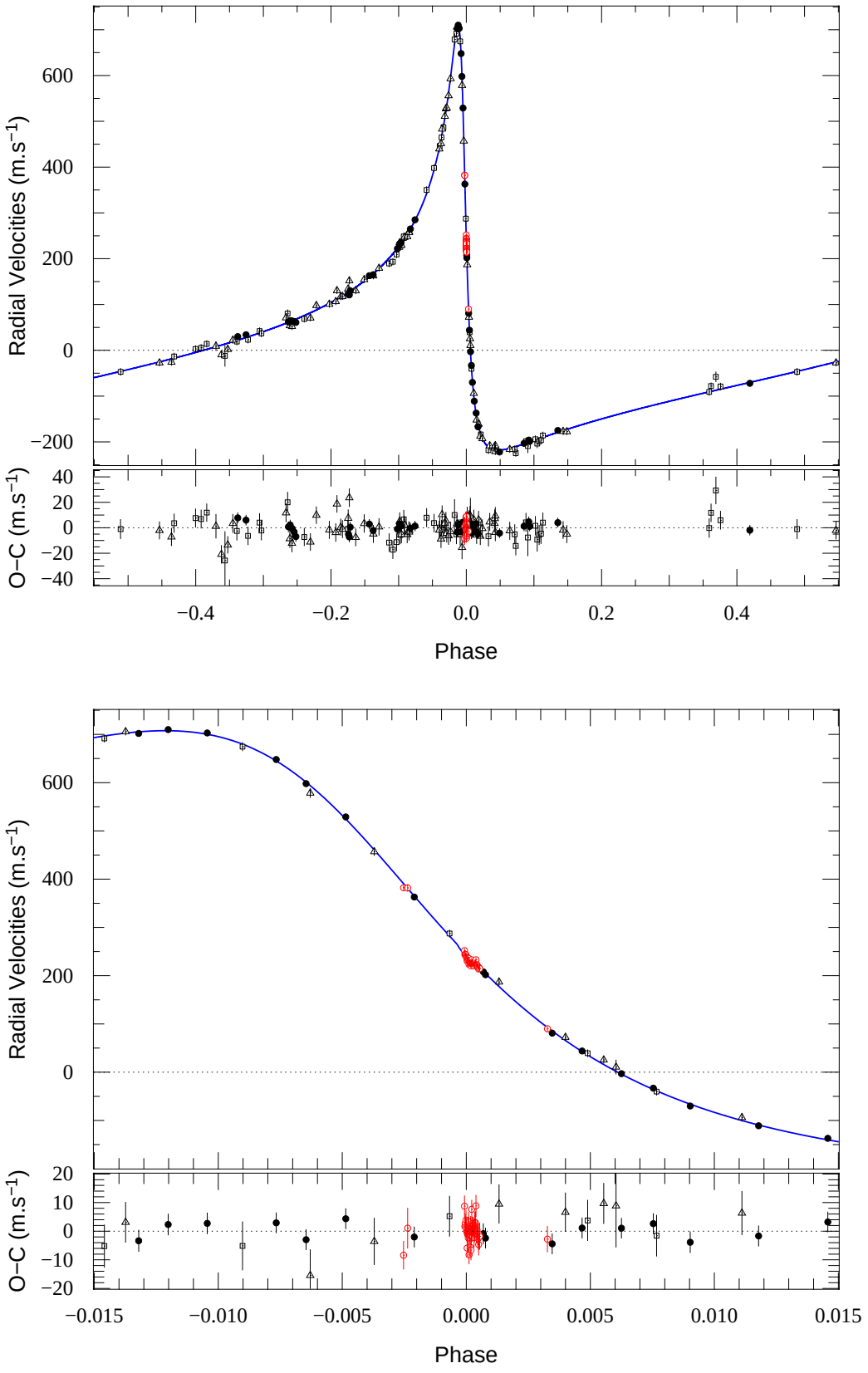


Figure 3.26: RV data on HD 156846. *top*: all orbit; *bottom*: zoom on periastron passage. Open symbols: CORALIE. Squares: CORALIE '98 data, triangle: CORALIE '07 data, red circle: CORALIE transit data. Filled circle: Keck HIRES data.

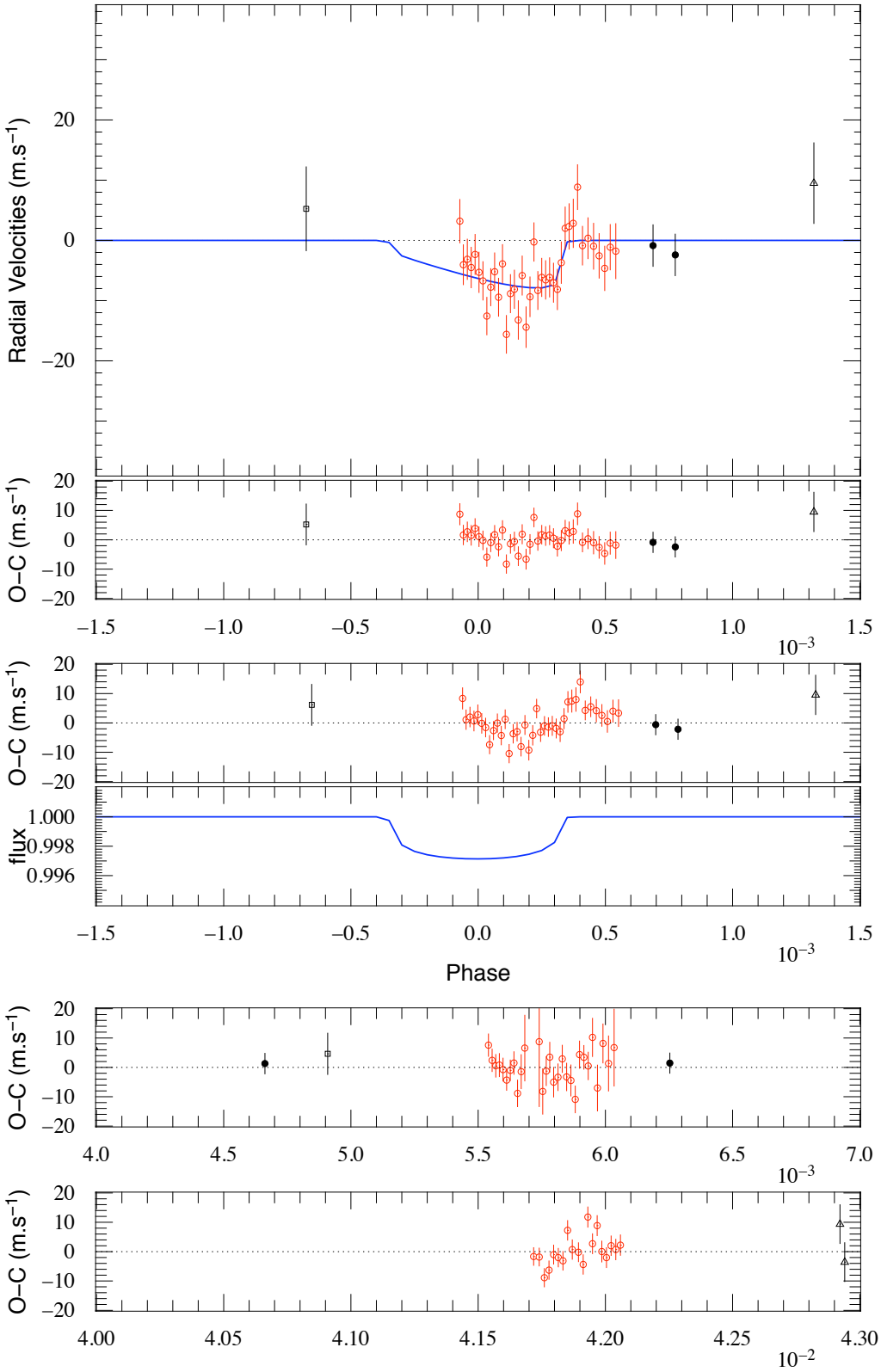


Figure 3.27: RV data on HD 156846. *top*: zoom on the transit RV sequence and its residuals. Open symbols: CORALIE. Squares: CORALIE '98 data, triangle: CORALIE '07 data, red circle: CORALIE transit data. Filled circle: Keck HIRES data. *middle*: RV residuals if not adjusting for the RM effect and predicted transit lightcurve. *bottom* two other series taken after the transit series to check the level of variability in the RVs.

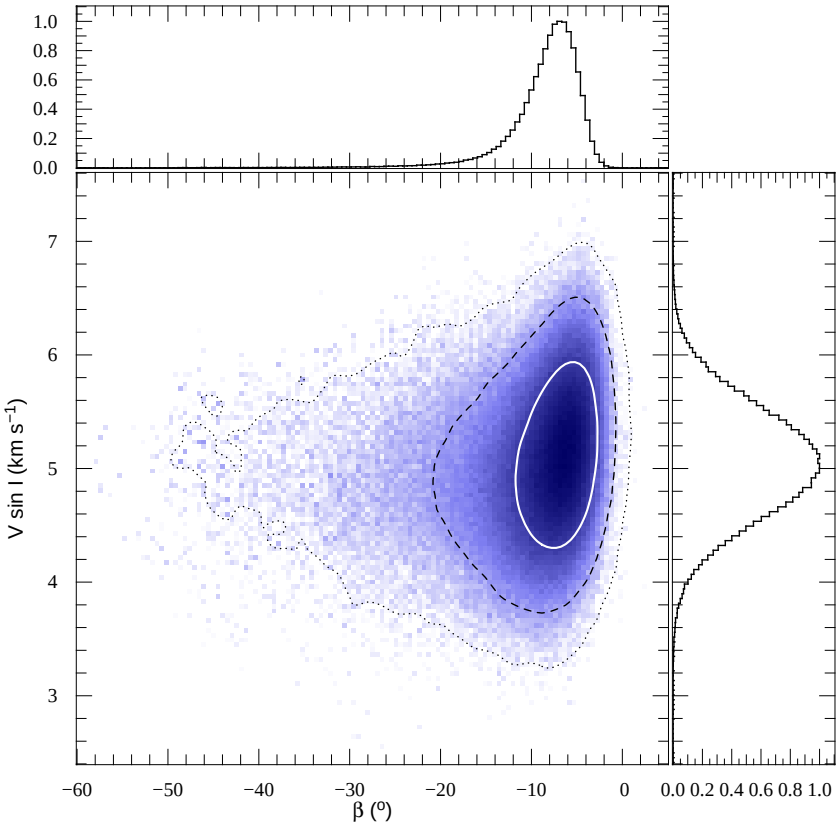


Figure 3.28: Joint probability distribution function, resulting from a Rossiter-McLaughlin effect adjustment to the data in ($V \sin I$, β) space. Marginalised distributions are in histograms. 1, 2 and 3 σ confidence intervals are drawn.

The radial velocity data from the transit night was downloaded from La Silla, and immediately inserted into the code where preliminary chains had been conducted and whose results matched those given by YORBIT. We had been monitoring the star to also ameliorate the precision in its orbital parameters and were obtaining data as often as possible during periastron passage (data is presented in figure 3.26). I was quick to spot a radial velocity anomaly in the Doppler curve and start adjusting an effect by fixing some parameters to credible values. The transit was not complete (see figure 3.27, top panel). To convince ourselves (Damien Ségransan and I) that we had detected a transit and not a systematic caused by a cloud, we asked the observer, Roi Alonso, to acquire a similar sequence in term of cadence and individual error bars. This was obtained two nights after, also in poor weather conditions thus providing a good comparison. Another timeseries was obtained a fortnight later. None of those show the level of correlation we observe, though the second control series is quite noisy (see figure 3.27, lower panels).

I then started running chains trying to adjust for the RV anomaly that we had observed. The data I had then, consisting mostly of CORALIE, was predicting a mid transit time which was quite loose and thus I could never be sure that the series we had observed was at ingress, or at egress or rightly, out of transit. Things stayed as they were, waiting to have more data for the orbit and maybe another chance to observe during the transit.

Kane's paper thus helped a great deal since they used HIRES on the Keck Telescope at the same time as we used CORALIE, though, not during transit. As soon as the paper appeared on the online archive ASTRO-PH, I read their refined transit ephemeris, and saw the two points that are located just after the transit (see figure 3.27) were compatible with our data. Combining everything and reanalysing, we realised our observations coincide well with the expected time of transit. Following is the analysis of that signal, taking the hypothesis that we indeed have observed a Rossiter-McLaughlin effect:

Using the MCMC, progressively more and more parameters were included, reaching the total number of parameters that can be adjusted for a transit. To help the chain avoid getting lost into unphysical parameter space, some priors were used on the stellar radius $R_\star = 2.12 \pm 0.12\, R_\odot$ (Kane et al. 2011) (well determined thanks to Hipparcos parallax measurements), the planet's radius $R_p = 1.0 \pm 0.1\, R_{\rm Jup}$, (thanks to our knowledge acquired since the discovery of the first transiting planets. The planet minimum mass being > 10 $M_{\rm Jup}$, its radius should not be inflated, plus that planet stays all the time further from the star than our hot Jupiters) and the much needed $v_\star \sin I = 5.05 \pm 0.5$ km s^{-1} (Kane et al. 2011).

Have we detected a signal? Residuals from the adjustment of the Rossiter-McLaughlin effect shown in figure 3.27 still show a fairly large scatter. Using the method described in section 2.2.5, we will compare two models: a straight line through the data (ie. no Rossiter-McLaughlin effect) that we call M_1, and a model with a Rossiter-McLaughlin effect, called M_2. We have 41 data points in the sample including two located a night earlier and one a night later (to adjust for the γ velocity). M_1 has only one parameter: the γ velocity, a scaling parameter for the MCMC. M_2 has six more parameters (T_0, D, W, b, $\sqrt{V}\sin I\cos\beta$ and $\sqrt{V}\sin I\sin\beta$). All other parameters are entirely constrained by the rest of the data.

Our results show that χ^2 over the transit series goes from 84.9 ± 13.0 to 48.9 ± 9.9 for the addition of 6 parameters and 41 measurements. Accounting for the variance of χ^2 and comparing (as described in the previous chapter) with the expected χ^2, we favour a Rossiter-McLaughlin model only with 85.4 % probability above a straight line through the data. This summons for additional observations.

While there is a chance the cloudy conditions affected the data to make us think there is a Rossiter-McLaughlin, this would have happened with the right shape and timing to be consistent with a Rossiter-McLaughlin effect for that planet and that particular star, a relatively fast rotating, evolved star. If - and only if - this is so, the planet is close to a coplanar orbit with $\beta = -6.5^\circ\,^{+5.5}_{-39.5}$ which error bars have been estimated for a $3\,\sigma$ confidence interval[26] (figure 3.28).

Now, apart from these considerations, this attempt at adjusting only a spectroscopic transit, without the help from photometry, shows it is hard business but doable. I was really surprised at how well the chain was behaving using the various priors and finally giving constraints on many parameters, even for the impact parameters b.

The following transit, in 2010 was not observable from La Silla. The next transit will happen on the night starting in 2011 August 23$^{\rm rd}$. If all goes well, my PhD defence will be a dozen hours earlier (that was not planned). Only the ingress will be observable from La Silla[27] while the egress could be observed from Hawai'i. In 2012 there should not be a visible transit from either place, and in 2013, the ingress will be observable from Hawai'i. Then it will remain unobservable from high resolution, stable spectrographs for 10 to 12 years.

the search for an Earth Twin

Let's now see how well the Rossiter-McLaughlin effect could be used as a detection method. If not using the traditional approach, certainly using the Doppler shadow as described in Cameron et al. (2010a). As the search for less massive and more habitable planets intensify, it will get harder and harder to confirm them using radial velocities. Our Earth causes a 9 cm s^{-1} semi-amplitude on the Sun, something very challenging to detect with the spectrographs projected to be built on the

[26] still a chance to be severely misaligned [corrections: the code used to fit had a wrong treatment of the eccentricity. This has now been corrected. Alvaro Gimènez inserted the correction in his code. The fit still allowed a Rossiter-McLaughlin effect with a very different β.]

[27] last minute corrections: HARPS radial velocities unfortunately do not confirm the transit

VLT and ELT. In addition to getting to the precision, correcting for stellar variability and to getting the observing time on those telescopes, phase coverage will be incomplete for an Earth twin as at most, half the orbit can be covered since only few stars remain visible at decent airmasses all year round from Chile. Now, the Rossiter-McLaughlin effect of an Earth over the Sun has a peak to peak amplitude of order 30 cm s^{-1} over 12 hours, assuming a coplanar orbit. Any inclined orbit will show a lower variation. Nevertheless, despite not helping in measuring the planet's mass, it could be a used as way to confirm candidates, as advocated in Gaudi & Winn (2007).

Apart from being higher in amplitude than the Doppler reflex motion, the Rossiter-McLaughlin effect has the advantage of being a relatively short observation over which the stellar noise can be more easily dealt with than over a year. Finally as demonstrated in the earlier chapters, if this detection is used to confirm a candidate found by a transit survey of bright stars such at the currently proposed mission to ESA, *PLATO*, one can use the well determined transit parameters that good space-based photometry can provide to help with the adjustment. Certainly this could be a tool to verify that the transit is indeed on target in order to decide then to invest some time trying to measure the Doppler reflex motion and obtain the mass.

I simulated what kind of observations could be conducted using an instrument similar to the announced ESPRESSO, to be installed at the VLT which aims to reach a stability and precision of order 10 cm s^{-1} on bright stars. Let's simulate two different strategies: the first would be to detect the Doppler reflex motion, the second to only detect the Rossiter-McLaughlin effect. Our aim is to compare the amount of data one needs to observe to obtain the same detection level (examples of the datasets and signals are found in figure 3.29):

To detect the Doppler reflex motion: one needs to observe in average three radial velocity points per night for about six months. Those data points were drawn randomly with an RMS around a model of 15 cm s^{-1}. Individual data points have variable error bars of 10 ± 2 cm s^{-1}. The RMS and 2 cm s^{-1} variation on the error bar account for systematic noise and variation due to night to night conditions and errors in removing stellar activity. In addition, I removed randomly some epochs from the observations to account for clouds and other observing programs taking up time. In total 406 RV measurements have been used. The analysis is made hard because $\chi^2_{\rm reduced} > 1$ due to systematics, needing a quadratic addition of 11 cm s^{-1} on error bars. Then we reach: $\chi^2_{\rm flat} = 1.18 \pm 0.08$ compared to $\chi^2_{\rm reflex} = 1.03 \pm 0.07$. About $2\,\sigma$ detection.

To detect the Rossiter-McLaughlin effect, one needs to observe continuously for 15 hours at a cadence of about 9 minutes. Since nights are shorter, only half a transit can be observed per year in average. Confirmation of an Earth twin would thus take several years but would require less data: with 80 RV points, 60 of which located inside the transit, one can have a tentative, independent detection of the Rossiter-McLaughlin effect. Using priors on $V \sin I$ thanks to a good knowledge of $v_\star$ from photometry and spectroscopic measurement, detection can be made much easier. The data was drawn similarly to above but with an RMS of 14 cm s^{-1}, for varying error bars of 12 ± 1 cm s^{-1}. Error bar is larger because we observe less time per data point (we need the cadence to observe the Rossiter-McLaughlin). Systematics are smaller because our timebase is smaller and stellar activity treated differently. We are also less sensitive to weather variations. Punching the numbers we would obtain: $\chi^2_{\rm flat} = 1.41 \pm 0.19$ compared to $\chi^2_{\rm RM} = 0.97 \pm 0.16$ without using additional error bars but again with only about $2\,\sigma$ confidence. Adding a bayesian penalty on $V \sin I = 2.25 \pm 0.25$ one raises the $\chi^2_{\rm flat}$ to 2.78 ± 0.39, a clear detection. All these efforts would confirm this is a target worth investigating more, notably to get its mass.

This simple approach should give an idea of what we will soon be confronted with. Finding such Earth twins with the Doppler method around smaller mass stars should be easier than presented here (notably due to the phase coverage, lower stellar activity and higher Doppler amplitude) and a confirmation via Rossiter-McLaughlin effect harder due to smaller $v_\star$ and smaller transit width.

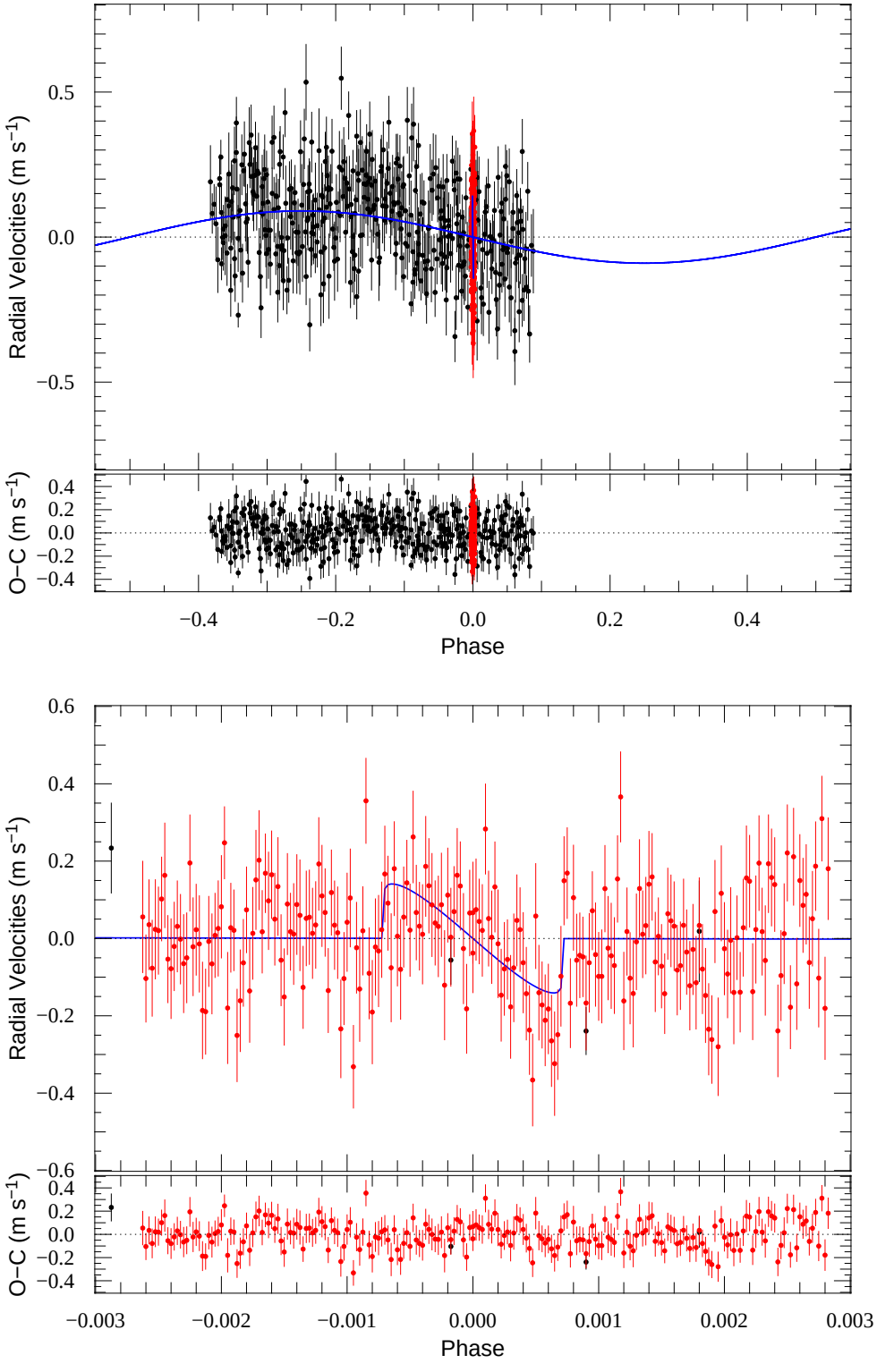


Figure 3.29: Simulated radial velocity data including the Rossiter-McLaughlin effect for an Earth twin. The data on the top graph cannot cover the entire orbit because of the time the star spends in the night sky. The data around transit, cannot be taken over one night (except if observing from several facilities spread in longitude), but the whole transit could in time be observed entirely. The data is comparable to expectations from the forthcoming ESPRESSO on the VLT, and include an extra source of noise to account for uncorrected weather, stellar and instrumental noise.



Earthly and Cosmological clouds;
the rise of the Galactic bulge over the Andes, from La Silla

Chapter 4

Rossiter-McLaughlin Observations

We arrive at the heart - the beating heart - of this thesis. The Rossiter-McLaughlin effect is a fascinating thing to study. There is the elegance of it: an additional shape on the otherwise monotonous planetary signal, there is the information it carries, be it about the rotation of the star, or as has proven a most valuable observable: the projection of the spin/orbit angle. But there is another beauty in it given by CORALIE and HARPS, thanks to their automated, fast, accurate and precise reduction softwares. You see, dear reader, if one can marvel at the heavens, even in dark La Silla, if one can walk solely lit by the galactic bulge, if one can see its shadow cast by the powerful Venus, and if one can drive with sole view the magnificent Milky Way, there is one thing an astronomer rarely sees: motion. Most of the beauty we capture is frozen. The Rossiter-McLaughlin effect is a dynamical observation.

Observing for the regular planet search (WASP or the CORALIE survey), one can get excited by a new velocity measurements differing from that of the previous night, or that from two nights before, or a year before. I get excited by watching live the planet pass over its star, changing its apparent colour and inducing the Rossiter-McLaughlin effect. Live! In the same instant one knows exactly where the planet is on the stellar disc, which part it covers and how fast it is moving. One can, live, know whether the orbit is coplanar or retrograde!

Every Rossiter-McLaughlin effect is an event, something to look forward to (I got so addicted that I started observing M dwarfs transiting their primary to observe more of them!). Some observers can tell you, how I can at some insane hour in Europe, be up, on SKYPE, collecting point after point and observe the effect appear on my computer screen[1]. Maybe the most funny observation that I carried was that of WASP-15 b. I was on duty at the *Euler* Telescope, and Gaël Chauvin was observing on HARPS for the consortium. That night I spent running between the *Euler* control room and the then *Ritz* where HARPS was controlled from, and saw live that planet orbit retrogradely its star. For WASP-17 b, the CORALIE transit, and for the HARPS transit later, I was on SKYPE with the observer to check it.

The work that follows, really comes from a deep deep deep love for the subject.

[1] I still have a life, so I did not follow each effect like that, be reassured, my insanity is still bounded by a slight bit of rationality

4.1 The Change that Came

The scientific adventure progresses by incremental steps, a few large changes and a handful of sweeping transformations. I think - I hope - this work is part of a change which is somewhere in that second category, that to which belong those moments bringing a new observable on the table and forcing a rethink and an adjustment of the current paradigm.

Since the discovery of the first of them, the origins of hot Jupiters have been debated. There are those supporting disc migration (eg. Lin et al. (1996)) and those supporting planet-planet scattering and other dynamical effect followed by tidal capture (eg. Rasio & Ford (1996)) (according to Bodenheimer et al. (2000), in-situ formation might be possible though hard, but this is the least currently favoured explanation). We will get into the details of these theories in next chapter, but their mention is relevant to make clear the aims behind our Rossiter-McLaughlin survey and that of other groups. What we are looking to answer: we want to learn about the origin of hot Jupiters.

Both in-situ formation and disc migration are expected to deposit planets on modest eccentric orbits, with orbital planes close to coplanar with their star's (Goldreich & Sari 2003; Ogilvie & Lubow 2003). Dynamical interactions (not limited just to planet-planet interactions) are expected to produce planets on orbits with eccentricity spanning from close to 0 to above 1 (in which case we can't observe them). In addition they are expected to be on a range of orbital inclinations (Wu & Murray 2003; Fabrycky & Tremaine 2007; Jurić & Tremaine 2008; Chatterjee et al. 2008; Nagasawa et al. 2008).

Hut (1981); Eggleton & Kiseleva-Eggleton (2001); Winn et al. (2005) point out that if eccentricity and semi-major axis can decay relatively quickly due to tidal dissipation and blur the distinction between disc migration and dynamical events followed by a tidal capture (tidal migration), the orbital obliquity ψ will be decaying on a timescale longer than the lifetime of the system. Thus getting information about orbital obliquities could provide a manner with which one could differentiate between different migration pathways. This is why the Rossiter-McLaughlin effect is so important. By observing it, we measure β, the projection of ψ on the sky[2]. Therefore, collecting those measurements, we may probe how hot Jupiters came to the orbits they now occupy.

The first Rossiter-McLaughlin effect was observed by Queloz et al. (2000). It took five years for the next to appear thanks to Winn et al. (2005). Josh Winn and Norio Narita produced most of the first measurements. I started working on it from a suggestion by Michel Mayor and a master's work with Andrew Collier Cameron in 2006-07, and started my thesis to work on that particular subject. By the beginning of the PhD thesis, about five measurements had been done, and all showed spin/orbit alignment.

In Autumn 2008, came a paper by Hébrard et al. (2008) on XO-3 showing the best evidence of an asymmetric Rossiter-McLaughlin effect, but a doubt remained because of an incomplete transit sequence. We had just started our campaign of observations to systematically observe the transiting planets in range of the HARPS instrument. WASP-8 was our first target (WASP-18 had actually been observed a few months prior with the HARPS GTO time). WASP-8 b was found on a retrograde orbit[3]. The signal is extremely clear and could not be doubted. We finished the first leg of our survey by WASP-17 in summer 2009, and the paper that follows shows six of the eight Rossiter-McLaughlin effect that we observed, as well as a statistical analysis of the whole known

[2] let's remind here to the reader that there are two conventions for the spin/orbit angle. I and Simon Albrecht use a formalism based on work by Hosokawa (1953) where the angle β is used. Josh Winn, and the majority of other authors use the formalism of Ohta et al. (2005) who defined that angle as λ. The only difference is that $\beta = -\lambda$.

[3] Guillaume Hébrard was actually the observer on HARPS for the consortium the night it transited

sample then, including three claims for retrograde planets. Fabrycky & Winn (2009) produced a paper summarising Rossiter-McLaughlin measurements on the eleven then known systems. In the meantime, while the paper was getting ready, Winn et al. (2009c) confirmed XO-3 b's misalignment, Moutou et al. (2009) found out that HD 80606 b was transiting by notably observing an asymmetric effect, Johnson et al. (2009) produced a misaligned Rossiter-McLaughlin effect on WASP-14 and Winn et al. (2009b) and Narita et al. (2009b) found Hat-P-7 b on a retrograde orbit too just as Anderson et al. (2010) showed officially in WASP-17 b's discovery paper the three suspicious points that indicated a retrograde orbit. In a little over a year, the idea that all planets were on coplanar orbits with their star's equatorial plane was gone.

In addition contrary to the misaligned planets XO-3 b and HD 80606 b, which were on highly eccentric orbits leading one to think they may have suffered some dynamical event in their history, WASP-15 b and WASP-17 b are retrograde, but on circular orbits. This confirmed that the circularisation timescale is probably much shorter than the realignement timescale.

If I was to reanalyse those Rossiter-McLaughlin effects presented in the following paper, a few things would change like the addition of stellar jitter to obtain a χ^2 closer to 1; the jump parameters would change to those taken in the WASP-23 paper using $\sqrt{V \sin I} \cos\beta$ and $\sqrt{V \sin I} \sin\beta$ instead of $V \sin I \cos\beta$ and $V \sin I \sin\beta$ which creating a prior proportional to $V \sin I$ biased this observable to a higher - more significant - value (see section 3.4.4); taking in account what the error bars on χ^2 were really showing for WASP-2, this Rossiter-McLaughlin effect is not really detected, nothing can then be said about its retrogradicity, we in fact have probably fitted a variation due to statistical noise that looked like a Rossiter-McLaughlin effect (and since confirmed in Albrecht et al. (2011)).

Yet the main point remains, there are too many misaligned systems, something which standard disc migration theory cannot explain. Our conclusions were that disc migration alone cannot explain the observations.

In the course of the refereeing, both the referee and the editor asked that in addition to comparing the whole distribution in β with theoretical predictions from Nagasawa et al. (2008) and Fabrycky & Tremaine (2007), I also attempt comparing how a mix of disc migration and dynamics + tidal migration would compare. This paper is primarily about observations. Those are compared in a simple fashion to theoretical predictions in order to raise questions and show our observations in context. As Didier Queloz put it: theories come and go, observations stay. Going deeper into comparing the β distribution with an array of theoretical predictions was to risk over-interpreting (50 % of disc migration, 30 % of planet-planet scattering, 20 % of Kozai cycles for example?) as well as using theoretical predictions which would later turn-out wrong (for example the treatment of the Kozai mechanism has been recently refined by Naoz et al. (2011) in the context of planet-planet interactions). Such an analysis was presented by Morton & Johnson (2011).

A&A 524, A25 (2010)
DOI: 10.1051/0004-6361/201014525
© ESO 2010

Astronomy & Astrophysics

Spin-orbit angle measurements for six southern transiting planets

New insights into the dynamical origins of hot Jupiters⋆,⋆⋆

A. H. M. J. Triaud[1], A. Collier Cameron[2], D. Queloz[1], D. R. Anderson[3], M. Gillon[4], L. Hebb[5], C. Hellier[3], B. Loeillet[6], P. F. L. Maxted[3], M. Mayor[1], F. Pepe[1], D. Pollacco[7], D. Ségransan[1], B. Smalley[3], S. Udry[1], R. G. West[8], and P. J. Wheatley[9]

[1] Observatoire Astronomique de l'Université de Genève, Chemin des Maillettes 51, 1290 Sauverny, Switzerland
e-mail: Amaury.Triaud@unige.ch
[2] School of Physics & Astronomy, University of St Andrews, North Haugh, St Andrews KY16 9SS, Fife, Scotland, UK
[3] Astrophysics Group, Keele University, Staffordshire ST55BG, UK
[4] Institut d'Astrophysique et de Géophysique, Université de Liège, Allée du 6 Août, 17, Bât. B5C, Liège 1, Belgium
[5] Department of Physics and Astronomy, Vanderbilt University, Nashville, TN37235, USA
[6] Laboratoire d'Astrophysique de Marseille, BP 8, 13376 Marseille Cedex 12, France
[7] Astrophysics Research Centre, School of Mathematics & Physics, Queens University, University Road, Belfast BT71NN, UK
[8] Department of Physics and Astronomy, University of Leicester, Leicester LE17RH, UK
[9] Department of Physics, University of Warwick, Coventry CV4 7AL, UK

Received 28 March 2010 / Accepted 11 August 2010

ABSTRACT

Context. Several competing scenarios for planetary-system formation and evolution seek to explain how hot Jupiters came to be so close to their parent stars. Most planetary parameters evolve with time, making it hard to distinguish between models. The obliquity of an orbit with respect to the stellar rotation axis is thought to be more stable than other parameters such as eccentricity. Most planets, to date, appear aligned with the stellar rotation axis; the few misaligned planets so far detected are massive ($>2\,M_J$).
Aims. Our goal is to measure the degree of alignment between planetary orbits and stellar spin axes, to search for potential correlations with eccentricity or other planetary parameters and to measure long term radial velocity variability indicating the presence of other bodies in the system.
Methods. For transiting planets, the Rossiter-McLaughlin effect allows the measurement of the sky-projected angle β between the stellar rotation axis and a planet's orbital axis. Using the HARPS spectrograph, we observed the Rossiter-McLaughlin effect for six transiting hot Jupiters found by the WASP consortium. We combine these with long term radial velocity measurements obtained with CORALIE. We used a combined analysis of photometry and radial velocities, fitting model parameters with the Markov Chain Monte Carlo method. After obtaining β we attempt to statistically determine the distribution of the real spin-orbit angle ψ.
Results. We found that three of our targets have β above 90°: WASP-2b: $\beta = 153^{\circ}{}^{+11}_{-15}$, WASP-15b: $\beta = 139.6^{\circ}{}^{+5.2}_{-4.3}$ and WASP-17b: $\beta = 148.5^{\circ}{}^{+5.1}_{-4.2}$; the other three (WASP-4b, WASP-5b and WASP-18b) have angles compatible with 0°. We find no dependence between the misaligned angle and planet mass nor with any other planetary parameter. All six orbits are close to circular, with only one firm detection of eccentricity $e = 0.00848^{+0.00085}_{-0.00095}$ in WASP-18b. No long-term radial acceleration was detected for any of the targets. Combining all previous 20 measurements of β and our six and transforming them into a distribution of ψ we find that between about 45 and 85% of hot Jupiters have $\psi > 30°$.
Conclusions. Most hot Jupiters are misaligned, with a large variety of spin-orbit angles. We find observations and predictions using the Kozai mechanism match well. If these observational facts are confirmed in the future, we may then conclude that most hot Jupiters are formed from a dynamical and tidal origin without the necessity to use type I or II migration. At present, standard disc migration cannot explain the observations without invoking at least another additional process.

Key words. binaries: eclipsing – stars: general – techniques: spectroscopic

1. Introduction

The formation of close-in gas giant planets, the so-called *hot Jupiters*, has been in debate since the discovery of the first example, 51 Peg b, by Mayor & Queloz (1995). Since then, more than 440 extrasolar planets have been discovered. Following the discovery of HD 209548b (Charbonneau et al. 2000; Henry et al. 2000), more than 70 have been found to transit. The known planets present a rich and growing diversity in planetary parameters, such as separation, mass, radius (hence density) and eccentricity.

While it is generally accepted that close-orbiting gas-giant planets do not form in-situ, their previous and subsequent evolution is still mysterious. Several processes can affect the planet's eccentricity and semi-major axis. Inward migration via angular momentum exchange with a gas disc, first proposed in Lin et al. (1996) from work by Goldreich & Tremaine (1980), is a natural and widely-accepted explanation for the existence of these hot Jupiters.

⋆ Using observations with the high resolution échelle spectrograph HARPS mounted on the ESO 3.6 m (under proposals 072.C-0488, 082.C-0040 & 283.C-5017), and with the high resolution échelle spectrograph CORALIE on the 1.2 m *Euler* Swiss Telescope, both installed at the ESO La Silla Observatory in Chile.
⋆⋆ RV data is only available at the CDS via anonymous ftp to cdsarc.u-strasbg.fr (130.79.128.5) or via http://cdsarc.u-strasbg.fr/viz-bin/qcat?J/A+A/524/A25

A&A 524, A25 (2010)

Migration alone does not explain the observed distributions of planetary eccentricities and semi-major axes. Alternative mechanisms have therefore been proposed such as the Kozai mechanism (Kozai 1962; Eggleton & Kiseleva-Eggleton 2001; Wu & Murray 2003) and planet scattering (Rasio & Ford 1996). These mechanisms can also cause a planet to migrate inwards, and may therefore have a role to play in the formation and evolution of hot Jupiters. These different models each predict distinctive distributions in semi-major axis and eccentricity. Discriminating between various models is done by matching the distributions they produce to observations. Unfortunately this process does not take into account the evolution with time of the distributions and is made harder by the probable combination of a variety of migration mechanisms.

Transiting planets permit measurement of β, the projection on the sky of the angle between the star's rotation axis and the planet's orbital axis. This parameter is potentially a sensitive tracer of past migration history. Dynamical studies indicate that the obliquity (the real spin-orbit angle ψ) of an orbit evolves only slowly and is not as strongly affected by the proximity of the star as the eccentricity (Hut 1981; Winn et al. 2005; Barker & Ogilvie 2009). Disc migration is expected to leave planets orbiting close to the stellar equatorial plane. Kozai cycles and planet scattering should excite the obliquity of the planet and should produce a population of planets on misaligned orbits with respect to their star's rotation.

As a planet transits a rotating star, it will cause an overall redshifting of the spectrum if it covers the blue-shifted half of the star and vice-versa on the other side. This is called the Rossiter-McLaughin effect (Rossiter 1924; McLaughlin 1924). It was first observed for a planet by Queloz et al. (2000). Several papers model this effect: Ohta et al. (2005), Giménez (2006), Gaudi & Winn (2007).

Among the 70 or so known transiting planets discovered since 2000 by the huge effort sustained by ground-based transiting planet searches, the Rossiter-McLaughlin (RM) effects have been measured for 20, starting with observations on HD 209458 by Queloz et al. (2000). This method has proven itself reliable at giving precise and accurate measurement of the projected spin-orbit angle with its best determination done for HD 189733b (Triaud et al. 2009). Basing their analysis on measurements of β in 11 systems, 10 of which are coplanar or nearly so, Fabrycky & Winn (2009) concluded that the angle distribution is likely to be bimodal with a coplanar population and an isotropically-misaligned population. At that time, the spin-orbit misalignment of XO-3b (Hébrard et al. 2008) comprised the only evidence of the isotropic population. Since then, the misalignment of XO-3b has been confirmed by Winn et al. (2009c), and significant misalignments have been found for HD 80606b (Moutou et al. 2009) and WASP-14b (Johnson et al. 2009). Moreover, retrograde orbital motion has been identified in HAT-P-7b (Winn et al. 2009b; Narita et al. 2009). Other systems show indications of misalignment but need confirmation. One such object is WASP-17b (Anderson et al. 2010) which is one of the subjects of the present paper.

The Wide Angle Search for Planets (WASP) project is designed to find transiting gas giants (Pollacco et al. 2006). Observing the northern and southern hemispheres with sixteen 11-cm refractive telescopes, the WASP consortium has published more than 20 transiting planets in a large range of period, mass and radius, around stars with apparent magnitudes between 9 and 13. The planet candidates observable from the South are confirmed by a large radial-velocity follow-up program using the CORALIE high resolution échelle spectrograph, mounted on the 1.2 m *Euler* Swiss Telescope, at La Silla, Chile. As part of our efforts to understand the planets that have been discovered, we have initiated a systematic program to measure the Rossiter-McLaughlin effect in the planets discovered by the WASP survey, in order to measure their projected spin-orbit misalignment angles β.

Table 1. List of observations.

Target	Date	Instrument	Paper
WASP-18b	2008/08/21	HARPS	this paper
WASP-8b	2008/10/05	HARPS	Queloz et al. (2010)
WASP-6b	2008/10/07	HARPS	Gillon et al. (2009a)
WASP-4b	2008/10/08	HARPS	this paper
WASP-5b	2008/10/10	HARPS	this paper
WASP-2b	2008/10/15	HARPS	this paper
WASP-15b	2009/04/27	HARPS	this paper
WASP-17b	2009/05/22	CORALIE	this paper
WASP-17b	2009/07/05	HARPS	this paper

Notes. The date indicates when the first point of the Rossiter-McLaughlin sequence was taken.

In this paper we report the measurement of β in six southern transiting planets from the WASP survey, and analyse their long term radial-velocity behaviour. In Sects. 2 and 3 we describe the observations and the methods employed to extract and analyse the data. In Sect. 4 we report in detail on the Rossiter-McLaughlin effects observed during transits of the six systems observed. In Sects. 5 and 6 we discuss the correlations and trends that emerge from the study and their implications for planetary migration models.

2. The observations

In order to determine precisely and accurately the angle β, we need to obtain radial velocities during planetary transits at a high cadence and high precision. We therefore observed with the high resolution échelle spectrograph HARPS, mounted at the La Silla 3.6 m ESO telescope. The magnitude range within which planets are found by the SuperWASP instruments allows us to observe each object in adequate conditions. For the main survey proposal 082.C-0040, we selected as targets the entire population of transiting planets known at the time of proposal submission to be observable from La Silla during Period 82, i.e. WASP-2b, 4b, 5b, 6b, 8b and 15b. The results for WASP-6b are presented separately by Gillon et al. (2009a) and for WASP-8b by Queloz et al. (2010). Two targets were added in separate proposals. A transit of WASP-18b was observed during GTO time (072C-0488) of the HARPS consortium allocated to this planet because of its short and eccentric orbit. During the long-term spectroscopic follow-up of WASP-17b undertaken for the discovery paper (Anderson et al. 2010), three CORALIE measurements fell during transit showing a probably retrograde orbit. Observations of the Rossiter-McLaughlin effect with CORALIE confirmed the conclusions of Anderson et al. (2010), and a follow-up DDT proposal (283.C-5017) was awarded time on HARPS.

The strategy of observations was to take two high-precision HARPS points the night before transit and the night after transit. The radial-velocity curve was sampled densely throughout the transit, beginning 90 min before ingress and ending 90 min after egress. The data taken before ingress and after egress allow any activity-related offset in the effective velocity of the system's centre of mass to be determined for the night of observation. In addition, radial velocity data from the high resolution

Table 2. Stellar parameters used in our model fitting.

Parameters	Units	WASP-2 (a,b)	WASP-4 (c)	WASP-5 (c)	WASP-15 (d)	WASP-17 (a,e)	WASP-18 (f)
Spectral Type		K1	G8	G5	F7	F4	F6
$T_{\rm eff}$	K	5150 ± 80	5500 ± 100	5700 ± 100	6300 ± 100	6650 ± 80	6400 ± 100
$B-V$	mag	0.86 ± 0.05	0.73 ± 0.05	0.66 ± 0.05	0.48 ± 0.05	0.38 ± 0.05	0.45 ± 0.05
$\log g$	dex	4.40 ± 0.15	4.5 ± 0.2	4.5 ± 0.2	4.35 ± 0.15	4.45 ± 0.15	4.4 ± 0.15
[Fe/H]	dex	−0.08 ± 0.08	−0.03 ± 0.09	+0.09 ± 0.09	−0.17 ± 0.11	−0.19 ± 0.09	0.00 ± 0.09
$\log R'_{\rm HK}$	dex	−4.84 ± 0.10	−4.50 ± 0.06	−4.72 ± 0.07	−4.86 ± 0.05	–	−4.85 ± 0.02
$\xi_{\rm t}$	km s^{-1}	0.9 ± 0.1	1.1 ± 0.2	1.2 ± 0.2	1.4 ± 0.1	1.7 ± 0.1	1.6 ± 0.1
$V_{\rm macro}$	km s^{-1}	1.6 ± 0.3	2.0 ± 0.3	2.0 ± 0.3	4.8 ± 0.3	6.2 ± 0.3	4.8 ± 0.3
$v \sin I$	km s^{-1}	1.6 ± 0.7	2.0 ± 1.0	3.5 ± 1.0	4.0 ± 2.0	9.8 ± 0.5	11.0 ± 1.5
$M_\star$	$M_\odot$	0.84 ± 0.11	0.93 ± 0.05	1.00 ± 0.06	1.18 ± 0.12	1.2 ± 0.12	1.24 ± 0.04

Notes. The $v \sin I$ (stellar spectroscopic rotation broadening) and stellar mass estimates are used as priors in the analysis. $\xi_{\rm t}$ is the microturbulence. $V_{\rm macro}$ is the macrotrubulence.

References. (a) this paper; (b) Collier Cameron et al. (2007); (c) Gillon et al. (2009c); (d) West et al. (2009); (e) Anderson et al. (2010); (f) Hellier et al. (2009).

échelle spectrograph CORALIE mounted on the Swiss 1.2 m *Euler* Telescope, also at La Silla was acquired to help search for a long term variability in the the periodic radial velocity signal.

All our HARPS observations have been conducted in the OBJO mode, without a simultaneous thorium-argon comparison spectrum. The velocities are estimated by a thorium-argon calibration at the start of the night. HARPS is stable within 1 m s^{-1} across a night. This is lower than our individual error bars and avoids contamination of stellar spectrum by the Th-Ar lamp, easing spectral analysis.

3. The data analysis

3.1. Radial-velocity extraction

The spectroscopic data were reduced using the online Data Reduction Software (DRS) for the HARPS instrument. The radial velocity information was obtained by removing the instrumental blaze function and cross-correlating each spectrum with one of two masks. This correlation is compared with the Th-Ar spectrum acting as a reference; see Baranne et al. (1996), Pepe et al. (2002) & Mayor et al. (2003) for details. Recently the DRS was shown to achieve remarkable precision (Mayor et al. 2009) thanks to a revision of the reference lines for thorium and argon by Lovis & Pepe (2007). Stars with spectral type earlier than G9 were reduced using the G2 mask, while those of K0 or later were cross-correlated with the K5 mask. A similar software package is used for CORALIE data. A resolving power $R = 110\,000$ for HARPS yields a cross-correlation function (CCF) binned in 0.25 km s^{-1} increments, while for CORALIE, with a lower resolution of 50 000, we used 0.5 km s^{-1}. The CCF window was adapted to be three times the size of the full width at half maximum (*FWHM*) of the CCF.

All our past and current CORALIE data on the stars presented here were reprocessed after removal of the instrumental blaze response, thereby changing slightly some radial velocity values compared to those already published in the literature. Correcting this blaze is important for extracting the correct RVs for the RM effect. The uncorrected blaze created a slight systematic asymmetry in the CCF that was translated into a bias in radial velocities.

1σ error bars on individual data points were estimated from photon noise alone. HARPS is stable long term within 1 m s^{-1} and CORALIE at less than 5 m s^{-1}. These are smaller than our individual error bars and thus have not been taken into account.

3.2. Spectral analysis

Spectral analysis is needed to determine the stellar atmospheric parameters from which limb darkening coefficients can be inferred. We carried out new analyses for two of the target stars, WASP-2 and WASP-17, whose previously-published spectroscopic parameters were of low precision. For our other targets, the atmospheric parameters were taken from the literature, notably the stellar spectroscopic rotation broadening $v \sin I$ [1].

The individual HARPS spectra can be co-added to form a composite spectrum with $SNR > 100$, suitable for photospheric analysis using the UCLSYN spectral synthesis package (Smith 1992; Smalley et al. 2001) and ATLAS9 models without convective overshooting (Castelli et al. 1997). The spectral analysis followed the method described in many discovery papers published by the WASP consortium (e.g.: Wilson et al. 2008).

The stellar rotational $v \sin I$ is determined by fitting the profiles of several unblended Fe I lines. The instrumental *FWHM* was determined to be 0.065 Å from the telluric lines around 6300 Å.

For WASP-2, a value for macroturbulence ($v_{\rm mac}$) of 1.6 ± 0.3 km s^{-1} was adopted (Gray 2008). A best fitting value of $v \sin I = 1.6 \pm 0.7$ km s^{-1} was obtained. On WASP-17, a value for macroturbulence ($v_{\rm mac}$) of 6.2 ± 0.3 km s^{-1} was used (Gray 2008). The analysis gives a best fitting value of $v \sin I = 9.8 \pm 0.5$ km s^{-1}. The error on $v_{\rm mac}$ is taken from the scatter around fit to Gray (2008) and is propagated to the $v \sin I$.

All stellar parameters, used as well as derived, are presented in Table 2. Stellar $B-V$ colours were estimated from the effective temperature and used in the calculations of the $\log R'_{\rm HK}$ (Noyes et al. 1984; Santos et al. 2000; Boisse et al. 2009). Errors refer to the photon noise: they do not include systematic effects likely to arise and affect low values of $\log R'_{\rm HK}$ due to the low signal to noise in the blue orders. WASP-17 does not have a value since this stellar activity indicator is only calibrated for $0.44 < B-V < 1.20$.

3.3. Model fitting

The extracted radial velocity data was fitted simultaneously with the transit photometry available at the time of analysis. Three

[1] Throughout this paper we use the symbol I to denote the inclination of the stellar rotation axis to the line of sight, while i represents the inclination of the planet's orbital angular momentum vector to the line of sight.

A&A 524, A25 (2010)

models are adjusted to the data: a Keplerian radial velocity orbit (Hilditch 2001), a photometric planetary transit (Mandel & Agol 2002), and a spectroscopic transit, also known as Rossiter-McLaughlin effect (Giménez 2006). This combined approach is very useful for taking into account all of the possible contributions to the uncertainties due to correlations among all relevant parameters. A single set of parameters describes both the photometry and the radial velocities. We use a Markov Chain Monte Carlo (MCMC) approach to optimize the models and estimate the uncertainties of the fitted parameters. The fit of the model to the data is quantified using the χ^2 statistic.

The code is described in detail by Triaud et al. (2009), has been used several times (e.g.: Gillon et al. 2009a) and is similar to the code described in Collier Cameron et al. (2007).

We fitted up to 10 parameters, namely the depth D of the primary transit, the radial velocity (RV) semi-amplitude K, the impact parameter b, the transit width W, the period P, the epoch of mid-transit T_0, $e\cos\omega$, $e\sin\omega$, $V\sin I\cos\beta$, and $V\sin I\sin\beta$. Here e is the eccentricity and ω the angle between the line of sight and the periastron, $V\sin I$ is the sky-projected rotation velocity of the star[2] while β is the sky-projected angle between the stellar rotation axis (Hosokawa 1953; Giménez 2006) and the planet's orbital axis[3].

These parameters have been chosen to reduce correlations between then. The use of uncorrelated parameters allows to explore parameter space more efficiently since the correlation length between jumps is smaller. Eccentricity and periastron angle were paired as were $V\sin I$ and β. This breaks a correlation between them (the reader is invited to compare Figs. 2d and 3 for a clear illustration for choosing certain jump parameters as opposed to others). This way we also explore solutions around zero more easily: $e\cos\omega$ and $e\sin\omega$ move in the $]-1,1[$ range while e could only be floating in $]0,1[$. For exploring particular solutions such as a circular orbit, parameters can be fixed to certain values.

We caution that, as noted by Ford (2006) that the choice of $e\cos\omega$ and $e\sin\omega$ as jump variables implicitly imposes a prior that is proportional to e. This approach thus has a tendency to yield a higher eccentricity than would be obtained with a uniform prior, in cases when e is poorly-constrained by the data. A similar argument applies to the use of $V\sin I\cos\beta$ and $V\sin I\sin\beta$ as jump variables, in cases where the impact parameter is low and there is a strong degeneracy between $V\sin I$ and β in modelling the Rossiter-McLaughlin effect. In such cases, however, the tendency to overestimate $V\sin I$ from the Rossiter-McLaughlin effect can effectively be curbed by imposing an independent, spectroscopically-determined $v\sin I$ prior on $V\sin I$, as we have done here.

In addition to the physical free floating parameters, we need to use one γ velocity for each RV set and one normalisation factor for each lightcurve as adjustment parameters. These are found by using optimal averaging and optimal scaling. γ velocities represent the mean radial velocity of the star in space with respect to the barycentre of the Solar System. Since our analysis had many datasets, the results for these adjustment parameters have been omitted, not adding anything to the discussion.

During these initial analyses we also fitted an additional acceleration in the form of an RV drift $\dot{\gamma}$ but on no occasion was it significantly different from zero. We therefore assumed there was no drift for any of our objects. We will give upper limits for each star in the following sections.

The MCMC algorithm perturbs the fitting parameters at each step i according to the formula:

$$P_{i,j} = P_{i-1,j} + f\sigma_{P_j} G(0,1) \quad (1)$$

where P_j is a free parameter, G is a Gaussian random number of unit standard deviation and zero mean, while σ is the step size for each parameter. A factor f is used to control the chain and ensures that 25% of steps are being accepted via a Metropolis-Hastings algorithm, as recommended in Tegmark et al. (2004) to give an optimal exploration of parameter space.

The step size is adapted by doing several initial analyses. They are adjusted to produce as small a correlation length as possible. Once the value is chosen, it remains fixed. Only f fluctuates.

A *burn-in* phase of 50 000 accepted steps is used to make the chain converge. This is detected when the correlation length of each parameter is small and that the average χ^2 does not improve anymore (Tegmark et al. 2004). Then starts the real chain, of 500 000 accepted steps, from which results will be extracted. This number of steps is used as a compromise between computation time and exploration. Statistical tests, notably by comparing χ^2 are used to estimate the significance of the results.

Bayesian penalties can be added to χ^2 to account for any prior information that we might have on any fitted or derived parameter. Stellar mass $M_\star$ can notably be contrained via a prior in the MCMC in order to propagate its error bars into the estimate of the the planet's mass. Because of the random nature of a Markov chain, sometimes a step yields an impact parameter close to zero. This can cause $V\sin I$ to wander to unphysical values because of the degeneracy between $V\sin I$ and β at low impact parameters. We therefore imposed the $v\sin I$ found by spectral analysis as a prior in some of our fits to ensure consistency with the spectral analysis and to determine whether this influenced the fitted value of β. The prior values are in Table 2.

We use a quadratic limb-darkening law with fixed values for the two limb darkening coefficients appropriate to the stellar effective temperature. They were extracted for the photometry from tables published in Claret (2000). For the radial velocity (the Rossiter-McLaughlin effect is also dependent on limb darkening) we use values for the V band. Triaud et al. (2009) showed that HARPS is centred on the V band. The coefficients were chosen for atmospheric parameters close to those presented in Table 2.

3.4. Extracting the results

For each star, we performed four analyses, each using a MCMC chain with 500 000 accepted steps:

- 1. a prior is imposed on $V\sin I$, eccentricity is fixed to zero;
- 2. no prior on $V\sin I$, eccentricity is fixed to zero;
- 3. a prior is imposed on $V\sin I$, eccentricity is left floating;
- 4. no prior on $V\sin I$, eccentricity is left floating.

This is to assess the sensitivity of the model parameters to a small but uncertain orbital eccentricity and to the $v\sin I$ value found by spectral analysis which, as demonstrated in Triaud et al. (2009), can seriously affect the fitting of the Rossiter-McLaughlin effect. The comparative tables holding the results of

[2] We make a distinction between $v\sin I$ and $V\sin I$: $v\sin I$ is the value extracted from the spectral analysis, the stellar spectroscopic rotation broadening, while $V\sin I$ denotes the result of a Rossiter-McLaughlin effect fit. Both can at times be different. Each, although caused by the same effect, is independently measured making the distinction worthwhile.

[3] $\beta = -\lambda$, another notation used in the literature for the same angle.

these various fits are available in the Appendices to support the conclusions we reach while allowing readers to form their own opinion. In addition, we also conducted control chains fixing the parameters controlled by the photometry in order to check whether this was a limiting source of errors in the determination of our most important parameter: β. The results from these chains are in the Appendices as well. Although different in their starting hypotheses all the chains are also useful at checking their respective convergence. Our final results are presented in Table 3.

The best solution is found in the best of the four fits by comparing χ^2 and using Ockham's principle of minimising the number of parameters for similar results: for fits with similar $\chi^2_{\rm reduced}$ we usually choose a circular solution with no prior on $V \sin I$. Results are extracted from the best fit by taking the median of the posterior probability distribution for each parameter, determined from the Markov chain. Errors bars are estimated from the 68.3% confidence region of the accepted steps. The best solution is not taken from the lowest χ^2 as it is dependent on the sampling and chance encounter of a – small – local minimum. Scatter plots will be presented with the positions of the best χ^2, the average and the median for illustration.

In the following section and in tables, several statistical values are used: χ^2 is the value found for all the data, while $\chi^2_{\rm RV}$ gives the value of χ^2 solely for the radial velocities. The reduced χ^2 for the radial velocities, denoted by $\chi^2_{\rm reduced}$, is used to estimate how well a model fits the data and to compare various fits and their respective significance. In addition we will also use the residuals, denoted as O–C. These estimates are only for radial velocities. The results from photometry are not mentioned since they are not new. They are only here to constrain the shape of the Rossiter-McLaughlin effect.

When giving bounds, for eccentricity and long term radial velocity drift, we quote the 95% confidence interval for exclusion. Times are expressed by calculating the Barycentric Julian Dates using the UTC time standard.

4. The survey results

4.1. WASP-2b

A sequence of 26 RV measurements was taken on WASP-2 using HARPS on 2008 October 15, with additional observations made outside transit as given in the journal of observations presented in the Appendices. The cadence during transit was close to a point every 430 s. The average photon noise error of that sequence is 5.7 m s^{-1}. We made additional observations with CORALIE to refine the orbital solution obtained by Collier Cameron et al. (2007) using the SOPHIE instrument on the 1.93 m telescope at Observatoire de Haute-Provence, and to look for long-term variability of the orbit. 20 measurements were taken with a mean precision of 13.9 m s^{-1} over close to 11 months between 2008 October 25 and 2009 September 23. All the RV data is available at the CDS along with exposure times.

To establish the photometric ephemeris and the transit geometry, we fitted the photometric datasets of Collier Cameron et al. (2007) (3 seasons by SuperWASP in the unfiltered WASP bandpass), Charbonneau et al. (2007) (a z band *Keplercam* lightcurve) and Hrudková et al. (2009) (a William Herschel Telescope *AG2 R* band transit curve).

WASP-2b's data were fitted with up to 10 free parameters plus 8 independent adjustment parameters: three γ velocities for the three RV data sets and five normalisation factors for photometry. This sums up to 58 RV measurements and 8951 photometric observations.

$\chi^2_{\rm reduced}$ does not improve significantly between circular and eccentric models. We therefore impose a circular solution. The presence of a prior on $V \sin I$ does not affect the results. We find $V \sin I = 0.99^{+0.27}_{-0.32}$ km s^{-1} in accordance with the $v \sin I$ value found in Sect. 3.2. The fit delivers $\beta = 153^{\circ}{}^{+11}_{-15}$. The overall root-mean-square (rms) scatter of the spectroscopic residuals about the fitted model is 11.73 m s^{-1}. During the HARPS transit sequence these residuals are at 6.71 m s^{-1}.

Figure 3 shows the resulting distribution as $V \sin I$ vs. β. We detect $V \sin I$ significantly above zero with confidence interval showing that 99.73% (3σ) of the posterior probability function has $V \sin I > 0.2$ km s^{-1} while $\beta > 77.26^{\circ}$. We have computed 6 additional chains in order to test the strength of our conclusions. Table A.1 shows the comparison between the various fits; we invite the reader to refer to it as only important results are given in the text.

In all cases, eccentricity is not detected, being below a 3σ significance from circular which is likely affected by the poor coverage of the phase by the HARPS points. Circular solutions are therefore adopted. We fix the eccentricity's upper limit to $e < 0.070$. In addition no significant long term drift was detected in the spectroscopy: $|\dot{\gamma}| < 36$ m s^{-1} yr^{-1}.

Using the spectroscopically-determined $v \sin I$ value of 1.6 km s^{-1} and forcing β to zero, $\chi^2_{\rm reduced}$ changes from 2.14 ± 0.27 to 3.49 ± 0.39, clearly degrading the solution. We are in fact 7.6σ away from the best-fitting solution, therefore excluding an aligned system with this large a $V \sin I$. This is also excluded by comparison to a fit with a flat RM effect at the 6.7σ. Similarly, a fit with an imposed $V \sin I = 0.9$ km s^{-1} and aligned orbit is found 5.6σ from our solution. In Fig 1b, we have plotted the various models tested and their residuals so as to give a visual demonstration of the degradation for each of the alternative solutions.

4.2. WASP-4b

We obtained a RM sequence of WASP-4b with HARPS on 2008 October 8; other, out of transit, measurements are reported in the journal of observations given in the Appendices. The RM sequence comprises 30 data points, 13 of which are in transit, taken at a cadence of 630 s^{-1} with a mean precision of 6.4 m s^{-1}. The spectrograph CORALIE continued monitoring WASP-4 and we add ten radial velocity measurements to the ones published in Wilson et al. (2008). These new data were observed around the time of the HARPS observations, about a year after spectroscopic follow-up started.

In photometry we gathered 2 timeseries in the WASP bandpass from Wilson et al. (2008) and an R band *C2 Euler* transit plus a *VLT/FORS2* z band lightcurve obtained from Gillon et al. (2009c) to establish the transit shape and timing.

The WASP-4b data were fitted with up to 10 free parameters to which 6 adjustment parameters were added: two γ velocities for RVs and four normalisation factors for the photometry. In total, this represents 56 radial velocity points and 9989 photometric measurements. Gillon et al. (2009c) let combinations of limb darkening coefficients free to fit the high precision *VLT* curve. We used and fixed our coefficients on their values.

Because the impact parameter is small, a degeneracy between β and $V \sin I$ appeared, as expected (see Figs. 2d and 3). The values on stellar rotation for our unconstrained fits reach unphysical values as high as $V \sin I = 150$ km s^{-1}. We imposed a

Table 3. Fitted and physical parameters found after fitting photometric and spectroscopic data of WASP-4b with a prior on $V \sin I$.

Parameters	Units	WASP-2b	WASP-4b	WASP-5b	WASP-15b	WASP-17b	WASP-18b
fitted parameters							
D		$0.01802^{+0.00027}_{-0.00025}$	$0.023334^{+0.000044}_{-0.000072}$	$0.01223^{+0.00040}_{-0.00014}$	$0.00969^{+0.00013}_{-0.00011}$	$0.01672^{+0.00020}_{-0.00016}$	$0.00916^{+0.00020}_{-0.00012}$
K	m s^{-1}	$153.6^{+3.0}_{-3.1}$	$242.1^{+2.8}_{-3.1}$	$268.7^{+1.8}_{-1.9}$	$64.6^{+1.20}_{-1.25}$	$52.7^{+3.0}_{-2.8}$	$1816.7^{+1.9}_{-1.9}$
b	$R_\star$	$0.737^{+0.012}_{-0.013}$	$0.051^{+0.023}_{-0.049}$	$0.37^{+0.11}_{-0.06}$	$0.525^{+0.037}_{-0.028}$	$0.400^{+0.043}_{-0.040}$	$0.527^{+0.052}_{-0.046}$
W	days	$0.07372^{+0.00065}_{-0.00068}$	$0.08868^{+0.00008}_{-0.000014}$	$0.0988^{+0.0013}_{-0.0005}$	$0.1547^{+0.0012}_{-0.0009}$	$0.1843^{+0.0013}_{-0.0010}$	$0.09089^{+0.00080}_{-0.00061}$
P	days	$2.1522254^{+0.0000015}_{-0.0000014}$	$1.3382299^{+0.0000023}_{-0.0000021}$	$1.6284229^{+0.0000043}_{-0.0000039}$	$3.752100^{+0.000009}_{-0.000011}$	$3.7354330^{+0.0000076}_{-0.0000075}$	$0.94145290^{+0.00000078}_{-0.00000086}$
T_0	Bjd−2 450 000	$3991.51428^{+0.00020}_{-0.00021}$	$4387.327787^{+0.000040}_{-0.000039}$	$4373.99601^{+0.00014}_{-0.00016}$	$4584.69819^{+0.00021}_{-0.00020}$	$4559.18096^{+0.00025}_{-0.00021}$	$4664.90531^{+0.00016}_{-0.00017}$
$e \cos \omega$		–	–	–	–	–	$-0.00030^{+0.00071}_{-0.00063}$
$e \sin \omega$		–	–	–	–	–	$-0.00845^{+0.00092}_{-0.00087}$
$V \sin I \cos\beta$		$-0.86^{+0.30}_{-0.32}$	$1.88^{+0.18}_{-0.16}$	$3.10^{+0.40}_{-0.20}$	$-3.24^{+0.27}_{-0.31}$	$-8.43^{+0.45}_{-0.52}$	$15.52^{+1.03}_{-0.67}$
$V \sin I \sin\beta$		$0.44^{+0.17}_{-0.18}$	$-0.13^{+1.65}_{-1.33}$	$-0.68^{+0.54}_{-0.48}$	$2.75^{+0.34}_{-0.36}$	$5.17^{+0.75}_{-0.81}$	$-1.10^{+0.68}_{-0.64}$
derived parameters							
$R_p/R_\star$		$0.1342^{+0.0010}_{-0.0009}$	$0.15275^{+0.00014}_{-0.00024}$	$0.1106^{+0.0018}_{-0.0006}$	$0.09842^{+0.00067}_{-0.00058}$	$0.12929^{+0.00077}_{-0.00061}$	$0.09576^{+0.00105}_{-0.00063}$
$R_\star/a$		$0.1248^{+0.0025}_{-0.0024}$	$0.18079^{+0.00037}_{-0.00040}$	$0.182^{+0.011}_{-0.004}$	$0.1342^{+0.0039}_{-0.0027}$	$0.1467^{+0.0033}_{-0.0025}$	$0.313^{+0.012}_{-0.009}$
$\rho_\star$	$\rho_\odot$	$1.491^{+0.088}_{-0.85}$	$1.2667^{+0.0084}_{-0.0077}$	$0.84^{+0.06}_{-0.14}$	$0.394^{+0.024}_{-0.032}$	$0.304^{+0.016}_{-0.020}$	$0.493^{+0.043}_{-0.051}$
$R_\star$	$R_\odot$	$0.825^{+0.042}_{-0.040}$	$0.903^{+0.016}_{-0.019}$	$1.060^{+0.076}_{-0.028}$	$1.440^{+0.064}_{-0.057}$	$1.579^{+0.067}_{-0.060}$	$1.360^{+0.055}_{-0.041}$
$M_\star$	$M_\odot$	$0.84^{+0.11}_{-0.12}$	$0.930^{+0.054}_{-0.053}$	$1.000^{+0.063}_{-0.064}$	$1.18^{+0.14}_{-0.12}$	$1.20^{+0.12}_{-0.12}$	$1.24^{+0.04}_{-0.04}$
$V \sin I$	km s^{-1}	$0.99^{+0.27}_{-0.32}$	$2.14^{+0.38}_{-0.35}$	$3.24^{+0.35}_{-0.27}$	$4.27^{+0.26}_{-0.36}$	$9.92^{+0.40}_{-0.45}$	$14.67^{+0.81}_{-0.57}$ *
R_p/a		$0.01675^{+0.00045}_{-0.00040}$	$0.027617^{+0.000064}_{-0.000083}$	$0.0201^{+0.0015}_{-0.0006}$	$0.01321^{+0.00047}_{-0.00030}$	$0.01897^{+0.00051}_{-0.00040}$	$0.0299^{+0.0016}_{-0.0010}$
R_p	R_J	$1.077^{+0.055}_{-0.058}$	$1.341^{+0.023}_{-0.029}$	$1.14^{+0.10}_{-0.04}$	$1.379^{+0.067}_{-0.058}$	$1.986^{+0.089}_{-0.074}$	$1.267^{+0.062}_{-0.045}$
M_p	M_J	$0.866^{+0.076}_{-0.084}$	$1.250^{+0.050}_{-0.051}$	$1.555^{+0.066}_{-0.072}$	$0.551^{+0.041}_{-0.038}$	$0.453^{+0.043}_{-0.035}$	$10.11^{+0.24}_{-0.21}$
a	AU	$0.0307^{+0.0013}_{-0.0015}$	$0.02320^{+0.00044}_{-0.00045}$	$0.02709^{+0.00056}_{-0.00059}$	$0.0499^{+0.0019}_{-0.0017}$	$0.0500^{+0.0017}_{-0.0017}$	$0.02020^{+0.00024}_{-0.00021}$
i	°	$84.73^{+0.18}_{-0.19}$	$89.47^{+0.51}_{-0.24}$	$86.1^{+0.7}_{-1.5}$	$85.96^{+0.29}_{-0.41}$	$86.63^{+0.39}_{-0.45}$	$80.6^{+1.1}_{-1.3}$
e		<0.070	<0.0182	<0.0351	<0.087	<0.110	$0.00848^{+0.00085}_{-0.00095}$
ω	°	–	–	–	–	–	$-92.1^{+4.9}_{-4.3}$
β	°	153^{+11}_{-15}	-4^{+43}_{-34}	$-12.1^{+10.0}_{-8.0}$	$139.6^{+5.2}_{-4.3}$	$148.5^{+5.1}_{-4.2}$	$-4.0^{+5.0}_{-5.0}$
$\lvert\dot{\gamma}\rvert$	(m s^{-1} yr^{-1})	<36	<30	<47	<11	<18	<43
O–C$_{RV}$	m s^{-1}	11.73	15.16	12.63	10.89	31.32	13.70
O–C$_{RM}$	m s^{-1}	6.71	6.71	7.72	7.35	31.87; 30.57	15.02

Notes. The value from eccentricity was found using information from other fits as explained in the text.
⋆ This value is not really a $V \sin I$ but more an amplitude parameter for fitting the Rossiter-McLaughlin effect. Please refer to Sect. 4.6 treating WASP-18b

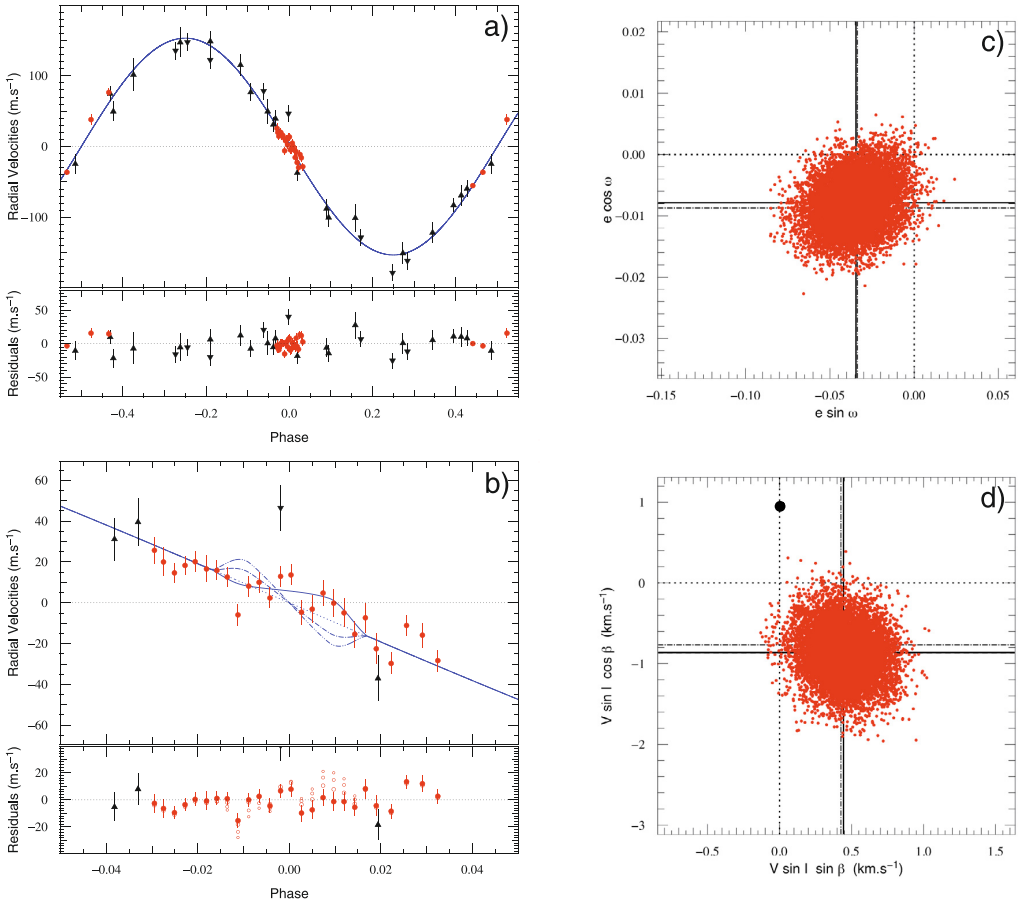


Fig. 1. Fit results for WASP-2b. **a)** Overall Doppler shift reflex motion of the star due to the planet and residuals. **b)** Zoom on the Rossiter-McLaughlin effect and residuals. Black inverted triangles are SOPHIE data, black triangles represent CORALIE points, red dots show the HARPS data. The best fit model is also pictured as a plain blue line. In addition to our best model found with $V \sin I = 0.99\,\mathrm{km\,s^{-1}}$ we also present models with no RM effect plotted as a dotted blue line, RM effect with $\beta = 0$ and $V \sin I = 0.9\,\mathrm{km\,s^{-1}}$ drawn with a dashed-dotted blue line and RM effect with $\beta = 0$ and $V \sin I = v \sin I = 1.6\,\mathrm{km\,s^{-1}}$ pictured with a dashed-double dotted blue line. In the residuals, the open symbols represent in the values with the size of the circle decreasing with the likelyhood of the model. **c)** Posterior probability distribution issued from the MCMC showing the distribution of points between $e \cos \omega$ and $e \sin \omega$. **d)** Posterior probability distribution issued from the MCMC showing the distribution of points between $V \sin I \cos \beta$ and $V \sin I \sin \beta$. The black disc shows where the distribution would be centred only changing to $\beta = 0$. The dotted line shows where zero is. The straight lines represent the median of the distribution, the dashed lines plot the position of the average values, the dash-dotted lines indicate the values with the lowest χ^2 (some lines can overlap). The size of boxes **c)** and **d)** represents 7 times the 1σ distance on either side of the median.

prior on the stellar rotation to restrict it to values consistent with the spectroscopic analysis.

The reduced χ^2 is the same within error bars whether eccentricity if fitted or fixed to zero. Therefore the current best solution, by minimising the number of parameters, is a circular orbit.

The eccentricity is constrained to $e < 0.0182$. Thanks to the long time series in spectroscopy we also investigated the presence of a long term radial velocity trend. Nothing was significantly detected: $|\dot{\gamma}| < 30\,\mathrm{m\,s^{-1}\,yr^{-1}}$.

Because of the small impact parameter the spin-orbit angle is poorly constrained with $\beta = -4^{\circ}{}^{+43}_{-34}$, even when a prior is imposed on $V \sin I$. The high S/N of the Rossiter-McLaughlin effect allows us to exclude a projected retrograde orbit.

4.3. WASP-5b

Using HARPS, we took a series of 28 exposures on WASP-5 at a cadence of roughly 630 s with a mean photon noise of $5.5\,\mathrm{m\,s^{-1}}$ on 2008 October 16. Other measurements were obtained at dates before and after this transit. Five additional CORALIE spectra were acquired the month before the HARPS observations. They were taken about a year after the data published in Anderson et al. (2008). All spectroscopic data is available from the Appendices.

To help determine transit parameters, published photometry was assembled and comprises three seasons of WASP data, two *C2 Euler* lightcurves in *R* band, and one *FTS i′* band lightcurve (Anderson et al. 2008).

WASP-5b's 49 RV measurements and 14 754 photometric points were fitted with up to 10 free parameters to which 8

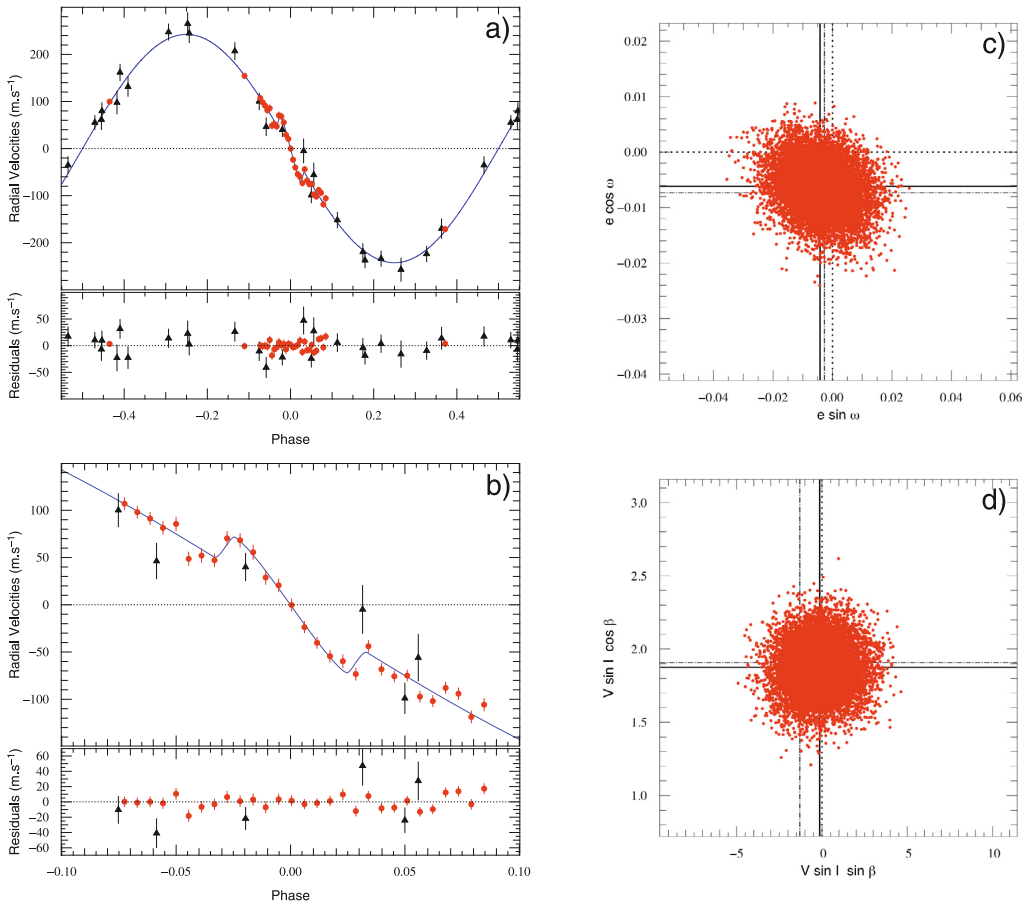


Fig. 2. Fit results for WASP-4b. Nota Bene: Legend similar to the legend in Fig. 1.

adjustment parameters had to be added: two γ velocities and six normalisation factors.

The imposition of a prior on $V \sin I$ prior has little impact on the final results (see Appendices) and their 1σ error bars but prevents $V \sin I$ from attaining unphysical values on occasions when, through the random process of the MCMC, the impact parameter b gets very close to zero. We constrain the solution using a prior. The priorless solution gives a $V \sin I$ fully consistent with $v \sin I$ thereby obtaining an independent measurement of the projected stellar equatorial rotation speed. Allowing eccentricity to float did not produce a significantly better fit. It has a 99.6% chance of being different from zero: at 2.9σ. Thus, minimising the number of parameters for a similar fit, we chose the solution with a circular orbit and simply place an upper limit on the eccentricity: $e < 0.0351$. No long term RV trend appears at this date: $|\dot{\gamma}| < 47\,\mathrm{m\,s^{-1}\,yr^{-1}}$.

Parameters extracted are similar to those that were published in Gillon et al. (2009c), and Anderson et al. (2008) and with Southworth et al. (2009) using a independent dataset. The projection of the spin-orbit angle is found to be: $\beta = -12.1^{\circ\,+10.0}_{\ -8.0}$ and we obtain an independent measurement of $V \sin I = 3.24^{+0.34}_{-0.35}\,\mathrm{km\,s^{-1}}$ fully compatible with the spectral value that was used as a prior in other fits. Results are presented in Table 3.

The $\chi^2_{\mathrm{reduced}}$ for spectroscopy (see Table A.1) is quite large, at 3.68 ± 0.44. The O–C for CORALIE data stand at $17.94\,\mathrm{m\,s^{-1}}$ to be compared with an average error bar of $18.13\,\mathrm{m\,s^{-1}}$. The badness of fit therefore comes from the HARPS sequence which has a dispersion of $8.98\,\mathrm{m\,s^{-1}}$ for an average error bar of $5.49\,\mathrm{m\,s^{-1}}$. From Fig. 4b we can see that residuals are quite important during the transit; Fig. 4d also shows that the MCMC does not produce a clean posterior distribution. This is mostly caused by impact parameter values nearing zero during parameter exploration and causing a degeneracy between V sin I and β. This can be observed in Fig. 3 with similitude to what occurs to WASP-4.

No better solution can be adjusted to the data: we remind that the RM effect is fitted in combination with six photometric sets which strongly constrain the impact parameter, depth and width of the Rossiter-McLaughlin effect. The $V \sin I \cos\beta$ vs. $V \sin I \sin\beta$ distribution is not centred on zero but close to it. This may come from the intrinsic dispersion in the data. Among the six data points which are spread over the rest of the phase, we have a dispersion of $11.92\,\mathrm{m\,s^{-1}}$. A likely cause to explain the data dispersion is stellar activity. Table 2 indicates that this star is moderately active. A longer discussion on $\chi^2_{\mathrm{reduced}} > 1$. is presented in Sect. 5.3. Santos et al. (2000) show that for the $\log R'_{\mathrm{HK}}$ that we find, we can expect a variation in velocities of the order of 7 to $12\,\mathrm{m\,s^{-1}}$.

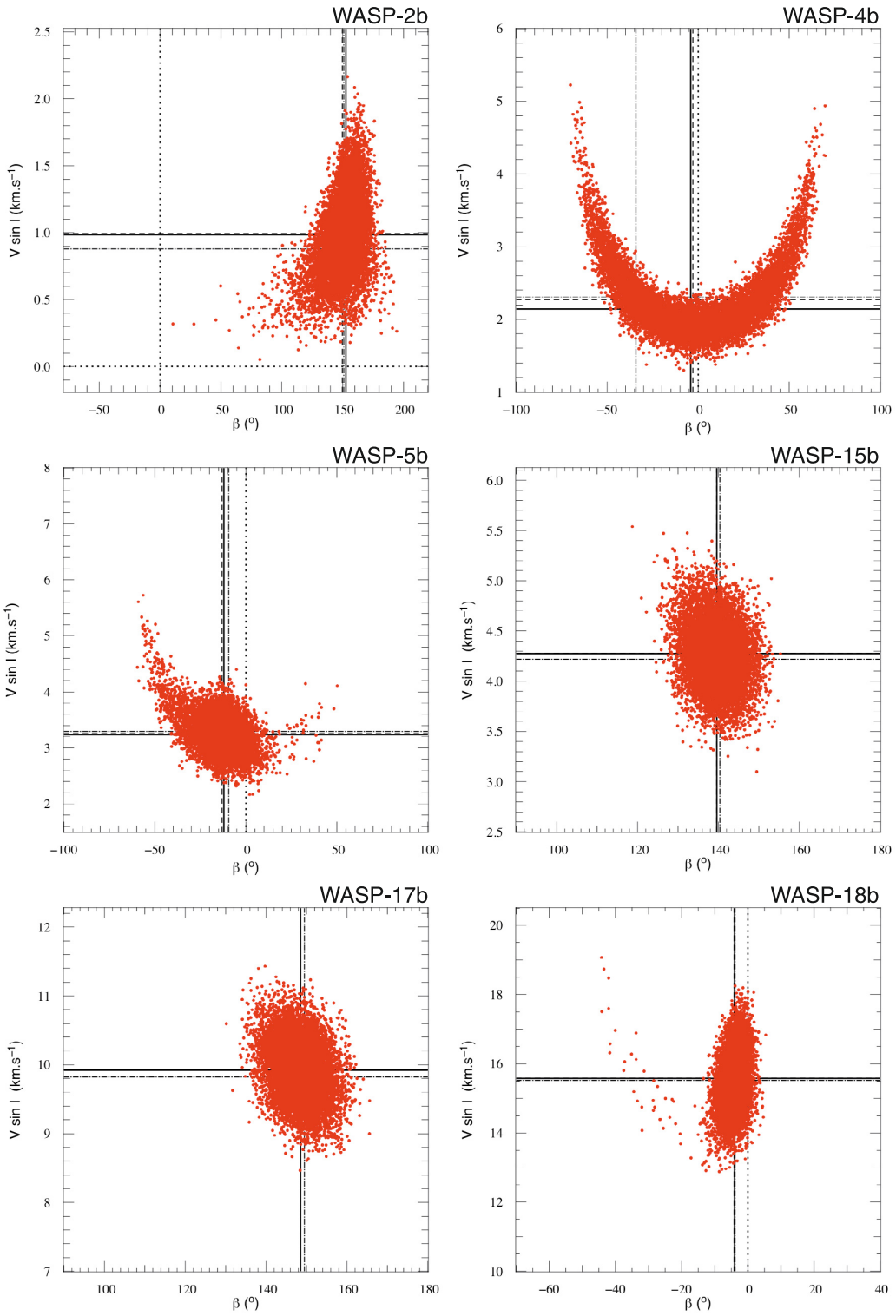


Fig. 3. Posterior probability distribution issued from the MCMC showing the resulting distributions of points between $V \sin I$ and β for our six WASP targets. These distributions are issued from the chains that gave our preferred solutions as explained in the text. The dotted lines show where zeros are, the straight lines represent the medians of the distributions, the dashed lines plot the positions of the average values, the dash-dotted lines indicate the values with the lowest χ^2 (some lines can overlap). The scale of the boxes was adapted to include the whole distibutions.

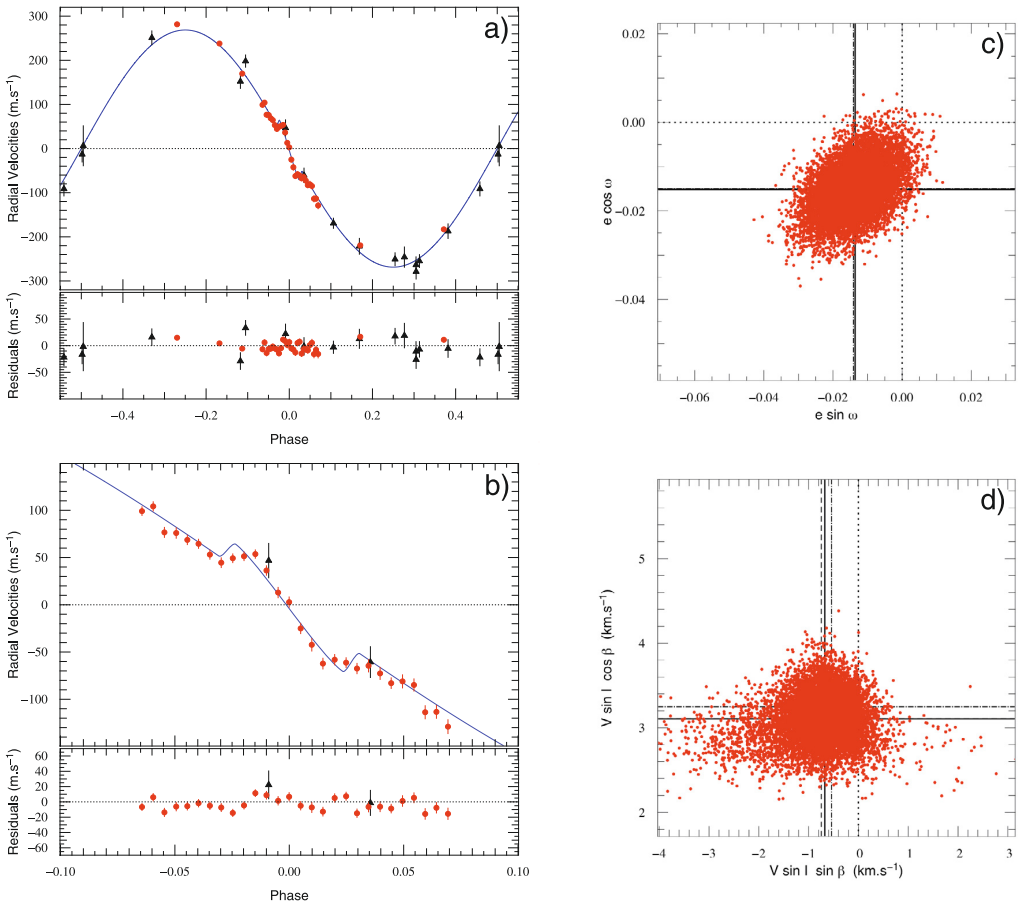


Fig. 4. Fit results for WASP-5b. Nota Bene: Legend similar to the legend in Fig. 1.

4.4. WASP-15b

Observations were conducted using the spectrographs CORALIE and HARPS. 23 new spectra have been acquired with CORALIE in addition to the 21 presented in West et al. (2009) and extending the time series from about a year to 500 days. We observed a transit with HARPS on 2009 April 27. 46 spectra were obtained that night, 32 of which are during transits with a cadence of 430 s. Additional observations have been taken as noted in the journal of observations.

The photometric sample used for fitting the transit has data from five time-series in the WASP bandpass, as well as one *I* and one *R* band transit from *C2 Euler* (West et al. 2009). The spectral data were partitioned into two sets: CORALIE and HARPS.

7 normalisation factors and 2 γ velocities were added to ten free floating parameters to adjust our models to the data which included a total of 95 spectroscopic observations and 23 089 photometric measurements.

For the various solutions attempted, $\chi^2_{\rm reduced}$ are found the same (Table A.2). We therefore choose the priorless, circular adjustment as our solution.

Compared to West et al. (2009), parameters have only changed little. Thanks to the higher number of points we give an upper limit on eccentricity: $e < 0.087$ (Fig. 5c shows results consistent with zero); there is no evident long term evolution in the radial velocities, which is constrained within: $|\dot{\gamma}| < 11\,{\rm m\,s^{-1}\,yr^{-1}}$. The projected spin-orbit angle is found rather large with $\beta = 139.6^{\circ\,+5.2}_{-4.3}$ making WASP-15b appear as a retrograde planet with a very clear detection. $V \sin I$ is found within 1σ of the spectrally analysed value of $v \sin I$ from West et al. (2009) at $4.27^{+0.26}_{-0.36}$ km s^{-1} and as such constitutes a precise independent measurement.

$\chi^2_{\rm reduced} = 1.51 \pm 0.19$ for the spectroscopy, indicating a good fit of the Keplerian as well as of the Rossiter-McLaughlin effect, the best fit in this paper. Full results can be seen in Table 3.

4.5. WASP-17b

On 2009 May 22, 11 CORALIE spectra were obtained at a cadence of 2030s with an average precision of 33.67 m s^{-1} to confirm the detection of retrograde orbital motion announced by Anderson et al. (2010). The sequence was stopped when airmass reached 2. HARPS was subsequently used and on 2009 July 5 a sequence of 42 spectra was acquired with a cadence of 630 s during transit. They have a mean precision of 19.02 m s^{-1}. In addition to these and to data already published 12 CORALIE spectra and 15 HARPS spectra were obtained. All the spectroscopic data is presented in the Appendices.

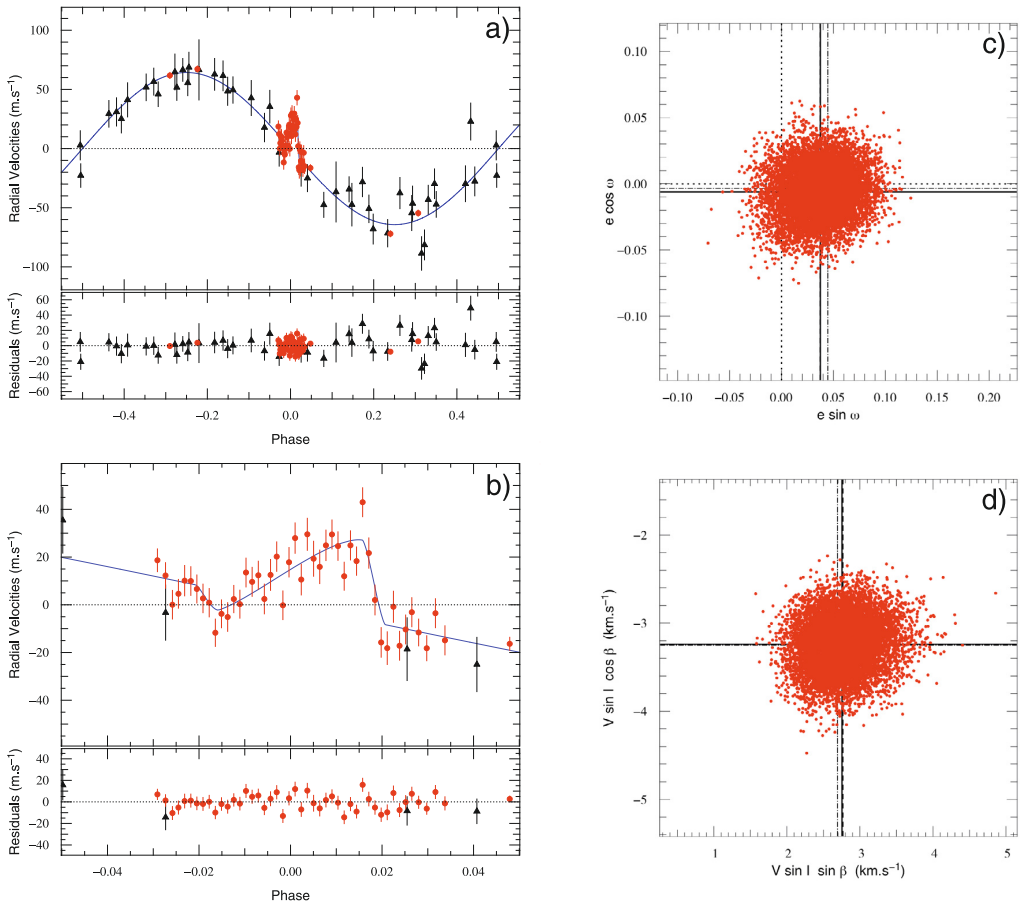


Fig. 5. Fit results for WASP-15b. Nota Bene: Legend similar to the legend in Fig. 1.

Table 4. List of γ velocities for WASP-17's RV sets.

Instrument	Dataset	γ (m s^{-1})
CORALIE	*Rossiter-McLaughlin effect*	$-49500.80^{+2.62}_{-1.57}$
CORALIE	*orbital Doppler shift*	$-49513.67^{+0.46}_{-0.37}$
HARPS	*Rossiter-McLaughlin effect*	$-49490.59^{+2.72}_{-1.64}$
HARPS	*orbital Doppler shift*	$-49491.68^{+0.17}_{-0.17}$

The photometry includes five timeseries of data in the WASP bandpass, and one *C2 Euler I* band transit (Anderson et al. 2010).

The model had to adjust up to 10 free floating parameters and 10 adjustment parameters (6 photometric normalisation factors and 4 radial velocity offsets) to 15 690 photometric data points and 124 spectroscopic points.

The RV was separated into four datasets fitted separately as detailed in Table 4. This was done to mitigate the possibility that the RM effect was observed at a particular activity level for the star. Stellar activity adds an additional RV variation. For a set where this data is taken randomly over some time, one expects activity to act like a random scatter around a mean which would be the true γ velocity of the star in space. But for a sequence such as the RM effect, we expect only a slowly-varying radial-velocity bias caused by the activity level on the star on the night concerned. This analysis method is explained in Triaud et al. (2009) which showed an offset in γ velocities between different Rossiter-McLaughlin sequences of HD 189733 which can only be attributed to stellar variability. The large number of CORALIE and HARPS measurements outside transit and their large temporal span allowed us to separate RV sets for WASP-17 but not for the other targets. Table 4 shows the four values of γ. We remark a difference of 13 m s^{-1} for CORALIE, justifying our segmentation of the data.

Among the four computed chains, we select the circular solution, with prior on V sin I since our results show eccentricity is not significantly detected but that the prior on V sin I prevents the MCMC from wandering to small impact parameters leading to the degeneracy between V sin I and β.

The non significant eccentricity presented by Anderson et al. (2010) was not confirmed, so a circular orbit was adopted. We confine to within $e < 0.110$. Eccentricity affects the derived value of the stellar density, and thereby also affects the planet's radius measurement. Our circular solution suggests that WASP-17b's radius is $1.986^{+0.089}_{-0.074}\,R_J$, making it the largest and least dense extrasolar planet discovered so far. We looked for an additional long term acceleration but found none: $|\dot{\gamma}| < 18$ m s^{-1} yr^{-1}.

The Rossiter-McLaughlin effect is well fitted. The residuals show some dispersion about the model during the HARPS

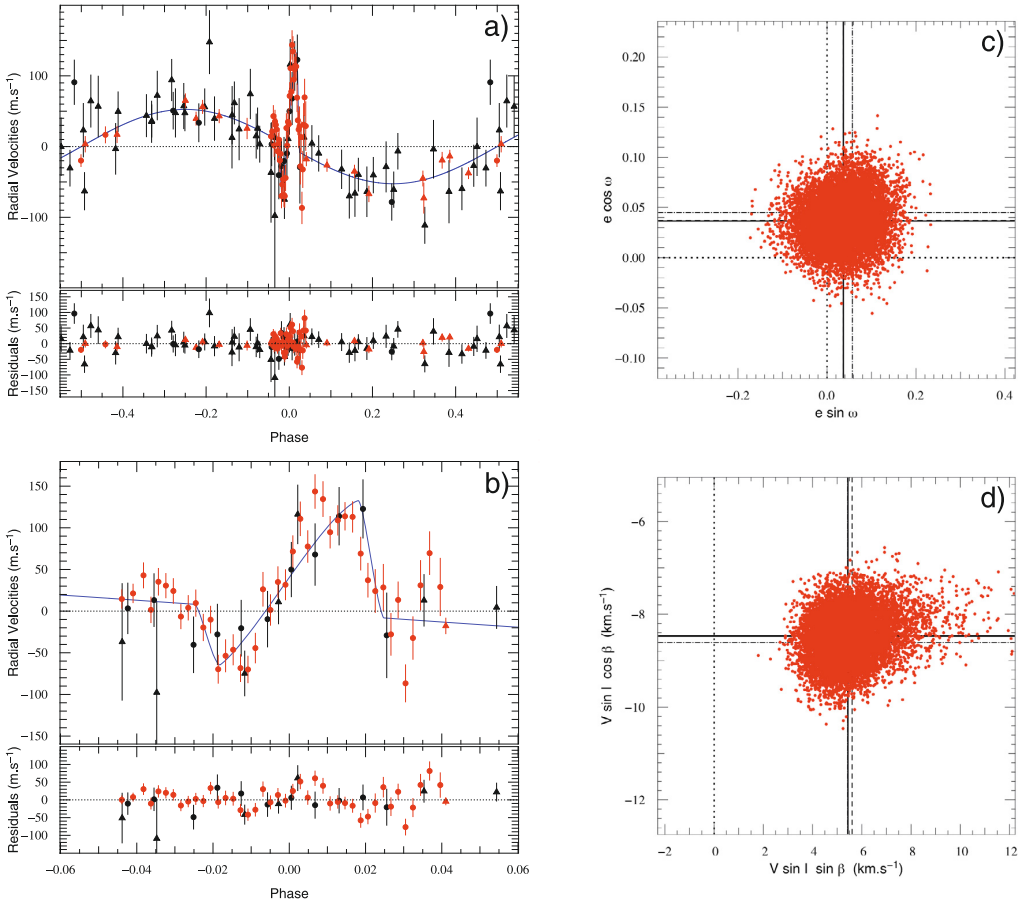


Fig. 6. Fit results for WASP-17b. On **a)** and **b)** black circles represent the RM effect taken with CORALIE, while black triangles picture the remaining CORALIE measurements; red dots show the HARPS RM data, red triangles are the remained HARPS points. Nota Bene: Legend similar to the legend in Fig. 1.

sequence. At the end of the HARPS transit, the airmass attained high values which account for the larger error bars, the sparser sampling and higher dispersion. By comparison the CORALIE sequence appears better: its longer exposures blurred out short-term variability. Both $V \sin I$ and β are unambiguously detected. WASP-17b is on a severely misaligned orbit: $V \sin I = 9.92\,\mathrm{km\,s^{-1}}$ and $\beta = 148.5^{\circ\,+5.1}_{-4.2}$. Full results are displayed in Table 3.

4.6. WASP-18b

Soon after WASP-18b was confirmed by the spectrograph CORALIE, a Rossiter-McLaughlin effect was observed with HARPS. We obtained 19 measurements at a cadence of 630s on 2008 August 21. The mean photon noise for the transit sequence is $6.99\,\mathrm{m\,s^{-1}}$. Seeing and airmass improved during the sequence, increasing the S/N and decreasing the individual error bars. Additional data were also acquired out of transit. Hellier et al. (2009) presented 9 RV measurements from CORALIE. 28 more have been taken and are presented in this paper. They span over three months. The total data timeseries spans close to 500 days. All RV measurements are presented in the journal of observations at the end of the paper.

Transit timing and geometry were secured by four photometric series: two SuperWASP seasons and two *C2 Euler* transits in *R* band, presented in Hellier et al. (2009).

The fitted data comprises 8593 photometric measurements and 60 radial velocities. Ten free parameters were used, with, in addition, four normalisation constants and two γ velocities.

Eccentricity is clearly detected, improving $\chi^2_{\mathrm{reduced}}$ from 5.58 ± 0.47 to 3.70 ± 0.36 (from 4.31 ± 0.46 to 2.00 ± 0.32 if we remove the RM effect from the calculation). We therefore exclude a circular solution.

The $V \sin I$ found in the priorless chain differs from the spectral analysis ($15.57^{+1.01}_{-0.69}$ instead of $11 \pm 1.5\,\mathrm{km\,s^{-1}}$), this solution is preferred so as to not produce biased results. For this particular case, we should consider $V \sin I$ more like a amplitude parameter in order to fit the Rossiter-McLaughlin effect rather than a bone fide measurement of projected rotation of the star. Therefore, the solution we favour is that of an eccentric orbit, without a prior on the $V \sin I$.

Results are presented in Table. 3, and the best fit is shown in Fig. 7. This Rossiter-McLaughlin effect is one of the largest so far measured, with an amplitude of nearly $185\,\mathrm{m\,s^{-1}}$. During the transit sequence $O - C = 15.02\,\mathrm{m\,s^{-1}}$ for a mean precision of $6.95\,\mathrm{m\,s^{-1}}$: the fit is poor; $\chi^2_{\mathrm{reduced}} = 3.70 \pm 0.36$. This is likely

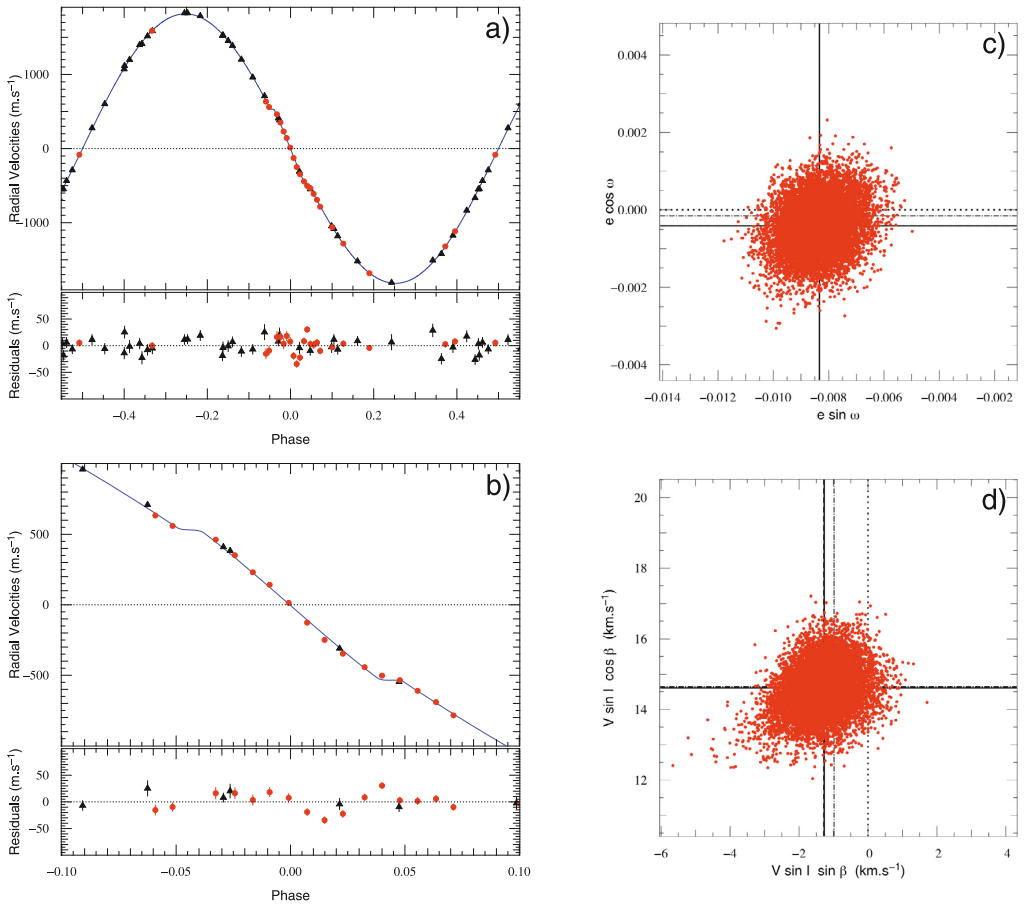


Fig. 7. Fit results for WASP-18b. Nota Bene: Legend similar to the legend in Fig. 1.

caused by a misfit of a symmetric Gaussian on a no longer symmetrical CCF[4]. We are in fact *resolving* the planet transit in front of the star like spots can be detected via Doppler tomography. This has recently been modelled and detected for HD 189733b, as a *Doppler shadow* by Collier Cameron et al. (2010). The uncertainty of the β parameter is not affected by the misfit since it is measured from the asymmetry of the Rossiter-McLaughlin effect. It is in essence estimated from the difference between the time spent in the approaching and receding hemispheres of the star.

All parameters can therefore be trusted except the $V \sin I$, including the much sought after β angle. We find it to be consistent with zero within 1.5σ: $\beta = -4.0^{\circ}{}^{+2.5}_{-2.5}$. The precision on this angle is the best we measured, something that is not reflected in the fit, we therefore doubled error bars to $\beta = -4.0^{\circ}{}^{+5.0}_{-5.0}$. This is in part thanks to the brightness of the star, allowing precise measurements of a large amplitude effect. Any departure from the model is quickly penalised in χ^2 by the data. Similarly, eccentricity is detected above 9σ with $e = 0.00848^{+0.00085}_{-0.00095}$ thanks to the large amplitude of the reflex motion. Note, that fitting $e \cos \omega$ and $e \sin \omega$ can correspond to fitting e proportional to e and tending to bias the search for solutions towards higher values. We attempted a few control fits exploring instead $\sqrt{e}\cos\omega$ & $\sqrt{e}\sin\omega$. The results showed there is no bias in our analysis, so strongly is the eccentricity constrained by the radial velocities. The spectroscopic coverage gives us the chance to put some limits on an undetected long term radial velocity drift: $|\dot{\gamma}| < 43\,\mathrm{m\,s^{-1}\,yr^{-1}}$.

The other parameters are consistent with the values published by Hellier et al. (2009) and are presented in Table 3.

5. Overall results

Our fits to the Rossiter-McLaughlin effect confirm the presence of planetary spectroscopic transit signatures in all six systems. While three of the six appear closely aligned, the other three exhibit highly-inclined, apparently retrograde orbits. The orbits of all six appear close to circular. Only the massive WASP-18b yields a significant detection of orbital eccentricity.

5.1. Orbital eccentricities

As Gillon et al. (2009b) noted, allowing eccentricity to float as a free fitting parameter increases the error bars on other parameters; we are exploring a larger parameter space. One might argue

[4] this was noted in Triaud et al. (2009) in the case of HD 189733b and CoRoT-3b, but can also be seen on fits of CoRoT-2b (Bouchy et al. 2008), Hat-P-2b (Loeillet et al. 2008) and others.

A&A 524, A25 (2010)

that allowing eccentricity to float is necessary since no orbit is perfectly circular, therefore making an eccentric orbit the simplest model available. We argue against this for the simple reason that if statistically we cannot distinguish between an eccentric and a circular model then the eccentric model is not detected. Actually, the mere fact of letting eccentricity float biases the result towards a small non zero number, a bias which can be larger than the actual physical value (Lucy & Sweeney 1971). Hence letting eccentricity float when it is not detected is to allow values of parameter space for all parameters to be explored which do not need to be. This is why, unless χ^2 is significantly improved by adding two additional parameters to a circular model, we consider the former as preferable. In addition to the risk of biasing, there is a strong assumption that due to tidal effects circularising the planet's orbit, eccentricities are really small and therefore undetectable for the majority of targets. It is therefore reasonable to assume a value of zero when the data does not contradict it. To facilitate comparison, we also present the results of fits with floating eccentricity. These are given in the Appendices; our preferred solutions are described in the text and in Table 3.

Only for WASP-18b, have we detected some eccentricity in the orbit, thanks primarily to the high amplitude of the RV signal and the brightness of the target. The amount of RV data taken on WASP-18b is not really more than for the other targets. In addition to a high semi-amplitude, sampling is another key to fixing eccentricity properly. The lack of measured eccentricities on our other targets shows how difficult it is to measure a small eccentricity for these planets as long as no secondary transit is detected to constrain it. Spurious eccentricities tend to appear in fits to data sets where the radial velocities are not sampled uniformly around the orbit, and where the amplitude is small compared to the stellar and instrumental noise levels.

A good example is the case of WASP-17b for which the doubling of high precision RV points solely permitted us to place a tighter constraint compared to Anderson et al. (2010).

5.2. Fitting the Rossiter-McLaughlin effect

Our observations yielded results from which five sky-projected spin-orbit angles β have been determined with precision better than 15°. Three of these angles appear to be retrograde: half our sample. Adding the two other stars from our original sample that have been published separately (WASP-6b and WASP-8b) we obtain 4 out of 8 angles being not just misaligned but also over 90°. The precision on the angle depends mostly on the spectroscopy as is shown by comparing fits where parameters controlled by the photometry are kept fixed (in the Appendices).

The error bar on WASP-4b's β is large. A degeneracy appears when the impact parameter is close to 0 between $V \sin I$ and β. The estimate of the spin-orbit angle therefore relies on a good estimate of the stellar rotational velocity as well as with getting a stronger constraint on the shape of the Rossiter-McLaughlin effect. WASP-5b, WASP-17b and WASP-18b are also affected by this degeneracy, with much lower consequences, when the MCMC takes a random step in low impact parameters. This is controlled by the use of a prior on $V \sin I$.

When the planet is large compared to the parent star, or the star rotates rapidly, the cross-correlation function develops a significant asymmetry during transit. This happens because the spectral signature of the light blocked by the planet is partially resolved. Fitting a Gaussian to such a profile yields a velocity estimate that differs systematically from the velocity of the true light centroid. Winn et al. (2005), and later Triaud et al. (2009) and Hirano et al. (2010) showed how this effect can lead to over-estimation of $V \sin I$. Hirano et al. (2010) have developed an analytic method to compensate for this bias. Collier Cameron et al. (2010) circumvent the problem altogether by modelling the CCF directly, decomposing the profile into a stellar rotation profile and a model of the light blocked by the planet.

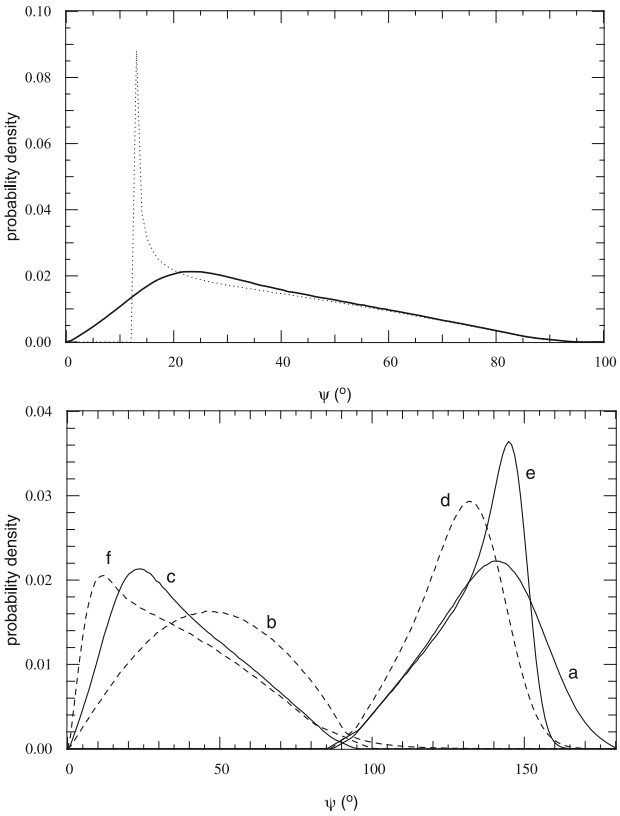


Fig. 8. *Top*: Smoothed histogram of the ψ distribution for WASP-5b. The dotted line is when errors on i and β are set to zero. The plain curve shows the same conversion from β to ψ but with all errors accounted for. *Bottom*: 6 smoothed histograms of the distribution in ψ our six targets: a) WASP-2b; b) WASP-4b; c) WASP-5b; d) WASP-15b; e) WASP-17b; f) WASP-18b. Bins are of 1°.

Only one star in our sample suffers from this misfit: WASP-18b where easily we see that the value the fit issues for the $V \sin I$ is above the estimated value taken via spectral analysis. WASP-17b is the second fastest rotating star. If affected, it is not by much: the fitted $V \sin I$ is found within 1σ of the $v \sin I$.

As shown in Fabrycky & Winn (2009), we can get an idea of the real angle ψ from β by using the following equation, coming only from the geometry of the system:

$$\cos\psi = \cos I \cos i + \sin I \sin i \cos\beta \quad (2)$$

where I is the inclination of the stellar spin axis and i the inclination of the planet's orbital axis to the line of sight.

Using the reasonable assumption that the stellar spin axis angle I is distributed isotropically, we computed the above equation using a simple Monte-Carlo simulation to draw a random uniform distribution in $\cos I$. We also inserted the error bars on i and β, using a Gaussian random number adjusted to the 1σ error bars printed in Table 5. Figure 8 shows the transformation from β to ψ for our targets, also illustrating the importance of including error bars in the calculation. We computed the lower ψ

Table 5. Comparative table of all Rossiter-McLaughlin effects published and parameters.

Planet	R_p (R_J)	M_p (M_J)	e	P (day)	i (°)	β (°)	$V \sin I$ (km s^{-1})	References
HD 17156b	$1.23^{+0.17}_{-0.20}$	$3.09^{+0.22}_{-0.17}$	$0.6719^{+0.0052}_{-0.0063}$	$21.21747^{+0.00070}_{-0.00067}$	$85.4^{+1.9}_{-1.2}$	-9.4 ± 9.3	6.3 ± 1.1	Cochran et al. (2008); Gillon et al. (2008)
HD 80606b	0.9 ± 0.1	4.0 ± 0.3	0.934 ± 0.003	111.436 ± 0.003	89.6 ± 0.4	-53^{+21}_{-34}	2.2	Moutou et al. (2009); Winn et al. (2009a)
HD 147506b	$0.951^{+0.039}_{-0.053}$	$8.62^{+0.39}_{-0.55}$	$0.5163^{+0.0025}_{-0.0023}$	5.63341 ± 0.00013	$90.00^{+0.85}_{-0.93}$	$-0.2^{+12.2}_{-12.5}$	$22.9^{+1.1}_{-1.2}$	Loeillet et al. (2008)
HD 149026b	0.718 ± 0.065	0.352 ± 0.025	0	$2.87618^{+0.00018}_{-0.00033}$	86.1 ± 1.4	12 ± 15	$6.2^{+2.1}_{-0.6}$	Wolf et al. (2007)
HD 189733b	$1.178^{+0.016}_{-0.023}$	$1.138^{+0.022}_{-0.025}$	$0.0041^{+0.0025}_{-0.0020}$	$2.21857312^{+0.00000036}_{-0.00000076}$	$85.51^{+0.10}_{-0.05}$	$0.85^{+0.28}_{-0.32}$	$3.316^{+0.017}_{-0.067}$	Triaud et al. (2009)
HD 209458b	1.355 ± 0.002	0.657 ± 0.006	0.0147 ± 0.0053	$3.52474859 \pm 0.00000038$	86.55 ± 0.03	4.4 ± 1.4	4.70 ± 0.16	Winn et al. (2005); Knutson et al. (2007)
XO-3b	1.5 ± 0.2	12.5 ± 1.9	0.2884 ± 0.0035	3.19161 ± 0.00014	82.5 ± 1.5	-37.3 ± 3.7	18.31 ± 1.3	Hébrard et al. (2008); Winn et al. (2009c)
HAT-P-1b	1.225 ± 0.059	0.524 ± 0.031	0	4.4652934 ± 0.0000093	86.28 ± 0.20	-3.7 ± 2.1	3.75 ± 0.58	Johnson et al. (2008)
HAT-P-7b	$1.363^{+0.195}_{-0.087}$	$1.776^{+0.077}_{-0.049}$	0	2.2047304 ± 0.0000024	$80.8^{+2.8}_{-1.2}$	-182.5 ± 9.4	$4.9^{+1.2}_{-0.9}$	Pál et al. (2008); Winn et al. (2009b); Narita et al. (2009)
TrES-1b	1.081 ± 0.029	0.61 ± 0.06	0	3.0300722 ± 0.0000002	88.4 ± 0.3	-30 ± 21	1.3 ± 0.3	Narita et al. (2007)
TrES-2b	$1.220^{+0.045}_{-0.042}$	1.198 ± 0.053	0	2.470621 ± 0.00017	83.62 ± 0.14	9 ± 12	1.0 ± 0.6	Winn et al. (2008); Daemgen et al. (2009)
TrES-4b	1.674 ± 0.094	0.84 ± 0.10	0	3.553945 ± 0.000075	82.81 ± 0.33	-7.3 ± 4.6	8.3 ± 1.1	Mandushev et al. (2007); Narita et al. (2010)
CoRoT-1b*	1.49 ± 0.08	1.03 ± 0.12	0	1.5089557 ± 0.0000064	85.1 ± 0.5	77 ± 11	5.2 ± 1.0	Barge et al. (2008); Pont et al. (2010)
CoRoT-2b	1.465 ± 0.029	3.31 ± 0.16	0	1.7429964 ± 0.0000017	87.84 ± 0.10	-7.1 ± 5.0	$11.46^{+0.29}_{-0.44}$	Alonso et al. (2008); Bouchy et al. (2008)
CoRoT-3b*	$0.9934^{+0.0058}_{-0.0058}$	$21.23^{+0.82}_{-0.59}$	$0.008^{+0.015}_{-0.005}$	$4.2567994^{+0.0000039}_{-0.0000031}$	$86.10^{+0.73}_{-0.52}$	$37.6^{+10.0}_{-22.3}$	$35.8^{+8.2}_{-8.3}$	Triaud et al. (2009)
Kepler-8b*	$1.419^{+0.056}_{-0.058}$	$0.60^{+0.13}_{-0.19}$	0	$3.52254^{+0.00003}_{-0.00005}$	84.07 ± 0.33	26.9 ± 4.6	10.5 ± 0.7	Jenkins et al. (2010)
WASP-2b	$1.077^{+0.055}_{-0.058}$	$0.866^{+0.076}_{-0.084}$	0	$2.1522254^{+0.0000015}_{-0.0000014}$	$84.73^{+0.18}_{-0.19}$	153^{+11}_{-15}	$0.99^{+0.27}_{-0.32}$	This paper
WASP-3b	$1.29^{+0.05}_{-0.07}$	$2.04^{+0.07}_{-0.07}$	0	1.846834 ± 0.000002	$84.93^{+1.32}_{-0.80}$	$-3.3^{+4.4}_{-2.5}$	$14.1^{+1.5}_{-1.3}$	Pollacco et al. (2008); Tripathi et al. (2010)
WASP-4b	$1.341^{+0.023}_{-0.029}$	$1.250^{+0.050}_{-0.051}$	0	$1.3382299^{+0.0000023}_{-0.0000021}$	$89.47^{+0.51}_{-0.24}$	-4^{+43}_{-34}	$2.14^{+0.38}_{-0.35}$	This paper
WASP-5b	$1.14^{+0.10}_{-0.04}$	$1.555^{+0.066}_{-0.072}$	0	$1.6284229^{+0.0000043}_{-0.0000039}$	$86.1^{+0.7}_{-1.5}$	$-12.1^{+10.0}_{-8.0}$	$3.24^{+0.35}_{-0.27}$	This paper
WASP-6b	$1.224^{+0.051}_{-0.052}$	$0.503^{+0.019}_{-0.038}$	0	$3.3610060^{+0.0000022}_{-0.0000035}$	$88.47^{+0.65}_{-0.47}$	11^{+14}_{-18}	$1.6^{+0.27}_{-0.17}$	Gillon et al. (2009a)
WASP-8b	$1.039^{+0.070}_{-0.048}$	$2.244^{+0.079}_{-0.093}$	$0.3101^{+0.0029}_{-0.0024}$	$8.158715^{+0.000016}_{-0.000015}$	$88.54^{+0.15}_{-0.17}$	$123.2^{+4.4}_{-3.4}$	$1.59^{+0.08}_{-0.10}$	Queloz et al. (2010)
WASP-14b	$1.281^{+0.075}_{-0.082}$	$7.34^{+0.51}_{-0.50}$	0.0903 ± 0.0027	2.23752 ± 0.000010	$84.32^{+0.67}_{-0.57}$	33.1 ± 7.4	2.89 ± 0.57	Joshi et al. (2009); Johnson et al. (2009)
WASP-15b	$1.379^{+0.067}_{-0.058}$	$0.551^{+0.041}_{-0.038}$	0	$3.752100^{+0.000009}_{-0.000011}$	$85.96^{+0.29}_{-0.41}$	$139.6^{+5.2}_{-4.3}$	$4.27^{+0.26}_{-0.36}$	This paper
WASP-17b	$1.986^{+0.089}_{-0.074}$	$0.453^{+0.043}_{-0.035}$	0	$3.7354330^{+0.0000076}_{-0.0000075}$	$86.63^{+0.39}_{-0.45}$	$148.5^{+5.1}_{-4.2}$	$9.92^{+0.40}_{-0.45}$	This paper
WASP-18b	$1.267^{+0.062}_{-0.045}$	$10.11^{+0.24}_{-0.21}$	$0.00848^{+0.00085}_{-0.00095}$	$0.94145290^{+0.00000078}_{-0.00000086}$	$80.6^{+1.1}_{-1.3}$	$-4.0^{+5.0}_{-5.0}$	$14.61^{+0.81\dagger}_{-0.57}$	This paper

Notes. Asterisks show claims of misalignments which remain to be confirmed.
(†) This values is not really a $V \sin I$ but more an amplitude parameter for fitting the Rossiter-McLaughlin effect. Please refer to Sect. 4.6 treating WASP-18b.

A&A 524, A25 (2010)

(at the 3σ limit) and found that in the stars we surveyed: WASP-15b is >90.3° and WASP-17b >91.7° therefore retrograde, while WASP-2b is >89.8° most probably retrograde.

Statistically we will fail to detect a Rossiter-McLaughlin effect (hence β and ψ) on stars nearly pole-on (with a low I). WASP-2b, with its small $V \sin I$ could be a close case. It could be one reason why its RM amplitude is so small (or stellar rotation so low). We observe that the spread in ψ is larger than for our other targets.

5.3. $\chi^2_{\rm reduced} > 1$

It can be remarked from the text or from the Appendices that a few of our objects have $\chi^2_{\rm reduced} > 1.$; in the case of WASP-5 notably. This shows the models are not adjusted perfectly to the data. As showcased by model fits to WASP-4, 15 and 17 (with $\chi^2_{\rm reduced} < 2.$) and in many publications using the CORALIE and HARPS spectrographs, produced error bars on individual radial velocity points are well estimated and understood and worth using as they are (Lovis et al. 2006).

An easy way to solve the problem would be to scale error bars so as to achieve an acceptable χ^2. By increasing error bars blindly, we risk hiding sources of error that we do not yet understand: if an extra signal is observed by the instruments, there may be useful;information in a bad χ^2. Error bars can be scaled with a value of *stellar jitter* added quadratically to individual errors, but this applies only if one samples randomly over long periods of time an extra stellar signal. In our case, part of our out-of-transit RVs would feel this *jitter*, but it would not apply in the same way to the Rossiter-McLaughlin sequences during which we are sensitive to a correlated noise of a different frequency. This renders the increase of error bars prone to errors of judgement, thus leading to a wrong computation of the model.

Hence, we decided to produce results without interfering with the way the data is estimated giving the best optimisation of the data that we could produce using known and substantiated physics. We leave to the reader the assessment of where this extra signal originates from.

5.4. Correlations between parameters

We present a compilation of results from all known observations of the Rossiter-McLaughlin effect in transiting exoplanetary systems in Table 5. No clear correlation is evident between important planetary parameters such as radii, masses, eccentricities, orbital periods, β and $V \sin I$, except that planets with $M < 2\,M_{\rm J}$ and $e > 0.1$ are rare among transiting systems (the only two are Neptunes around M dwarfs); this remark is independent from having a Rossiter-McLaughlin measurement or not. It is hard to see if this is really a result, or a bias due to observations (eg: transits harder to extract from the survey photometry, or to confirm via radial velocity), or a lack of precision during follow-up making eccentricity hard to detect with confidence. WASP-17b, for example, was previously thought to be the most eccentric transiting planet with $M < 2\,M_{\rm J}$ but our analysis yields only an upper limit $e < 0.110$. Eccentricities with as great as $e = 0.1$ have been published for some planets with masses less that $2\ M_{\rm J}$, none of these results are significant at more than the $\sim 2\sigma$ level.

The current ($M_{\rm p} \sin i$, e) distribution in radial velocity does not show this result, but these masses are only minimum masses.

Amongst planets where eccentricity is firmly detected, four out of seven are misaligned. Some of the hot Jupiters appear to be in multiple systems but this appears unrelated to other parameters such as eccentricity or misalignment. Examples are: HD 80606 (Naef et al. 2001), HD 189733 (Bakos et al. 2006), Hat-P-1 (Bakos et al. 2007), WASP-8 (Queloz et al. 2010), Hat-P-7 (Winn et al. 2009b), WASP-2, TrES-2 and TrES-4 (Daemgen et al. 2009).

6. Discussion

After a long sequence of closely-aligned planets (Fabrycky & Winn 2009), the sudden appearance of so many misaligned planets is somewhat surprising if not unpredicted. In a collapsing gas cloud, conservation of angular momentum will create a disc from which a star can form. Thus it is expected that star and disc rotate in the same direction with parallel spin axes. If planets form in and migrate through the disc, we can extend the idea that planets' orbital axes and stellar rotation axes ought to be parallel. Tides alone cannot make a planet retrograde (Hut 1981). Therefore it is expected that the creation of retrograde planets involves another body: planetary or stellar. Several papers (Wu et al. 2007; Fabrycky & Tremaine 2007; Nagasawa et al. 2008; Chatterjee et al. 2008; Jurić & Tremaine 2008; Bate et al. 2000, 2009) produce via various processes, orbits which are not coplanar with the host star's equator. Of these papers Wu et al. (2007), Fabrycky & Tremaine (2007) and Nagasawa et al. (2008) produce the largest range of angles.

When combining the 26 RM effects that have been observed, we now see that eight planets are severely misaligned: XO-3b (Hébrard et al. 2008; Winn et al. 2009c), HD 80606b (Moutou et al. 2009; Pont et al. 2009; Winn et al. 2009a), WASP-14b (Johnson et al. 2009), Hat-P-7b (Winn et al. 2009b; Narita et al. 2009), WASP-8b (Queloz et al. 2010) and WASP-2b, WASP-15b and WASP17b. Of these eight, five have been found to be in retrograde orbits, four from our survey.

Three additional targets may be misaligned: Kepler-8b (Jenkins et al. 2010), CoRoT-1b (Pont et al. 2010) and CoRoT-3b (Triaud et al. 2009). All three are around faint stars and fairly fast rotators making it hard to determine the angle. All β measurements have been plotted in Fig. 9a. Because we only measure the sky-projection of the angle, the planets can in fact be in a variety of configurations. What is their real angle ψ distribution?

Deconvolving the whole β distribution into ψ is hypothesis dependent. Hence, to compare the observational data and theoretical predictions we chose to produce cumulative histograms of observational and theoretical β angles in Fig. 9b. We transformed predictions from Fabrycky & Tremaine (2007) and Nagasawa et al. (2008), by taking their ψ histograms and transforming them geometrically into observable β, with the assumption that I is isotropic. For a fixed ψ, we define an azimuthal angle α measured from a zero point where the star's north pole is tilted towards the observer. If we precess the star for $\alpha \in [0, 2\pi[$ we obtain β via a Monte Carlo simulation from solving:

$$\tan\beta \simeq \tan\psi \sin\alpha \qquad (3)$$

using the conservative assumption that $i = 90°$ since these systems are transiting.

Results from this transform are in Fig. 9b. The observational data have been overplotted. Both observations and models by Fabrycky & Tremaine (2007) agree that about 55% of planets should appear with $\beta < 30°$[5]. Overall the theoretical distribution is a little steeper than the observations. We clearly remark that

[5] This criterion of misalignement of $\beta > 30°$, is a limit where, with current error bars on β, one can generally have a significant detection of a misalignment.

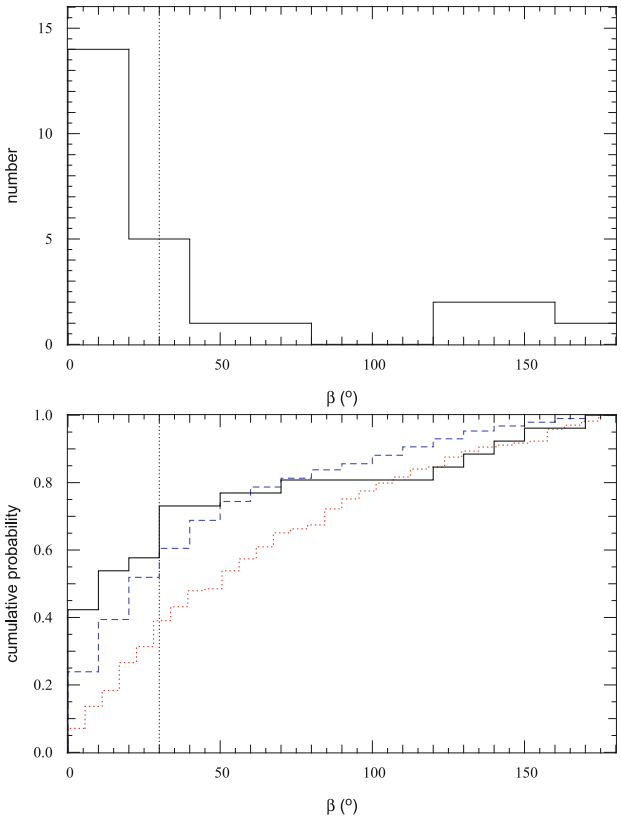


Fig. 9. *Top*: histogram of all the β measured, binned by 20°. *Bottom*: cumulative probability function for models by Fabrycky & Tremaine (2007) (blued dashed) and Nagasawa et al. (2008) (red dotted) converted from ψ to β, compared with current observations of β (plain black). The vertical black dotted line shows $\beta = 30°$. Above that, planets are considered misaligned.

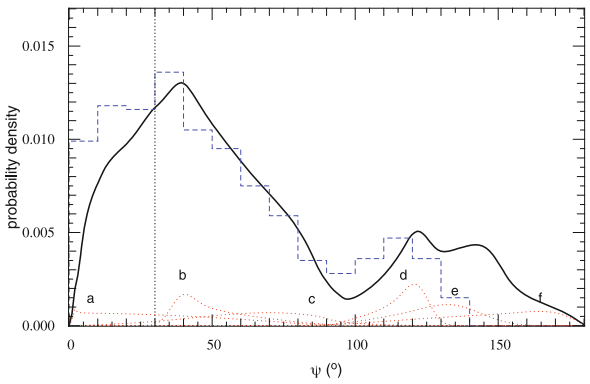


Fig. 10. The above histogram transformed into the real angle ψ in solid line and smoothed to bins of 1°. Red dotted curves show key individual objects in order to illustrate some of the features of the overall distribution. The blue dashed histogram is the reproduction of the theoretical histogram published by Fabrycky & Tremaine (2007) and solely plotted over. a) HD 189733b; b) XO-3b; c) HD 80606b; d) WASP-8b; e) WASP-15b; f) Hat-P-7b. The black dotted line shows $\psi = 30°$. Above that, planets are considered misaligned.

predictions by Nagasawa et al. (2008) agree in range but not in the shape of distribution of observed β, notably, it lacks enough aligned systems. This model is handy to illustrate the difference between the observations and a distribution isotropic in ψ.

Disc migration models would only produce a steep distribution reaching unity before 30°. A combination of several models is not attempted here because of the vast amount of possibilities and the likelihood that models will evolve.

The theoretical ψ distribution published by Fabrycky & Tremaine (2007), transformed into β, shown along the angle distribution obtained from observations, in Fig. 9b gives a remarkably close match. If the form of this distribution is borne out by future observations, we may then conclude that hot Jupiters are formed by this very mechanism. Wu et al. (2007) predictions are essentially the same as those from Fabrycky & Tremaine (2007).

We also attempted to generalise the method explained in Sect. 5.2 to all objects presented in Table 5: we are going to assume two distributions for the stellar spin axis in order to derive a distribution of real obliquity ψ. Two hypotheses were tested. The first was to assume an isotropy of the stellar axis orientation, by taking a uniform distribution in $\cos I$ from 0 to 1; the second was to assume stellar axes are aligned with the plane of the sky. For this last hypothesis we assumed all $\cos I$ followed a Gaussian distribution centred on 0 with a variance of 0.1, an error bar corresponding to the best of what observations can give us at the moment to constrain the stellar I. Taking these hypotheses allows us to test for extremes and get an idea of the true proportion of misaligned planetary systems.

The first hypothesis is shown in Fig. 10 plotted in comparison with the theoretical predictions by Fabrycky & Tremaine (2007). Inferring an isotropic distribution in stellar axes gives us as an upper bound that 86.2% of the probability density distribution is at $\psi > 30°$. The other hypothesis gives a proportion of 43.6% of misaligned systems. The effect of constraining the stellar I makes every individual contribution narrower in range. Taking a stricter constraint does not change this proportion much.

Both hypotheses are at the extremes of what the real distribution of I is. We interpret these results as showing that between 45 and 85% of systems are misaligned with $\psi > 30°$. Aligned systems are no longer the norm, radically altering our view on how these hot Jupiters formed.

Fabrycky & Tremaine (2007) and Wu et al. (2007) use the Kozai mechanism (Kozai 1962; Wu & Murray 2003) induced by an outer binary companion to the inner planet, to move the planet from the ice line where it is thought to form, to the inner stellar system. As the planet gets closer to the primary, tidal friction helps to break the Kozai cycles and finalise the planet's orbital parameters. Their equations are extracted from work by Eggleton & Kiseleva-Eggleton (2001). The resulting ψ distribution extends from 0° up to 150° away from the primary's rotation axis (see Fig. 10). In this scenario, the planet can be created in a binary star system, or around a single star which acquired a companion through interactions in its cluster of origin (Pfahl & Muterspaugh 2006). Fabrycky & Tremaine (2007) following on a paper by Malmberg et al. (2007), also predict that in multi-planetary systems undergoing Kozai cycles thanks to a nearby star, the most massive planet would survive the resulting planet-planet scattering. Although Kozai cycles are usually associated with high eccentricities, we should not be surprised by the presence of so many misaligned planets on circular orbits. As simulated in the case of HD 80606b in Fabrycky & Tremaine (2007),

A&A 524, A25 (2010)

the Kozai cycle has ended (is responsible the close proximity of the planet to the central star at periastron making precession dominated by general relativity rather than by the action of the third body). The planet appears now in a process of circularisation that will take ~0.7 Gyr, while its angle ψ remains almost constant.

Nagasawa et al. (2008) model scattering processes between planets creating a pair where one planet is on a close orbit and the other around 40 to 100 AU which then drives Kozai cycles on the inner planet. They also use tidal friction with the star. These authors predict with orbits with a wide range distribution of inclinations and eccentricities which does not reproduce our observations as closely as Fabrycky & Tremaine (2007) do. All other authors fall short of the wide range of angles that we detect. This, however does not mean that the processes they describe do not happen in combination with those talked about here. In addition we cannot rule out that each of the current theoretical distributions will evolve thanks to greater scrutiny of their starting hypotheses leading to new simulations. Typically, tidal interactions between the star and the planet have been understudied. Any change in the way tidal processes are treated will alter the rate at which planets would realign the stellar spin axis (Winn et al. 2010). New effects are also likely to be imagined such as these Kozai cycles between a misaligned planet and a disc presented in Terquem & Ajmia (2010).

If the Kozai effect were found to be the dominant process leading to the creation of hot Jupiters, there is no reason why longer period planets should not have undergone similar cycles. The only difference would be that having greater periastron distances, tidal friction was less active. It would then be expected that lone Jupiters on large eccentric orbits be misaligned as well. HD 80606b would be part of that population. We could then have a *lone Jupiter* population of which *hot Jupiters* are a subset, and another planet population where dynamical interactions and tidal migration did not act.

7. Conclusions

The observations reported here bring the total number of transiting planets with known sky-projected obliquities from 20 to 26. Among this enlarged sample, eight show significant projected spin-orbit misalignments; and of these eight, five show apparent retrograde motion. This projected angle β can be transformed statistically into the real spin-orbit angle ψ. Although 1/3 of planets have $\beta \neq 0°$, the distribution in ψ shows that up to 85% of hot Jupiters are misaligned. The angle range and shape of the overall ψ distribution appears consistent with the predictions of models by Fabrycky & Tremaine (2007) and Wu et al. (2007) using the Kozai mechanism to make planets move inwards and tidal friction to reduce their semi-major axis and eventually, circularise them.

Our evidence therefore points towards a dynamical – not limited to Kozai – and tidal origin for making hot Jupiters so close to their host star. This evidence is the strongest yet to suggest that processes others than type I or II migration (using exchange of angular momentum between a planet and a disc) are responsible for the creation of hot Jupiters. Disc migration alone cannot explain the observations; we need to invoke another process. Our interpretation is supported by other facts such as how different hot Jupiters are spread in semi-major axis compared to multiple systems (Wright et al. 2009), on how lonely hot Jupiters are, and the rarity of hot Jupiters at orbital distances less than two Hill radii from the star (Ford & Rasio 2006). These results and conclusions should also be a call to account for environmental effects on planetary systems in planet formation simulations. These systems are not in isolation and interact with their neighbours.

We are seeing the coming of a new diversity in planetary parameters, coming after large diversities in mass, period, eccentricity and radius. The variety of angles β, transformed into ψ, is an indication of the physical processes that happened before, during and after planet formation. Once again the measurement of a new observable has brought a large variety of values reflecting how rich nature is.

As more transiting systems are discovered in wide-field surveys, and follow-up observations of the kind reported here are made, the statistical picture that is beginning to emerge will become clearer.

Acknowledgements. The authors would like to acknowledge the use of ADS and *Simbad* but foremost, the help and the kind attention of the ESO staff at La Silla. As a small show of our immense gratitude, we would like to underline the enormous work and constant support, upkeep and maintenance of the *Euler* observing station at La Silla, as well as the quick and useful help given by engineers, mechanical and IT staff from the Observatoire de Genève. Without you, a lot of this work would not have been possible. This station is like a jewel, thanks!
An extensive use of the `exoplanet.eu` encyclopaedia was made; many thanks to Jean Schneider for the continuous update and upkeep of this database.
We would also like to thank G. Ogilvie, M. Davies, A. Barker, D. Malmberg, R. Alonso, S. Matsumura, G. Laughlin, D. Fabrycky, T. Guillot and E. Ford for their helpful and interesting conversations and to the battery of observers that helped obtain the data on HARPS and CORALIE, notably X. Bonfils, G. Chauvin, G. Hébrard, G. Lo Curto, C. Lovis, M. Marmier, C. Moutou and D. Naef.
Our final thanks go to Josh Winn, our referee, who helped greatly to refine this paper, its results and their interpretation.
This work is supported by the Swiss Fond National de Recherche Scientifique.

References

Alonso, R., Auvergne, M., Baglin, A., et al. 2008, A&A, 482, L21
Anderson, D. R., Gillon, M., Hellier, C., et al. 2008, MNRAS, 387, L4
Anderson, D. R., Hellier, C., Gillon, M., et al. 2010, ApJ, 709, 159
Bakos, G. Á., Pál, A., Latham, D. W., Noyes, R. W., & Stefanik, R. P. 2006, ApJ, 641, L57
Bakos, G. Á., Noyes, R. W., Kovács, G., et al. 2007, ApJ, 656, 552
Baranne, A., Queloz, D., Mayor, M., et al. 1996, A&A, 119, 373
Barge, P., Baglin, A., Auvergne, M., et al. 2008, A&A, 482, L17
Barker, A. J., & Ogilvie, G. I. 2009, MNRAS, 395, 2268
Bate, M. R., Bonnell, I. A., Clarke, C. J., et al. 2000, MNRAS, 317, 773
Bate, M. R., Lodato, G., & Pringle, J. E. 2010, MNRAS, 401, 1505
Boisse, I., Moutou, C., Vidal-Madjar, A., et al. 2009, A&A, 495, 959
Bouchy, F., Queloz, D., Deleuil, M., et al. 2008, A&A, 482, L25
Collier Cameron, A., Bouchy, F., Hébrard, G., et al. 2007, MNRAS, 375, 951
Collier Cameron, A., Bruce, V. A., Miller, G. R. M., Triaud, A. H. M. J., & Queloz, D. 2010, MNRAS, 403, 151
Castelli, F., Gratton, R. G., & Kurucz, R. L. 1997, A&A, 318, 841
Charbonneau, D., Brown, T. M., Latham, D. W., & Mayor, M. 2000, ApJ, 529, L45
Charbonneau, D., Winn, J. N., Everett, M. E., et al. 2007, ApJ, 658, 1322
Chatterjee, S., Ford, E. B., Matsumura, S., & Rasio, F. A. 2008, ApJ, 686, 580
Claret, A. 2000, A&A, 363, 1081
Cochran, W. D., Redfield, S., Endl, M., & Cochran, A. L. 2008, ApJ, 683, L59
Daemgen, S., Hormuth, F., Brandner, W., et al. 2009, A&A, 498, 567
Eggleton, P. P., & Kiseleva-Eggleton, L. 2001, ApJ, 562, 1012
Fabrycky, D., & Tremaine, S. 2007, ApJ, 669, 1298
Fabrycky, D. C., & Winn, J. N. 2009, ApJ, 696, 1230
Ford, E. B. 2006, ApJ, 642, 505
Ford, E. B., & Rasio, F. A. 2006, ApJ, 638, L45
Gaudi, B. S., & Winn, J. N. 2007, ApJ, 655, 550
Gillon, M., Triaud, A. H. M. J., Mayor, M., et al. 2008, A&A, 485, 871
Gillon, M., Anderson, D. R., Triaud, A. H. M. J., et al. 2009a, A&A, 501, 785
Gillon, M., Demory, B. O., Triaud, A. H. M. J., et al. 2009b, A&A, 506, 359
Gillon, M., Smalley, B., Hebb, L., et al. 2009c, A&A, 496, 259
Giménez, A. 2006, ApJ, 650, 408
Goldreich, P., & Tremaine, S. 1980, ApJ, 241, 425
Gray, D. F. 2008, The Observation and Analysis of Stellar Photospheres
Hébrard, G., Bouchy, F., Pont, F., et al. 2008, A&A, 488, 763
Hellier, C., Anderson, D. R., Cameron, A. C., et al. 2009, Nature, 460, 1098

Henry, G. W., Marcy, G. W., Butler, R. P., & Vogt, S. S. 2000, ApJ, 529, L41
Hilditch, R. W. 2001, An Introduction to Close Binary Stars
Hirano, T., Suto, Y., Taruya, A., et al. 2010, ApJ, 709, 458
Hosokawa, Y. 1953, PASJ, 5, 88
Hrudková, M., Skillen, I., Benn, C., et al. 2009, Transiting Planets, 253, 446
Hut, P. 1981, A&A, 99, 126
Jenkins, J. M., Borucki, W. J., Koch, D. G., et al. 2010, ApJ, 724, 1108
Johnson, J. A., Winn, J. N., Narita, N., et al. 2008, ApJ, 686, 649
Johnson, J. A., Winn, J. N., Albrecht, S., et al. 2009, PASP, 121, 1104
Joshi, Y. C., Pollacco, D., Cameron, A. C., et al. 2009, MNRAS, 392, 1532
Jurić, M., & Tremaine, S. 2008, ApJ, 686, 603
Knutson, H. A., Charbonneau, D., Noyes, R. W., Brown, T. M., & Gilliland, R. L. 2007, ApJ, 655, 564
Kozai, Y. 1962, AJ, 67, 591
Lin, D. N. C., Bodenheimer, P., & Richardson, D. C. 1996, Nature, 380, 606
Loeillet, B., Shporer, A., Bouchy, F., et al. 2008, A&A, 481, 529
Lovis, C., & Pepe, F. 2007, A&A, 468, 1115
Lovis, C., Mayor, M., Pepe, F., et al. 2006, Nature, 441, 305
Lucy, L. B., & Sweeney, M. A. 1971, AJ, 76, 544
Malmberg, D., Davies, M. B., & Chambers, J. E. 2007, MNRAS, 377, L1
Mandel, K., & Agol, E. 2002, ApJ, 580, L171
Mandushev, G., O'Donovan, F. T., Charbonneau, D., et al. 2007, ApJ, 667, L195
Mayor, M., & Queloz, D. 1995, Nature, 378, 355
Mayor, M., Pepe, F., Queloz, D., et al. 2003, The Messenger (ISSN0722-6691), 114, 20
Mayor, M., Bonfils, X., Forveille, T., et al. 2009, A&A, 507, 487
McLaughlin, D. B. 1924, ApJ, 60, 22
Moutou, C., Hébrard, G., Bouchy, F., et al. 2009, A&A, 498, L5
Naef, D., Latham, D. W., Mayor, M., et al. 2001, A&A, 375, L27
Nagasawa, M., Ida, S., & Bessho, T. 2008, ApJ, 678, 498
Narita, N., Enya, K., Sato, B., et al. 2007, PASJ, 59, 763
Narita, N., Sato, B., Hirano, T., & Tamura, M. 2009, PASJ, 61, L35
Narita, N., Sato, B., Hirano, T., et al. 2010, PASJ, 62, 653
Noyes, R. W., Hartmann, L. W., Baliunas, S. L., Duncan, D. K., & Vaughan, A. H. 1984, AJ, 279, 763
Ohta, Y., Taruya, A., & Suto, Y. 2005, ApJ, 622, 1118
Pál, A., Bakos, G. Á., Torres, G., et al. 2008, ApJ, 680, 1450
Pepe, F., Mayor, M., Galland, F., et al. 2002, A&A, 388, 632
Pfahl, E., & Muterspaugh, M. 2006, ApJ, 652, 1694
Pollacco, D. L., Skillen, I., Cameron, A. C., et al. 2006, PASP, 118, 1407
Pollacco, D., Skillen, I., Cameron, A. C., et al. 2008, MNRAS, 385, 1576
Pont, F., Hébrard, G., Irwin, J. M., et al. 2009, A&A, 502, 695
Pont, F., Endl, M., Cochran, W. D., et al. 2010, MNRAS, 402, L1
Queloz, D., Eggenberger, A., Mayor, M., et al. 2000, A&A, 359, L13
Queloz, D., Anderson, D., Cameron, A. C., et al. 2010, A&A, 517, L1
Rasio, F. A., & Ford, E. B. 1996, Science, 274, 954
Rossiter, R. A. 1924, ApJ, 60, 15
Santos, N. C., Mayor, M., Naef, D., et al. 2000, A&A, 361, 265
Smalley, B., Smith, K. C., & Dworetsky, M. M. 2001, UCLSYN Userguide
Smith, K. C. 1992, Ph.D. Thesis, University of London
Southworth, J., Hinse, T. C., Jørgensen, U. G., et al. 2009, MNRAS, 396, 1023
Tegmark, M., Strauss, M. A., Blanton, M. R., et al. 2004, PhRvD, 69, 103501
Terquem, C., & Ajmia, A. 2010, MNRAS, 404, 409
Triaud, A. H. M. J., Queloz, D., Bouchy, F., et al. 2009, A&A, 506, 377
Tripathi, A., Winn, J. N., Johnson, J. A., et al. 2010, ApJ, 715, 421
West, R. G., Anderson, D. R., Gillon, M., et al. 2009, AJ, 137, 4834
Wilson, D. M., Gillon, M., Hellier, C., et al. 2008, ApJ, 675, L113
Winn, J. N., Noyes, R. W., Holman, M. J., et al. 2005, ApJ, 631, 1215
Winn, J. N., Johnson, J. A., Narita, N., et al. 2008, ApJ, 682, 1283
Winn, J. N., Howard, A. W., Johnson, J. A., et al. 2009a, ApJ, 703, 2091
Winn, J. N., Johnson, J. A., Albrecht, S., et al. 2009b, ApJ, 703, L99
Winn, J. N., Johnson, J. A., Fabrycky, D., et al. 2009c, ApJ, 700, 302
Winn, J. N., Fabrycky, D., Albrecht, S., & Johnson, J. A. 2010, ApJ, 718, L145
Wolf, A. S., Laughlin, G., Henry, G. W., et al. 2007, ApJ, 667, 549
Wright, J. T., Upadhyay, S., Marcy, G. W., et al. 2009, ApJ, 693, 1084
Wu, Y., & Murray, N. 2003, ApJ, 589, 605
Wu, Y., Murray, N. W., & Ramsahai, J. M. 2007, ApJ, 670, 820

Appendix A: Comparative tables for each star

Here, for transparency, are the tables recording the results from the various fits that were done for each star, which, par comparing them, led to the choice of our solutions. χ^2 have been tabulated only for the radial velocity data that was used for our analysis. In addition, to show where the most important contributions come from, χ^2 have also been added for each set of radial velocities separately, as they are presented in the journal of observations in the following Appendix. Finally, because our aim was to measure β, a line with the χ^2 only during the Rossiter-McLaughlin effect has been added. Comparisons between the χ^2 contributions of the overall reflex motion of the star with contributions during the Rossiter-McLaughlin will show that we tend to fit better during transit than outside. The number of points during the Rossiter-McLaughlin effect have been chosen as all the points measured during transit, plus one point immediately on either side when available.

A&A 524, A25 (2010)

Table A.1. Differences between fits of WASP-2b, 4b & 5b. $\chi^2_{\rm reduced}$ has been estimated for the radial velocities only.

WASP-2b						
					Fixed Photometry	
$V \sin I$ Prior	On	Off	On	Off	Off	
$V \sin I$ (km s^{-1})	$1.08^{+0.26}_{-0.31}$	$0.99^{+0.27}_{-0.32}$	$1.02^{+0.28}_{-0.25}$	$0.93^{+0.26}_{-0.30}$	$0.99^{+0.29}_{-0.33}$	
β (°)	154^{+10}_{-12}	153^{+11}_{-15}	145^{+12}_{-15}	143^{+12}_{-18}	152^{+12}_{-16}	
e	–	–	$0.035^{+0.016}_{-0.014}$	$0.036^{+0.017}_{-0.015}$	–	
ω (°)	–	–	-103^{+6}_{-12}	-103^{+6}_{-11}	–	
all 58 RVs, 3 sets						
$\chi^2_{\rm RV}$	100.6 ± 14.2	100.5 ± 14.2	93.2 ± 13.6	92.9 ± 13.6	100.5 ± 14.2	
$N_{\rm d.o.f.}$	47	47	45	45	47	
$\chi^2_{\rm reduced}$	2.14 ± 0.30	2.14 ± 0.30	2.07 ± 0.30	2.06 ± 0.30	2.14 ± 0.30	
$\chi^2_{\rm SOPHIE,\,8\,RVs}$	28.1 ± 7.5	27.9 ± 7.5	26.9 ± 7.3	27.0 ± 7.4	27.9 ± 7.5	
$\chi^2_{\rm CORALIE,\,20\,RVs}$	15.6 ± 5.6	15.5 ± 5.6	21.8 ± 6.6	21.4 ± 6.5	15.7 ± 5.6	
$\chi^2_{\rm HARPS,\,30\,RVs}$	56.9 ± 10.7	57.1 ± 10.7	44.4 ± 9.4	44.5 ± 9.4	57.0 ± 10.7	
$\chi^2_{\rm HARPS,\,RM,\,17\,RVs}$	20.7 ± 6.4	20.7 ± 6.4	20.9 ± 6.5	20.7 ± 6.4	20.7 ± 6.4	
	no RM	RM fixed	RM fixed	no RM	RM fixed	RM fixed
$V \sin I$ (km s^{-1})	–	1.6	0.9	–	1.6	0.9
β (°)	–	0	0	–	0	0
e	–	–	–	$0.041^{+0.015}_{-0.016}$	$0.044^{+0.016}_{-0.014}$	$0.044^{+0.014}_{-0.016}$
ω (°)	–	-	–	-96^{+5}_{-6}	-98^{+5}_{-6}	-97^{+5}_{-6}
all 58 RVs, 3 sets						
$\chi^2_{\rm RV}$	113.7 ± 15.1	164.0 ± 18.1	135.8 ± 16.5	105.7 ± 14.5	154.0 ± 17.6	126.4 ± 15.9
$N_{\rm d.o.f.}$	49	47	47	47	45	45
$\chi^2_{\rm reduced}$	2.32 ± 0.31	3.49 ± 0.39	2.89 ± 0.35	2.25 ± 0.31	3.42 ± 0.39	2.81 ± 0.35
$\chi^2_{\rm SOPHIE,\,8\,RVs}$	31.0 ± 7.9	29.3 ± 7.7	30.1 ± 7.7	31.3 ± 7.9	30.4 ± 7.8	30.8 ± 7.8
$\chi^2_{\rm CORALIE,\,20\,RVs}$	15.7 ± 5.6	15.4 ± 5.5	15.4 ± 5.6	21.5 ± 6.6	23.0 ± 6.8	22.8 ± 6.8
$\chi^2_{\rm HARPS,\,30\,RVs}$	67.0 ± 11.6	119.4 ± 15.5	90.4 ± 13.4	52.8 ± 10.3	100.6 ± 14.2	72.8 ± 12.1
$\chi^2_{\rm HARPS,\,RM,\,17\,RVs}$	30.8 ± 7.8	82.7 ± 12.9	53.9 ± 10.4	29.0 ± 7.6	79.1 ± 12.6	51.1 ± 10.1
WASP-4b						
					Fixed Photometry	
$V \sin I$ Prior	On	Off	On	Off	On	
$V \sin I$ (km s^{-1})	$2.14^{+0.38}_{-0.35}$	4^{+46}_{-2}	$2.15^{+0.45}_{-0.39}$	78^{+41}_{-75}	$2.19^{+0.35}_{-0.45}$	
β (°)	-4^{+43}_{-34}	4^{+84}_{-80}	$0.^{+34}_{-41}$	28^{+118}_{-0}	-5^{+39}_{-38}	
e	–	–	$0.0105^{+0.0036}_{-0.0072}$	$0.0106^{+0.0038}_{-0.0074}$	–	
ω (°)	–	–	-108^{+282}_{-58}	-107^{+280}_{-61}	–	
all 56 RVs, 2 sets						
$\chi^2_{\rm RV}$	77.8 ± 12.5	78.0 ± 12.5	75.3 ± 12.4	75.3 ± 12.3	77.8 ± 12.5	
$N_{\rm d.o.f.}$	46	46	44	44	46	
$\chi^2_{\rm reduced}$	1.69 ± 0.27	1.70 ± 0.27	1.71 ± 0.28	1.71 ± 0.28	1.69 ± 0.27	
$\chi^2_{\rm CORALIE,\,24\,RVs}$	28.4 ± 7.5	29.1 ± 7.6	27.6 ± 7.4	28.0 ± 7.5	28.6 ± 7.6	
$\chi^2_{\rm HARPS,\,32\,RVs}$	49.4 ± 9.9	48.9 ± 9.9	47.8 ± 9.8	47.3 ± 9.7	49.2 ± 9.9	
$\chi^2_{\rm HARPS,\,RM,\,15\,RVs}$	12.6 ± 5.0	12.5 ± 5.0	12.2 ± 4.9	12.0 ± 4.9	12.7 ± 5.0	

Table A.2. Differences between fits of WASP-5b & 15b. $\chi^2_{\rm reduced}$ has been estimated for the radial velocities only.

WASP-5b					
					Fixed Photometry
$V \sin I$ Prior	On	Off	On	Off	Off
$V \sin I$ (km s^{-1})	$3.24^{+0.35}_{-0.27}$	$3.24^{+0.34}_{-0.35}$	$3.32^{+0.30}_{-0.32}$	$3.36^{+0.32}_{-0.46}$	$3.18^{+0.26}_{-0.31}$
β (°)	$-12.1^{+10.0}_{-8.0}$	$-12.4^{+11.9}_{-8.2}$	$-14.1^{+10.8}_{-7.8}$	$-16.1^{+14.2}_{-9.3}$	$-12.0^{+7.7}_{-7.3}$
e	–	–	$0.0209^{+0.0081}_{-0.0075}$	$0.0209^{+0.0071}_{-0.0087}$	–
ω (°)	–	–	-137^{+14}_{-16}	-137^{+12}_{-17}	–
all 49 RVs, 2 sets					
$\chi^2_{\rm RV}$	143.7 ± 17.0	144.3 ± 17.0	136.8 ± 16.5	136.7 ± 16.5	145.1 ± 17.0
$N_{\rm d.o.f.}$	39	39	37	37	39
$\chi^2_{\rm reduced}$	3.69 ± 0.43	3.70 ± 0.44	3.70 ± 0.45	3.70 ± 0.45	3.72 ± 0.44
$\chi^2_{\rm CORALIE,\ 16\ RVs}$	20.4 ± 6.4	20.5 ± 6.4	26.3 ± 7.2	26.0 ± 7.2	20.4 ± 6.4
$\chi^2_{\rm HARPS,\ 33\ RVs}$	123.3 ± 15.7	123.8 ± 15.7	110.6 ± 14.9	110.7 ± 14.9	124.8 ± 15.8
$\chi^2_{\rm HARPS,\ RM,\ 15\ RVs}$	42.8 ± 9.2	43.9 ± 9.4	40.6 ± 9.0	40.7 ± 9.0	43.9 ± 9.4
WASP-15b					
					Fixed Photometry
$V \sin I$ Prior	On	Off	On	Off	Off
$V \sin I$ (km s^{-1})	$4.26^{+0.27}_{-0.32}$	$4.27^{+0.26}_{-0.36}$	$4.37^{+0.29}_{-0.32}$	$4.36^{+0.27}_{-0.34}$	$4.26^{+0.28}_{-0.31}$
β (°)	$139.8^{+5.1}_{-4.5}$	$139.6^{+5.2}_{-4.3}$	$142.6^{+5.3}_{-4.5}$	$142.7^{+5.3}_{-5.0}$	$139.7^{+4.0}_{-4.0}$
e	–	–	$0.043^{+0.020}_{-0.022}$	$0.043^{+0.022}_{-0.023}$	–
ω (°)	–	–	96^{+45}_{-22}	96^{+38}_{-26}	–
all 95 RVs, 2 sets					
$\chi^2_{\rm RV}$	133.1 ± 16.3	133.3 ± 16.3	130.3 ± 16.1	130.1 ± 16.1	133.1 ± 16.3
$N_{\rm d.o.f.}$	85	85	83	83	85
$\chi^2_{\rm reduced}$	1.57 ± 0.19	1.57 ± 0.19	1.57 ± 0.19	1.57 ± 0.19	1.57 ± 0.19
$\chi^2_{\rm CORALIE,\ 44\ RVs}$	53.7 ± 10.4	53.4 ± 10.3	53.5 ± 10.3	54.4 ± 10.4	53.9 ± 10.4
$\chi^2_{\rm HARPS,\ 51\ RVs}$	79.4 ± 12.6	79.8 ± 12.6	76.7 ± 12.4	75.8 ± 12.3	79.2 ± 12.6
$\chi^2_{\rm HARPS,\ RM,\ 33\ RVs}$	47.3 ± 9.7	47.3 ± 9.7	46.9 ± 9.7	46.5 ± 9.6	47.1 ± 9.7

A&A 524, A25 (2010)

Table A.3. Differences between fits of WASP-17b and 18b. $\chi^2_{\rm reduced}$ has been estimated for the radial velocities only.

WASP-17b					
					Fixed Photometry
$V \sin I$ Prior	On	Off	On	Off	Off
$V \sin I$ (km s^{-1})	$9.92^{+0.40}_{-0.45}$	$10.14^{+0.58}_{-0.79}$	$9.95^{+0.45}_{-0.43}$	$10.27^{+0.68}_{-0.84}$	$10.03^{+0.63}_{-0.63}$
β (°)	$148.5^{+5.1}_{-4.2}$	$147.3^{+5.9}_{-5.5}$	$150.9^{+5.2}_{-5.9}$	$150.5^{+6.1}_{5.7}$	$147.5^{+4.2}_{-4.0}$
e	–	–	$0.062^{+0.024}_{-0.039}$	$0.066^{+0.030}_{-0.043}$	–
ω (°)	–	–	34^{+34}_{-72}	45^{+30}_{-77}	–
all 124 RVs, 4 sets					
$\chi^2_{\rm RV}$	190.1 ± 19.5	190.4 ± 19.5	187.3 ± 19.4	186.9 ± 19.3	191.6 ± 19.6
$N_{\rm dof}$	112	112	110	110	112
$\chi^2_{\rm reduced}$	1.70 ± 0.17	1.70 ± 0.17	1.70 ± 0.17	1.70 ± 0.17	1.71 ± 0.17
$\chi^2_{\rm CORALIE,\,49\,RVs}$	47.6 ± 9.8	47.4 ± 9.7	47.2 ± 9.7	47.7 ± 9.8	47.5 ± 9.7
$\chi^2_{\rm CORALIE,\,15\,RVs}$	15.0 ± 5.5	15.0 ± 5.5	16.2 ± 5.7	16.9 ± 5.8	15.0 ± 5.5
$\chi^2_{\rm HARPS,\,16\,RVs}$	23.6 ± 6.9	23.7 ± 6.9	23.5 ± 6.9	23.7 ± 6.9	23.9 ± 6.9
$\chi^2_{\rm HARPS,\,44\,RVs}$	103.8 ± 14.4	104.3 ± 14.4	100.4 ± 14.2	98.6 ± 14.0	105.2 ± 14.5
$\chi^2_{\rm CORALIE,\,RM,\,13\,RVs}$	9.8 ± 4.4	9.5 ± 4.4	9.9 ± 4.4	10.1 ± 4.5	9.8 ± 4.4
$\chi^2_{\rm HARPS,\,RM,\,28\,RVs}$	59.3 ± 10.9	59.8 ± 10.9	59.4 ± 10.9	58.7 ± 10.8	60.7 ± 11.0
WASP-18b					
					Fixed Photometry
$V \sin I$ Prior	On	Off	On	Off	Off
$V \sin I$ (km s^{-1}) *	$14.04^{+0.73}_{-0.52}$ *	$14.66^{+0.86}_{-0.58}$*	$14.67^{+0.81}_{-0.57}$ *	$15.57^{+1.01}_{-0.69}$ *	$15.59^{+0.56}_{-0.57}$ *
β (°)	$-11.1^{+6.6}_{-5.8}$	$-10.1^{+6.2}_{-5.8}$	$-5.0^{+6.2}_{-5.6}$	$-4.0^{+5.0}_{-5.0}$	$-4.2^{+4.6}_{-4.6}$
e	–	–	$0.0084^{+0.0008}_{-0.0010}$	$0.0085^{+0.0009}_{-0.00010}$	$0.0085^{+0.0010}_{-0.0010}$
ω (°)	–	–	$-92.8^{+5.2}_{-3.9}$	$-92.1^{+4.9}_{-4.3}$	$-92.5^{+2.7}_{-3.0}$
all 60 RVs, 2 sets					
$\chi^2_{\rm RV}$	283.3 ± 23.8	279.3 ± 23.6	179.7 ± 18.9	177.8 ± 18.9	178.4 ± 18.9
$N_{\rm d.o.f.}$	50	50	48	48	48
$\chi^2_{\rm reduced}$	5.67 ± 0.48	5.58 ± 0.47	3.74 ± 0.39	3.70 ± 0.39	3.72 ± 0.39
$\chi^2_{\rm CORALIE,\,37\,RVs}$	132.4 ± 16.3	131.2 ± 16.2	69.2 ± 11.8	66.7 ± 11.5	67.5 ± 10.4
$\chi^2_{\rm HARPS,\,23\,RVs}$	150.9 ± 17.4	148.1 ± 17.2	110.5 ± 14.9	111.1 ± 14.9	110.9 ± 14.9
$\chi^2_{\rm HARPS,\,RM,\,12\,RVs}$	113.7 ± 15.1	110.2 ± 14.8	98.7 ± 14.0	98.0 ± 14.0	98.6 ± 14.0

Notes. * These values are not really $V \sin I$ but more an amplitude parameter for fitting the Rossiter-McLaughlin effect. Please refer to Sect. 4.6 treating WASP-18b.

4.2 Newer Results

Soon after the appearance of the preprint of the paper on SUPERWASP.ORG and ASTRO-PH, a number of other papers have been published. From 26 measurements that were then known, we have now reached beyond 50, and more are coming with the passing months. The tables and graphs should be mostly up to date. The HARPS Rossiter-McLaughlin survey continued with WASP-24 shown in Simpson et al. (2011), WASP-19 was published by Hellier et al. (2011), Three more planets are being prepared in a paper from David Brown (soon to be submitted). Two more are being prepared by David Anderson (submitted), an additional two by Andrew Collier Cameron. WASP-30 will be analysed by myself. A few more measurements are being observed this observing season (and hopefully the next). This is a fast expanding field.

The aim now is the review our newer results as well as those published by our competitors and get a view on the current situation and on how it evolved to that given in the paper shown in previous section.

Out of the 54 measurements presented in table 4.1, 42 are deemed "secured" meaning the final value for the angle might change a little but not dramatically. The other ten have issues: low signal-to-noise (WASP-2), uncertainty about the angle (WASP-23), low cadence (CoRoT-3). Figure 4.1 shows the current situation. With a doubling of the sample, we obtain pretty much the same distribution as that presented in Figure 9 from Triaud et al. (2010). We remark here that adding or removing the "unsure" measurements does not affect the distribution, showing a certain robustness. The two theoretical predictions producing obliquity angles on the range of the observations which are drawn for comparison are from Nagasawa et al. (2008) and Fabrycky & Tremaine (2007). It is interesting in that neither predict enough aligned system and neither do they seem to explain the high level of fully retrograde planets. The observations are not entirely reproduced by the theory. It may be useful to point that numerical experiments such as those can heavily depend on which initial conditions one inputs (two separate studies of the Kozai mechanism nevertheless managed to produce two ψ distributions which are essentially the same, namely: Wu et al. (2007) and Fabrycky & Tremaine (2007). I am using more often the latter paper, but the previous is equal in its results).

Fabrycky & Winn (2009) had already noted with only one misaligned angle known then, that the distribution in projected spin/orbit angle was bimodal and resembled a Γ function around 0°, combined with an isotropic component. Morton & Johnson (2011) analysed the 26 measurements presented in Triaud et al. (2010) and confirmed this. The newer results, here shown, seem to comfort this view. This then makes trickier an interpretation of the cumulative distribution as one may need to insert two models. As will be outlined later, another complication comes from the fact that ψ (and thus β) may change with time.

Maybe one of the most influential papers was published by Winn et al. (2010a) showing the clearest pattern so far observed within the current data: plotting β against the stellar effective temperature, $T_{\rm eff}$, we obtain a deficit of aligned systems around stars hotter than 6250 K. Behind these authors' idea was that it was odd that the first ten Rossiter-McLaughlin measurements were all aligned, when now we know that about 25 % of hot Jupiters have $\beta > 30^\circ$. This is explained by realising that the first measurements were observed primarily for planets discovered using the Doppler method and then found to transit, while the latter measurements only came primarily from transit surveys, which find planets on hotter stars in average. Another effect might come from target selection as hotter stars being faster rotators give poorer radial velocity precision.

From Figure 4.2 we observe that about one star (colder than 6250 K) in six has a misaligned hot Jupiter, while only one star (hotter than 6250 K) in four has an aligned system, and those are

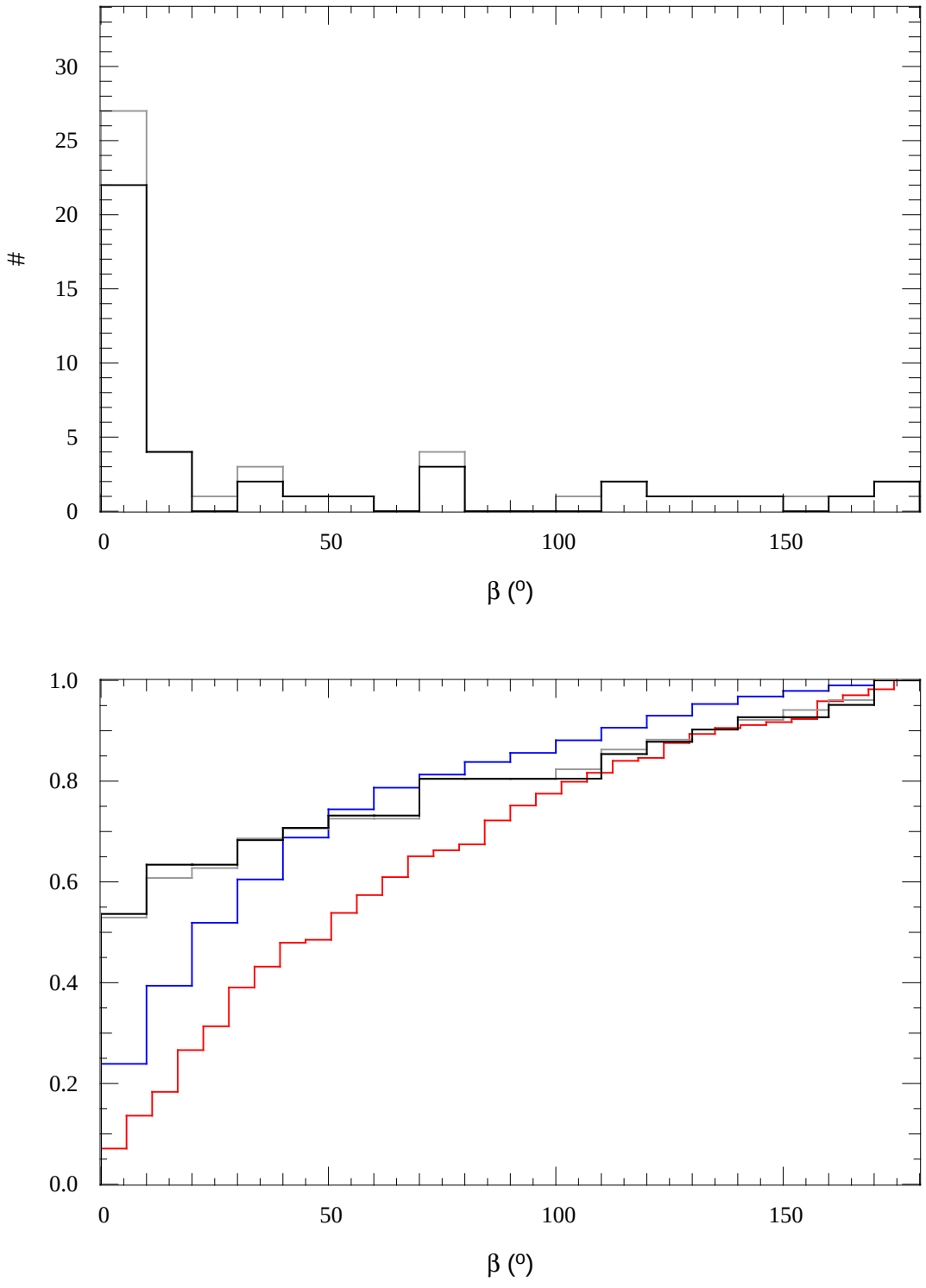


Figure 4.1: *top*: recent histogram of all β measurements (taking the absolute value as it is the only one that really matters). *bottom*: cumulative distribution. In black the secured measurements. Grey, adding the unsure measurements. Blue model is taken from Fabrycky & Tremaine (2007) (and pretty much the same as in Wu et al. (2007)), Red model from Nagasawa et al. (2008). The addition of the unsure measurements does not change the general shape.

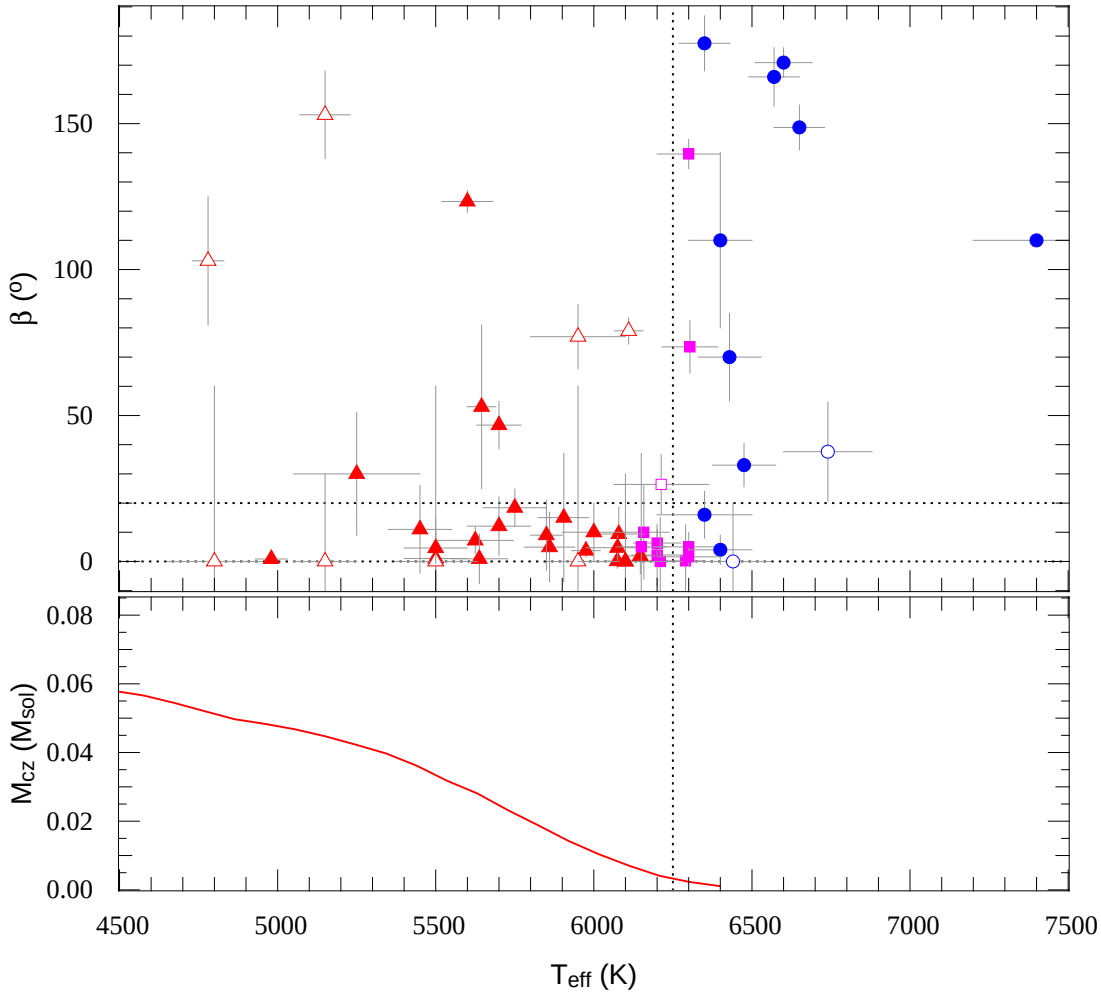


Figure 4.2: *top* Projected spin/orbit angle β against the stellar $T_{\rm eff}$. We observe a lack of aligned system around stars hotter than 6250 K. Open symbols indicate the unsure measurements. Several data points are yet unpublished results and likely to move. Triangles are objects < 6150 K, circles > 6350 K, squares are in between. *bottom* The Pinsonneault law showing the of the outer convective layer's mass $M_{\rm cz}$ as a function of $T_{\rm eff}$ (Pinsonneault et al. 2001).

grouped near the temperature limit. This cold/hot divide is confirmed in a statistical paper by Schlaufman (2010) where stars more massive than $1.2\,M_{\odot}$ hosting a transiting hot Jupiter have a *rotation deficit* compared to what would be predicted from the general stellar population by hypothesising that the stellar spin axis I is similar to the orbital inclination i, around $90°$. This can be easily understood if one thinks that they tend to be more pole-on which would happen only if they have misaligned planets around them. The stellar mass value corresponds well to the effective temperature boundary. I won't go into the details now (they are in next chapter), but Winn et al. (2010a) conclude that β may decay more rapidly for planets around stars colder than 6250 K for planets around stars that are hotter. If this is just, a more realistic comparison of the observations to theory might be to take only the planets whose host star are on the hot side since their β would be "frozen". Figure 4.1 is reproduced in figure 4.3 but only for the "hot" subsample. Theory and observations now clearly disagree.

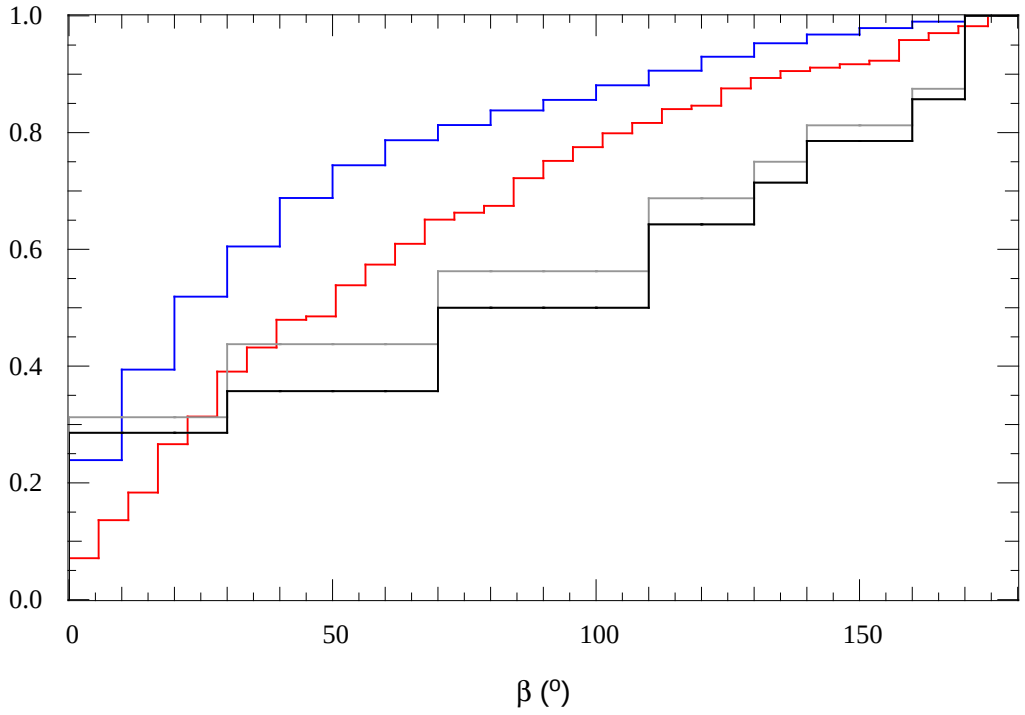


Figure 4.3: Similar to figure 4.1 but only taking the objects found around star with $T_{\rm eff}$ > 6250 K.

Another interesting feature was brought to my attention by Guillaume Hébrard which was recently renewed in a paper by Moutou et al. (2011). Something odd is happening in relation to the mass of the planet (or brown dwarf). We do not see retrograde systems for planets with mass $> 5M_{\rm Jup}$. Maybe a statistical fluke, but the distribution in $\beta > 20^{\circ}$ appears isotropic as outlined in figure 4.1. If this gap is confirmed, it could have three origins: the mechanism that makes retrograde planets for some reason cannot make planets $> 5M_{\rm Jup}$ retrograde, or that they were and have since been realigning, or that two mechanisms operate to make misalignments, which would have a mass dependence. This is despite the fact that those massive planets are mostly discovered around more massive stars, thus more likely to be hotter than 6250 K... Food for thoughts.

Hat-P-11 b is a Neptune around a rather cold star. Winn et al. (2010c) have observed its Rossiter-McLaughlin effect and concluded the planet is on near pole-on orbit. I have classified it as "unsure". Reviewing the paper, there is a strong degeneracy between $V \sin I$ and β as in the case of WASP-23 and requires the use of a prior on $V \sin I$ in the analysis. Thus the angle could vary by quite a lot. Nevertheless this planet - and hopefully more of that type coming - is very interesting as it shares the same orbital characteristics as hot Jupiters despite being of lower mass. Despite being an unsure measurements it is interesting to think that the first such object for which the Rossiter-McLaughlin effect is observed is found severely misaligned. More observations in this mass range are desperately needed. Another interesting thing is that this planet appears to be eccentric. The only other transiting hot Neptune for which we have that measurement is GJ 436 b, also eccentric, an eccentricity which is still unexplained as it ought to circularise quickly. A search for a perturbing companion has led to no results. More generally, nothing very clear emerges by comparing eccentricity and β . HD 17156 b is very well aligned and so is Hat-P-2 b despite large eccentricities. Most of the misaligned systems have no detectable eccentricity. WASP-8 b and 14 b are misaligned and eccentric.

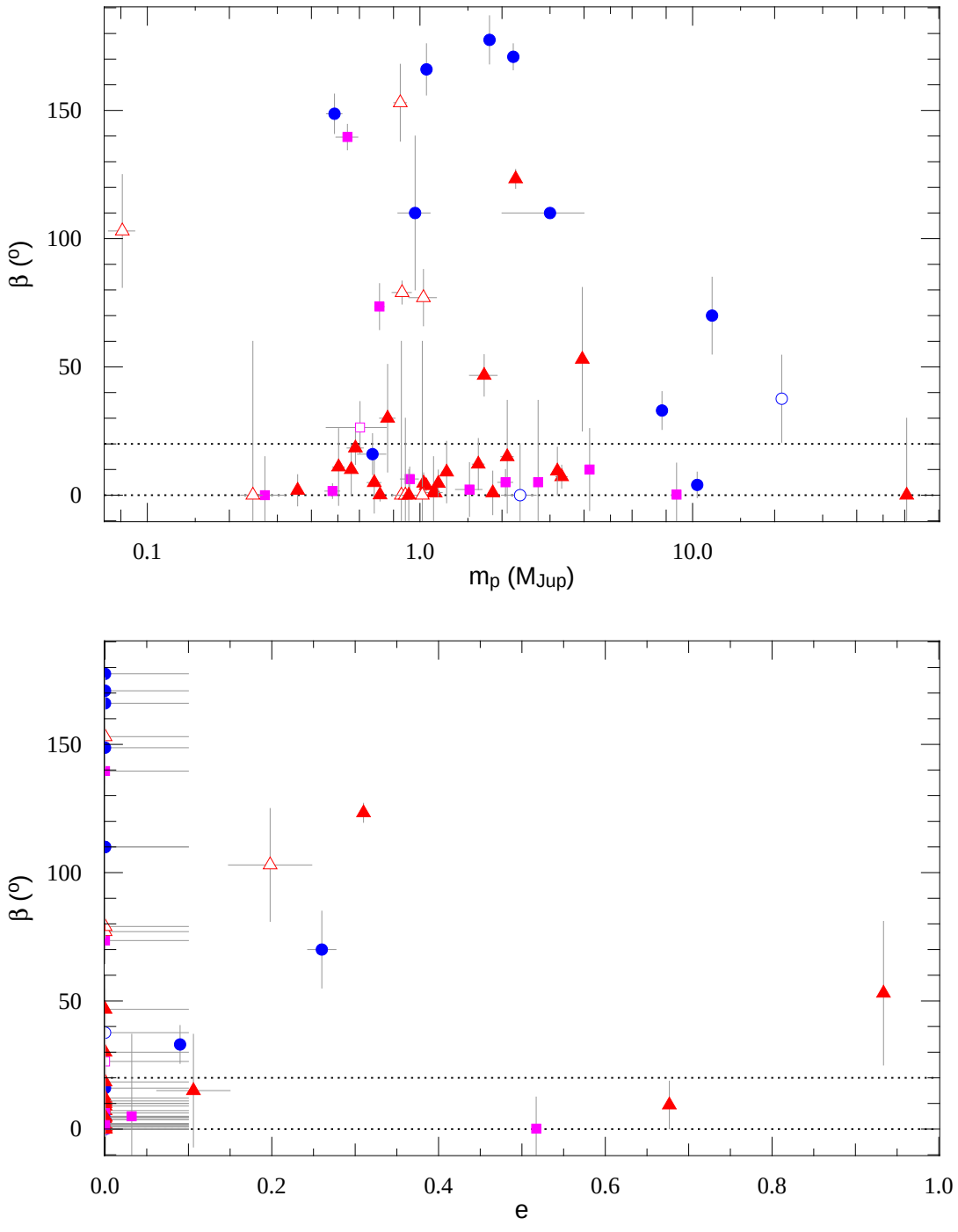


Figure 4.4: Same as figure 4.2 but instead *top*: β as a function of planet mass $m_{\rm p}$ and *bottom*: β as a function of eccentricity

Table 4.1: Rossiter-McLaughlin measurements sorted in order of host star $T_{\rm eff}$. The multiple column shows those systems for which we know of other stellar or substellar companions. The confidence column shows if I consider this measurement sure or unsure (meaning likely to change). References to the angle are given, other values taken from exoplanet.eu. Some figures are preliminary.

target	$T_{\rm eff}$	$\pm$	β	$\pm$	$M_{\rm p}$	$R_{\rm p}$	$M_\star$	$R_\star$	e	multiple	confidence	$M_{\rm cz}$	$\log \tau_{\rm cz}$	$\log \tau_{\rm tot}$	ref.
Hat-P-11	4780	50	103.0	22.0	0.081	0.452	0.810	0.750	0.198	N	N	0.0518	9.790	10.984	(1)
WASP-X	4800	150	0.0	60.0	0.244	0.792	0.825	0.846	0.	N	N	0.0513	8.734	9.940	(2)
HD 189733	4980	50	0.8	0.3	1.138	1.178	0.820	0.788	0.	Y	Y	0.0481	7.246	8.478	(3)
WASP-2	5150	80	0.	60.	0.847	1.079	0.840	0.834	0.	Y	N	0.0447	7.191	8.465	(4)
WASP-23	5150	100	0.0	30.0	0.884	0.962	0.780	0.765	0.	N	N	0.0447	7.869	9.111	(5)
TrES-1	5250	200	30.0	21.0	0.761	1.099	0.880	0.850	0.	N	Y	0.0422	7.749	9.069	(6)
WASP-6	5450	100	11.0	15.0	0.503	1.224	0.888	0.870	0.	N	Y	0.0355	7.973	9.371	(7)
WASP-4	5500	100	1.0	14.0	1.122	1.363	0.930	1.150	0.	N	Y	0.0331	5.306	6.754	(4)
WASP-X	5500	130	0.0	60.0	0.855	1.008	1.022	0.946	0.	N	N	0.0331	7.494	8.984	(8)
WASP-19	5500	100	4.6	5.2	1.168	1.383	0.970	0.990	0.	N	Y	0.0331	4.807	6.274	(9)
WASP-8	5600	80	123.3	3.7	2.244	1.038	1.033	0.953	0.31	Y	Y	0.0295	8.373	9.917	(10)
CoRoT 2	5625	120	7.2	4.5	3.310	1.465	0.970	0.982	0.	N	Y	0.0282	5.686	7.222	(11)
Hat-P-13	5638	90	0.9	8.5	1.850	1.280	1.220	1.560	0.	Y	Y	0.0275	5.806	7.453	(12)
HD 80606	5645	45	53.0	28.0	3.940	0.921	0.980	0.980	0.93366	Y	Y	0.0272	8.216	9.773	(13)
WASP-5	5700	100	12.1	10.0	1.637	1.171	1.000	1.084	0.	N	Y	0.0245	5.598	7.208	(4)
XO-4	5700	70	46.7	8.1	1.720	1.340	1.320	1.550	0.	N	Y	0.0245	6.494	8.225	(14)
WASP-X	5750	100	18.4	6.4	0.580	1.260	1.000	0.950	0.	N	Y	0.0221	7.786	9.441	(8)
TrES-2	5850	50	9.0	12.0	1.253	1.169	0.980	1.000	0.	Y	Y	0.0174	6.464	8.215	(15)
Hat-P-4	5860	80	4.9	11.9	0.680	1.270	1.260	1.590	0.	N	Y	0.0169	6.099	7.971	(16)
Hat-P-23	5905	80	15.0	22.0	2.090	1.368	1.130	1.203	0.106	N	Y	0.0149	4.544	6.424	(17)
CoRoT 1	5950	150	77.0	11.0	1.030	1.490	0.950	1.110	0.	N	N	0.0129	5.270	7.138	(18)
WASP-X	5950	100	0.0	60.0	1.020	1.320	1.120	1.340	0.	Y	N	0.0129	5.967	7.906	(19)
Hat-P-1	5975	45	3.7	2.1	1.053	1.217	1.133	1.115	0.	Y	Y	0.0119	7.155	9.134	(20)
WASP-X	6000	100	22.0	16.0	0.560	1.120	1.100	1.130	0.	Y	Y	0.0110	7.011	9.012	(19)
HD 209458	6074	33	0.1	2.4	0.714	1.380	1.148	1.146	0.	N	Y	0.0082	6.780	8.925	(21)
WASP-24	6075	100	4.7	4.0	1.032	1.104	1.129	1.147	0.	N	Y	0.0082	5.932	8.072	(22)

Table continues next page...

Table 4.1: Rossiter-McLaughlin measurements, continued...

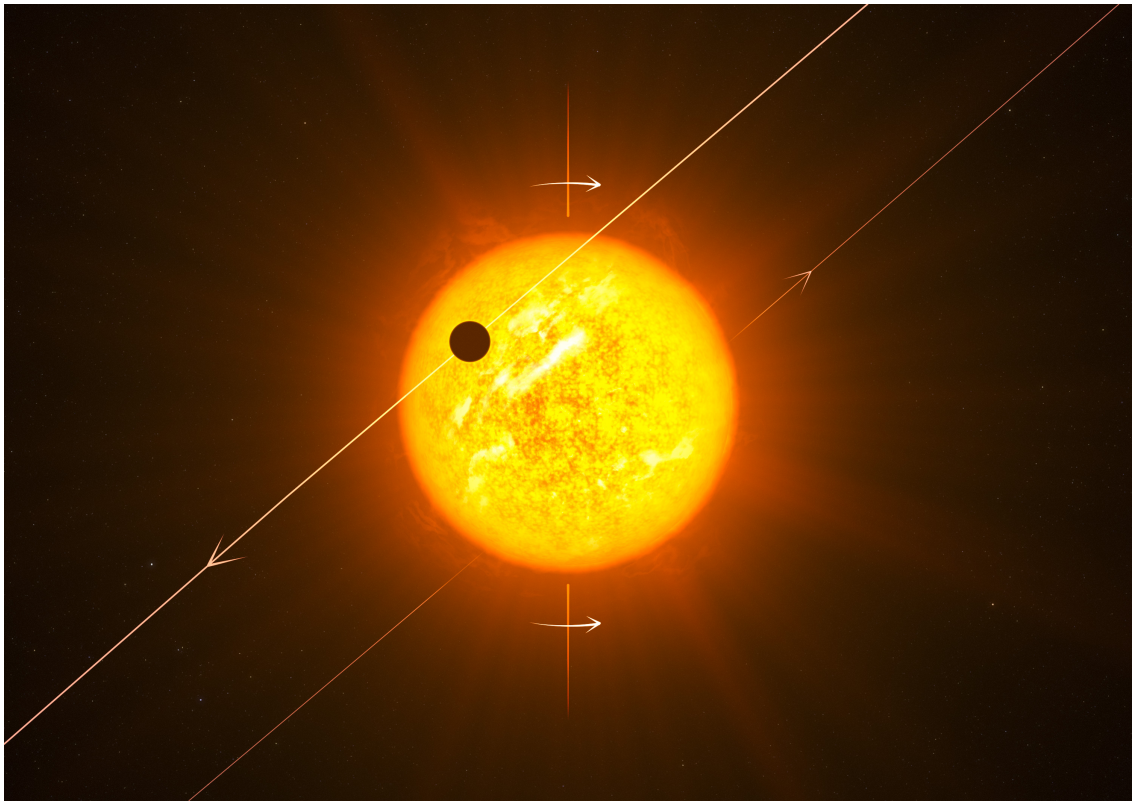
target	$T_{\rm eff}$	$\pm$	β	$\pm$	$M_{\rm p}$	$R_{\rm p}$	$M_\star$	$R_\star$	e	multiple	confidence	$M_{\rm cz}$	$\log \tau_{\rm cz}$	$\log \tau_{\rm tot}$	ref.
HD 17156	6079	80	9.4	9.3	3.191	1.095	1.275	1.508	0.6768	N	Y	0.0080	7.022	9.222	(23)
WASP-X	6100	150	0.0	10.0	0.910	1.120	1.080	1.050	0.	N	Y	0.0074	6.748	8.911	(2)
WASP-30	6100	100	0.0	30.0	61.000	0.889	1.166	1.295	0.	N	Y	0.0074	4.785	6.981	(24)
WASP-1	6110	45	79.0	4.5	0.860	1.484	1.240	1.382	0.	N	N	0.0070	5.577	7.824	(22)
HD 149026	6147	50	1.9	6.1	0.356	0.718	1.300	1.497	0.	N	Y	0.0057	5.964	8.321	(25)
WASP-38	6150	80	5.0	32.0	2.712	1.079	1.216	1.365	0.032	N	Y	0.0056	6.786	9.121	(22)
Hat-P-16	6158	80	10.0	16.0	4.193	1.289	1.218	1.237	0.	N	Y	0.0054	5.266	7.620	(17)
Hat-P-8	6200	80	2.2	10.5	1.520	1.500	1.280	1.580	0.	N	Y	0.0043	5.397	7.874	(22)
TrES4	6200	75	6.3	4.7	0.917	1.706	1.388	1.798	0.	Y	Y	0.0043	5.392	7.904	(26)
WASP-20	6210	140	0.0	15.0	0.270	1.200	1.260	1.210	0.	N	Y	0.0040	3.685	6.181	(2)
Kepler 8	6213	150	26.4	10.1	0.603	1.419	1.214	1.486	0.	N	N	0.0039	5.903	8.391	(27)
Hat-P-2	6290	60	0.2	12.3	8.740	0.951	1.360	1.640	0.5171	N	Y	0.0025	4.283	7.020	(28)
WASP-3	6300	100	5.0	5.0	2.060	1.454	1.230	1.310	0.	N	Y	0.0023	4.342	7.061	(29)
WASP-15	6300	100	139.6	5.0	0.542	1.428	1.180	1.477	0.	N	Y	0.0023	5.824	8.526	(4)
WASP-X	6300	100	1.6	2.9	0.478	1.537	1.160	1.240	0.	Y	Y	0.0023	6.154	8.849	(8)
Hat-P-30	6304	88	73.5	9.0	0.711	1.340	1.242	1.215	0.	N	Y	0.0023	5.746	8.484	(30)
Hat-P-7	6350	80	177.5	9.4	1.800	1.421	1.470	1.840	0.	Y	Y	0.0016	3.843	6.811	(31)
Hat-P-9	6350	150	16.0	8.0	0.670	1.368	1.280	1.320	0.	N	Y	0.0016	6.012	8.919	(17)
WASP-7	6400	100	110.0	30.0	0.960	1.330	1.276	1.432	0.	N	Y	0.0011	5.870	8.945	(24)
WASP-18	6400	100	4.0	5.0	10.400	1.165	1.240	1.230	0.	N	Y	0.0011	2.356	5.419	(4)
XO-3	6429	100	70.0	15.0	11.790	1.217	1.213	1.377	0.26	N	Y	0.0001	2.835	6.919	(32)
CoRoT 11	6440	120	0.0	20.0	2.330	1.430	1.270	1.370	0.	N	N	0.0001	3.665	7.769	(33)
WASP-14	6475	100	33.0	7.4	7.725	1.259	1.319	1.297	0.09	N	Y	0.0001	2.833	6.953	(34)
Hat-P-6	6570	80	166.0	10.0	1.057	1.330	1.290	1.460	0.	N	Y	0.0001	4.319	8.430	(35)
Hat-P-14	6600	90	170.9	5.1	2.200	1.200	1.386	1.468	0.	N	Y	0.0001	4.316	8.458	(14)
WASP-17	6650	80	148.7	7.7	0.486	1.991	1.200	1.380	0.	N	Y	0.0001	4.761	8.840	(4)
CoRoT 3	6740	140	37.6	17.0	21.230	0.099	1.370	1.560	0.	N	N	0.0001	3.061	7.198	(3)
WASP-33	7400	200	110.0	0.7	3.000	1.438	1.495	1.444	0.	N	Y	0.0001	2.029	6.203	(36)

Table continues next page...

Table 4.1: Rossiter-McLaughlin measurements, continued...

target	$T_{\rm eff}$	$\pm$	β	$\pm$	$M_{\rm p}$	$R_{\rm p}$	$M_\star$	$R_\star$	e	multiple	confidence	$M_{\rm cz}$	$\log \tau_{\rm cz}$	$\log \tau_{\rm tot}$	ref.
		Total:	54 measurements												

Notes: 1-Winn et al. (2010c) 2-Collier Cameron et al. (in prep) 3-Triaud et al. (2009) 4-Triaud et al. (2010) 5-Triaud et al. (2011)
6-Narita et al. (2007) 7-Gillon et al. (2009a) 8-Brown et al. (in prep) 9-Hellier et al. (2011) 10-Queloz et al. (2010) 11-Bouchy et al. (2008)
12-Winn et al. (2010b) 13-Moutou et al. (2009) 14-Narita et al. (2010a) 15-Winn et al. (2008) 16-Winn et al. (2011a) 17-Moutou et al. (2011)
18-Pont et al. (2010) 19-Anderson et al. (submitted) 20-Johnson et al. (2008) 21-Winn et al. (2005) 22-Simpson et al. (2011) 23-Narita et al. (2009a)
24-Triaud et al. (in prep) 25-Wolf et al. (2007) 26-Narita et al. (2010b) 27-Jenkins et al. (2010) 28-Loeillet et al. (2008) 29-Miller et al. (2010)
30-Johnson et al. (2011b) 31-Winn et al. (2009b) 32-Winn et al. (2009c) 33-Gandolfi et al. (2010) 34-Johnson et al. (2009)
35-Hébrard et al. (2011) 36-Cameron et al. (2010b)



Artist impression of WASP-8 b. Image courtesy ESO/L. Calçada

Chapter 5

Interpretation regarding the Origins of hot Jupiters

Now, on to the controversial stuff. If observations can lead to some controversy - some measurements are sure, others not, for example - nothing unleashes more passion than explaining nature through a theory. Nevertheless the lure is great: the possibility of understanding the laws of nature from the power of the human imagination is something fascinating and appealing, certainly very satisfying to the brain. The understanding of planet formation and orbital evolution is complex. The challenge is beautiful!

I will tread carefully in those murky waters. Theory regarding planetary systems is lagging the observations. Those have been laid out in this thesis in great length and I hope enough details; they are as sure as I care to be. Now, let's move on to places where I am much less sure, and where my mind wanders, sometimes fixing itself on an explanation and another day, on another. I will first try to showcase fairly what is present in the literature before trying to combine it in an idea. The topic will be focused on the hot Jupiters, those planets for which we have gathered a lot of information. But some of the results extend to other planet classes, and will be presented as those might carry the observables needed to understand the whole thing.

5.1 The Origins of hot Jupiters

Several explanations about the origin of hot Jupiters exist. They come broadly in two categories: disc migration and planet-planet scattering or as I prefer calling it: dynamical interactions and tidal dissipation[1]. I will try to show that neither are exclusive of each other as they happen, well, at different times in the lifetime of a planet. Both pathways appeared in the literature very early after the discovery of 51 Peg b, mostly because they had been theorised earlier, in case of Saturn's satellites for disc migration (Goldreich & Tremaine 1980), and in the case of close binary stars for dynamical interactions (Mazeh & Shaham 1979). Although hot Jupiters are rare (Howard et al. 2011), because they are so easy to find, many have been found. This biased the theoretical development which tried actively to explain those objects sometimes at the expense of what did

[1] or tidal friction, tidal circularisation, tidal migration... something tidal

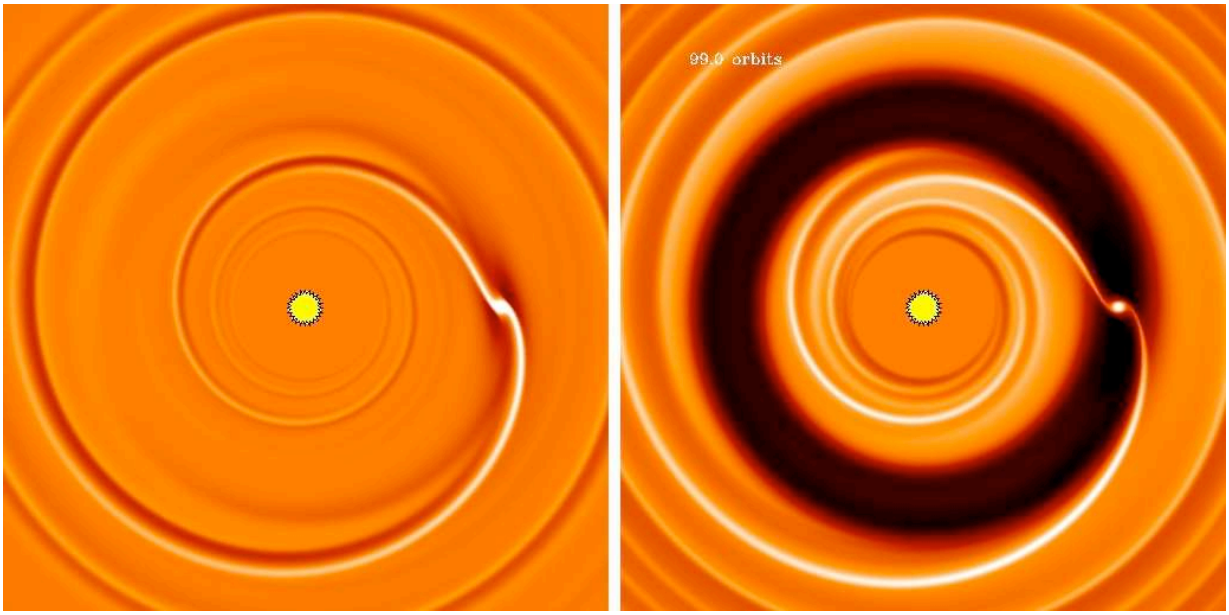


Figure 5.1: Two discs showing a planet and the effect it has on the density of the gas. Light shows over-densities, dark, under-densities. Left is an terrestrial planet (type I migration), right is a gas giant having opened a gap in the disc (Type II migration). In both cases we clearly see a spiral density wave developed, which will exert a torque on the planet. Figure obtained from Crida (2011) from a figure by Masset.

not happen in our own Solar System. The increase in observational timespan and precision in radial velocity, and the more recent results from the *Kepler* space satellite have clarified things a little. Theory has matured a lot.

There is a third alternative to the two proposed pathways: in-situ formation, or more precisely, formation of giant planets on shorter orbit than the traditional snow line. After formation the two pathways can nevertheless act on them. I could not find many references on this subject except one showing it is not an impossible thing (Bodenheimer et al. 2000); the only person I had discussion with on this subject was Günther Wuchterl.

disc migration

First theorised in the context of satellites and planets by Goldreich & Tremaine (1979, 1980), it was applied to planets in protoplanetary discs by Lin et al. (1996) and Ward (1997). Under the words *disc migration* hide all the interactions that a planet has with the disc in which it formed. Since disc migration has first been described, it has reveted several forms (for review please read Lubow & Ida (2010) and Crida (2011)), including three main type of migration: type I, a planet imbedded in a dust and gas disc, type II, a planet opening a gap in a dusty and gaseous (there is a type III if gas crosses the gap. Type III is a runaway type II migration). Another mechanism is planetesimal driven planet migration (Ida et al. 2000; Levison et al. 2008).

As it forms, a planet grows in mass and arrives a time when it will create a density wave in the gas of the surrounding disc. This wave develops into a spiral arm and exerts a torque onto the planet in the form of a Lindblad resonance. This process has been revised by Tanaka et al. (2002)

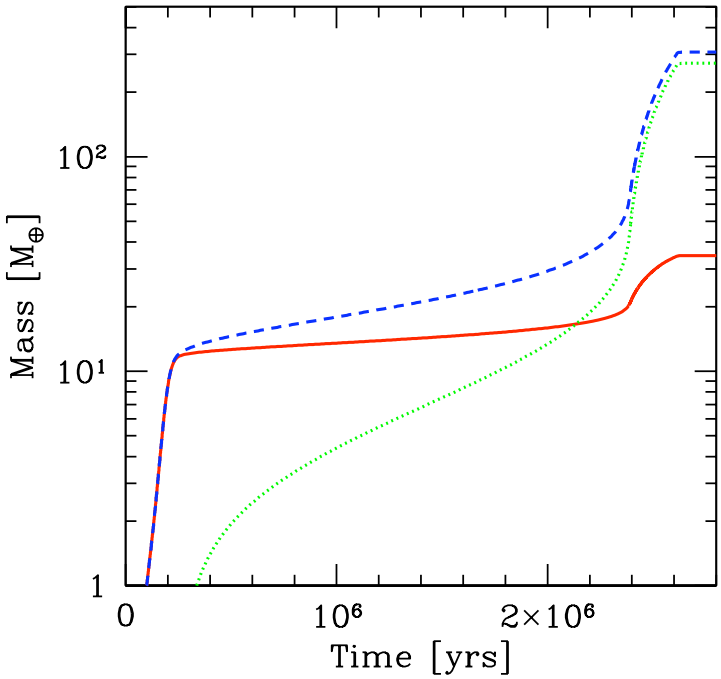


Figure 5.2: Planet mass as a function of time as the planet forms. First a core is created from accretion of ice and dust, then, past a critical mass, gas starts being accreted. Past a second threshold runaway gas accretion happen and the planet reaches is current mass. Figure obtained from Mordasini et al. (2010).

and is the type I prescription which is mostly used at the moment despite some heavy shortcomings: a ten Earth mass planet would plunge into its star in a few 1 000 years after formation. It also predicts that migration gets faster as mass grows (until mass $> 0.1 M_{\rm Jup}$ then we reach another regime: type II). One can be saved via the development of a corotation torque that will trap the planet at one particular orbit (Masset et al. 2006). For this torque to develop one needs a permanent, strong, outward, positive density gradient in the disc maintained by a certain physical process that remains to be determined. Some serious possibilities are given in Paardekooper & Mellema (2006) and Kley & Crida (2008). The addition of this process can lead to outward migration for a planet in the inner optically thin parts of the disc and inward migration for one planet situated in the outer optically thick parts.

A core made of ices and dust grows in mass before it reaches a critical mass where it starts accreting gas in a runaway process (Pollack et al. 1996; Alibert et al. 2005)) becoming a gas giant type planet. With enough mass the planet will open a gap into the disc (Crida et al. 2006) which slows down mass accretion and make the planet follow a type II migration. The planet then migrates at the viscous evolution timescale of the disc: inwards, slower than the Tanaka migration rate, but still too fast. Typical timescale are of the order 10^5 years depending on the planet's mass, the location where it opens the gap (it should undergo type I migration before becoming big enough to open a gap) and when in the disc's lifetime it does so. As the ratio between the planet's and the local disc's mass decrease with time and become comparable, migration slows down before finally stopping (Alexander & Armitage 2009; Mordasini et al. 2009a).

Nelson & Papaloizou (2004) advocate that discs being turbulent, an embedded planet will perceive different density gradients exerting different torques, outwards as much as inwards. One then should not see a monotonous migration. This also implies that migration rates as described in Tanaka et al. (2002) should be slower.

Planets are rarely born on their own, our Solar System is a good example, and an increasing number of system show that having several gas giants in a system is not rare. The presence of

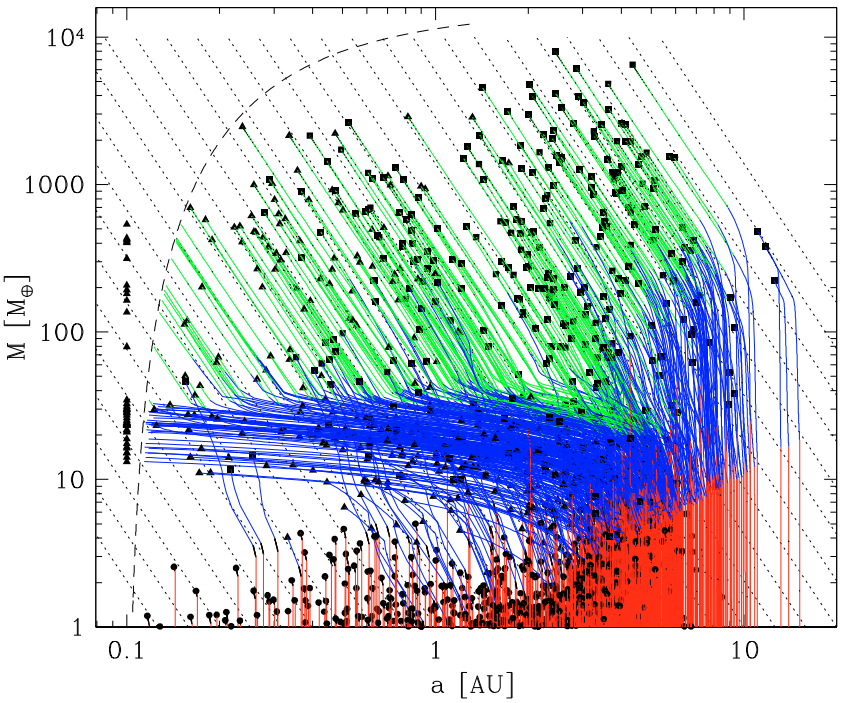


Figure 5.3: Result from a planet population synthesis code. Planet embryos start at the bottom of the graph at various orbital distances. They accrete mass and migrate. Colours represent different migration mechanisms: (red) reduced Type I, (blue) Type II disc dominated, (green) Type II at breaking phase. The simulation is stopped when the disc has dissipated and the resulting distribution can be compared to data. Various initial conditions can be thus tried and tested. Figure obtained from Mordasini et al. (2009a).

two planets in a disc disrupts seriously the rates described above. At first one can assume that the planets migrate as if they were alone, but migrating at different rate they can fall in mean motion resonances (including Trojan configurations (Thommes 2005)) and then migrate as a pair. Some configurations are unstable but the presence of the disc can dampen eccentricities and inclinations leaving the system in a stable configuration when the disc dissipates (Papaloizou & Larwood 2000; Crida et al. 2008) though this is challenged by Matsumura et al. (2010b). The opening of a common gap to both planets with the most massive being on an inner orbit, leads to an outward planet migration like described in Masset & Snellgrove (2001). This outward migration can go back $\sim$ 100 AU if the disc is viscous enough and large enough (Crida et al. 2009). This scenario is at the core of the Nice-model (eg. Levison et al. (2008)) which attempts at explaining the planets and asteroid belts configuration in our own Solar System.

None of these migration scenarii give a stopping mechanism: what happens when a planet reaches the inner edge of the disc is mostly unknown territory. In addition most of the papers above depend heavily on α-discs (as in Shakura & Sunyaev (1973)) to describe a mostly unknown parameter: the viscosity of the disc. The initial conditions such as the disc mass and distribution is also something being debated. The only stopping mechanism besides when the disc's mass is small enough that the planet does not perceive it anymore, is a mechanism developed by Rice et al. (2008) and involving the magnetospheric gap creating the inner edge of the disc. Furthermore a host of effects at present neglected could be shown to affect migration rates. But, the picture where migration was a one way route to the star and quite fast at that, has now changed. The different inwards and outwards rate give rise to convergence zones where planets can gather. Attempts to apply the physics of disc migration into codes exploring a vast array of initial conditions are being pursued by Ida & Lin (2004) and subsequent papers as well as by Mordasini et al. (2009a) and subsequent papers... If the migration rates needed to be tweaked to avoid all planets falling into the star and none surviving, the addition of the recent developments outlined above allowed the removal of those fudge factors, as presented by Mordasini et al. (2011), the unfortunate consequence being that to explain the population of gas giants beyond orbital separation of 1 AU, only half the hot Jupiters that are observed can now be produced (Mordasini, priv. comm.).

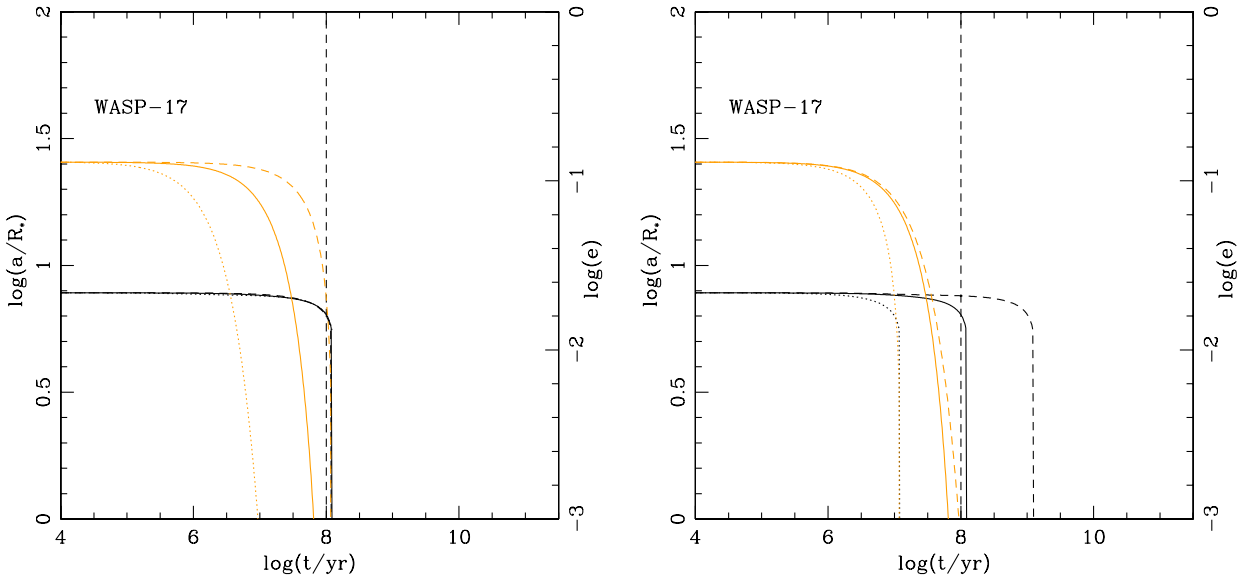


Figure 5.4: Tracks follow the orbital decay of WASP-17 b due to tidal dissipation. In orange, evolution of the eccentricity, in black, evolution of the semimajor axis for various tidal Q'. The planet is Darwin unstable: it is spiralling towards the star. Left: three different planet $Q'_{\rm p}$ for one stellar tidal $Q'_\star$ kept constant. Right: three different tidal $Q'_\star$ while keeping the planet's tidal $Q'_{\rm p}$ constant. WASP-17's age has been estimated to be $< 3\,10^9$ years. Figure from Matsumura et al. (2010a).

Attempts to check the physics describing those *population synthesis* simulations are made by comparing the simulated planet distributions with observed planet distribution (eg. Mordasini et al. (2009b)). In my mind those models are still lacking an essential feature (what will now follow): evolution and multiplicity. At the moment only one planet at a time is placed in a disc and migrated when we know multiplanetary systems exist. As the disc dissipates, configurations that may have been stable could no longer be, giving rise to planet-planet scattering changing the shape of the planet distributions. Thommes et al. (2008) attempted a few of those features in a limited capacity. I have heard that the next generation of population synthesis code will include those effects.

dynamical interactions and tidal friction

Under this title hide several mechanisms, but all are concerned with the gravitational interactions of more than two bodies. Very quickly after the discovery of 51 Peg b, it has been suggested by Rasio & Ford (1996) that planet-planet interactions could lead to the scatter of one giant planet towards the inner parts of its system. Since a series of papers have tried to simulate this interactions with various initial conditions and applied physics.

Often people people think of planet-planet scattering as a one-off event of two planet's skimming each others. This image is wrong. Planet-planet interactions can happen on secular timespan and can happen from before the disc disperses entirely to well after the disc is gone. A system which was stable when the disc transformed the repartition of mass can go unstable when the disc disappears (Matsumura et al. 2010b).

Those dynamical events place a planet on highly eccentric orbit. At periastron passage the

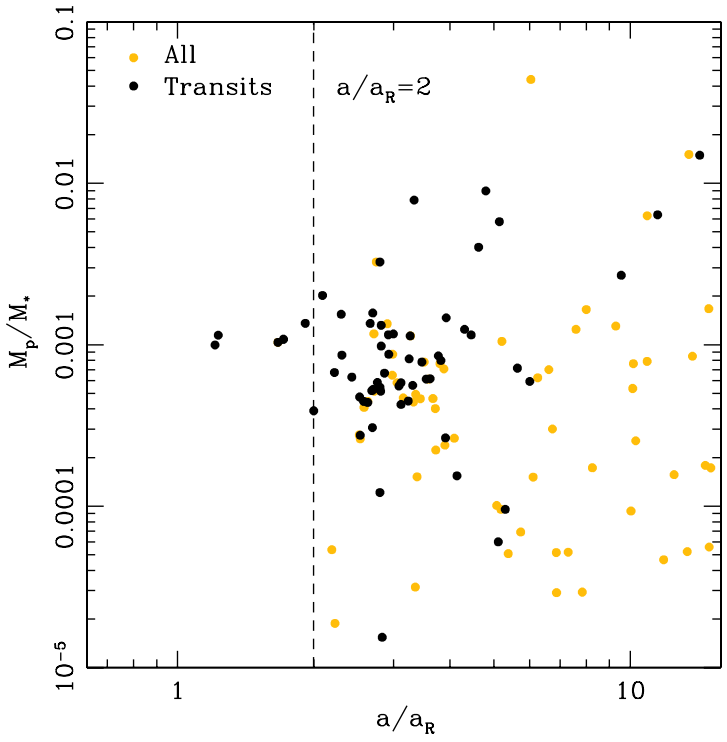


Figure 5.5: Planet mass as a function of orbital separation in units of Roche radii. In black transiting systems. In orange planets found using the Doppler technique for which a radius is assumed. Figure obtained from Matsumura et al. (2010a).

planets feels strong tidal forces, which dissipates part of the orbital energy away, heating up the planet in the process. The planet is *tidally captured*. The semimajor axis thus reduces and the orbit circularises in what we may call *tidal migration*. For orbits with e > 0.7 and a starting semimajor axis of a few AU, periastron is about one Roche limit from the star. After circularisation one expects to find planets beyond two Roche radii from the star (Ford & Rasio 2006). Planets which periastron was not within the "hot Jupiter Parking zone" felt weaker tides. Those planets are still eccentric, and if transiting, should follow the predicted distribution of orbital obliquities. In the meantime, planet-planet scattering explains well the distribution in orbital eccentricities (Jurić & Tremaine 2008; Chatterjee et al. 2008; Ford & Rasio 2008).

After being parked on circular orbits of a few days, in most cases their orbit, being within the stellar corotation orbit, will decay due to being tidally "Darwin unstable" (Darwin 1879; Levrard et al. 2009; Matsumura et al. 2010a). Thus the few planets whose orbital separation is within two Roche radii, such as WASP-19 are on in-spiralling orbits. Matsumura et al. (2010a) shows that a number of planets should fall into their star in a time shorter than the estimated age of the star around which they orbit. This points towards dynamical events happening well after disc dispersion, sometimes even several Gyr later. The treatment of tides could also impact the results.

The major current source of uncertainty comes from the treatment of tides and the use and values of the tidal Q' which is obtained from a tidal dissipation quality factor Q as defined in Goldreich (1963) not unlike the quality factor of a damped harmonic oscillator (Murray & Dermott 2000). Q quantifies the dissipated energy for each oscillation and is thus linked to the forcing frequency, which here is given by synodic period between the stellar rotation and the orbital period of the planet. Q' also includes information about the internal structure of the studied object by way of a Love number k (Barker & Ogilvie 2009). Ogilvie & Lin (2004, 2007) remark that although most papers assume a constant Q' in their treatment of tides, it has a complex relation with the orbital frequency, which is changing as the planet's orbit decays. This area of research is very active.

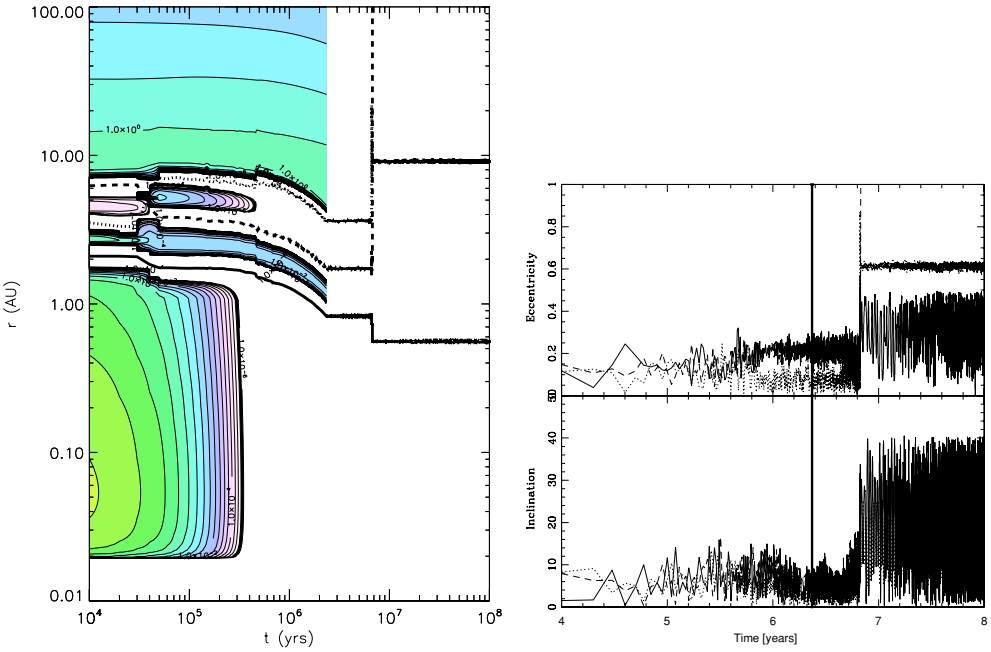


Figure 5.6: Simulation following the orbital evolution of a three planet system. The simulation followed the three planets in the disc and after the disc dispersed. An instability developped and a planet collides with the central star. The other two are left on eccentric and inclined orbits. Left: colours contours represent the disc's surface density and the planet's orbital evolution. Right: evolution of orbital eccentricity and inclination. Figure obtained from Matsumura et al. (2010b).

A possible hurdle was solved by Guillochon et al. (2011) and Matsumura et al. (2010a): as the planet circularises, an enormous amount of energy needs to be dissipated. Critics of tidal circularisation of highly eccentric orbit were saying that the dissipated energy is greater than the binding energy of the planet. Circularisation would lead to the planet's disruption. Guillochon et al. (2011) take this into account and manage to tidally bring almost all known hot Jupiters to their current orbit from another orbit which initial conditions were a semimajor axis reaching beyond the snow line and a high eccentricity. According to these authors, only a dozen of the known hot Jupiters could not have arrived on their current orbit through such a process but would have needed a smaller initial semimajor axis. This dozen includes all those planets which current orbital distance is smaller than two Roche radii. Since we know those are on infalling orbits, they are not a contradiction as they could have circularised at larger periods and decayed ever since. Anyway, dynamical events and tidal migration do not contradict disc migration, they can supplement it and basically take over from where the planets got deposited, in some grand orbital redistribution. Furthermore, let's remark here that planets with orbital period < 3 days are very rare; we find them very easily in transit surveys thanks to their short period and higher Doppler amplitude (see Hellier et al. (2011) for a estimate of the chance to catch a planet on its infall). Matsumura et al. (2010a) find that energy dissipation in the star is greater than in a planet, alleviating the problem.

Various dynamical events leading to an eccentric orbit can be:

- Interactions between a planet and the second star of a binary system can lead to an increase of the planet's orbital eccentricity. This eccentricity is exchanged cyclically for a change in orbital inclination of the binary orbital plane. This interaction start at a critical angle where the planetary orbital plane and binary orbital plane have an obliquity $\psi > 39.2°$. This is called the Kozai mechanism (Kozai 1962) which can lead to *Kozai migration* (Wu & Murray

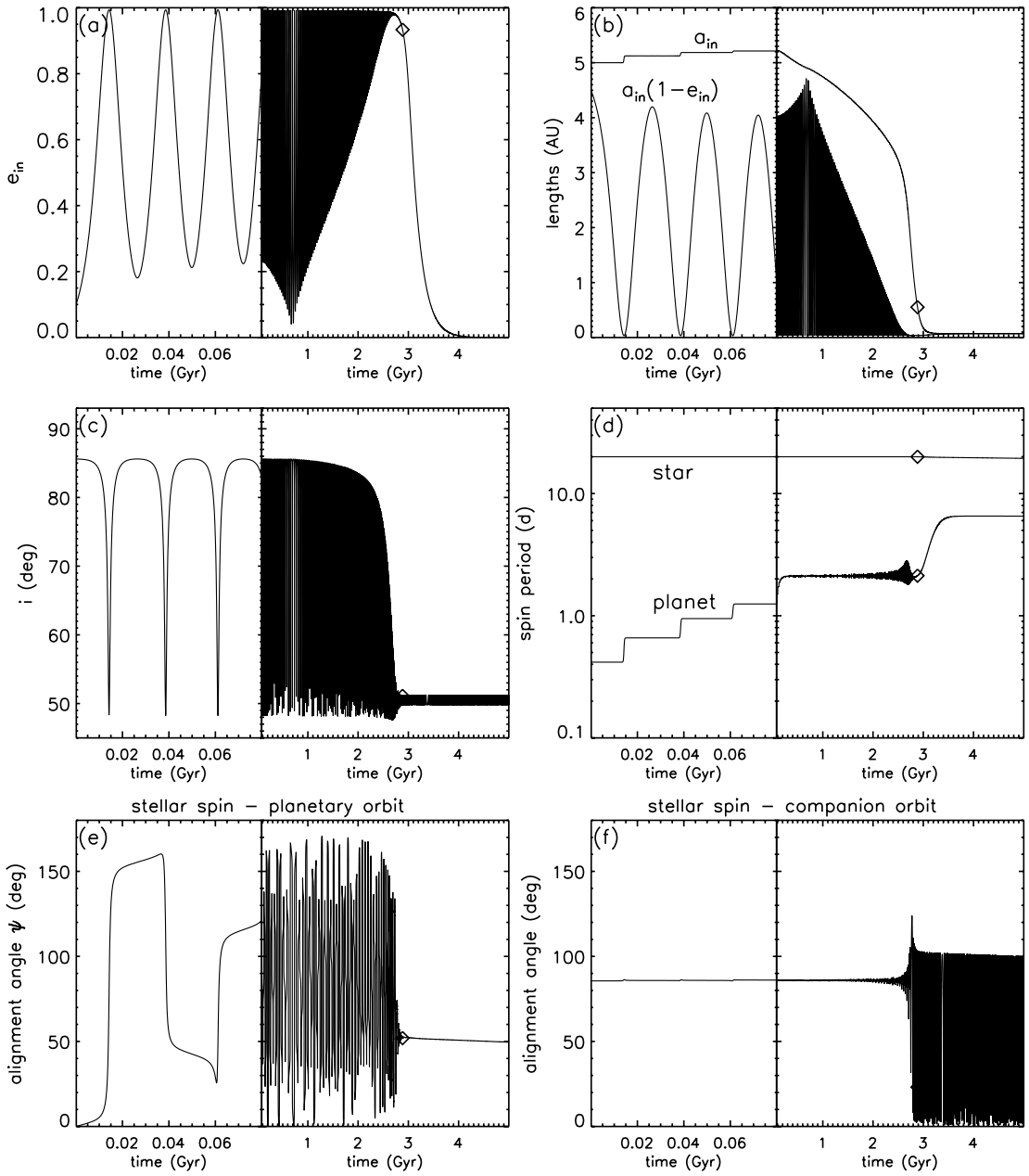


Figure 5.7: Simulation of the orbital evolution of a planet inside a wide binary system resembling HD 80606. For each subfigure, the left hand side shows a zoom on the first steps of what is shown on the right hand side. Top left we see the evolution of the planet's eccentricity. Top right, we see the evolution of the semimajor axis of the planet $a_{\rm in}$, and of its periastron $a_{\rm in}(1-e)$. Every time e is close to 1, $a_{\rm in}$ changes. Eventually it leads the planet to fall towards the star. The obliquity of the planet ψ with respect to the stellar spin axis is shown at the bottom left. What we measure is β the projection on the sky of ψ. Figure obtained from Fabrycky & Tremaine (2007).

2003; Wu et al. 2007; Fabrycky & Tremaine 2007). Binaries which are separated by more than 40 AU have random orbital planes inclinations with respect to their individual rotational planes (Hale 1994). Any planetary system born in a widely separated binary thus has a strong chance to experience Kozai cycles. Those can lead a planet to have periodically an orbit eccentric enough to experience strong tidal interactions with its host star. After a while precession due to General Relativity become dominant over the influence of the binary and Kozai oscillations stop. Malmberg et al. (2007a) and Malmberg & Davies (2009) show the action of the Kozai mechanism on multiplanetary systems: most of the planets are ejected. We would expect to still be able to detect the binary companions. Those can be located quite far, up to a few 1 000 AU.

- Planet-planet interactions can lead to a rearrangement of one planet towards shorter orbital radii and one to larger periods. Through the scatter, it can happen that both orbital plane are oblique by more than the Kozai criterion in which case further changes in the orbits will occur as outlined in Nagasawa et al. (2008). It can also happen that planets are ejected from the system. From this we expect a population of planets on inclined eccentric orbits with semimajor axis of order 100 AU.

- Many simulations used for planet-planet scattering often start with several planets which orbits are unstable to start with. Scattering thus happens on quite short timescales. More recent developments about planet-planet scattering treat secular effects between planets which a priori looks like being in stable configurations. A revised treatment of the Kozai mechanism (for smaller mass perturbers) leading to secular variations in the inclinations of planetary orbital plane is presented in Naoz et al. (2011). These authors produce retrograde planets, but still need to start with an outside perturber on an inclined orbit. Why that perturber is on an inclined orbit is unclear but could be the result of a past planet-planet interaction as described above. Another secular process is secular chaos theory as outlined in Lithwick & Wu (2010) in the case of Mercury (see also Laskar (2008) and Laskar & Gastineau (2009)) as well as in Wu & Lithwick (2010) for the production of hot Jupiters. This secular process again places a planet on a highly eccentric orbit which then tidally migrates. In this particular case the produced hot Jupiter used to be the innermost gas giant of a multiplanetary system which orbital inclinations are only slightly different (very much like in our own Solar System). If this is true, hot Jupiters should come with planetary companions on circular orbits. Those could be positioned quite far out but still within a typical protoplanetary disc size.

Finally, external events can lead a stable system to go unstable. This is work notably presented in Malmberg et al. (2007b) and Malmberg et al. (2011). They argue that a stellar fly by within 100 AU can insert a perturbation which grows during a few Gyr and leads to an instability and a scattering event. Those events can happen from the very beginning of a system's history: in the birth cluster where stellar densities are large, but also at later stages such as inside open clusters, or when stars cross spiral arms. From N body simulation of open clusters Malmberg et al. (2007b) show that a third of stellar systems in their simulation have had dynamical interactions, either due to a close fly-by by another star, or even by getting inserted into binaries during the lifetime of the cluster.

As Dan Fabrycky once told me, in system dynamics, configurations that cannot be obtain are rare. They are many ways to "mess up" planetary systems. Hot Jupiters are found only around one star in 200. A very low number.

5.2 Observational Clues

Let's now review some of the observational evidence in the light of the theoretical developments outlined just earlier.

5.2.1 Using the multiplicity argument

Different migration pathways could be expected to deposit planets at different semimajor axes. Thus, can we expect anything from this distribution?

There has been a strong observational effort to try and detect planets via Transit Timing Variations (TTV) which method is described in Holman & Murray (2005) and Agol et al. (2005), with the aim to find non transiting planets which could not be detected via the Doppler method. TTVs are mostly sensitive to the presence of a second planet in mean motion resonance with the one we see transiting. These configurations could have happened during the migration of a system in a disc (Kley et al. 2005), but not in the case of multi body dynamics and subsequent tidal circularisation. A few papers report detections of TTVs but none have undoubtedly detected a small planet in a system where a hot Jupiter is present[2]. This simple observational fact is something confirmed in the results by the satellite *Kepler* which would have been able to detect small transiting bodies on orbits of a few days. Out of the 65 hot Jupiter candidates they detected, not one is in a multiplanetary system (the only candidate they produced with close-in gas giants was KOI-961, with a Jupiter at 0.45 day, a Neptune at 1 day and another Jupiter on a 2 day orbit (Borucki et al. 2011; Lissauer et al. 2011b). But a refined analysis of this system (hard to characterise because of the shortness of the orbit and the 30 minutes integration time of the *Kepler* satellite) appears to show that the size of those planets is probably much smaller than that announced. They are more likely Neptune-sized objects than Jupiter-sized (Darin Ragozzine, Flagstaff conference, April 2011)).

If the lack of observed TTVs for hot Jupiters is not contradicting disc migration (there are number of reasons why no such planet should exist, for example the planets formed at completely different times, or an orbital tidal decay could have disrupted the resonance), it also goes along the way of dynamical interactions where we expect not to see them.

Radial velocity observations also show a dearth of multiplanetary system whose innermost planet is a hot Jupiter. Those can be counted on one hand: υ Andromeda (McArthur et al. 2010) and HD 187123 (Wright et al. 2009b). Other systems could be: HD 217107 (Wright et al. 2009b), HIP 14810 (Wright et al. 2009a) and 55 Cancri (Dawson & Fabrycky 2010), but their inner gas giant has an orbit > 6 days and often mildly eccentric so that their periastron does not correspond to a hot Jupiter's semimajor axis. In fact they resemble a lot WASP-38 b which I have trouble naming a hot Jupiter[3]. 55 Cancri, υ Andromeda, HIP 14810 have their second gas giant within 1 AU. In HD 187123 and HD 217107, the second planet is out at around 5 AU and thus unlikely to have migrated much.

Strong dynamical events are disruptive for planetary systems as we saw earlier. Although the Kozai mechanism gives little chance to planets other than the one that would have circularised to have survived, the other mechanisms do predict that hot Jupiters ought to be found in multiplanetary systems. Strong planet-planet scattering for example predicts the presence of an outer

[2] Else transit timing variations have been observed on a number of *Kepler* candidates, but those are not hot Jupiters, but smaller mass planets and/or at larger orbital radii (Holman et al. 2010; Lissauer et al. 2011a).

[3] the definition of a hot Jupiter is a little fuzzy, is it determined in semimajor axis, periastron passage or orbital period? I usually take periastron passage within 0.05 AU; a definition based on the tidal influence might be good too. Barker & Ogilvie (2009) indicate that tides dominate orbital evolution for orbits < 6 days.



Figure 5.8: All the *Kepler* systems where transits from two different planet candidates are detected. Figure courtesy Dan Fabrycky, present in Lissauer et al. (2011b).

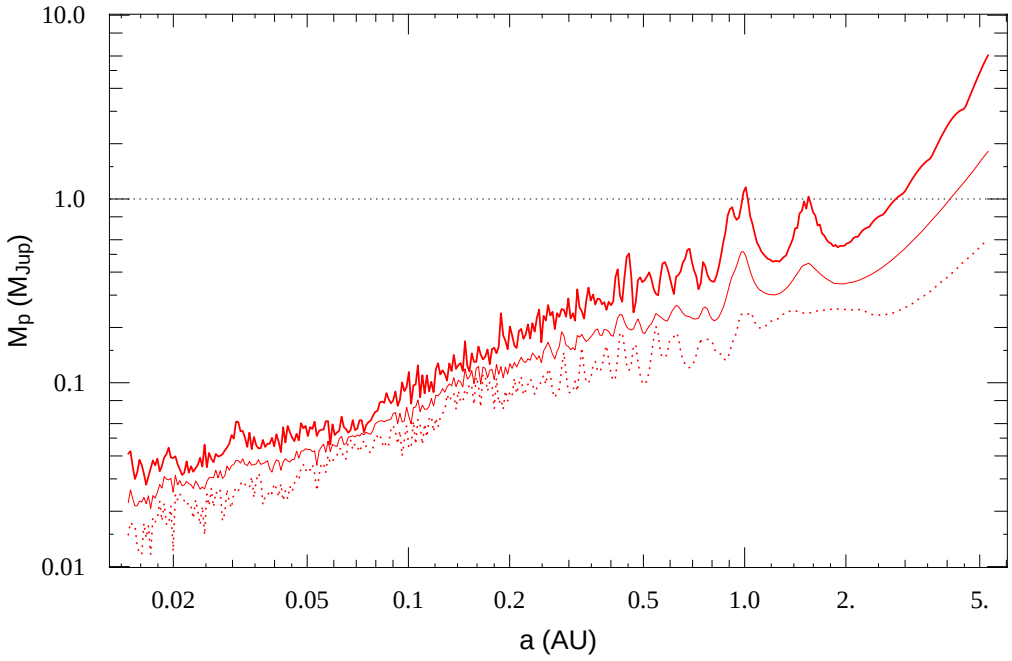


Figure 5.9: Detection limits for WASP-16. In bold, the 99 % detection limit. Any planet in the space above would have been detected. Dotted line: same limit but taking the best phase configuration possible. Thin line: average of the 20 phases that were considered. This plot shows we are reaching the precision and timespan necessary to detect another gas giant in the midst of the $2^{\rm nd}$ rise in planet numbers shown in figure 5.10. Such an analysis planned for each of the WASP planets with enough baseline and RV precision. For details on the computation needed to realise this plot, see Maxime Marmier's thesis. The methodology used is similar to that found in Naef et al. (2005) and Cumming et al. (2008), which will also appear in Mayor et al. (in prep)

planet on a highly eccentric orbit (Nagasawa et al. 2008). Those are too far for us to detect via the radial velocity method. Maybe direct detection might image them in the near future. Secular chaos theory predicts we should find at least two other planets on circular orbits, also quite far from the central star but on orbits similar to the gas giants in our own system. Those should also be more massive (Wu & Lithwick 2010).

HD 187123 has an architecture expected from secular chaos; 55 Cancri, υ Andromeda, HIP 14810 have probably disc migrated, having several gas giants within the ice line. The presence of an Earth size planet inside 55 Cancri b's orbit is a strong constraint (Winn et al. 2011b; Demory et al. 2011) for that scenario. So is the apsidal alignment of two of the planets around υ Andromeda (Chiang et al. 2001). HD 217107 is a bit of a mystery: the inner gas giant looks like one that could have migrated (it is a little too far from the star to have circularised from a longer, eccentric orbit), but then, why has not its companion migrated too?

Transit surveys have had less time to complete the detection of extra planets at long periods. Only two multiplanetary systems have been announced: Hat-P-13, which looks a lot like υ Andromeda (a hot Jupiter on a 3 day period and a second $15\,M_{\rm Jup}$ planet immediately after), and Hat-P-17 which looks like a good candidate for secular chaos theory. So far no WASP multiplanetary system has been announced though several long term drifts have been announced. Those may be caused by planets or stellar objects. An example of a detection limit to the presence of a second planet in the WASP-16 system is given in figure 5.9. We could have detected a planet of

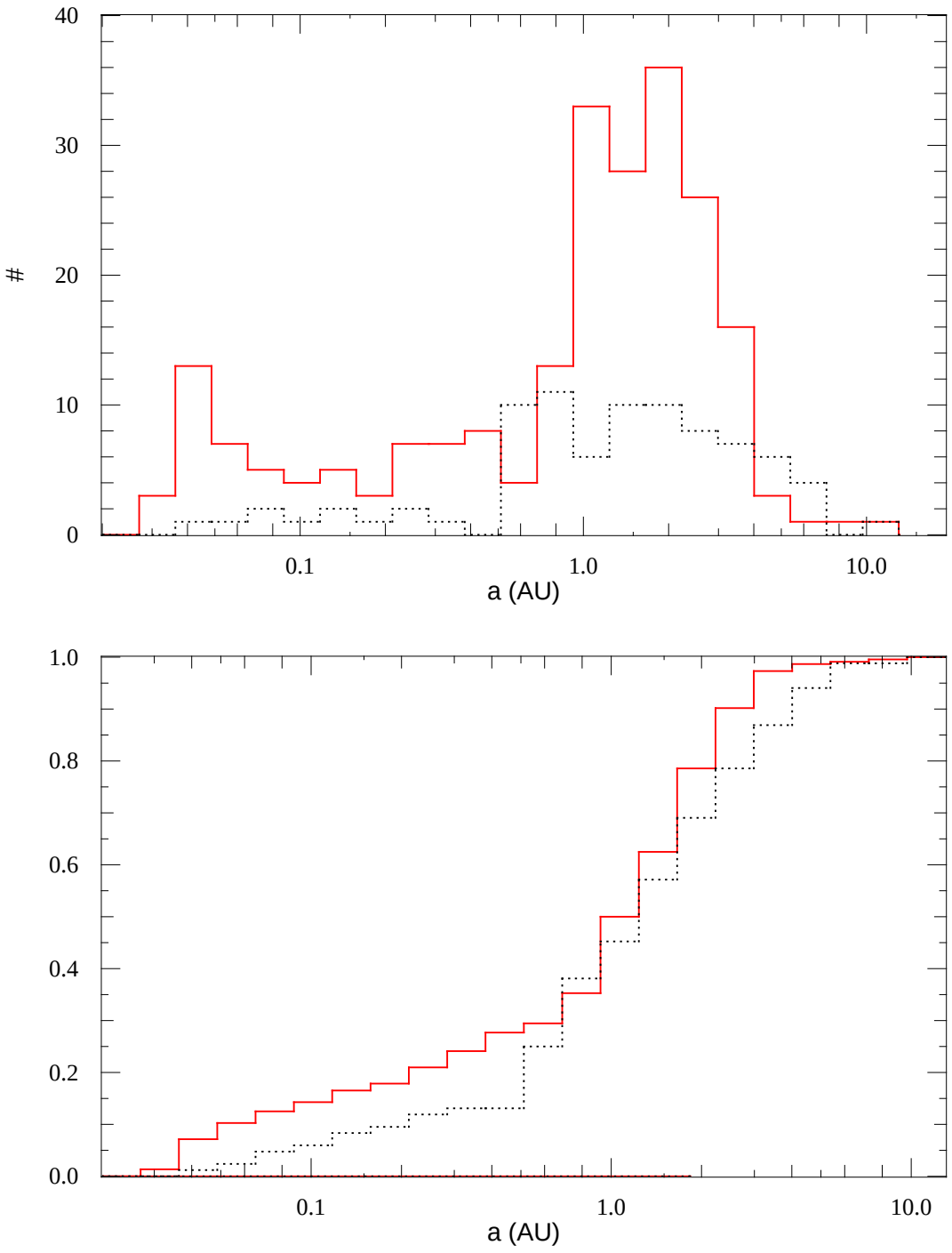


Figure 5.10: Only planets found using the Doppler method with masses > 0.1 $M_{\rm Jup}$ orbiting stars > 0.6 $M_{\odot}$ *top*: Plain red histogram shows the distribution in semimajor axis of planets for which no other planetary companion has been found to date. Dotted histogram shows the distribution in semimajor axis of planets which are found in multiplanetary sytems. In the case that the system had planets <0.1$M_{\rm Jup}$, these have not been included. We only compare gas giants. *bottom*: Same but as a cumulative distribution. Data obtained from `exoplanet.eu`, and graph updated from Wright et al. (2009b).

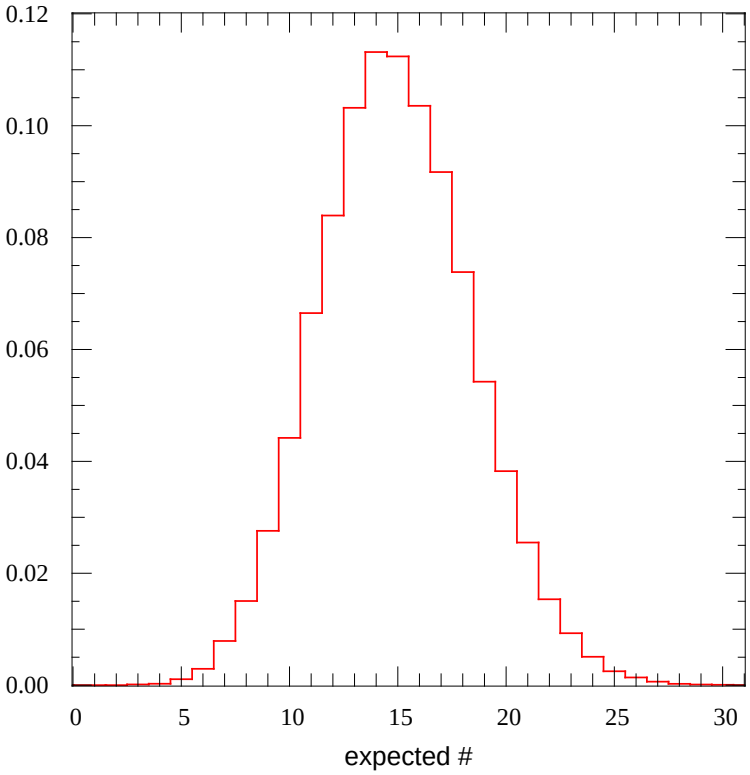


Figure 5.11: 100 000 random trials to match the multiplanetary distribution shown in figure 5.10 to the single planet population. For the seven inner bins (<0.12 AU) we would expect to have observed about 15 ± 4 gas giants. Only five have been discovered and announced.

about $1\,M_{\rm Jup}$ out at 3 AU. Increasing to longer period will take some time.

Wright et al. (2009b) have analysed the distribution of semimajor axes of planets found via the Doppler method and concluded that the distribution of planets in single systems is not the same than that which characterises the multiplanetary systems. I have updated the graphs to the current situation, which are presented in figure 5.10. I have only selected planet found on stars with masses > $0.6\,M_{\odot}$ and planets with masses > $0.1\,M_{\rm Jup}$. We still observe the so-called "3-day peak" characteristic of the hot Jupiter population. I ran a Monte-Carlo simulation to test if both distributions were the same. Thus, assuming both distributions are the same I drew randomly from the single planet population, a simulated population of planets in multiplanetary system. I obtained a distribution of the number of gas giants within 0.12 AU that should have been observed if both distribution where the same. Figure 5.11 shows the resulting distribution. This result is to take with caution. Some surveys were biased in metallicity to discovery more planets, and their completeness is uncertain. Both distributions are also correlated: if a Neptune mass planet were to be found in a system where only one Jupiter was known before, it would take away a planet from the single planet population and add one in the "gas giant in multiplanetary system" population.

To illustrate that doubt, I should point out that the three day peak is not at all evident in the analysis of the distribution of gas giant planets from the *Kepler* data, done by Howard et al. (2011).

A final point ought to be made. As shown by Dan Fabrycky (at the OHP conference), there are a number of systems with gas giants in mean motion resonances. Removing the GJ 876 system which is around an M dwarf[4], among all the other systems showing mean motion resonances between two of their gas giants, the innermost of these giants are located at about 250 day period,

[4]its snow line was closer to its star than for solar type stars and its planets might have migrated far less than gas giants around solar type stars

slightly inward to the 1 AU peak that can be noticed in figure 5.10. Mean motion resonances are expected to be created while multiple planets are disc migrating, each a slightly different rate (Kley et al. 2005). The presence of those resonances could then be interpreted as a signpost for disc migration having been at work. Because we do not see such systems closer than around 1 AU, we may interpret it has a marker of where most planets stop disc migrating (one system does not obey that rule: Kepler-9 (Holman et al. 2010)).

5.2.2 The metallicity correlation

Santos et al. (2004) showed there is a correlation between the presence of gas giants and the metallicity of the star. Population synthesis codes such as Mordasini et al. (2009a,b) reproduce such a correlation and interpret it as being the sign of a more efficient planet formation. Having more metals in the disc would facilitate core accretion and thus the presence of gas giants. I'll remark here, that having more gas giants in a system may trigger more easily some planet-planet interactions, those which eventually can lead to the formation of hot Jupiters.

5.2.3 The eccentricity distribution

Wright et al. (2009b) claim that planets which are observed as being single tend to have higher eccentricities than planets observed in multiplanetary systems (excluding hot Jupiters to avoid contamination from tidal circularised planets). It is hard to point to one particular phenomenon. This result is one that could be expected out of strong planet-planet scattering and Kozai migration, but likewise in secular chaos theory where we would expect other gas giants further out. Jurić & Tremaine (2008) reproduce the eccentricity distribution well for e > 0.2, meaning another mechanism might be responsible for the mildly eccentric orbits. Planet-disc interactions could do that (Goldreich & Sari 2003). Eccentricity could vary due to secular interactions between the planets as outlined for the case of υ Andromeda by Chiang et al. (2001). Planet-planet scattering simulations also eject a large number of planets that we may one day detect as free floaters (a recent detection claim of such a population is presented in Sumi et al. (2011)).

Furthermore, the highest eccentricities (> 0.8) are at the moment only found in single planet systems, which are found often in wide binary systems (HD 80606, HD 156846, HD20782) suggestive of the Kozai mechanism; Ford & Rasio (2008) point out that those could also well be explained with planet-planet scattering, but that a combination of several dynamical effect is not unlikely.

5.2.4 The study of our own Solar System

We fortunately have gas giants in our System (for example we won't have the same luck when studying the *mini-Neptunes* and *super-Earths* that are being found around other stars. Thanks to the *Cassini* spacecraft still in orbit around Saturn, an intense work had been produced to understand that planet and its satellites and provided interesting clues about its formation. Nearing the end of its mission, the probe will probably be placed on a grazing eccentric orbit, to study the gravitational field of Saturn (Lunine, priv. comm.) and measure the presence of a core, which would come as a confirmation of the core accretion scenario, as presented for example in Alibert et al. (2005). Meanwhile, the study of one of its satellites, Iapetus, has given strong constraints about the time that Saturn formed. Its rotation, its overall shape, and notably its equatorial ridge which makes Iapetus stand out amongst all other satellites, along with the radioactive decay of ^{26}Al, all depend on a precise chain of events which allowed Castillo-Rogez et al. (2007, 2009) to give an age at which it formed: 3.4 to 5.4 Myr into the history of our System. Iapetus is thought to have formed from an accretion disc around Saturn, and thus leads to an age estimate at which Saturn existed. This age would give it ample time to have disc migrated.

Now this result is interesting to put into context, notably by studying stars similar to our Sun. Two of the closest spectroscopic solar analogues (Soubiran & Triaud 2004), 47 Ursa Major, and 16 Cygni B, have planetary systems very different from our own. Yet, the initial conditions, presumably the discs (since most of the matter in the disc ends up onto the star), were sufficiently similar that they created very similar stars, while in the meantime creating different planetary systems. Both those systems appear to have had some sort of orbital migration. The Nice model (eg. Levison et al. (2008)) also allows some disc migration for Jupiter and Saturn, which opening a joint gap and using the Masset-Snellgrove mechanism, migrated outwards. This mechanism requires the inner planet to be the more massive of the pair. Such is the set-up around 47 Uma: the inner gas giant is found at 2 AU. 16 Cyg could be understood as being different: it is a binary system.

5.2.5 Spin/orbit angles

All previous evidence were the tools that people had at their disposal about two years ago. Since, the fast past of observations of the Rossiter-McLaughlin effect have brought a new observable to play with: β.

There is at the moment very little evidence that a star with a planetary system around it could change its spin axis from aligned to misaligned. The only such mention I heard about was made at a conference at the Observatoire de Haute-Provence. The subject was brought up by Claire Moutou and is presented in Cébron et al. (2011). They argued that a tidal instability caused by the hot Jupiter raising tides on the star, can develop and affect the stellar spin axis. If this is indeed what happens, it may invalidate much of my conclusions. I will assume henceforth that the stellar spin axis cannot be moved away from alignment.

Lai et al. (2011) show that accretion discs could become misaligned with respect to the central star if the magnetic field produced by the star had a dipole misaligned with the stellar spin axis. Thus, disc migrating planets inside those disc would be left on inclined orbits. This is unlikely to the be norm: using the distribution of projected spin/orbit angles as a function of stellar effective temperature presented in figure 4.2 we see that gas giants around hot stars are mostly misaligned. If the mechanism described in Lai et al. (2011) was the primary route for creating misaligned planets, one would expect most discs to be misaligned. Watson et al. (2011) did that analysis and showed disc are consistent with being coplanar with their star's equator. Thus this leaves only dynamical events as being responsible for non coplanarity. Those events must have happened after the disc dispersal as otherwise eccentricity and obliquity would have been damped by the disc as the planet crosses it (Kley, priv. comm.).

An interesting interferometric measurement can be found in Bouquin et al. (2009) who conclude the mis-centrered outer disc which triggered observation leading to the direct detection of Fomalhaut b (Kalas et al. 2008), is aligned with the star's equator.

Matsumura et al. (2010a) affirm that if an observed orbital misalignment for a hot Jupiter indicates a dynamical event, an orbital alignment does not reject that a dynamical event happened in the past. This is for two reasons:

- Chatterjee et al. (2008); Jurić & Tremaine (2008); Wu et al. (2007); Fabrycky & Tremaine (2007) and Nagasawa et al. (2008) produced distributions of orbital inclinations thanks to numerical experiments involving dynamical interactions between planets, or between a planet and an outer perturber. While their results show a large dispersion in orbital inclinations, they also produce a number of systems which remained aligned despite the fact they went through dynamical interactions.

- In addition, planets will tend to tidally realign with their star by transferring their angular momentum by raising a tidal bulge onto the star which will torque its spin axis towards the orbital spin axis (eg. Winn et al. (2010a) and Barker & Ogilvie (2009)). Matsumura et al. (2010a) indicate this is especially the case when the orbital evolution is dominated by tidal dissipation inside the star. Most hot Jupiters do not have enough angular momentum to fully realign and would thus plunge into the star as they realign. Matsumura et al. (2010a) show that under certain conditions (high rotation rate for the star and mild orbital inclination) some planets could reach a stable tidal equilibrium state in which the planet can remain and be saved from further orbital decay. Barker & Ogilvie (2009) point out that because of magnetic breaking, all stars rotate slower with time (Skumanich 1972), and thus no true stable equilibrium state exist.

Winn et al. (2010a) reflect on why there is a such a divide in the distribution of spin orbit angle as a function of effective temperature. Their interpretation is that at effective temperatures above 6250 K stars do not have an outer convective layer (see figure 4.2) while colder stars do. Planets, carrying most of the angular momentum, tend to realign their host star. One then could understand a process where planets around colder stars can tidally realign the outer convective layer, while keeping the stellar interior misaligned, while for planets around hotter stars, the planet would have to realign the entire object. It would mean planets around hot stars have a realignment timescale different from planets around cold stars. This also implies that while around hotter stars planets do not have the necessary angular momentum to realign entirely the star (leading to their destruction), planets around cold star may have just what is necessary to realign the outer layer and avoid complete orbital decay. This is of course under condition that the outer layer is decoupled from the inner radiative layer. A similar argument was made to explain the apparent synchronous rotation of τ Bootis with the orbital period of its planet (Butler et al. 1997). Interestingly, τ Boo is a 6309 K star with an estimated mass of $1.3\,M_{\odot}$ (Nordström et al. 2004). Donati et al. (2008), assuming the corotation is not coincidental, indicate that it is possible that the planet has forced the outer convective layer into corotation leaving the central parts of the star rotating slower. This would presuppose that τ Boo b would be observed as aligned with the stellar spin, for reasons somewhat in contradiction with the argumentation used by Winn et al. (2010a) who would see this planet on a misaligned orbit.

Winn et al. (2010a) note that while there is a pattern involving β and $T_{\rm eff}$, it is unsure whether the real parameter is not $M_{\star}$, since both are intrinsically linked.

Several mitigating factors can be found: a third parameter could influence. Because stars with masses above $1.2\,M_{\odot}$ cool down as they age, stellar age may be an issue. In addition the time available for realignment is of importance too. A cold star can spend 7 to 15 Gyr on the Main Sequence while more massive stars only stay between 3 and 4 Gyrs, so planets could easily have time to realign around cold stars, but not around hot stars. Following these ideas, a graph was realised showing evidence for a pattern between β and stellar age. The divide between where aligned and misaligned systems are is currently as pronounced than the pattern involving $T_{\rm eff}$ as in Winn et al. (2010a). From this graph we can now quote a realignment timescale of $\sim$ 2.5 Gyr. Observations are in accordance with the tidal timescales showed in Barker & Ogilvie (2009).

Part of this section was compiled in a paper written the weeks after submitting this thesis to the jury and since submitted to Astronomy & Astrophysics. As I write these words, the third version has been sent to the referee who recommends publication. Being more concise and presenting a better analysis, that paper has now replaced the original text.

Astronomy & Astrophysics manuscript no. BetaAgeLetterV3nobold
September 3, 2011
© ESO 2011

Letter to the Editor

The Time Dependence of hot Jupiters' Orbital Inclinations

Amaury H. M. J. Triaud

Observatoire Astronomique de l'Université de Genève, Chemin des Maillettes 51, CH-1290 Sauverny, Switzerland

Received date / accepted date

ABSTRACT

Via the Rossiter-McLaughlin effect, it is possible to measure the sky-projected angle between the stellar spin and a planet's orbital spin. Observed orbital inclinations have been found to range over all possible angles. A correlation between the dispersion in spin/orbit angle and the youth of the system is revealed, using spin/orbit measurements for hot Jupiters around stars with masses $\geq 1.2\,M_{\odot}$ for which age estimates are more accurately determined. This appears in accordance with tidal dissipation where non-coplanar hot Jupiters' orbits tidally realign. The results show they would do so within about 2.5 Gyr. For the considered sample, the results give support to hot Jupiters being placed on non coplanar orbits early in their history rather than this happening late. Such events could involve strong planet-planet scattering.

Key words. binaries: eclipsing – planets and satellites: dynamical evolution and stability, planet-star interactions – planetary systems

1. Introduction

For transiting planets, the Rossiter-McLaughlin effect (Holt 1893; Rossiter 1924; McLaughlin 1924; Queloz et al. 2000; Gaudi & Winn 2007), allows the measure of β (also called λ in the literature), which is the projection on the sky of the obliquity ψ, between the stellar spin axis and the orbital spin axis.

Up until recently planets were thought to be mostly on orbits coplanar with their star's equator (Fabrycky & Winn 2009), something in line with predictions of disc migration (Lin et al. 1996; Ward 1997). More recently a number of papers have shown that hot Jupiters on non coplanar orbits are common, including some planets on retrograde orbits (Hébrard et al. 2008; Moutou et al. 2009; Narita et al. 2009b; Winn et al. 2009a; Anderson et al. 2010; Queloz et al. 2010; Triaud et al. 2010). Those measurements have been interpreted as showing that dynamical events are probably not uncommon and that not all systems can be understood by disc migration alone. Strong dynamical events such as planet-planet scattering (Rasio & Ford 1996; Jurić & Tremaine 2008; Chatterjee et al. 2008), or more secular processes such as Kozai-Lidov oscillations (Wu et al. 2007; Fabrycky & Tremaine 2007; Nagasawa et al. 2008; Naoz et al. 2011), or chaotic interactions (Wu & Lithwick 2010) would place a planet on a highly eccentric orbit, whose passage at periastron is sufficiently close that tidal dissipation causes the planet to lose angular momentum and circularise around its star.

Understanding the origin of hot Jupiters is one of the keys to shedding light onto the processes that act during planet formation as well as those acting after planets have formed. Those processes allow us to place constraints on what happened and did not happen in our own Solar System. They will also help us match more accurately theoretical predictions of planet formation done in population synthesis simulations to the parameter space that planets currently occupy, as given by the observations (eg. Ida & Lin (2004) and Mordasini et al. (2009)).

Send offprint requests to: Amaury.Triaud@unige.ch

Matsumura et al. (2010a) remark that if misaligned hot Jupiters do not require disc migration, aligned planets are not in contradiction with a scenario involving dynamical interactions and tidal migration, as planets will tend to realign with the star (see also Hut (1981) and Barker & Ogilvie (2009)).

Winn et al. (2010a) point out a correlation between the stellar effective temperature and the spin/orbit angle. For stars with $T_{\rm eff} > 6250\,$K, fewer aligned systems are found compared to stars with lower effective temperatures. They also propose a theory according to which planets orbiting cooler stars need only realign the outer convective layer whereas planets around hotter stars have to realign an entire star, a process taking longer. Schlaufman (2010) presents an independent confirmation of that correlation, using a different methodology.

The aim of this letter is to combine the observational facts and offer an explanation. The results will then be discuss in light of the currently available theoretical framework.

2. Motivation

The lack of aligned systems for stars with $T_{\rm eff} > 6250\,$K that is noticed in Winn et al. (2010a) could be explained by stellar physics combined with an observational bias: as predicted by stellar evolution, stars with masses greater than about $1.2\,M_{\odot}$ start on the Zero Age Main Sequence with temperatures higher than 6250 K. When H-core burning stops, they have cooled by several hundred Kelvin (fig. 1). They do so in 3 to 4 Gyrs. This means that, while the planet and the star progressively realign, the star itself cools down. We are thus left with an aligned planet around an older, cooler star. Some, more massive, stars will cool to temperatures above 6250 K, but the timescale for realignment might be longer than the Main Sequence lifetime. Once they leave the Main Sequence, stars becomes too large for planets to be discovered by ground-based transit surveys as the contrast becomes too small. We thus have a bias to see misaligned planets around hot stars, notably because we may not detect their aligned population.

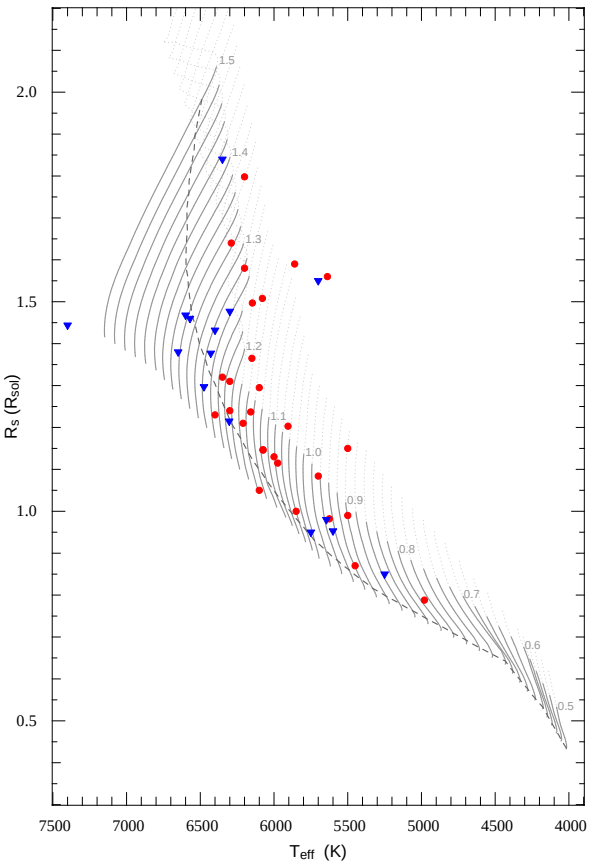


Fig. 1. Main Sequence showing the Geneva stellar evolution tracks for solar metallicity as presented in Mowlavi et al. (submitted) and plotted using $R_\star$ (in $R_\odot$) as a function of $T_{\rm eff}$. Tracks are labelled in units of $M_\odot$. Dashed line show the 2 Gyr isochrone. Overplotted are the systems for which we have Rossiter-McLaughlin measurements. Aligned systems are red circles, misaligned systems are blue triangles. Higher metallicities will move the tracks to the right. Data obtained from Exoplanet.eu

This explanation could be combined to the different realignment timescales described in Winn et al. (2010a) since, as the star ages and cools, its convective zone would become larger too. But while it is not certain that convective and radiative layer can become decoupled, the cooling down of a star is based on the established physics of stellar evolution. If that explanation is right, we should expect a correlation between stellar age and alignment.

The average stellar density, $\rho_\star$, is obtained directly from the planetary transit signal (Sozzetti et al. 2007), the effective temperature, $T_{\rm eff}$, and metallicity, Z, can be obtained via spectral analysis. Stellar mass and stellar age can be estimated from interpolating the stellar evolution tracks in $(\rho_\star, T_{\rm eff}, Z)$ space. Interestingly, stars $> 1.2\,M_\odot$ spend less time on the Main Sequence, but increase their radii more than solar mass stars do. We thus have a higher resolution on the tracks to estimate ages on more massive stars than on solar mass stars. Such a subsample should give the most precise and accurate ages that we can get. This is the sample used in this letter.

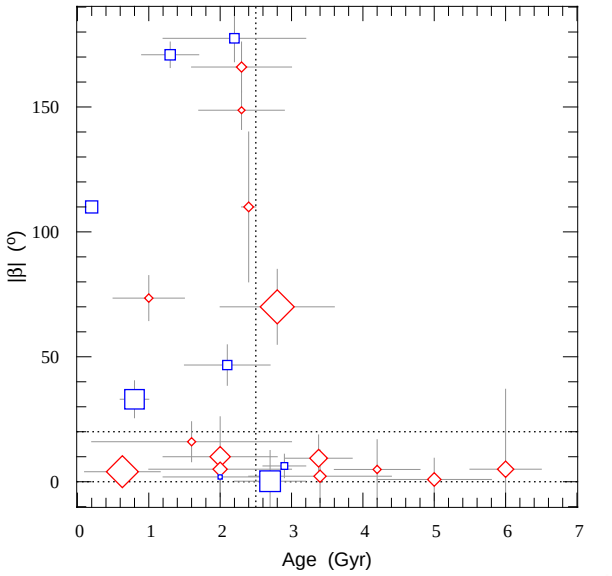


Fig. 2. Secure, absolute values of β against stellar age (in Gyr), for stars with $M_\star \geq 1.2\,M_\odot$. Size of the symbols scales with planet mass. In blue squares, stars with $M_\star \geq 1.3\,M_\odot$; in red diamonds $1.3 > M_\star \geq 1.2\,M_\odot$. Horizontal dotted line show where aligned systems are. Vertical dotted line shows the age at which where misaligned planets start to disappear.

3. Sample selection

Let us take only the most secure measurements for the projected spin/orbit angle[1], for planets with stars $\geq 1.2\,M_\odot$. There are 22 objects in the sample (table 1). The sample is divided in two: stars $\geq 1.3\,M_\odot$ (8 stars) and stars between 1.2 and $1.3\,M_\odot$ (14 stars). The angle and age estimates were obtained from the literature, but for WASP-17, whose error bar on the age was large. It was re-estimated for this letter, using the stellar parameters and density presented in Triaud et al. (2010) and interpolating in the Geneva tracks (Mowlavi et al. submitted). The new age estimate is 2.3 ± 0.6 Gyr. Its error bar is consistent with age measurements made by other teams. The new value is presented along with all other values in table 1.

Plotting the absolute values of the measured projected spin/orbit angle β against stellar age (fig. 2), a pattern is obvious and as sharp as that presented in Winn et al. (2010a). While observationally, there should be no bias to preferentially detect aligned systems instead of misaligned systems at any age, stars older than ~ 2.5 Gyr show mostly aligned systems (rms = 22°, median = 5°). For stars that are younger we have a large range of obliquities (rms = 66°, median = 60°). Figure 3 displays the cumulative distributions on either side of the 2.5 Gyr age limit.

To test the robustness of the pattern, a Monte Carlo simulation was performed taking the data with ages < 2.5 Gyr as a fiducial zone into which random samples of 8 measurements were drawn, allowing for repetitions. There is < 4% chance to draw a sample with median < 10° and rms < 60° which would allow a sample having seven aligned systems and one retrograde system. If restricting the rms within 30°, similar to

[1] Some measurements have been omitted for the following reasons: CoRoT-3 (sampling is poor (Triaud et al. 2009)), CoRoT-11 and Kepler-8 (transits are incomplete (Gandolfi et al. 2010; Jenkins et al. 2010)) and WASP-1 (angle is unsure (Albrecht et al. 2011)).

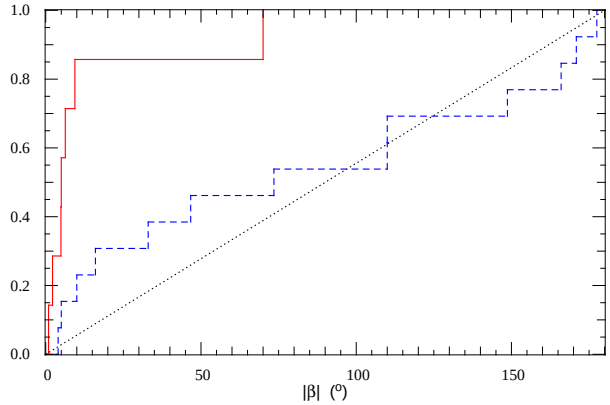


Fig. 3. Cumulative distributions in orbital inclinations for systems younger than 2.5 Gyr (dashed blue), and older (plain red). For comparison, a uniform distribution (dotted black).

that observed, there is a probability $< 1\%$ that the distributions on either side of the 2.5 Gyr age are the same. In addition a Kolmogorov-Smirnov test was carried out, also comparing the distribution in β on either side of the 2.5 Gyr limit. A $D = 0.661$ is obtained corresponding to a probability of 1.2% that both distributions are the same[2]. The same test shows that the distribution of angles around stars younger than 2.5 Gyr has about 22% chance to be compatible with a uniform distribution, while for the older sample, this chance is of order 10^{-5}. Finally, drawing randomly in the overall sample, there is a 2.6% chance to obtain a cluster containing 7 aligned systems and another at any angle $> 20°$. It can be affirmed there is tentative evidence of a pattern in the data.
We see that stars with masses $\geq 1.3\,M_{\odot}$ are all younger than 3 Gyr. Thus, when observing few aligned systems on stars with $T_{\rm eff} > 6250\,K$, Winn et al. (2010a) were in fact detecting an effect due to stellar age, or rather, time since planet formation.

Like for all multivariate problems, figure 2 offers an incomplete picture: it only shows two quantities in relation with time. At the moment orbital separations and mass ratios are quite similar since the bulk of the discoveries have been done by ground-based transit search programs. With increasing numbers of measurements over a larger parameter space we will eventually need to account for those extra parameters.

4. Discussion

The large variety of angles around the younger stars suggests that some misaligning mechanism happens during the youth of planetary systems. Notably, in combination with results by Watson et al. (2011) showing no evidence for misaligned protoplanetary discs, it lends strong support to a planet-planet scattering scenario occurring during the last stages of planet formation or soon in the aftermath of the disc dispersal like described in Matsumura et al. (2010b).

When preparing figure 2, reason dictated that a dearth of old, misaligned systems was expected, not an absence. The complete lack of misaligned planets orbiting stars older than 2.5 Gyr in the current sample came somewhat as a surprise as secular interactions could place planets on inclined orbits well after the disc dissipated. A system presenting such characteristics can be found among the "older" systems: HAT-P-13, whose current configuration may have originated from secular interactions (Mardling 2010). If that history is right, its observed coplanarity may be a chance alignment. Chance alignments can occur easily since firstly, we observe a projected angle, β, and not the real obliquity ψ and secondly, theoretical predictions such as Wu et al. (2007), Fabrycky & Tremaine (2007) and Nagasawa et al. (2008) predict very high orbital inclinations, but also a number of aligned systems.

There is great interest in matching those theoretical distributions to observations (notably for young hot Jupiters), but the evolving nature of the spin/orbit angle distribution makes this a tricky task. Multi-body dynamics are less concerned about absolute masses than about mass ratio. In systems where no Jupiter has formed, we would expect planet-planet scattering between Neptune-mass planets producing an inclined hot Neptune population. If the inital stages will be similar, the later ones will not: tidal circularisation and realignment timescales will be different. Spin/orbit angles for planets of masses $< 0.1\,M_{\rm Jup}$ will be less affected by tidal realignment and as such offer a closer picture of the initial spin/orbit angle distribution than would hot Jupiters. Such a hot Neptune, Hat-P-11 b has been recently detected misaligned by Winn et al. (2010c) and confirmed by Sanchis-Ojeda & Winn (2011).

This work has focused on stars with masses $\geq 1.2\,M_{\odot}$. If age is what determines primarily whether a hot Jupiter is observed aligned or misaligned, since solar mass stars are detected in average older than more massive stars, it is not surprising that their planets are coplanar. There nevertheless is an interest in looking at that population carefully which stems from work by Burkert & Ida (2007), Currie (2009) and Alibert et al. (2011) who argue that discs around the more massive stars are not long lived enough to produce an aligned hot Jupiter population via disc migration. In the mean time, if planet formation is more efficient in more massive discs (found around more massive stars), then one could expect a higher occurrence of planet-planet scattering around such stars. If this is true, it could point towards two pathways for bringing hot Jupiters to their observed location which would be dependent on stellar mass. Unfortunately stellar ages are less precisely determined for solar mass stars as illustrated by the isochrone on figure 1.

The change in the shape of the distribution of spin/orbit angles with time is indicative of some orbital evolution, presumably through tidal interactions between the star and the planet. Barker & Ogilvie (2009) show that retrograde planets decay into their star on timescales two to three times shorter than prograde planets would do, for given initial conditions. Incidentally, their infall timescale for a typical, retrograde, hot Jupiter are of order of a few Gyrs. Winn et al. (2010a) present similar behaviour. In addition they show that, for a given stellar mass, a more massive planet will realign and in-spiral faster than a lighter one[3]. In both papers the retrograde planets realign with the star but only very shortly before falling into it. It would thus be unlikely to observe them at these very particular phases. Nevertheless such examples could be found in WASP-12, 18 and 19 (eg. Hellier et al. (2011)). Matsumura et al. (2010a) describe how planets initially placed on mildly inclined or aligned orbits, are less likely to in-

[2] the same test on the pattern presented in Winn et al. (2010a) gives 6.1% chance that the distributions on either side of 6250 K are the same.

[3] Incidentally, this could explain a second observed feature in relation to the angle β. As shown in Moutou et al. (2011), there is a lack of retrograde massive planets ($> 5\,M_{\rm Jup}$), something expected if retrograde, massive planets realign faster to their star than other planets do.

fall and more likely to survive until observed. Nevertheless, in most cases tidal realignment corresponds to the disappearance of the planet.

If retrograde planets plunge into their star as they tidally realign, a decreasing number of hot Jupiters should be observed with time. No such decreasing trend can be found when considering all the hot Jupiters presented in the literature around stars in the mass range considered for this paper. This is at odds with evidence of a trend between semimajor axis and stellar age showing a lack of very short orbits around older stars as presented by Jackson et al. (2009) who interpreted it as evidence of the destructive tidal orbital decay of hot Jupiters. Looking at the semimajor axes of the targets in table 1, a similar trend appears. This may indicate we do not have enough objects yet to detect the expected decreasing fraction of hot Jupiters with time.

Finding out about the ultimate fate of hot Jupiters is of great interest and a subject of intense on-going research, fraught with challenges. For example, the tidal circularisation and realignment timescales notably depend on the orbital obliquity ψ, the ratio of masses, the scaled radius $(a/R_\star)$ and the tidal quality factors, in the planet Q'_p and in the star, $Q'_\star$ (Hut 1981; Barker & Ogilvie 2009). Most of the theoretical work currently assumes constant Q' values when Ogilvie & Lin (2004) showed they depend on the tidal frequency. Similarly $R_\star$ is often assumed constant when clearly, in figure 1 a 1.3 $M_\odot$ star increases its radius by about 30% in about 4 Gyrs.

Stellar age estimates are notoriously difficult to obtain. The estimates that have been used here have been extracted by a variety of authors using different techniques on different sets of evolution models. The pattern resisted a blurring caused by systematic effects, displaying a certain robustness. Nevertheless, this letter should also be an incentive to continue obtaining Rossiter-McLaughlin measurements as well as check those stellar ages and derive them in a uniform manner. Similarly, accurate and precise age estimates for solar mass stars are dearly needed. One can access those via good determination of stellar parameters, using higher resolution spectroscopy for the T_eff and Z, and high precision photometry which will give $\rho_\star$. Stellar ages can also be estimated from asteroseismologic timeseries underlying the interest in having a planet-finding space mission with such capacity, like the proposed PLATO. Astrometric distance measurements from the GAIA satellite will soon give us an independent access to stellar radii.

Acknowledgements. Many thanks are given to those that gave feedback on this work and those with whom the many discussions helped me in producing this work, especially Rosemary Mardling, Soko Matsumura and Johannes Sahlmann, but also Christoph Mordasini, Michaël Gillon, Pedro Figueira and Damien Ségransan. Thanks to Nami Mowlavi and the Geneva stellar evolution group for preparing stellar tracks to my specifications. Eternal recognition also go to Didier Queloz, my PhD supervisor for teaching me how to research while giving me freedom and independence. I would also like to acknowledge the use of Jean Schneider's EXOPLANET.EU and René Heller's encyclopaedia for the Rossiter-McLaughlin effect. This work is supported by the Swiss Fond National de Recherche Scientifique.

References

Albrecht, S., Winn, J. N., Johnson, J. A., et al. 2011, eprint arXiv, 1106, 2548, accepted for publication in ApJ
Alibert, Y., Mordasini, C., & Benz, W. 2011, A&A, 526, 63
Anderson, D. R., Hellier, C., Gillon, M., et al. 2010, ApJ, 709, 159
Bakos, G. Á., Howard, A. W., Noyes, R. W., et al. 2009, ApJ, 707, 446
Barker, A. J. & Ogilvie, G. I. 2009, MNRAS, 395, 2268
Barros, S. C. C., Faedi, F., Cameron, A. C., et al. 2011, A&A, 525, 54
Buchhave, L. A., Bakos, G. Á., Hartman, J. D., et al. 2010, ApJ, 720, 1118
Burkert, A. & Ida, S. 2007, ApJ, 660, 845
Cameron, A. C., Guenther, E., Smalley, B., et al. 2010, MNRAS, 407, 507
Chan, T., Ingemyr, M., Winn, J. N., et al. 2011, AJ, 141, 179
Chatterjee, S., Ford, E. B., Matsumura, S., & Rasio, F. A. 2008, ApJ, 686, 580
Currie, T. 2009, ApJ, 694, L171
Fabrycky, D. & Tremaine, S. 2007, ApJ, 669, 1298
Fabrycky, D. C. & Winn, J. N. 2009, ApJ, 696, 1230
Gandolfi, D., Hébrard, G., Alonso, R., et al. 2010, A&A, 524, 55
Gaudi, B. S. & Winn, J. N. 2007, ApJ, 655, 550
Hébrard, G., Bouchy, F., Pont, F., et al. 2008, A&A, 488, 763
Hébrard, G., Ehrenreich, D., Bouchy, F., et al. 2011, A&A, 527, L11
Hellier, C., Anderson, D. R., Cameron, A. C., et al. 2009, Nature, 460, 1098
Hellier, C., Anderson, D. R., Collier-Cameron, A., et al. 2011, ApJ, 730, L31
Holt, J. 1893, Astronomy & Astrophysics, XII, 646
Hut, P. 1981, A&A, 99, 126
Ida, S. & Lin, D. N. C. 2004, ApJ, 604, 388
Jackson, B., Barnes, R., & Greenberg, R. 2009, ApJ, 698, 1357
Jenkins, J. M., Borucki, W. J., Koch, D. G., et al. 2010, ApJ, 724, 1108
Johns-Krull, C. M., McCullough, P. R., Burke, C. J., et al. 2008, ApJ, 677, 657
Johnson, J. A., Winn, J. N., Albrecht, S., et al. 2009, PASP, 121, 1104
Johnson, J. A., Winn, J. N., Bakos, G. Á., et al. 2011, ApJ, 735, 24
Joshi, Y. C., Pollacco, D., Cameron, A. C., et al. 2009, MNRAS, 392, 1532
Jurić, M. & Tremaine, S. 2008, ApJ, 686, 603
Kovács, G., Bakos, G. Á., Torres, G., et al. 2007, ApJ, 670, L41
Latham, D. W., Bakos, G. Á., Torres, G., et al. 2009, ApJ, 704, 1107
Lin, D. N. C., Bodenheimer, P., & Richardson, D. C. 1996, Nature, 380, 606
Loeillet, B., Shporer, A., Bouchy, F., et al. 2008, A&A, 481, 529
Mardling, R. A. 2010, MNRAS, 407, 1048
Matsumura, S., Peale, S. J., & Rasio, F. A. 2010a, ApJ, 725, 1995
Matsumura, S., Thommes, E. W., Chatterjee, S., & Rasio, F. A. 2010b, ApJ, 714, 194
McCullough, P. R., Burke, C. J., Valenti, J. A., et al. 2008, eprint arXiv, 0805, 2921, 27 pages, 7 figures, submitted to ApJ
McLaughlin, D. B. 1924, ApJ, 60, 22
Miller, G. R. M., Cameron, A. C., Simpson, E. K., et al. 2010, A&A, 523, 52
Mordasini, C., Alibert, Y., Benz, W., & Naef, D. 2009, A&A, 501, 1161
Moutou, C., Diaz, R. F., Udry, S., et al. 2011, eprint arXiv, 1105, 3849, accepted in A&A
Moutou, C., Hébrard, G., Bouchy, F., et al. 2009, A&A, 498, L5
Nagasawa, M., Ida, S., & Bessho, T. 2008, ApJ, 678, 498
Naoz, S., Farr, W. M., Lithwick, Y., Rasio, F. A., & Teyssandier, J. 2011, Nature, 473, 187
Narita, N., Hirano, T., Sanchis-Ojeda, R., et al. 2010a, PASJ, 62, L61
Narita, N., Hirano, T., Sato, B., et al. 2009a, PASJ, 61, 991
Narita, N., Sato, B., Hirano, T., & Tamura, M. 2009b, PASJ, 61, L35
Narita, N., Sato, B., Hirano, T., et al. 2010b, PASJ, 62, 653
Noyes, R. W., Bakos, G. Á., Torres, G., et al. 2008, ApJ, 673, L79
Nutzman, P., Gilliland, R. L., McCullough, P. R., et al. 2011, ApJ, 726, 3
Ogilvie, G. I. & Lin, D. N. C. 2004, ApJ, 610, 477
Pál, A., Bakos, G. Á., Torres, G., et al. 2010, MNRAS, 401, 2665
Pál, A., Bakos, G. Á., Torres, G., et al. 2008, ApJ, 680, 1450
Pollacco, D., Skillen, I., Cameron, A. C., et al. 2008, MNRAS, 385, 1576
Queloz, D., Anderson, D., Cameron, A. C., et al. 2010, A&A, 517, L1
Queloz, D., Eggenberger, A., Mayor, M., et al. 2000, A&A, 359, L13
Rasio, F. A. & Ford, E. B. 1996, Science, 274, 954
Rossiter, R. A. 1924, ApJ, 60, 15
Sanchis-Ojeda, R. & Winn, J. N. 2011, eprint arXiv, 1107, 2920, submitted to ApJ [9 pages]
Sato, B., Fischer, D. A., Henry, G. W., et al. 2005, ApJ, 633, 465
Schlaufman, K. C. 2010, ApJ, 719, 602
Shporer, A., Bakos, G. Á., Bouchy, F., et al. 2009, ApJ, 690, 1393
Simpson, E. K., Pollacco, D., Cameron, A. C., et al. 2011, MNRAS, 600
Southworth, J., Dominik, M., Jørgensen, U. G., et al. 2011, A&A, 527, 8
Sozzetti, A., Torres, G., Charbonneau, D., et al. 2007, ApJ, 664, 1190
Torres, G., Bakos, G. Á., Hartman, J., et al. 2010, ApJ, 715, 458
Triaud, A. H. M. J., Cameron, A. C., Queloz, D., et al. 2010, A&A, 524, 25
Triaud, A. H. M. J., Queloz, D., Bouchy, F., et al. 2009, A&A, 506, 377
Ward, W. R. 1997, Icarus, 126, 261
Watson, C. A., Littlefair, S. P., Diamond, C., et al. 2011, MNRAS, 413, L71
Winn, J. N., Fabrycky, D., Albrecht, S., & Johnson, J. A. 2010a, ApJ, 718, L145
Winn, J. N., Howard, A. W., Johnson, J. A., et al. 2011, AJ, 141, 63
Winn, J. N., Johnson, J. A., Albrecht, S., et al. 2009a, ApJ, 703, L99
Winn, J. N., Johnson, J. A., Fabrycky, D., et al. 2009b, ApJ, 700, 302
Winn, J. N., Johnson, J. A., Howard, A. W., et al. 2010b, ApJ, 718, 575
Winn, J. N., Johnson, J. A., Howard, A. W., et al. 2010c, ApJ, 723, L223
Wolf, A. S., Laughlin, G., Henry, G. W., et al. 2007, ApJ, 667, 549

Table 1. Stellar and planetary parameters used to create figure 2. Values obtained using Exoplanet.eu. The values of β here are the absolute values. Error bars for the age are consistently the lower error bars presented in papers.

Name	$M_\star$ ($M_\odot$)	$R_\star$ ($R_\odot$)	β (°)	Age (Gyr)	M_p (M_{Jup})	references
HAT-P-2	1.36	1.64	0.2 ± 12.3	2.7 ± 0.5	8.7	(Pál et al. 2010; Loeillet et al. 2008)
HAT-P-4	1.26	1.59	4.9 ± 11.9	4.2 ± 0.6	0.7	(Kovács et al. 2007; Winn et al. 2011)
HAT-P-6	1.29	1.46	166 ± 10	2.3 ± 0.7	1.1	(Noyes et al. 2008; Hébrard et al. 2011)
HAT-P-7	1.47	1.84	178 ± 9	2.2 ± 1.0	1.8	(Pál et al. 2008; Winn et al. 2009a)
HAT-P-8	1.28	1.58	2.2 ± 10.5	3.4 ± 1.0	1.5	(Latham et al. 2009; Moutou et al. 2011)
HAT-P-9	1.28	1.32	16 ± 8	1.6 ± 1.4	0.7	(Shporer et al. 2009; Moutou et al. 2011)
HAT-P-13	1.22	1.56	0.9 ± 8.5	5.0 ± 0.8	1.9	(Bakos et al. 2009; Winn et al. 2010b)
HAT-P-14	1.38	1.47	171 ± 5	1.3 ± 0.4	2.2	(Torres et al. 2010; Winn et al. 2011)
HAT-P-16	1.22	1.24	10 ± 16	2.0 ± 0.8	4.2	(Buchhave et al. 2010; Moutou et al. 2011)
HAT-P-30	1.24	1.22	74 ± 9	1.0 ± 0.5	0.7	(Johnson et al. 2011)
HD 17156	1.28	1.51	9.4 ± 9.3	3.4 ± 0.5	3.2	(Narita et al. 2009a; Nutzman et al. 2011)
HD 149026	1.30	1.50	1.9 ± 6.1	2.0 ± 0.8	0.4	(Sato et al. 2005; Wolf et al. 2007)
TrES 4	1.39	1.80	6.3 ± 4.7	2.9 ± 0.3	0.9	(Narita et al. 2010b; Chan et al. 2011)
WASP-3	1.23	1.31	5 ± 5	2.0 ± 1.0	2.1	(Pollacco et al. 2008; Miller et al. 2010)
WASP-7	1.28	1.43	110 ± 30	2.4 ± 0.1	1.0	(Southworth et al. 2011, Triaud et al. in prep)
WASP-14	1.32	1.30	33 ± 7	0.8 ± 0.2	7.7	(Joshi et al. 2009; Johnson et al. 2009)
WASP-17	1.20	1.38	149 ± 8	2.3 ± 0.6	0.5	(Triaud et al. 2010); this paper
WASP-18	1.24	1.23	4 ± 5	0.6 ± 0.5	10.4	(Hellier et al. 2009; Triaud et al. 2010)
WASP-33	1.50	1.44	110 ± 0.3	0.2 ± 0.2	< 4	(Cameron et al. 2010)
WASP-38	1.22	1.37	5 ± 32	6.0 ± 0.5	2.7	(Barros et al. 2011; Simpson et al. 2011)
XO-3	1.21	1.38	70 ± 15	2.8 ± 0.8	11.8	(Johns-Krull et al. 2008; Winn et al. 2009b)
XO-4	1.32	1.55	47 ± 8	2.1 ± 0.6	1.7	(McCullough et al. 2008; Narita et al. 2010a)

Wu, Y. & Lithwick, Y. 2010, eprint arXiv, 1012, 3475, submitted to ApJ
Wu, Y., Murray, N. W., & Ramsahai, J. M. 2007, ApJ, 670, 820

The fact that β evolves in time makes of any attempt to match the cumulative distribution of β compared to theoretical predictions (as in figures 4.1 and 4.3) a tricky business as they would need to be debiased for the effect of stellar evolution, tidal realignment and observational biases. We should therefore not be surprised that our current observations do not match those that have been predicted. Nevertheless this explanation implies that all hot Jupiters could have been misaligned in the past, favouring a dynamical origin as being the dominant effect at work to explain the existence of those planets. Some planets are still realigning: those found around the older stars, such as WASP-8, or HD 80606, which may also have suffered secular dynamical interactions while the majority of hot Jupiters might come from stronger gravitational interactions, which happened in the early history of their planetary system. A few planets, I expect could have disc migrated right down to a hot Jupiter's orbit. Those could be differentiated from the *dynamical* hot Jupiters from the architecture of their multi-planetary system as outlined briefly in section 5.2.1.

Obviously, we should also try discover other systems similar to WASP-33 b. In general the discovery of any planet around stars more massive than $1.2\,M_{\odot}$ would be interesting as their age are more accurately determined thanks to the large increase of their radius and the short time they spend on the main sequence. From the study of planets around those more massive stars, it would also nice if we could one day compare the frequency of systems around stars as a function of age to get to an observational estimate of the tidal in-fall timescale leading to the destruction of those planets. Currently the only evidence for the destruction of planets has been brought by Jackson et al. (2009) in the form of a lack of short period planets on older stars.

Further interesting targets are those for which tidal evolution is slow and β is close to frozen. Smaller planets, such as Saturn-mass, or Neptune mass are better as they don't carry as much angular momentum as the more massive planets. Longer orbits are also of great interest, especially those with periastron passage far enough from the star. β measurements from those systems may provide a more valuable sample to compare to theoretical predictions than the current one.

Discovering multiplanetary systems quite densely packed (indicating low mutual inclinations) where at least one planet is retrograde with the stellar equator would cast serious doubt on all that I have just written.

5.3 Planets' history

Thanks to the gathered observational evidence and the theoretical work notably presented in Matsumura et al. (2010a), disc migration does not appear to explain the inclined hot Jupiter population. In fact, disc migration does not need to explain it at all. Disc migration can set the initial conditions for dynamical interactions which will rearrange the orbital distribution as outlined in Matsumura et al. (2010b). In some extreme (and rare) cases hot Jupiters are produced, of which a fraction will survive to be observed. The emerging picture is as such:

Stars formed with discs around them. Inside those discs, dust starts to coalesce forming larger and larger bodies (eg. Johansen et al. (2007)). Beyond the iceline, those grow faster and more easily. They become protocores and move about due to interactions with the gas around them (eg. D'Angelo et al. (2010)). Some start accreting gas. The process takes a few millions years (eg. Pollack et al. (1996) and Alibert et al. (2005)). Planets appear within the disc at different orbital distances. Interactions with the disc change as it dissipates and as planets grow, some lock into resonances (eg. Kley et al. (2005)). Most do not migrate much; all move, some inwards, some

outwards[5] (eg. Crida (2011)).

The disc gets thinner and planets feel less and less its presence (eg. Armitage (2007)). The dissipation also changes the repartition of mass, some resonances get broken. Less gas means that planetesimals start scattering more effectively, creating other torques leading to further migration (eg. Levison et al. (2008)). All in all, gas giants are spread out. Around solar mass stars they usually stop their inward migration around 1 AU if we follow the argument developed at the end of section 5.2.1; in some instances a few migrate further in and are found in multiplanetary systems. Some protocores which did not accrete fast enough stayed as Neptune mass planets (eg. Mordasini et al. (2009a)). The lack of too much inward migration leaves material and time to create planets like our terrestrial planets from the remaining planetesimal disc (eg. Chambers (2010) and Walsh et al. (2011)).

Following this (it could also start late in the disc phase), there is an orbital reorganisation (eg. Matsumura et al. (2010b)):

Most systems have mild interactions where eccentricities are being slightly increased (eg. Chiang et al. (2001) and Mardling (2010)) and the planets stay approximately where they were when the gas disc and planetesimal disc dissipated. In a small fraction of systems, more violent interactions happen leading to a complete reorganisation (eg. Rasio & Ford (1996), Nagasawa et al. (2008) and others already mentioned). Those are positioned on a variety of orbits, inclined and eccentric. The misaligning events are expected to happen quite early in the history of the system, in light of the evidence presented in section 5.2.5.

Other more secular effects can take their time to create the conditions leading to instability (eg. Wu & Lithwick (2010)). Outside perturbers could in a number of systems be the originator of a perturbation growing into an instability well after the perturbation occurred (eg. Malmberg et al. (2011)). In wide binaries, Kozai cycles are long, and the disc can retain its integrity. Once gone, planets can start feeling the presence of the perturber. In this case the most massive planets have more chance to eject all others from the system very much like in strong planet-planet scattering (eg. Malmberg et al. (2007a)). Depending on the eccentricity and inclination of the last remaining planet, Kozai oscillations will continue. Some configurations can bring that planet close enough that it is tidally captured (eg. Wu et al. (2007) and Fabrycky & Tremaine (2007)). They are left alone in their system on a highly eccentric, and inclined orbit.

In both instances, tidal forces acting on those planets whose periastron passage are close enough, start reducing the eccentricity and orbital inclination (eg. Barker & Ogilvie (2009) and Matsumura et al. (2010a)). They become hot Jupiters. Those of higher mass or (and) on retrograde orbits decay rapidly to the star. Some of those on prograde or aligned orbit follow too, with a delay, some around stars where tidal dissipation exceeds that of the planet can move towards equilibrium (made precarious due to magnetic breaking).

Some issues remain since planet-planet scattering predicts a population of planets scattered to the outer reaches of their system, thus far still undetected. In addition the understanding of the final orbital evolution of hot Jupiters is incomplete: notably can planets realign before they decay into the star? If not, where is the aligned population around cold (or old stars) coming from? The exact role of disc migration and its (apparently modest) contribution to the hot Jupiter population is also something worth further investigation. We have also seen that stellar mass is probably an important factor affecting the distribution of planets and migration rates. The proportion of hot Jupiters as a function of stellar mass compared with the orbital angle distribution would help our

[5] Some discs could be disrupted early on due to a stellar fly-by while still in the birth cluster, due to a nearby hot star irradiating the disc, or to a supernova, all of which could participate in the diversity of planet masses and orbital distributions

understanding of whether the pathway described above is dominant for all stars, or only for some stars.

Help may come from the study of smaller mass planets, such as the population of Neptunes and SuperEarths uncovered by the HARPS survey (Mayor et al. 2009b) and the *Kepler* spacecraft (Borucki et al. 2011). Their frequent presence in multiplanetary systems and close to mean motion resonances is a good indication of planetary migration (Lissauer et al. 2011b)).

Dynamical interactions do not care so much about absolute masses but about mass ratios between interacting bodies. For stars where Neptune mass planets primarily got formed, we should expect that the same processes that created hot Jupiters would produce hot Neptunes. Those should have orbits with similar characteristics: eccentric initially and tidally circularising (to about two Roche radii) and inclined as well as observing a void of other planets in their immediate vicinity.

Smaller mass planets do not have the capacity to tidally realign, meaning their orbital angle is closer to the initial distribution than would hot Jupiters'. By careful selection it should then be possible to compare the angle distribution of lone "hot Neptunes" and of Neptunes in multiplanetary systems and see if there are any differences.

Chapter 6

Conclusion

Three and a half years of efforts, about four months of gathering most of the information that I accumulated since the beginning of the work. A few more months till the defence. Now is time I suppose for some closure. I started writing because I needed too. The start was good and then it drew on me, this was all about stuff that felt so normal to do that it was strange to have to explain it all, and do it plainly (well I hope). New ideas kept coming from the papers that appeared on ASTRO-PH, from newer data (which really keeps coming fast[1]), but also from interactions with people, in conferences, by electronic mail, or directly at the institute. All this made it hard to continue writing about things done instead of producing new. But at the end, very much as Didier had warned me, this was a useful exercise.

It combined most of my past activities into one document for one thing, which made it way easier to show people about what I do, and much easier to find the relevant graphs and figures when asked for them, or when needed for newer projects. The thesis was written in - I am not ashamed of it - in a Monte-Carlo fashion: a bit here, another there as envy and inspiration came along. Graphs and words from one part, and another kept flashing by as I was looking for a spot where I could continue the writing. Then followed a review process revealing some gaps in information, some lack of continuity, but also connected all the information and ideas that had been gathered. Having passed over the same diagrams so many times, finally some connections happened. I don't think I would have found that quickly about why some planets are aligned while others are not, if I had not written that thesis. A useful exercise indeed.

Thus in those three and half years, I have, with the help and great expertise of many people, discovered almost 50 new worlds[2], started characterising them, created a new problem to solve, and days before closing the shop, proposed a solution for it which give clues on the history of how planetary systems form and evolve, informing us about our own origins and how those can compare with the general way with which planets form. In the meantime I caught a liking for statistics[3], the way data behaves, how to choose a hypothesis over another while avoiding one's biases. There has long been a debate as to why hot Jupiters existed and about what did not happen in our system. I hope I have now presented the necessary evidence (using my data, that of others, and bibliography notably regarding theoretical development) in the necessary amount to give an answer to this question:

[1] no less than three newer Rossiter-McLaughlin effects measured, and about ten newer planets for WASP

[2] and I am not getting the least bored of discovering more: actually it was my daily hour of rest from the thesis: jumping on the previous night's data arriving from La Silla to find more

[3] who would have known!

The creation of hot Jupiters is a fairly rare event needing the concourse of several phenomena: a gravitational instability, the insertion on an eccentric orbit and tides to bring in the planet close by, but not too fast so we get a chance to observe some of them as they get progressively engulfed within their star.

As most often, answering a question can lead to another: how often do systems get unstable enough to disrupt the overall architecture elevated by the time the protoplanetary disc dissipates? This question is linked to a more fundamental one, one that many others try to get a grasp on: how probable could other Earths have formed, but then also, how likely could they have survived long enough on orbits allowing life to develop and evolve on their surface?

I hope I can stay in the game long enough to help answering those questions.

Along the interest, it was also good fun. Discovering a new planet, finding something no one knows exist else than you gives quite a thrill. The many missions to Chile in the beautiful region of the southern Atacama have a been delight despite some terrible weather and technical conditions at times. But the sky is so gorgeous, the Milky Way and the zodiacal light so evident in the night sky, than returning there is always a pleasure!

Even higher up in the fun, was observing unlikely events. For example we know that hot Jupiters are around about one star in 200, and thus only one in 2000 will show a transit. Yet, observing continuously in photometry a WASP target that I suspected was a false positive during a night that CORALIE was offline, we caught a complete transit signal on a nearby star, which turned out to be another WASP candidate which was confirmed later the same month as a genuine planet (WASP-29)!

When one observes long enough, the integrated probability of catching those object by luck alone comes close to 1. This is also a good illustration on how ubiquitous planets are. They are everywhere!

I think I had a lot of luck (beside observing oddities). I arrived in a team where the instrumentation was ready and the closest to perfection as is now possible, with automated reliable data reduction and a target list from a group of hard working people. I only had to use all those various tools to produce the results that came out. In addition, being responsible for most of the time allocated on CORALIE for the WASP survey, it gave quite a few opportunities to try and find other objects of interest than planets. With *Euler*, I could experiment, try a hunch. The freedom to be able to do that is something quite unique when usually we have to go through committees and explain what you are looking for. And I am glad I had that opportunity.

6.1 Prospects

Time now for a few prospects, ideas that I did not have the time to develop, others which were not quite ready for this thesis but should lead to publications in the coming months.

6.1.1 The future of WASP

As outlined in the text, WASP is doing good, certainly in the South, where a combination of high amount of observing time allocated on CORALIE and the lack of competitors have allowed us to be the most effective ground based survey. A comparison between targets found by Hat and WASP (eg. graph 2.42) shows that they discover smaller planets on bigger stars on longer orbits than we do. The chance to catch those is lower than to catch the easier ones, and we find a lot of those easier ones. I can conclude from that, that WASP is indeed a very good planet finding project, but that even a slight increase in precision would allow to find way more planets, exploring a larger parameter space.

Now as confirmed by *Kepler*, there are many Neptune sized planets on short orbits. Finding those would be of great interest. A newer instrument able to find such planets would inevitably find the bigger planets too, notably detecting those that we missed which are on orbits of 10 days and above, whose periods could easily be confirmed by searching the WASP archive. The NGTS project being launched between Genève and some of our British colleagues aims to do just that: a wide angle search for planets with increased precision to reach down to Neptune radius.

6.1.2 WASP and binaries

Every research is bent on future prospect, on seeking new questions and new answers. One of those many questions is: how to find more planets and how learn more about them. One can build new facilities, or often as researchers all over our world often do by lack of financial resources, we can resort to grey matter and being clever.

Planets in multistellar systems are interesting laboratories for planetary formation. How much influence has the companion of the the disc around the primary (and vice-versa). Does it alter the formation of planets? Does its disrupt it more easily once they have formed? Additionally, binaries often are of different spectral type, which makes it interesting to fit within an HR diagram to get the age. Now also, if one of the two components has a planet, could the other have also? Would they be transiting (ie, are their orbital planes the same?)? Those questions apply to wide binaries, where one can measure both components

Another line of investigation which is opening is that of finding planets in close visual binaries and blended double lined binaries. If one takes the Santos et al. (2002) paper on HD 41004 at face value, one can deduce the presence of an additional body in the brown dwarf mass range thanks to the variation of the bissector. The transit method gives us a short list of candidates. We know the transit is there, which period it is in: something must be moving in the system. Assuming the transit signal is confirmed, observing only one peak in the CCF could be one of three solutions:

- we have one or several, either very hot, or very fast rotating bodies which CCFs are so diluted that we cannot detect them traditionnally. One method to find them is through Doppler imaging as in the case of WASP-9 (section 3.3.5).
- we have a wide binary system with similar stars, thus both velocities are close to each other and we can't separate their respective peaks. If one of them has an orbiter, it should oscil-

late. That oscillation will be diluted by the other peak but should be reflected by a similar frequency in the bissector span and FWHM.

- we have a solar type primary, and another lower mass companion such as an M dwarf. This one will not produce a detectable CCF and can be on any orbit. If close enough we will soon detect a linear or quadratic drift in the peak of the primary corresponding to that object. If this one is being transited one could infer its upper mass from the lack of detection in the spectrum, and lower mass via radial velocity. Using these as priors, it should be possible to infer the size of the transiter whose transit will be heavily diluted and get an idea of its mass (eg: a Jupiter around a small M dwarf produces a nearly 100 % transit which will be diluted to 1 % by a star 5 magnitude brighter).

Modelling this and starting hunting for those should be possible, but I lacked the time.

6.1.3 The WASP transiting M-dwarfs

This is a subject only lightly touched here and there in text (like in section 3.6.2) because of the incompleteness of the analysis. As we searched for planets and brown dwarfs such as WASP-30. Using CORALIE we confirmed and characterised the orbits of about 50 SB1 binaries which secondary mass is lower 0.5 $M_{\odot}$. The aims is to study how they compare with planets in orbital parameters, a, e, and β. On about 15 of those we observed the Rossiter-McLaughlin effect. The underlying idea is to test their formation and provide a good comparison sample to the planet propulation. According notably to Fabrycky & Tremaine (2007) and references there-in, high mass ratio close binaries are thought to form thanks to Kozai migration and thus should be misaligned. Preliminary results show that all appear aligned. If tidal theory is right, being aligned does not mean you were not misaligned before. This notably can participate in showing that being aligned does not equate to disc migration as M dwarfs cannot migrate in a disc like planet do.

All in all these M dwarfs provide a good comparison for our capacity to detect object, but also to be compared directly to the properties to planets with similar observation biases. It will also be interesting to check how those object distribute compare to planets. Do they have a dependence with the mass of the primary for example?

6.1.4 Treating the Rossiter-McLaughlin effect better

Having shown that adjusting a Rossiter-McLaughlin effect onto Gaussian extracted radial-velocities was not always the most perfect way to proceed (section 2.5.2), work was started to search for a better way. In this I had only little part to play unfortunately as this is mostly work by Andrew Collier Cameron and his collaborators notably in Cameron et al. (2010a). Yet, this is a development which I intend to follow and had actually started to briefly in the aftermath of the paper presented in section 2.5.2.

The Doppler shadow method is elegant: finding the missing velocity information on the CCF, hidden by the transiting planet. By notably using the CCF when undisturbed - out of transit - one can adjust a model to all CCFs and make appear the contribution hidden by the planet. Then one can fit that contribution. This method also allows for a precise estimate of the impact parameter b as one detect onto which isovelocity on the stellar surface the planet is orbiting in front of. This is also a way to estimate precisely the $v_{\star} \sin I$.

As progress are made, I am convinced this is the way to proceed in the future: adjust directly on the CCFs which contain much more information than the sole value of the radial velocity. This in principle could be used for the entire Doppler motion as well.

Setting aside those future prospects, this method also proved to be a fantastic diagnosis tool. Indeed by detecting the signal of the transiter, one knows exactly that it transits that particular CCF, thus that particular star, and not that of a background eclipsing binary. Twice it happened in our search for new planets that bissector was not showing correlated variations with the radial-velocities. Some Doppler imaging quickly showed another broad CCF was sweeping by what had looked like the single peak of an SB1, creating just enough disturbance to move the centre of mass of the CCF.

6.1.5 Calibrating stellar evolution models

We currently use $T_{\rm eff}$, $\rho_\star$ and $[M/H]$ as input to determine stellar mass and age. Eventually one could also easily include parallactic distances when those will become readily available thanks to the GAIA mission and other age estimates (if those are not biased by the presence of a hot Jupiter) such as Lithium content, or using gyrochronology. The flexibility of the MCMC allows to insert them as Bayesian priors which can be switched on and off to compare their effects on the results. In addition, since one knows the time it takes a star to evolve over one track compared to another one, it should be possible to use that information using a decision maker similar to the Metropolis-Hastings algorithm, to choose a new step according to the effective chance of observing our object at this particular moment of its evolution compared to that other. This would be mostly effective when the star moves from H-core burning to H-shell burning.

At the moment we have to assume the models are just. It would also be a natural thing to check their accuracy. Using the tools developed in section 2.6 and the many objects found from the transit surveys, one may be able to test stellar evolution models and help in a finer understanding of stellar physics:

Currently they are checked using eclipsing binaries which if they are too close have radii and evolution different from field singletons (which the models assume), or because of the transit geometry caused by two rotating eclipsing light emitters of similar size, their physical parameters, such as radii are hard to estimate. This could be improved: the ultimate objects to study are systems for which we can cross our various observables several times over: imagine systems for which we have parallactic information each with a transiting object smaller than the primary, in open clusters of different ages. To make it better, having astrometric or(and) direct detection of orbital motion would help.

The orbital motion informs on the total mass of the system, the parallax and luminosity would give us the stellar radius, a small transiter in a non grazing transit informs us on the primary's density precisely and accurately. That transiter can be a planet up to low mass M dwarfs on sufficiently long orbits to insure that the primary has not been much influenced by its orbiter. A small dark transiter insures that the error in density estimation due to it non spherical shape is negligible. Having an occultation also helps in resolving the system. Density could also come from asteroseismology, but the requirement of having those objects in open clusters make them faint and consequently harder to observe asteroseismologically.

Acknowledgments

I acknowledge having used a lot the exoplanet encyclopaedia http://www.exoplanet.eu maintained by Jean Schneider and the Holt-Rossiter-McLaughlin encyclopaedia which is compiled by René Heller and made available at http://www.aip.de/People/rheller/. Similarly, online data repositories and tools such Simbad, Aladin and VizieR found at CDS-Strasbourg http://cds.u-strasbg.fr/ have been of a great help. Notably for finding references and helping in writing the historical background I have used the online encyclopaedia http://www.wikipedia.org and the book *Tycho & Kepler* written by Kitty Ferguson (ISBN 0-8027-7688-4). I also picked up many things from my classes at St Andrews and Genève, but also from public conferences and general reading.

FINISHED WRITING AND SUBMITTED: 2011 JUNE 29
ACCEPTED: 2011 AUGUST 23
FINAL CORRECTIONS: 2011 SEPTEMBER 10

Appendix A

Publications related to this thesis

Here are presented the majority of papers that I authored and co-authored during the time I spent in Genève as a PhD student. Being at the crossroad of the data in an active international collaboration explains the numbers.

Refereed articles

WASP-23b: a transiting hot Jupiter around a K dwarf and its Rossiter-McLaughlin effect
Triaud, A. H. M. J., Queloz, D., Hellier, C., Gillon, M., Smalley, B., Hebb, L., Collier Cameron, A., Anderson, D., Boisse, I., Hébrard, G., Jehin, E., Lister, T., Lovis, C., Maxted, P. F. L., Pepe, F., Pollacco, D., Ségransan, D., Simpson, E., Udry, S., West, R.
2011 A&A **531**, 24

WASP-39b: a highly inflated Saturn-mass planet orbiting a late G-type star
Faedi, F., Barros, S. C. C., Anderson, D. R., Brown, D. J. A., Collier Cameron, A., Pollacco, D., Boisse, I., Hébrard, G., Lendl, M., Lister, T. A., Smalley, B., Street, R. A., **Triaud, A. H. M. J.**, Bento, J., Bouchy, F., Butters, O. W., Enoch, B., Haswell, C. A., Hellier, C., Keenan, F. P., Miller, G. R. M., Moulds, V., Moutou, C., Norton, A. J., Queloz, D., Santerne, A., Simpson, E. K., Skillen, I., Smith, A. M. S., Udry, S., Watson, C. A., West, R. G., Wheatley, P. J.
2011 A&A **531**, 40

WASP-31b: a low-density planet transiting a metal-poor, late-F-type dwarf star
Anderson, D. R., Collier Cameron, A., Hellier, C., Lendl, M., Lister, T. A., Maxted, P. F. L., Queloz, D., Smalley, B., Smith, A. M. S., **Triaud, A. H. M. J.**, West, R. G., Brown, D. J. A., Gillon, M., Pepe, F., Pollacco, D., Ségransan, D., Street, R. A., Udry, S.
2011 A&A **531**, 60

WASP-40b: Independent Discovery of the 0.6 M_{Jup} Transiting Exoplanet HAT-P-27b
Anderson, D. R., Barros, S. C. C., Boisse, I., Bouchy, F., Collier Cameron, A., Faedi, F., Hebrard, G., Hellier, C., Lendl, M., Moutou, C., Pollacco, D., Santerne, A., Smalley, B., Smith, A. M. S., Todd, I., **Triaud, A. H. M. J.**, West, R. G., Wheatley, P. J., Bento, J., Enoch, B., Gillon, M., Maxted, P. F. L., McCormac, J., Queloz, D., Simpson, E. K., Skillen, I.
2011 PASP **123**, 555

WASP-41b: A Transiting Hot Jupiter Planet Orbiting a Magnetically Active G8V Star
Maxted, P. F. L., Anderson, D. R., Collier Cameron, A., Hellier, C., Queloz, D., Smalley, B., Street, R. A., **Triaud, A. H. M. J.**, West, R. G., Gillon, M., Lister, T. A., Pepe, F., Pollacco, D., Ségransan, D., Smith, A. M. S., Udry, S.
2011 PASP **123**, 547

The spin-orbit angles of the transiting exoplanets WASP-1b, WASP-24b, WASP-38b and HAT-P-8b from Rossiter-McLaughlin observations
Simpson, E. K., Pollacco, D., Cameron, A. Collier; Hébrard, G., Anderson, D. R., Barros, S. C. C., Boisse, I., Bouchy, F., Faedi, F., Gillon, M., Hebb, L., Keenan, F. P., Miller, G. R. M., Moutou, C., Queloz, D., Skillen, I., Sorensen, P., Stempels, H. C., **Triaud, A.**, Watson, C. A., Wilson, P. A.
2011 MNRAS accepted

On the Orbit of the Short-period Exoplanet WASP-19b
Hellier, Coel, Anderson, D. R., Collier-Cameron, A., Miller, G. R. M., Queloz, D., Smalley, B., Southworth, J., **Triaud, A. H. M. J.**
2011 ApJ **730**, 31

WASP-34b: a near-grazing transiting sub-Jupiter-mass exoplanet in a hierarchical triple system
Smalley, B., Anderson, D. R., Collier Cameron, A., Hellier, C., Lendl, M., Maxted, P. F. L., Queloz, D., **Triaud, A. H. M. J.**, West, R. G., Bentley, S. J., Enoch, B., Gillon, M., Lister, T. A., Pepe, F., Pollacco, D., Segransan, D., Smith, A. M. S., Southworth, J., Udry, S., Wheatley, P. J., Wood, P. L., Bento, J.
2011 A&A **526**, 130

WASP-25b: a 0.6 M_J planet in the Southern hemisphere
Enoch, B., Cameron, A. Collier; Anderson, D. R., Lister, T. A., Hellier, C., Maxted, P. F. L., Queloz, D., Smalley, B., **Triaud, A. H. M. J.**, West, R. G., Brown, D. J. A., Gillon, M., Hebb, L., Lendl, M., Parley, N., Pepe, F., Pollacco, D., Segransan, D., Simpson, E., Street, R. A., Udry, S.
2011 MNRAS **410**, 1631

Thermal emission at 4.5 and 8 micron of WASP-17b, an extremely large planet in a slightly eccentric orbit
Anderson, D. R., Smith, A. M. S., Lanotte, A. A., Barman, T. S., Campo, C. J., Collier Cameron, A., Gillon, M., Harrington, J., Hellier, C., Maxted, P. F. L., Queloz, D., **Triaud, A. H. M. J.**, Wheatley, P. J.
Accepted in MNRAS (arXiv:1101.5620)

WASP-30b: A 61 M_{Jup} Brown Dwarf Transiting a V = 12, F8 Star
Anderson, D. R., Collier Cameron, A., Hellier, C., Lendl, M., Maxted, P. F. L., Pollacco, D., Queloz, D., Smalley, B., Smith, A. M. S., Todd, I., **Triaud, A. H. M. J.**, West, R. G., Barros, S. C. C., Enoch, B., Gillon, M., Lister, T. A., Pepe, F., Ségransan, D., Street, R. A., Udry, S.
2011 ApJ **726**, 19

WASP-37b: A 1.8 M_J Exoplanet Transiting a Metal-poor Star
Simpson, E. K., Faedi, F., Barros, S. C. C., Brown, D. J. A., Collier Cameron, A., Hebb, L., Pollacco, D., Smalley, B., Todd, I., Butters, O. W., Hébrard, G., McCormac, J., Miller, G. R. M., Santerne, A., Street, R. A., Skillen, I., **Triaud, A. H. M. J.**, Anderson, D. R., Bento, J., Boisse, I., Bouchy, F., Enoch, B., Haswell, C. A., Hellier, C., Holmes, S., Horne, K., Keenan, F. P., Lister, T. A., Maxted, P. F. L., Moulds, V., Moutou, C., Norton, A. J., Parley, N., Pepe, F., Queloz, D., Segransan, D., Smith, A. M. S., Stempels, H. C., Udry, S., Watson, C. A., West, R. G., Wheatley, P. J.
2011 AJ **141**, 8

AN EDUCATED SEARCH FOR TRANSITING HABITABLE PLANETS:. TARGETTING M DWARFS WITH KNOWN TRANSITING PLANETS
Gillon, M., Bonfils, X., Demory, B.-O., Seager, S., Deming, D., **Triaud, A. H. M. J.**
2011 A&A **525**, 32

WASP-38B: A TRANSITING EXOPLANET IN AN ECCENTRIC, 6.87D PERIOD ORBIT
Barros, S. C. C., Faedi, F., Collier Cameron, A., Lister, T. A., McCormac, J., Pollacco, D., Simpson, E. K., Smalley, B., Street, R. A., Todd, I., **Triaud, A. H. M. J.**, Boisse, I., Bouchy, F., Hébrard, G., Moutou, C., Pepe, F., Queloz, D., Santerne, A., Segransan, D., Udry, S., Bento, J., Butters, O. W., Enoch, B., Haswell, C. A., Hellier, C., Keenan, F. P., Miller, G. R. M., Moulds, V., Norton, A. J., Parley, N., Skillen, I., Watson, C. A., West, R. G., Wheatley, P. J.
2011 A&A **525**, 54

WASP-32B: A TRANSITING HOT JUPITER PLANET ORBITING A LITHIUM-POOR, SOLAR-TYPE STAR
Maxted, P. F. L., Anderson, D. R., Collier Cameron, A., Gillon, M., Hellier, C., Queloz, D., Smalley, B., **Triaud, A. H. M. J.**, West, R. G., Enoch, R., Lister, T. A., Pepe, F., Pollacco, D. L., Ségransan, D., Skillen, I., Udry, S.
2010 PASP **122**, 1465

WASP-22 B: A TRANSITING "HOT JUPITER" PLANET IN A HIERARCHICAL TRIPLE SYSTEM
Maxted, P. F. L., Anderson, D. R., Gillon, M., Hellier, C., Queloz, D., Smalley, B., **Triaud, A. H. M. J.**, West, R. G., Wilson, D. M., Bentley, S. J., Cegla, H., Collier Cameron, A., Enoch, B., Hebb, L., Horne, K., Irwin, J., Lister, T. A., Mayor, M., Parley, N., Pepe, F., Pollacco, D., Segransan, D., Udry, S., Wheatley, P. J.
2010 AJ **140**, 2007

SPIN-ORBIT ANGLE MEASUREMENTS FOR SIX SOUTHERN TRANSITING PLANETS. NEW INSIGHTS INTO THE DYNAMICAL ORIGINS OF HOT JUPITERS
Triaud, A. H. M. J., Collier Cameron, A., Queloz, D., Anderson, D. R., Gillon, M., Hebb, L., Hellier, C., Loeillet, B., Maxted, P. F. L., Mayor, M., Pepe, F., Pollacco, D., Ségransan, D., Smalley, B., Udry, S., West, R. G., Wheatley, P. J.
2010 A&A **140**, 25

WASP-29B: A SATURN-SIZED TRANSITING EXOPLANET
Hellier, Coel; Anderson, D. R., Collier Cameron, A., Gillon, M., Lendl, M., Maxted, P. F. L., Queloz, D., Smalley, B., **Triaud, A. H. M. J.**, West, R. G., Brown, D. J. A., Enoch, B., Lister, T. A., Pepe, F., Pollacco, D., Ségransan, D., Udry, S.
2010 ApJ **723**, 60

THE DOPPLER SHADOW OF WASP-3B. A TOMOGRAPHIC ANALYSIS OF ROSSITER-MCLAUGHLIN OBSERVATIONS
Miller, G. R. M., Collier Cameron, A., Simpson, E. K., Pollacco, D., Enoch, B., Gibson, N. P., Queloz, D., **Triaud, A. H. M. J.**, Hébrard, G., Boisse, I., Moutou, C., Skillen, I.
2010 A&A **523**, 52

WASP-24 B: A NEW TRANSITING CLOSE-IN HOT JUPITER ORBITING A LATE F-STAR
Street, R. A., Simpson, E., Barros, S. C. C., Pollacco, D., Joshi, Y., Todd, I., Collier Cameron, A., Enoch, B., Parley, N., Stempels, E., Hebb, L., **Triaud, A. H. M. J.**, Queloz, D., Segransan, D., Pepe, F., Udry, S., Lister, T. A., Depagne, É., West, R. G., Norton, A. J., Smalley, B., Hellier, C., Anderson, D. R., Maxted, P. F. L., Bentley, S. J., Skillen, I., Gillon, M., Wheatley, P., Bento, J., Cathaway-Kjontvedt, P., Christian, D. J.
2010 ApJ **720**, 337

WASP-26B: A 1-JUPITER-MASS PLANET AROUND AN EARLY-G-TYPE STAR
Smalley, B., Anderson, D. R., Collier Cameron, A., Gillon, M., Hellier, C., Lister, T. A., Maxted, P. F. L., Queloz, D., **Triaud, A. H. M. J.**, West, R. G., Bentley, S. J., Enoch, B., Pepe, F., Pollacco, D. L., Segransan, D., Smith, A. M. S., Southworth, J., Udry, S., Wheatley, P. J., Wood, P. L., Bento, J.
2010 A&A **520**, 56

WASP-21b: a hot-Saturn exoplanet transiting a thick disc star
Bouchy, F., Hebb, L., Skillen, I., Collier Cameron, A., Smalley, B., Udry, S., Anderson, D. R., Boisse, I., Enoch, B., Haswell, C. A., Hébrard, G., Hellier, C., Joshi, Y., Kane, S. R., Maxted, P. F. L., Mayor, M., Moutou, C., Pepe, F., Pollacco, D., Queloz, D., Ségransan, D., Simpson, E. K., Smith, A. M. S., Stempels, H. C., Street, R., **Triaud, A. H. M. J.**, West, R. G., Wheatley, P. J.
2010 A&A **519**, 98

WASP-8b: a retrograde transiting planet in a multiple system
Queloz, D., Anderson, D., Collier Cameron, A., Gillon, M., Hebb, L., Hellier, C., Maxted, P., Pepe, F., Pollacco, D., Ségransan, D., Smalley, B., **Triaud, A. H. M. J.**, Udry, S., West, R.
2010 A&A **517**, 1

H-band thermal emission from the 19-h period planet WASP-19b
Anderson, D. R., Gillon, M., Maxted, P. F. L., Barman, T. S., Collier Cameron, A., Hellier, C., Queloz, D., Smalley, B., **Triaud, A. H. M. J.**
2010 A&A **513**, 3

Line-profile tomography of exoplanet transits - I. The Doppler shadow of HD 189733b
Collier Cameron, A., Bruce, V. A., Miller, G. R. M., **Triaud, A. H. M. J.**, Queloz, D.
2010 MNRAS **403**, 151

WASP-17b: An Ultra-Low Density Planet in a Probable Retrograde Orbit
Anderson, D. R., Hellier, C., Gillon, M., **Triaud, A. H. M. J.**, Smalley, B., Hebb, L., Collier Cameron, A., Maxted, P. F. L., Queloz, D., West, R. G., Bentley, S. J., Enoch, B., Horne, K., Lister, T. A., Mayor, M., Parley, N. R., Pepe, F., Pollacco, D., Ségransan, D., Udry, S., Wilson, D. M.
2010 AJ **709**, 159

WASP-19b: The Shortest Period Transiting Exoplanet Yet Discovered
Hebb, L., Collier-Cameron, A., **Triaud, A. H. M. J.**, Lister, T. A., Smalley, B., Maxted, P. F. L., Hellier, C., Anderson, D. R., Pollacco, D., Gillon, M., Queloz, D., West, R. G., Bentley, S., Enoch, B., Haswell, C. A., Horne, K., Mayor, M., Pepe, F., Segransan, D., Skillen, I., Udry, S., Wheatley, P. J
2010 AJ **708**, 224

Transiting exoplanets from the CoRoT space mission. VII. The "hot-Jupiter"-type planet CoRoT-5b
Rauer, H., Queloz, D., Csizmadia, Sz., Deleuil, M., Alonso, R., Aigrain, S., Almenara, J. M., Auvergne, M., Baglin, A., Barge, P., Bordé, P., Bouchy, F., Bruntt, H., Cabrera, J., Carone, L., Carpano, S., de La Reza, R., Deeg, H. J., Dvorak, R., Erikson, A., Fridlund, M., Gandolfi, D., Gillon, M., Guillot, T., Guenther, E., Hatzes, A., Hébrard, G., Kabath, P., Jorda, L., Lammer, H., Léger, A., Llebaria, A., Magain, P., Mazeh, T., Moutou, C., Ollivier, M., Pätzold, M., Pont, F., Rabus, M., Renner, S., Rouan, D., Shporer, A., Samuel, B., Schneider, J., **Triaud, A. H. M. J.**, Wuchterl, G.
2009 A&A **506**, 281

VLT transit and occultation photometry for the bloated planet CoRoT-1b
Gillon, M., Demory, B.-O., **Triaud, A. H. M. J.**, Barman, T., Hebb, L., Montalbán, J., Maxted, P. F. L., Queloz, D., Deleuil, M., Magain, P.
2009 A&A **506**, 359

The Rossiter-McLaughlin effect of CoRoT-3b and HD 189733b
Triaud, A. H. M. J., Queloz, D., Bouchy, F., Moutou, C., Collier Cameron, A., Claret, A., Barge, P., Benz, W., Deleuil, M., Guillot, T., Hébrard, G., Lecavelier Des Étangs, A., Lovis, C., Mayor, M., Pepe, F., Udry, S.
2009 A&A **506**, 377

WASP-16b: A New Jupiter-Like Planet Transiting a Southern Solar Analog
Lister, T. A., Anderson, D. R., Gillon, M., Hebb, L., Smalley, B. S., **Triaud, A. H. M. J.**, Collier Cameron, A., Wilson, D. M., West, R. G., Bentley, S. J., Christian, D. J., Enoch, R., Haswell, C. A., Hellier, C., Horne, K., Irwin, J., Joshi, Y. C., Kane, S. R., Mayor, M., Maxted, P. F. L., Norton, A. J., Parley, N., Pepe, F., Pollacco, D., Queloz, D., Ryans, R., Segransan, D., Skillen, I., Street, R. A., Todd, I., Udry, S., Wheatley, P. J.
2009 ApJ **703**, 752

An orbital period of 0.94days for the hot-Jupiter planet WASP-18b
Hellier, Coel; Anderson, D. R., Collier Cameron, A., Gillon, M., Hebb, L., Maxted, P. F. L., Queloz, D., Smalley, B., **Triaud, A. H. M. J.**, West, R. G., Wilson, D. M., Bentley, S. J., Enoch, B., Horne, K., Irwin, J., Lister, T. A., Mayor, M., Parley, N., Pepe, F., Pollacco, D. L., Segransan, D., Udry, S., Wheatley, P. J.
2009 Nature **460**, 1098

Discovery and characterization of WASP-6b, an inflated sub-Jupiter mass planet transiting a solar-type star
Gillon, M., Anderson, D. R., **Triaud, A. H. M. J.**, Hellier, C., Maxted, P. F. L., Pollaco, D., Queloz, D., Smalley, B., West, R. G., Wilson, D. M., Bentley, S. J., Collier Cameron, A., Enoch, B., Hebb, L., Horne, K., Irwin, J., Joshi, Y. C., Lister, T. A., Mayor, M., Pepe, F., Parley, N., Segransan, D., Udry, S., Wheatley, P. J.
2009 A&A **501**, 785

The Low Density Transiting Exoplanet WASP-15b
West, R. G., Anderson, D. R., Gillon, M., Hebb, L., Hellier, C., Maxted, P. F. L., Queloz, D., Smalley, B., **Triaud, A. H. M. J.**, Wilson, D. M., Bentley, S. J., Collier Cameron, A., Enoch, B., Horne, K., Irwin, J., Lister, T. A., Mayor, M., Parley, N., Pepe, F., Pollacco, D., Segransan, D., Spano, M., Udry, S., Wheatley, P. J.
2009 AJ **137**, 4834

Improved parameters for the transiting hot Jupiters WASP-4b and WASP-5b
Gillon, M., Smalley, B., Hebb, L., Anderson, D. R., **Triaud, A. H. M. J.**, Hellier, C., Maxted, P. F. L., Queloz, D., Wilson, D. M.
2009 A&A **496**, 259

WASP-7: A Bright Transiting-Exoplanet System in the Southern Hemisphere
Hellier, Coel; Anderson, D. R., Gillon, M., Lister, T. A., Maxted, P. F. L., Queloz, D., Smalley, B., **Triaud, A. H. M. J.**, West, R. G., Wilson, D. M., Alsubai, K., Bentley, S. J., Collier Cameron, A., Hebb, L., Horne, K., Irwin, J., Kane, S. R., Mayor, M., Pepe, F., Pollacco, D., Skillen, I., Udry, S., Wheatley, P. J., Christian, D. J., Enoch, R., Haswell, C. A., Joshi, Y. C., Norton, A. J., Parley, N., Ryans, R., Street, R. A., Todd, I.
2009 ApJ **690**, 89

Improved parameters for the transiting planet HD 17156b: a high-density giant planet with a very eccentric orbit
Gillon, M., **Triaud, A. H. M. J.**, Mayor, M., Queloz, D., Udry, S., North, P.
2008 A&A **485**, 871

Transiting exoplanets from the CoRoT space mission. III. The spectroscopic transit of CoRoT-Exo-2b with SOPHIE and HARPS
Bouchy, F., Queloz, D., Deleuil, M., Loeillet, B., Hatzes, A. P., Aigrain, S., Alonso, R., Auvergne, M., Baglin, A., Barge, P., Benz, W., Bordé, P., Deeg, H. J., de La Reza, R., Dvorak, R., Erikson, A., Fridlund, M., Gondoin, P., Guillot, T., Hébrard, G., Jorda, L., Lammer, H., Léger, A., Llebaria, A., Magain, P., Mayor, M., Moutou, C., Ollivier, M., Pätzold, M., Pepe, F., Pont, F., Rauer, H., Rouan, D., Schneider, J., **Triaud, A. H. M. J.**, Udry, S., Wuchterl, G.
2008 A&A **482**, 25

Submitted articles

WASP-44b, WASP-45b and WASP-46b: three short-period, transiting extrasolar planets
D. R. Anderson, A. Collier Cameron, M. Gillon, C. Hellier, E. Jehin, M. Lendl, P. F. L. Maxted, D. Queloz, B. Smalley, A. M. S. Smith, **A. H. M. J. Triaud**, R. G. West, F. Pepe, D. Pollacco, D. Ségransan, I. Todd, S. Udry
submitted to MNRAS (arXiv:1105.3179)

WASP-35b, WASP-48b and WASP-51b: Two new planets and an independent discovery of HAT-P-30b
Enoch, B., Anderson, D. R., Barros, S. C. C., Brown, D. J. A., Collier Cameron, A., Faedi, F., Gillon, M., Hébrard, G., Lister, T. A., Queloz, D., Santerne, A., Smalley, B., Street, R. A., **Triaud, A. H. M. J.**, West, R. G., Bouchy, F., Bento, J., Butters, O., Fossati, L., Haswell, C. A., Hellier, C., Holmes, S., Jehen, E., Lendl, M., Maxted, P. F. L., McCormac, J., Miller, G. R. M., Moulds, V., Moutou, C., Norton, A. J., Parley, N., Pepe, F., Pollacco, D., Segransan, D., Simpson, E., Skillen, I., Smith, A. M. S., Udry, S., Wheatley, P. J.
submitted to AJ (arXiv:1104.2827)

WASP-43b: The closest-orbiting hot Jupiter
Hellier, Coel, Anderson, D. R., Collier Cameron, A., Gillon, M., Jehin, E., Lendl, M., Maxted, P. F. L., Pepe, F., Pollacco, D., Queloz, D., Segransan, D., Smalley, B., Smith, A. M. S., Southworth, J., **Triaud, A. H. M. J.**, Udry, S., West, R. G.
submitted to A&A (arXiv:1104.2823)

Publications in conference proceedings

Spin-Orbit Angles: Reflections of Dynamics in Systems
Triaud, A. H. M. J., Queloz, D., Collier Cameron, A.
in OHP colloquium 2010: *Detection and Dynamics of Transiting Exoplanets*, Eds F. Bouchy, R. Díaz, C. Moutou
PJ Web of Conferences, **Volume 11**, 05003

List of Figures

1.1 Direct Detection of four planets around HR 8799 . . . 10
1.2 First extrasolar planet . . . 11
1.3 Observed photometric flux from an orbiting, transiting exoplanet . . . 12
1.4 Geometry of a transiting planet . . . 13
1.5 The transit of HD 209458 b . . . 14
1.6 The transits of WASP-4 . . . 16
1.7 Illustrating the shape of the Rossiter-McLaughlin effect . . . 17
1.8 The Rossiter-McLaughlin effect on HD 209458 . . . 18

2.1 Transit Diagram . . . 24
2.2 Multiband transits on HD 209458 . . . 25
2.3 Rossiter-McLaughlin diagram . . . 26
2.3 Parameter vs Parameter . . . 33
2.4 W vs b and contours . . . 36
2.5 $R_{\rm p}$ vs b and contours . . . 37
2.6 First toy model . . . 37
2.7 An MCMC with burn-in and stationary state . . . 38
2.8 χ^2 MCMC output . . . 40
2.9 χ^2 vs parameters . . . 40
2.10 The variance of χ^2 . . . 42
2.11 Second toy model . . . 43
2.12 χ^2 MCMC output for 2 models . . . 43
2.13 Obtained and expected $\chi^2_{\rm PDF}$ . . . 44
2.14 Difference from expected $\chi^2_{\rm PDF}$ . . . 44
2.15 Output $\chi^2_{\rm PDF}$ for WASP-8 . . . 46
2.16 Output $\chi^2_{\rm PDF}$ for WASP-23 . . . 46
2.17 Output $\chi^2_{\rm PDF}$ for WASP-23, CORALIE data . . . 47
2.18 Output $\chi^2_{\rm PDF}$ vs K for WASP-23, CORALIE data . . . 47
2.19 Output $\chi^2_{\rm PDF}$ for WASP-23, HARPS data . . . 48
2.20 Output $\chi^2_{\rm PDF}$ vs K for WASP-23, HARPS data . . . 48
2.21 Output $\chi^2_{\rm PDF}$ for WASP-23, Photometric data . . . 49
2.22 Output $\chi^2_{\rm PDF}$ vs K for WASP-23, Photometric data . . . 49
2.23 Traditional Herzsprung-Russell diagram . . . 90
2.24 Herzsprung-Russell diagram showing $R_\star$ vs $T_{\rm eff}$ . . . 91
2.25 Herzsprung-Russell diagram showing $\rho_\star$ vs $T_{\rm eff}$ . . . 92
2.26 Herzsprung-Russell diagram showing $\rho_\star^{-1/3}$ vs $T_{\rm eff}$ . . . 93
2.27 How Z changes the position of the main sequence . . . 94
2.28 $(\rho_\star/\rho_\odot)^{-1/3}$ vs $T_{\rm eff}$ joint posterior distribution in stellar tracks, WASP-8 . . . 96
2.29 $(\rho_\star/\rho_\odot)^{-1/3}$ vs $T_{\rm eff}$ joint posterior distribution in stellar tracks, WASP-8 . . . 96
2.30 Interpolated $M_\star$ posterior distribution for WASP-8 . . . 97
2.31 Interpolated stellar age posterior distribution for WASP-8 . . . 97
2.32 Interpolated $T_{\rm eff}$ posterior distribution for WASP-8 . . . 98

2.33 Interpolated metallicity posterior distribution for WASP-8 . . . 98
2.34 $\rho_\star$ posterior distribution for WASP-8 . . . 99
2.35 $(\rho_\star/\rho_\odot)^{-1/3}$ vs $T_{\rm eff}$ joint posterior distribution in stellar tracks, WASP-23 . . . 100
2.36 $(\rho_\star/\rho_\odot)^{-1/3}$ vs $T_{\rm eff}$ joint posterior distribution in stellar tracks, WASP-23 . . . 100
2.37 Interpolated $M_\star$ posterior distribution for WASP-23 . . . 101
2.38 Interpolated stellar age posterior distribution for WASP-23 . . . 101
2.39 Interpolated $T_{\rm eff}$ posterior distribution for WASP-23 . . . 102
2.40 Interpolated metallicity posterior distribution for WASP-23 . . . 102
2.41 $\rho_\star$ posterior distribution for WASP-23 . . . 103
2.42 Host stars in the HR diagram . . . 104

3.1 The WASP instrument . . . 106
3.2 The sky according to WASP . . . 107
3.8 The Euler Telescope . . . 108
3.3 Candidate List from the *hunter* webpage . . . 109
3.4 Candidate page from the *hunter* webpage . . . 110
3.5 Nearby Candidate page . . . 111
3.6 Transit Scheduler page . . . 112
3.7 Proper Motion-Colour diagram . . . 113
3.9 Possible Scenarii . . . 114
3.10 On/Off example . . . 115
3.11 This is an SB3 . . . 117
3.12 Unresolved Blended SB2 . . . 117
3.13 Resolved Blended SB2 . . . 117
3.14 Triple system . . . 118
3.15 Triple system, second phase . . . 118
3.16 Fast rotator at telescope . . . 119
3.17 Fast rotator at telescope, zoom . . . 119
3.18 Fast rotator, blaze corrected . . . 119
3.19 Repartition of objects in the sky . . . 182
3.20 Repartition of objects in the sky . . . 183
3.21 CORALIE effort to WASP . . . 185
3.22 Sky position of transiting planets . . . 186
3.23 Mass-Radius diagram, according to WASP and CORALIE . . . 187
3.24 Evolution of WASP in time . . . 189
3.25 Depth versus Period for transiting planets and M dwarfs in WASP . . . 190
3.26 The orbit of HD 156846b . . . 192
3.27 Is that a Rossiter-McLaughlin effect? . . . 193
3.28 Joint posterior probability between $V \sin I$ and β for HD 156846 b . . . 194
3.29 trucmachin . . . 197

4.1 Histogram and Cumulative distribution of current β measurements . . . 225
4.2 Plotting the projected spin/orbit β against the effective temperature of its host star . . . 226
4.3 Cumulative distribution of β for planets around hot stars . . . 227
4.4 β as a function of eccentricity and planetary mass . . . 228

5.1 A planet opening a gap in a protoplanetary disc . . . 234
5.2 Formation of a gas giant . . . 235
5.3 Population Synthesis . . . 236
5.4 Orbital decay of WASP-17 b . . . 237
5.5 Hot Jupiters park at two Roche radii from their star . . . 238
5.6 Planet-planet scattering after disc dispersal . . . 239
5.7 Kozai cycles on HD 80606 b . . . 240
5.8 Kepler Systems . . . 243
5.9 Detection limits for an additional companion to WASP-16 . . . 244
5.10 Distribution of gas giants in single or multiplanetary systems . . . 245
5.11 Expected hot Jupiters . . . 246

List of Tables

3.1 WASP resuts 184

4.1 Rossiter-McLaughlin measurements composing the figures 229
4.1 Rossiter-McLaughlin measurements, continued... 230
4.1 Rossiter-McLaughlin measurements, continued... 231

Bibliography

Agol, E., Steffen, J., Sari, R., & Clarkson, W. 2005, MNRAS, 359, 567

Albrecht, S., Reffert, S., Snellen, I. A. G., & Winn, J. N. 2009, Nature, 461, 373

Albrecht, S., Winn, J. N., Johnson, J. A., et al. 2011, eprint arXiv, 1106, 2548, accepted for publication in ApJ

Alexander, R. D. & Armitage, P. J. 2009, ApJ, 704, 989

Alibert, Y., Mordasini, C., Benz, W., & Winisdoerffer, C. 2005, A&A, 434, 343

Alonso, R., Aigrain, S., Pont, F., Mazeh, T., & Team, T. C. E. S. 2009, Transiting Planets, 253, 91

Anderson, D. R., Cameron, A. C., Hellier, C., et al. 2011, ApJ, 726, L19

Anderson, D. R., Gillon, M., Hellier, C., et al. 2008, MNRAS, 387, L4

Anderson, D. R., Hellier, C., Gillon, M., et al. 2010, ApJ, 709, 159

Armitage, P. J. 2007, ApJ, 665, 1381

Bakos, G., Noyes, R. W., Kovács, G., et al. 2004, PASP, 116, 266

Baraffe, I., Chabrier, G., Allard, F., & Hauschildt, P. H. 1998, A&A, 337, 403

Baranne, A., Queloz, D., Mayor, M., et al. 1996, A&A, 119, 373

Barbieri, M., Alonso, R., Laughlin, G., et al. 2007, A&A, 476, L13

Barker, A. J. & Ogilvie, G. I. 2009, MNRAS, 395, 2268

Batygin, K. & Stevenson, D. J. 2010, ApJ, 714, L238

Benedict, G. F., McArthur, B. E., Gatewood, G., et al. 2006, AJ, 132, 2206

Bodenheimer, P., Hubickyj, O., & Lissauer, J. J. 2000, Icarus, 143, 2

Bodenheimer, P., Laughlin, G., & Lin, D. N. C. 2003, ApJ, 592, 555

Borucki, W. J., Koch, D. G., Basri, G., et al. 2011, ApJ, 728, 117

Bouchy, F., Deleuil, M., Guillot, T., et al. 2011, A&A, 525, 68

Bouchy, F., Queloz, D., Deleuil, M., et al. 2008, A&A, 482, L25

Bouchy, F., Udry, S., Mayor, M., et al. 2005, A&A, 444, L15

Bouquin, J.-B. L., Absil, O., Benisty, M., et al. 2009, A&A, 498, L41

Brown, T. M. 2003, ApJ, 593, L125

Butler, R. P., Marcy, G. W., Williams, E., Hauser, H., & Shirts, P. 1997, ApJL, 474, L115

Cameron, A. C., Bouchy, F., Hébrard, G., et al. 2007a, MNRAS, 375, 951

Cameron, A. C., Bruce, V. A., Miller, G. R. M., Triaud, A. H. M. J., & Queloz, D. 2010a, MNRAS, 403, 151

Cameron, A. C., Guenther, E., Smalley, B., et al. 2010b, MNRAS, 407, 507

Cameron, A. C., Pollacco, D., Street, R. A., et al. 2006, MNRAS, 373, 799

Cameron, A. C., Wilson, D. M., West, R. G., et al. 2007b, MNRAS, 380, 1230

Castillo-Rogez, J., Johnson, T. V., Lee, M. H., et al. 2009, Icarus, 204, 658

Castillo-Rogez, J. C., Matson, D. L., Sotin, C., et al. 2007, Icarus, 190, 179

Cébron, D., Moutou, C., Bars, M. L., Gal, P. L., & Farès, R. 2011, Detection and Dynamics of Transiting Exoplanets, 11, 03003

Chabrier, G., Baraffe, I., Allard, F., & Hauschildt, P. 2000a, ApJ, 542, L119

Chabrier, G., Baraffe, I., Allard, F., & Hauschildt, P. 2000b, ApJ, 542, 464

Chambers, J. 2010, Exoplanets, 297

Charbonneau, D., Brown, T. M., Latham, D. W., & Mayor, M. 2000, ApJ, 529, L45

Charbonnel, C., Däppen, W., Schaerer, D., et al. 1999, A&AS, 135, 405

Chatterjee, S., Ford, E. B., Matsumura, S., & Rasio, F. A. 2008, ApJ, 686, 580

Chiang, E. I., Tabachnik, S., & Tremaine, S. 2001, AJ, 122, 1607

Claret, A. 2000, A&A, 363, 1081

Claret, A. 2004, A&A, 424, 919

Correia, A. C. M., Couetdic, J., Laskar, J., et al. 2010, A&A, 511, 21

Cox, A. N. 2000, Allen's astrophysical quantities, iSBN: 0387987460

Crida, A. 2011, Detection and Dynamics of Transiting Exoplanets, 11, 04002

Crida, A., Masset, F., & Morbidelli, A. 2009, ApJ, 705, L148

Crida, A., Morbidelli, A., & Masset, F. 2006, Icarus, 181, 587

Crida, A., Sándor, Z., & Kley, W. 2008, A&A, 483, 325

Cumming, A., Butler, R. P., Marcy, G. W., et al. 2008, PASP, 120, 531

D'Angelo, G., Durisen, R. H., & Lissauer, J. J. 2010, Exoplanets, 319

Darwin, G. H. 1879, Proceedings of the Royal Society of London, 29, 168

Dawson, R. I. & Fabrycky, D. C. 2010, ApJ, 722, 937

Deeg, H. J., Ocaña, B., Kozhevnikov, V. P., et al. 2008, A&A, 480, 563

Deleuil, M., Deeg, H. J., Alonso, R., et al. 2008, A&A, 491, 889

Demory, B. O., Gillon, M., Deming, D., et al. 2011, eprint arXiv, 1105, 415, submitted to A&A

Donati, J.-F., Moutou, C., Farès, R., et al. 2008, MNRAS, 385, 1179

Eggenberger, P., Maeder, A., & Meynet, G. 2010a, A&A, 519, L2

Eggenberger, P., Meynet, G., Maeder, A., et al. 2008, Astrophysics and Space Science, 316, 43

Eggenberger, P., Miglio, A., Montalban, J., et al. 2010b, A&A, 509, 72

Eggleton, P. P. & Kiseleva-Eggleton, L. 2001, ApJ, 562, 1012

Enoch, B., Cameron, A. C., Parley, N. R., & Hebb, L. 2010, A&A, 516, 33

Fabrycky, D. & Tremaine, S. 2007, ApJ, 669, 1298

Fabrycky, D. C. & Winn, J. N. 2009, ApJ, 696, 1230

Fischer, D. A., Vogt, S. S., Marcy, G. W., et al. 2007, ApJ, 669, 1336

Ford, E. B. 2006, ApJ, 642, 505

Ford, E. B. & Rasio, F. A. 2006, ApJ, 638, L45

Ford, E. B. & Rasio, F. A. 2008, ApJ, 686, 621

Fossey, S. J., Waldmann, I. P., & Kipping, D. M. 2009, MNRAS, 396, L16

Gandolfi, D., Hébrard, G., Alonso, R., et al. 2010, A&A, 524, 55

Garaud, P. 2011, ApJ, 728, L30

Garcia-Melendo, E. & McCullough, P. R. 2009, ApJ, 698, 558

Gaudi, B. S. 2010, Exoplanets, 79

Gaudi, B. S. & Winn, J. N. 2007, ApJ, 655, 550

Gillon, M., Anderson, D. R., Triaud, A. H. M. J., et al. 2009a, A&A, 501, 785

Gillon, M., Deming, D., Demory, B.-O., et al. 2010, A&A, 518, 25

Gillon, M., Jehin, E., Magain, P., et al. 2011, Detection and Dynamics of Transiting Exoplanets, 11, 06002

Gillon, M., Pont, F., Demory, B.-O., et al. 2007, A&A, 472, L13

Gillon, M., Smalley, B., Hebb, L., et al. 2009b, A&A, 496, 259

Giménez, A. 2006a, A&A, 450, 1231

Giménez, A. 2006b, ApJ, 650, 408

Goldreich, P. 1963, MNRAS, 126, 257

Goldreich, P. & Sari, R. 2003, ApJ, 585, 1024

Goldreich, P. & Tremaine, S. 1979, ApJ, 233, 857

Goldreich, P. & Tremaine, S. 1980, ApJ, 241, 425

Gray, D. F. 2008, The Observation and Analysis of Stellar Photospheres, 978052 10668 15

Gregory, P. C. 2005, Bayesian Logical Data Analysis for the Physical Sciences: A Comparative Approach with 'Mathematica' Support., iSBN: 0-521-84150-X

Guillochon, J., Ramirez-Ruiz, E., & Lin, D. 2011, ApJ, 732, 74

Hale, A. 1994, AJ, 107, 306

Hebb, L., Collier-Cameron, A., Loeillet, B., et al. 2009, ApJ, 693, 1920

Hébrard, G., Bouchy, F., Pont, F., et al. 2008, A&A, 488, 763

Hébrard, G., Ehrenreich, D., Bouchy, F., et al. 2011, A&A, 527, L11

Hellier, C., Anderson, D. R., Collier-Cameron, A., et al. 2011, ApJ, 730, L31

Hilditch, R. W. 2001, An Introduction to Close Binary Stars, iSBN: 0521241065

Hirano, T., Suto, Y., Taruya, A., et al. 2010, ApJ, 709, 458

Holman, M. J., Fabrycky, D. C., Ragozzine, D., et al. 2010, Science, 330, 51

Holman, M. J. & Murray, N. W. 2005, Science, 307, 1288

Holt, J. 1893, Astronomy & Astrophysics, XII, 646

Hosokawa, Y. 1953, PASJ, 5, 88

Howard, A. W., Bakos, G. Á., Hartman, J., et al. 2010, arXiv, astro-ph.EP, submitted to ApJ, 13 pages, 6 figures, 6 tables

Howard, A. W., Marcy, G. W., Bryson, S. T., et al. 2011, eprint arXiv, 1103, 2541, submitted to ApJ

Huber, K. F., Czesla, S., Wolter, U., & Schmitt, J. H. M. M. 2010, A&A, 514, 39

Huélamo, N., Figueira, P., Bonfils, X., et al. 2008, A&A, 489, L9

Hut, P. 1981, A&A, 99, 126

Ida, S., Bryden, G., Lin, D. N. C., & Tanaka, H. 2000, ApJ, 534, 428

Ida, S. & Lin, D. N. C. 2004, ApJ, 604, 388

Jackson, B., Barnes, R., & Greenberg, R. 2009, ApJ, 698, 1357

Jenkins, J. M., Borucki, W. J., Koch, D. G., et al. 2010, ApJ, 724, 1108

Johansen, A., Oishi, J. S., Low, M.-M. M., et al. 2007, Nature, 448, 1022

Johnson, J. A., Apps, K., Gazak, J. Z., et al. 2011a, ApJ, 730, 79

Johnson, J. A., Winn, J. N., Albrecht, S., et al. 2009, PASP, 121, 1104

Johnson, J. A., Winn, J. N., Bakos, G. Á., et al. 2011b, ApJ, 735, 24

Johnson, J. A., Winn, J. N., Narita, N., et al. 2008, ApJ, 686, 649

Jurić, M. & Tremaine, S. 2008, ApJ, 686, 603

Kalas, P., Graham, J. R., Chiang, E., et al. 2008, Science, 322, 1345

Kane, S. R., Howard, A. W., Pilyavsky, G., et al. 2011, ApJ, 733, 28

Kane, S. R., Mahadevan, S., von Braun, K., Laughlin, G., & Ciardi, D. R. 2009, PASP, 121, 1386

Kley, W. & Crida, A. 2008, A&A, 487, L9

Kley, W., Lee, M. H., Murray, N., & Peale, S. J. 2005, A&A, 437, 727

Knutson, H. A., Charbonneau, D., Cowan, N. B., et al. 2009, ApJ, 690, 822

Knutson, H. A., Charbonneau, D., Noyes, R. W., Brown, T. M., & Gilliland, R. L. 2007, ApJ, 655, 564

Knutson, H. A., Madhusudhan, N., Cowan, N. B., et al. 2011, eprint arXiv, 1104, 2901

Kopal, Z. 1942, ApJ, 96, 399

Kovács, G., Bakos, G. Á., Hartman, J. D., et al. 2010, ApJ, 724, 866

Kozai, Y. 1962, AJ, 67, 591

Lagrange, A.-M., Bonnefoy, M., Chauvin, G., et al. 2010, Science, 329, 57

Lagrange, A.-M., Gratadour, D., Chauvin, G., et al. 2009, A&A, 493, L21

Lai, D., Foucart, F., & Lin, D. N. C. 2011, MNRAS, 412, 2790

Laskar, J. 2008, Icarus, 196, 1

Laskar, J. & Gastineau, M. 2009, Nature, 459, 817

Latham, D. W., Stefanik, R. P., Mazeh, T., Mayor, M., & Burki, G. 1989, Nature, 339, 38

Laughlin, G., Deming, D., Langton, J., et al. 2009, Nature, 457, 562

Levison, H. F., Morbidelli, A., Vanlaerhoven, C., Gomes, R., & Tsiganis, K. 2008, Icarus, 196, 258

Levrard, B., Winisdoerffer, C., & Chabrier, G. 2009, ApJ, 692, L9

Lin, D. N. C., Bodenheimer, P., & Richardson, D. C. 1996, Nature, 380, 606

Lissauer, J. J., Fabrycky, D. C., Ford, E. B., et al. 2011a, Nature, 470, 53

Lissauer, J. J., Ragozzine, D., Fabrycky, D. C., et al. 2011b, eprint arXiv, 1102, 543

Lithwick, Y. & Wu, Y. 2010, eprint arXiv, 1012, 3706, submitted to ApJ

Loeillet, B., Shporer, A., Bouchy, F., et al. 2008, A&A, 481, 529

Lovis, C. & Pepe, F. 2007, A&A, 468, 1115

Lovis, C., Ségransan, D., Mayor, M., et al. 2011, A&A, 528, 112

Lubow, S. H. & Ida, S. 2010, Exoplanets, 347

Maeder, A. & Meynet, G. 1989, Astronomy and Astrophysics (ISSN 0004-6361), 210, 155

Malmberg, D. & Davies, M. B. 2009, MNRAS, 394, L26

Malmberg, D., Davies, M. B., & Chambers, J. E. 2007a, MNRAS, 377, L1

Malmberg, D., Davies, M. B., & Heggie, D. C. 2011, MNRAS, 411, 859

Malmberg, D., de Angeli, F., Davies, M. B., et al. 2007b, MNRAS, 378, 1207

Mandel, K. & Agol, E. 2002, ApJ, 580, L171

Mardling, R. A. 2010, MNRAS, 407, 1048

Marois, C., Macintosh, B., Barman, T., et al. 2008, Science, 322, 1348

Marois, C., Zuckerman, B., Konopacky, Q. M., Macintosh, B., & Barman, T. 2010, Nature, 468, 1080

Masset, F. & Snellgrove, M. 2001, MNRAS, 320, L55

Masset, F. S., Morbidelli, A., Crida, A., & Ferreira, J. 2006, ApJ, 642, 478

Matsumura, S., Peale, S. J., & Rasio, F. A. 2010a, ApJ, 725, 1995

Matsumura, S., Thommes, E. W., Chatterjee, S., & Rasio, F. A. 2010b, ApJ, 714, 194

Mayor, M., Bonfils, X., Forveille, T., et al. 2009a, A&A, 507, 487

Mayor, M. & Queloz, D. 1995, Nature, 378, 355

Mayor, M., Udry, S., Lovis, C., et al. 2009b, A&A, 493, 639

Mazeh, T. & Shaham, J. 1979, A&A, 77, 145

McArthur, B. E., Benedict, G. F., Barnes, R., et al. 2010, ApJ, 715, 1203

McLaughlin, D. B. 1924, ApJ, 60, 22

Miller, G. R. M., Cameron, A. C., Simpson, E. K., et al. 2010, A&A, 523, 52

Mordasini, C., Alibert, Y., & Benz, W. 2009a, A&A, 501, 1139

Mordasini, C., Alibert, Y., Benz, W., & Naef, D. 2009b, A&A, 501, 1161

Mordasini, C., Dittkrist, K. M., Alibert, Y., et al. 2011, eprint arXiv, 1101, 3238

Mordasini, C., Klahr, H., Alibert, Y., Benz, W., & Dittkrist, K.-M. 2010, eprint arXiv, 1012, 5281

Morton, T. D. & Johnson, J. A. 2011, ApJ, 729, 138

Moutou, C., Diaz, R. F., Udry, S., et al. 2011, eprint arXiv, 1105, 3849, accepted in A&A

Moutou, C., Hébrard, G., Bouchy, F., et al. 2009, A&A, 498, L5

Murray, C. D. & Dermott, S. F. 2000, Solar System Dynamics, iSBN: 0521575974

Naef, D., Mayor, M., Beuzit, J.-L., et al. 2005, Proceedings of the 13th Cambridge Workshop on Cool Stars, 560, 833

Nagasawa, M., Ida, S., & Bessho, T. 2008, ApJ, 678, 498

Naoz, S., Farr, W. M., Lithwick, Y., Rasio, F. A., & Teyssandier, J. 2011, Nature, 473, 187

Narita, N., Enya, K., Sato, B., et al. 2007, PASJ, 59, 763

Narita, N., Hirano, T., Sanchis-Ojeda, R., et al. 2010a, PASJ, 62, L61

Narita, N., Hirano, T., Sato, B., et al. 2009a, PASJ, 61, 991

Narita, N., Sato, B., Hirano, T., & Tamura, M. 2009b, PASJ, 61, L35

Narita, N., Sato, B., Hirano, T., et al. 2010b, PASJ, 62, 653

Narita, N., Sato, B., Ohshima, O., & Winn, J. N. 2008, PASJ, 60, L1

Nelson, R. P. & Papaloizou, J. C. B. 2004, MNRAS, 350, 849

Nordström, B., Mayor, M., Andersen, J., et al. 2004, A&A, 418, 989

Ogilvie, G. I. & Lin, D. N. C. 2004, ApJ, 610, 477

Ogilvie, G. I. & Lin, D. N. C. 2007, ApJ, 661, 1180

Ogilvie, G. I. & Lubow, S. H. 2003, ApJ, 587, 398

Ohta, Y., Taruya, A., & Suto, Y. 2005, ApJ, 622, 1118

Paardekooper, S.-J. & Mellema, G. 2006, A&A, 459, L17

Papaloizou, J. C. B. & Larwood, J. D. 2000, MNRAS, 315, 823

Pepe, F., Mayor, M., Galland, F., et al. 2002, A&A, 388, 632

Petrie, R. M. 1938, Journal of the Royal Astronomical Society of Canada, 32, 257

Pinsonneault, M. H., DePoy, D. L., & Coffee, M. 2001, ApJ, 556, L59

Pollacco, D., Skillen, I., Cameron, A. C., et al. 2008, MNRAS, 385, 1576

Pollacco, D. L., Skillen, I., Cameron, A. C., et al. 2006, PASP, 118, 1407

Pollack, J. B., Hubickyj, O., Bodenheimer, P., et al. 1996, Icarus, 124, 62

Pont, F., Endl, M., Cochran, W. D., et al. 2010, MNRAS, 402, L1

Pont, F., Gilliland, R. L., Moutou, C., et al. 2007, A&A, 476, 1347

Queloz, D., Anderson, D., Cameron, A. C., et al. 2010, A&A, 517, L1

Queloz, D., Eggenberger, A., Mayor, M., et al. 2000, A&A, 359, L13

Queloz, D., Henry, G. W., Sivan, J. P., et al. 2001, A&A, 379, 279

Rasio, F. A. & Ford, E. B. 1996, Science, 274, 954

Rice, W. K. M., Armitage, P. J., & Hogg, D. F. 2008, MNRAS, 384, 1242

Rossiter, R. A. 1924, ApJ, 60, 15

Sahlmann, J., Lovis, C., Queloz, D., & Ségransan, D. 2011a, A&A, 528, L8

Sahlmann, J., Ségransan, D., Queloz, D., et al. 2011b, A&A, 525, 95

Sanchis-Ojeda, R., Winn, J. N., Holman, M. J., et al. 2011, ApJ, 733, 127

Santos, N. C., Israelian, G., & Mayor, M. 2004, A&A, 415, 1153

Santos, N. C., Mayor, M., Naef, D., et al. 2002, A&A, 392, 215

Schaller, G., Schaerer, D., Meynet, G., & Maeder, A. 1992, A&ASS, 96, 269

Schlaufman, K. C. 2010, ApJ, 719, 602

Schlesinger, F. 1910, Publications of the Allegheny Observatory of the University of Pittsburgh ; v. 1, 1, 123

Seager, S. 2011, Exoplanets by Sara Seager. University of Arizona Press

Seager, S. & Mallén-Ornelas, G. 2003, ApJ, 585, 1038

Ségransan, D., Udry, S., Mayor, M., et al. 2010, A&A, 511, 45

Seneta, E. 1996, Int Stat Rev, 64, 255

Shakura, N. I. & Sunyaev, R. A. 1973, A&A, 24, 337

Silvotti, R., Schuh, S., Janulis, R., et al. 2007, Nature, 449, 189

Simpson, E. K., Pollacco, D., Cameron, A. C., et al. 2011, MNRAS, 600

Skumanich, A. 1972, ApJ, 171, 565, a&AA ID. AAA007.114.020

Smalley, B., Anderson, D. R., Cameron, A. C., et al. 2010, A&A, 520, 56

Smith, A. M. S., Cameron, A. C., Christian, D. J., et al. 2006, MNRAS, 373, 1151

Snellen, I. A. G., de Kok, R. J., de Mooij, E. J. W., & Albrecht, S. 2010, Nature, 465, 1049

Soubiran, C. & Triaud, A. 2004, A&A, 418, 1089

Southworth, J. 2009, MNRAS, 394, 272

Southworth, J., Wheatley, P. J., & Sams, G. 2007, MNRAS, 379, L11

Sozzetti, A., Torres, G., Charbonneau, D., et al. 2007, ApJ, 664, 1190

Steinmetz, M., Zwitter, T., Siebert, A., et al. 2006, AJ, 132, 1645

Sumi, T., Kamiya, K., Bennett, D. P., et al. 2011, Nature, 473, 349

Tamuz, O., Ségransan, D., Udry, S., et al. 2008, A&A, 480, L33

Tanaka, H., Takeuchi, T., & Ward, W. R. 2002, ApJ, 565, 1257

Tegmark, M., Strauss, M. A., Blanton, M. R., et al. 2004, PhRvD, 69, 103501

Thommes, E. W. 2005, ApJ, 626, 1033

Thommes, E. W., Matsumura, S., & Rasio, F. A. 2008, Science, 321, 814

Torres, G., Andersen, J., & Giménez, A. 2010, A&AR, 18, 67

Torres, G., Fressin, F., Batalha, N. M., et al. 2011, ApJ, 727, 24

Triaud, A. H. M. J., Cameron, A. C., Queloz, D., et al. 2010, A&A, 524, 25

Triaud, A. H. M. J., Queloz, D., Bouchy, F., et al. 2009, A&A, 506, 377

Triaud, A. H. M. J., Queloz, D., Hellier, C., et al. 2011, A&A, 531, 24

Walsh, K. J., Morbidelli, A., Raymond, S. N., O'Brien, D. P., & Mandell, A. M. 2011, Nature, 475, 206

Ward, W. R. 1997, Icarus, 126, 261

Watson, C. A., Littlefair, S. P., Diamond, C., et al. 2011, MNRAS, 413, L71

Wilson, D. M., Gillon, M., Hellier, C., et al. 2008, ApJ, 675, L113

Winn, J. N. 2010, Exoplanets, 55

Winn, J. N., Fabrycky, D., Albrecht, S., & Johnson, J. A. 2010a, ApJ, 718, L145

Winn, J. N., Holman, M. J., Henry, G. W., et al. 2009a, ApJ, 693, 794

Winn, J. N., Howard, A. W., Johnson, J. A., et al. 2011a, AJ, 141, 63

Winn, J. N., Johnson, J. A., Albrecht, S., et al. 2009b, ApJ, 703, L99

Winn, J. N., Johnson, J. A., Fabrycky, D., et al. 2009c, ApJ, 700, 302

Winn, J. N., Johnson, J. A., Howard, A. W., et al. 2010b, ApJ, 718, 575

Winn, J. N., Johnson, J. A., Howard, A. W., et al. 2010c, ApJ, 723, L223

Winn, J. N., Johnson, J. A., Narita, N., et al. 2008, ApJ, 682, 1283

Winn, J. N., Matthews, J. M., Dawson, R. I., et al. 2011b, eprint arXiv, 1104, 5230

Winn, J. N., Noyes, R. W., Holman, M. J., et al. 2005, ApJ, 631, 1215

Wolf, A. S., Laughlin, G., Henry, G. W., et al. 2007, ApJ, 667, 549

Wolszczan, A. & Frail, D. A. 1992, Nature, 355, 145

Wolszczan, A. & Kuchner, M. 2010, Exoplanets, 175

Wright, J. T., Fischer, D. A., Ford, E. B., et al. 2009a, ApJ, 699, L97

Wright, J. T., Upadhyay, S., Marcy, G. W., et al. 2009b, ApJ, 693, 1084

Wu, Y. & Lithwick, Y. 2010, eprint arXiv, 1012, 3475, submitted to ApJ

Wu, Y. & Murray, N. 2003, ApJ, 589, 605

Wu, Y., Murray, N. W., & Ramsahai, J. M. 2007, ApJ, 670, 820